DIETRICH
Geology & Geophysics

MECHANICS OF SEDIMENT MOVEMENT

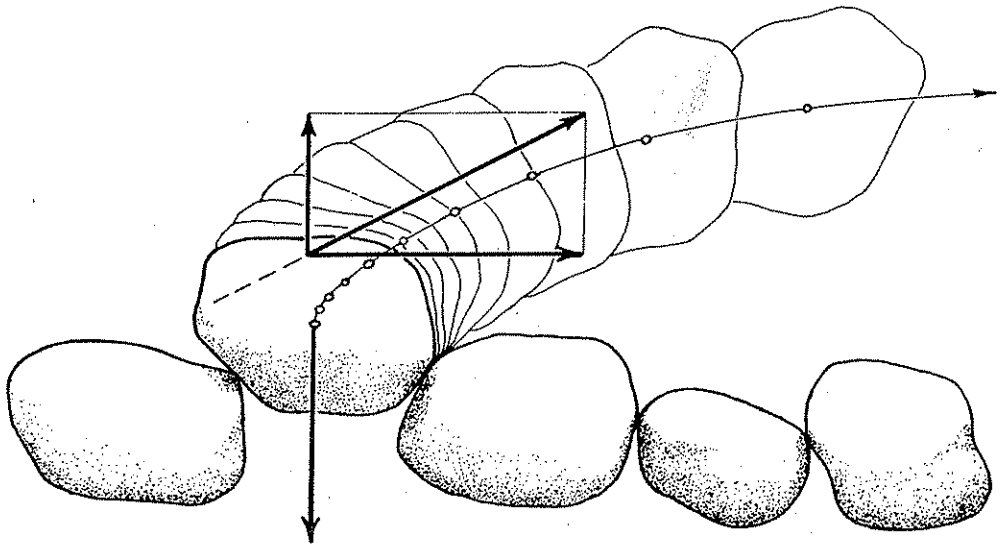

S.E.P.M. SHORT COURSE NUMBER 3
2nd Edition, PROVIDENCE 1984
SPONSORED BY THE EASTERN SECTION S.E.P.M.

MECHANICS OF SEDIMENT MOVEMENT

Lecture notes for Short Course No. 3, sponsored by the Eastern Section of the Society of Economic Paleontologists and Mineralogists, and given in Providence, Rhode Island, March 13-14, 1984

Gerard V. Middleton, McMaster University

John B. Southard, Massachusetts Institute of Technology

SECOND EDITION

MARCH 1984

CONTENTS

LIST OF COMMONLY USED SYMBOLS

A	cross-sectional area normal to the flow; inverse of von Kármán constant; area of ripple in streamwise profile
A_o	constant in analysis of bed-form shape
A_1	constant of integration in analysis of the law of the wall for smooth flow; constant in analysis of bed-form shape
a_1	coefficient in analysis of incipient movement
a_2	coefficient in analysis of incipient movement
B	constant term in law of wall for smooth flow; Bingham number
B'	constant term in law of wall for fully rough flow
$b.$	distance between clefts along gravity-flow head
C	fractional volume concentration of grains in a fluid; Chézy coefficient; cohesion; speed of sound
C_D	drag coefficient
C_L	lift coefficient
c	celerity of surface gravity waves
c_1	constant of integration; coefficient in analysis of incipient movement
c_2	constant of integration; coefficient in analysis of incipient movement
D	diameter
D_n	nominal diameter
D^o	dimensionless sediment diameter
d	flow depth
d^o	dimensionless flow depth
E	energy
E_w	energy per unit weight of fluid
F	shear stress exerted by flow on saltation carpet or traction carpet
Fr	Froude number
Fr'	Froude number based on reduced gravity g'
F_D	drag force
F_G	gravity force
F_L	lift force
F_R	resistance force
f	function symbol; friction factor
f_o	friction factor associated with lower surface of density current
f_i	friction factor associated with upper surface of density current
g	acceleration due to gravity
g'	reduced gravity, $g' = g(\rho_s-\rho)/\rho$ or $g' = g[\rho_s-\rho)/\rho_s]$
H	mean height of grain rise in saltation; height of bed forms
H_o	specific head
H^o	dimensionless ripple height
H_L	head loss
h	elevation above datum; elevation head; thickness of gravity-flow head
h_o	elevation of channel bottom
h_s	elevation of water surface
h_n	height to overhang of turbidity-current head
I	moment of inertia

K constant in analysis of bed-form shape
K_1 constant in analysis of incipient movement; porosity correction factor in sediment conservation equation, $K_1 = 1/(1-\lambda)$
K_2 constant in analysis of incipient movement; constant in analysis of bed-form shape
K_3 constant in analysis of bed-form shape
k_s equivalent sand roughness
L length dimension; characteristic length scale; bed-form spacing; dimensionless sediment concentration, $L = D/S$
L^o dimensionless bed-form spacing
M mass dimension
m mass
N dimensionless number of grains in motion per unit area and unit time
n number of grains in motion per unit area and unit time
P wetted perimeter; flow power; normal stress transmitted by grain collisions
p fluid pressure; pore pressure
Q discharge
q discharge per unit width
q_f volumetric bed-form transport rate per unit width
q_s volumetric sediment transport rate per unit width
q_{sb} volumetric bed-load transport rate per unit width
R derivative of sediment transport rate with respect to bed elevation, $R = dq_s/dh$
Re Reynolds number
Re_* boundary Reynolds number, $Re_* = u_*D/\nu$
R_H hydraulic radius
S slope, $S = \tan\phi$; average spacing of particles
$S.F.$ Corey Shape Factor
T time dimension; period of bursts; shear stress transmitted by grain collisions
T_r passage time for a bed form past a station
t_s shear stress transmitted by both grain collisions and fluid thickness of traction carpet
U flow velocity averaged over a cross section, $U = Q/A$
U_B bed-form velocity
U_G grain velocity
U^o dimensionless flow velocity
U_{max} maximum or surface velocity
U_s surface velocity in open channel flow
u instantaneous fluid velocity in the x direction
$\overline{u}$ time-average fluid velocity in the x direction
u' instantaneous deviation from $\overline{u}$, $u' = u - \overline{u}$
u_* shear velocity, $u_* = (\tau_o/\rho)^{1/2}$
u_{*c} value of u_* at threshold of sediment movement
V fluid velocity, used in various ways; characteristic velocity scale
v instantaneous fluid velocity in the y direction
$\overline{v}$ time-average fluid velocity in the y direction
v' instantaneous deviation from $\overline{v}$, $v' = v - \overline{v}$
W work
W' submerged weight of saltating grains per unit area of bed

w	settling velocity (fall velocity); instantaneous fluid velocity in the z direction
$\overline{w}$	time-average fluid velocity in the z direction
w'	instantaneous deviation from $\overline{w}$, $w' = w - \overline{w}$
x	streamwise coordinate direction
y	cross-stream coordinate direction normal to boundary
y_o	roughness length
y_1	displacement length
y^+	dimensionless distance from boundary
z	cross-stream coordinate parallel to boundary; Rouse number, $z = w/\beta\kappa u_*$
α	angle of internal friction; angle of imbrication; ripple slip-face angle
β	Shields parameter; coefficient relating ε_s and ε, $\varepsilon_s = \beta\varepsilon$
β_c	value of Shields parameter at threshold of sediment movement
γ	weight per unit volume (specific weight) of fluid, $\gamma = \rho g$
γ_s	weight per unit volume (specific weight) of solid, $\gamma_s = \rho_s g$
γ_x	downchannel component of γ
γ'	submerged weight per unit volume of solid, $\gamma' = \gamma_s - \gamma$
δ	thickness of boundary layer
δ_v	thickness of viscous sublayer
ε	eddy diffusion coefficient (kinematic eddy viscosity)
ε_s	eddy diffusion coefficient for sediment
η	eddy viscosity
κ	von Kármán constant
λ	porosity
μ	dynamic viscosity of fluid
μ_s	viscosity of sediment-fluid mixture
ν	kinematic viscosity, $\nu = \mu/p$
ρ	fluid density
ρ_s	solid density
σ	standard deviation; normal stress
τ	shear stress
τ_o	boundary shear stress
τ_c	critical or threshold boundary shear stress; yield stress for granular medium
τ_i	shear stress at upper surface of density current
ϕ	angle of inclination
ψ	Wadell sphericity
ψ_p	maximum projection sphericity

CHAPTER 1. BEHAVIOR OF FLUIDS

INTRODUCTION

Some knowledge of fluid dynamics is essential to an adequate understanding of sediment movement. We're not assuming any previous knowledge on your part. Chapters 1, 3, and 5 present a very selective treatment of some of the topics in fluid dynamics that are important in the study of sediment movement. This material is not a substitute for a more substantial background in fluid flow, but it allows a level of discussion of many of the important ideas in the mechanics of sediment transport that would not otherwise be possible.

Fluids are substances that deform continuously and permanently when subjected to forces that vary in magnitude or direction from point to point. The nature of the relationship between the deforming forces and the geometry of deformation varies from fluid to fluid; as discussed in this chapter, the relationship is a simple linear one for air and water, the two fluids most important in sedimentology.

Liquids and gases differ greatly in their structure on the molecular scale. How is it that the macroscopic motions of these two kinds of fluid need not be considered separately? The answer is that fluids can be treated as if they were continua--as if their constituent matter, which is actually distributed discontinuously as atoms and molecules, were smeared uniformly throughout space. The justification for this approach is that it works extremely well for fluid flows on scales that are much larger than the intermolecular spacing. This includes most problems in sediment movement down to the range of colloidal sizes (fractions of a micrometer).

In this chapter we'll develop some ideas in fluid mechanics by looking at three kinds of flow: shearing of fluid between parallel plates, flow past a sphere, and flow down an inclined plane. The last two are of direct importance to sedimentology, and we'll build upon the results in later chapters.

SHEARING A FLUID BETWEEN PARALLEL PLATES

For a first look at how fluids behave when they are deformed, make a pencil-and-paper experiment. Imagine two parallel plates, spaced a distance L apart, with a fluid at rest between them (Figure 1.1). The upper plate is rapidly accelerated to a constant velocity parallel to itself by applying a force per unit area F over its entire surface, while the lower plate is held fixed by applying to it an equal and opposite force per unit area. This kind of flow is called Couette flow. (Never mind that in real life this would be a difficult experiment because of loss of fluid around the edges.) The fluid is set in motion by friction

from the moving plate. How will the fluid move? More specifically, how will velocity in the fluid vary along a line normal to the plates? After an initial transient period of adjustment during which progressively lower layers of the fluid are brought into motion, the velocity would vary linearly from zero at the stationary plate to V at the moving plate (Figure 1.2).

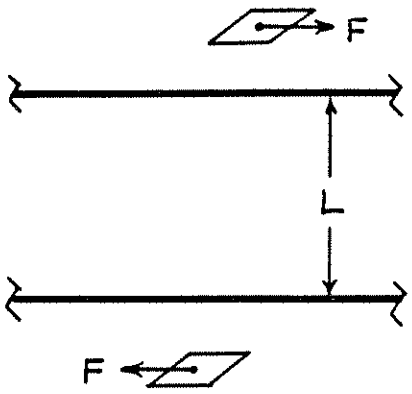

Figure 1.1 Hypothetical experimental arrangement for shearing a fluid between two parallel plates. Cross-sectional view shows the two plates, spaced a distance L apart and extending indefinitely in all directions, with equal and opposite forces per unit area F exerted uniformly over the outer surfaces of the plates.

Note that the fluid in contact with each of the plates has exactly the same velocity as the plates themselves. This is a manifestation of what is known as the no-slip condition: fluid in contact with a solid boundary has exactly the same velocity as that boundary. This is a fact of observation, although it can be justified by considerations on intermolecular forces.

To see why the velocity distribution between the plates is linear, pass an imaginary plane, parallel to the plates, anywhere through the fluid. Since the fluid contained between this plane and either plate is not being accelerated after the steady state is attained, the fluid on either side of this plane must exert on the fluid on the other side of the plane the same force per unit area F as that on the plates themselves. Since the imaginary plane can be located anywhere between the two plates, the shear force per unit area across all such planes in the fluid, called the shear stress τ, must be the same. And because the fluid must be expected to shear or deform at the same rate for the same applied shearing force, the rate of change of velocity normal to the plates must be constant; assuming the y axis to be normal to the plates, $du/dy = k$. So the velocity itself must vary linearly: taking $y = 0$ at the lower plate,

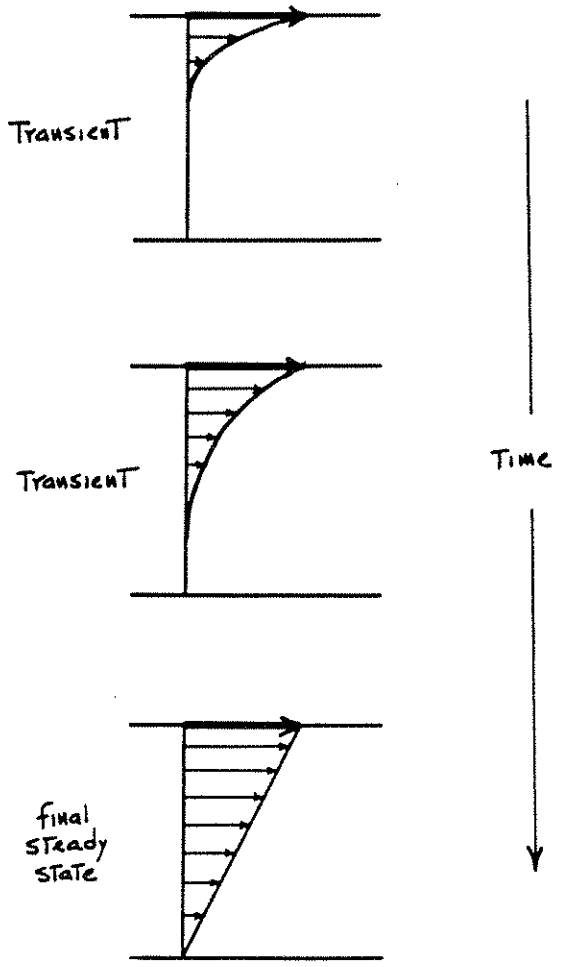

Figure 1.2 Development of velocity distribution in the fluid between the plates after the upper plate is rapidly accelerated to a constant velocity V. In each picture the succession of fluid velocities along the arrows represents the continuous distribution of fluid velocities along the line shown normal to the plates.

$$u = \int k\,dy = ky + c$$

Evaluating the constant of integration using the no-slip condition that $u = 0$ at $y = 0$, we find $c = 0$, so

$$u = ky \tag{1.1}$$

What determines the value of F needed to produce a given difference in velocity between the two plates? For many fluids, including air and water, the ratio of F to the quantity V/L would be found to be the same for all values of F: $F/(V/L) = \text{const}$. It was shown above that the shear stress is exactly F everywhere in the fluid, and since du/dy is the same everywhere it must be equal to V/L, the average velocity gradient. So

$$\frac{\tau}{du/dy} = \text{const} = \mu \tag{1.2}$$

This constant ratio μ is called the viscosity of the fluid, and is the property that characterizes the resistance of the fluid to deformation. And it's indeed an intrinsic property of the fluid, in that it does not depend on the state of motion but only on the nature of the fluid itself. Different fluids have different viscosities, and for a given fluid the viscosity is a function of temperature. Equation (1.2) tells you that the velocity gradient at every point in the fluid is proportional to the ratio of the shear stress to the viscosity.

You can see now the significance of k in the linear velocity distribution in Equation (1.1). Combining Equation (1.2) with the condition that $du/dy = k$,

$$\frac{du}{dy} = k = \frac{\tau}{\mu} \tag{1.3}$$

and integrating as before (and remembering that τ isn't a function of y in this special flow),

$$u = \frac{\tau}{\mu} y \tag{1.4}$$

The parallel-plate experiment is a specialized case of shearing in a fluid. In a more general flow, the deformation of the fluid in any tiny volume can be visualized in the same way, but both the rate of shearing and the orientation of the shear planes are likely to vary from point to point. A relationship like Equation (1.2) holds at every point in a sheared fluid, no

matter how much the rate and orientation of the shearing vary from place to place:

$$\frac{\tau}{du/dy} = \mu, \quad \tau = \mu \frac{du}{dy} \tag{1.5}$$

where τ is the shear stress exerted across the shearing surfaces at some point in the fluid, and du/dy is the rate of change of the local fluid velocity u in the direction y normal to the shearing surfaces at the point (Figure 1.3).

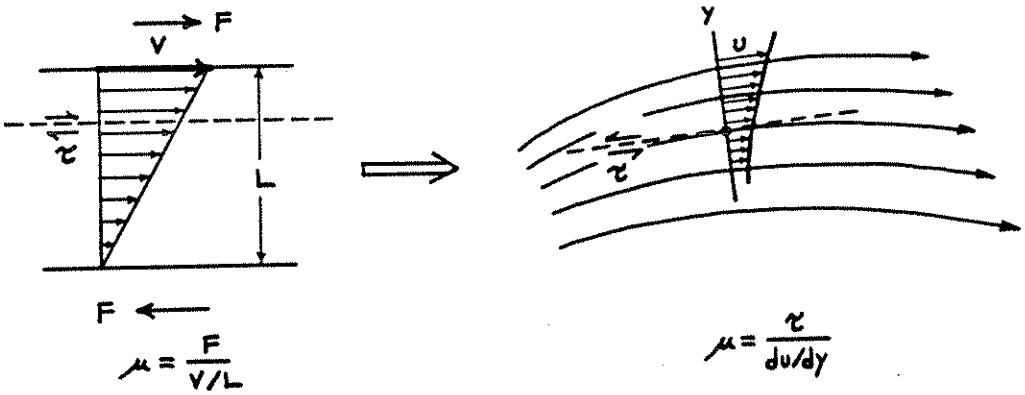

Figure 1.3 How shear stress and viscosity in the parallel-plate experiment generalize to shear stress and viscosity at a point in any sheared region of the fluid.

FLOW PAST A SPHERE: AN INTRODUCTION TO DIMENSIONAL ANALYSIS

Introduction

Flow past a sphere is of obvious importance in sedimentology. Rounded sediment particles settling through still fluid see almost exactly the same flow. And what's just as important, it's a good guide to the forces and motions involved in flow over particles at rest on the bed of a flowing fluid. We'll make a start on the drag exerted by flow past a sphere here--just enough to show how the problem can best be approached--and then consider the physical effects more closely in Chapters 2 and 4. Another motivation for this section is to convince you, by example, of the importance and utility of careful dimensional reasoning about fluid-flow problems.

Just from considerations of space and motion, it's clear that the approaching fluid must both move faster and be displaced laterally as it flows past the sphere. On the other hand, the no-slip condition requires that the fluid velocity go to zero

everywhere at the surface of the sphere; this implies the existence of velocity gradients, very sharp under some conditions, at and near the surface of the sphere. These velocity gradients produce a shear stress on the surface of the sphere; see Equation (1.5). When summed over the surface, the shear stress exerted by the fluid on the sphere represents the part of the total drag force on the sphere called the viscous drag. Your intuition probably tells you (correctly in this case) that the pressure of the fluid, the normal force per unit area, is greater on the front of the sphere than on the back. The sum of the pressure over the entire surface of the sphere represents the other part of the drag force, called the pressure drag or form drag. You'll see later that the relative importance of viscous drag and pressure drag, as well as the qualitative flow patterns and the distance out into the fluid the sphere makes its presence felt, are greatly different in different ranges of flow. Even in such a seemingly simple flow there's a great variation in flow phenomena. This should put you on your guard against facile theorizing in sediment transport, for there are few kinds of sediment-transporting flows without an even greater degree of variety and complexity.

It does not make much difference whether the sphere is held motionless relative to moving fluid, or is towed through still fluid, or settles under its own weight; what's important is the movement of the sphere relative to the fluid. The differences among these three situations is explored in a little more detail in Chapter 2. For the sake of definiteness we'll assume here that the sphere is being towed or pushed through still fluid (Figure 1.4). All that's said here about the flow is then with reference to a point fixed relative to the moving sphere.

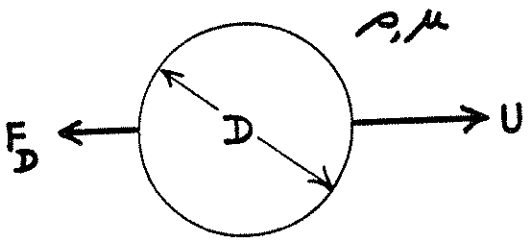

Figure 1.4 Definition sketch for variables involved in the motion of a sphere through still fluid.

Which Variables Are Important?

Think first about the resultant drag force F_D exerted on the sphere by the fluid. To account fully for the value assumed by F_D for a given sphere in a given fluid, we have to specify the values of certain other variables. (This carefully phrased sentence should not be interpreted as implying that F_D is necessarily the "dependent variable" in the problem; for a sphere settling under its own weight, it's more natural to think of F_D as an independent

variable and settling velocity as the dependent variable. What's important here is that there is a one-to-one correspondence between the value of F_D and the values of those other variables, irrespective of their dependence or independence. That said, however, for convenience we'll refer to such variables as independent variables.) The velocity U of the sphere relative to the fluid is important because it affects the shear in the fluid near the surface of the sphere, and therefore by Equation (1.5) the shear stress. Sphere diameter D is important for the same reason. Viscosity μ is important because it determines the shear force associated with a given rate of shear. Fluid density ρ must also be included, because the forces associated with the accelerations in the fluid depend upon ρ. If the sphere is in steady motion far from solid walls or a free surface, you can assume that no other variables are important. So

$$F_D = f(U, D, \rho, \mu) \tag{1.6}$$

where f is some function with one or more terms involving the four independent variables. (We'll often use the same symbol f for unrelated functions. In Chapter 5, f will also be used for a quantity called the friction factor.)

You might reasonably ask why neither sphere density nor acceleration of gravity are on the list. These are relevant only if the sphere settles under its own weight, and then only because they determine the weight of the sphere, to which F_D is then equal. Variables that enter the problem only by their effect on other variables already on the list and not because of some separate effect need not be included in the analysis. And there's no reason to think that either of these has any such significance.

If we're lucky in problems like this, we can use theory to derive an analytical form for the function in Equation (1.6) that agrees well with observation. If not, we must rely solely on experiment. For flow past a sphere there is indeed an analytical solution, described in Chapter 2, that agrees beautifully with experimental data, but it holds over only a limited range of the independent variables; over the rest of the range we have to obtain the function by experiment, as is commonly the case in problems of sediment movement. With flow past the sphere as an example, we need to consider how we can best go about organizing both data and thought by resorting to dimensional reasoning.

Some Dimensional Reasoning, and Its Consequences

Like every physically correct equation, Equation (1.6) must represent equality not only of magnitudes but also of dimensions. In most mechanical systems three basic dimensions are needed to express forces, motions, and system properties; these are usually

taken to be mass, length, and time. So whatever the form of the term or terms on the right side of Equation (1.6), the variables U, D, ρ, and μ must combine in such a way that each term has the dimensions of force, because the left side has the dimensions of force. The following list gives the dimensions of each of the five variables involved in flow past a sphere, in terms of mass M, length L, and time T:

F_D ---- ML/T^2

U ---- L/T

D ---- L

ρ ---- M/L^3

μ ---- M/LT

The only variable here whose dimensions are not straightforward is μ; the dimensions M/LT are obtained by use of Equation (1.5), by which μ is defined.

It's advantageous to rewrite equations like Equation (1.6) in dimensionless form. To do this, first make the left side dimensionless by dividing F_D by some product of independent variables that itself has the dimensions of force. Using the list of dimensions above, you can verify that ρU^2D^2 has the dimensions of force:

$$\rho U^2D^2 \text{ ----- } (M/L^3)(L/T)^2(L)^2 = ML/T^2$$

So dividing the left side of Equation (1.6) by ρU^2D^2 makes the left side of the equation dimensionless. The result, $F_D/\rho U^2D^2$, can be viewed as a dimensionless form of F_D. That leaves the right side of Equation (1.6) to be made dimensionless. There is one and only one way the four variables U, D, ρ, and μ can be combined into a dimensionless variable, namely $\rho UD/\mu$:

$$\frac{\rho UD}{\mu} \qquad (M/L^3)(L/T)(L)/(M/LT) \qquad \begin{matrix}\text{dimensionless} \\ \text{(M,L,T all cancel)}\end{matrix}$$

(That statement is not strictly true--but all the other possibilities are just $\rho UD/\mu$ raised to some power, and they're not independent of $\rho UD/\mu$.) So whatever the form of the function f, the right side of the dimensionless form of Equation (1.6) can be written using just one dimensionless variable:

$$\frac{F_D}{\rho U^2 D^2} = f\left(\frac{\rho UD}{\mu}\right) \qquad (1.7)$$

Equation (1.7) is an equivalent but dimensionless form of Equation (1.6). The great advantage of the dimensionless equation is that it involves only two variables--a dependent dimensionless variable $F_D/\rho U^2 D^2$ and an independent dimensionless variable $\rho UD/\mu$--instead of the original five. Think of the enormous saving in effort this implies for an experimental program to characterize the drag force. If you had to measure F_D as a function of each one of the four variables while holding the other three constant, you'd generate mountains of data and graphs. But Equation (1.7) tells you that U, D, ρ, and μ need only be varied so as to make $\rho UD/\mu$ vary. All of the experimental points for $F_D/\rho U^2 D^2$ obtained by varying $\rho UD/\mu$ should plot as a curve in a two-dimensional graph with these two variables along the axes. Whatever the value of U, D, ρ, and μ, all possible realizations of flow past a sphere are expressed by just one curve. This curve is shown in Figure 1.5 together with some of the experimental points that have been used to define it. The physics behind the curve is discussed in Chapters 2 and 4. And you could find the curve by varying only <u>one</u> of the four variables U, D, ρ, and μ--although you may not be able to get a very wide range of values of $\rho UD/\mu$ by varying only one of the variables. A fairly small number of experiments involving values of the original independent variables that combined to span a wide range of $\rho UD/\mu$ would suffice to characterize all other possible combinations of the independent variables. This is because each point in the dimensionless graph represents a great many different possible combinations of the original variables--an infinity of these, in fact. You thus gain a far-reaching predictive capability on the basis of relatively little observational effort.

A skeptic might find all this too good to be true. But the fact is that this is how things work, and the analysis of flow past a sphere is just one good example. A note of caution is in order, however. It's prudent to vary as many of the variables over as wide a range as possible; this doesn't take an enormous number of observations, and it's a check on the correctness of your analysis. You'll see below in more detail that if there's a larger number of important variables than you think, your data points would form a scattered band rather than a single curve. If you varied just one variable to try to find the curve, you'd indeed get a curve, but it wouldn't be the curve you were after; you'd be missing the scatter that would manifest itself if you varied the other variables as well.

Several notes are in order here:

(1) Variables of the form $\rho UD/\mu$ are called <u>Reynolds numbers</u>, usually denoted by Re or bold-faced R. Whenever both density and

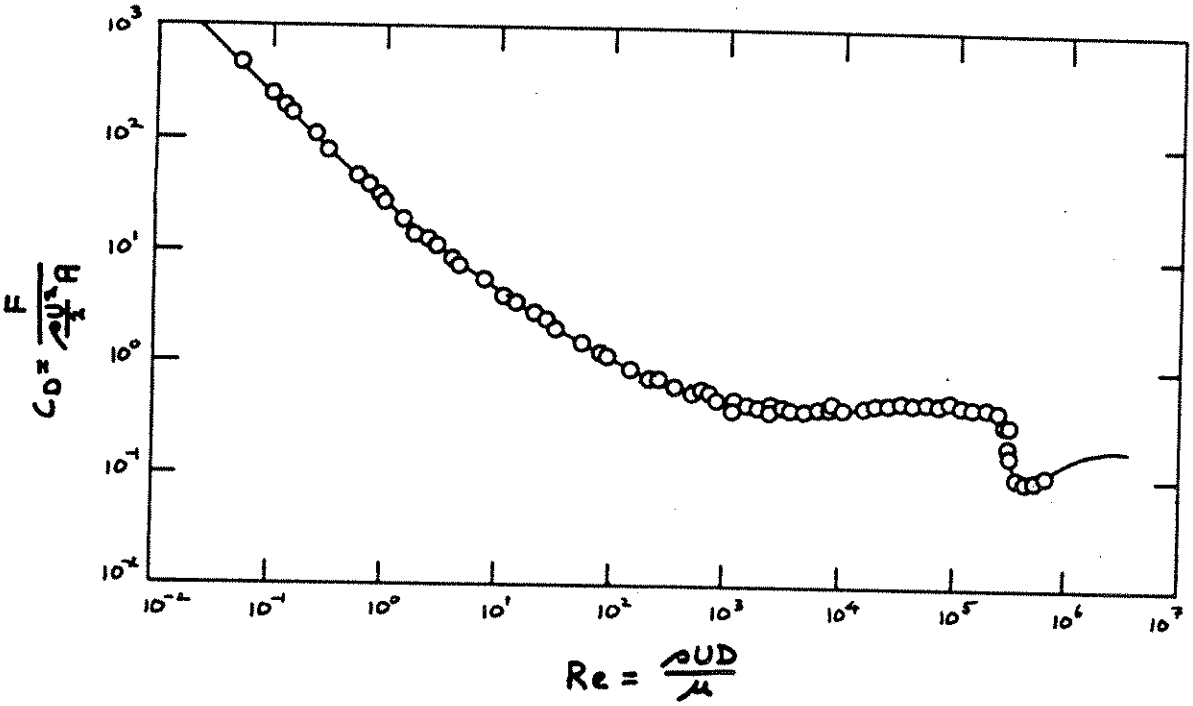

Figure 1.5 Plot of dimensionless drag force against $\rho UD/\mu$ for steady motion of a sphere through a viscous fluid. Instead of $F_D/\rho U^2 D^2$, an equivalent variable $F_D/(\rho U^2/2)A$ is plotted on the vertical axis, where A is the cross-sectional area of the sphere; see text. Experimental points are from several sources, and are somewhat generalized. Some of the experiments involve settling of a sphere through a still fluid, and others involve flow past a sphere held at rest. For a more detailed plot, see Schiller (1932).

viscosity are important in a problem and both a length variable and a velocity are involved, a Reynolds number can be formed and used. There are thus many different Reynolds numbers, with different length and velocity variables depending on the particular problem. You'll encounter others later in the notes.

(2) For the steady flow we've assumed, the variables U, D, ρ, and μ characterize not only everything about the distributions of shear stress and pressure over the entire surface of the sphere, which add up to F_D, but also the distributions of shear stress, pressure, and fluid velocity at every point in the surrounding fluid. Since $\rho UD/\mu$ replaces these four variables on the right side of Equation (1.7), the same can be said of the Reynolds number. Anything about forces and motions you might want to consider can be viewed as being specified completely by the Reynolds number.

(3) There's a further important consequence of the fact that each point on the curve of $F_D/\rho U^2D^2$ vs. $\rho UD/\mu$ represents an infinity of combinations of U, D, ρ, and μ. Suppose you wanted to find the drag force exerted by a certain flow on a sphere that's too large to fit into your laboratory. You could work with a much smaller sphere by adjusting the values of U, ρ, and μ so that $\rho UD/\mu$ is the same as in the flow in question past the large sphere. Then from the curve in Figure 1.5 the value of $F_D/\rho U^2D^2$ is also the same, and from it you could find the drag force F_D on the large sphere by substituting the corresponding values of U, D, and ρ. Or, on the other hand, you could study the flow around a very small sphere by use of a much larger sphere, with the same complete confidence in the results; an example is worked out in Appendix I. This is the essence of scale modeling. Viewed in this way, each point on the curve of $F_D/\rho U^2D^2$ vs. $\rho UD/\mu$ represents an infinite number of possible experiments, each of which is a scale model of all the others.

(4) In Figure 1.5 the dimensionless drag force is written in a conventional form that is slightly different from that derived above: $F_D/(\rho U^2/2)A$, where A is the cross-sectional area of the sphere, equal to $\pi D^2/4$. This differs from $F_D/\rho U^2D^2$ by the factor $\pi/8$, but its dimensions are exactly the same. It's usually called a drag coefficient, denoted by C_D; you can see why by writing

$$F_D = C_D \frac{\rho U^2}{2} A \tag{1.8}$$

where the factor $(\rho U^2/2)A$ on the right side has dimensions of force. The functional relationship between dimensionless drag force and Reynolds number in Equation (1.7) can be written in an entirely equivalent form using C_D:

$$C_D = \frac{F_D}{\frac{\rho U^2}{2} A} = f\left(\frac{\rho UD}{\mu}\right) \tag{1.9}$$

(5) There are alternative versions of the dependent dimensionless variable. Dividing by ρU^2D^2 isn't the only way to nondimensionalize F_D. You can check for yourself that $F_D/\mu UD$, $\rho F_D/\mu^2$, and $F/\mu U$ are other possibilities, obtained by combining F with the four variables ρ, μ, U, and D taken three at a time. (You'll see in a minute how to derive such variables.) Sometimes, as in the last two cases, one of the variables drops out; this happens when M or L or T appears in only one of the four variables chosen. Any of these three alternative dependent dimensionless

variables would serve just as well as $F/\rho U^2D^2$ to represent the data. You'll see below, however, that sometimes one is more revealing than the others.

How to Construct Dimensionless Variables

You may be wondering about how you could have constructed the dimensionless variable $\rho UD/\mu$ on your own instead of having it presented to you. Start with a very general product $\rho^a U^b D^c \mu^d$. The exponents a through d have to be adjusted so that the M, L, and T dimensions of the product cancel out. One of the exponents can be chosen arbitrarily, say d = 1, but then a, b, and c have to be adjusted by solving three equations, one each for M, L, and T, expressing the condition that the product be dimensionless. Using length as an example, you can see from the list of dimensions above that length enters into ρ to the power -3, into U to the power +1, into D to the power +1, and into μ to the power -1. So for L to cancel out of $\rho^a U^b D^c \mu$, the following condition must be met: $-3a + b + c - 1 = 0$. (Remember that we've already chosen d to be 1.) Two more conditions, one for M and one for T, give three linear equations in the three unknowns a,b,c:

$$\begin{aligned} -3a + b + c - 1 &= 0 \quad \text{(for L)} \\ a \qquad\quad + 1 &= 0 \quad \text{(for M)} \\ -b \qquad - 1 &= 0 \quad \text{(for T)} \end{aligned}$$

The solution is a = -1, b = -1, c = -1, so the product takes the form $\mu/\rho UD$. This is the inverse of the Reynolds number introduced above. If d had been taken as -1 at the outset, the result would have been the Reynolds number itself.

What If You Choose the Wrong Variables?

What would be the consequences of including an irrelevant variable in analyzing the dimensional structure of a problem like that of flow past a sphere? Suppose, just for the sake of discussion, that viscosity is not important in determining F_D. Then the functional relationship for F_D would be

$$F_D = f(U, D, \rho)$$

As before, you can start to make this equation dimensionless by forming the same dimensionless drag force $F_D/\rho U^2D^2$ on the left-hand side. But how about the right-hand side? The three variables U, D, and ρ can't be combined to form a dimensionless variable, because there isn't enough freedom to adjust exponents

to make a product $U^aD^b\rho^c$ dimensionless; this should be clear from the formal procedure outlined above for obtaining $\rho UD/\mu$. Then what takes the place of the Reynolds number on the right side? The answer is that the right side must be a numerical constant; there is no independent dimensionless variable. So if μ were not important in flow past a sphere, the dimensionless force $F_D/\rho U^2D^2$ would be a constant rather than a function of the Reynolds number. To generalize: if one original variable is eliminated from the problem, one dimensionless variable must be eliminated as well. In a graph of C_D vs. Re the experimental points would fall along a straight line parallel to the Re axis, as shown schematically in Figure 1.6. Now look back at the actual graph of C_D vs. Re in Figure 1.5. Over a wide range of Reynolds numbers from about 10^3 to greater than 10^5, C_D is nearly independent of the Reynolds number. Since μ is the only variable that appears in the Reynolds number but not in C_D, this tells you that μ is indeed not important in determining F_D at high Re. The reasons for this will be discussed in Chapter 4.

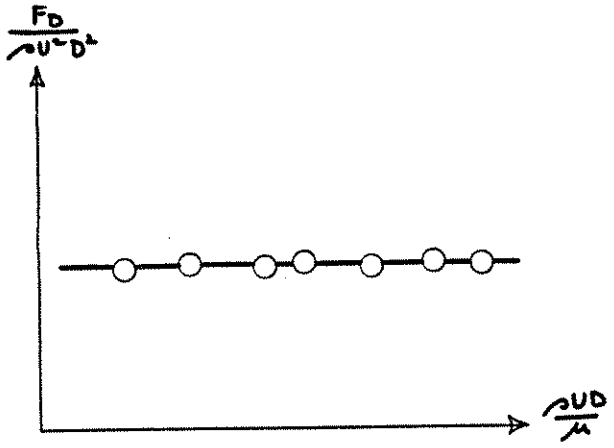

Figure 1.6. Sketch of what a graph of C_D vs. Re would look like for flow past a sphere if the drag force on the sphere did not depend on viscosity μ.

Now you can see why there's some practical advantage to using $F/\rho U^2D^2$ as the dependent dimensionless variable. The other three mentioned above contain μ, and so in a plot of any one of them against $\rho UD/\mu$ the segment of the curve for which μ is not important would plot as a sloping line rather than as a horizontal line, and the unimportance of μ would be harder to spot.

You should also consider the consequences of omitting an important variable from consideration. For example, if you had not been careful to keep the sphere well away from the wall of the vessel containing the fluid, you would find that the experimental points plot in a scattered band around the curve of C_D vs. Re in Figure 1.5, as shown in Figure 1.7. This tells you that some other variable is important in determining F_D and that you've inadvertently let it vary--assuming, of course, that your

measurements are free of errors in the first place. The obvious culprit is y, the distance of the center of the sphere from the wall (Figure 1.8). (This curve would differ somewhat depending on whether it's the sphere or the fluid that's moving relative to the wall, because of the inevitable development of a boundary layer at the wall in the latter case; more on boundary layers in Chapter 5.) With y included in the analysis, the functional relationship for F_D is of the form

$$F_D = f(U, D, \rho, \mu, y) \qquad (1.10)$$

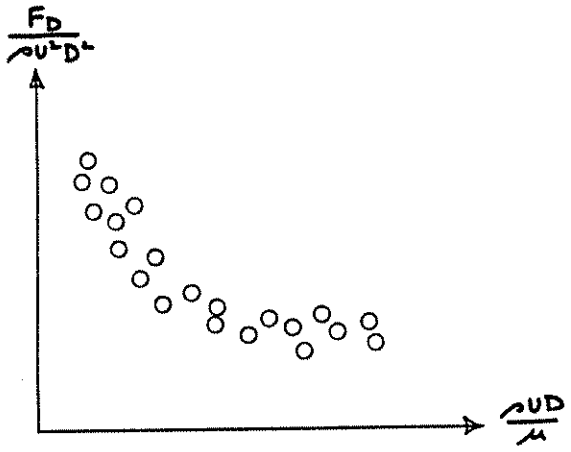

Figure 1.7 Sketch of what a graph of C_D vs. Re would look like for flow past a sphere if the sphere is located a short and experimentally uncontrolled distance from the wall of the vessel.

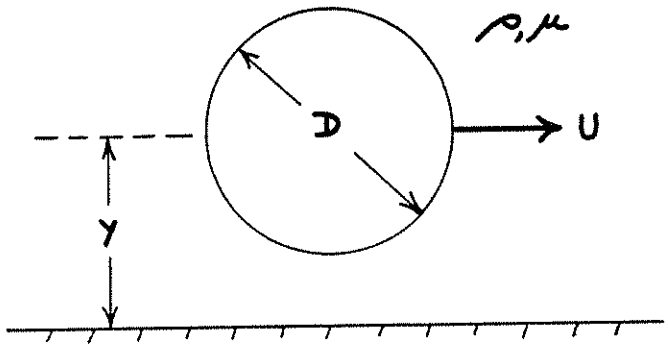

Figure 1.8 A sphere moving through fluid near a solid boundary.

In nondimensionalizing Equation (1.10) you should again expect to have a dimensionless drag force on the left and the Reynolds number on the right. But what happens to the new

variable y? You can use it to form one more independent dimensionless variable, in the same way you formed the Reynolds number. There has to be at least one other such variable, because y has to appear somewhere on the right side of the nondimensionalized version of Equation (1.10). A natural choice for this new variable is y/D (or D/y). You could instead form another Reynolds number, $\rho Uy/\mu$. But only two of the three variables $\rho UD/\mu$, $\rho Uy/\mu$, and y/D are independent of each other. (For example, you can arrive at this second Reynolds number by multiplying the first by the new dimensionless variable y/D. This is an illustration of the principle that you can always replace a dimensionless variable in a set of dimensionless variables by another one formed by multiplying or dividing it by one of the others.) So addition of one new independent variable to the problem adds only one new independent dimensionless variable. In dimensionless form Equation (1.10) is then

$$\frac{F_D}{\rho U^2 D^2} = f\left(\frac{\rho UD}{\mu}, \frac{y}{D}\right) \qquad (1.11)$$

The function in Equation (1.11) would plot as a curved surface in a three-dimensional graph with C_D, Re, and y/D along the axes (Figure 1.9). The two planes perpendicular to the y/D axis in Figure 1.9 show the range over which y/D varied in your experiments without your realizing it's important. The projection of the segment of the surface between these two planes onto the C_D-Re plane is the band in which your experimental points would fall. The intersection of the surface with the plane y/D = 0, also shown on the projection, represents the curve you would have gotten if you had always kept the sphere very far away from the wall; it's the same as the curve in Figure 1.7.

Finally, you could carry the analysis one step further by moving the sphere horizontally just beneath the free surface of a liquid at rest in a gravitational field (Figure 1.10). Of importance now is not only the distance y of the sphere below the free surface but also the acceleration of gravity g: if the movement of the sphere distorts the free surface, unbalanced gravity forces will tend to flatten the surface again, and surface gravity waves may be generated. Then

$$F_D = f(U, D, \rho, \mu, y, g) \qquad (1.12)$$

This adds still another independent dimensionless variable, and that variable must include g. There are five possibilities: $\mu g/\rho U^3$, $\rho^2 gD^3/\mu^2$, $\rho^2 gy^3/\mu^2$, U^2/gD, and U^2/gy, plus obvious variants obtained by inversion and exponentiation. (You could try constructing these by combining U, ρ, μ, D, and y three at a time with g and going through the procedure described above for Re.

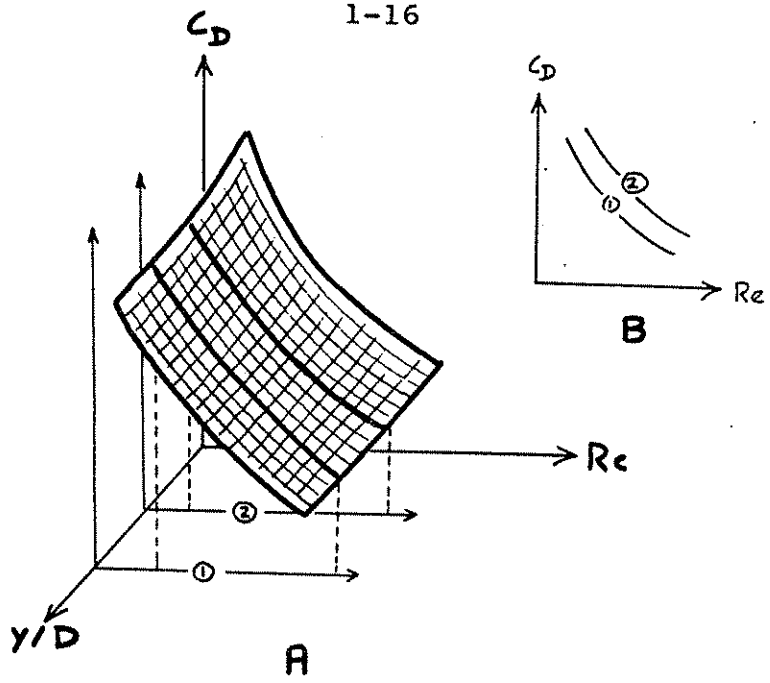

Figure 1.9 A. Schematic plot of C_D vs. Re and y/D for a sphere moving through still fluid near a planar wall. The two planes perpendicular to the y/D axis bracket the range of y/D values for which the hypothetical experimental points in Figure 1.7 were obtained. B. Plot of C_D vs. Re from Figure 1.7 obtained by projection of the function surface between the two y/D = const planes onto a plane of C_D vs. Re.

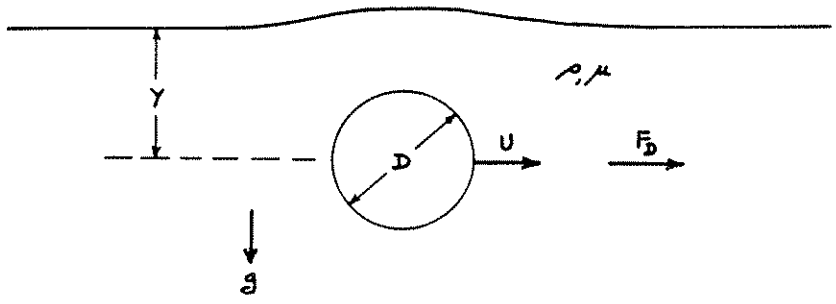

Figure 1.10 Definition sketch for flow past a sphere moving horizontally just below the free surface of a liquid.

You would also get y/D again in the process.) Any one of these five would suffice to express the effect of g on the drag force. Again only one is independent, because the others can all be obtained by combining that one (whichever you choose) with either $\rho UD/\mu$ or y/D. It's worth noting here that the square root of a variable like U^2/gy or U^2/gD, with a velocity, a length variable, and g, is called a Froude number, usually denoted by Fr or

bold-faced F. It's natural, although not essential, to use U^2/gD here because then each of the four dimensionless variables in the functional relationship can be viewed as being formed by combining F_D, μ, y, and g in turn with the three variables ρ, U, and D; see the following paragraph for details.

$$\frac{F_D}{\rho U^2 D^2} = f\left(\frac{\rho UD}{\mu}, \frac{U^2}{gy}, \frac{y}{D}\right) \qquad (1.13)$$

The function would plot as a four-dimensional "surface" in a graph of C_D vs. Re, Fr, and y/D. It's difficult for human beings to visualize such a graph. A good substitute would be to plot a three-dimensional graph for each of a series of values of one of the independent dimensionless variables. The trouble is that there's an infinite number of these three-dimensional graphs.

Suppose you had realized at the outset that all seven variables in Equation (1.12) were important in the problem. The systematic way of obtaining four dimensionless variables all at once is just an extension of the method described in an earlier section for obtaining the Reynolds number. Form four products by choosing three of the seven variables (the "repeating" variables) to be those raised to the exponents a, b, and c and using each of the remaining four variables in turn as the one that's raised to the exponent 1 (or any other fixed exponent, for that matter). You can verify for yourself that if you choose ρ, U, and D as the three repeating variables, the four products $\rho^a U^b D^c F_D$, $\rho^a U^b D^c \mu$, $\rho^a U^b D^c y$, and $\rho^a U^b D^c g$ would produce the four dimensionless variables in Equation (1.13), except that U^2/gD appears instead of U^2/gy. It turns out that for this procedure to work, the constraints on the choice of the three repeating variables are that (i) among them they include all three dimensions M, L, T, and (ii) they be dimensionally independent of each other, in the sense that you can't obtain the dimensions of any one by multiplying together the dimensions of the other two after raising them to some exponents. These constraints just ensure that you get solvable sets of simultaneous equations.

Conclusion

Most kinds of fluid flow that are important in natural environments don't lend themselves to analytical solutions, even when no sediment is moved, so one has to rely on experiment and observation to learn something about them. We've expatiated upon dimensionless variables and their use in expressing experimental results because this sort of analysis, usually called dimensional analysis, is so useful in dealing with problems of fluid flow and sediment movement. Dimensional analysis is a way of getting some useful information about a problem when you can't obtain an analytical solution and may not even know anything about the form of the solution, but you have some ideas about important physical

effects or variables. You'll encounter many examples of its use in later chapters.

Suppose that you're dealing with a fluid-flow problem that ca be simplified somehow, perhaps in geometry or in time variability to be manageable but still representative. Use your experience and physical intuition to identify the important variables. Form a set of dimensionless variables by which the observational results can be expressed. This represents the most efficient means of dealing with experimental data, and usually makes it possible to get some idea of the ranges in which certain physical effects are important or unimportant. Don't worry too much about guessing wrong about important variables; the example of flow past a sphere shows how you can find out and change course.

This approach was first systematized by Buckingham (1914, 1915) in two papers that are still very readable. The number of dimensionless variables equivalent to a given set of original variables is given by the Pi theorem, also called Buckingham's theorem. By the Pi theorem, the number of dimensionless variables corresponding to a number n of original variables that describe some physical problem is equal to n-m, where m is the number of dimensions by which the problem must be expressed. We haven't proved this here, but we've come close in demonstrating its application to flow past a sphere. More detailed discussions of dimensional analysis are given by Langhaar (1951), Sedov (1960), and Kline (1965), as well as most textbooks in fluid mechanics.

FLOW DOWN AN INCLINED PLANE

Steady and uniform flow of liquid down an inclined plane is a simplified but useful model for many natural flows that transport sediment. (A steady flow does not change with time; a uniform flow is the same at all cross-sections down the flow. It won't be until Chapter 5 that we deal with the problem of what the slope of the plane must be to produce uniform flow in the first place.) The freely deformable upper surface of the liquid, called the free surface, is open to the air. We'll neglect the minor forces exerted by the overlying air on the moving liquid. This kind of flow is called open-channel flow. The plane has no sidewalls, but we can think of it as an infinitely wide channel.

Again by the no-slip condition, the velocity at the very bottom of the flow is zero, so the velocity must increase upward in the flow. You might also guess that the flow is everywhere directed straight down the plane. This must certainly be true on the average, but you need to keep in mind the possibility of random fluctuations in velocity caused by passage of the swirls and eddies characteristic of fluid turbulence. Suffice it to say here that turbulence is of crucial importance in a wide range of flow conditions. You'll eventually see in Chapters 3 and 5 that turbulence develops in the flow at sufficiently high values of a Reynolds number based on the flow depth and the mean or maximum

velocity. A sedimentologist from a low-Reynolds-number planet would have the surprise of its life when it encountered the complexities of high-Reynolds-number flow, because the phenomena are difficult even to account for when observed, much less to predict.

Before trying to derive the velocity distribution in the flow from first principles, let's make a dimensional analysis, as for flow past a sphere. Taking the x direction down the plane and the y direction normal to the plane, let the flow velocity a distance y above the plane be the dependent variable u, let the flow depth be d, and let the downslope component of the weight per unit volume γ of the fluid, which is the driving force for the flow, be $\gamma_x = \gamma \sin\phi$, where ϕ is the angle of inclination of the plane (Figure 1.11).

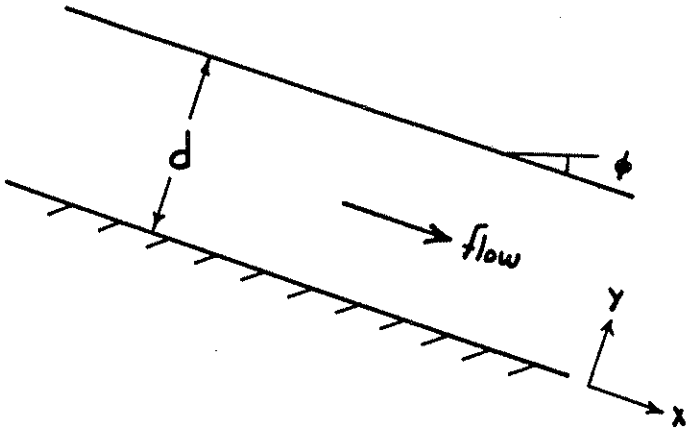

Figure 1.11 Uniform flow of liquid down an inclined plane.

Upon which variables does u depend? Obviously γ_x is important because it's responsible for the flow in the first place. Both flow depth d and viscosity μ are important because they affect the shear in the fluid, and the height y above the bottom is important because from the no-slip condition you should expect u to vary with distance above the bottom. Finally, ρ must also be included if fluid accelerations are present, and you've already seen that this is the case in some ranges of flow. So $u = f(\rho, \mu, \gamma_x, d, y)$, and by the Pi theorem you can write this functional relationship in a dimensionless form with three dimensionless variables, one dependent and two independent.

There are five possibilities for the dependent variable, obtained by combining three of the four variables ρ, μ, γ_x, d, and y with u in a product that is adjusted to be dimensionless. Disregarding two that contain y, these are:

$$\left(\frac{\rho^2}{\mu\gamma_x}\right)^{1/2} u, \quad \frac{\rho u d}{\mu}, \quad \frac{\mu u}{\gamma_x d^2}$$

(Note that the second is a Reynolds number.) None of these is inherently better than the others. As discussed in the last section, if you suspect that one of the original independent variables becomes unimportant in some range of conditions, use the dimensionless variable from which that independent variable is absent, because that best reveals the effect when the function is plotted. The best one here is thus $\mu u/\gamma_x d^2$, because under some conditions there are no accelerations in the flow, and ρ is then irrelevant.

The two independent dimensionless variables involve ρ, μ, γ_x, d, and y; one is naturally y/d or d/y, and the other is a dimensionless combination of ρ, μ, γ_x, and either d or y. You can check that this comes out to be $\rho\gamma_x d^3/\mu^2$. So

$$\frac{\mu}{\gamma_x d^2} u = f\left(\frac{\rho\gamma_x d^3}{\mu^2}, \frac{y}{d}\right) \tag{1.14}$$

(You could have derived the three dimensionless variables in Equation (1.14) by choosing μ, d, and γ_x as repeating variables, except that $\rho\gamma_x d^3/\mu^2$ comes out to the one-third power.) You can use this to express the results of theory or experiment by plotting a three-dimensional graph of dimensionless velocity against y/d and $\rho\gamma_x d^3/\mu^2$. The entire range of the phenomenon can be characterized by a well-defined surface in a three-dimensional graph, or (what's the same) by the way a two-dimensional graph of, say, $\mu u/\gamma_x d^2$ vs. y/d changes as $\rho\gamma_x d^3/\mu^2$ is varied.

Writing Newton's second law for the balance of forces on a suitably chosen element of fluid in the flow and using Equation (1.2) for the relationship between shear stress and velocity gradient, we can obtain analytical solutions for the variation of both shear stress and velocity in the flow, provided only that u is everywhere in the x direction and is independent of x as well as of time. Think about the forces acting on the fluid contained at a given instant in the rectangular volume formed by the free surface, the bottom boundary, and two pairs of imaginary planes normal to the bottom and with unit spacing, one pair parallel to the flow and spaced a distance B apart, and the other normal to the flow and spaced a distance L apart (Figure 1.12).

Because the fluid is not accelerating, the downslope component $\gamma_x BLd$ of the weight of the fluid in the volume must be balanced by the frictional force $\tau_o BL$ exerted by the bottom

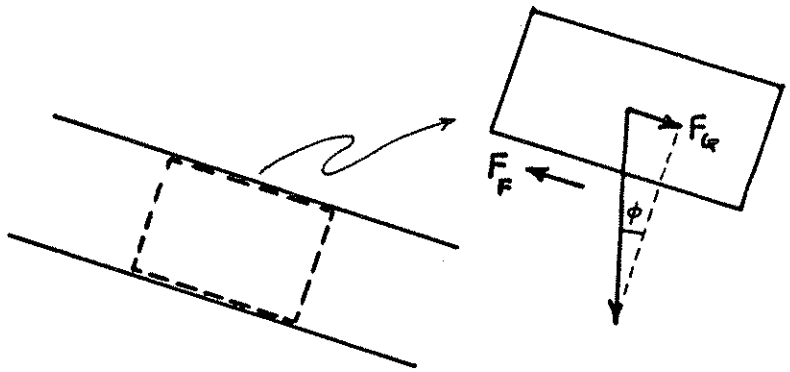

F_G = downslope component of fluid weight = (1)(1)$d\rho g \sin\phi$
F_F = bottom frictional force per unit area = (1)(1)τ_o

Figure 1.12 Balance of streamwise-oriented forces exerted on a body or "block" of fluid in the flow (with imaginary side boundaries) down the inclined plane.

boundary on the fluid in the volume, where τ_o, called the boundary shear stress, is the shear stress (with dimensions of force per unit area) acting at the bottom boundary:

$$\tau_o = \gamma_x d \qquad (1.15)$$

(There are also pressure forces that act parallel to the flow direction on the upstream and downstream boundaries of the volume. But since by our assumption of uniformity the vertical distribution of these pressure forces is the same at every cross section, they cause no net force on the fluid in the body.) Since $\gamma_x = \gamma \sin\phi$, Equation (1.15) can also be written

$$\tau_o = \gamma d \sin\phi \qquad (1.16)$$

The slope $S = \tan\phi$, but for very small ϕ (the usual case), the approximation $\sin\phi \approx \tan\phi$ is a good one, and Equation (1.16) is often written

$$\tau_o = \gamma d S \qquad (1.17)$$

Equations (1.16) and (1.17) can easily be generalized for a straight channel with arbitrary cross-sectional shape. Let the cross-sectional area be A and the wetted perimeter be P (Figure

1.13). Then corresponding to Equation (1.15) the balance of forces is $\tau_o P = \gamma_x A$. Defining the hydraulic radius R_H to be A/P, this becomes

$$\tau_o = \gamma_x R_H \qquad (1.18)$$

Equation (1.18) or its equivalent, $\tau_o = \gamma R_H \sin\phi$, is the basic resistance equation for steady uniform flow in open channels. Not many useful results in fluid mechanics are so easily derived. It's applicable not just to flows that are strictly steady and uniform at all points, but also to flows that are steady and uniform in a time-average sense but show turbulent fluctuations in velocity, because nothing was assumed about the internal details of the flow in deriving the equation. Equation (1.18) thus gives the time-average bottom shear stress; the instantaneous bottom shear stress would fluctuate turbulently with time.

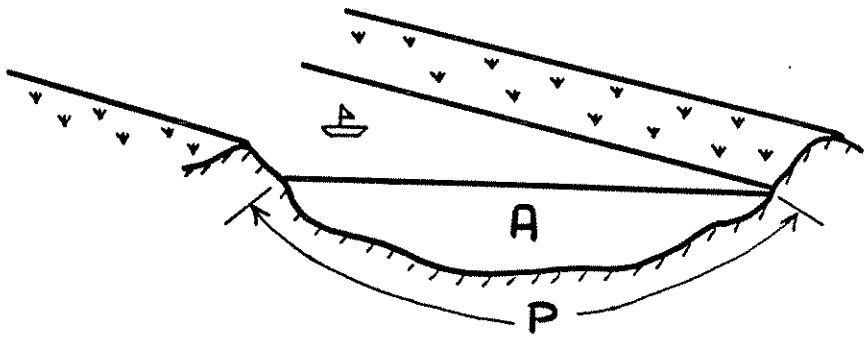

Figure 1.13 Definition sketch for resistance equation for open-channel flow in a channel of arbitrary cross section.

To see what the flow is like away from the boundary, you can apply this same force-balancing procedure to a body of fluid similar to that used above but with its lower face formed by an imaginary plane a variable distance y above the bottom and parallel to it (Figure 1.14). The shear stress τ across the plane is given directly by the force balance:

$$\tau = \gamma_x (d-y) \qquad (1.19)$$

Using Equation (1.15) to eliminate γ_x from Equation (1.19), we can write τ in terms of the boundary shear stress τ_o:

$$\tau = \tau_o\left(1 - \frac{y}{d}\right) \qquad (1.20)$$

Equation (1.20) shows that τ varies linearly from a maximum of $\gamma_x d$ at the bottom to zero at the surface (Figure 1.15).

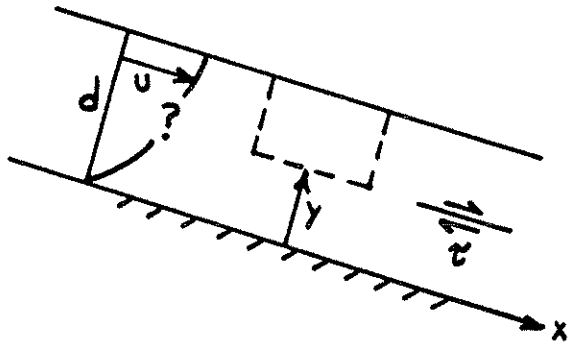

Figure 1.14 Use of a differently defined body of fluid to aid in solving for velocity distribution in flow down an inclined plane.

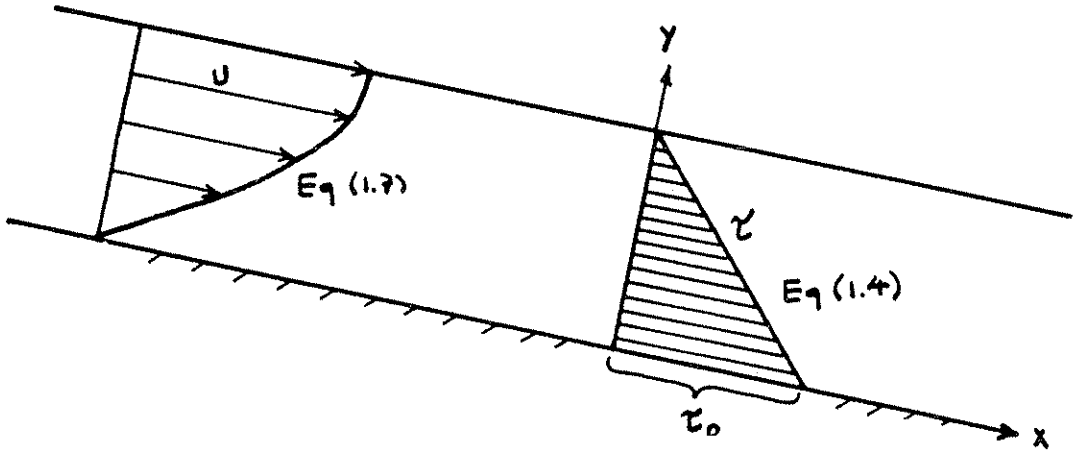

Figure 1.15 Distributions of (A) velocity and (B) shear stress in steady uniform laminar flow down an inclined plane.

Eliminating τ from Equation (1.19) by use of Equation (1.5) gives an expression for the velocity gradient du/dy:

$$\frac{du}{dy} = \frac{\gamma_x}{\mu} (d - y) \qquad (1.21)$$

A simple integration with respect to y then gives the vertical distribution of fluid velocity:

$$u = \int \frac{du}{dy}\, dy = \frac{\gamma_x}{\mu} \int (d-y)\, dy = \frac{\gamma_x}{\mu} \left(yd - \frac{y^2}{2}\right) + c \qquad (1.22)$$

The constant of integration c is found to be zero by using the no-slip condition that u = 0 at y = 0, so Equation (1.22) becomes

$$u = \frac{\gamma_x}{\mu} \left(yd - \frac{y^2}{2}\right) \qquad (1.23)$$

For given values of γ_x, μ, and d, the velocity u thus varies parabolically from zero at the bottom boundary to a maximum at the surface (Figure 1.15A). On the other hand, from Equation (1.21) the velocity gradient du/dy varies linearly from a maximum at the bottom to zero at the free surface, since it's directly proportional to the shear stress (Figure 1.15B).

Does Equation (1.23) represent real flows, at least in some limited range of conditions? If we experimented with a uniform flow of liquid down an inclined plane we would find that for combinations of shallow depths, low velocities, and high viscosities the velocity distribution predicted by Equation (1.23) would correspond very closely to the experimental results. A good example of this kind of flow in nature is the runoff of water in thin sheets over an even ground surface after a heavy rain. But if the flow is too deep or too fast, or the viscosity too small, we would find a markedly different velocity distribution (Figure 1.16). If we could also observe patterns of motion within the flow in the two cases, we would find that in the former the fluid glides along regular linear paths characteristic of laminar flow, whereas in the second the fluid moves in irregular and sinuous paths characteristic of turbulent flow, with the velocity changing unpredictably from time to time at any point. The nature of turbulence and turbulent flow, and in particular the complicated picture of velocity distribution in turbulent flow, are discussed in more detail in Chapters 3 and 5. Here we only make some initial comments on why Equation (1.23) breaks down for turbulent flow. The simplest answer, although not the most fundamental, is that we can no longer assume that the shear stress

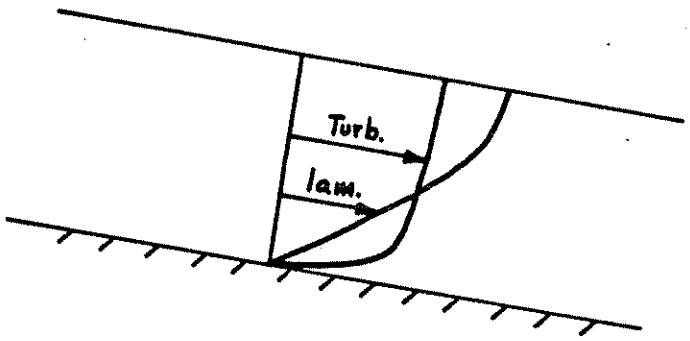

Figure 1.16 Comparison of velocity profiles in laminar and turbulent flow down an inclined plane. The profiles are drawn so that they represent about the same total discharge, or volume rate of flow, per unit width of the plane (that is, the areas under the two curves are about the same). There is a certain range of flow conditions for which the flow could be either laminar or turbulent depending on experimental conditions (although the slope needed for uniform flow would then be different in the two cases).

across planes in the flow parallel to the bottom boundary is given by Equation (1.5), and so we can no longer eliminate τ and perform the integration as in Equation (1.21). Because of the irregularity of the fluid motion in the turbulent case, the surfaces of local shear are oriented differently at each point on such a plane, and the rate or intensity of shear varies as well.

If Equation (1.23) is a correct equation it must have the dimensions of velocity on the right side as well as on the left. Dividing both sides by $\gamma_x d^2/\mu$,

$$\frac{\mu}{\gamma_x d^2} u = \frac{y}{d} - \frac{1}{2}\left(\frac{y}{d}\right)^2 \qquad (1.24)$$

This is the analytical relationship for velocity distribution written in dimensionless form; it's plotted in Figure 1.17. If you compare this with Equation (1.14), the functional relationship for u derived by dimensional analysis, you see two differences: the function is now specific rather than general (it's a polynomial in y/d), and the independent dimensionless variable $\rho\gamma_x d^3/\mu^2$ doesn't appear on the right side. The reason for the latter difference is that ρ does not enter independently into Equation (1.21).

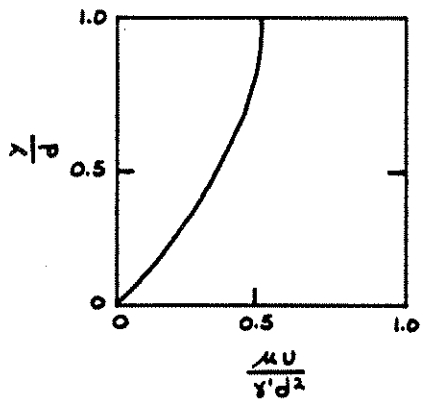

Figure 1.17 Plot of dimensionless velocity $\mu u/\gamma_x d^2$ vs. y/d from Equation (1.22), the dimensionless analytical solution for velocity distribution in laminar flow down an inclined plane.

So density ρ must be taken into account explicitly in steady uniform turbulent flow down a plane but not in steady uniform laminar flow down a plane. In the turbulent flow, small masses of fluid experience accelerations as they follow their irregular paths. Forces on accelerating fluid elements depend not only on the acceleration but also on the mass of the fluid, so ρ must be treated as a separate variable. In the laminar flow, on the other hand, there are no accelerations because the fluid moves in straight paths and the velocity profile does not vary either with time or in the flow direction; ρ is then of no importance outside of its effect on the specific weight of the fluid. But keep in mind that ρ is important in laminar flows that are nonuniform, because then there are accelerations in the fluid. Flow past a sphere is a good example.

Recall that by Equation (1.14) all the velocity profiles observed in steady uniform flow down a plane, laminar or turbulent, can be plotted in a three-dimensional graph. The best way to do this is to plot graphs of dimensionless velocity $\mu u/\gamma_x d^2$ vs. y/d for a series of values of $\rho\gamma_x d^3/\mu^2$, as shown in Figure 1.18. From Figure 1.18 you can picture the general shape of the three-dimensional surface that represents the function. The curves of $\mu u/\gamma_x d^2$ vs. y/d change progessively in shape as $\rho\gamma_x d^3/\mu^2$ is varied. In laminar flow, for which ρ is not a variable of independent significance, $\rho\gamma_x d^3/\mu^2$ is irrelevant and has no effect on the shape of the curve of $\mu u/\gamma_x d^2$ vs. y/d. The curves in the left-hand part of Figure 1.18, for $\rho\gamma_x d^3/\mu^2$ less than a certain value, are therefore all the same, and project or collapse upon one another to give the curve already shown in Figure 1.17. At a certain value of $\rho\gamma_x d^3/\mu^2$ the profile changes its shape drastically and abruptly in the change from laminar flow to turbulent flow. Beyond that point the profile continues to change

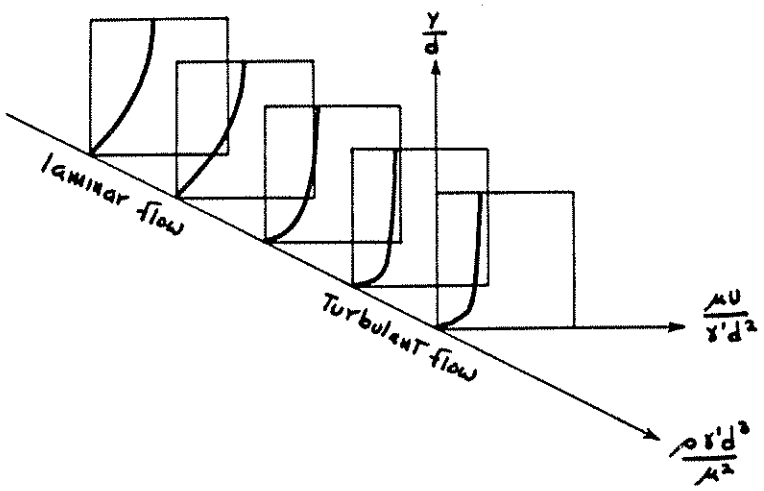

Figure 1.18 Schematic three-dimensional plot of dimensionless velocity $\mu u/\gamma_x d^2$ against $\rho\gamma_x d^3/\mu^2$ and y/d for steady uniform flow down an inclined plane. The plot is shown in the form of a number of sections or two-dimensional graphs normal to the axis of $\rho\gamma_x d^3/\mu^2$. For small values of $\rho\gamma_x d^3/\mu^2$ the flow is laminar, and for large values, turbulent.

with $\rho\gamma_x d^3/\mu^2$, but not greatly. We'll return to this last point in Chapter 5 in the course of a more extended discussion of velocity profiles in turbulent flow.

SIGNIFICANCE OF REYNOLDS NUMBERS AND FROUDE NUMBERS

We can gain some further insight into the significance of Reynolds numbers and Froude numbers by showing that dimensionless variables of this form always arise in problems involving viscous forces and gravity forces. Think about the balance of forces on some small element of fluid in any fluid-flow problem (for example, that of a sphere moving near a free surface) that involves fluid shear forces and also gravity forces that are not simply balanced out by hydrostatic pressure. Whatever the exact nature of the problem, Newton's second law must hold for this small element of fluid, so we can write for it a general equation of motion in words:

$$\text{viscous force} + \text{gravity force} + \text{any other forces} = \text{rate of change of momentum} \tag{1.25}$$

All the terms in this equation have the same dimensions, so we can divide all the terms by any one of them to obtain an equation with all terms dimensionless. Dividing by the term on the right,

$$\frac{\text{viscous force}}{\text{R.O.C. of momentum}} + \frac{\text{gravity force}}{\text{R.O.C. of momentum}} + \frac{\text{any other forces}}{\text{R.O.C. of momentum}} = 1 \qquad (1.26)$$

What will be the form of the first two dimensionless terms on the left, in terms of representative variables that might be involved in any given flow problem? Assuming that there is some characteristic length variable L in the problem like a sphere size or flow depth, and some characteristic velocity V like the approach velocity in flow past a sphere or the mean velocity or surface velocity in flow down a plane, then the rate of change of momentum, which has dimensions of momentum divided by a characteristic time T, can be written $\rho L^3 V/T$. (Remember that the mass can be expressed as density times volume and the volume as the cube of a length.) And this can further be written $\rho L^2 V^2$, because velocity has the dimensions L/T. The viscous force is the product of the viscous shear stress and the area over which it acts. Since area is proportional to the square of the characteristic length, and by Equation (1.5) the shear stress is proportional to the viscosity and the velocity gradient, viscous force is proportional to μVL. The first term in Equation (1.26) is then proportional to $\mu VL/\rho L^2 V^2$, or $\mu/\rho LV$. This is simply the inverse of a Reynolds number. The Reynolds number in any fluid problem is therefore inversely proportional to the ratio of a viscous force and a quantity with the dimensions of a force, the rate of change of momentum, which is usually viewed as an "inertial force."

How about the second term in Equation (1.26)? The gravity force is the weight of the fluid element, which is proportional to $\rho g L^3$. The second term is then proportional to $\rho g L^3/\rho L^2 V^2$, or gL/V^2. This is the square of the inverse of a Froude number. The square of the Froude number is therefore proportional to the ratio of a gravity force and a rate of change of momentum or an "inertial force."

This probably strikes you as not a very rigorous exercise. It's intended only to give you an initial feel for the significance of Reynolds numbers and Froude numbers. If we had more space we would derive the general differential equation of motion for flow of a viscous fluid and then make it dimensionless by introducing the same characteristic length and characteristic velocity, and a reference pressure as well. You'd see that the Reynolds number and the Froude number then emerge as coefficients of the dimensionless viscous-force term and gravity-force term, respectively. This is done especially lucidly by Tritton (1977,

p. 75-77). The value of such an exercise is that then the magnitudes of the Reynolds number and Froude number tell you whether the viscous-force term or the gravity-force term in the equation of motion can be neglected relative to the mass-times-acceleration term. This is a productive way of simplifying the equation of motion to gain some insight into the physics of the flow.

When you're deciding which set of dimensionless variables to work with in problems like those of flow past a sphere or flow down a plane, introduced above, it makes sense to use dimensionless variables that have their own physical significance, like Reynolds numbers and Froude numbers. In later chapters we'll be introducing other dimensionless variables that represent ratios of two forces in specific problems.

CHAPTER 2. SETTLING OF SPHERES

INTRODUCTION

This chapter deals with some basic ideas about settling of sediment particles through fluids. This is a good topic in sediment transport to start with in these notes, because settling is an important aspect of sediment transport, and Chapter 1 has provided enough background for substantial progress. But complexities that require greater understanding of fluid flow will soon arise, and Chapter 3 is therefore devoted to several important topics in fluid flow. Chapter 4 is a continuation of material on settling.

If placed in suspension in a viscous fluid, a sediment particle will settle toward the lower boundary of the fluid, provided that the weight of the particle is not much smaller than the random forces exerted on the particle by bombardment by the fluid molecules in thermal motion. All mineral particles larger than colloidal sizes of hundredths of a micrometer are in this category. When such a particle is released from rest in a still fluid, it accelerates in response to the force of gravity, but as its velocity increases, the oppositely directed drag force exerted by the fluid grows until it equals the weight of the particle. When the weight and the drag are in balance the particle no longer accelerates but falls at its terminal velocity, called the fall velocity or settling velocity. Particles of sand size and smaller attain terminal velocity over very short times and distances.

With respect to natural sedimentary environments, the settling of a sphere in a still fluid is obviously a great oversimplification with respect both to particle shape and to the state of motion of the fluid, but it will lead to development of some important ideas and point the way toward consideration of nonspherical particles and flowing fluids.

TOWING VS. SETTLING

In Chapter 1 we used the example of the drag force on a sphere moved or towed at constant velocity through a still fluid as an illustration of dimensional analysis, and we showed a graph of dimensionless drag force, or drag coefficient, as a function of a Reynolds number (Figure 1.5) without saying much about the nature or significance of the curve. It should make sense that towing a sphere at velocity U through a still fluid by exerting a force F_D on it is equivalent to passing a steady and uniform stream of fluid at velocity U around a sphere that is held fixed by exerting a force F_D on it. This is largely true, but there are two complications. First, if the sphere is held fixed and the flow passes by it, the drag force can be influenced by even weak turbulence in the approaching flow, whereas if the sphere is towed through still fluid there can be no such effect. Second, in some ranges of relative velocity, eddies can form behind the sphere and

break away irregularly; if the sphere is fixed and the fluid is flowing by, this causes the force to fluctuate about some average value but does not affect the relative velocity, whereas if the sphere is towed, either the velocity fluctuates along with the force or (if by definition we tow with a constant force) the velocity fluctuates but the force is steady.

Settling of a sphere through still fluid under its own weight is exactly like towing the sphere vertically downward: the weight of the sphere, which is simply the Earth's gravitational attractive force on the sphere, is constant and totally independent of the state of motion, and the sphere responds by settling downward at some velocity through the fluid. (As noted above, this velocity may fluctuate slightly with time.) For spheres the differences between the fixed-sphere case and the settling-sphere case are usually assumed to be minor. In fact, some of the data in Figure 1.5 for dimensionless drag force as a function of Reynolds number are from settling experiments and some are from wind-tunnel experiments with fixed spheres, and it can be seen that there is very little scatter of the combined experimental curve. But we'll see in Chapter 4 that for nonspherical particles this effect can be very significant.

SETTLING SPHERES: FLOW AND FORCES

Flow lines relative to the falling sphere should be expected to look about as shown in Figure 2.1. They are straight and uniform in the free stream well ahead of the sphere, but as they pass around the sphere they become more closely spaced, and then they return to the straight and uniform pattern behind the sphere. Velocity varies not only in direction but also in magnitude in the neighborhood of the sphere. Think of the space between two adjacent flow lines as a conduit: the smaller the conduit becomes, the faster the fluid must move in order to maintain the same volume rate of flow. Around the midsection of the sphere, velocity relative to the sphere is therefore substantially greater than the free-stream velocity.

In describing the flow pattern shown in Figure 2.1 we've largely appealed to your intuition; we haven't given you much basis for thinking about why the pattern looks the way it does. It turns out that the flow actually does look like this in the limiting case of very low Reynolds numbers $\rho UD/\mu$ but gradually becomes different as the Reynolds number is increased, and at high Reynolds numbers the pattern is grossly different, with important consequences. The picture at low Reynolds numbers is considered at some length later in this chapter, and the progressive changes in flow pattern with increasing Reynolds number are discussed in more detail in Chapters 3 and 4.

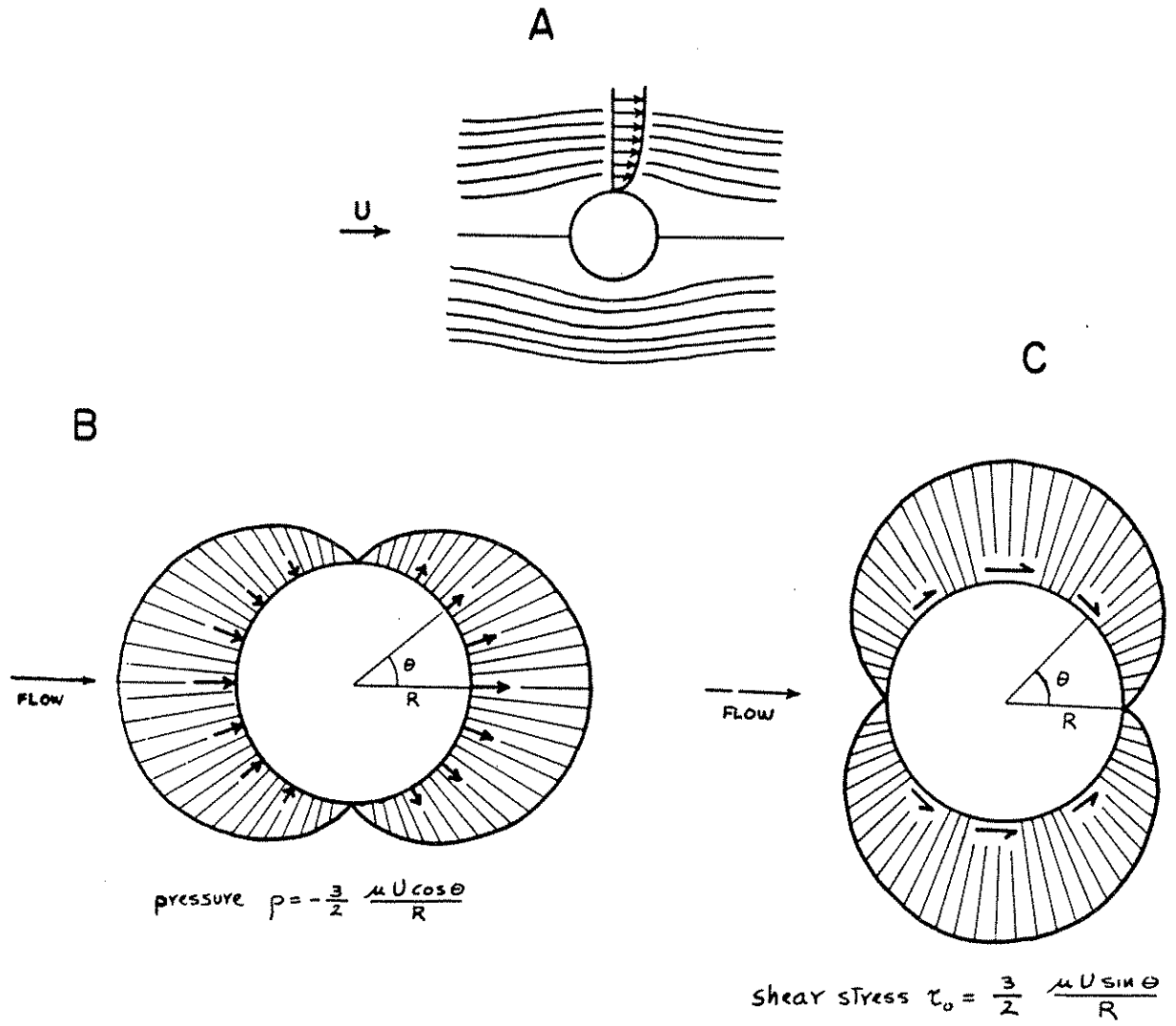

Figure 2.1 (A) Streamlines of flow of real fluid around a sphere at very low Reynolds numbers (in the Stokes range), and distribution of (B) pressure p (relative to free-stream pressure) and (C) viscous shear stress τ_o on the surface of the sphere.

At every point on the surface of the sphere there is a definite value of fluid pressure (normal force per unit area) and of viscous shear stress (tangential force per unit area). Figure 2.1 gives an idea of the distribution of these forces. It is easy to see why the viscous shear stress should be greatest around the midsection and least on the front and back surfaces of the sphere; the distribution of pressure (more on this later) is not so obvious. You can imagine adding up both pressures and viscous shear stresses over the entire surface, remembering that both magnitude and direction must be taken into account, to obtain a

resultant pressure force and a resultant viscous force on the sphere. Because of the symmetry of the flow, both of these resultant forces are directed downstream. You can then add them together to obtain a grand resultant, the total drag force F_D.

SETTLING SPHERES: DIMENSIONAL ANALYSIS

To obtain an experimental curve for settling velocity we can simply transform the curve in Figure 1.5 for drag coefficient vs. Reynolds number for towed spheres into a curve based on settling velocity. In fact, much of this curve, especially for low Reynolds numbers, was obtained by settling experiments in the first place, with the experimental results recast into the form of drag coefficients. When a sphere falls at terminal velocity the drag force F_D is equal to the submerged weight of the particle, $(1/6)\pi D^3\gamma'$, where γ' is the submerged weight per unit volume of the particle, equal to $\gamma_s-\gamma$ or $g(\rho_s-\rho)$. Substituting this for F_D in the definition of the drag coefficient C_D in Equation (1.8), using settling velocity w in place of U, and then solving for C_D,

$$C_D = \frac{4}{3}\frac{\gamma' D}{\rho w^2}$$

This expression for C_D, which can be viewed as the settling drag coefficient, can be used in the relationship for dimensionless drag force as a function of Reynolds number (Equation 1.9) for spheres moving through a viscous fluid:

$$\frac{\gamma' D}{\rho w^2} = f\left(\frac{\rho w D}{\mu}\right) \qquad (2.1)$$

where the factor 4/3 has been absorbed into the function, just for convenience. Figure 2.2, which is the same as Figure 1.5 with axes relabeled and adjusted in scale to take account of the factor 4/3, is the corresponding graph of this function. No data points are shown, because the curve is exactly the same as in Figure 1.5. Figure 2.2 gives settling velocity w as an implicit function of ρ, μ, D, and γ'.

The curve in Figure 2.2 is still not very convenient for finding settling velocity. This is because both w and D appear in the dimensionless variables along both axes. Finding w in an actual problem would necessitate laborious trial-and-error computation. To get around this problem the graph can be further recast into a more convenient form in which w appears in only one

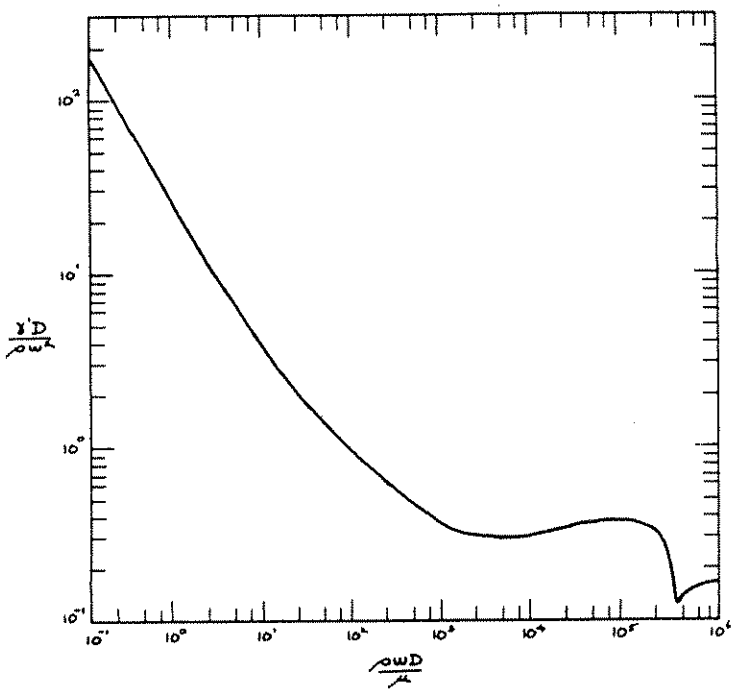

Figure 2.2 Plot of $\gamma' D/\rho w^2$ against Reynolds number $\rho wD/\mu$ for settling of spheres in a still fluid.

of the two dimensionless variables. Also, since usually what's desired is w as a function of D, or vice versa, it's convenient to arrange for D to appear only in the other variable. Remember from Chapter 1 that if you have a set of dimensionless variables for a problem you can multiply or divide any one of them by any others in the set to get a new variable to replace the old one. To get a dimensionless variable with w but not D, invert the left-hand variable in Equation (2.1) and multiply the result by the right-hand variable:

$$\left(\frac{\rho w^2}{\gamma' D}\right)\left(\frac{\rho wD}{\mu}\right) = \frac{\rho^2 w^3}{\gamma' \mu}$$

To get a dimensionless variable with D but not w, square the right-hand variable in Equation (2.1) and multiply it by the left-hand variable:

$$\left(\frac{\rho wD}{\mu}\right)^2\left(\frac{\gamma' D}{\rho w^2}\right) = \frac{\rho \gamma' D^3}{\mu^2}$$

It's convenient, but not necessary, to take these two variables to the one-third power, so that w and D appear to the first power; $w(\rho^2/\gamma'\mu)^{1/3}$ can be viewed as a dimensionless settling velocity, and $D(\rho\gamma'/\mu^2)^{1/3}$ as a dimensionless sphere diameter. Since these two new variables are equivalent to C_D and Re, the functional relationship for C_D vs. Re can just as well be written

$$\left(\frac{\rho^2}{\gamma'\mu}\right)^{1/3} w = f\left(\frac{\rho\gamma'}{\mu^2}\right)^{1/3} D \qquad (2.2)$$

The usefulness of Equation (2.2) is that settling velocity appears only on the left side and sphere diameter appears only on the right side.

It's now a simple matter to find w for a given fluid, sphere size, and submerged specific weight by use of Figure 2.3, which is a plot of dimensionless setting velocity vs. dimensionless sphere diameter. This curve is obtained directly from that in Figure 2.2; you can imagine taking the original data points and forming the new dimensionless variables rather than the old ones to plot the curve in the new coordinate axes of Figure 2.3. This emphasizes that these two curves are equivalent because they are based on the same set of experimental data.

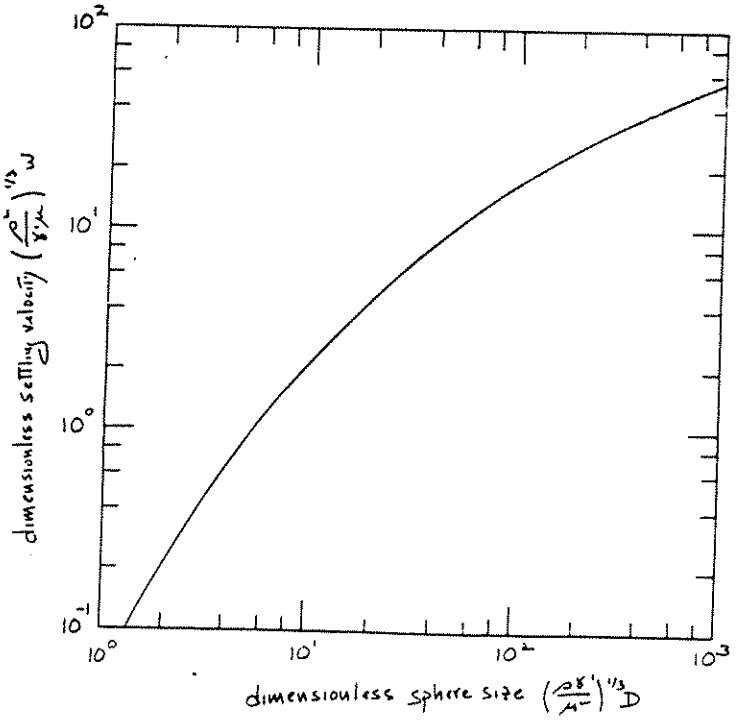

Figure 2.3 Plot of dimensionless settling velocity $w(\rho^2/\gamma'\mu)^{1/3}$ against independent dimensionless variable $D(\rho\gamma'/\mu^2)^{1/3}$ for settling of spheres in a still fluid.

If you are unsatisfied by the roundabout way of arriving at the functional relationship expressed in Equation (2.2), you might consider making a fresh start on dimensional analysis of the problem of settling of a sphere through a still fluid at terminal velocity. Settling velocity w, the dependent variable, must depend on fluid density ρ, fluid viscosity μ, sphere diameter D, and submerged weight per unit volume γ' of the sphere. Each of these must be included for the reasons given in Chapter 1. As before, acceleration of gravity and sphere density do not have to appear separately in the list of variables because they are important only by virtue of their combined effect on γ'. The five variables w, ρ, μ, D, and γ' should then combine into two dimensionless variables, as in Equation (2.2) above.

SETTLING AT LOW REYNOLDS NUMBERS: STOKES' LAW

We said that fluid density ρ is needed as a variable to describe the drag force on a sphere because accelerations are produced in the fluid as the sphere moves through it. If these accelerations are small enough, it's reasonable to expect that their effect on the drag force can be neglected. Flows of this kind are called creeping flows. The reason, which can't be examined in detail here, is that in the differential equation of motion for flow of an incompressible viscous fluid (nothing more than Newton's second law F = ma written per unit volume of fluid) the term for rate of change of momentum per unit volume, $\rho(Du/Dt)$, gets small faster than the two remaining terms for viscous forces and pressure forces as the Reynolds number decreases. These matters are discussed in many books in fluid dynamics; see, for example, Tritton (1977, Chapter 8).

If you remove ρ from the list of important variables that characterize the settling velocity, you're left with four variables: w, D, μ, and γ'. You can form only one dimensionless variable out of these four: $\mu w/\gamma' D^2$. So the functional relationship for w becomes

$$\frac{\mu w}{\gamma' D^2} = \text{const} \qquad (2.3)$$

Solving Equation (2.3) for w,

$$w = \text{const} \ \frac{\gamma' D^2}{\mu} \qquad (2.4)$$

All you would need to do to obtain a completely determined expression for w in this special case of creeping flow is find the value of the constant by experiment.

For creeping flow around a sphere it turns out that an analytical solution can be obtained for the constant in Equation (2.4). This solution was first obtained by Stokes in the 1840s. The approach is to specialize the equation of motion for low-Reynolds-number flow past a sphere by omitting the $\rho(Du/Dt)$ term, as noted above. The equation is then more tractable mathematically; Stokes solved it to obtain the distribution of pressure and shear stress at all points on the surface of the sphere, shown in Figure 2.1. Then by integrating these forces over the entire surface of the sphere he obtained

$$F_D = 3\pi D\mu U \tag{2.5}$$

This result, called Stokes' law, is in perfect agreement with experiment. It turns out that exactly one-third of F is due to the pressure force and two-thirds is due to the viscous force. Density does not appear in Stokes' law because it enters the equation of motion only in the mass-times-acceleration term, which is neglected. The constant in Equation (2.4) can now be found easily by setting the weight of the particle, $(1/6)\pi D^3\gamma'$, equal to the drag force given by Equation (2.5) and solving for w:

$$w = \frac{1}{18}\,\frac{D^2\gamma'}{\mu} \tag{2.6}$$

Stokes' solution also gives velocity, pressure, and shear stress at every point in the fluid away from the surface of the sphere. (Remember that by the no-slip condition the fluid velocity is zero at the surface of the sphere; this constitutes a boundary condition that Stokes used in solving the equation of motion.) The flow pattern shown in Figure 2.1 is based on these results for velocity. We'll return to the pressure distribution around the sphere after introducing the Bernoulli equation in the next chapter.

Figure 2.4 is an expanded graph of the low-Reynolds-number part of the experimentally determined curve for drag coefficient in Figure 1.5. Superimposed on this curve is the straight line (Equation 2.6) derived from Stokes' law. For low Reynolds numbers, Stokes' law fits the experimental points perfectly. But with increasing Reynolds number the experimental curve diverges from the straight line given by Stokes' law, because the effects of fluid acceleration gradually become too large to ignore. Stokes' law thus breaks down with increasing Reynolds number, but not at any definite value. A Reynolds number of one is usually

taken to be the upper limit of applicability. For Re = 1 the actual settling velocity is about 12% lower than predicted by Stokes' law. How far use of Stokes' law can be extended depends on the accuracy needed. There have been some attempts to extend the analytical solution by taking partial account of the acceleration term, but these lead to only slight improvement. Beyond this range you have to rely entirely upon experiment.

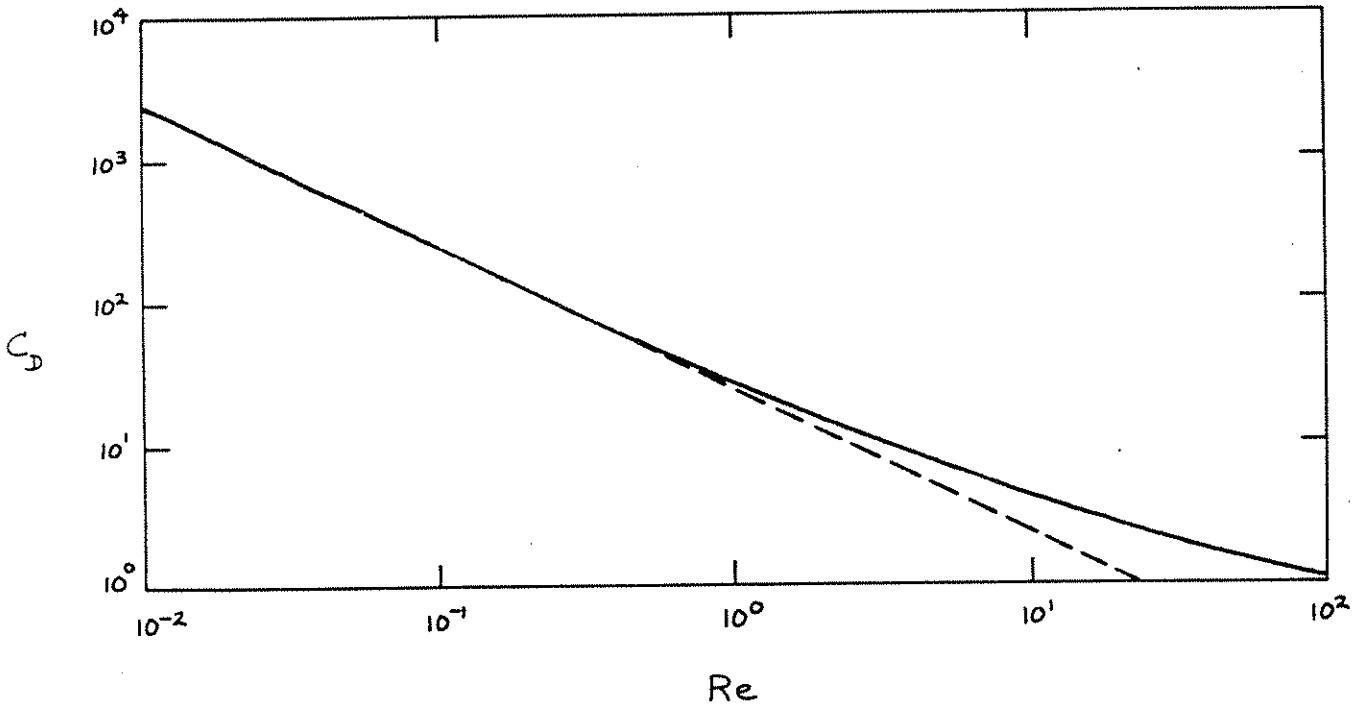

Figure 2.4 Plot of drag coefficient (dimensionless drag force) C_D against Reynolds number for settling of spheres in a still fluid, within and slightly above the Stokes range of settling. This is an expanded version of the left-hand part of the plot in Figure 1.5.

You might be interested in a comparison of the diameters of the largest quartz-density spheres that settle according to Stokes' law in water and in air. This can easily be done by substituting Equation (2.6) for w as a function of γ', D, and μ based on Stokes' law into the condition that the Reynolds number $\rho wD/\mu$ be equal to one (thereby eliminating w), solving for D,

$$D = \left(\frac{18\mu^2}{\rho\gamma'}\right)^{1/3} \qquad (2.7)$$

and then substituting the values of ρ, μ, and γ' for air and water into the resulting Equation (2.7). The density of water at 20°C is 0.998 g/cm^3, the viscosity is 1.005 x 10^{-2} poise (a poise is the unit of viscosity in the cgs system of units), and the specific weight of quartz in water is

$$\gamma' = g(\rho_s - \rho) = (0.98 \times 10^3 \text{ cm/s}^2)(2.65 \text{ g/cm}^3 - 0.998 \text{ g/cm}^3) \approx 1.62 \times 10^3 \text{ g/cm}^2\text{-s}^2$$

Substituting these values into Equation (2.7), D ≈ 0.10 mm for the conventional upper limit of Stokes'-law settling in water. The density of air at 20°C and atmospheric pressure is 1.20 x 10^{-3} g/cm^3, the viscosity is 1.81 x 10^{-4} poise, and the specific weight of quartz in air is

$$\gamma' = g(\rho_s - \rho) = (0.98 \times 10^3 \text{ cm/s}^2)(2.65 \text{ g/cm}^3 - 1.20 \times 10^{-3} \text{ g/cm}^3) \approx 2.65 \times 10^3 \text{ g/cm}^2\text{-s}^2$$

Substituting into Equation (2.7), D ≈ 0.06 mm for the upper limit of Stokes'-law settling in air. The values for water and air are not greatly dissimilar. The corresponding settling velocities, which can be found by substituting into Equation (2.6), are not much different either: at Re = 1 the Stokes'-law settling velocity of a 0.10 mm quartz sphere in water is 1.0 cm/s, and that of a 0.06 mm quartz sphere in air is 2.6 cm/s.

We note in passing that Stokes' law can also be put into a form involving the drag coefficient C_D as a function of Reynolds number, as introduced in Chapter 1. Combining the definition of the drag coefficient (Equation 1.9) with Stokes' law (Equation 2.5) to eliminate drag force F_D and then rearranging the variables into the form of a Reynolds number,

$$C_D = \frac{24}{Re} \tag{2.8}$$

In Figure 2.4 the dashed straight line sloping downward to the right is what Stokes' law in this form looks like in a graph of drag coefficient vs. Reynolds number.

A WORD ON HIGHER REYNOLD NUMBERS

At the much higher Reynolds numbers corresponding to the almost horizontal part of the curve in Figure 1.5 the pattern of flow around the sphere is radically different from that shown in Figure 2.1. Although the flow in front of the sphere is qualitatively similar to that at low Reynolds numbers, near the midsection of the sphere (halfway around) the flow departs tangentially from the sphere along a surface of very strong fluid shear. This phenomenon, called flow separation, is an important aspect of high-Reynolds-number flows past solid boundaries that diverge or curve away from the mean flow direction. The separation surface encloses behind the sphere a zone of irregularly eddying fluid called the wake. Fluid pressure exerted on the back surface of the sphere is very low relative to the pressure exerted on the front surface. The very large drag force on the sphere in this regime of flow is caused mainly by pressure forces rather than viscous forces. After covering some more ground in fluid mechanics in the next chapter, we'll return to flow around spheres at high Reynolds numbers in Chapter 4.

CHAPTER 3. FLUID FLOW

INTRODUCTION

So far we've been able to cover a lot of ground with a minimum of material on fluid flow. At this point we need to present some more topics in fluid dynamics before returning in the next chapter to flow past spheres at Reynolds numbers higher than the Stokes range. We'll look at inviscid fluid flow, the Bernoulli equation, turbulence, boundary layers, and flow separation. This material will also provide some of the necessary background for discussion of dynamics of sediment movement in Chapter 6.

INVISCID FLOW

Over the past hundred and fifty years a vast body of mathematical analysis has been devoted to a kind of fluid that exists only in the imagination: an ideal or inviscid fluid, in which no viscous forces act. This fiction allows a level of mathematical progress not possible for viscous fluids. Although mathematical solutions for flow of an inviscid fluid are mostly beyond the scope of these notes, you can appreciate why they are so much more easily attainable simply by reference to a generalized equation of motion written in words. For a flow in which the effect of gravity is unimportant, and the only forces are viscous forces and pressure forces, Equation (1.23) becomes

$$\text{viscous force} + \text{pressure force} = \text{rate of change of momentum} \qquad (3.1)$$

The difficulties in the equation this represents (called the Navier-Stokes equation) come about partly because of the presence of the viscous-force term. If the fluid is inviscid this term is absent and the equation becomes more tractable. The major outlines of mathematical analysis of the resulting simplified equation were well worked out by late in the 1800s. Since then, fluid dynamicists have been extending the results and applying or specializing them to problems of interest in a great many fields.

The pattern of inviscid flow around a sphere is shown in Figure 3.1. The arrangement of flow lines is qualitatively similar to that in the viscous creeping flow shown in Fig. 2.1. Flow lines are again symmetrical with respect to a plane through the midsection of the sphere and normal to the overall flow direction. But for inviscid flow this symmetry is present not just for very low velocities but for all velocities. Figure 3.2 is a plot of fluid velocity along the particular flow line that meets the sphere at its front point, passes back along the surface of the sphere, and leaves the sphere again at the rear point. The

velocity varies symmetrically with respect to the midsection of the sphere: it falls to zero at the front point, accelerates to a maximum at the midsection, falls to zero again at the rear point, and then attains its original value again dowstream. The front and rear points are called stagnation points, because the fluid velocity is zero there. Note that elsewhere the velocity is not zero on the surface of the sphere, as it is in viscous flow. Don't let this unrealistic finite velocity on the surface of the sphere bother you; it's a consequence of the unrealistic assumption that viscous effects are absent, so that the no-slip condition is not applicable.

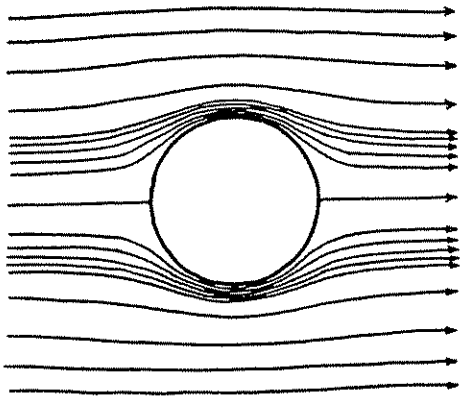

Figure 3.1 Steady flow of inviscid fluid around a sphere. Streamlines are shown from the standpoint of an observer stationary relative to the sphere.

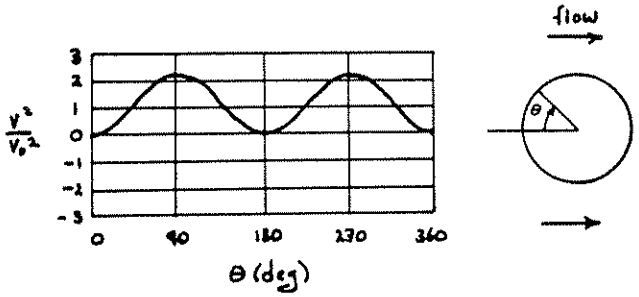

Figure 3.2 Distribution of fluid velocity on the sphere surface in flow of inviscid fluid around a sphere.

Figure 3.3 shows the distribution of fluid pressure around the surface of a sphere moving relative to an inviscid fluid. As with velocity, pressure is distributed symmetrically with respect to the midsection, and its variation is just the inverse of that of the velocity: relative to the uniform pressure far away from the sphere it's greatest at the stagnation points and least at the

midsection. One seemingly ridiculous consequence of this symmetrical distribution is that the flow exerts no net pressure force on the sphere, and therefore, since there are no viscous forces either, it exerts no resultant force on the sphere at all! In contrast, the distribution of pressure on the surface of a sphere moving very slowly relative to a viscous fluid shows a strong front-to-back asymmetry (Figure 2.1); it is this uneven distribution of pressure, together with the existence of viscous shear forces on the boundary, that gives rise to the drag force.

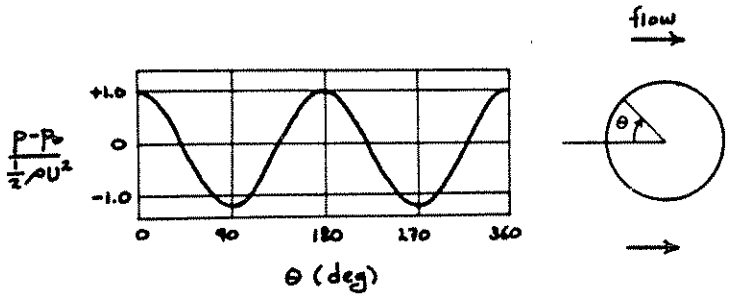

Figure 3.3 Distribution of fluid pressure on the sphere surface in flow of inviscid fluid around a sphere.

So the distributions of velocity and pressure in inviscid flow around a sphere, and therefore of the fluid forces on the sphere, are grossly different from the case of slow flow of viscous fluid around the sphere, even though the pattern of flow lines is not grossly different. Then what's the value of the inviscid approach? You'll see in the section on flow separation below that at higher real-fluid velocities the boundary layer in which viscous effects are concentrated next to the surface of the sphere is thin, and outside this thin layer the flow patterns and the distributions of both velocity and pressure are approximately as given by the inviscid theory. Moreover, the boundary layer is so thin for high flow velocities that the pressure on the surface of the sphere is approximately the same as that given by the inviscid solution just outside the boundary layer. And since at these high velocities the pressure forces are the main determinant of the total drag force, the inviscid approach is useful in dealing with forces on the sphere after all. Behind the sphere the flow patterns given by inviscid theory are grossly different from the real pattern mentioned at the end of the last chapter (and discussed more fully in a later section of this chapter), but you'll see that one of the advantages of the inviscid assumption is that it aids in a rational explanation for the existence of this great difference.

In many kinds of flows around well streamlined bodies like airplane wings, agreement is much better than for flow around blunt bodies like spheres. In flow of air around an airplane wing, viscous forces are important only in a very thin layer

immediately adjacent to the wing, and outside this layer the pressure and velocity are almost exactly as given by inviscid theory (Figure 3.4). It is these inviscid solutions that allow prediction of the lift on the airplane wing: although drag on the wing is governed largely by viscous effects within the boundary layer, lift is largely dependent upon the inviscid distribution of pressure that holds just outside the boundary layer. To some extent this is true also for flow around sediment grains resting on the bottom; lift and drag forces on sediment grains will be pursued in detail in Chapter 4 and 6.

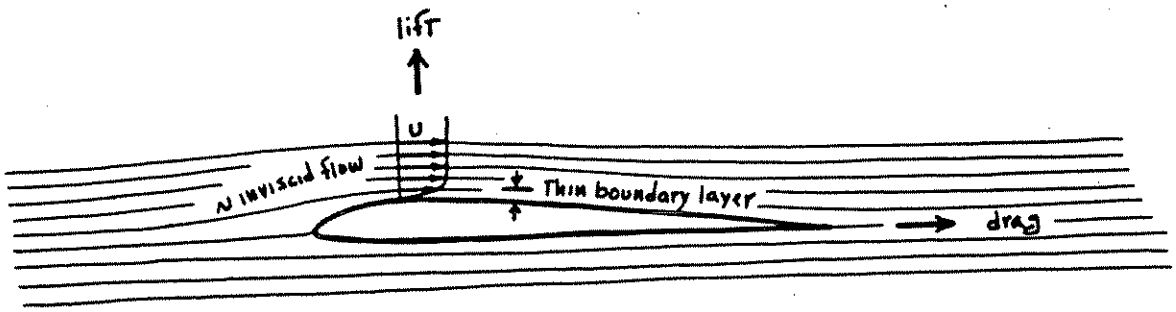

Figure 3.4 Schematic streamlines and forces in flow around an airplane wing.

THE BERNOULLI EQUATION

In the example of inviscid flow past a sphere described above, the pressure is high at points where the velocity is low, and vice versa. It is not difficult to derive an equation, called the Bernoulli equation, that accounts for this relationship. Because this will be useful later on, we'll show here how it comes about.

First we have to be more specific about what we've casually been calling flow lines. Fluid velocity is a vector quantity, and since the fluid behaves as a continuum, a velocity vector can be associated with every point in the flow. Continuous and smooth curves that are everywhere tangent to these velocity vectors (Figure 3.5) are called streamlines. One and only one streamline passes through each point in the flow, and at any given time there is only one such set of curves in the flow. If the flow is steady, the streamline pattern doesn't change with time; if the streamline pattern changes with time, the flow is unsteady. (But note that the converse of each of these statements is not necessarily true, because an unsteady flow can exhibit an unchanging pattern of streamlines as velocities everywhere increase or decrease with time.)

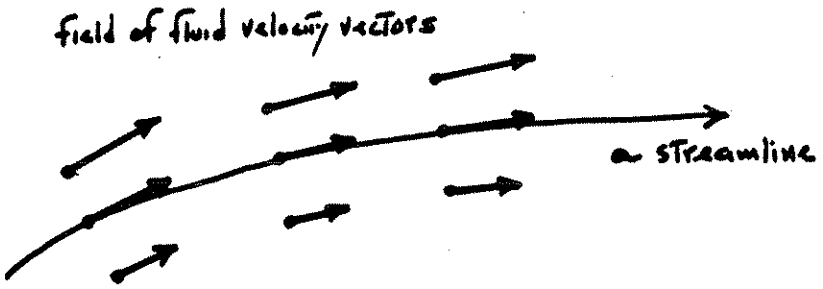

Figure 3.5 A streamline.

There obviously is an infinity of streamlines passing through any region of flow, no matter how small; usually only a few representative streamlines are shown in sketches and diagrams. An important property of streamlines follows directly from their definition: the flow can never cross streamlines. We can imagine a tubelike surface formed by streamlines (Figure 3.6), called a stream tube, passing through some region; this surface or set of streamlines can be viewed as functioning as if it were a real tube or conduit, in that there is flow through the tube but there is no flow either inward or outward across its surface.

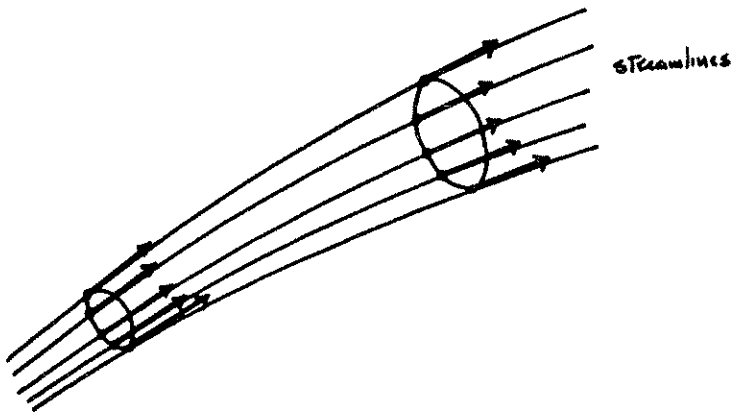

Figure 3.6 A stream tube.

Consider a short segment of one such tiny stream tube in a fluid flow (Figure 3.7). Write Newton's second law for the fluid contained at some instant in this stream-tube segment. The cross-sectional area of the tube is ΔA, and the length of the segment is Δs. If the pressure at cross section 1, at the left-hand end of the segment, is p, then the force exerted on this end of the segment is $p\Delta A$. It's not important that the area of the cross section might be slightly different at the two ends (if

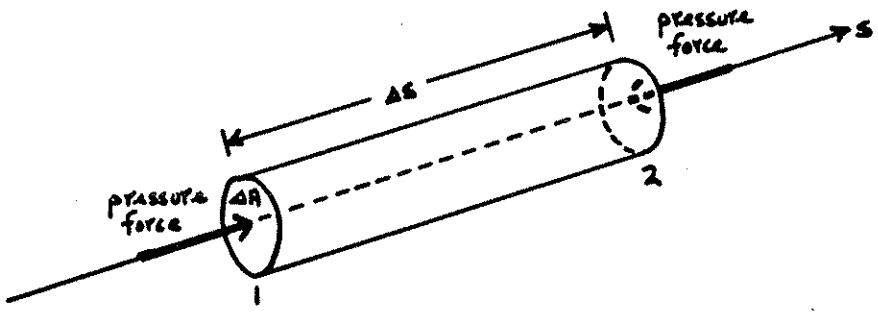

Figure 3.7 Segment of a stream tube, for derivation of the Bernoulli equation.

the flow is expanding or contracting), or that p might vary slightly over the cross section, because you can make the cross-sectional area of the stream tube as small as you please. What is the force on the other end of the tube? The pressure at cross section 2 is different from that at cross section 1 by $(\partial p/\partial s)\Delta s$, the rate of change of pressure in the flow direction times the distance between the two cross sections, so the force on the right-hand end of the tube is

$$\left(p + \frac{\partial p}{\partial s}\,\Delta s\right)\Delta A$$

The net force on the stream tube in the flow direction is then

$$p\Delta A - \left(p + \frac{\partial p}{\partial s}\right)\Delta A = -\frac{\partial p}{\partial s}\Delta s\Delta A$$

The pressure on the lateral surface of the tube is of no concern, because the pressure force on it acts normal to the flow direction. Newton's second law, $F = d(mv)/dt$, for the fluid in the segment of the stream tube, where v is the velocity of the fluid at any point, is then

$$-\frac{\partial p}{\partial s}\Delta s\Delta A = \frac{d}{dt}[v(\rho\Delta s\Delta A)]$$

or

$$-\frac{\partial p}{\partial s} = \rho \frac{dv}{dt} \tag{3.3}$$

where we have assumed that ρ is constant and so can be moved outside the derivative. (In this section v is used not as the component of velocity in the y direction but as the component of velocity tangent to the streamline at a given point .) The derivative on the right side of Equation (3.3) can be put into more convenient form by use of the chain rule and a simple "undifferentiation" of one of the resulting terms:

$$\begin{aligned} -\frac{\partial p}{\partial s} &= \rho \frac{dv}{dt} \\ &= \rho \frac{\partial v}{\partial t}\frac{dt}{dt} + \frac{\partial v}{\partial s}\frac{ds}{dt} \\ &= \rho \frac{\partial v}{\partial t} + v \frac{\partial v}{\partial s} \\ &= \rho \frac{\partial v}{\partial t} + \frac{1}{2}\frac{\partial (v^2)}{\partial s} \end{aligned} \tag{3.4}$$

This equation is strictly true only for the single streamline to which the stream tube collapses as we let $\Delta A \to 0$, because only then need we not worry about possible variation of either p or v over the cross sections. Assuming further that the flow is steady, $\partial v/\partial t = 0$, and Equation (3.4) becomes

$$-\frac{\partial p}{\partial s} = \frac{\rho}{2}\frac{\partial (v^2)}{\partial s} \tag{3.5}$$

It's easy to integrate this equation between two points 1 and 2 on the streamline (remember that this equation holds for any streamline in the flow):

$$-\int_1^2 \frac{\partial p}{\partial s}\, ds = \frac{\rho}{2}\int_1^2 \frac{\partial (v^2)}{\partial s}\, ds$$

$$p_2 - p_1 = -\frac{\rho}{2}(v_2^2 - v_1^2) \tag{3.6}$$

or

$$p + \frac{\rho v^2}{2} = \text{const}$$

So you see that if the flow is steady and incompressible there is an inverse relationship between fluid pressure and fluid velocity along any streamline. Equation (3.6) is called the Bernoulli equation. Remember that it holds only along individual streamlines, not through the entire flow. (In other words, the constant in the alternative form of the equation above is generally different for each streamline in the flow.) And it holds only for inviscid flow, because if the fluid is viscous there are shearing forces across the lateral surfaces of stream tubes, and Newton's second law cannot be written and manipulated so simply. But often in flow of a real fluid the viscous forces are small enough outside the boundary layer that the Bernoulli equation is a good approximation.

Note that the right-hand side of Equation (3.6) is the negative of the increase in kinetic energy per unit volume of fluid between point 1 and point 2. The Bernoulli equation is just a statement of the work-energy theorem, whereby the work done by a force acting on a body is equal to the change in kinetic energy of the body. In this case fluid pressure is the only force acting on the fluid.

In discussing inviscid flow around a sphere we called the front and rear points of the sphere the stagnation points, because velocities relative to the sphere are zero there. Using the Bernoulli equation it's easy to find the corresponding stagnation pressures. Taking the free-stream values of pressure and velocity to be p_o and v_o, writing Equation (3.6) in the form

$$p - p_o = -\frac{\rho}{2}(v^2 - v_o^2)$$

and substituting $v = 0$ at the stagnation points, the stagnation pressure (the same for front and rear points) is

$$p = p_o + \frac{\rho v_o^2}{2}$$

TURBULENCE

Almost all fluid flows of sedimentological interest are turbulent. Because of the range and complexity of problems in turbulent flow, our approach will necessarily continue to be selective. The introductory material on the description and origin of turbulence in this section is background for the important topic of turbulent flow in boundary layers in the following section and in Chapter 5. The emphasis in all this material on turbulence is on the most important physical effects. Mathematics will be held to a minimum, although some is unavoidable in the derivation of useful results on flow resistance and velocity profiles.

What is Turbulence?

It's not easy to devise a satisfactory definition of turbulence. Turbulence might be loosely defined as an irregular or random or statistical component of motion that under certain conditions becomes superimposed on the mean or overall motion of a fluid when that fluid flows past a solid surface or past an adjacent stream of the same fluid with different velocity. This definition does not convey very well what turbulence is really like; it's much easier to describe turbulence than to define it.

Our goal in this section is to present as clear a picture as possible of what turbulence is like. Suppose that you were in possession of a magical instrument that allowed you to make an exact and continuous measurement of the fluid velocity at any point in a turbulent flow as a function of time. We're calling the instrument magical because all of the many available methods of measuring fluid velocity at a point, some of them fairly satisfactory, inevitably suffer from one or both of two drawbacks: (i) the presence of the instrument distorts or alters the flow we're trying to measure; (ii) the effective measurement volume is not small enough to be regarded as a "point." What would your record of velocities look like? Figure 3.8 is an example of such a record, for the component u of velocity in the downstream direction. The outstanding characteristic of the velocity is its uncertainty: there is no way of predicting at a given time what the velocity at some future time will be. But note that there is a readily discernible (although not precisely definable) range into which most of the velocity fluctuations fall, and the same can be said about the time scales of the fluctuations.

Turbulence measurements present a rich field for statistical treatment. First of all, a mean velocity u can be defined from the record of u by use of an averaging time interval that is very long with respect to the time scale of the fluctuations but not so long that the overall level of the velocity drifts upward or downward during the averaging time (Figure 3.9). A fluctuating

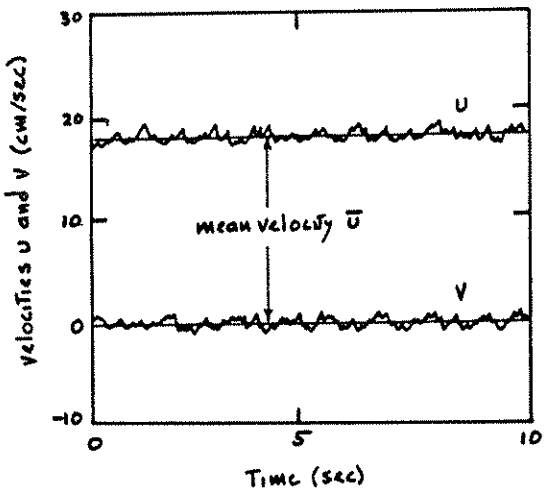

Figure 3.8 Typical records of streamwise component u and normal-to-boundary component v of instantaneous fluid velocity in turbulent flow past a solid boundary. The horizontal line representing the mean velocity u has the property that the areas under the velocity curve above and below the line are equal.

velocity u' can then be defined as the difference between the instantaneous velocity u and the mean velocity $\bar{u}$:

$$u' = u - \bar{u}$$

where the overbar denotes a time average. The time-average value of u' must be zero. Now look at the component of velocity in any direction normal to the mean flow direction (Figure 3.8). You'd see a similar record, except that the average value would always have to be zero; the normal-to-boundary velocity is usually called v, and the cross-stream velocity (parallel to the boundary and normal to flow) is usually called w.

$$v' = v - \bar{v} = v$$

$$w' = w - \bar{w} = w$$

A good measure of the intensity of the turbulence is the root-mean-square value of the fluctuating components of velocity:

$$RMS(u') = (\overline{u'^2})^{1/2}$$

$$RMS(v') = (\overline{v'^2})^{1/2}$$

$$RMS(w') = (\overline{w'^2})^{1/2}$$

These are formed by taking the square root of the time average of the squares of the fluctuating velocities; for those who are familiar with statistical terms, the rms values are simply standard deviations of instantaneous velocities. They are always positive quantities, and their magnitudes are a measure of the strength or intensity of the turbulence, or the spread of instantaneous velocities around the mean. Turbulence intensities are typically something like five to ten percent of the mean velocity $\bar{u}$ (i.e., the coefficient of variation of velocity is 5-10%).

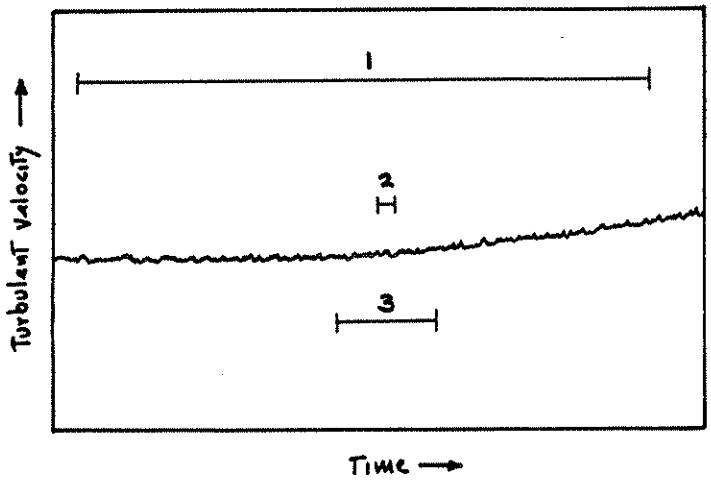

Figure 3.9 Choice of an averaging time interval for turbulent velocity. Time interval 1 is too long, because the velocity has drifted considerably. Time interval 2 is too short, because it does not include enough fluctuations to provide a stable or representative average. Time interval 3 is acceptable, because it includes a sufficiently large number of fluctuations but the velocity has drifted very little. An appropriate averaging interval like this can usually be found.

Statistical analysis of turbulence can be carried much further than this. But now suppose that you measured velocity in a different way, by following the trajectories of fluid "points"

or markers as they travel with the flow and measuring the velocity components as a function of time. It is straightforward, though laborious, to do this sort of thing by photographing tiny neutrally buoyant marker particles that represent the motion of the fluid well, and then measuring their travel and computing velocities. Velocities measured in this way, called Lagrangian velocities, are related to those measured at a fixed point, called Eulerian velocities, and the records would look generally similar. The trajectories themselves would be three-dimensionally sinuous and highly irregular, as shown schematically in Figure 3.10, although angles between tangents to trajectories and the mean flow direction are usually not very large, because u' is usually small relative to u. You can imagine releasing fluid markers at some fixed point in the flow and watching a succession of trajectories traced out at different times (Figure 3.11). Each trajectory would be different in detail, but they would show similar features.

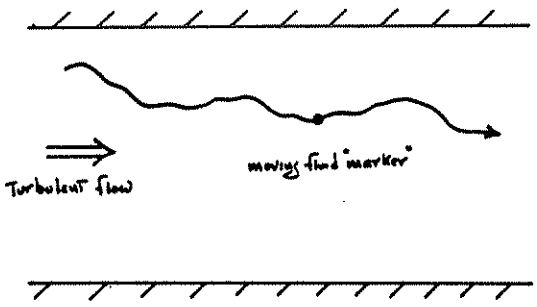

Figure 3.10 Typical trajectory of a small fluid element or "marker" in a turbulent flow. The trajectory is slightly exaggerated in the direction normal to the flow.

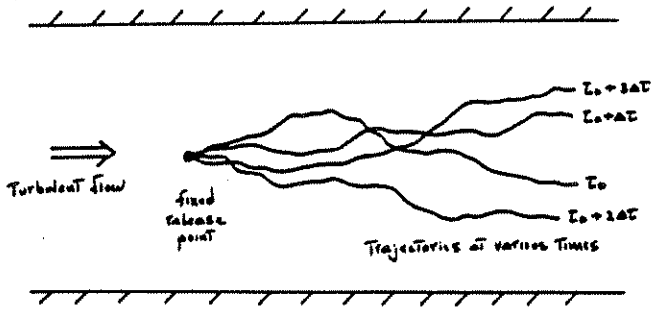

Figure 3.11 A succession of trajectories of fluid markers released at the same point but at different times in a turbulent flow. Trajectories are slightly exaggerated in the direction normal to the flow.

One thing you can do to learn something about the spatial scale of the fluctuations revealed by velocity records like the

one in Figure 3.8 is to think about the distance over which the velocity becomes "different" or uncorrelated with distance away from a given point. Suppose that you measured the velocity component u simultaneously at two points 1 and 2 a distance x apart in the flow and computed the correlation coefficient by forming products of a large number of pairs of velocities, each measured at the same time, taking the average of all the products, and then scaling by dividing by the rms value. If the two points are close together compared to the scale of the turbulence, the velocities at the two points will be nearly the same, and the coefficient will be nearly one. But if the points are far apart the velocities will be uncorrelated (that is, they will have no tendency to be similar), and the coefficient will be zero or nearly so. The distance over which the coefficient falls to a value close to zero is roughly representative of the spatial scale of the turbulent velocity fluctuations. A similar correlation coefficient can be computed for Lagrangian velocities, and correlation coefficients can also be based on time rather than on space.

One of the very best ways to get a qualitative idea of the physical nature of turbulent motions is to put some very fine flaky reflective material into suspension in a well illuminated flow. The flakes tend to be brought into parallelism with local shearing planes, and variations in reflected light from place to place in the flow give a fairly good picture of the turbulence. Although it's easier to appreciate than to describe the pattern that results, the general picture is one of intergrading swirls of fluid, with highly irregular shapes and with a very wide range of sizes, that are in a constant state of development and decay. These swirls are called turbulent eddies. Even though they're not sharply delineated, they have a real physical existence. The swirly nature of the eddies is most readily perceived when the eye attempts to follow points moving along with the flow; if instead the eye attempts to fix upon a point in the flow that is stationary with respect to the boundaries, fluid elements (if there are some small marker particles contained in the fluid to represent them) are seen to pass by with only slightly varying velocities and directions, in accordance with the Eulerian description of turbulent velocity at a point.

Each eddy has a certain sense and intensity of rotation that tends to set it off, at least momentarily, from surrounding fluid. The property of solid-body-like rotation of fluid at a given point in the flow is termed vorticity. Think in terms of the rotation of a small element of fluid as the volume of the element shrinks toward zero around the point. The vorticity varies smoothly in both magnitude and orientation from point to point. The eddy structure of the turbulence can be described by how the vorticity varies throughout the flow; the vorticity in an eddy varies from point to point, but it tends to be more nearly the same there than in neighboring eddies.

Origin of Turbulence

You saw in Chapter 1 that steady uniform flow down a plane is laminar under some conditions and turbulent under other conditions. This is characteristic of most kinds of flows. Now that you have some idea of the kinematics of turbulent flow, you might consider what it is that governs whether the flow is laminar or turbulent in the first place, and what the transition from laminar to turbulent flow is like. Osborne Reynolds did the pioneering work on these questions in the 1880s in an experimental study of flow through tubes with circular cross-section (Reynolds, 1883). Think first about the variables important in such a flow (Figure 3.12). Density ρ and viscosity μ must be taken into account, for the same reasons as in flow down a plane. A variable that describes the speed of movement of the fluid is important, because this governs both fluid inertia and rates of shear. A good variable of this kind is the mean velocity of flow in the tube; this can be found either by averaging the local fluid velocity over the cross section of the tube or by dividing the discharge (i.e., the volume rate of flow) by the cross-sectional area of the tube. The diameter D of the tube is important because it affects both the shear rate and the scale of the turbulence. Gravity need not be considered explicitly in this kind of flow because no deformable free surface is involved. As discussed in Chapter 1, the four variables U, D, ρ, and μ can be combined into a single dimensionless variable $\rho UD/\mu$ on which all the characteristics of the flow, including the transition from laminar to turbulent flow, depend. Reynolds first deduced the importance of this variable, now called the Reynolds number Re, by considering the dimensional structure of the equation of motion in the way we discussed briefly at the very end of Chapter 1.

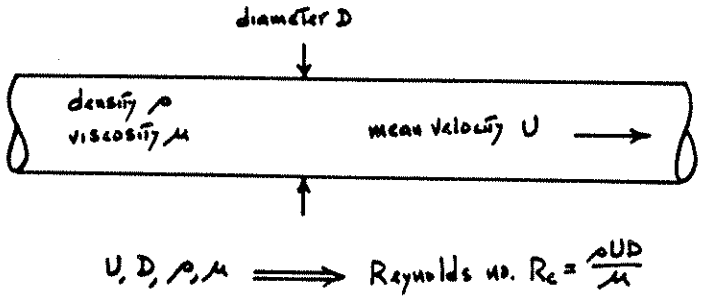

Figure 3.12 Variables that characterize the transition from laminar flow to turbulent flow in a straight tube with circular cross section.

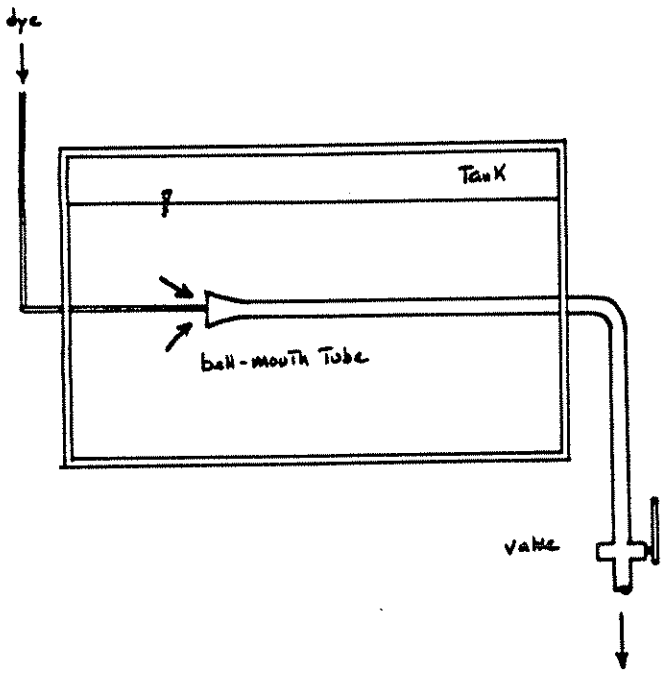

Figure 3.13 Apparatus of the kind used by Reynolds to study the transition from laminar flow to turbulent flow downstream of the inlet to a straight circular tube.

Reynolds made two kinds of experiments. The first, to study the development of turbulent flow from an originally laminar flow, was made in an apparatus like that shown in Figure 3.13: a long tube leading from a reservoir of still water by way of a trumpet-shaped entrance section, through which a flow with varying mean velocity could be passed with a minimum of disturbance. Three different tube diameters (1/4", 1/2", and 1") and water of two different temperatures, and therefore of two different viscosities, were used. For each combination of D and μ the mean velocity was gradually increased until the originally laminar flow became turbulent. The transition was observed with the aid of a streak of colored water introduced at the entrance of the tube.

> When the velocities were sufficiently low, the streak of color extended in a beautiful straight line through the tube [Figure 3.14A].... As the velocity was increased by small stages, at some point in the tube, always at a considerable distance from the trumpet or entrance, the color band would all at once mix up with the surrounding water, and fill the rest of the tube with a mass of colored water [Figure 3.14B].... On viewing the tube by the light of an electric spark, the mass of water resolved itself into a mass of more or less distinct curls, showing eddies [Figure 3.14C]

(Reynolds, 1883, p. 942). Reynolds found that for each combination of D and μ the point of transition was characterized by almost exactly the same value of Re, around 12,000. Subsequent experiments have since confirmed this over a much wider range of U, D, ρ, and μ.

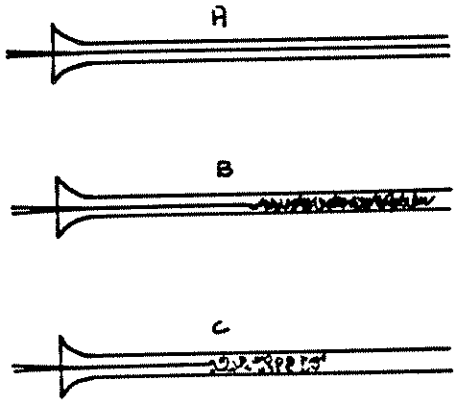

Figure 3.14 Patterns of flow observed by Reynolds in his experiments on transition from laminar flow to turbulent flow in a straight circular tube. (A) Laminar flow through the tube; (B) transition from laminar flow to turbulent flow in the tube; (C) transition from laminar flow to turbulent flow illuminated by a spark to reveal the eddy structure of the turbulent flow.

Since the transition from laminar to turbulent flow was so abrupt and the resulting turbulence was so well developed, Reynolds suspected that the laminar flow became potentially unstable to large disturbances at a much lower value of Re than he found for the transition when he minimized external disturbances, and in fact he observed that the transition took place at much lower values of Re if there was residual turbulence in the supply tank or if the apparatus was disturbed in any way. Similar experiments made with even greater care in eliminating such disturbances have since shown that laminar flow can be maintained to much higher values of Re, up to about 40,000, than in Reynolds' original experiments.

To circumvent the persistence of laminar flow into the range of Re for which it is unstable, Reynolds made a separate set of experiments to study the transition of originally turbulent flow to laminar flow as the mean velocity in the tube was gradually decreased. To do this he passed turbulent flow through a very long metal pipe and gradually decreased the mean velocity until at some point along the pipe the flow became laminar. The occurrence of the transition was detected by measuring the drop in fluid pressure between two stations about two meters apart near the downstream end of the pipe. (It had been known long before Reynolds' work that in laminar flow through a horizontal pipe the rate at which fluid pressure drops along the pipe is directly

proportional to the mean velocity, whereas in turbulent flow it is approximately proportional to the square of the mean velocity. Thus, although Reynolds could not see the transition he had a sensitive means of detecting its occurrence.) Again many different combinations of pipe diameter and fluid viscosity were used; in every case the transition from turbulent to laminar flow occurred at values of Re close to 2000. This is the value for which laminar flow can be said to be unconditionally stable, in the sense that no matter how great a disturbance is introduced, the flow will always revert to being laminar.

Mathematical theory for the origin of turbulence is intricate, and only partly successful in accounting for the transition to turbulent flow at a certain critical Reynolds number. One of the most successful approaches involves analysis of the stability of a laminar shear flow against very-small-amplitude disturbances. The mathematical technique involves introducing a small wavelike disturbance of a certain frequency into the equation of motion for the flow and then seeing whether the disturbance grows in amplitude or is damped. The assumption is that if the disturbance tends to grow it will eventually lead to development of turbulence. Although a satisfactory explanation would take us off the track at this point, in laminar flow there is a tendency for a wave-shaped distortion as in Figure 3.15 to be amplified with time: applying the Bernoulli equation along the streamlines shows that fluid pressure is lowest where the velocity is greatest in the region of crowded flow lines, and highest where the velocity is smallest in the region of uncrowded flow lines, and the resulting unbalanced pressure force tends to accelerate the fluid in the direction of convexity and thereby accentuate the distortion. But at the same time the viscous resistance to shearing tends to weaken the shearing in the high-shear part of the distortion and thus tends to make the flow revert to uniform shear. It should therefore seem natural that the Reynolds number, which is a measure of the relative importance of viscous shear forces and accelerational tendencies, should indicate whether disturbances like this are amplified or damped.

Figure 3.16 is a stability diagram for a laminar shear layer or boundary layer (see next section) developed next to a planar boundary. The diagram shows the results of both the mathematical stability analysis described above (Lin, 1955) and experimental observations on stability (Schubauer and Skramstad, 1947). The experiments were made by causing a small metal band to vibrate next to the planar boundary at a known frequency and observing the resulting velocity fluctuations in the fluid. Agreement between theory and experiment is good but not perfect; if the experimental results were completely in agreement with the calculated curve, they would all fall on it. The diagram shows that there is a well-defined critical Reynolds number, Re_{crit}, below which the laminar flow is always stable but above which there is a range of frequencies at any Reynolds number for which the disturbance is amplified, so that the laminar flow is potentially unstable and

will become turbulent provided that disturbances with frequencies in that range are present.

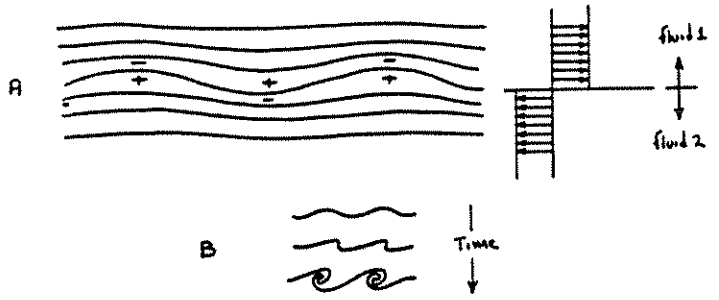

Figure 3.15 Amplification of a wave-shaped disturbance on an interface of velocity discontinuity in laminar flow (schematic). (A) Pressure forces acting to deform the interface. Plus and minus signs indicate high and low pressures, respectively, acting on each side of the velocity discontinuity. (B) Evolution of the disturbance with time in a series of vortices.

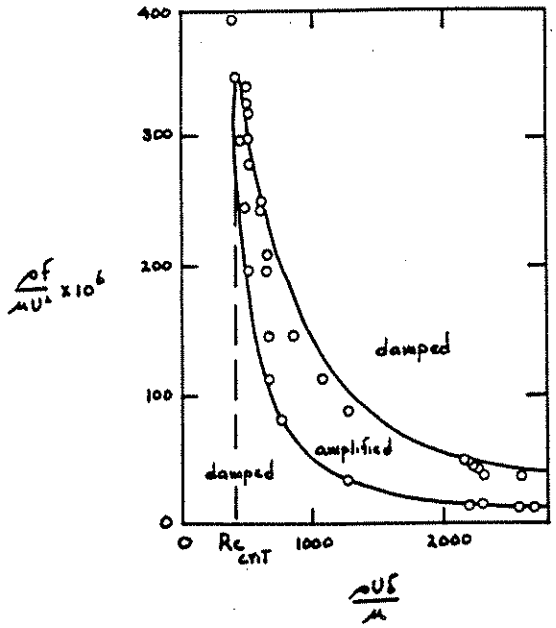

Figure 3.16 Diagram showing stability of a laminar shearing layer (boundary layer) developed next to a planar boundary. The vertical axis is a dimensionless measure of the frequency f of the imposed small-amplitude disturbances. The horizontal axis is a Reynolds number based on thickness δ of the boundary layer and free-stream velocity at the outer edge of the boundary layer. The solid curve is the calculated curve for neutral stability (Lin, 1955); the points represent experimental determinations of neutral stability (Schubauer and Skramstad, 1947).

BOUNDARY LAYERS

A boundary layer is the zone of flow in the immediate vicinity of a solid surface or boundary in which the motion of the fluid is affected by the frictional resistance exerted by the boundary. The no-slip condition requires that the velocity of fluid in direct contact with solid boundary be exactly the same as the velocity of the boundary; the boundary layer is the region of fluid next to the boundary across which the velocity of the fluid grades from that of the boundary to that of the unaffected part of the flow (often called the free stream) some distance away from the boundary.

A good example is the boundary layer that develops on both surfaces of a stationary flat plate held parallel to a uniform free stream of fluid (Figure 3.17). Just downstream of the leading edge of the plate the boundary layer is very thin, and the shearing necessitated by the transition from zero velocity to free-stream velocity is compressed into a thin zone of strong shear, and so the shear stress at the surface of the plate is large. Farther along the plate the boundary layer is thicker, because the motion of a greater thickness of fluid is retarded by the frictional influence of the plate, in the form of shear stresses exerted from layer to layer in the fluid; the shearing is therefore weaker, and the shear stress at the surface of the plate is smaller.

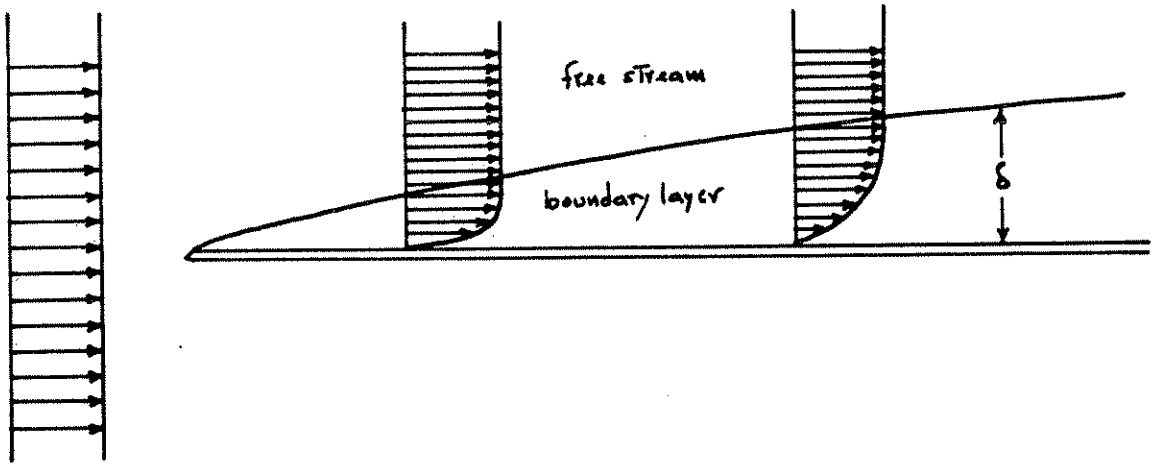

Figure 3.17 Development of a laminar boundary layer downstream of the leading edge of a flat plate held parallel to a uniform stream of fluid. A boundary layer is developed on both sides of the plate; only one is shown. Rate of growth of the boundary layer downstream is exaggerated.

Boundary layers develop on objects of any shape immersed in a fluid moving relative to the object: flat plates as discussed above, airplane wings and other streamlined shapes, and blunt or bluff bodies like spheres or cylinders or sediment grains. Boundary layers also develop next to the external boundaries of a flow: the walls of pipes and ducts, the beds and bottoms of channels, the ocean bottom, and the land surface under the moving atmosphere. In every case the boundary layer has to start somewhere, as at the front surface or leading edge of a body immersed in the flow or at the upstream end of any solid boundary to the flow. And in every case it grows or expands downstream, either until the flow passes by the body (the shearing motion engendered in the boundary layer is then degraded by viscous forces), or until it meets another boundary layer growing from some other surface, or until it reaches a free surface.

Flow in boundary layers may be either laminar or turbulent. A boundary layer typically starts out as a laminar flow, but if it has a chance to grow for a long enough distance along the boundary it abruptly becomes turbulent. In the example of a flat-plate boundary layer, we can define a Reynolds number $Re_\delta = \rho U\delta/\mu$ based on free-stream velocity U and boundary-layer thickness δ (Figure 3.18); just as in flow in a tube or down a plane, past a certain critical value of Re_δ the laminar boundary layer is potentially unstable and may become turbulent. If there are no large turbulent eddies in the free stream, the laminar boundary layer may persist to very high Reynolds numbers; if the free stream is itself turbulent, or if the surface of the plate is very rough, the boundary layer may become turbulent a very short distance downstream of the leading edge. Turbulence in the form of small spots develops at certain points in the laminar boundary layer, spreads rapidly, and soon engulfs the entire boundary layer. Once the boundary layer becomes turbulent it thickens faster, because fluid from the free stream is incorporated into the boundary layer at its outer edge in much the same way that clear air is incorporated into a turbulent plume of smoke (Figure 3.19). But the thickness of even a turbulent boundary layer grows fairly slowly relative to downstream distance--the angle between the average position of the outer edge of the boundary layer and the boundary itself is not very large, typically something like a few degrees.

A question that might be bothering you at this point is: How thick can a boundary layer grow? In the case of objects immersed in the flow, the boundary layer develops only in the immediate vicinity of the object. Downstream of the object the fluid that was retarded in the boundary layer is gradually reaccelerated by the free stream, until far downstream the velocity profile in the free stream no longer shows any evidence of the presence of the object upstream. The zone of retarded and often turbulent fluid downstream of the object is called the <u>wake</u>.

The boundary layer that grows along an external boundary of the flow itself keeps growing until it encounters a free surface

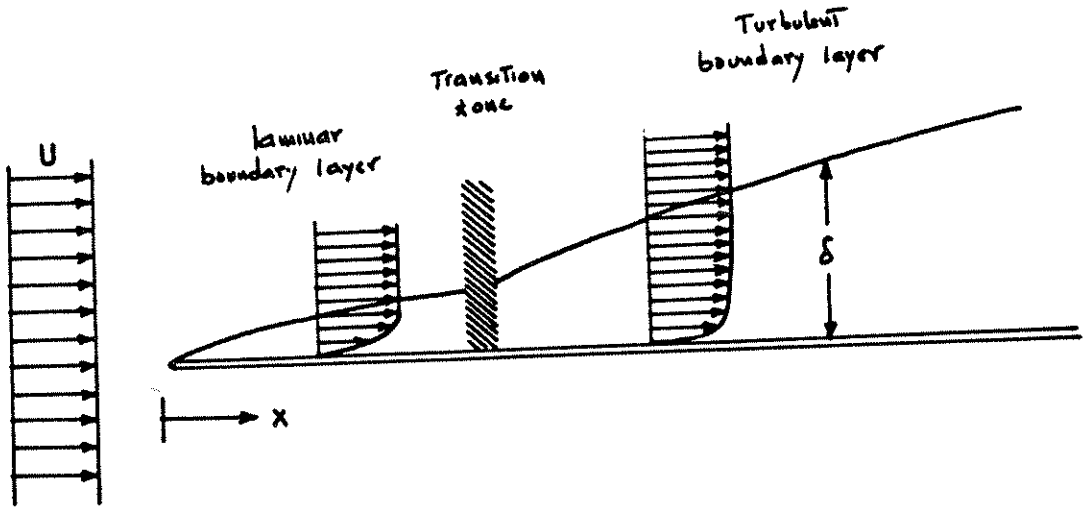

Figure 3.18 Transition from laminar flow to turbulent flow in the boundary layer developed next to a flat plate held parallel to the flow.

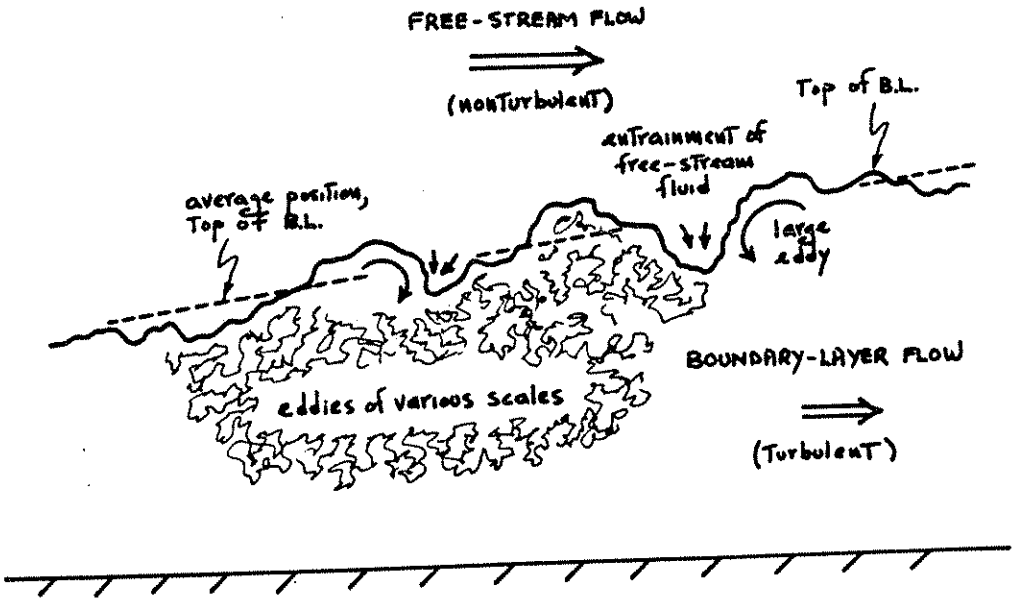

Figure 3.19 Mixing of ambient free-stream fluid into the outer part of a turbulent boundary layer.

or another boundary layer growing from the opposite boundary. It's instructive to consider how the boundary layer in flow down a plane develops if the flow actually has a well defined starting

point, as at the sill or spillway of a large reservoir of still fluid (Figure 3.20). A boundary layer starts to develop at the head of the planar channel bottom and grows upward toward the surface. At some point downstream the boundary layer becomes so thick that it reaches the free surface. Past this point the flow is all boundary layer! Boundary-layer development is typically complete in a length of channel equivalent to something like a few tens of flow depths. Upstream, in the zone of boundary-layer growth, the boundary layer is nonuniform, in that it is different at each section; downstream, in the zone of fully established flow, the boundary layer is uniform. In the same sense, a fairly straight river or tidal-channel flow is all boundary layer. Of course, since objects can be immersed in such flows, local boundary layers, called internal boundary layers, can be developed within larger boundary layers. One example is that of the boundary layer developed on a sediment grain on the bed of a turbulent boundary-layer flow or settling through the flow; another, discussed in more detail in Chapters 5 and 7, is that of the boundary layer that develops locally in the accelerating flow over the back of a ripple or a dune.

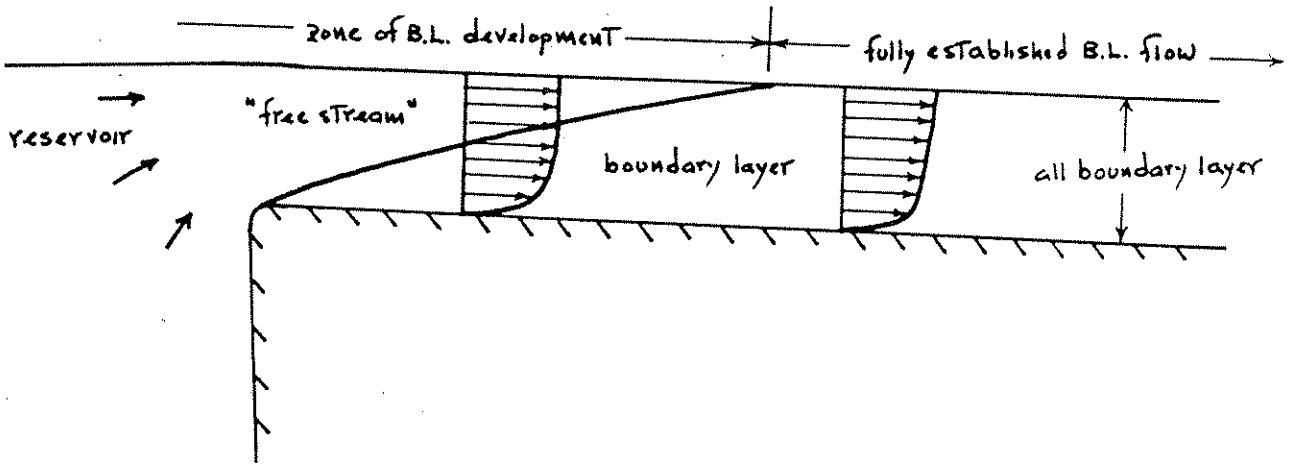

Figure 3.20 Development of a turbulent boundary layer at the head of an open channel.

FLOW SEPARATION

The overall pattern of flow at fairly high Reynolds numbers past blunt bodies or through sharply expanding channels or conduits is radically different from the pattern expected from inviscid theory, which we've said is often a good guide to the real flow patterns. Figure 3.21 shows two examples of such flow patterns, one for a sphere and one for a duct or pipe that has a downstream expansion at some point. Near the point where the solid boundary begins to diverge from the direction of the mean

flow, the boundary layer separates or breaks away from the boundary. This phenomenon is called flow separation. In all cases the flow separates from the boundary in such a way that the fluid keeps moving straight ahead as the boundary surface falls away from the direction of flow just upstream. The main part of the flow, outside the boundary layer, diverges from the solid boundary correspondingly. If you look only at the regions enclosed by the dashed curves in Figure 3.21 you can appreciate that flow separation is dependent not so much on the overall flow geometry as on the change in the orientation of the boundary relative to the overall flow--a change that involves a curving away of the boundary from the overall flow direction. Separation takes place at or slightly downstream of the beginning of this curving away.

Downstream of the separation point is a region of stagnant fluid with about the same average velocity as the boundary itself. In this region the fluid has an unsteady eddying pattern of motion, with only a weak circulation as shown in Figure 3.21. As soon as the boundary layer leaves the solid boundary it is in contact with this slower-moving fluid across a surface of strong shear. This shearing surface is unstable, and a short distance downstream of the separation point it becomes wavy and then breaks down to produce turbulence. This turbulence is then mixed or diffused both into the main flow and into the stagnant region, and is eventually damped out by viscous shearing within eddies, but its effect extends for a great distance downstream. The stagnant region of fluid inside the separation surface, together with the region of strong turbulence developed on the separation surface, is called a wake. Far downstream from a blunt body like a sphere (Figure 3.21A) the wake turbulence is weak and the average fluid velocity along a profile across the mean flow is slightly less than the free-stream velocity. In flow past an expansion in a duct or channel (Figure 3.21B), the expanding zone of wake turbulence eventually impinges upon the boundary; downstream of this point, where the flow is said to reattach to the boundary, the flow near the boundary is once again in the downstream direction, and a new boundary layer develops until far downstream of the expansion the flow is once again fully established.

You can understand why flow separation takes place by reference to steady inviscid flow around a sphere (Figure 3.1). Remember that variations in fluid velocity can be deduced qualitatively just from variations in spacing of neighboring streamlines. As a small mass of fluid approaches the sphere along a streamline that will take it close to the surface of the sphere (Figure 3.22), it decelerates slightly from its original uniform velocity and then accelerates to a maximum velocity at the midsection of the sphere (Figure 3.23). Beyond the midsection it experiences precisely the reverse variation in velocity: it decelerates to minimum velocity and then accelerates slightly back to the free-stream velocity. We can apply the Bernoulli equation (Equation 3.6) to find the corresponding variation in fluid pressure. The pressure is slightly greater than the free-stream value at points just upstream and just downstream of the sphere

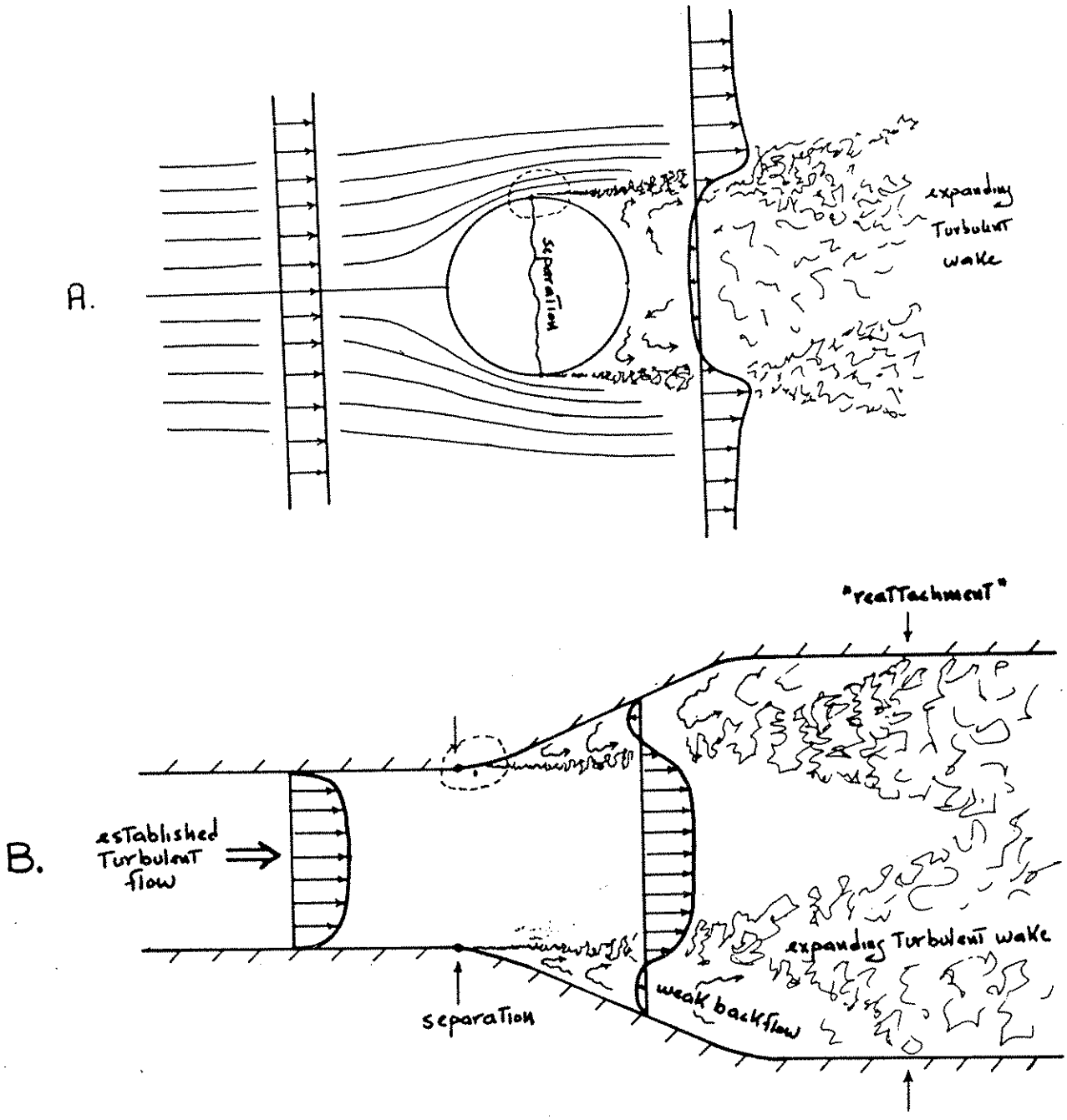

Figure 3.21 Flow separation developed in (A) flow past a sphere and (B) flow through a duct or pipe.

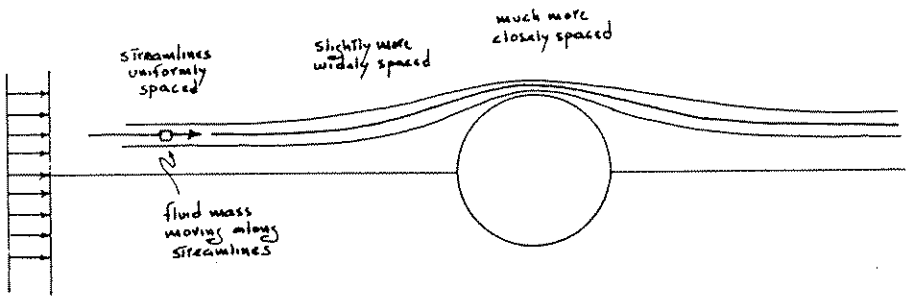

Figure 3.22 Steady inviscid motion of a small mass of fluid passing close to a sphere.

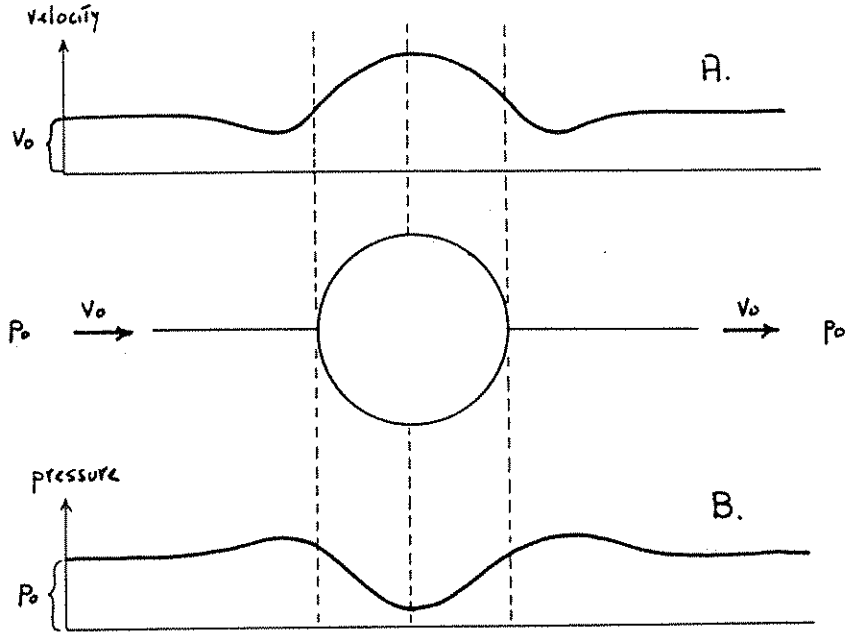

Figure 3.23 Schematic variation in (A) velocity and (B) pressure along a streamline passing close to the sphere, for steady inviscid flow around a sphere.

but shows a minimum at the midsection (Figure 3.23). It is this variation in pressure that causes strong accelerations and decelerations as the fluid passes around the sphere. In front of the sphere the pressure decreases along the streamline (the spatial rate of change or gradient of pressure is said to be negative or favorable), so there is a net force on the fluid mass in the direction of motion, causing an acceleration. In back of the sphere the pressure increases along the streamline (the pressure gradient is positive or adverse), so there is a net force opposing the motion, and the fluid mass decelerates.

In inviscid flow the pressure is the only force in the fluid. But in the real world of viscous fluids, a boundary layer develops next to the sphere. If the boundary layer is thin, the streamwise variation in fluid pressure given by the Bernoulli equation along streamlines just outside the boundary layer is approximately the same as the pressure on the boundary. (The pressure outside the boundary layer is said to be impressed on the boundary.) If now you follow the motion of a fluid mass along a streamline that is close enough to the sphere to become involved in the boundary layer, a viscous force as well as the impressed pressure force acts on the fluid mass. Because the viscous force everywhere opposes the motion, the fluid mass cannot ultimately regain its uniform velocity after passing the sphere, as in inviscid flow. The fluid cannot accelerate as much in front of the sphere as in the inviscid flow, and reaches the midsection with lower velocity; then the adverse pressure gradient in back of the sphere, which is augmented by the viscous retardation, decelerates the fluid to zero velocity and causes it to start to move in reverse (Figure 3.24). This reverse flow forms a barrier to the continuing flow from the front of the sphere, and so the flow must break away from the boundary to pass over the obstructing fluid. Because velocities are small along streamlines close to the boundary, this deceleration to zero velocity occurs only a short distance downstream of the onset of the adverse pressure gradient where the boundary curves away from the mean flow direction.

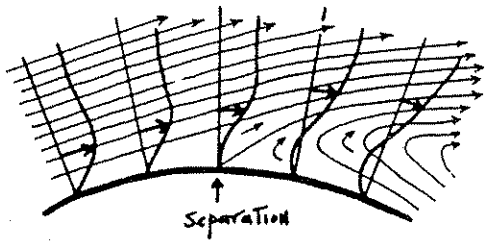

Figure 3.24 Development of reverse flow and boundary-layer separation in the region of adverse pressure gradient where the solid boundary curves away from the mean flow direction. Profiles show component of fluid velocity parallel to the boundary.

You might justifiably ask why this same explanation should not hold just as well for slow flow around a sphere at Reynolds numbers small enough to be in the Stokes range. A superficial answer would be that according to Stokes' law for slow viscous flow around a sphere the distributions of pressure and shear stress are such that the flow passes around the sphere without reversal. A more basic explanation, which is qualitatively true but may not be very helpful, is as follows. As noted in Chapter 2, flow around a sphere at low velocities is characterized by fluid accelerations that are everywhere so small compared to

fluid velocities that the viscous forces are everywhere closely balanced by pressure forces, so that there is no tendency for fluid to decelerate to a stall. At these low velocities, vorticity generated by shearing in the fluid caused by the presence of the solid boundary is spread uniformly for a great distance away from the surface of the sphere rather than being concentrated near the boundary. As the velocity around the sphere increases, the vorticity is to a progressively greater extent swept or convected back around the sphere in a progressively thinner layer rather than being distributed in all directions (or, in other words, shearing is more concentrated near the solid boundary), and the pressure distribution in the surrounding fluid is more and more like that predicted by inviscid theory. Ultimately flow separation develops for the reasons outlined above.

CHAPTER 4. MORE ON DRAG AND SETTLING

INTRODUCTION

In Chapter 2 we outlined the basic law for settling of a spherical grain through a still, viscous fluid. This was done by establishing, partly on theoretical grounds but mainly from dimensional analysis and experimentation, a relationship between drag coefficient and Reynolds number for a sphere moving through a viscous fluid. It was seen that the nature of the relationship changes as the Reynolds number increases, corresponding to a change from a viscous regime of flow to a regime in which the motion of the particle results in the formation of a turbulent wake.

In this chapter we will examine a little more closely the phenomenon of wake formation, and then consider the modifications of settling behavior that arise from changes in shape and concentration of the settling grains.

MORE ON FLOW REGIMES

Flow separation is the basic physical process leading to the formation of a wake behind a settling grain. Even before a wake is developed, there are deviations of the observed drag coefficient from that predicted by Stokes' Law, but after flow separation begins, the deviations from Stokes' Law become very large (Figure 4.1).

For spheres, flow separation begins at a Reynolds number of about 24. The point of separation is at first close to the rear of the sphere, and separation results in the formation of a ring eddy attached to the rear surface of the sphere. Flow within the eddy is at first quite regular and predictable, thus not turbulent, but as the Reynolds number increases the point of separation moves to the side of the sphere, and the ring eddy is drawn out in the downstream direction and begins to oscillate and become unstable. At Reynolds numbers larger than about 100, turbulence begins to develop in the wake of the sphere. At first turbulence develops mainly in the thin zone of strong shearing produced by flow separation and then spreads out downstream, but as the Reynolds number reaches values of the order of 1000, the entire wake is filled with a mass of turbulent eddies. In the range of Reynolds numbers from about 1000 to about 200,000 there are few major changes in the pattern of flow. The flow separates at a position about 80° from the front stagnation point, and there is a fully developed turbulent wake. The drag is due mainly to the pressure distribution on the surface of the sphere, with only a minor contribution from viscous shear stress. The pressure distribution is as shown in Figure 4.2 and does not vary much with Reynolds number in this range (1000-200,000), so the drag coefficient remains almost constant at about 0.5.

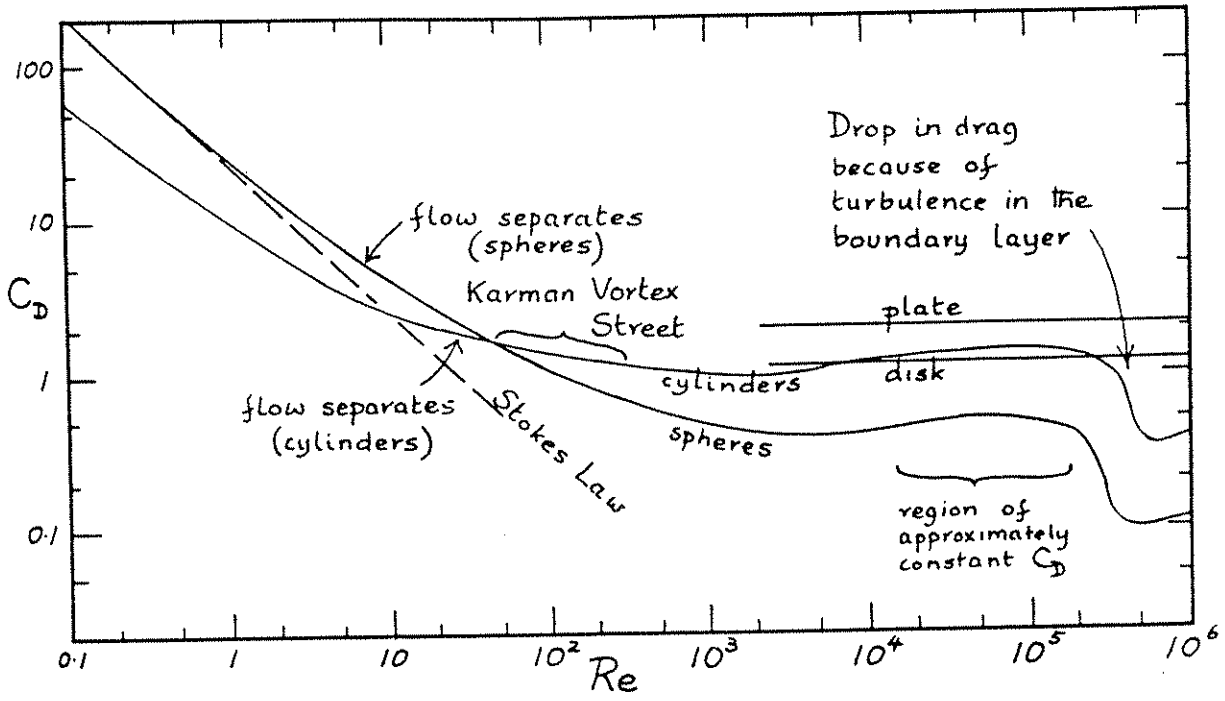

Figure 4.1 Diagram of drag coefficient vs. Reynolds number for spheres, cylinders, spherical plates, and two-dimensional plates normal to the flow.

At very high Reynolds numbers, above about 200,000 (this value corresponds to a quartz sphere of about 16 cm diameter settling in water), the boundary layer becomes turbulent before separation takes place, and there is a sudden change in the flow pattern. Separation takes place at the rear of the sphere (at a position about 120-130° from the front stagnation point), the wake contracts in size, and consequently the pressure distribution changes markedly over the rear of the sphere (Figure 4.2). The result is a sudden drop in drag coefficient, to a minimum of about 0.1. This is sometimes called the "drag crisis."

This sequence of different flow patterns or regimes for spheres is very similar to that observed for flow past many other blunt bodies, i.e., bodies without a good streamlined shape. It is actually easier to observe and measure the flow patterns and drag for circular cylinders normal to the flow than for spheres. A detailed sequence of the flow regimes for cylinders is shown in Figure 4.3, and we will discuss it briefly below, as it illustrates some features not shown by spheres.

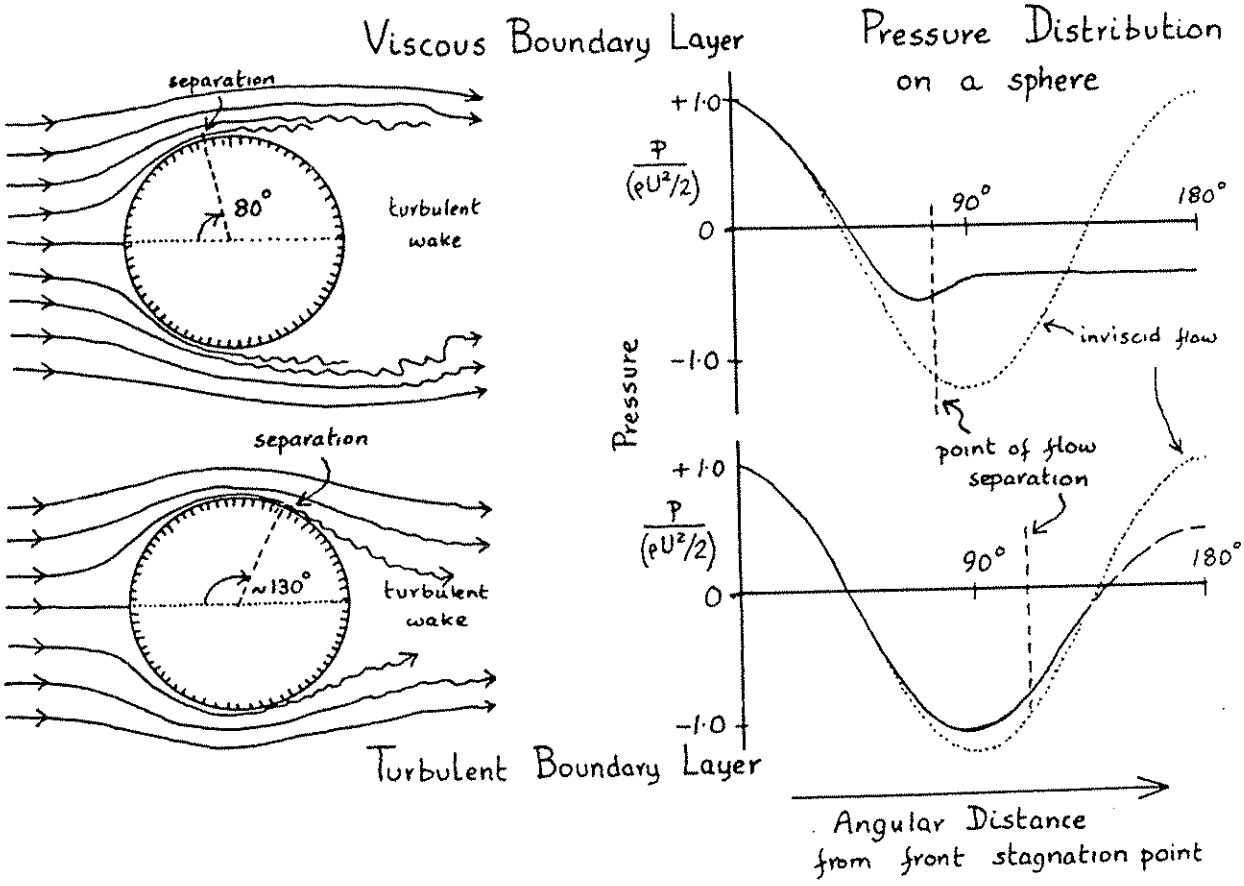

Figure 4.2 Flow pattern and pressure distribution around a sphere at high Reynolds numbers. Upper part of diagram shows experimental results for viscous boundary layer on the front of the sphere; lower part of diagram shows results for a turbulent boundary layer on the front of the sphere. Theoretical pressure distribution for inviscid flow shown for comparison. Pressure is scaled by the stagnation pressure ($\rho U^2/2$).

For cylinders, flow separation begins at a Reynolds number of about 6. At first two regular eddies form, and the point of separation is well around toward the rear of the cylinder (for Re = 40, at an angle of 127° from the front stagnation point). In the range of Reynolds numbers from 40 to 120 there is a regular shedding of the eddies, first from one side of the cylinder and then from the other, to produce a wake consisting of a row of alternating regular eddies or vortices moving downstream. This phenomenon is called the Kármán vortex street. Shedding of the eddies tends to make the cylinder oscillate or vibrate normal to the flow direction--an effect that produces the humming of wires and cables in the wind (Simpson, 1983). At Reynolds numbers of about 120, the vortex street starts to become unstable, leading to development of turbulence in the downstream part of the wake. The

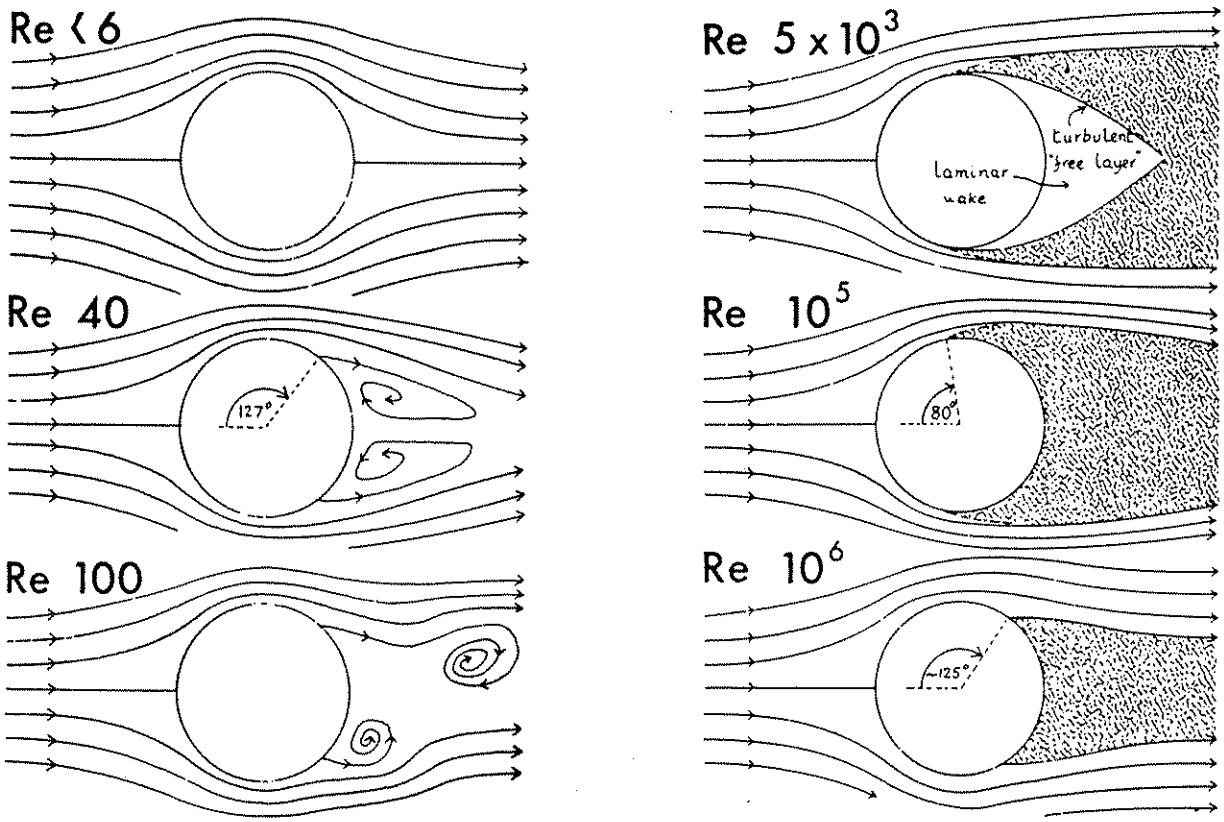

Figure 4.3 Flow patterns around circular cylinders normal to the flow, for Reynolds numbers from less than six to about 10^6.

point of separation moves forward to an angle of about 100° from the front stagnation point, and the wake gradually becomes filled with turbulent eddies, except at first in a region immediately behind the cylinder. At Reynolds numbers greater than 15,000 the entire wake is turbulent, and the point of flow sepration has moved upstream to a point about 80° from the front stagnation point. Further increase in Reynolds number does not produce any other major change in flow pattern until a Reynolds number of about 200,000, when a turbulent boundary layer develops for cylinders just as it does for spheres, and with about the same results.

For both spheres and cylinders the observed control of the drag coefficient by the Reynolds number can therefore be related to just a few factors. Deviations from the slow viscous theory appear even before flow separation in both cases, and can be predicted by a more advanced theoretical treatment that takes more acount of inertial forces (Batchelor, 1967, p. 244-246; O'Neill,

1981). As the Reynolds number rises the drag due to asymmetrical pressure distribution over the surface becomes more and more important, and the drag due to viscous shearing less important.

At high Reynolds numbers the pressure distribution over the front of a blunt body may be predicted reasonably well by inviscid flow theory (e.g., Figure 4.2), but it is almost impossible to predict the pressure distribution developed within the wake, and it is also very difficult to predict exactly where separation will take place. Therefore the pressure distribution at high Reynolds numbers can be determined only experimentally. If this is done, for example by measuring the pressure at a number of small holes (called pressure taps) drilled through the surface of a hollow model of the body, then the total drag force due to the pressure distribution can be calculated from the vector sum of the measured pressure forces. We will see later in this chapter that this has been done for several cases of sedimentological interest. At high Reynolds numbers most of the drag is due to the pressure distribution, but this is not true at low Reynolds numbers. In the case of settling grains the drag coefficient can simply be calculated from the terminal settling velocity, but in other situations (for example, a sphere resting on a bed of spheres, with flow parallel to the bed) it is much more difficult to investigate the drag coefficient experimentally.

As we have seen, most of the drag at high Reynolds numbers results from the formation of a turbulent wake. The pressure within the wake is generally negative relative to the ambient or free-stream pressure (this is called suction) and has a magnitude almost as large as the maximum pressure (positive relative to ambient pressure) reached at the stagnation point at the front of the body. The combination of a large positive pressure on the front of a blunt body and a large negative pressure on the rear of the body results in a high drag coefficient.

Given that the pressure is positive on the front of the sphere and negative in the wake, and that the average magnitude of the pressure in both of these regions is some fraction of the stagnation pressure, we can predict that the total drag force is proportional to the stagnation pressure, the area of the body surface, and the proportion of that surface that is covered by the wake:

$$F_D = (\text{constant})\ \left(\begin{matrix}\text{proportionate}\\ \text{size of wake}\end{matrix}\right)\left(\begin{matrix}\text{surface}\\ \text{area}\end{matrix}\right)\left(\begin{matrix}\text{stagnation}\\ \text{pressure}\end{matrix}\right)$$

$$= (\text{coefficient})\ A_S\ (\rho u^2/2)$$

The only difference between this and the conventional equation for drag (Equation 1.11) is that we have substituted the surface area for the cross-sectional area of the body. Some authors (e.g., Komar and Reimers, 1978) prefer this form of the equation anyway,

because at lower Reynolds numbers the surface area also determines the viscous component of the drag. From the form of the equation given above, we can readily see that one of the main factors determining the size of the drag coefficient is the proportion of the surface covered by the wake. (Vanoni and Hwang, 1967, suggested that the resistance due to bed forms could similarly be predicted by the proportion of the bed covered by separation zones.) The slight increase in drag coefficient at Reynolds numbers of about 10,000 can be attributed to an increase in the size of the wake, as separation takes place closer to the front of the grain. It might be predicted (as observed) that this increase would not be observed for sharp-edged geometrical bodies or for highly irregular grains, on which points of separation are likely to be fixed by the geometry.

Changes in the shape of the rear of a body can produce major reductions in drag, if the changes prevent or reduce flow separation, because such changes eliminate the area of negative pressures acting on the rear of the body. The shapes necessary to do this are, of course, "streamlined" shapes, such as the cigar-like shapes developed for airships. These forms may have drag coefficients less than 0.1.

Many natural grains approximate elongated ellipsoids, and it might be thought that they would have much lower drag coefficients than those of spheres and equant grains. This would be true if an elongate or flat grain settled with its long axis vertical, but as we will see in the next section, this position is unstable and the grain is generally rotated into a position with the long axis (and maximum projection area) transverse to the flow. In this position, the drag coefficient is somewhat larger than that of a sphere with the same maximum projection area.

EFFECT OF SHAPE

Basically the same kinds of flow regimes as those developed around spheres and cylinders are developed around many other shapes. The details of motion and the exact values of drag coefficients and of the Reynolds numbers for the transition from one regime to another differ somewhat from one shape to another. At high Reynolds numbers, values for C_D vary from less than 0.1 for well streamlined shapes to more than one for flat disks transverse to the flow. Compilations of existing experimental data are given by Hoerner (1965) and Vogel (1981). Most of the experimental results were obtained at high Reynolds numbers by holding the test shape stationary in a wind tunnel or water tunnel and measuring the drag force that results from a measured flow.

For a sphere, one would expect that drag coefficients obtained in this way could be applied directly to calculate the settling velocity, as was shown in Chapter 2. Even in this ideal case, however, a recent investigation by Boillat and Graf (1981) has suggested that the settling velocities calculated from the

commonly accepted Re-C_D diagram in Figure 1.5 might not coincide with those measured directly at high Reynolds numbers. They observed that settling velocities of spheres in still water corresponded to slightly larger drag coefficients than indicated by the generally accepted curve. There are two possible reasons for this discrepancy:

(i) in wind and water tunnels, the fluid moving past the sphere is in turbulent motion, and this may affect the development of the boundary layer and wake, and therefore the drag;

(ii) shedding of vortices, even from the lee of regular symmetric bodies like spheres, is not perfectly regular and symmetric, but shares some of the characteristics of the irregular, turbulent wake that is produced. As a result, spheres do not settle along a perfectly vertical trajectory, even in still water, nor are they subject to a perfectly constant drag force.

For grains of irregular shape, there is no simple relationship between laws of resistance and laws of settling:

(i) the resistance varies with the orientation of the grain relative to the flow;

(ii) a varying sequence of orientations may be assumed by a settling grain, with the pattern of fall determined not only by the Reynolds number but also by the moment of inertia of the grain;

(iii) nonspherical grains do not necessarily settle along a straight, vertical path: they may, for example, adopt a side-to-side oscillating ("falling-leaf") type of motion. The vertical settling velocity is then not the same as the speed at which the grain is moves through the fluid. The grain is not in steady motion and its drag coefficient is continually changing as its orientation changes, so a simple equating of drag and gravity forces is no longer possible.

Therefore, we do not expect that the settling of nonspherical grains can be fully represented by a single diagram of drag coefficient vs. Reynolds number. Nevertheless, we do expect that for grains of a given size, shape, and density settling in a given fluid there is a sphere of the same density whose average vertical settling velocity is the same as that of the grain; the diameter of this sphere has long been defined by sedimentologists as the equivalent diameter or sedimentation diameter. The "true" diameter of a nonspherical grain differs from the equivalent diameter, and is generally defined as the diameter of the sphere with the same volume as the grain (the nominal diameter). The practical problem, therefore, is to find some measurable property of the grain shape ("shape factor") that expresses the relationship between the equivalent diameter and the nominal diameter.

ORIENTATION

Particles settling freely in a fluid generally tend to reorient themselves with their maximum projection area normal to the flow. To understand why this is so, consider Figure 4.4, which shows the flow past a disk-shaped particle oriented oblique to the flow direction.

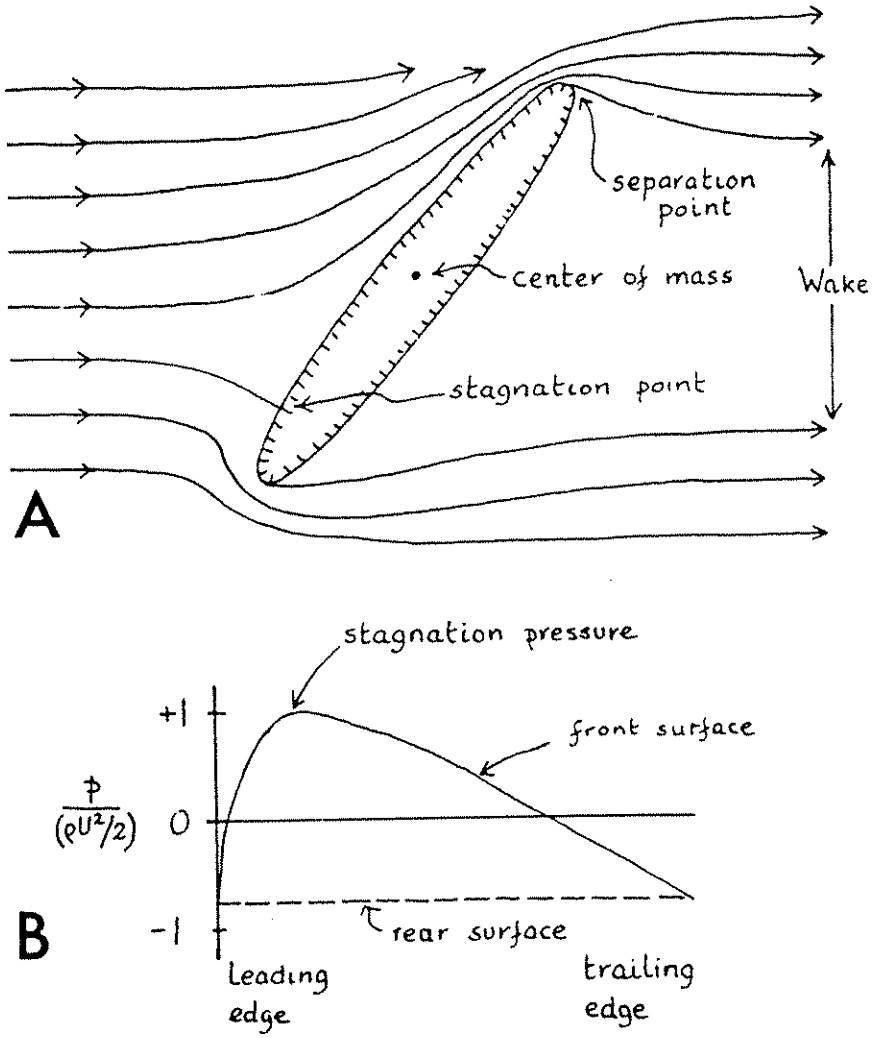

Figure 4.4 Flow and pressure distribution around a disk inclined at a large angle to the flow direction (hypothetical).

Except at very low Reynolds numbers, separation takes place at the edges of the disk, producing an almost uniform negative pressure on the lee side of the disk. There is a stagnation point on the front of the disk, situated close to the "leading edge" (as shown in the diagram): this point is also the point of the highest pressure, the stagnation pressure, equal to $\rho U^2/2$ from the Bernoulli equation. Flow on either side of the stagnation point is convergent almost to the edge of the disk, where it becomes

divergent just upstream of the points of separation. Almost the whole front part of the disk is therefore an area of positive pressure relative to the free stream, and the pressure decreases from a maximum at the stagnation point to negative values near the edge (where the velocity is higher than it is far from the grain and therefore the pressure must be lower). It is evident that although the negative pressure in the wake is almost uniformly distributed over the rear surface, the positive pressures on the front surface of the disk are not at all uniformly distributed, but concentrated near the leading edge. The resultant pressure on the disk therefore acts to the leading side of the center of mass, and tends to swing the disk around to adopt an orientation normal to the flow.

The response of the disk to the force moment produced by form drag depends on the moment of inertia. Four different responses have been noted by Willmarth et al. (1964) and Stringham et al. (1969): (i) Steady-flat fall, with the disk oriented normal to the flow. This takes place at Reynolds numbers less than 100, when the viscous forces are large enough to damp out the oscillations that tend to be produced by the pressure moment. (ii) Regular oscillation about a position normal to the flow, with little deviation of the settling disk from a straight vertical line of fall. (iii) Glide-tumble, in which the disk swings from side to side as it falls, and assumes a high angle to the vertical, or actually tumbles over, at the end of each swing (the "falling-leaf" pattern). (iv) Tumble, a pattern of fall in which the disk continously tumbles end-over-end, and moves along a path that is almost straight but oblique to the vertical. Typical examples of each pattern are shown in Figure 4.5.

The tumble pattern of flow is an example of a phenomenon called autorotation by Riabouchinsky (1935; for references and a review of the literature see Lugt, 1983). A body is said to be autorotating if it exhibits continuous rotation in a parallel flow, even though one or more stable positions exist at which the fluid flow exerts no torque on the resting body.

Willmarth et al. (1964) found that the stability and pattern of fall of disks correlated not only with Reynolds number but also with the following dimensionless form of the moment of inertia:

$$I = \frac{\text{moment of inertia}}{\rho D_L^{\,5}}$$

where D_L is the long (maximum) diameter of the disk. The moment of inertia of a disk is given by

$$\text{moment of inertia} = \frac{\pi}{64}\ \rho_s D_s D_L^4$$

where D_S is the short diameter (thickness) of the disk and ρ_S is the density of the solid. So for disks

$$I = \frac{\pi \rho_s D_s}{64 \rho D_L}$$

Experimental results on the settling of disks are summarized on the C_D-Re-I diagram shown in Figure 4.6. The dimensionless moment of inertia becomes important in determining the drag coefficent and pattern of fall for Reynolds numbers greater than about 2000. Larger values of dimensionless moment of inertia tend to produce the tumbling pattern of fall, and give rise to higher drag coefficients for a given Reynolds number. In almost all cases, however, the drag coefficient for freely falling disks is less than that for a disk fixed in a position normal to the flow, provided that computations of drag coefficient and Reynolds number are based on path velocity. If they are based on the vertical component of velocity only (i.e., on net settling velocity) then the drag coefficients are higher for a freely falling disk than for a fixed disk.

Experimental results for a variety of different regular geometric shapes, calculated from the nominal diameter and the path velocity, are shown in Figure 4.7.

Most natural grains do not have regular geometrical shapes. It is the almost universal practice of sedimentologists to devise measures of the shape by combining measurements of the three principal diameters of the grain: the long (D_L), intermediate (D_I), and short (D_S) diameters. Explicitly or implicitly, therefore, most sedimentologists assume that a grain can be approximated by a regular triaxial ellipsoid.

For such grains, Wadell suggested use of sphericity ψ as an index of shape:

$$\psi = \left(\frac{D_I D_S}{D_L^2}\right)^{1/3}$$

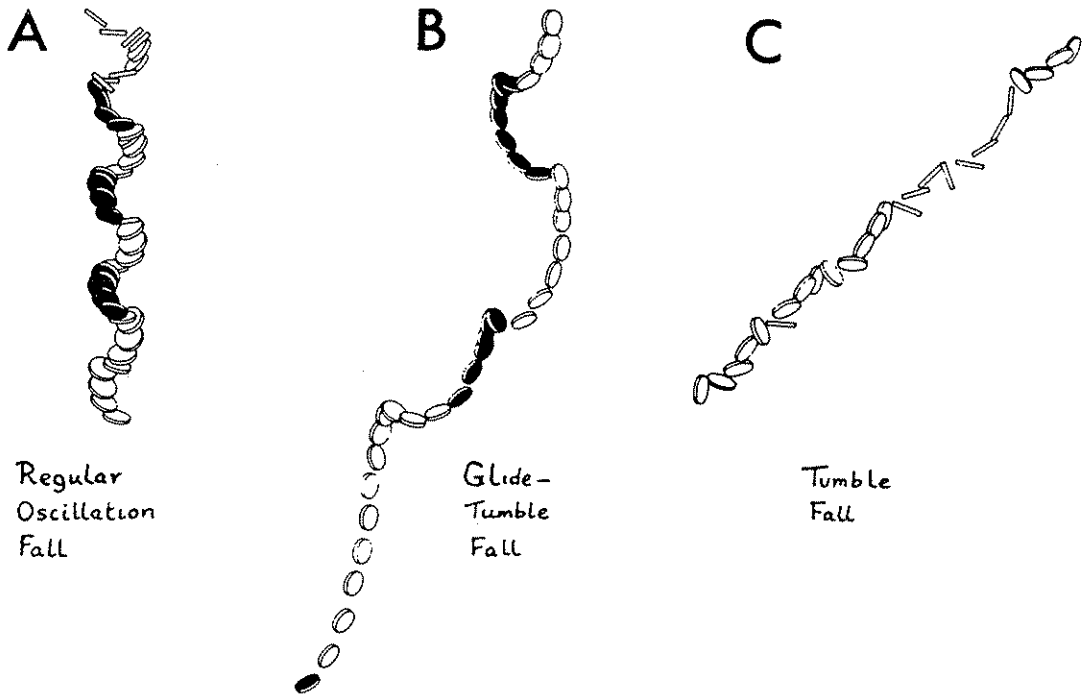

Figure 4.5 Pattern of fall of a disk (from Stringham et al., 1969). A, Regular oscillation pattern; B, glide-tumble pattern; C, tumble pattern. In C, note the large angle between the path of the falling disk and the vertical direction.

Sneed and Folk (1958) and Corey (see American Society of Civil Engineers, 1962) independently concluded that Wadell sphericity was unlikely to be a good index of settling behavior. Sneed and Folk pointed out that, because a grain tends to become oriented with its maximum projection area normal to the flow, the drag force is proportional to the area $D_L D_I$, whereas for a sphere with the same volume as the grain it would be proportional to $(D_L D_I D_S)^{2/3}$. The settling velocities might therefore be expected to be related in the same proportion, and the appropriate shape factor would be the Maximum Projection Sphericity ψ_p:

$$\psi_p = \frac{(D_L D_I D_S)^{2/3}}{D_L D_I}$$

$$= \left(\frac{D_S^2}{D_L D_I}\right)^{1/3}$$

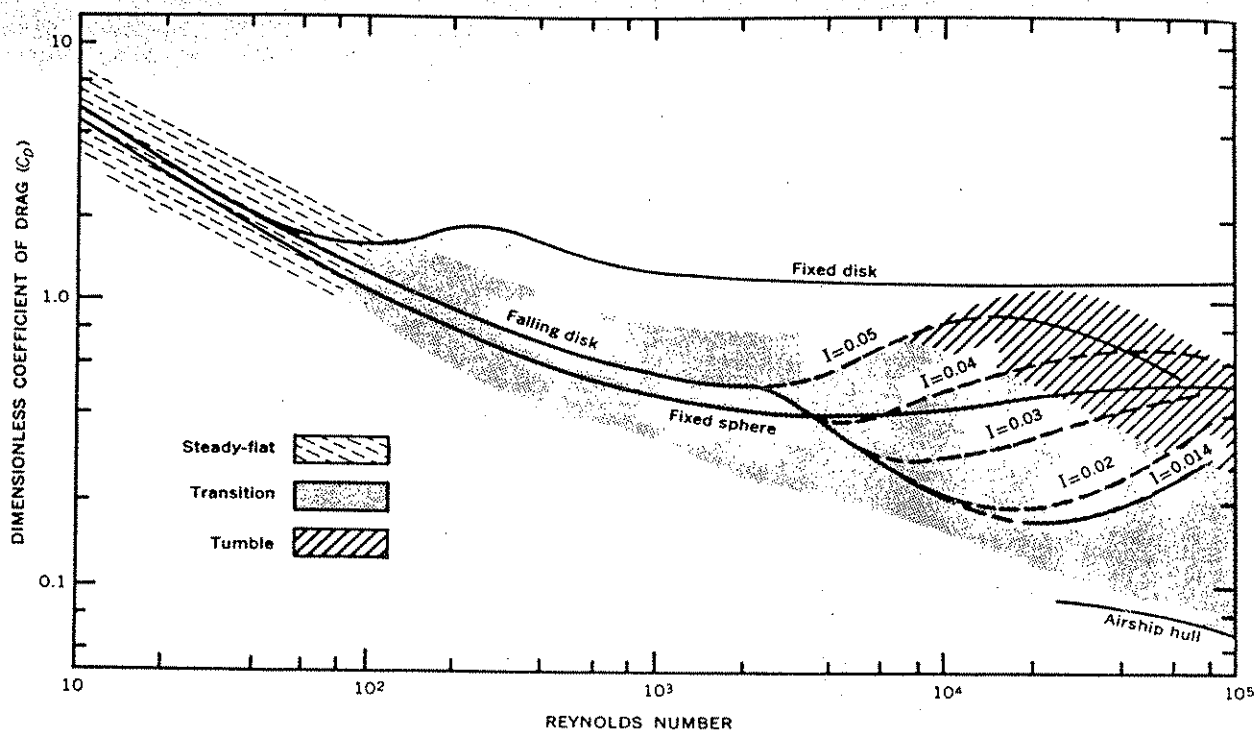

Figure 4.6 Diagram of drag coefficient vs. Reynolds number for fixed and falling disks (fixed sphere shown for comparison). Fall pattern shown by shading. At high Reynolds numbers both the pattern and the drag coefficient depend on moment of inertia (see text). Computations are based on maximum diameter of disk and path velocity. (From Stringham et al., 1969.)

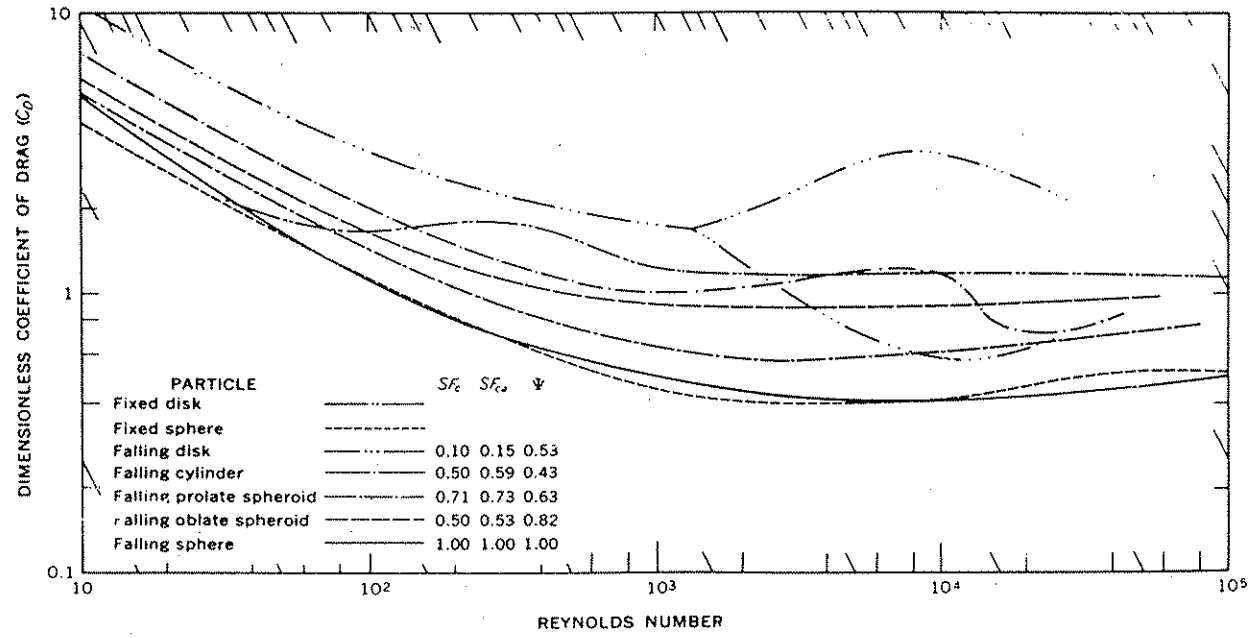

Figure 4.7 Diagram of drag coefficient vs. Reynolds number for various falling shapes (from Stringham et al., 1969). Computations are based on nominal diameter and path velocity. $S.F._C$ is Corey Shape Factor, ψ is Waddell sphericity.

The Corey Shape Factor (S.F.) has a similar definition:

$$S.F. = \frac{D_S}{(D_L D_I)^{1/2}}$$

$$= \psi_p^{3/2}$$

It is clear from the discussion given above that such measures of shape cannot be expected to provide an exact correction for the effect of shape upon the settling velocity of nonspherical particles; but for natural grains, the range of shapes and densities is so large that the best that can be expected is an approximate correction, and for this purpose the Maximum Projection Sphericity or Corey Shape Factor is certainly adequate, and an improvement over the Wadell sphericity (Komar and Reimers, 1978; see also Baba and Komar, 1981a). Figure 4.8 shows a graph of Shape Factor against sieve diameter and standard settling diameter (the equivalent diameter, determined in water at 24°C) determined empirically for natural sands. Most quartz sands have a Shape Factor of about 0.6 to 0.7; the natural variation in average shape is not large, because the shape of quartz grains is determined largely by the ultimate source of the grains.

The fact that natural sands do not vary greatly in shape suggests that it might be useful to have an empirical formula that can be used to calculate the settling velocity of grains of known size and density in a fluid of known density and viscosity. Rubey (1933b) provided such a formula, and this formula was widely used before it became clear that it gives results that are too slow for most natural grains. A corrected form of Rubey's equation has been given by Watson (1969), but Riley and Bryant (1979) found that the corrected equation did not work well with their beach sands. Older experimental data on natural sands were summarized by Graf (1971, p. 35-63), and more recent studies include those of Baba and Komar (1981b) and Hallermeier (1981). For spheres accurate settling data and empirical formulas have been given by Gibbs et al. (1971), Warg (1973), and Boillat and Graf (1981). The use of the Gibbs formula has been discussed by Komar (1981) and Slingerland (1982).

Biogenic grains are especially variable in shape, and may also differ from mineral grains in density, because of structural porosity and the incorporation of organic substrates. Experimental studies of these grains have been published by Maiklem (1968), Futterer (1978), Mehta et al. (1980), and Fok-Pun and Komar (1983).

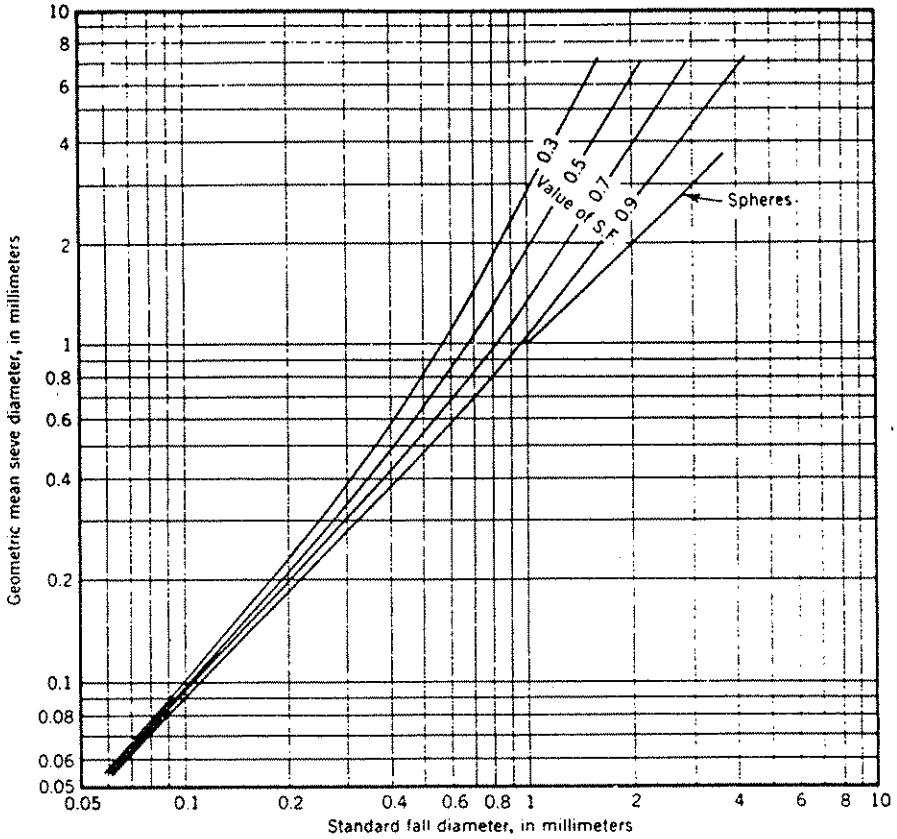

Figure 4.8 Relationship among shape factor, sieve diameter, and standard settling diameter. (From American Society of Civil Engineers, 1962.)

Very fine grains may not settle as predicted by Stokes' law for several reasons: they may be flocculated into low-density aggregates (Kranck, 1975), they may be bound together by or coated with organic matter (Johnson, 1974; Smith and Syvitski, 1982), or they may be electrically charged and interact with ions or polar water molecules (Chase, 1979). The settling velocity of natural aggregates has been studied by Hawley (1982).

DRAG FORCES ON GRAINS RESTING ON A BED

At this point it may be useful to digress slightly to consider another case of some practical importance: the drag forces exerted by a flow on a grain that is resting on a flat bed (or a bed composed of similar grains) rather than being freely suspended in a fluid. We will return to this topic again in Chapter 6, when we consider movement of grains on a bed.

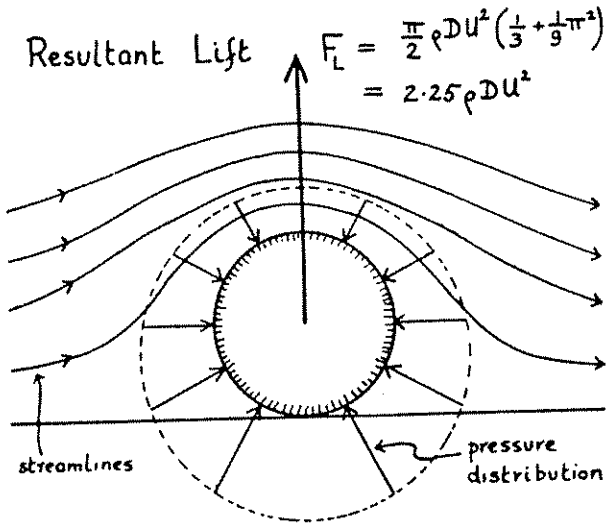

Figure 4.9 Flow pattern and pressure distribution for inviscid flow over a cylinder normal to the flow direction and lying on a flat bed.

Consider first the case of a cylinder resting on a plane surface (Figure 4.9). For inviscid fluids the flow would be symmetrical about the cylinder and the velocity would increase as the streamlines crowd together where the flow passes over the top of the cylinder. For this we can predict the pressure distribution shown, which indicates that although the flow is theoretically not subject to any drag force in this ideal case, it is subject to a lift force, directed vertically away from the bed. This lift can be calculated, and corresponds to $C_L = 4.5$.

A more realistic case, corresponding to relatively large Reynolds numbers, is shown in Figure 4.10. In this case there is flow separation behind the cylinder, so there is a drag as well as a lift component. The exact pressure distribution is not known, but its general character can be inferred from pressure distributions measured on freely suspended cylinders. The maximum positive pressure on the front of the cylinder is slightly less than the stagnation pressure, and the (negative) pressure in the wake also has a magnitude somewhat less than the stagnation pressure. There is likely to be a region of high negative pressure on the upper front part of the cylinder (as shown in Figure 4.10) because of the high velocities produced by flow convergence in this region. It is clear that the resultant pressure distribution must include large components of both drag (parallel to the flow) and lift (transverse to the flow).

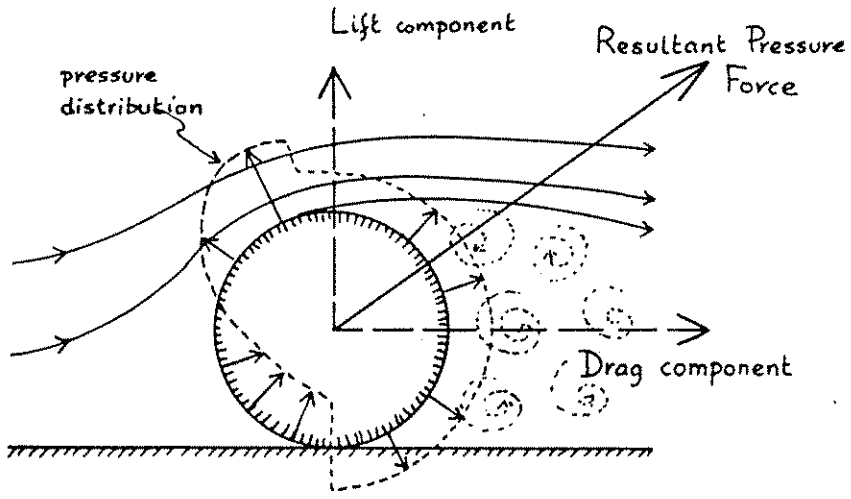

Figure 4.10 Flow pattern and pressure distribution (hypothetical) for flow of a viscous fluid past a cylinder normal to the flow direction and lying on a flat bed (for moderately large Reynolds numbers).

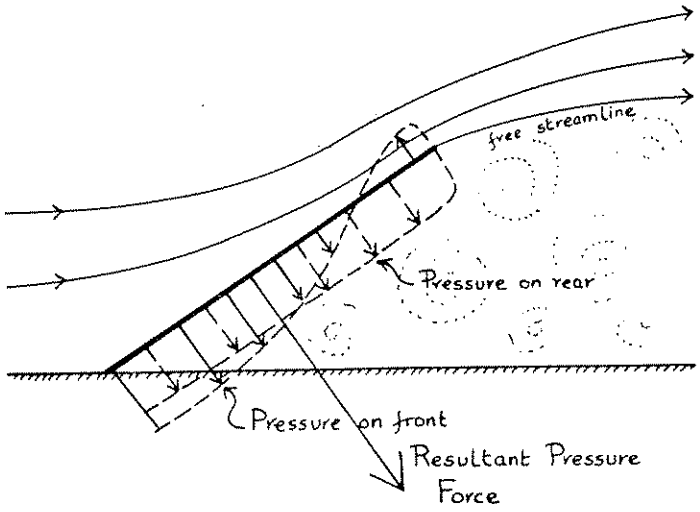

Figure 4.11 Flow pattern and pressure distribution (hypothetical) for flow of a viscous fluid past an imbricated flat plate (for moderately large Reynolds numbers).

It is also instructive to consider the case of a thin plate inclined at an angle α to the downstream direction, and with the leading edge in contact with the bed. (Such a plate is an idealization of an imbricated blade-shaped grain lying on the bed.) The flow pattern and hypothetical pressure distribution are shown in Figure 4.11. The resultant pressure force in this case

is directed downstream and towards the bed. In general, therefore, the flow tends to press imbricated flat grains down onto the bed rather than lifting them off as it does most other grains. Only if grain shape and flow conditions are such that large negative pressures are developed on the upper trailing surface might imbricated flat grains be subject to a net lift force; a hypothetical example is shown in Figure 4.12. Perhaps such conditions might be achieved for some grain shapes when a turbulent boundary layer is developed at high Reynolds numbers. Under normal circumstances, however, a tightly packed bed of well imbricated flat grains should be very difficult to dislodge.

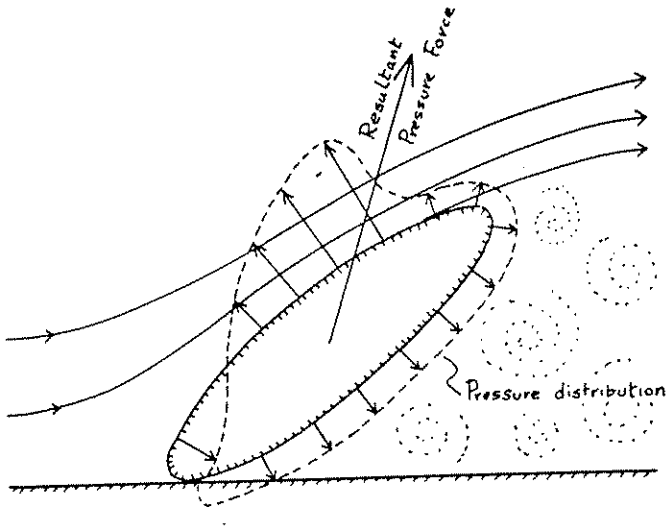

Figure 4.12 Flow pattern and pressure distribution (hypothetical) for flow of a viscous fluid past an imbricated disk-shaped pebble (moderately large Reynolds numbers).

For small grains it is to be expected that imbrication is less effective in stabilizing the grain, because the viscous component of drag is as important as form drag, and for flat imbricated grains the viscous forces have an upward as well as a downstream component.

EFFECT OF CONCENTRATION

Up to this point we have been considering the settling of only a single grain, or we have at least assumed that if there is more than one grain settling in a fluid, the grains are sufficiently far from each other that they do not interact in any way. In nature this assumption is often not valid: the concentration of grains often exceeds one percent by volume, and may reach very high values, so that some interaction between grains is inevitable.

Two opposite bulk effects are possible. (i) Group settling, due to local concentrations of grains. A high concentration of grains locally raises the bulk density of the suspension, and may cause it to move through the surrounding fluid as a "density current." (ii) Hindered settling, due to interactions between the grains and an overall reduction in the cross section available for the upward movement of the fluid that is displaced by the downward movement of grains.

Group settling is important in settling tubes of the type in which the sample is introduced at the top of the tube; the effect can be minimized only by making use of a very small sample and a large tube diameter. Also, Jopling (1964) has reported group settling of grains in the "heavy fluid layer" formed by the high concentration of grains close to the bed on the stoss side of a dune, as this layer moves over the brink of the dune (Figure 4.13).

Hindered settling is generally the more important of the two effects. A pioneer study was made of the settling of metallurgical slurries by Coe and Clevenger (1916). They observed two types of settling phenomena in concentrated fine-grained suspensions (Figure 4.14). In the first type, two interfaces develop: one with clear liquid above and the other with the settled sediment below. The zone between is mostly of constant concentration. The upper interface moves down at a constant rate, and the sedimentation rate is also constant. After the two interfaces meet (i.e., after all the sediment has settled) there is some slight further lowering of the sediment-water interface due to consolidation of the bed. The second and less common type of hindered settling is found in fine suspensions, particularly where there is a wide range in particle sizes (greater than six to one). In this type the concentration and size composition of the suspension change progressively during the settling; there may be a zone of constant concentration above the zone of variable concentration (see further discussion by Wallis, 1969).

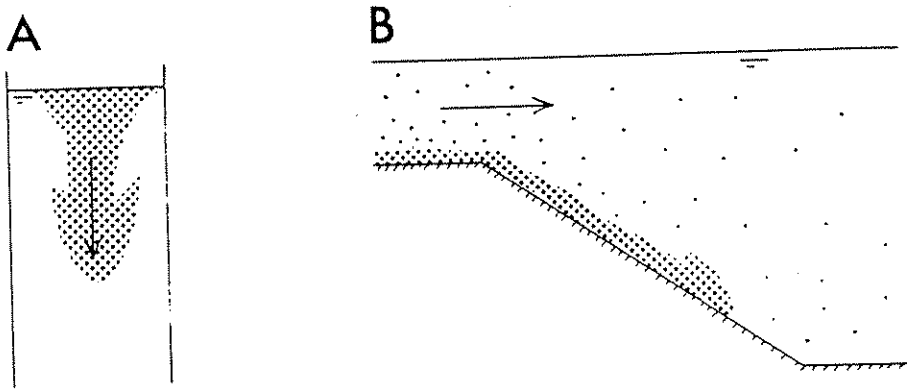

Figure 4.13 Two examples of group settling: A, at the top of a settling tube; B, on the lee slope of a dune (megaripple).

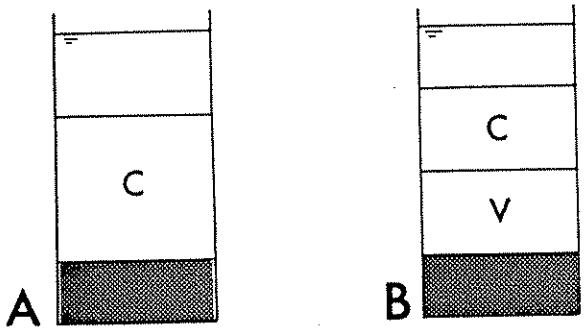

Figure 4.14 Two types of hindered settling: A, settling from a dispersion with constant concentration; B, settling from a dispersion showing zones of constant (C) and variable (V) concentration.

In the first type of hindered settling, the constant concentration of the grain dispersion indicates that a segregation of grains by their individual sizes or settling velocities is no longer possible at the high concentrations involved. The bed deposited therefore shows no size grading. In the second type, some segregation of grains is still taking place within the zone of variable concentration. It is expected, therefore, that the bed should show some size grading, although the degree of size segregation, and therefore grading, should depend on the absolute concentration. In some cases, where a zone of uniform concentration is found above a zone of variable concentration, the size grading is restricted to the base of the bed.

The main reasons for the modification of settling behavior in hindered settling have been well summarized by Coulson and Richardson (1955):

(i) Large grains are settling relative to a suspension of fine grains, and this suspension has a higher viscosity and density than the pure fluid, thus tending to reduce the settling velocity.

(ii) Fluid displaced by settling grains flows upward between the grains, so that the settling velocity is less than the true relative velocity between the grain and the fluid. If there is a large range in grain sizes, finer grains may actually be swept upwards by the fluid rising up through the spaces between the larger settling grains.

(iii) Velocity gradients close to the grains are increased as a result of the proximity of other grains.

(iv) For cohesive grains, proximity and resulting random collisions between grains may trigger flocculation.

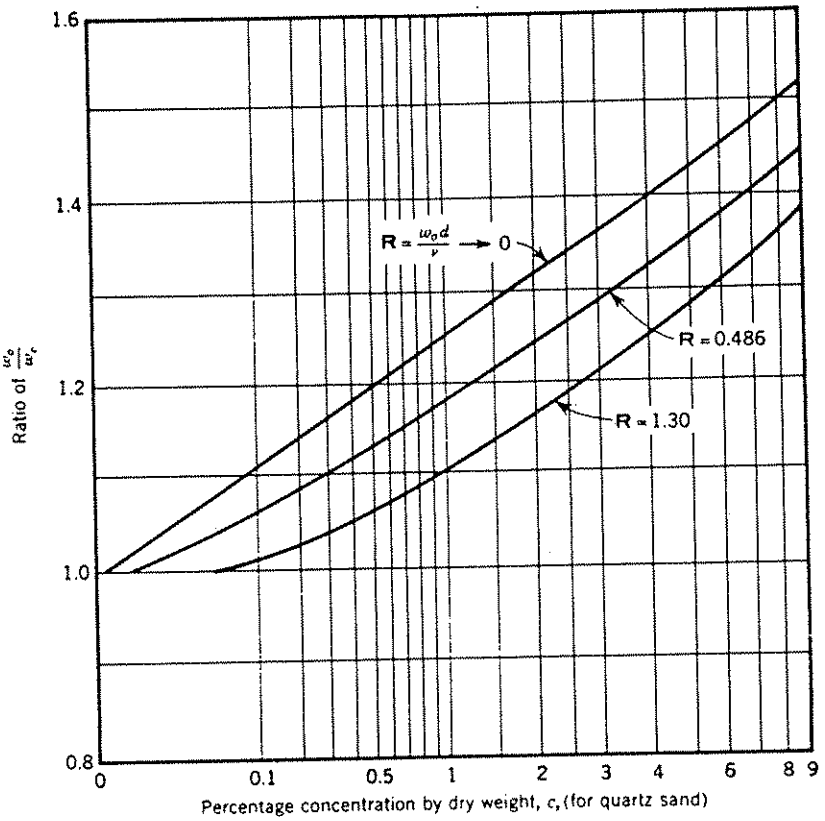

Figure 4.15 Effect of concentration on settling at low Reynolds numbers (after McNown and Lin, 1952). w_o is settling velocity at zero concentration, w_c is settling velocity at a concentration c, and d is the diameter of the grains.

For low Reynolds numbers the problem of hindered settling has been studied theoretically as well as experimentally. McNown and Lin (1952) used a modification of the Stokes creeping-flow theory to study the effect of low concentrations, and calculated the result numerically for selected Reynolds numbers (Figure 4.15). The effect is large at low Reynolds (as also is the effect of the side wall of the settling tube) because for slow viscous flow the presence of a moving grain changes the pattern of flow relatively far away from the grain, and the pattern of flow is what determines the magnitude of the viscous drag. The effect of a sidewall, for example, is detectible at low Reynolds numbers for ratios of tube diameter to grain diameter as large as 100. The effect of a sidewall or of other particles is much less at large Reynolds numbers, for which the drag is determined mainly by the pressure distribution, which changes only slightly in response to major changes in the pattern of flow round the grain.

Experimental results for Reynolds numbers greater than one have been determined by Richardson and Zaki (1954) and Thorpe (1965). Thorpe studied the settling of uniform sand in water for concentrations up to about 10 percent, and Richardson and Zaki studied even higher concentrations. Richardson and Zaki (1954) found that the ratio between the observed settling velocity and the settling velocity w_o of a single grain (i.e., of grains at vanishingly small concentration) was

$$w/w_o = (1 - C)^n$$

where C is the fractional volume concentration and n is a coefficient that varies at low Reynolds numbers but reaches a constant (minimum) value of 2.4 for Reynolds numbers greater than 500.

Thorpe (1965) found that for concentrations between 0.5 and 10 percent the settling velocity of sand in water is directly proportional to the diameter of the grains, a result not predicted by settling theory for single grains. He concluded that at these concentrations viscous drag on the grains is more important than inertial effects, even though the grains are individually well beyond the range of validity of Stokes' Law.

LIQUEFACTION AND FLUIDIZATION

The two similar terms liquefaction and fluidization have been used by different groups of engineers (in soil mechanics and chemical engineering, respectively) to refer to phenomena related to the settling of grains at very large concentrations.

Liquefaction refers to the sudden loss of strength of a loosely packed sand, when the grains temporarily lose contact with each other and become suspended in the pore fluid. Contact between grains, and the strength of the mass of sand, is restored when the grains settle down again through the interstitial fluid, a part of which escapes vertically upward to the surface.

Fluidization is a process developed by chemical engineers to promote rapid chemical reaction in a column filled with loose grains. (The high surface area of the grains tends to catalyze certain reactions.) Fluid is introduced at the base of the column until the mass of grains is expanded so that the individual grains are no longer in contact, and their weight is supported by the rising fluid. At this point there is a sudden drop in the pressure required to force the fluid up through the column, and the grains are said to be fluidized (Figure 4.16). A whole range of conditions of fluidization exists, from the minimum flow required for fluidization through progressive expansion of the bed (i.e., decrease in concentration of the suspension) to the point where a single particle is freely suspended in the rising fluid.

Under certain conditions grains are uniformly suspended ("particulate fluidization"), but under other conditions (more common in fluidization by gases than in fluidization by liquids) small or large bubbles ("slugs") or channels of almost grain-free fluid rise up through the suspension.

Etymologically, the terms liquefaction and fluidization have an almost identical meaning, which derives from the observation that when the grains in a concentrated mass are no longer in contact the mass loses its strength and behaves like a viscous fluid rather than like a solid material. Because of this, the two terms were used almost synonymously by Middleton (1969, 1970b) and by Middleton and Hampton (1973, 1976). Lowe (1976a) has recently argued that the term "fluidized bed" should be restricted to cases where there is an upward movement of fluid through grains which themselves are not moving downward. If the upward movement of fluid is produced by the downward movement of grains, the bed should be described as liquefied rather than fluidized.

The question arises whether or not fluidization, in the strict sense, ever takes place in nature. One obvious possibility is in volcanic vents (Reynolds, 1954). In ash flows, where the hot particles are still releasing volcanic gases, there is also a possibility of an upward flow of fluid which is not simply due to the settling of the grains (McTaggart, 1960). In flows of concentrated suspensions of sand, however, there can generally be no upward flow of fluid except that produced by settling out of grains. A possible exception might be the case of movement over a basal fluid layer, a mechanism invoked by Shreve (1968) to explain the high mobility of some rock slides in air.

Fluid escaping from a liquefied sand does not generally do so uniformly; generally it moves preferentially up nearly vertical planes or tubes, thereby producing the range of structures described as sheet structures (Laird, 1970) or pillar structures (Lowe, 1975). As pointed out by Lowe (1975), velocities of fluid escaping upward within these confined regions may locally exceed those needed to fluidize the grains. Evidence from sedimentary structures indicates that this happened in some pillars but not in others.

Flows that originate by liquefaction may become turbulent if they reach sufficiently large Reynolds numbers. The effective viscosity of highly concentrated grain dispersions is as much as several thousand times that of water, so relatively deep flows and high velocities are needed to achieve turbulence, but these conditions are likely to be found in natural environments like the heads of submarine canyons. Turbulence and trapping of water under the head of the flow (see Chapter 8) may mix water into the suspension, so there may be all transitions from liquefied flows of very high concentration to flows of much lower concentration in which the grains are supported mainly by fluid turbulence.

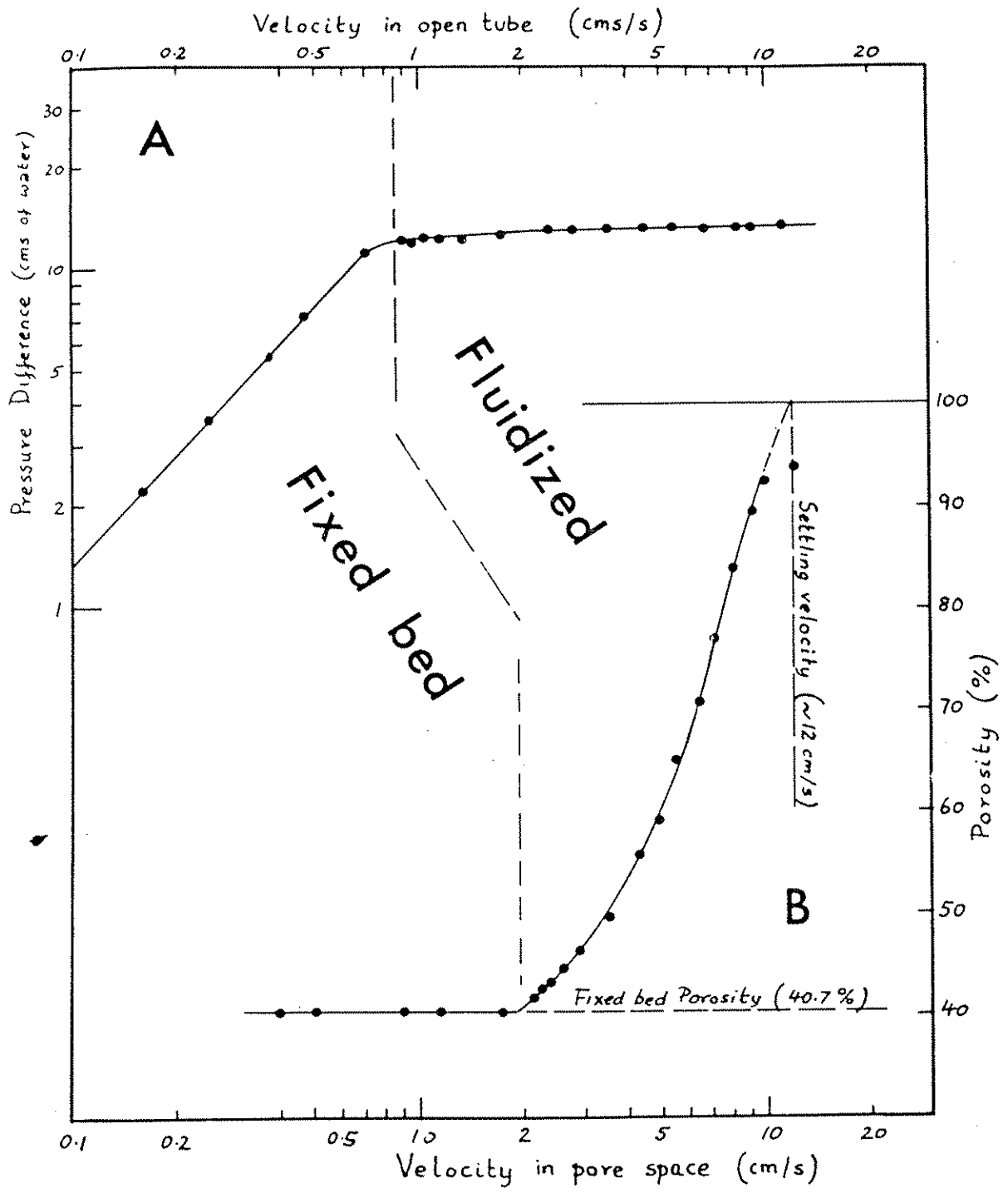

Figure 4.16 Result of an experiment on the fluidization of sand by water (data from Wilhelm and Kwauk, Table 10). The experiment was performed with 1 mm sand in a tube 7.5 cm wide. The fixed bed was initially 15 cm high. (A) the drop in pressure across the bed as the vertical velocity of water in the tube is increased; (B) the same data but plotted as porosity of the bed vs. mean fluid velocity in the pore space.

Sedimentation from high-concentration liquefied flows should be somewhat similar to static hindered settling, as discussed in the previous section. At sufficiently high concentrations and with only a small range in grain sizes there will be little size segregation, so little grading will be observed in the deposit. But with lower concentrations and a larger range of grain sizes a well-developed grading is possible.

Some unusual patterns of grain segregation might possibly result from the settling of concentrated dispersions of particles of different densities, sizes, and shapes. Richardson and Meikle (1961) studied the settling of concentrated dispersions composed of two different types of grains having the same settling velocity. The types were glass ballotini (beads), with a density of 2.92 g/cm^3 and a diameter of 0.07 mm, and polystyrene, with a density of 1.04 g/cm^3 and a diameter of 0.39 mm (both types of grains had a settling velocity of 0.324 cm/s). Settling from dispersions of very low concentration produced a sediment consisting of a mixture of both types of grains, but sedimentation from dispersions at a concentration of more than 10 percent produced a complete separation of the grain types, with a bed of pure ballotini below a bed of pure polystyrene. Segregation of the two types of grains took place within the concentrated dispersion during settling: at an intermediate stage of settling (Figure 4.17) the dispersion consisted of a lower zone of glass ballotini, an intermediate mixed zone, and an upper zone of polystyrene. The result was explained by Richardson and Meikle in terms of the difference in density betwen the grains and the dispersion--for very light grains, like polystyrene, the dispersion may actually have a bulk density larger than that of the light grains, so that they tend to float upwards in the dispersion rather than settling out. It is possible too (though not considered by Richardson and Meikle) that the large size difference between the grains might be important: the glass grains were small enough to pass through the interstitial spaces between even a closely packed layer of polystyrene grains.

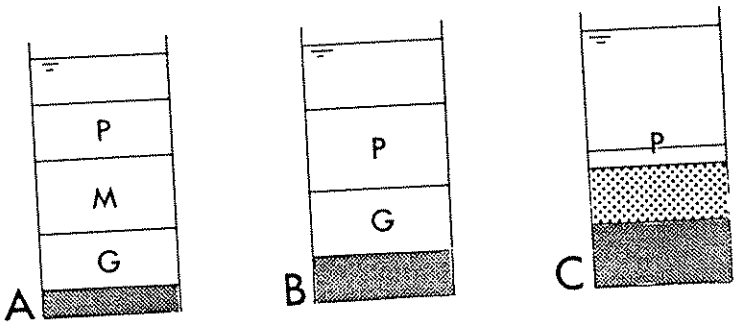

Figure 4.17 Results of an experiment by Richardson and Meikle (1961) on the settling of a concentrated disperion of mixed glass and polystyrene grains. P, dispersion of polystyrene only; M, mixed dispersion; G, dispersion of glass only.

Obviously these results cannot be transferred directly to the interpretation of natural sedimenting systems, where the range of sizes and densities is more complex than in the experiments, and where turbulence may inhibit complete grain segregation, but the experiments do indicate the sort of complexities that are possible. It is not unrealistic to suppose that grains in natural systems (intraclasts of little-consolidated fine sediment, for example) may have densities less than those of highly concentrated sand-water mixtures (as pointed out by Kuenen, 1950). The presence of large "floating" shale clasts within a sandstone bed has sometimes been cited as evidence for a particular mechanism of sand transport (e.g., Stauffer, 1967)--but perhaps it is simply evidence for the high density of the dispersion, whatever the mechanism of flow.

CHAPTER 5. TURBULENT FLOW

INTRODUCTION

Almost all flows that transport sediment are turbulent. We've mentioned turbulence at several points already and devoted an introductory section in Chapter 3 to it; this chapter deals in more detail with some aspects of turbulent flow most relevant to sediment transport. We'll concentrate on two related problems: the nature of the resistance force exerted on the turbulent flow by the boundary, and the profile of time-average velocity along a line normal to the boundary. With turbulent flow it's not possible to solve the equations of motion to obtain exact solutions for such things as boundary resistance or velocity profiles. The reason for this is basically similar to, although more general than, the reason why in Chapter 1 we weren't able to obtain a solution for turbulent flow down a plane: we know what equations we have to solve but we can't solve them because of the uncertainty that turbulence introduces into the application of these equations. The great number of equations to be found in textbooks and papers on turbulent flow are semi-empirical: the general form of the equation may be suggested by physical reasoning, but the numerical constants in the equation, and therefore its specific form, must be found from experiments. And in many cases not even the general form of the equation is known, and the curve must be obtained entirely by experiment.

TURBULENT SHEAR STRESS

One of the most significant effects of turbulence is the transport of such things as heat, solute, or suspended matter--things that can be viewed as carried passively by the fluid--across planes parallel to the mean flow by the random motions of fluid masses back and forth across these planes. The mean velocity across such planes is by definition zero, so the net mass of fluid transferred back and forth in this way must balance to zero on the average. But if the property passively associated with the fluid is on the average unevenly distributed--if its average value varies in a direction normal to the mean motion--then the balanced turbulent transfer of fluid across the planes causes a transport or "flow" of this property in the direction of decreasing average value. To see this, think about the result of an exchange of two fluid parcels or eddies with equal mass across a plane of mean shear parallel to the boundary in a turbulent boundary layer (Figure 5.1). The eddy traveling from the side of the plane with higher average value of some property P tends to arrive on the other side with a higher value of P than its new surroundings, and conversely the eddy traveling from the side with lower average value will tend to arrive with a lower value than its surroundings. The exchange thus tends to even out the distribution of P by means of a net transport of P in the direction of decreasing average value. This process is an example of <u>turbulent diffusion</u>.

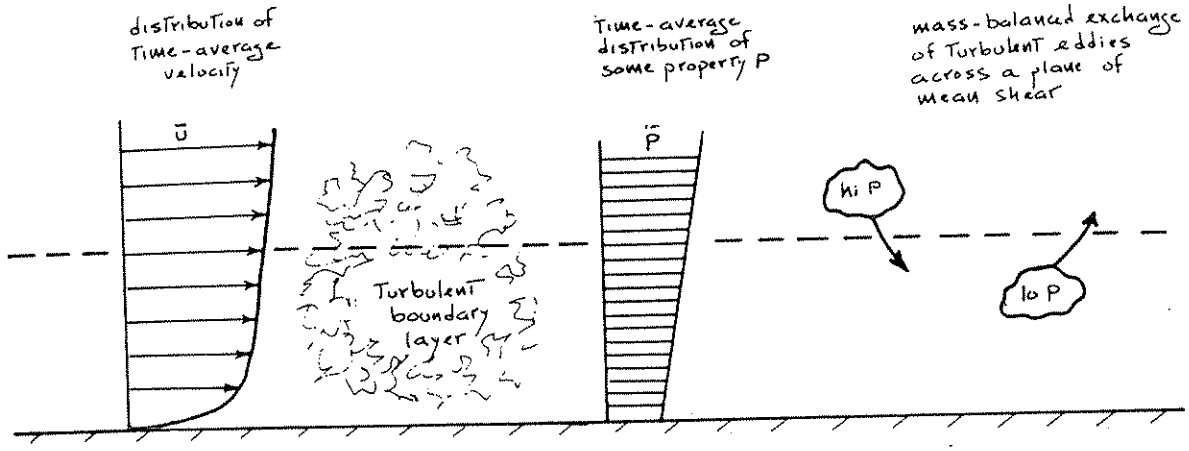

Figure 5.1 Physical basis for turbulent diffusion.

An irregular or nonuniform distribution of the property P at the scale of individual eddies is to be expected by the very nature of the diffusion process. An average gradient of P is maintained in some way unrelated to diffusion that need not concern us here, but diffusion is always randomly disrupting this gradient. So not every eddy that crosses the plane of mean shear shown in Figure 5.1 from the side with higher average P will arrive on the other side with a value of P higher than the new surroundings, and conversely not every eddy crossing in the other direction will arrive with a lower value of P. But the important thing is that there's a tendency for this to happen because there's a statistical correlation between values of P and position normal to the plane. An example, the correlation between suspended-sediment concentration and distance above the bottom in a horizontal boundary-layer flow, is shown schematically in Figure 5.2. Here, sediment is diffused upward in the flow by turbulent motions while the average upward gradient is maintained by settling. The nature of the resulting vertical distribution will be explored more fully in the next chapter.

We can use the idea of diffusion of fluid momentum to account for the velocity distribution in flow down an inclined plane, discussed in Chapter 1. In laminar flow there are no eddies to be exchanged across shear planes parallel to the bottom, but the molecules themselves hurtle or weave randomly back and forth across these planes in loose analogy with the picture outlined above for the random motions of turbulent eddies. Since on the average the molecules have a greater downchannel velocity in the region above a given shear plane than below it, molecular exchange across the plane tends to even out the distribution of fluid momentum and therefore also of fluid velocity. Fluid momentum is continuously

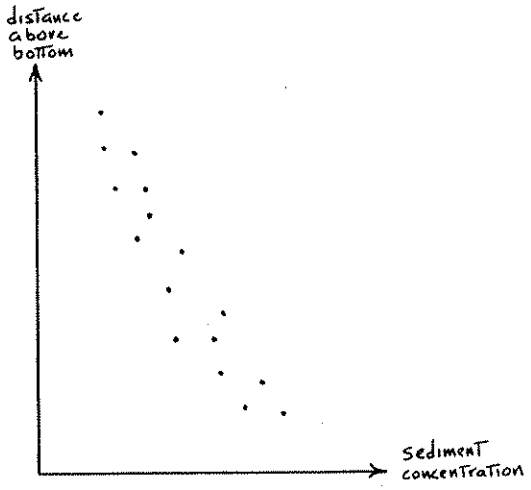

Figure 5.2 Correlation between suspended-sediment concentration and distance above bottom in a sediment-transporting turbulent boundary layer (schematic).

created by the downslope forces of gravity, then transported toward the bottom boundary by molecular diffusion, and in the process is consumed by the resistance force at the bottom boundary. This is just a different way of looking at the nature of the velocity distribution derived in Chapter 1. The tendency for molecular motions to even out the velocity distribution in a sheared fluid is in part the physical cause of the resistance of a fluid to shearing. In liquids the effect of transient molecular attractions in resisting shear is more important, but in gases the diffusive effect is the dominant one. The viscosity of a fluid is simply a measure of the effectiveness of molecular motions and/or molecular attractions in smoothing out an uneven velocity distribution or in maintaining the velocity distribution against the tendency for the fluid to accelerate downslope and intensify the shearing. The continuum hypothesis allows us to disregard the details of molecular forces and diffusion and regard the resulting shear stress as a point quantity.

In turbulent flow, on the other hand, there is an additional diffusional mechanism for transport of fluid momentum toward the boundary: exchange of macroscopic fluid eddies across the planes of mean shear parallel to the bottom tends to even out the velocity distribution by diffusion of momentum toward the bottom. By Newton's second law this rate of transport of momentum by the turbulent motions is equivalent to a shear stress across the plane. This is called the turbulent shear stress (or, usually, the Reynolds stress). It has exactly the same physical effect as an actual frictional force exerted directly between the two layers of fluid on either side of the plane: the faster-moving fluid above the plane exerts an accelerating force on the slower-moving fluid below the plane, and conversely the fluid below exerts an equal

and opposite retarding force on the fluid above. It is true that the "range of operation" of this force is smeared out indefinitely for some distance on either side of the plane, but the result is the same as that of a force exerted directly across the plane.

The total shear stress across a shear plane in the flow is the sum of the turbulent shear stress, caused by macroscopic diffusion of fluid momentum, and the viscous shear stress, caused in part by molecular diffusion of fluid momentum and in part by attractive forces between molecules at the shear plane. Owing to its macroscopic nature the turbulent shear stress can be associated with a given point on a shear plane only in a formal way; the viscous shear stress, although it has real physical meaning from point to point, must be regarded as an average over the area of the shear plane, because in turbulent flow both the magnitude and the orientation of shearing vary from point to point.

In Chapter 1 we derived an expression (Equation 1.20) for the shear stress across shear planes in laminar channel flow. In turbulent channel flow the shear stress in Equation (1.20) is the sum of the turbulent shear stress and the viscous shear stress. You may protest that the result in Equation (1.20) was obtained for laminar flow only. But in deriving the equation we didn't assume anything at all about the internal nature of the flow, only that the flow is steady and uniform on the average. (This is in contrast to the result for velocity distribution, Equation (1.23), which involves the assumption that the shear stress across a shear plane is given by Equation (1.2)--an assumption inadmissible for turbulent flow because of the importance of the additional turbulent shear stress.) The linear distribution of shear stress from zero at the surface to a maximum at the bottom should therefore hold just as well for turbulent flow as for laminar flow, provided only that the flow is steady and uniform on the average.

Except very near the solid boundary, where the vertical component of the turbulent velocity must go to zero, the turbulent shear stress is far greater than the viscous shear stress. This is because turbulent exchange of fluid masses acts on a much larger scale than the molecular motions involved in the viscous shear stress, and therefore transports momentum much more efficiently. Figure 5.3 is a plot of the distribution of turbulent shear stress and viscous shear stress in steady uniform flow down a plane. The total shear stress is given by the straight line, and the turbulent shear stress is given by the curve that is almost coincident with the straight line all the way from the surface to fairly near the bottom but then breaks sharply away to become zero right at the bottom. The difference between the straight line for total shear stress and the curve for turbulent shear stress represents the viscous shear stress; this is important only very near the boundary.

Because the turbulent shear stress is so much larger than the viscous shear stress except near the boundary, differences in time-average velocity from layer to layer in turbulent flow are

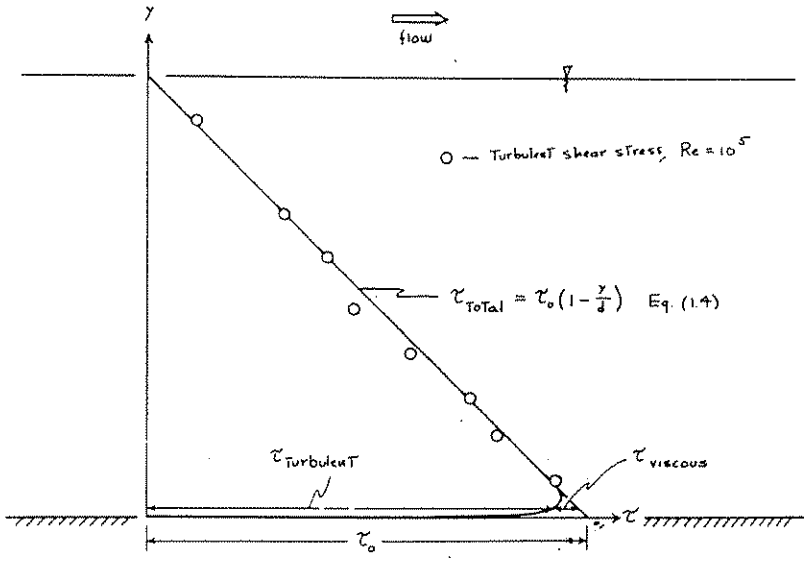

Figure 5.3 Distributions of total shear stress, turbulent shear stress, and viscous shear stress in steady uniform flow down a plane.

much more effectively ironed out over most of the flow depth than in laminar flow. This accounts for the much gentler velocity gradient $d\bar{u}/dy$ in turbulent flow than in laminar flow; go back and look at Figure 1.16. But as a consequence of this gentle velocity gradient over most of the flow depth, near the bottom boundary (where viscous effects rather than turbulent effects control the flow) the velocity gradient is much steeper than in laminar flow, because the shearing necessitated by the no-slip condition is compressed into a thin layer immediately adjacent to the boundary.

STRUCTURE OF TURBULENT BOUNDARY LAYERS

Introduction

We've said quite a lot about what turbulence looks like in a general way. We now need to be more specific about the structure of turbulence in turbulent boundary layers, because most flows that transport sediment are turbulent boundary-layer flows, and the forces exerted on sediment grains, both those resting on the bed and those in transport, are governed by the characteristics of the turbulence. We'll also have to deal with the opposite effect: if the concentration of sediment in transport is great enough, even if only in a thin layer near the bed, the turbulence characteristics themselves must be substantially different from those in clear flows.

Many of the important things about turbulence in boundary layers have been known for a long time. Workable techniques for reliable measurement of instantaneous velocities in air were worked out many years ago, in the 1940s and 1950s. Comparable laboratory techniques for water flows became available only in the 1960s, and reliable field measurements in water flows have become possible even more recently. It is still very difficult to make detailed observations of the scales, shapes, motions, and interactions of turbulent eddies, especially the relatively small eddies near the boundary. Only since the late 1960s has observational knowledge of the dynamics of near-boundary turbulent structure advanced from the stage of point measurements of velocities and their statistical treatment, to observations of the eddy structure of the turbulent flow as a whole by means of various flow-visualization techniques. Studies on the structure and organization of turbulent fluid motions in boundary layers is now a large and actively growing branch of fluid dynamics, and has resulted in much deeper understanding of the dynamics of turbulent flows.

Since knowledge of the important features of turbulent motions is so important to the study of sediment transport, we'll present some of the most important facts and observations here. We'll continue to use steady uniform flow down a plane as a reference case, but the differences between this kind of boundary-layer flow and that in a straight open channel with irregular cross-section shape, or flow in a straight closed conduit like a circular pipe, or a boundary layer developing on a surface the flow has just encountered, lie only in minor details and not in important effects.

Vertical Organization

First of all, you should expect the nature of turbulence to vary strongly from surface to bottom in the flow, because the boundary is the place where the vertical turbulent fluctuations must go to zero and where by the no-slip condition the fluid velocity itself must go to zero. You've already seen that the relative contributions of turbulent shear stress and viscous shear stress change drastically in the vicinity of the boundary.

If the bottom boundary is physically smooth, or is rough but the height of the roughness elements is less than a certain value to be discussed presently, three qualitatively different but intergrading zones of flow can be recognized (Figure 5.4): a thin viscous sublayer next to the boundary, a turbulence-dominated layer occupying most of the flow depth, and a buffer layer between. If the boundary is too rough, the viscous sublayer is missing. Here we'll only give a qualitative description of the flow in these layers; in later sections we'll show their implications for flow resistance and velocity profiles.

The viscous sublayer is a thin layer of flow next to the boundary in which viscous shear stress predominates over turbulent

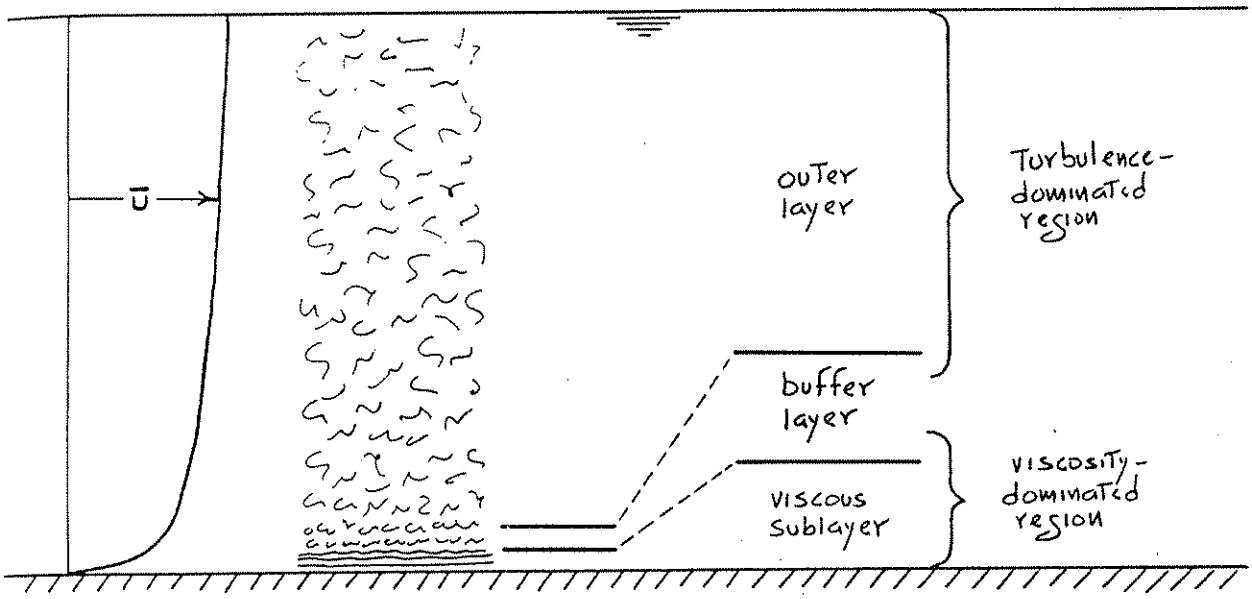

Figure 5.4 Zones of turbulence structure in steady uniform turbulent flow down a smooth plane. Eddy structure (schematic) is as seen by an observer moving with flow.

shear stress. Shear in the viscous sublayer, as characterized by the rate of change of average fluid velocity away from the wall, is very high, because fast-moving fluid is mixed right down to the top of the viscous sublayer by turbulent diffusion.

The thickness of the viscous sublayer depends on the characteristics of the particular flow and fluid; it's typically in the range of a fraction of a millimeter to many millimeters. The flow is not strictly laminar in the viscous sublayer because it experiences random fluctuations in velocity. But since fluctuations in velocity normal to the boundary must become zero at the boundary itself molecular transport of fluid momentum is dominant over turbulent transport of momentum near the boundary. Fluctuations in velocity very close to the boundary must therefore be largely parallel to the boundary. Fluctuations in shear stress at and near the boundary caused by these fluctuations in velocity can be substantial and must have an important bearing on sediment transport. Normal-to-boundary velocity fluctuations in the viscous sublayer can, however, be important in diffusion of sediment toward or away from the boundary even though they are unimportant in diffusion of fluid momentum. The turbulent fluctuations in velocity in the viscous sublayer are the result of advection of eddies from regions farther way from the wall; these eddies are damped out by viscous shear stresses in the sublayer.

When the boundary is physically smooth the thickness of the viscous sublayer can easily be defined, but when the boundary is covered with closely spaced roughness elements like sediment particles with heights greater than the thickness of the viscous sublayer (or, more properly, what the sublayer thickness would be in

the absence of the roughness), then no sublayer is actually present at all, and turbulence extends all the way to the boundary, in among the roughness elements.

The buffer layer is a zone just outside the viscous sublayer in which the gradient of time-average velocity is still very high but the flow is strongly turbulent. Its outstanding characteristic is that both viscous shear stress and turbulent shear stress are too important to be ignored. With reference to Figure 5.3 you can see that this is the case only in a thin zone close to the bottom. Very energetic small-scale turbulence is generated here by instability of the strongly sheared flow, and there is a sharp peak in the conversion of mean-flow kinetic energy to turbulent kinetic energy, and also in the dissipation of this turbulent energy; for this reason the buffer layer is often called the turbulence-generation layer. Some of the turbulence produced here is carried outward into the broad outer layer of flow and some is carried inward into the viscous sublayer. The buffer layer is fairly thin, but thicker than the viscous sublayer.

The broad region outside the buffer layer and extending all the way to the free surface is called the outer layer. (In pipe flow this is more naturally called the core region.) This layer occupies most of the flow depth, from the free surface down to fairly near the boundary. Here the turbulent shear stress is predominant, and the viscous shear stress can be neglected. Except down near the buffer layer, turbulence in this zone is of much larger scale than nearer the boundary. Because of their large size the turbulent eddies here are more efficient at transporting momentum normal to the flow direction than are the much smaller eddies nearer the boundary; this is why the profile of mean velocity is much gentler in this region than nearer the bottom. However, the eddies contain much less kinetic energy per unit volume of fluid than in the buffer layer. The normal-to-bottom dimension of the largest eddies in this outer layer is a large fraction of the flow depth.

In terms of the relative importance of turbulent shear stress and viscous shear stress, it's convenient to divide the flow in a somewhat different way into a viscosity-dominated region, which includes the viscous sublayer and the lower part of the buffer layer, where viscous shear stress is more important than turbulent shear stress, and a turbulence-dominated region, which includes the outer layer and the outer part of the buffer layer, where the reverse is true. In a thin zone in the middle part of the buffer layer the two kinds of shear stress are about equal. It's worth emphasizing that there are no sharp divisions in all this profusion of layers and regions: they grade smoothly one into another.

Bursting

Up until the 1960s the emphasis in turbulence research was statistical: turbulence was largely viewed as a strictly random

phenomenon, one that can be analyzed only by statistical methods. Since the late 1960s there have been many studies with emphasis less on statistical analysis than on the characteristic patterns of eddy motion and eddy structure near the boundary in a turbulent shear flow past a solid wall; for a good review, see Cantwell (1981). Studies of this kind have mostly used three techniques of flow visualization: (i) dye injection, (ii) generation of lines of tiny hydrogen bubbles in water by passing a current through a fine platinum wire immersed in the flow, and (iii) high-speed motion-picture photography of very small opaque solid particles suspended in the flow.

Flow-visualization studies of turbulent boundary layers have shown the importance of quasi-ordered or quasi-deterministic patterns or sequences of movement of certain structures or elements in the flow. These structures are parcels of fluid, with distinctive dynamics, that probably follow a consistent sequence of development in time. The structures are never precisely the same in detail, however, and because they develop randomly in space, observations made at any one place show only a crude periodicity in properties and sequence. Although the details (to say nothing of the underlying causes) are not yet clear, it is generally agreed that turbulent flow near the boundary is characterized by the following sequence of events. A high-velocity eddy or vortex (called a sweep) moves toward the boundary and interacts with low-velocity fluid near the boundary to cause acceleration, increase in shear, and development of small-scale turbulence; this accelerated fluid is then lifted from the boundary and ejected as a turbulent burst into a region of flow farther from the boundary. The entire sequence of events is usually called bursting.

Close to the boundary the high-velocity and low-velocity vortices or eddies tend to be elongated or streaked out in the streamwise direction, and their manifestation is a streaky or ribbon-like pattern of high and low fluid velocities, and therefore of boundary shear stresses as well. The scale of the motions involved in bursting is of the same order as the thickness of the viscous sublayer and the buffer layer. Owing to the substantial changes in velocity, shear, and turbulence above a given point on the boundary occasioned by the bursting cycle, the effective thickness of the viscous sublayer varies with time. The periodicity of events seems to be controlled by the velocity and scale of the main flow outside the near-boundary zone, perhaps because the periodicity of large eddies is controlled by these properties of the main flow (Jackson, 1976). It is not yet clear to what extent similar quasi-ordered patterns are also characteristic of the region of flow farther away from the boundary. In any case, appropriate measurements of turbulent velocities have shown that this ordered sequence of eddy motions accounts for most of the turbulent shear stress in the lower part of the flow. A final significant point is that the same bursting cycle is observed near the boundary in flows with a boundary so rough that no viscous sublayer is present. So, whatever the physics of bursting, it's not related to the existence of a viscous sublayer.

FLOW RESISTANCE

Introduction

In this section we take account of what is known about the mutual forces exerted between a turbulent flow and its solid boundary. As you saw in Chapter 1, flow of real fluid past a solid boundary exerts a force on that boundary, and the boundary must exert an equal and opposite force on the flowing fluid. It is thus immaterial whether you think in terms of resistance to flow or drag on the boundary.

Forces Exerted by a Flow on Its Boundary

What is the physical nature of the mutual force between the flow and the boundary? Remember that at every point on the solid boundary, no matter how intricate in detail the geometry of that boundary may be, two different kinds of fluid forces act: pressure, acting normal to the local solid surface at the point, and viscous shear stress, acting tangential to the local solid surface at the point. If the boundary is physically smooth (Figure 5.5A) the downstream component of force the fluid exerts on the boundary can result only from the action of the viscous shear stresses, because the pressure forces can then have no component in the direction of flow. But the boundary may be strongly uneven or rough on a small scale at the same time it is planar or smoothly curving on a large scale; this unevenness or roughness might involve arrays of various kinds of bumps, corrugations, protuberances, or sediment particles. Then the picture is more complicated (Figure 5.5B), because there is a downstream component of pressure force on the boundary in addition to a downstream component of viscous force: just as with the drag on blunt bodies considered in Chapter 3, if roughness elements are present on the boundary, local pressure forces are greater on the upstream sides than on the downstream sides, and so each element is subjected to a resultant pressure force with a component in the downstream direction.

The details of pressure forces on roughness elements are complicated, because they depend not only on some Reynolds number based on the size of the roughness elements and the local velocity of flow around the elements, but also on the shape, arrangement, and spacing of the elements. Qualitatively, however, the picture is clear: at low Reynolds numbers the pressure force on an element is of the same order as the viscous force, as in creeping flow past a sphere, whereas at higher Reynolds numbers the pressure forces are much greater than the viscous forces, as in separated flow past a sphere.

The sum of all the forces on individual roughness elements on the boundary (or, in the case of a physically smooth boundary, the sum of the viscous shear stresses at all points of the boundary) consitutes the overall drag on the boundary, or conversely the

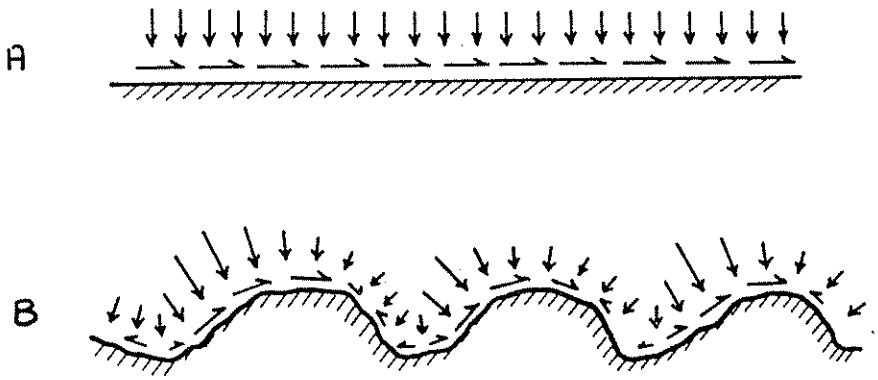

Figure 5.5 Pressure forces (double-barbed arrows) and viscous forces (single-barbed arrows) exerted by flow over (A) a physically smooth boundary, (B) a physically rough boundary. (Highly schematic.)

overall resistance to the flow. When expressed as force per unit area this boundary resistance is called the boundary shear stress τ_o. It's important to remember that τ_o refers not to the viscous shear stress at any given point on the flow boundary (which, after all, fits the description of "boundary shear stress" perfectly) but to the average force per unit area, viscous plus pressure, over an area of the boundary large enough that the variations in local forces from point to point are suitably averaged out. The word "suitably" calls for some explanation. If you're interested in the overall boundary shear stress, you average over an expanse of bed large enough to include a fair number of the largest roughness elements present (which could range from sediment particles to bed forms). If you're interested in some small local area on or among roughness elements that are much larger than the sediment particles, you have to average over an area that's small relative to those large elements but still large relative to the grain roughness.

It's worth considering at this point how boundary shear stress is actually measured in channel flows. Direct measurement is extremely difficult even in the laboratory: mechanical shear plates set flush with the boundary tend to cause some disturbance to the flow because of the inevitable gap or step at the edges. Hot-film sensors, which measure the shear at the fluid-solid interface indirectly via the conductive heat transfer from a heated solid surface, get around this problem nicely for smooth boundaries, but they don't work well when sediment is transported as bed load over a granular bed, and they can measure only the local boundary shear stress anyway. Direct measurement has so far been out of the question under field conditions or in the presence of abundant transported sediment. Fortunately, there are other

ways to measure boundary shear stress. If the flow is steady and uniform we can use Equation (1.16), the resistance equation for channel flow, to find τ_o without concern for the internal details of the flow simply by measuring the slope of the water surface; although not always a simple matter, this is possible in both field and laboratory with the proper surveying equipment. The problem is that the value of τ_o obtained is the average around the wetted perimeter of the cross section. Another method, suitable only for laboratory experiments with smooth flow, is to measure the velocity profile within the viscosity-dominated zone of flow very near the boundary, using various techniques, in order to determine velocity gradient at the boundary, which by Equation (1.5) is proportional to τ_o. Finally, we'll see presently, after considering velocity profiles in turbulent flow, that τ_o can also be found indirectly in both rough and smooth flow by means of less demanding measurement of the velocity profile through part or all of the flow depth. This last method is the most useful and important of all.

If the fluid forces on the individual grains that form a loose sediment bed become momentarily large enough, they may set some of the grains into motion. For now we're interested only in the average of the pressure forces and viscous forces over the entire surface of the boundary, and in how the mean velocity of flow depends upon this average force. Chapter 6 provides more detail on fluid forces on sediment particles exposed on the bed, and on the nature of particle motions when the forces are large enough to entrain the particles.

Smooth Flow and Rough Flow

Two fundamentally different but intergrading cases of turbulent boundary-layer flow can be distinguished by comparing the thickness of the viscous sublayer and the height of granular roughness elements. (What we'll say here will be for sand-grain roughness, but the situation is about the same for close-packed roughness of any geometry.) The roughness elements may be small compared to the thickness of the sublayer and therefore completely enclosed within it (Figure 5.6A). Or they may be larger than what the sublayer thickness would be for the given flow if the boundary were physically smooth rather than rough (Figure 5.6B). In the latter case, flow over and among the roughness elements is turbulent, and the structure of this flow is dominated by effects of turbulent momentum transport. There can then be no overall viscous sublayer in the sense described in an earlier section, although a thin viscosity-dominated zone with thickness much smaller than the roughness size must still be present at the very surface of all the elements. In the transitional case the roughness elements poke up through a viscous sublayer that is of about the same thickness as the size of the elements.

If, in flow over a rough bed, sublayer thickness is much greater than roughness size, the overall resistance to flow turns

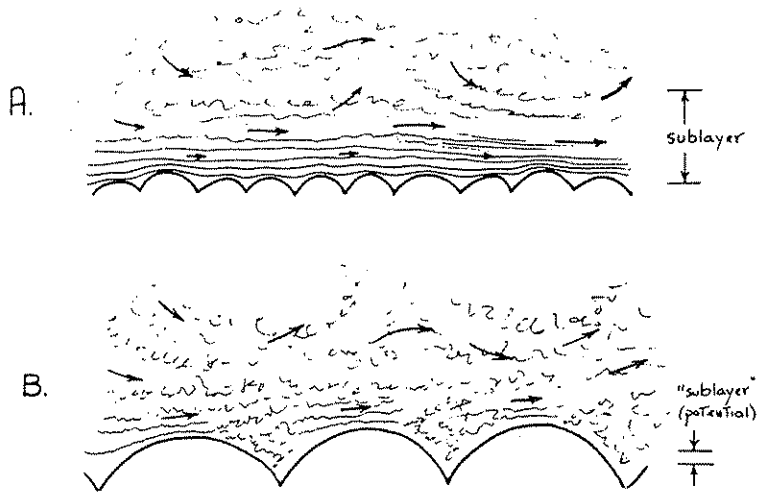

Figure 5.6 Relationship between viscous-sublayer thickness and height of roughness elements. (A) Roughness elements much smaller than sublayer thickness. (B) Roughness elements much larger than sublayer thickness.

out to be almost the same as if the boundary were physically smooth; such flows are said to be dynamically smooth (or hydraulically or hydrodynamically or aerodynamically smooth), even though they are in fact geometrically rough. (Obviously, flow over physically smooth boundaries is also dynamically smooth.) This is a consequence of the argument, introduced above, that if the Reynolds number of flow around individual roughness elements is small, as must be the case if the elements are much smaller than the viscous sublayer, pressure forces and viscous forces are of about the same magnitude, so that the presence of roughness makes little difference in the overall resistance to flow. If the elements are much larger than the potential thickness of the viscous sublayer, however, Reynolds numbers of local flow around the elements are large enough that pressure forces on the elements are much larger than viscous forces, and then the roughness has an important effect on flow resistance. Such flows are said to be dynamically rough.

It's convenient to have a dimensionless measure of distance from the boundary that can be used to specify the thicknesses of the viscous sublayer and the buffer layer. For this purpose, assume that the mechanics of flow near the boundary is controlled only by the shear stress τ_o and the fluid properties ρ and μ. This should seem at least vaguely reasonable to you, in that the dynamics of turbulence and shear stress in the viscous sublayer and buffer layer are a local phenomenon related to the presence of the boundary but not much affected by the weaker large-scale

eddies in the outer layer. (There will be more on this in the later section on velocity profiles.) You can readily verify that the only possible dimensionless measure of distance y from the boundary would then be $\rho^{1/2}\tau_o^{1/2}y/\mu$, often denoted by y^+. A similar dimensionless variable $\rho^{1/2}\tau_o^{1/2}D/\mu$, involving the height D of roughness elements or sediment grains on the boundary, can be derived based on the same line of reasoning about variables important near the boundary. This latter variable is called the boundary Reynolds number or roughness Reynolds number Re*. It's useful in dealing with fluid forces and motions near a sediment bed.

The dimensionless distance y^+ and the roughness Reynolds number Re* can be written in a more convenient and customary form by introduction of two new variables. The quantity $(\tau_o/\rho)^{1/2}$, usually denoted by u* (pronounced u-star), has the dimensions of a velocity; it's called the shear velocity or friction velocity. (Unimportant footnote: The asterisk should be a subscript but we couldn't manage to make it look right on our word processor.) The quantity μ/ρ, which you may have noticed always appears in Reynolds numbers, is called the kinematic viscosity, denoted by ν. The word kinematic is used because the dimensions of ν involve only length and time, not mass. Remember that the two variables u* and ν are nothing more than convenience variables; u* is not actually a velocity, only a disguised boundary shear stress. If y^+ as defined above is rearranged slightly it can be written $u*y/\nu$, and the roughness Reynolds number can be written $u*D/\nu$. Stare at these two dimensionless variables for a few seconds now, because you'll be seeing them often.

When expressed in the dimensionless form y^+, the transition from the viscous sublayer to the buffer layer is at a y^+ value of about 5, and the transition from the buffer layer to the turbulence-dominated layer is at a y^+ value of about 30. These transition values are about the same whatever the values of boundary shear stress τ_o and fluid properties ρ and μ; this confirms the supposition made above that over a wide range of turbulent boundary-layer flows the variables τ_o, ρ, and μ suffice to characterize the flow near the boundary. These values are known not from watching the flow but from plots of velocity profiles, as will be discussed presently.

The relative magnitude of the viscous-sublayer thickness and the roughness height D can be expressed in terms of the roughness Reynolds number $u*D/\nu$. To see this, take the top of the viscous sublayer to be at $u*\delta_v/\nu \approx 5$, meaning that $\delta_v \approx 5\nu/u*$ is the distance from the boundary to the top of the viscous sublayer. Here we've replaced y by δ_v, the thickness of the viscous sublayer. The ratio of particle size to sublayer thickness is then $D/\delta_v \approx (u*D/\nu)/5$. In other words, sublayer thickness and particle size are about the same when the roughness Reynolds number has a value of about 5. (But remember that if the particles are this large or larger, there won't be any well developed viscous sublayer in the first place.) Another way of looking at this is that we can compare the particle size D with

$\nu/u*$, a quantity with dimensions of length called the viscous length scale, which is proportional to the thickness of the viscous sublayer.

The limits of smooth and rough flow can also be specified by values of the roughness Reynolds number. The upper limit of smooth flow is associated with the condition that the height of the viscous sublayer is about equal to that of the roughness elements. As noted above, at the top of the viscous sublayer $y^+ = u*\delta_v/\nu \simeq 5$, so the upper limit of roughness Reynolds number for smooth flow should be $u*D/\nu \simeq 5$, and in fact the value of 5 is in good agreement with results based on both boundary resistance and velocity profiles. Likewise, the lower limit of roughness Reynolds numbers for fully rough flows is found to be about 60. In between these values ($5 < u*D/\nu < 60$) the flow is said to be transitionally rough.

Some further discussion of smooth and rough flow can be found in the latter part of this chapter in the section on velocity profiles.

Dimensional Analysis of Flow Resistance

One circumstance that tends to make the standard treatments of flow resistance in fluid-dynamics textbooks seem more complicated than they really are is that the details of the equations for flow resistance (although not their general form) depend not only on the boundary roughness but also on the overall geometry of the flow. On the one hand, the flow may be a turbulent boundary layer growing into a free stream; on the other hand, it may be a fully established turbulent boundary layer that occupies all of a conduit or channel. In terms of flow mechanics in the boundary layer itself these two kinds of flow may be treated together. In the latter case any number of boundary geometries are possible. Most engineering applications involve flow in a closed conduit of some cross-sectional shape or a turbulent boundary layer growing from a surface, as on an airplane wing. An application more relevant to our purposes is flow in an open channel with a planar bottom boundary that is very wide compared to the flow depth. But since the classic experiments on flow resistance were made using circular pipes with inside surfaces coated with uniform sand, and not much systematic work has been done on channel flow, the discussion here will focus on pipe flow, with the understanding that both the principles and the general form of the results will be the same for any steady uniform flow whatever the boundary geometry.

In common with other aspects of turbulent boundary-layer flow, there is no theory upon which we can draw in finding relationships for flow resistance. It is therefore again natural to start with a dimensional analysis of resistance to flow through a circular pipe or tube (Figure 5.7) in order to develop a framework in which experimental data can provide dimensionless

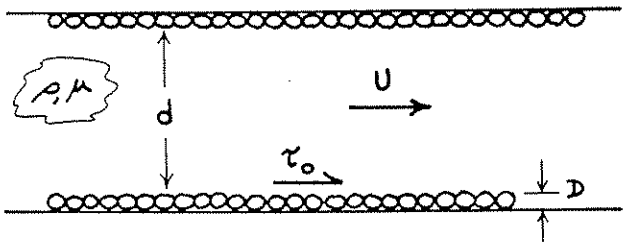

Figure 5.7 Flow through a circular pipe coated with uniform sand.

relationships that are expressible in the form of essentially empirical equations valid in certain ranges of flow.

What variables must be specified in order that the boundary shear stress τ_o be fully characterized or determined? Pipe diameter d and mean flow velocity U are important because they affect the rate of shearing in the flow, both directly and through their effect on the structure of turbulence. Viscosity μ is obviously important because of its role in determining viscous shear stress at the boundary. Fluid density ρ is important because if the flow is turbulent there must be local fluid accelerations. Finally, the size of boundary roughness elements may affect the turbulent forces and motions near the boundary. There are thus two important length scales in the problem of flow resistance: pipe diameter and roughness height. We'll have to assume that shape, spacing, and arrangement of the roughness elements are either always the same or, if variable, are of secondary importance in determining flow resistance. Neither assumption is justified, but they form a good place to start. Never mind that if the boundary is rough there is some haziness about where the position of the wall should be taken in defining the pipe diameter; at least with respect to flow resistance, any reasonable choice will produce consistent results provided that consideration is limited to geometrically similar roughness.

Assuming that all the important variables have been included, τ_o can be viewed as a function of the five variables U, d, D, ρ, and μ. You should then expect to have a dependent dimensionless variable as a function of two independent dimensionless variables. It should occur to you immediately that one of the independent dimensionless variables can be a Reynolds number based on U and d, which we'll call the mean-flow Reynolds number. The other independent dimensionless variable is most naturally d/D, the ratio of pipe diameter to roughness height. This variable is called the relative roughness. The dependent dimensionless variable, which must involve τ_o, has exactly the same form and physical significance as the dimensionless drag force or drag coefficient that characterizes the drag on a sphere moving relative to a fluid (Chapter 1), except that here we're dealing

with a force per unit area rather than with a force. You can verify that one possible dimensionless variable involving τ_o is $8\tau_o/\rho U^2$, and although this is not the only one possible (there are two others) it's the most useful, and it's the one that's conventionally used. (The factor 8 is present for reasons of convenience that need not concern us here.) This dimensionless boundary shear stress is called the friction factor, denoted by f; it is one kind of flow-resistance coefficient.

The functional relationship for flow resistance can thus be written

$$f = \frac{8\tau_o}{\rho U^2} = F\left(\frac{\rho U d}{\mu}, \frac{d}{D}\right) \qquad (5.1)$$

where F is a function which for turbulent flow must be ascertained by experiment.

Resistance Diagrams

The relationship expressed in Equation (5.1) can be shown in a two-dimensional graph most easily by plotting curves of f vs. Reynolds number for a series of values of d/D. Figure 5.8 shows a graph of this kind, called a resistance diagram. The data were obtained by Nikuradse (1933) for flows through circular pipes lined with closely spaced sand grains of approximately uniform size. A version of Figure 5.8 is shown in just about all books on flow of viscous fluids.

Leaving aside the steeply sloping part of the curve on the far left (it holds for laminar flow in the pipe, for which an exact solution can be obtained), you see that at fairly low Reynolds numbers the curve of f vs. Re for any given d/D in Figure 5.8 at first slopes gently down to the right, then breaks away, and finally levels out to a horizontal straight line. The larger the relative roughness d/D the greater the Reynolds number at which the breakaway takes place. Physically smooth boundaries, for which D/d = 0, follow the descending curve to indefinitely high Reynolds numbers. Flows that plot on this descending curve are those we earlier termed dynamically smooth. Note that flows over physically rough boundaries can be dynamically smooth, so long as d/D is sufficiently large. If Re is fairly small and the pipe is fairly large, D can be absolutely large--millimeters or even centimeters--in smooth water flows. Flows that plot on the horizontal straight lines to the right are those we called fully rough, and those at intermediate points are those we called transitionally rough. For a given d/D the flow is smooth at low Reynolds numbers but rough at sufficiently high Reynolds numbers.

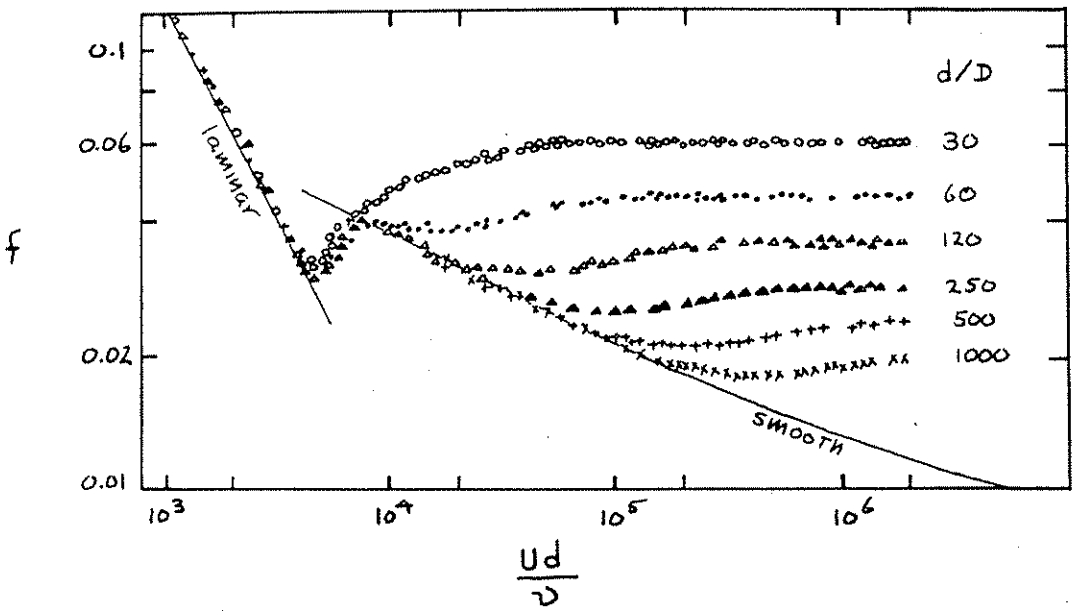

Figure 5.8 Plot of friction factor f against mean-flow Reynolds number Ud/ν for several values of relative roughness d/D in fully developed pipe flow. Data are from experiments by Nikuradse (1932, 1933) on flow through pipes with inside surfaces smooth or artificially roughened with closely spaced uniform sand grains.

Two questions need to be discussed at this point: How would the results in Figure 5.8 change for kinds of roughness elements different from glued-down uniform sand grains, and how would the results change for conduits or channels with geometry different from that of a circular pipe? The answer to both of these questions is that the results are qualitatively the same, provided that the characteristics of the roughness are not grossly different and that the size of the roughness elements remains a small fraction of the conduit diameter or channel depth. The curves are merely shifted slightly in position or differ slightly in shape. To adapt the uniform-sand-roughness results to other kinds of roughness a quantity called the equivalent sand roughness, denoted by k_s, is defined as the fictitious roughness height that would make the results for the given kind of roughness expressible by the same plot as in Figure 5.8 for uniform-sand-roughness pipes. (We'll have a little more to say about k_s later in the section on velocity profiles.) And to compare the pipe results with those for conduits or channels with different geometry, it's customary to use the hydraulic radius in place of the pipe radius, although the results can't be expected to be exactly the same. By applying the definition of hydraulic radius given in Chapter 1 you can verify that for a circular pipe the hydraulic radius specializes to one-fourth the pipe diameter, and for infinitely wide flow down a plane, to the flow depth (see Appendix 2).

How then can you predict the friction factor for a given sand-transporting flow in a laboratory flume or a natural channel? It's all right to use the graph in Figure 5.8 for channel flow over motionless planar sediment beds (unless the particle size is a substantial fraction of the flow depth, as could be the case in gravel-bed streams). But usually the bed is covered with bed forms like ripples or dunes whose shape, spacing, and arrangement are drastically different from sand-grain roughness and whose height might be a substantial fraction of the flow depth. Also, even when the bed is planar in very strong flows, the abundance of sediment in transport changes the frictional characteristics of the flow substantially. So you shouldn't expect Figure 5.8 to help you much with resistance in most natural flows. The obvious thing to do would be to develop a similar graph for the frictional characteristics of equilibrium flow-generated bed roughness over a wide range of conditions in natural channels. But only a start has been made on that formidable task. We'll return briefly to the problem in Chapter 7.

There's an equivalent way of expressing resistance that's used specifically for open-channel flow. Combining the equation $\tau_o = (f/8)\rho U^2$ that defines the friction factor f with the equation $\tau_o = \gamma_x d$ (Equation 1.15) for boundary shear stress in steady uniform flow down a plane, eliminating τ_o from the two equations, and then solving for U (remembering that $\gamma_x = \rho g \sin\phi$),

$$U = \left(\frac{8g}{f}\, d \sin\phi\right)^{1/2} \qquad (5.2A)$$

This is usually written

$$U = C(d \sin\phi)^{1/2} \qquad (5.2B)$$

where

$$C = \left(\frac{8g}{f}\right)^{1/2} \qquad (5.2C)$$

This formula, which relates mean velocity, flow depth, and slope for uniform flow in wide channels, is called the Chézy equation, after the eighteenth-century French hydraulic engineer who first developed it. The coefficient C, called the Chézy coefficient, is not a dimensionless number like f; it has the dimensions $g^{1/2}$. But since g is virtually a constant at the Earth's surface, C can be viewed as being a function only of f. We've introduced the Chézy C because it's in common use in work on open-channel flow, but you should understand that it adds nothing new.

VELOCITY PROFILES

Introduction

You've already seen that the profile of time-average local fluid velocity $\bar{u}$ from the bottom to the surface in turbulent flow down a plane is much blunter over most of the flow depth than the corresponding parabolic profile for laminar flow (Figure 1.18). This difference is a consequence of the efficient transport of fluid momentum across planes of mean shear by motions of turbulent eddies. Here we continue the treatment of velocity profiles in steady uniform turbulent flow down a plane. Remember from what we said about the structure of turbulent boundary layers that the results should be almost the same as for flow in a closed conduit or for a boundary layer growing into a free stream. Can an equation for velocity profile in turbulent flow be found by writing an equation like Equation (1.5) for turbulent flow and solving for the velocity profile by integration?

Equation (1.19) or (1.20), for the distribution of total shear stress in the flow, is valid for turbulent flow as well as for laminar flow because no assumptions were made about the nature of internal fluid motions in its derivation, just that the flow must be steady and uniform on the average. And an expression of the same kind as Equation (1.5), defining the shear stress, can also be written for turbulent flow:

$$\tau = \mu \frac{d\bar{u}}{dy} + \eta \frac{d\bar{u}}{dy} \qquad (5.3)$$

The term $\mu(d\bar{u}/dy)$ is the viscous shear stress due to the mean shear across planes parallel to the boundary. (Actually it's a spatial average over an area of such a plane that's large relative to eddy scales, because fluid shear varies from point to point in a turbulent flow.) The term $\eta(d\bar{u}/dy)$ is a way of writing the turbulent shear stress across these planes that involves an artificial quantity η, called the eddy viscosity, that's formally like the molecular viscosity μ. Everywhere in a turbulent shear flow except very near the solid boundary the eddy viscosity is much larger than the molecular viscosity, because turbulent momentum transport is dominant over molecular momentum transport. (Often η is written as $\rho\varepsilon$, where ε can be viewed as the kinematic eddy viscosity, in analogy with ν; ε is also called the eddy diffusion coefficient.) Just as for laminar flow, the expressions for τ_o in Equation (5.3) and Equation (1.20) can be set equal to give a differential equation for $\bar{u}$ as a function of distance y from the boundary:

$$(\mu + \eta)\frac{d\bar{u}}{dy} = \gamma_x(d - y) \qquad (5.4)$$

Unfortunately there's always an insuperable problem in integrating Equation (5.4), or any other equation like it for turbulent flow in a conduit or channel with some other geometry, to find the velocity distribution: η is not a property of the fluid, as is μ, but depends upon the flow: it varies with height above the boundary, because the turbulent shear stress it represents is a function of the flow itself, for which we're trying to solve. We're therefore always forced to find the velocity distribution in turbulent flow by experiment. It's important to realize, however, that the approach doesn't have to be blindly empirical: physical reasoning can be used to guess which effects and therefore which variables are important in governing the velocity distribution in the various layers of the flow. If the functional relationships thus specified by the dimensional structure of the problem are consistent with the observational results, then the correctness of that qualitative view of the physics is confirmed. In fact, much of what's known about turbulent flow past solid boundaries has been learned in this way.

We made a dimensional analysis of the velocity distribution in turbulent flow down a plane in Chapter 1 (see Equation 1.14), but we didn't show any data to indicate whether the approach is valid. It is, but we'd like to backtrack a little and repeat the analysis here in a slightly different way that leads more directly toward the equations for velocity profiles usually found in the literature. To this end we'll use not the driving force γ_x, the downslope component of the weight per unit volume of the fluid, but instead τ_o, which in steady uniform flow must balance the driving force (Figure 5.9). We'll also extend the analysis slightly to flow over physically rough boundaries; if for now we stick to the roughness represented only by planar beds of loose sediment, and not worry about sorting and grain shape, this adds the mean sediment size D to the problem. Then $\bar{u}$ can be viewed as a function of boundary stress τ_o, flow depth d, sediment size D, the fluid properties ρ and μ, and of course the distance y above the bottom:

$$\bar{u} = f(\tau_o,\ \rho,\ \mu,\ D,\ d,\ y) \qquad (5.5)$$

The dimensionless functional relationship for $\bar{u}$ is then

$$\frac{\bar{u}}{u_*} = f\left(\frac{u_* D}{\nu},\ \frac{d}{D},\ \frac{y}{d}\right) \qquad (5.6)$$

where we've made use of the shear velocity u_* and the kinematic viscosity ν introduced earlier in this chapter. Equation (5.6) says that $\overline{u}/u_*$, a dimensionless version of u (often denoted y^+), should be a function only of the roughness Reynolds number u_*D/ν and the relative roughness d/D for a given dimensionless position y/d in the flow. There are alternative possibilities for the three independent dimensionless variables (for example, all three could be put into the form of a Reynolds number, each with a different one of the three length variables), but this is the most natural.

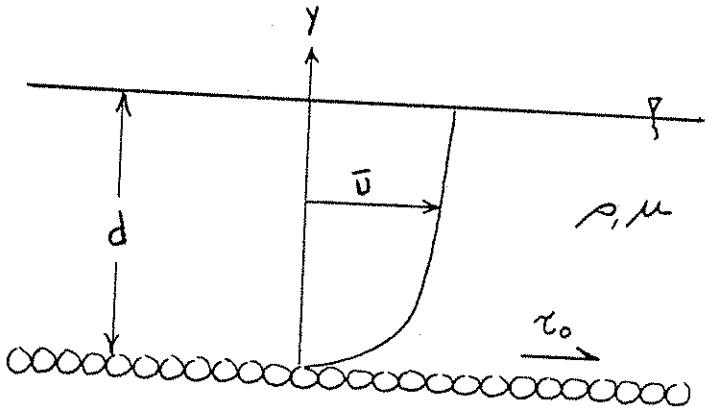

Figure 5.9 Definition sketch for dimensional analysis of velocity profiles in turbulent flow down a plane.

We're sure that all the velocity data you could get your hands on would plot very nicely in a four-dimensional graph using the variables $\overline{u}/u_*$, u_*D/ν, d/D, and y/d. But even though the number of variables has been reduced from seven to four you'd still have a burdensome plotting job and a product that would be unwieldy for practical use. Moreover, further careful study would be needed to decipher what the graph is telling you about the physics of the phenomenon. This is a good place to think about whether the problem can be simplified further by a divide-and-conquer approach wherein certain of the variables are eliminated or modified in certain ranges of conditions to arrive at simpler functions that represent the data well under those conditions. This serves two purposes: it provides useful results, and it helps to clarify the physical effects that are important.

First off, in the next two sections, we'll present some ideas about energy in turbulent flow. This may seem out of place here, but it leads to two conclusions that are of great importance for velocity profiles in turbulent flow: that of the existence of overlapping inner and outer layers of the flow, in which separate equations for velocity profiles hold, and that of the approximate independence of these profiles on the mean-flow Reynolds number. Five further subsections are devoted to the details of velocity profiles in the inner and outer layers of flows for which the diameter of the sediment on the bed is far smaller than the flow

depth. As you read these sections, refer to Figure 5.10, which provides a key or road map for the relationships that will be developed for velocity profiles under various conditions of flow and in various parts of the flow. The level of detail might strike you as excessive--but it's hard to find this fundamental material spelled out explicitly in the literature, so we've chosen to include it. If you're not interested in this much detail you can skip those five sections and read instead a following summary section. A less detailed section then covers flows over beds with sediment particles or bed forms (roughness elements, in the fluid dynamicist's parlance) whose height is a larger fraction of the flow depth and/or whose spacing is more open. A final section presents some field measurements of velocity profiles.

Upon first exposure to the great variety of equations for velocity profiles in most fluid-dynamics textbooks, a common reaction of the student is, "How will I keep them straight and know when to use them?" You may well have the same reaction. But we've worried about that, and we've tried to develop carefully the reasoning that leads to the equations and their applicability. A few especially important and useful equations are put in boxes and given names or descriptive phrases.

Energy

In making some simplifying assumptions it helps to take a closer look at the nature of turbulence in a channel flow. We'll present some arguments we hope will make some sense to you even though they can't be developed rigorously here. In what follows, keep in mind that kinetic energy, a quantity $mv^2/2$ associated with a body with mass m moving with velocity v, is changed only when an unbalanced force does work on the body, and the change in kinetic energy is equal to the work done. The change in kinetic energy caused by the action of certain forces like gravity can be recaptured without any loss of mechanical energy--think of throwing a ball straight up and watching it as it passes you on the way back down--but the work done by frictional forces represents conversion of mechanical energy into heat.

We'll start with laminar flow because the energy bookkeeping is simpler. The viscous shear stress acting across the shear planes does work against the moving fluid. (Remember that a force does work on a moving body provided that there's a component of the force in the direction of movement of the body, as is true here.) The viscous shear stress is counterbalanced by the downslope component of the weight of the fluid, so no net work is done and the kinetic energy doesn't change. But you can think in terms of potential energy being converted to kinetic energy, and kinetic energy then being converted to heat at the same rate. So in terms of energy the flow is a mechanism that converts potential energy into heat, the heat then being transferred to the surroundings at the same rate by conduction or radiation. The particular magnitude of kinetic energy in the flow in the process of this conversion is an outcome of the dynamics of the flow.

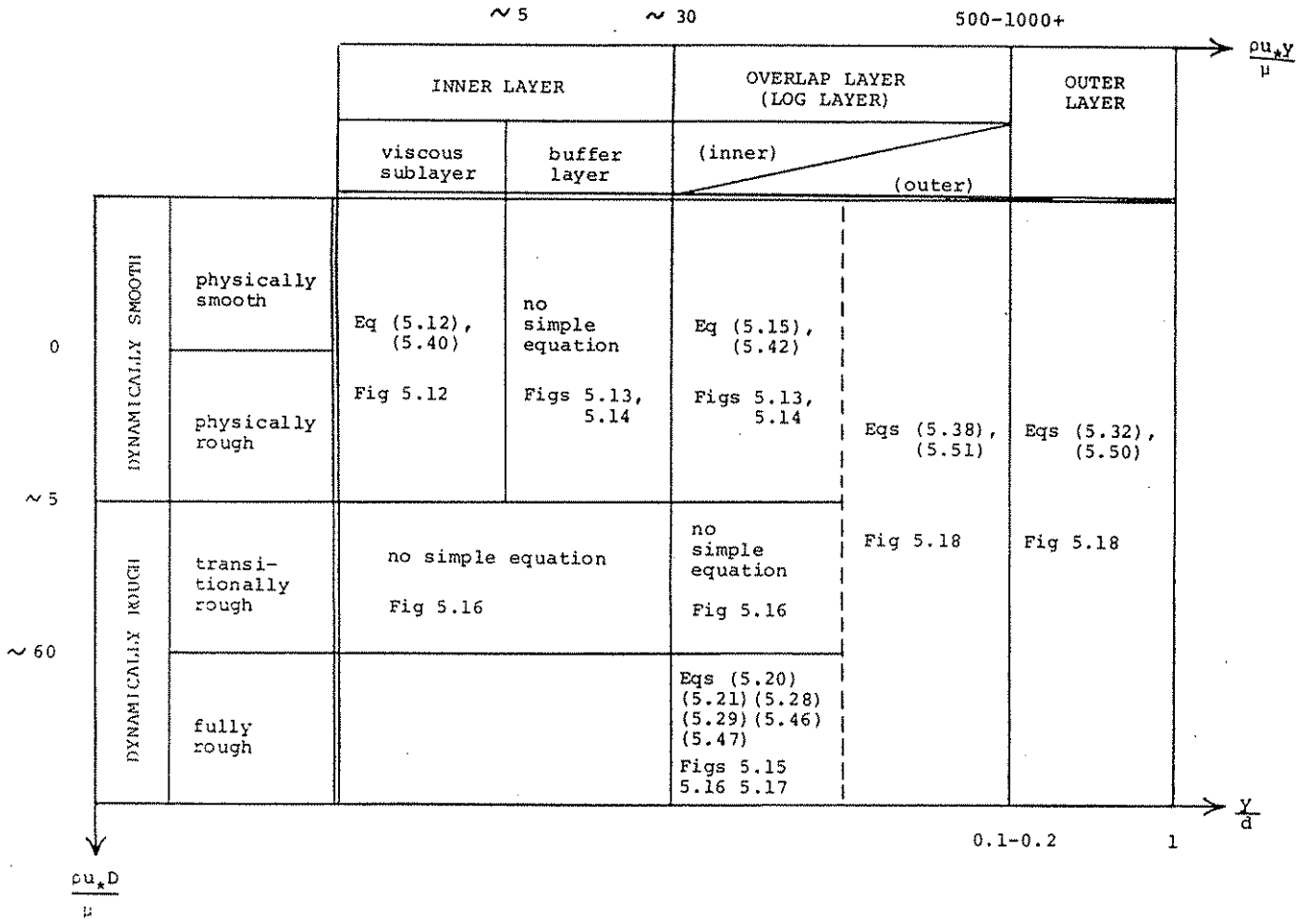

Figure 5.10 Key to profiles of time-average velocity as a function of distance from the boundary in turbulent boundary layers. Equations and figures cited are discussed in the following sections.

In turbulent flow, kinetic energy is contained not just in the mean flow but also in the turbulent fluctuations. Potential energy is again converted to heat, but the way the flow mediates this conversion, and therefore the picture of kinetic energy in the flow, is more complicated. This is because energy is extracted mainly by the work done against the mean motion by the turbulent shear stress rather than by the viscous stress, because at all levels in the flow except very near the bottom the former greatly overshadows the latter. This work done by the turbulent shear stress transforms the kinetic energy of the mean motion into kinetic energy associated mostly with the largest eddies, which

have the dominant role in the turbulent shear stress because they are the longest-range carriers of fluid momentum. But not much of this turbulent kinetic energy is converted directly into heat in these large eddies, because they are so large relative to the velocity differences across them that shear rates in them are very small.

Then where does the kinetic energy go? Answer: it's handed down to smaller eddies. This phrase "handed down" might strike you as plausible but unilluminating. Large eddies degenerate or become distorted into smaller eddies in ways not elaborated here, and when this happens the kinetic energy that was associated with the large eddies becomes transferred to the smaller eddies. But the odds are all against smaller eddies organizing themselves again into larger eddies--just watch the breakup of regular flow in a smoke plume to get the sense that the natural tendency in turbulent motions is from regular motion to irregular motion. So in terms of kinetic energy, turbulence is largely a one-way street: it passes energy mostly from large scales to small scales, not in the other direction. This effect is called an energy cascade. Shear rates are greatest in the smallest eddies because of their small size relative to the velocity differences across them, and it's in these smallest eddies that most of the kinetic energy is finally converted into heat. In fact, the reason there's a lower limit to eddy size is that below a certain scale the viscous shear stresses are so strong that they damp out the velocity fluctuations.

A very significant consequence is that viscosity has a direct effect on turbulence only at the smallest scales of turbulent motion. If the mean-flow Reynolds number is increased, the energy cascade is lengthened at the smallest scales by development of even smaller eddies, but the structure of turbulence at larger scales is not much changed. So any bulk characteristic of the flow that is governed by the large-scale turbulence--like the velocity profile, which depends mainly on the turbulent exchange of fluid momentum--should be only slightly dependent on the Reynolds number. This effect is called Reynolds-number similarity.

Inner and Outer Layers

Now back to velocity profiles. We want to convince you that two different but overlapping regions or layers of the flow can be recognized (Figure 5.11) in which the velocity profile depends not on the full list of variables τ_o, ρ, μ, D, y, and d used in the dimensional analysis above, but on certain subsets. The advantage is that in each of these layers there's then a simpler functional relationship for the velocity profile, one that leads to a curve in a two-dimensional graph that holds very well for almost the entire range of turbulent channel flows. We'll wave our arms a little about the various variables, but of course the most convincing evidence is that this is how things actually work out, as you'll see.

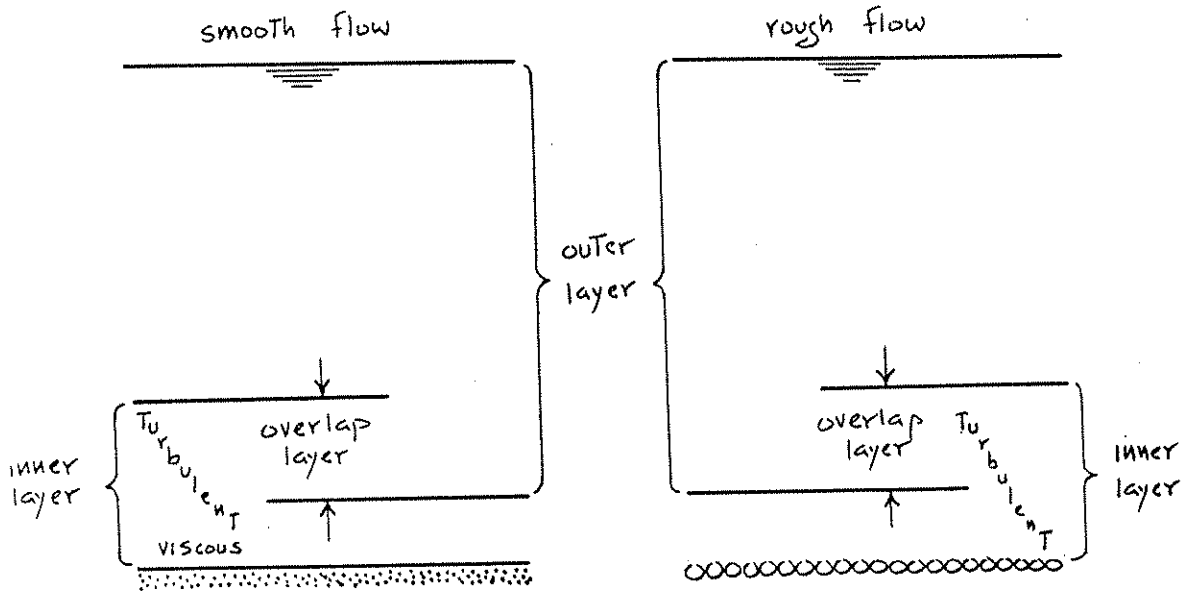

Figure 5.11 Inner and outer layers in turbulent channel flow. See also Figure 5.4.

Near the bottom boundary, in what we called the buffer zone and for a ways outside it, the turbulence is small-scale and intense, and both production and dissipation of turbulent kinetic energy are known from actual measurements to be at a peak. It's reasonable to view the dynamics of the turbulence, and therefore the nature of the velocity profile, as being controlled by local effects and substantially independent of the nature of the turbulence in the rest of the flow, all the way up to the free surface. This is also true of the viscous sublayer, if one is present, because there the velocity profile is controlled by the strong viscous shear adjacent to the solid boundary. The velocity profile in this inner layer thus depends on τ_o, D, ρ, μ, and y, but not on d.

On the other hand, over most of the flow depth, from the free surface all the way down to the top of the buffer layer in smooth flow, you've seen already from the discussion of turbulent energy that the velocity profile should be largely independent of μ. If the boundary is rough the profile should be independent of D as well as of μ down to a position just far enough above the roughness elements that the turbulence shed by the elements is not important in the turbulence dynamics. But you should expect the profile to depend on d, because the size of the largest eddies is proportional to the flow depth. The velocity profile in this outer layer (here we've generalized the significance of the outer-layer concept introduced in an earlier section) should thus depend on τ_o, ρ, d, and y, but not on D or μ.

If you scrutinize the definitions of the inner and outer layers in the last two paragraphs in the light of what we've said about the structure of the flow, you'll see that they are likely to overlap. In other words, there's a zone where the velocity

profile is at the same time independent of all three variables d, μ, and D. This should be true so long as the mean-flow Reynolds number is high enough (well beyond the laminar-turbulent transition) that the viscosity-dominated zone near the boundary is very thin relative to the flow depth. (Remember that the thickness of the viscous sublayer decreases as the Reynolds number increases, because the Reynolds number is a measure of the relative importance of inertial forces and viscous forces.) This is usually the case in sediment-transporting turbulent flows of sedimentological interest.

You're probably thinking by now that we've presented you with a confusion of layers. We'll summarize them at this point. On the one hand, in terms of the relative importance of viscous shear stress and turbulent shear stress it's natural to recognize three intergrading but well defined zones (the viscous sublayer, the buffer layer, and the outer layer) or, more generally, a viscosity-dominated layer below and a turbulence-dominated layer above. On the other hand, in terms of importance or unimportance of variables (a related but not identical matter) two overlapping layers can be recognized: an inner layer in which the mean velocity (and other mean characteristics of the flow as well) depends on μ or D (or both) but not d, and the same outer layer in which the mean velocity depends on d but not on μ or D. In rough flow the entire thickness of the flow is dominated by turbulence, and there's no viscosity-dominated layer--but there are still inner and outer layers.

The Law of the Wall for Smooth Boundaries

Look first at the inner-layer velocity profile over a physically smooth bottom. From what was just said about the inner layer,

$$\bar{u} = f(\tau_o, \rho, \mu, y) \tag{5.7}$$

or in dimensionless form,

$$\frac{\bar{u}}{u_*} = f\left(\frac{\rho u_* y}{\mu}\right) \tag{5.8}$$

Equation (5.8) states that the velocity $\bar{u}$, nondimensionalized using u_*, depends only on y^+, the dimensionless distance from the bottom. So the velocity profile should be expressible as a single curve for all turbulent channel flows with smooth bottoms. Equation (5.8) is the general form of what's called the law of the wall for smooth boundaries.

You should expect the velocity profile expressed in Equation (5.8) to be in two different parts, one corresponding to the viscous sublayer and the other to the outer part of the inner layer, where turbulent shear stress predominates over viscous shear stress. These two parts of the profile have to pass smoothly one from the other in the intervening buffer layer.

Because fluid accelerations are unimportant in the viscous sublayer, $\overline{u}$ there depends on τ_o, μ, and y, but not on ρ:

$$\overline{u} = f(\tau_o, \mu, y) \tag{5.9}$$

The only way to write Equation (5.9) in dimensionless form is

$$\frac{\mu\overline{u}}{\tau_o y} = \text{const} \tag{5.10}$$

because there's only one way to form a dimensionless variable from the four variables u, τ_o, μ, and y. Equation (5.10) can be juggled algebraically a little by introducing ρ on both sides, for no other reason than to put it in the same form as Equation (5.8):

$$\frac{\overline{u}}{u_*} = \text{const}\ \frac{\rho u_* y}{\mu} \tag{5.11}$$

The constant in Equation (5.11) turns out to be unity. To get an idea why, go back to Equation (1.22), the exact solution for the velocity profile in laminar channel flow. It's reasonable to expect that the velocity profile in the viscous sublayer of a turbulent channel flow is like the velocity profile near the boundary in a laminar channel flow. Points near the boundary in laminar flow, where the velocity gradient $d\overline{u}/dy$ is very large, are way out on the limb of the parabola in Equation (1.22), so the second term on the right in Equation (1.22) can be neglected and $\overline{u}$ assumed to be a linear function of y/d:

$$\overline{u} = \frac{\tau_o}{\mu d}(yd) = \frac{\tau_o y}{\mu} \tag{5.12A}$$

When cast in the same form as Equation (5.11), this becomes

$$\boxed{\frac{\bar{u}}{u_*} = \frac{\rho u_* y}{\mu}}$$

the law of the wall
for a smooth boundary
inside the viscous sublayer (5.12B)

Figure 5.12 shows that Equation (5.12) is in good agreement with careful velocity measurements in the viscous sublayer. It turns out that Equation (5.12) holds for all turbulent boundary layers next to smooth boundaries, not just for open-channel flows. Equation (5.12) provides a way of finding τ_o in flow over smooth boundaries: if you have available a very small velocity sensor, measure the velocity profile in the viscous sublayer, fit Equation (5.12) to it, and find u_* given μ and ρ.

In the outer, turbulence-dominated part of the inner layer over a physically smooth bottom we can assume that $d\bar{u}/dy$ does not depend on μ, because the shear stress and therefore the velocity gradient is determined almost entirely by turbulent momentum exchange (see Equation 5.3). On the other hand, $\bar{u}$ itself must depend on μ, because the velocity profile in the turbulence-dominated part of the inner layer must be connected to that in the viscosity-dominated part, and you've just seen that the velocity profile in the viscous sublayer depends on μ. In other words, the velocity at the base of the turbulence-dominated part of the inner layer depends on the velocity at the top of the viscous sublayer, which in turn depends on μ. The viscosity-dominated part of the profile can be viewed as anchoring the turbulence-dominated part of the profile to the bottom, where the velocity is zero by the no-slip condition. So to get the velocity profile we have to start with the velocity gradient, rather than the velocity itself, and write $d\bar{u}/dy = f(\tau_o, \rho, y)$ in dimensionless form as

$$\frac{y}{u_*}\frac{d\bar{u}}{dy} = A \tag{5.13}$$

(where A is a dimensionless constant that should hold in this particular layer for all turbulent channel flows over smooth boundaries) and then integrate to obtain the dimensionless velocity profile:

$$\frac{\bar{u}}{u_*} = A \ln y + A_1 \tag{5.14}$$

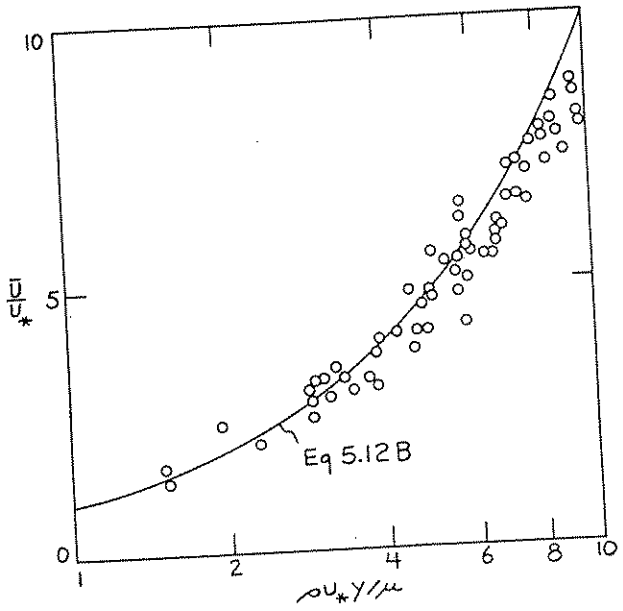

Figure 5.12 Arithmetic plot of $\bar{u}/u*$, ratio of local time-average velocity to shear velocity, against $\rho u*y/\mu$, dimensionless distance from the boundary, for the viscous sublayer over smooth boundaries. This plot represents the law of the wall inside the viscous sublayer. Equation (5.12) is given by the solid line. Data points are from several sources, and cover a fairly wide range of mean-flow Reynolds numbers and outer-layer flow geometries.

where A_1, also dimensionless, is a constant of integration. By the concept of Reynolds-number similarity discussed above, A should be very nearly constant provided that the Reynolds number is high enough for the turbulence to be fully developed.

Note that Equation (5.14) doesn't contain μ explicitly, but from what we said above, μ has to be in there somewhere. The resolution of this seeming paradox is that the constant of integration A_1 must depend upon μ. You can verify that this is so by noting that Equation (5.14) can be put into the general form for the law of the wall given by Equation (5.8) if and only if A_1 is equal to $A \ln(\rho u*/\mu) + B$: putting this expression for A_1 into Equation (5.14),

$$\frac{\bar{u}}{u_*} = A \ln y + A \ln \frac{\rho u_*}{\mu} + B$$

$$= A \ln \frac{\rho u_* y}{\mu} + B \qquad (5.15A)$$

The constant B is just the residuum of the constant of integration after A $\ln(\rho u_*/\mu)$ has been extracted.

If the argument leading from Equation (5.14) to Equation (5.15A) leaves you a bit unsatisfied, you can look at the matter in a way that is physically more revealing although mathematically more taxing. Assume that Equation (5.12) holds to a height δ' that's about in the middle of the buffer layer and that Equation (5.14) holds above that; δ' is thus the height at which the curves given by the two equations intersect. This ignores the smooth transition in velocity profile through the buffer layer, but it leads to evaluation of the constant of integration A_1 in Equation (5.14) in a natural way by use of the fact that Equations (5.12) and (5.14) must both hold at the point of intersection. This is what we meant when we said above that the viscosity-dominated profile anchors the turbulence-dominated profile to the bottom. The outcome is that B in Equation (5.15A) is a function of $\rho u_* \delta'/\mu$, the dimensionless form of δ', which like the dimensionless thickness of the viscous sublayer or of the buffer layer is largely independent of the mean-flow Reynolds number if the flow is fully turbulent. If you're interested in the mathematical details, see Appendix 3.

Equation (5.15A) shows that the velocity profile is expressed by a single curve for the turbulence-dominated part of the inner layer, just as was the case for the viscosity-dominated part. It's the profile given by Equation (5.15A) that's usually called the law of the wall, although that term more properly describes the whole inner-layer profile, viscosity-dominated and turbulence-dominated, plus the transition between. The logarithmic form of the velocity profile was prefigured way back in Chapter 1, in Figure 1.16.

There's no universal agreement in the literature on the values of the constants A and B: A is usually taken to be between 2.4 and 2.5, and B is taken to be between 5 and 6. The small differences in A and the larger differences in B from source to source are an understandable result of fitting straight lines in semilogarithmic plots of slightly scattered data from diverse experimental studies. Discussions on the values of these constants can be found in Monin and Yaglom (1971) and Hinze (1975). With the commonly used values A = 2.5, B = 5.1, Equation (5.15A) becomes

$$\frac{\overline{u}}{u_*} = 2.5 \ln \frac{\rho u_* y}{\mu} + 5.1 \qquad (5.15B)$$

the law of the wall for a smooth boundary outside the viscous sublayer and buffer layer

In summary, time-average velocity $\overline{u}$ in the inner layer over a smooth boundary, when nondimensionalized by dividing by u_*, should plot as a single curve as a function of y^+, the dimensionless distance above the bottom. Figure 5.13, which incorporates the

data already plotted in Figure 5.12 for the viscous sublayer, shows the velocity profile through the whole of the inner layer over a smooth boundary. This profile represents the complete law of the wall for smooth boundaries. The data points in the viscosity-dominated part of the inner layer follow Equation (5.12); the data points in the turbulence-dominated part of the inner layer follow Equation (5.15B), which plots here as a straight line because of the semilogarithmic coordinates.

Between y^+ values of about 5 and about 30 in Figure 5.13 there is a smooth transition between the viscosity-dominated profile (Equation 5.12B) and the turbulence-dominated profile (Equation 5.15B). This is the buffer layer, where viscous shear stress and turbulent shear stress are both important. For $y^+ < 5$ the turbulent shear stress is negligible, and Equation (5.12B) describes the profile; for $y^+ > 30$ the viscous shear stress is negligible, and Equation (5.15B) describes the profile. It's in wall-law plots like Figure 5.13 that the lower and upper limits of the buffer layer are most clearly manifested. You'll see a variety of lower and upper limiting y^+ values mentioned in the literature; this is understandable, because the divergence of the curves given by Equations (5.12B) and (5.15B) from the actual profile is gradual. Although it's of no great physical significance, the height of intersection δ' of equations (5.12B) and (5.15B) in the buffer layer is at $y^+ \approx 11$, as you can see from Figure 5.13, so $\rho u_* \delta'/\mu \approx 11$. What's of greater significance is that the turbulent shear stress and the viscous shear stress are found experimentally to be equal at a slightly larger y^+ value of about 12; this is in a sense the "middle" of the buffer layer.

The dimensionless height y^+ above the boundary at which $\overline{u}/u_*$ begins to deviate from the law of the wall depends on the mean-flow Reynolds number Re; it ranges upward from around 500 at small Re to over 1000 at larger Re (Figure 5.14). For y^+ greater than this, $\overline{u}/u_*$ is greater than predicted by the law of the wall.

How thick is the inner layer? The upper limit of y^+ for the law of the wall at high Reynolds numbers for open-channel flow is not well established, but assume a y^+ value of 1000 in a flow of room-temperature water 1 m deep at a mean flow velocity of 0.5 m/s. Then y at the outer limit of the inner layer is about 5 cm. (To figure this out, compute Re, use the smooth-flow curve in Figure 5.8 to get f and therefore τ_o, and put this into y^+.) So the inner layer occupies only a small percentage of the flow depth, no more than 10-20%. And the viscous sublayer in this flow is only a fraction of a millimeter thick. Note that the logarithmic abscissa axis in plots like Figures 5.13 and 5.14 crowds the whole outer layer, in which Equation (5.15B) no longer holds, into a small part of the graph.

Most of the data points in Figure 5.13 are from flows in circular pipes and rectangular ducts rather than from open-channel flows. But data from open-channel flows, and from boundary layers developing on flat plates as well, are consistent with those from

flow in pipes and ducts. This emphasizes the important point that the law of the wall holds for a wide variety of geometries of outer-layer flow. From the earlier discussion of variables important in the inner and outer layers, this should be no surprise: the flow in the inner layer is governed by local

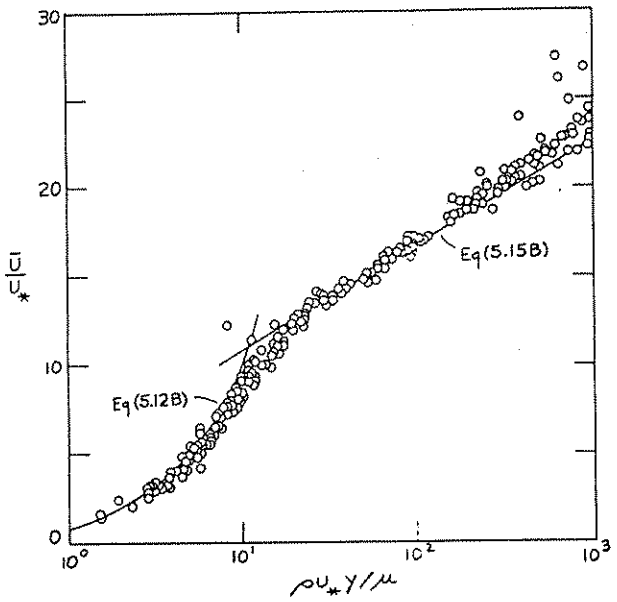

Figure 5.13 Plot of $\bar{u}/u*$, ratio of local time-average velocity to shear velocity, against the logarithm of $\rho u*y/\mu$, dimensionless distance from the boundary, for the inner layer over smooth boundaries. This plot represents the complete law of the wall for dynamically smooth turbulent boundary layers. Equations (5.12B) and (5.15B), for the viscosity-dominated and turbulence-dominated parts of the inner layer, are given by the solid curves. Data points are from several sources, and cover a fairly wide range of mean-flow Reynolds numbers and various outer-layer flow geometries. The intersection of Equations (5.12B) and (5.15B) at δ' is discussed in the text.

effects and is independent of the nature of the outer flow. In fact, the law of the wall is even more general: although we won't pursue the matter here, the law of the the wall holds even when there is a substantial pressure gradient (negative or positive) in the direction of flow, resulting in downstream acceleration or deceleration.

The Law of the Wall for Rough Boundaries

Introduction

If the bottom is occupied by or consists of roughness elements of some kind, the velocity profile depends on the size, shape, and arrangement of those roughness elements as well as on

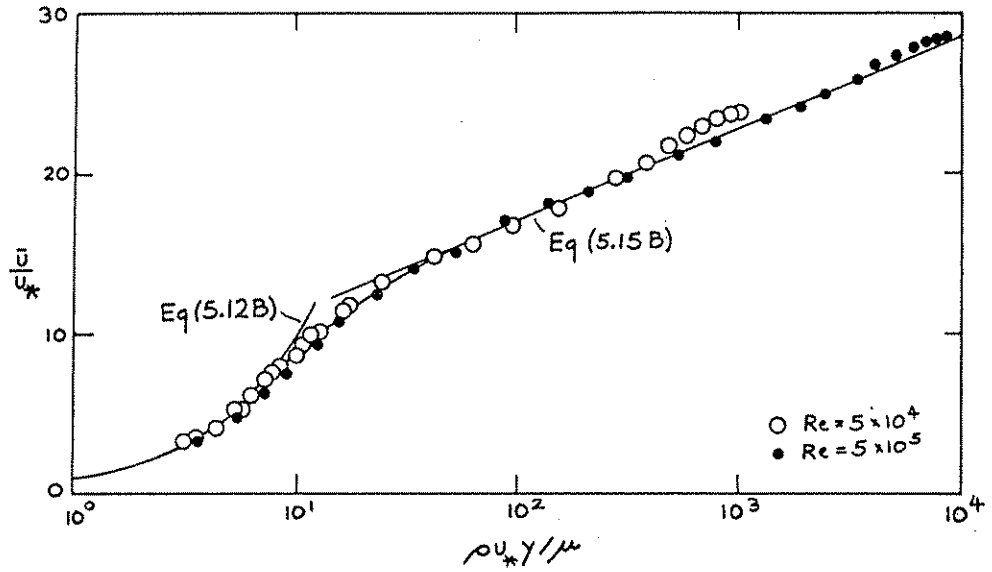

Figure 5.14 Inner-layer velocity profiles in pipe flow for two different mean-flow Reynolds numbers. Data are from Laufer (1954).

τ_o, ρ, μ, and y:

$$\bar{u} = f(\tau_o, \rho, \mu, y, \text{roughness geometry}) \qquad (5.16)$$

where the roughness geometry is specified by the size distribution, the shape distribution, and the arrangement of the roughness elements. To make any progress we have to be specific about the nature of the roughness. We'll assume here that the roughness is composed of fairly well sorted mineral sediment particles with the usual natural range of particle shape and roundness, and that the particles form a full sediment bed that's planar on a large scale. This kind of roughness, called close-packed granular roughness, is fairly well characterized by the single variable D, the mean or median particle size. It may seem as though we're defining most of the phenomenon away, but this case is of obvious importance to sediment transport. Fortunately, it's also the best studied. It's not the only important case, however; eventually we'll have to deal with bed-form roughness. With the above simplifications, Equation (5.16) becomes

$$\bar{u} = f(\tau_o, \rho, \mu, y, D) \qquad (5.17)$$

or, in dimensionless form,

$$\frac{\overline{u}}{u_*} = f\left(\frac{\rho u_* y}{\mu}, \frac{\rho u_* D}{\mu}\right) \qquad (5.18)$$

The dimensionless velocity $\overline{u}/u_*$ depends not only on y^+ but also on the boundary Reynolds number. Equation (5.18), which could also be written using y/D instead of $\rho u_* D/\mu$, is the law of the wall for granular-rough boundaries.

Two different aspects of the effect of the roughness on the velocity profile become apparent upon examination of Equation (5.18). First, the size of the roughness elements relative to the thickness of the viscous sublayer is important. Remember from the section on smooth flow and rough flow earlier in this chapter that if D is much smaller than the viscous length scale $\mu/\rho u_*$ the particles are embedded in the viscous sublayer, whereas if D is much larger than $\mu/\rho u_*$ there's no viscous sublayer, and the particles are enveloped in turbulence generated by flow separation around upstream particles. You should suspect, then, that for very small $\rho u_* D/\mu$ (less than about 5, for which viscous-sublayer thickness and particle size are about equal), the roughness has no effect on the velocity profile. Under these conditions the velocity profile over physically rough boundaries is indeed found to coincide with that over physically smooth boundaries--provided that we don't place our velocity meter so close to the bed that individual grains distort the velocity field. The law of the wall for smooth boundaries, Equations (5.12) and (5.15) together with the transition between them through the buffer layer, therefore holds for flows with $\rho u_* D/\mu < 5$ over physically rough boundaries also. These are the flows that in the section on flow resistance were termed dynamically smooth even though physically rough and were shown to fall on the curve for physically smooth boundaries in the resistance diagram in Figure 5.8. For very large $\rho u_* D/\mu$, however, there's no viscous sublayer and therefore no effect of μ on the velocity profile, and you should expect to see a velocity profile rather different from the wall law for smooth flow. The next two subsections are devoted to the velocity profile in these dynamically rough flows, which are sedimentologically so important.

Second, in the case of rough flow the value of y relative to D is important. For $y \approx D$, at points in the flow that are nestled among the uppermost particles or just a few diameters above, the velocity depends in a complicated way on the shape and packing of the particles and on the position of the profile relative to individual particles, and we shouldn't expect to find any generally applicable profile; the velocity profile could be said to be spatially disunified. A bit higher in the flow, several diameters above the tops of the particles, the wakes shed by individual particles can be expected to blend together in such a way that the velocity profile is about the same at all positions,

but the flow structure is still affected by the roughness-generated turbulence. Far above the tops of the particles, however, for y >> D, it's reasonable to expect that the turbulence structure is governed by local dynamics, as in smooth flow, and not by the wakes from the little particles far below. If D is sufficiently smaller than the flow depth d, there should then be a layer of the flow for which y << d and y >> D at the same time--that is, a part of the inner layer in which roughness-generated turbulence is not of direct importance. Remember, however, that by analogy with what was said about smooth flow above, this part of the profile still has to be anchored at its lower end to that part of the velocity profile controlled by the roughness-generated turbulence.)

In the following we examine in some detail the velocity profile in rough flows for which there's indeed a zone for which y << d but at the same time is above the near-bed layer of spatial disunification of the profile. The treatment will be in two sections, one for the region farther from the bed, where the bed grains don't affect the profile shape, and the other for the region nearer the bed, where the turbulence shed by the grains has a direct effect on the profile. We'll return briefly later to the equally important flows in which there's no such zone, examples being shallow flows over gravels and flows over bed forms whose height is not very small relative to the flow depth.

Inner Layer Far Above the Grains

In the part of the inner layer for which y >> D, neither μ nor D affects the slope of the velocity profile. We can therefore make exactly the same statement as for the turbulence-dominated part of the inner layer in physically smooth flow: the velocity gradient $d\overline{u}/dy$ depends only on τ_o, ρ, and y. This leads again to Equation (5.13), and upon integration, to Equation (5.14). We should even expect the constant A to be the same, because it is a manifestation of the vertical turbulent transport of streamwise fluid momentum, and we just concluded that sufficiently far from the boundary the structure of the turbulence depends only on local effects and is independent of the turbulence shed by the bed roughness. The constant of integration A_1, however, is different, because it depends on the nature of the connecting velocity profile nearer the boundary, which is different from that in smooth flow. This latter difference has to do with the relative importance of viscous shear stress and turbulent shear stress near the boundary, and with the relative importance of viscous drag and pressure drag at the boundary; if $D >> \mu/\rho u_*$ (we've termed such flows fully rough), viscous shear stress in the flow and viscous drag on the boundary are negligible, so not only the velocity gradient but also the velocity itself is unaffected by μ in the layer under consideration here.

We can rearrange Equation (5.14) to obtain Equation (5.15A) just as in the case of smooth flow, but with one important

difference: by comparison with the general form of the law of the wall for rough flow (Equation 5.18), the term B is now not a constant but instead a function of the boundary Reynolds number:

$$\frac{\bar{u}}{u_*} = A \ln \frac{\rho u_* y}{\mu} + f\left(\frac{\rho u_* D}{\mu}\right) \qquad (5.19)$$

This can be put into an equivalent but more revealing and more useful form by splitting $f(\rho u_* D/\mu)$ into two parts: $-A \ln(\rho u_* D/\mu)$ plus a remainder that's some different function of $\rho u_* D/\mu$, which we'll call B'. The only reason for this otherwise arbitrary choice is that now Equation (5.19) can be written

$$\frac{\bar{u}}{u_*} = A \ln\left[\frac{\rho u_* y}{\mu} - \ln \frac{\rho u_* D}{\mu}\right] + B' = A \ln \frac{y}{D} + B' \qquad (5.20A)$$

This is neater than Equation (5.19), but remember that B' is a function of $\rho u_* D/\mu$. If $\rho u_* D/\mu$ is sufficiently large, however, so that D is large relative to what the viscous-sublayer thickness would be, turbulence extends down among the roughness elements and there's no viscosity-dominated layer next to the bottom. The velocity profile then cannot depend on μ and therefore not on $\rho u_* D/\mu$, so B' in Equation (5.20A) is a constant, which has a value of about 8.5 for uniform, close-packed sand-grain roughness. (There's about as much uncertainty about this constant as there is about the constant B in Equation 5.15B.) The value of B has indeed been found experimentally to become constant for $\rho u_* D/\mu > 60$. It's under these conditions that the flow was termed fully rough in the earlier section on flow resistance. Equation (5.20A) can then be written as Equation (5.20B), the law of the wall for fully rough flow:

$$\boxed{\frac{\bar{u}}{u_*} = 2.5 \ln \frac{y}{D} + 8.5}$$

The law of the wall for fully rough flow over granular-rough boundaries (5.20B)

Figure 5.15 shows Equation (5.20B) together with the data from Nikuradse (1933) on which the value of 8.5 for B' was originally derived. Nikuradse's data were obtained for a particular geometry of granular roughness manufactured by gluing a somewhat open monolayer of subrounded and almost single-size sand

to the inner walls of circular pipes. You should expect the value of B' for full, loose beds of less well sorted sand to be different, even if the mean size is the same, because the effective height and spacing of the "tallest" roughness elements (i.e., the largest and most protrusive bed grains) are different. As is commonly done, you can preserve the value of 8.5 in Equation (5.20B) and use for D the fictitious diameter of single-size sand grains in a uniform monolayer that makes Equation (5.20B) fit the velocity data best. That size is called the equivalent sand roughness, usually denoted k_s. (A more descriptive term would be the "equivalent Nikuradse-style sand roughness.") In other words, k_s for any given bed roughness is the uniform-sand-grain height that gives the same wall-law velocity distribution for a given value of τ_o.

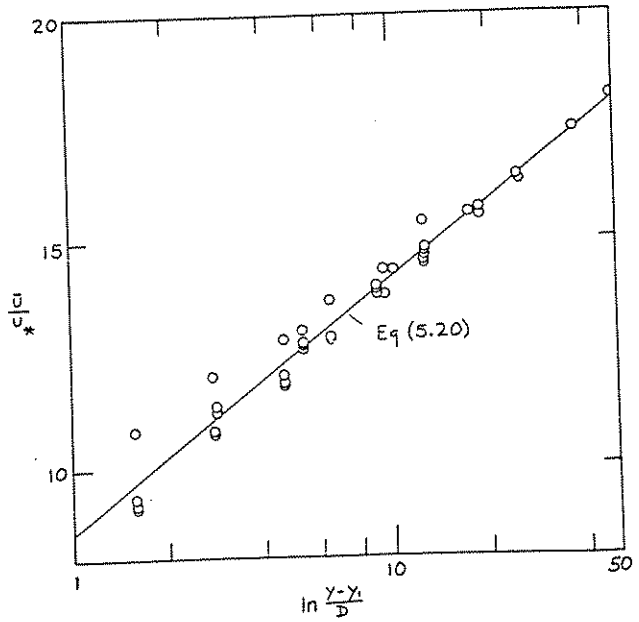

Figure 5.15 Plot of $\bar{u}/u_*$ against y/D for the inner layer over granular-rough boundaries. Data are from Nikuradse (1933) for runs with pipe radius > 60 D. Only data for which $Re_* > 60$ are shown, so this plot represents the law of the wall for dynamically fully rough flow. All points up to 0.2 times the pipe radius are shown. Equation (5.20) is shown by the straight line, with A = 2.43 and B' = 8.56 obtained by a least-squares fit. Included are 8 profiles from 4 sand-lined pipes. As described in a later section, the y = 0 level has been adjusted downward from the tops of the grains a distance $y_1/D = -0.36$ to extend the straight-line fit as close to the bed as possible.

One further comment about Figure 5.15: in pipe flow, and also in open-channel flow, it happens that the velocity profile doesn't deviate greatly from Equation (5.20B) even at positions far out from the boundary toward the centerline of the pipe or the free surface of the channel. So you can safely fit your rough-flow velocity profile to Equation (5.20B) without great error. But you shouldn't expect the value of τ_o derived therefrom (for how to do

that, see a later section) to be exactly the same as that derived from just the inner part of the velocity profile; from Nikuradse's original pipe data, for example, estimates of τ_o based on almost the entire profile, out to 90% of the pipe radius from the wall, are greater on the average by a factor of 1.07 than the actual measured values, when the value of 2.46 for A determined from only the lowest 20% of the profile is used also in the case of the entire profile. (We could just change the value for A a little in the equation for the whole profile to make the value for τ_o come out right. But since least-squares fits of the entire velocity profile are not as good as those of just the inner layer, and A is of fundamental physical significance, it's better simply to view as slightly erroneous the use of the entire profile.) Unfortunately, we don't know of any data good enough for the same comparison for open-channel flow.

For $5 < \rho u_* D/\mu < 60$ the flow is said to be transitionally rough. The velocity profile is still a semilog straight line for $y >> D$, whether $\overline{u}/u_*$ is plotted against $\rho u_* y/\mu$ as in Figure 5.13 or against y/D as in Figure 5.15, and it still has the same slope given by the universal constant A. But the position of the straight line varies as the near-bed part of the profile changes from the smooth-flow profile shown in Figure 5.13 to the fully rough profile shown in Figure 5.15. For transitionally rough flows, the law of the wall in the innermost region, where there's some dependence on μ, can't be derived in the form of a simple equation like Equation (5.12) or Equation (5.20); keep in mind, however, that some form of the general law of the wall for rough boundaries (Equation 5.18) holds there nonetheless.

Figure 5.16, a combined plot of the law of the wall in smooth and rough flows, summarizes much of what's in the last two subsections. The three-dimensional surface in Figure 5.16, drawn by use of Equations (5.12), (5.15), and (5.20), shows $\overline{u}/u_*$ as a function of y^+ and Re_*. In smooth flows, represented by the left-hand part of the surface, the velocity profiles don't depend on Re_*, so the surface is a cylinder whose elements are parallel to the Re_* axis. Each of the several profiles shown (which represent intersections of the surface with planes for which $Re_* = \text{const}$) is exactly the same as that in Figure 5.13. In fully rough flows, represented by the region to the right of the plane $Re_* = 60$, the velocity profiles depend only on y/D. To see why the right-hand part of the surface slopes downward to the right, write $\ln(y/D)$ as $\ln(\rho u_* y/\mu) - \ln(\rho u_* D/\mu)$, or $\ln y^+ - \ln Re_*$; thus, the larger the value of Re_*, the smaller the value of $\overline{u}/u_*$ for a given value of y^+. Since there's no viscous sublayer or buffer layer to contend with, the profiles are straight lines all the way down to positions not far above the tops of the roughness elements. You'll see in the next section that unless the $y = 0$ level is chosen carefully the rough-wall profile deviates from a semilog straight line within several grain diameters above the tops of the grains--to say nothing of the spatial disunification of the velocity profile that sets in below the tops of the grains. Only at points on the surface well above the dashed curve that

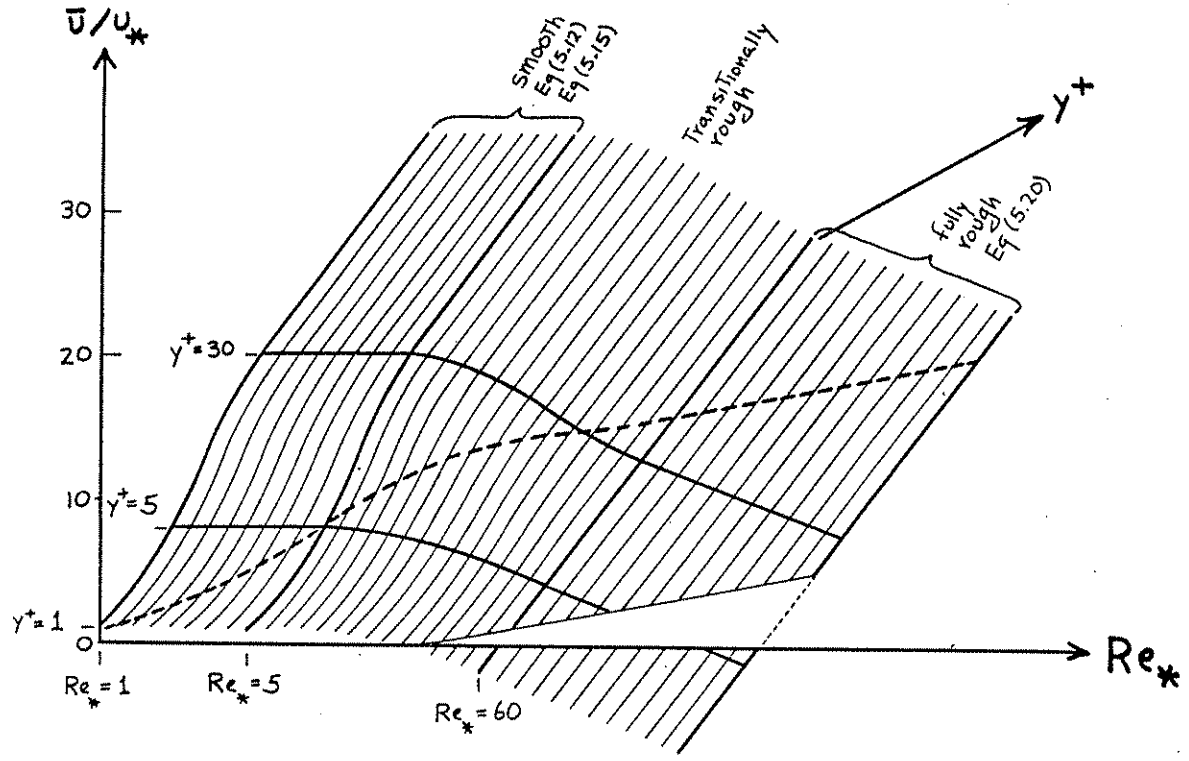

Figure 5.16 Combined plot of the law of the wall in smooth, transitionally rough, and fully rough flows. See text for explanation.

expresses the condition y = D are the profiles valid; the part of the surface shown in the lower right is therefore useful only hypothetically, for displaying for you the nature of the relationships. Finally, in the middle part of the surface the profiles are transitional between the smooth and the fully rough profiles. Here the lines for $y^+ = 5$ and $y^+ = 30$ shown on the left-hand part of the surface lose their physical significance as the viscous sublayer disappears.

Note in Figure 5.16 that at any value of y^+ well up in the inner layer $\bar{u}/u*$ in any rough flow is less than $\bar{u}/u*$ in any smooth flow, although the slopes of the profiles for the two flows are the same at that height. This is because nearer the bottom the velocity increases more sharply with distance from the bottom in smooth flow than in rough flow. Subtract Equation (5.20B) from Equation (5.15B) to find the difference in $\bar{u}/u*$ between smooth and rough flow:

$$\frac{\Delta\overline{u}}{u_*} = \left(\frac{\overline{u}}{u_*}\right)_{smooth} - \left(\frac{\overline{u}}{u_*}\right)_{rough} = A \ln\left[\frac{\rho u_* y}{\mu} - \ln\frac{y}{D}\right] + B - B'$$

$$= A \ln \frac{\rho u_* D}{\mu} + B - B'$$

It's easy to verify that $\Delta\overline{u}/u*$ is indeed always positive for any fully rough flow: B is about 5 and B' is about 8.5 (see above), and since $\rho u*D/\mu > 60$, $\ln(\rho u*D/\mu)$ is always greater than about 4.

A conventional additional step that's taken with Equation (5.20A) is to write B' in the form $-A \ln(y_o/D)$, where the quantity y_o, with the dimensions of length, is called the roughness length. (Outdoors fluid dynamicists like meteorologists take the normal-to-boundary coordinate direction to be z, so they deal with z_o, not y_o.) This allows B' to be completely absorbed into the log term in Equation (5.20A):

$$\frac{\overline{u}}{u_*} = A \ln\frac{y}{D} - A \ln\frac{y_o}{D} = A \ln\frac{y}{y_o} \qquad (5.21)$$

By the definition of the natural logarithm, y_o can be written in terms of B' as $y_o = D \exp(-B'/A)$.

If the flow is only transitionally rough, y_o is a function of $\rho u*D/\mu$, as is B'. If the flow is fully rough, however, y_o is independent of $\rho u*D/\mu$ for the same reason that B' in Equation (5.20A) is independent of $\rho u*D/\mu$. Don't confuse y_o with the actual roughness height D: for a given geometry of roughness in fully rough flow y_o is proportional to D (for close-packed uniform sand-grain roughness $y_o \approx D/30$) but the proportionality coefficient varies with roughness geometry.

Setting y equal to y_o in Equation (5.21) gives $\overline{u}/u* = 0$. So another way of looking at y_o is that it's the height at which the velocity would become zero if the logarithmic rough-wall equation for the velocity profile could be extended down to that height. It's important to remember, however, that Equation (5.21) becomes inapplicable far above that position, which is nestled in amongst the grains. In fact, we'll see below that Equation (5.21) has to be corrected at positions even well above the tops of the grains.

Inner Layer Not Far Above the Grains

We still haven't considered the lowermost part of the inner layer, not far above the tops of the grains. For sand-size bed roughness this region isn't much more than a few millimeters thick, but for water flowing over gravels or for wind blowing over large ground-surface roughness it may be decimeters or even meters thick, and no sophisticated, miniaturized velocity meters are needed to include it in measured velocity profiles. At positions this close to the bed there's a troublesome problem we've avoided up to now: where's the origin for y? It seems reasonable to suppose that the y = 0 level lies somewhere between the bases and the tops of the surface particles. A natural choice would be the average surface elevation--the spatial average of the heights, normal to the mean plane of the bed, at which a solid surface is first encountered in descending onto the bed. You'll see, however, that this doesn't produce the best fit of velocity to Equations (5.20) or (5.21). And it's not a very practical choice anyway. With close-packed granular roughness, the plane through the tops of the grains (which itself is not very well defined) is usually taken as the y = 0 level for velocity measurements.

For a given dimensionless distance y^+ from the boundary, $\overline{u}/u_*$ is not the same in rough and smooth flow, because the second term on the right side of Equation (5.19) always has a value different from B in Equation (5.15A). But the shape and slope of the velocity profile are the same: if you differentiate Equation (5.19) for the rough-flow velocity profile with respect to y, you get

$$\frac{d\overline{u}}{dy} = \frac{Au_*}{y} \qquad (5.22)$$

which is exactly the same as Equation (5.13) for flow over a smooth bottom. You might expect, however, that at positions closer down to the tops of the grains, the grains have some effect on the shape as well as the position of the velocity profile, making the shape different from the smooth-flow case. In other words, when y is not much greater than D, the velocity gradient depends not only on τ_o, ρ, and y but also on D: $d\overline{u}/dy = f(\tau_o, \rho, y, D)$, or in dimensionless form (cf. Equation 5.13), $(y/u_*)d\overline{u}/dy = f(D/y)$. It's convenient to extract the same constant A from the function on the right, so that the effect of proximity to the bed grains can be viewed as a correction function by which the right side of Equation (5.22) must be multiplied:

$$\frac{d\bar{u}}{dy} = \frac{Au_*}{y} f\left(\frac{D}{y}\right) \qquad (5.23)$$

There's no simple way of dealing with the physics behind the correction function f(D/y) in Equation (5.23). The only thing we can say with certainty is that as y gets smaller (and D/y gets larger) the correction gets larger. To investigate the correction function further we can expand it as a power series in D/y (Monin and Yaglom, 1971; remember that any function can be approximated in this way by an appropriate power series.) Equation (5.23) can then be written

$$\frac{d\bar{u}}{dy} = \frac{Au_*}{y}\left[1 + a\frac{D}{y} + b\left(\frac{D}{y}\right)^2 + \text{---}\right] \qquad (5.24)$$

As the boundary is approached from above, and the correction gets larger, the term aD/y, the dominant term while the correction is still small, gets less important relative to terms of higher order in D/y. In the following we'll consider only positions higher than one to two diameters above the tops of the roughness elements. (Measurements are seldom made closer to the bed anyway, because to get a representative value for the mean velocity a large number of profiles must be taken at different places relative to the roughness elements and then spatially averaged.) To conform to the usual practice in dealing with the grain-proximity correction we have recast Equation (5.24) into a slightly different form by introducing a new variable $y-y_1$ for the vertical coordinate, where y_1 is a small constant that's in the same ballpark as D itself. We also need the following algebraic identity:

$$\frac{1}{y} = \left(\frac{1}{y-c}\right)\left(\frac{y-c}{y}\right) = \left(\frac{1}{y-c}\right)\left(1 - \frac{c}{y}\right)$$

where y is some variable and c is a constant. Then, replacing 1/y in Equation (5.24) with the right side of the identity above and letting the constant be y_1,

$$\frac{d\bar{u}}{dy} = \frac{Au_*}{y - y_1}\left(1 - \frac{y}{y_1}\right)\left[1 + a\frac{D}{y} + b\left(\frac{D}{y}\right)^2 + \text{---}\right]$$

$$= \frac{Au_*}{y - y_1}\left(1 - \frac{y_1}{y} + a\frac{D}{y} + \text{terms in } \frac{1}{y^2} \text{ etc.}\right) \qquad (5.25)$$

Neglecting terms of order higher than 1/y on the right side, Equation (5.25) becomes

$$\frac{d\bar{u}}{dy} = \frac{Au_*}{y - y_1}\left(1 + \frac{aD - y_1}{y}\right) \qquad (5.26)$$

We're at liberty to adjust the definition of y_1 at the outset in such a way that $y_1 = aD$; then Equation (5.26) becomes

$$\frac{d\bar{u}}{dy} = \frac{Au_*}{y - y_1} \qquad (5.27)$$

Equation (5.27) can be integrated in the same way as the rough-flow equivalent of Equation (5.13) to be in the same form as Equation (5.20),

$$\frac{\bar{u}}{u_*} = A \ln \frac{y - y_1}{D} + B' \qquad (5.28)$$

and Equation (5.28) can be manipulated into the same form as Equation (5.21), with y_o and no separate constant of integration,

$$\frac{\bar{u}}{u_*} = A \ln \frac{y - y_1}{y_o} \qquad (5.29)$$

(See Appendix 4 for details.)

Equations (5.28) and (5.29) are the conventional way of dealing with the correction function f(D/y) that appears in Equation (5.23). Shifting the origin of the y coordinate by the small quantity y_1 usually straightens out the velocity profile in

a semilog plot down to positions not far above the tops of the roughness elements. What's commonly done with wind-velocity profiles above the land surface is to take y = 0 at the base of the roughness elements--the ground on which the observer is standing--and then find the value of y_1 which when subtracted from y gives the best straight-line fit of data to Equation (5.29). The distance y_1 (often denoted by d) is called the displacement height or the zero-plane displacement. The situation is a little different with close-packed granular roughness, which is of greater interest here: usually the velocity profile is measured with respect to the tops of the grains, and then the apparent origin for y is lowered to produce the best straight-line fit to Equation (5.29). (The plane through the tops of the grains isn't ideally well defined, but it's impossible to define a dynamically natural plane that represents the bases of the grains in a full bed of loose sediment.) So the value of y_1 depends not only on the physics of the problem but also on the y origin chosen at the outset.

To see whether Equation (5.29) represents the velocity profile well, consider an actual example of a measured profile. Profile A in Figure 5.17 shows one of the original velocity profiles measured by Nikuradse (1933) in his classic experiments on flow resistance in sand-roughened pipes. (You might object that sedimentologists aren't much interested in pipe flow, but remember that the law of the wall holds just as well in sand-roughened open channels as in sand-roughened pipes.) Profile A shows $\overline{u}$ vs. ln y for a flow with a cross-section mean velocity U of 5.75 m/s through a pipe with diameter 0.1 m onto which uniform 0.4 mm sand had been glued (Nikuradse, 1933, Table 10, Column 7). The flow was fully rough, the boundary Reynolds number being 154, and the value of about 125 for the ratio of pipe radius to grain diameter is comfortably within the range for which there's a zone with $y >> D$ and $y/r << 1$ at the same time. The origin for y is taken here at the tops of the grains.

From the preceding section on the outer part of the inner layer, far above the grains, you should expect the profile to be a straight line for $y >> D$ and y/r about 0.2 or less. In Profile A in Figure 5.17 only a few points, from Point 3 out to Point 6, meet these conditions. Because of the way y_1 enters into Equations (5.28) and (5.29), changing the origin by y_1 shifts the points more and more as the bed is approached. So it should be possible to find a value for y_1 that shifts Points 1 and 2 onto to the extension of the straight line that can be passed approximately through Points 3 through 6. We hunted by trial and error for the value of y_1 that produces the best straight-line fit (in a least-squares sense) to the curve of $\overline{u}$ vs. ln y for Points 1 through 6, which extend up to a height y/r = 0.2. The value of y_1 that produces the best straight line is 0.26 mm. So the new origin is below the tops of the grains by 0.26 mm, or about half a grain diameter. For a wide variety of roughness geometries, this distance has been found to be between 0.2 and 0.4 roughness diame-

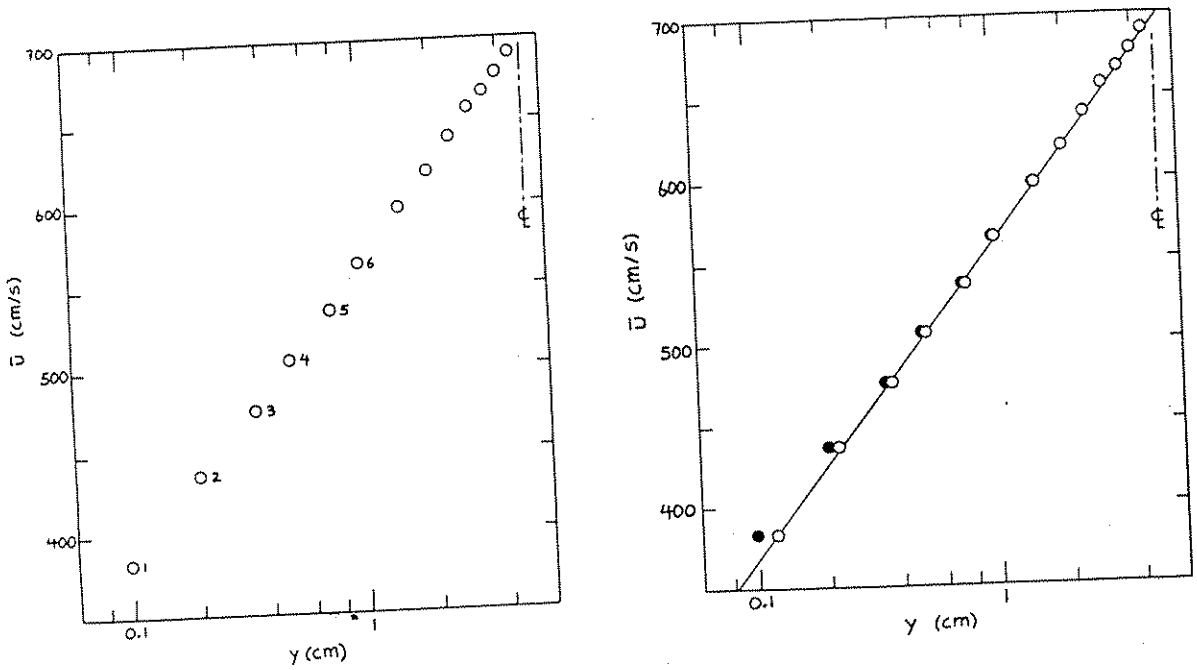

Figure 5.17 Velocity profile measured by Nikuradse (1933) in a sand-roughened pipe. A. Raw profile of $\bar{u}$ vs. ln y, based on points out to 90% of the pipe radius toward the center line. B. The same profile after the origin for y is shifted a distance y_1 of 0.21 mm (≈ 0.5D) toward the boundary, producing the best least-squares straight-line fit of the lowermost six points of the velocity profile, up to 20% of the pipe radius. The solid circles in B are corresponding points transferred directly from A.

ters below the tops of the roughness elements (Jackson, 1981). For this value of y_1, the velocity profile is as shown in Figure 5.17B. You can see that the profile becomes almost a straight line. Using the independently measured value of u* for this profile the constant A comes out to be 2.44, within the range of accepted values. If the same thing is done using all the profile points up to 90% of the pipe radius, about as good a straight line is obtained but the value for A is higher, 2.49.

We're fooling you a little here: when the other fully rough profiles taken in the very same pipe are considered, values for A range from 2.31 to 2.57, and y_1, which is especially sensitive to errors in velocity measurement, ranges from almost zero to twice the roughness diameter. When the measured points in all three profiles are lumped together, however, A comes out to be a respectable 2.43 and y_1 comes out to be 0.26 mm, again putting the new origin a little below the tops of the grains. This serves as a reminder that unless your profiles are based on a lot of accurately measured points, the results for any one profile can be misleading when used to find τ_0, as described in the next section.

The physical significance of the displacement height y_1 has never been clear. There's some experimental evidence that the height y_1 above the origin is the level in the flow at which the boundary shear stress τ_o appears to act (Thom, 1971). The horizontal component of the force per unit area the flow exerts on its bed has not only a magnitude but also a line of action. In other words, if we could measure τ_o with enough accuracy and detail we would find that it appears to act on some plane parallel to the bed. (Presumably this plane would lie somewhere between the bases and tops of the roughness elements.) Choose an arbitrary plane above or below the bed and find the moment M per unit bed area associated with the force τ_o per unit bed area. Dividing M by τ_o gives a quantity with the dimensions of length, and this length is just the distance above or below the arbitrary plane at which τ_o acts. Jackson (1981) reasons that this distance is none other than the displacement height y_1.

Using the Law of the Wall to Find τ_o

An important practical reason for measuring mean-velocity profiles, in addition to finding the cross-section mean velocity U, is to obtain the bed shear stress τ_o. The first thing to remember is that, as will become clear when you reach Equation (5.30) below, you can't obtain both A and τ_o from a measured profile, no matter how good the profile is; all you get is the product Au*. If you have a trustworthy independent measurement of τ_o you can get your own estimate of A by looking at the slope of the velocity profile in the outer part of the inner layer, well above the tops of the roughness elements. If no sediment is in motion on or above the bed, then your estimate should be close to 2.5. But if τ_o is what you want but don't have, you must assume the accepted value of 2.5 for A and use the slope of the profile to obtain τ_o. It doesn't make any difference whether the flow is smooth or rough, because the slope of the wall-law profile in the outer part of the inner layer is always the same.

An important note of caution: the value of the constant A seems to change when sediment is being transported--although the nature and magnitude of the change is still a matter of debate (Coleman, 1981; Gust and Southard, 1983). Unfortunately, therefore, obtaining τ_o from the velocity profile when the flow is transporting sediment is a less straightforward matter than outlined below for an immobile sediment bottom.

The easiest way to find τ_o, alias u*, is to use the differential form of the law of the wall, $(y/u*)d\overline{u}/dy = A$, which holds for both smooth and rough flows (Equations 5.13 and 5.22). Plot $\overline{u}$ against ln y, and from that graph find the slope $d\overline{u}/d(\ln y)$ of the straight-line part of the law of the wall in the outer part of the inner layer. By the chain rule

$$\frac{d\bar{u}}{d(\ln y)} = \frac{dy}{d(\ln y)} \frac{d\bar{u}}{dy} = y \frac{d\bar{u}}{dy}$$

so Equations (5.13) and (5.22) can be written

$$u_* = \frac{y \, d\bar{u}/dy}{A} = \frac{d\bar{u}/d(\ln y)}{A} \qquad (5.30)$$

(Be careful about the base of the logarithms. If you want to work with logs to the base ten, A is larger by the factor 2.3. This is why you often see the value 5.75 instead of 2.5 for A in fluid-mechanics textbooks.) An example of finding τ_o from a measured wall-law velocity profile is given in Appendix 5.

Aside from the practicalities of measuring a good velocity profile (see the later section on field measurements), you have to make sure that there actually is a straight-line outer part of the inner layer. This means that $\overline{D}/d$, the ratio of roughness height D to flow depth d, must be small enough for you to work with a range of y such that two conditions hold at the same time: $y << d$ (y/d less than, say, 0.2-0.3), and $y >> D$ (this latter requirement can be made less stringent by choosing $y = 0$ so as to extend the straight-line part of the wall law as close to the bed as possible, as described above in the discussion of the displacement height y_1).

In addition to finding τ_o (and also the displacement height y_1 as a byproduct) there are three other things you might want to find from your velocity profile: (i) the roughness length y_o (Equations 5.21 and 5.29); (ii) the constant B' (Equations 5.20 and 5.28); and (iii) the equivalent sand roughness k_s, obtained by using the conventional value of 8.5 for the constant B' in Equations (5.20) and (5.28); this value corresponds to the reference case of a glued-down monolayer of subrounded and almost single-size sand grains, studied by Nikuradse (1933). Details are given in Appendix 6.

Velocity-Defect Law

Now look at the velocity profile in the outer layer. There the velocity is most naturally specified relative to that at the free surface, because we've seen that the inner layer, with a different relationship for the velocity, intervenes between the outer layer and the bottom boundary. In other words, if we look at the velocity relative to that at the surface we don't have to worry about how the velocity is anchored to the bottom through the

inner layer. So instead of $\overline{u}$ we use $U_s - \overline{u}$, called the velocity defect, where U_s is the surface (i.e., maximum) velocity.

If you go back and review the discussion in the section on inner and outer layers you'll see that the structure of the turbulence in the outer layer should depend on τ_o, ρ, y, and d, but not on μ, for the same reason that the velocity profile in the turbulence-dominated part of the inner layer doesn't depend on μ. Since this is true from the free surface down to the bottom of the outer layer, and $U_s - \overline{u}$ characterizes the velocity relative to the free surface rather than the bottom, not just the velocity gradient $d\overline{u}/dy$ (as in the turbulent part of the inner layer) but also $U_s - \overline{u}$ itself is independent of μ. Turbulence structure and $U_s - \overline{u}$ shouldn't depend on D either, provided that $D \ll d$. So the general form of the velocity-defect profile is

$$U_s - \overline{u} = f(\tau_o, \rho, y, d) \tag{5.31}$$

or in dimensionless form

$$\frac{U_s - \overline{u}}{u_*} = f\left(\frac{y}{d}\right) \tag{5.32}$$

The dimensionless velocity defect depends only on the dimensionless height above the bottom. This relationship for the velocity profile in the outer layer is called the velocity-defect law. We'll defer further discussion of velocity profiles in the outer part of the flow until the following section, where an examination of the region of overlap between the inner and outer layers affords further insight into the form of the velocity-defect law.

The Overlap Layer; More on the Velocity-Defect Law

One more matter to consider in this exposition of velocity profiles has to do with the overlap layer, where at sufficiently high mean-flow Reynolds numbers the conditions defining the inner and outer layers hold simultaneously; we refer you once more to the earlier section on inner and outer layers. This overlap layer is far enough from the bottom that the flow structure is independent of both viscosity and the characteristics of the bottom roughness but close enough to the bottom that the flow structure is independent of the flow depth. Here the inner-layer and outer-layer velocity profiles must match--that is, the velocities $\overline{u}$ given by the law of the wall and by the velocity-defect law at any level in the overlap layer must be the same. The upper limit of the overlap layer is at the top of the inner layer. In smooth flow the lower limit is at the top of the

buffer layer. With regard to the lower limit in rough flow, presumably the velocity-defect representation of the velocity profile, which looks downward from the free surface and can ignore the details of the bottom roughness, must start to break down when it reaches the lower part of the inner layer, where you've seen that the roughness causes the inner-layer profile to curve away from a semilog straight line. (But you won't find much discussion of this point in the literature.)

The constraints imposed by the matching requirement on the form of both the wall law and the velocity-defect law in the overlap layer were first perceived by Izakson (1937) and Millikan (1939). One way to show the consequences of the matching is to equate the velocity gradients $d\bar{u}/dy$ given by the outer-layer profile and the inner-layer profile (see, e.g., Tennekes and Lumley, 1972, p. 153-155). Differentiate with respect to y the profile given by Equation (5.32) in the outer layer to obtain $d\bar{u}/dy$,

$$\frac{d\bar{u}}{dy} = -\frac{u_*}{d}\frac{df_1}{d(y/d)} \tag{5.33}$$

(remember the chain rule), and also the profile given by Equation (5.8) for smooth flow or by Equation (5.18) for rough flow in the inner layer,

$$\frac{d\bar{u}}{dy} = \frac{\rho u_*^2}{\mu}\frac{df_2}{d(\rho u_* y/\mu)} \tag{5.34}$$

The functions on the right in Equations (5.33) and (5.34) have been distinguished here as f_1 and f_2 to keep them straight, although we'll see in a moment that in fact they're the same. Set the expressions for $d\bar{u}/dy$ in Equations (5.33) and (5.34) equal and multiply by y/u_*:

$$-\frac{y}{d}\frac{df_1}{d(y/d)} = \frac{\rho u_* y}{\mu}\frac{df_2}{d(\rho u_* y/\mu)} \tag{5.35}$$

The left side of Equation (5.33) is a function only of y/d and not $\rho u_* y/\mu$, and the right side is a function only of $\rho u_* y/\mu$ (and also $\rho u_* D/\mu$, for rough flow) but not of y/d. The only way these two statements can be true at the same time is for both sides to be equal to some constant; we'll call this constant A. You'll see presently that this is the same as the constant A in the law of the wall. Each of the resulting equations can be integrated, the

first with respect to the variable y/d and the second with respect to the variable $\rho u_* y/\mu$ (for clarity and economy we'll call these two variables q_1 and q_2, respectively):

$$\int \frac{df_1}{dq_1}\, dq_1 = f(q_1) = \frac{U_s - \bar{u}}{u_*} = -A\int \frac{dq_1}{q_1} = -A \ln q_1 + c_1 = A \ln \frac{y}{D} + c_1 \qquad (5.36)$$

$$\int \frac{df_2}{dq_2}\, dq_2 = f(q_2) = \frac{\bar{u}}{u_*} = A\int \frac{dq_2}{q_2} = A \ln q_2 + c_2 = A \ln \frac{\rho u_* y}{\mu} + c_2 \qquad (5.37)$$

where c_1 and c_2 are constants of integration.

First examine Equation (5.37) for the inner-layer profile. It holds for both smooth flow and rough flow, because the expression for $d\bar{u}/dy$ in Equation (5.34) holds for both. It's the same as Equation (5.15) for smooth flow if c_2 is identified with B, and it's the same as Equation (5.20) for rough flow if c_2 is identified with $f(\rho u_* D/\mu)$; in the former case c_2 is really a constant, and in the latter case it's a function of $\rho u_* D/\mu$, because the integration is in fact a partial integration. In both cases this exercise shows in a different way that the law of the wall in the turbulence-dominated part of the inner layer has to be logarithmic.

Now look at Equation (5.36), for the outer-layer profile in the overlap layer, the end result being

$$\frac{U_s - \bar{u}}{u_*} = - A \ln \frac{y}{D} + c_1 \qquad (5.38)$$

This is just a specialization of the velocity-defect law given by Equation (5.32). It holds only in the overlap layer, up to y/d values that correspond to the top of the inner layer; keep in mind that this extends no more than about 20% of the way from the bottom to the surface. Equation (5.38) shows that in the overlap layer--but not farther out, beyond the inner layer--the velocity-defect law too is of logarithmic form. The overlap layer is often called the logarithmic layer, because in it both the wall law and the defect law are logarithmic.

(A slightly different way of matching inner-layer and outer-layer velocity profiles in the overlap layer, leading to the same result as above, is to add the two profiles given by Equations (5.18) and (5.32), differentiate the resulting equation twice, once with respect to $\rho u_* y/\mu$ and then with respect to y/d, solve the resulting differential equation to get the law of the

wall, and then compare this solution to the original equation obtained by addition to get the logarithmic form of the velocity-defect law in the overlap layer. See Appendix 5.) Figure 5.18 shows velocity-defect profiles on flat plates and in pipes, wide planar ducts, and open channels. The open-channel data, from Coleman (1981), are for a width-to-depth ratio of only about 2, but we could find no better data; the scarcity of good published data on complete velocity profiles from surface to bottom in steady uniform open-channel flows at large ratios of width to depth is amazing. In each graph in Figure 5.18 the data points define a single curve that holds for a wide range of mean flow Reynolds numbers, indicating that our assumptions about the controls on velocity and turbulence in the outer layer are justified. In each graph there's a well defined straight-line segment for fairly small y/d corresponding to Equation (5.38). Toward the position of maximum velocity at y/d = 1 the profile breaks away from the semilog straight line to reach the point $(U_s-\overline{u})/u* = 0$ at the position of maximum velocity. The velocity farthest from the solid boundary is thus greater than that given by the extension of Equation (5.19), which holds in the logarithmic part of the outer layer. The different intercepts of these straight lines with the right-hand vertical axis in Figure 5.18 reflect different values for c_1 in the three cases.

The differing shape of the outer part of the velocity-defect profile in different geometries of flow is to be expected because of differing physical effects in the movement and geometry of large eddies in the region of the flow farthest from the solid boundary. Since the outer edge of a freely growing turbulent boundary layer is highly irregular in shape (Chapter 3), at any point near the outer edge passage of large turbulent eddies alternates with passage of nonturbulent fluid, so the efficacy of turbulent momentum exchange is less and the velocity gradient correspondingly steeper than in regions closer to the boundary; this presumably explains the large divergence of the profile from the semilog straight-line segment in Figure 5.18A. In pipes and planar ducts the similar but smaller divergence might be explained by the free passage of large eddies across the centerline or center plane from the opposite side of the flow. In open-channel flow a similar effect might be produced by flattening of large eddies moving toward the free surface. The meager data from open channels suggest an effect similar in magnitude to that in pipes and planar ducts, or perhaps even smaller. There seems to be no reason to expect a perfectly logarithmic profile all the way to the free surface, but the deviations clearly are insubstantial, at least for practical work.

Note that as a consequence of the matching of inner and outer velocity profiles the coefficient A of the log term in the velocity-defect law in the overlap layer, Equation (5.38), is exactly the same as the coefficient A in the law of the wall smooth or rough (Equations 5.15 and 5.20). This constant A, which as noted earlier is a reflection of the nature of turbulent momentum transport in the inner layer, is usually written $1/\kappa$, and κ is called

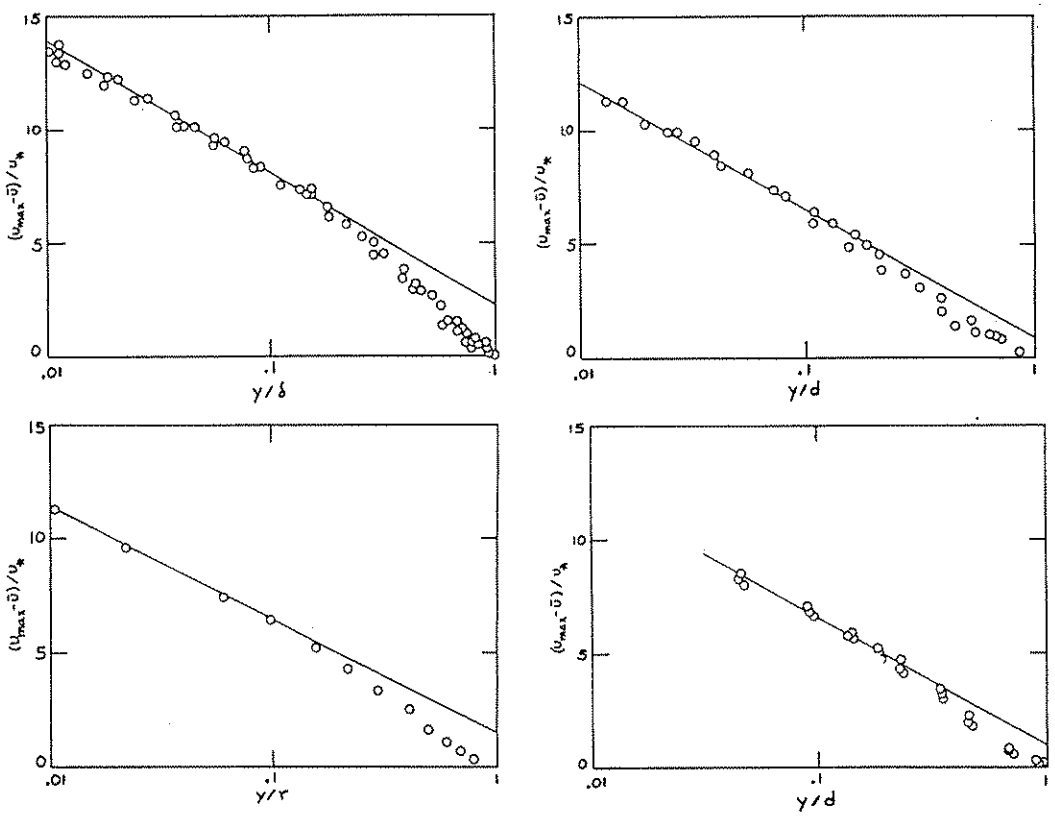

Figure 5.18 Velocity-defect profiles: plots of $(U_s-\overline{u})/u*$ vs. y/d in boundary-layer flows with four geometries: A, flat plate; B, circular pipe; C, wide planar duct; D, open channel. After Monin and Yaglom (1971; various sources) and Coleman (1981). Straight lines with slopes of -A (=-1/κ) are fitted to points for y/d < 0.2.

von Karman's constant. Thus, κ has a value very nearly 0.4. (The reason A is written as 1/κ is historical, not fundamental.) You'll see values other than 0.4 cited, because the accuracy with which A is known is not ideal, being dependent upon fitting measured profiles to the equations. Also, you should expect a weak dependence of κ on the mean-flow Reynolds number. The exact value of κ and its variation with Reynolds number have been controversial (see, for example, Simpson, 1970; Huffman and Bradshaw, 1972). The variation of κ with the concentration of sediment in transport--an even more controversial matter--is discussed in Chapter 6.

Summary on Velocity Profiles

This section summarizes the preceding three sections; you might as well skip it if you're satisfied with what you got out of those sections. If not, then before reading it you might review the earlier section on inner and outer layers.

Remember that we're concentrating on high-Reynolds-number flows over physically smooth surfaces or granular sediment beds

whose size is far smaller than the flow depth. When the bottom is physically smooth, the profile of velocity as a function of distance above the bottom in the inner layer depends on τ_o, ρ, and μ but not on d, so

$$\frac{\bar{u}}{u_*} = f\left(\frac{\rho u_* y}{\mu}\right) \tag{5.39}$$

This relationship, called the law of the wall, is in two parts. In the viscous sublayer adjacent to the bottom, where viscous shear stress predominates over turbulent shear stress, $\bar{u}$ doesn't depend on ρ, so $\bar{u} = f(\tau_o, \mu, y)$, or in dimensionless form, $\mu\bar{u}/\tau_o y = \text{const}$. In terms of u_* and with some rearrangement, this can be written $\bar{u}/u_* = \text{const}(\rho u_* y/\mu)$. The constant here can be shown to be unity by going back to Equation (1.22) for the velocity profile in a laminar open-channel flow and neglecting the quadratic term because y is small near the boundary. Then the law of the wall in the viscous sublayer becomes

$$\frac{\bar{u}}{u_*} = \frac{\rho u_* y}{\mu} \tag{5.40}$$

Equation (5.39) can be specialized for the turbulence-dominated part of the inner layer by use of the fact that $d\bar{u}/dy$ doesn't depend on μ there, because the shear stress and therefore the velocity gradient depends on turbulent rather than viscous momentum exchange. So $d\bar{u}/dy = f(\tau_o, \rho, y)$, or in dimensionless form $(y/u_*)d\bar{u}/dy = A$, where A is a fundamental constant that expresses the nature of the turbulent momentum exchange. Integrating with respect to y,

$$\frac{\bar{u}}{u_*} = A \ln y + A_1 \tag{5.41}$$

where A_1 is a constant of integration. By writing A_1 as $A \ln(\rho u_*/\mu + B)$, Equation (5.41) can be put into the form of the law of the wall, Equation (5.39):

$$\frac{\bar{u}}{u_*} = A \ln \frac{\rho u_* y}{\mu} + B \tag{5.42A}$$

This is the law of the wall for a smooth bottom outside the viscosity-influenced layer adjacent to the bottom. It shouldn't surprise you that μ appears explicitly here, because $\overline{u}$ itself must depend on μ even though $d\overline{u}/dy$ doesn't: the velocity at the base of the turbulence-dominated part of the inner layer depends on the velocity at the top of the viscous sublayer, which in turn depends on μ. With commonly used values for A and B, Equation (5.42A) becomes

$$\frac{\overline{u}}{u_*} = 2.5 \ln \frac{\rho u_* y}{\mu} + 5.1 \qquad (5.42B)$$

For values of $\rho u_* y/\mu$ in an intermediate range of about 5 to 30 the velocity profile grades smoothly from that given by Equation (5.40) to that given by Equation (5.42); this is the region we earlier called the buffer layer.

When the bottom is rough the velocity profile in the inner layer depends not only on τ_o, ρ, μ, and y but also on the size, shape, and arrangement of the roughness elements. Assume that $D \ll d$, so that the distinction between the inner layer and the outer layer is valid in the first place, and assume further that the bottom is covered with rounded and well sorted grains. Then $\overline{u} = f(\tau_o, \rho, \mu, y, D)$, or

$$\frac{\overline{u}}{u_*} = f\left(\frac{\rho u_* y}{\mu}, \frac{\rho u_* D}{\mu}\right) \qquad (5.43)$$

Equation (5.43) is the most general form of the law of the wall for granular-rough boundaries. To see what specific form it takes, we have to worry about two important matters. First, what's the size of the grains relative to the thickness of the viscous sublayer (which is proportional to the viscous length scale $\mu/\rho u_*$)? If the ratio of D to $\mu/\rho u_*$ is very small ($\rho u_* D/\mu$ less than about 5), the grains are embedded in the viscous sublayer and have no effect on the velocity profile. The profile is the same as if the boundary were physically smooth, and the flow is said to be dynamically smooth even though physically rough. But for large values of D relative to $\mu/\rho u_*$ ($\rho u_* D/\mu$ greater than about 60), viscous forces on the boundary are negligible, the velocity profile doesn't depend on μ, and the flow is said to be dynamically rough as well physically rough. In the intermediate range of $\rho u_* D/\mu$, μ can't be neglected, and the flow is said to be transitionally rough.

Second, what's the value of y relative to D? Far above the grains, for $y \gg D$, the turbulence structure depends only on local dynamics, and is independent of the turbulence shed by the

bed grains, whereas for y not much greater than D the velocity profile is strongly influenced by the turbulence shed by the bed grains. So we have to consider the inner layer in two parts. (Even closer to the bed, within a grain diameter or two above the grains, the velocity profile depends on position relative to the individual bed grains.)

High up in the inner layer neither μ nor D affects the velocity gradient $d\overline{u}/dy$. So we can again write $d\overline{u}/dy = f(\tau_o, \rho, y)$ and integrate to obtain Equation (5.41), just as for smooth flow. The constant A is the same, because it expresses the nature of vertical turbulent momentum transport far above the bed, and that's the same as in smooth flow. The constant A_1 is different, however, because it depends on how the velocity profile connects with the boundary, and that's different in smooth and rough flow.

Equation (5.41) can again be put into the form of Equation (5.42A), but now, by comparison with the form of the law of the wall for rough flow (Equation 5.43), B must be a function of $\rho u_* D/\mu$:

$$\frac{\overline{u}}{u_*} = A \ln \frac{\rho u_* y}{\mu} + f\left(\frac{\rho u_* D}{\mu}\right) \qquad (5.44)$$

This can be made more useful by splitting $f(\rho u_* D/\mu)$ into two parts, $-A \ln(\rho u_* D/\mu) + B'$, where B' is just a different function of $\rho u_* D/\mu$. Then Equation (5.44) can be written

$$\frac{\overline{u}}{u_*} = A \ln \frac{y}{D} + B' \qquad (5.45)$$

In fully rough flow B' is a constant, which for a glued-down monolayer of well rounded and almost single-size grains is about 8.5. So the law of the wall for dynamically rough flow over granular-rough boundaries is

$$\frac{\overline{u}}{u_*} = 2.5 \ln \frac{y}{D} + 8.5 \qquad (5.46)$$

Some points about Equation (5.45): (i) B' is different for other roughness geometries owing to differences in sorting and arrangement of surface roughness elements. Commonly the value of 8.5 is nonetheless retained for B', and D is taken to be the fictitious diameter of single-size grains in a uniform monolayer

that makes Equation (5.45) fit the data best. That size is called the equivalent sand roughness k_s. (ii) Equation (5.45) shouldn't be expected to hold outside the inner layer--something like the lowermost 20% of the flow depth--but in both open channels and closed ducts it fits the velocity profile without great error all the way to the free surface or pipe centerline. (iii) For transitionally rough flow the velocity profile is still a semilog straight line outside the near-bed layer of viscous influence, but the equation for the profile is not so simple because B' in Equation (5.45) is a function of the boundary Reynolds number rather than being a constant. (iv) By writing $B' = -A \ln(y_o/D)$ Equation (5.45) can be put into the equivalent form

$$\frac{\bar{u}}{u_*} = A \ln \frac{y}{y_o} \tag{5.47}$$

where y_o is called the roughness length. Like B', y_o is a function of the boundary Reynolds number for transitionally rough flow but is a constant for fully rough flow. For close-packed uniform sand-grain roughness, y_o is found to be approximately D/30.

In the lower part of the inner layer (but above the zone of spatial disunification of the velocity profile within one or two grain diameters above the tops of the grains) the grains should be expected to have an effect on the gradient as well as on the magnitude of the velocity. So $d\bar{u}/dy$ depends not only on τ_o, ρ, and y, as in the outer part of the inner layer, but also on D. In dimensionless form, $(y/u_*)d\bar{u}/dy = f(D/y)$. From the function on the right we can extract the same constant A as before,

$$\frac{d\bar{u}}{dy} = \frac{Au_*}{y} f\left(\frac{D}{y}\right) \tag{5.48}$$

so by comparison with the expression $d\bar{u}/dy = Au_*/y$ obtained by differentiating Equation (5.44) the effect of proximity to the bed grains can be viewed as wrapped up in a multiplicative correction factor f(D/y). Upward from the bed f(D/y) gets smaller and eventually becomes negligible.

The way the correction function f(D/y) is usually handled is to shift the origin for y up or down by trial and error until the profile expressed by Equation (5.45) comes out closest to a semilog straight line. (You might expect the most natural origin to lie somewhere between the tops and bases of the grains, but the best choice is not immediately obvious.) You can look at this from the standpoint of the derivative $d\bar{u}/dy$ in the equation

$$\frac{d\overline{u}}{dy} = \frac{Au_*}{y - y_1} \qquad (5.49)$$

where y_1, called the displacement height or the zero-plane displacement, usually puts the best origin for y a short distance below the tops of grains, something like 25% of the grain diameter. It's shown in the preceding main text that the introduction of y_1 in Equation (5.49) is equivalent to keeping just the linear part of the correction function f(D/y) in Equation (5.48). There seems to be a good physical reason why things work this way: the height y_1 above the origin seems to be the level in the flow at which τ_o appears to act. (Remember that the drag component of τ_o has not only a magnitude but also a line of action.)

Now consider the outer layer. If we look at the velocity relative to that at the free surface we don't have to worry about how the velocity profile is anchored to the bottom through the inner layer. Then the velocity defect $U_s-\overline{u}$, the difference between the velocity at the free surface and that at a distance y above the bottom, shouldn't depend on μ. Neither should it depend on D, so long as $D \ll d$. So $U_s-\overline{u} = f(\tau_o, \rho, y, d)$, or

$$\frac{U_s - \overline{u}}{u_*} = f\left(\frac{y}{d}\right) \qquad (5.50)$$

Equation (5.50) is called the velocity-defect law.

Remember that so long as the mean-flow Reynolds number is large enough there's an overlap layer where the conditions defining the inner and outer layers hold simultaneously. This overlap layer extends upward from the top of the buffer layer to the top of the inner layer, which depending on conditions is 10% to 20% of the way up through the flow. Here the velocity profile given by the wall law and that given by the velocity-defect law must match, because they're equivalent ways of expressing the velocity. A consequence of this matching (see an earlier section for details) is that within the overlap layer the velocity-defect law is of semilogarithmic form with the same constant A:

$$\frac{U_s - \overline{u}}{u_*} = -A \ln\frac{y}{d} + c_1 \qquad (5.51)$$

For this reason the overlap layer is also called the logarithmic

layer. Above the overlap layer the velocity-defect law shouldn't be expected to be logarithmic, although in both pipe flow and open-channel flow the deviations from logarithmic form are not substantial.

Effects of Roughness Height and Spacing

It's in some ways horrifying to sit back and consider that just about everything said so far about velocity profiles is limited to the case of sediment-free flow over close-packed granular roughness whose size is a tiny fraction of the flow depth. Except for threshold of movement on a planar sediment bed, most problems in sediment transport go beyond this limited case: sediment is moved on or above the bed, thereby altering the turbulence structure in certain fundamental but poorly understood ways, and the bed is often molded into bed forms whose dimensions are orders of magnitude larger than the particle size and often a sizable fraction of the flow depth. In these important cases, velocity profiles have not been nearly as well studied. The discussion in this section emphasizes mostly the qualitative effects to be expected as the roughness height increases relative to the flow depth and as the roughness spacing increases relative to roughness height.

Figure 5.19 summarizes the changes in velocity profile as the size of close-packed granular roughness increases relative to flow depth. In Figure 5.19A the sediment is so small (or, more precisely, the roughness Reynolds number $\rho u_* D/\mu$ is so small) that the sediment is embedded in a viscous sublayer, and the flow is dynamically smooth. In Figure 5.19B the sediment is larger and the flow is dynamically rough, but the sediment size is still so small relative to the flow depth that there is a well developed outer layer beyond the overlap layer in which the velocity-defect profile expressed by Equation (5.32) holds but the inner-layer profile expressed by Equation (5.20) does not. These first two cases are covered by the preceding detailed treatment of velocity profiles.

In Figure 5.19C, as the ratio of flow depth to grain size decreases still further, the distinction between inner and outer layers begins to be blurred, and eventually a situation is reached where the entire profile, from bottom to free surface, is affected by the details of the roughness. The whole profile then looks like just the lower part of the wall-law profile in flows with very large values of d/D. This effect begins to become appreciable at d/D values of something like 10 to 15. Fortunately it seems that even in this situation the law of the wall for rough flow represents the velocity profile fairly well through the entire flow depth provided that the origin is adjusted by an appropriate displacement height, as in Equation (5.28), although experimental evidence on this point is scanty.

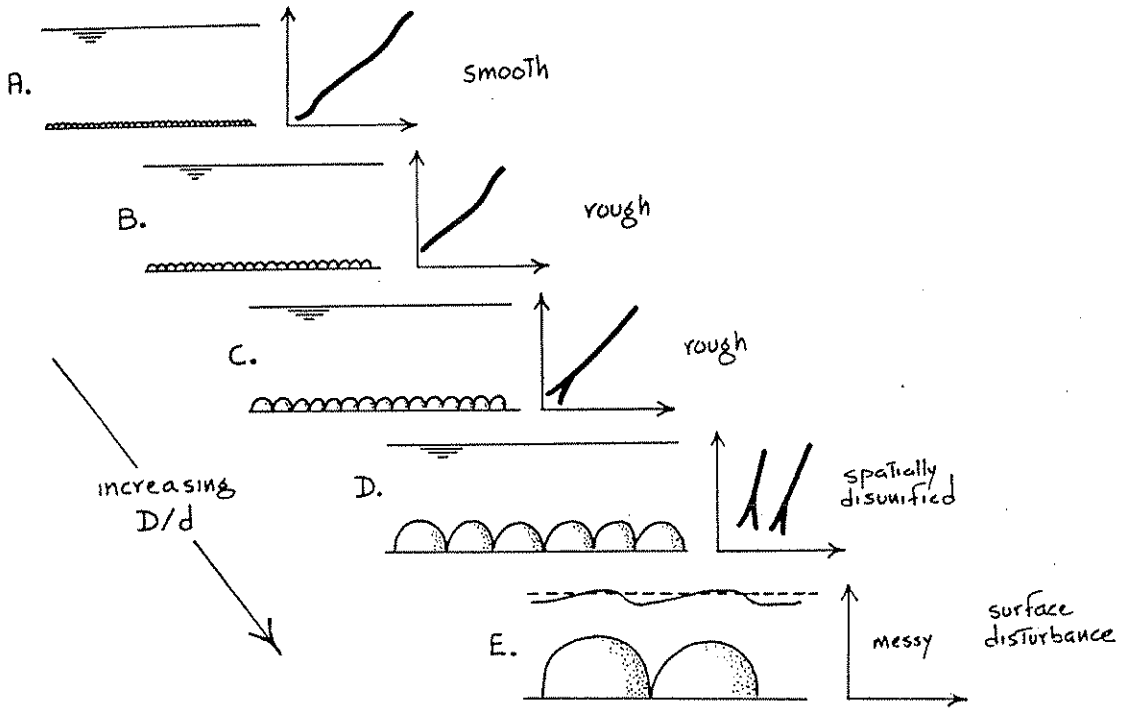

Figure 5.19 Changes in velocity profile as the size of close-packed granular roughness increases relative to flow depth.

As d/D decreases, an increasingly large fraction of the total flow depth is occupied by the zone of the flow (within one or perhaps two grain diameters above the tops of the bed grains) where the velocity profile is spatially disunified in the sense that it varies with position relative to the layout of the grains. As shown in Figure 5.19D in exaggerated form, for d/D values below about 2 or 3 most or all of the velocity profile is spatially variable in this way. It's not well known whether the inner-layer representation of the velocity profile after adjustment by the displacement height breaks down before this stage of total disunification is reached.

What happens as d/D decreases further (Figure 5.19E) depends on the value of the mean-flow Froude number $U/(gD)^{1/2}$. (For full appreciation of this point you'll have to jump ahead to the section on subcritical and supercritical flow in Chapter 7.) For Froude numbers close to or greater than one (i.e., for supercritical or nearly supercritical flow), the free surface is strongly deformed by the presence of the grains just below the surface; think of a shallow fast-flowing mountain stream with a bed of cobbles and boulders. For the same very small d/D but low Froude numbers, however, the grains sit just beneath a relatively placid water surface, or in the extreme case project above the surface as islands.

Figure 5.20 is a cartoon showing the changes in the structure of the flow as the roughness spacing decreases relative to the roughness height. Start with a physically smooth and planar bottom; the flow is dynamically smooth, and y = 0 is naturally taken at the planar bottom. Now take a set of roughness elements whose heights are a very small fraction of the flow depth and begin to place them either randomly or in a regular pattern on the bed. The elements could be three-dimensional bluff bodies or two-dimensional ridges transverse to the flow; the effects are qualitatively the same, at least until the ratio of spacing to height becomes very small.

Provided that the roughness Reynolds number (based on the height of the roughness elements being added) is sufficiently large, each element creates a wake as the flow separates around it. From the discussion of flow separation in Chapter 3 you can see that the flow structure downstream of each roughness element is very complicated: the smooth-flow boundary layer is profoundly modified by the development of a highly turbulent shear layer that extends downstream from the separation point. Downstream from each element the flow gradually readjusts toward the boundary-layer structure that would exist in the absence of roughness; the wakes shed by the elements are said to relax. This readjustment or relaxation takes the form of a new lowest layer of the flow, expanding upward at the expense of the turbulent shear layer, in which a turbulence-dominated wall-law profile is established in just the same way as in a boundary layer growing on a flat plate. It takes a surprisingly large number of element heights downstream, something of the order of a hundred, for the process to be completed, whereupon the local structure of the flow shows no trace of the presence of the roughness element upstream and the wall-law layer extends without interruption from the planar bottom up into the region of the flow far above the level of the tops of the large roughness elements. The case of low roughness Reynolds numbers is of less interest here, because then the elements are embedded in a viscous sublayer, but in that case also a deficit in fluid momentum is created downstream of each element even though the flow doesn't separate, and this deficit is ironed out downstream by viscous shear until the original viscosity-dominated velocity profile is reestablished.

If the roughness elements are sufficiently far apart (Figure 5.20A) each has a long wake extending downstream, but the flow is able to return to normal before it encounters the next roughness element. This is called isolated-roughness flow (Morris, 1955). The velocity profile measured above a given point on the bed depends on the position of that point relative to the wakes behind the elements. You'd have to measure a large number of profiles and average them spatially to obtain a profile that represents the entire flow. Compared with the original smooth-flow profile before emplacement of any roughness elements, the spatially averaged profile shows a deficit of velocity within one or two roughness heights of the bed.

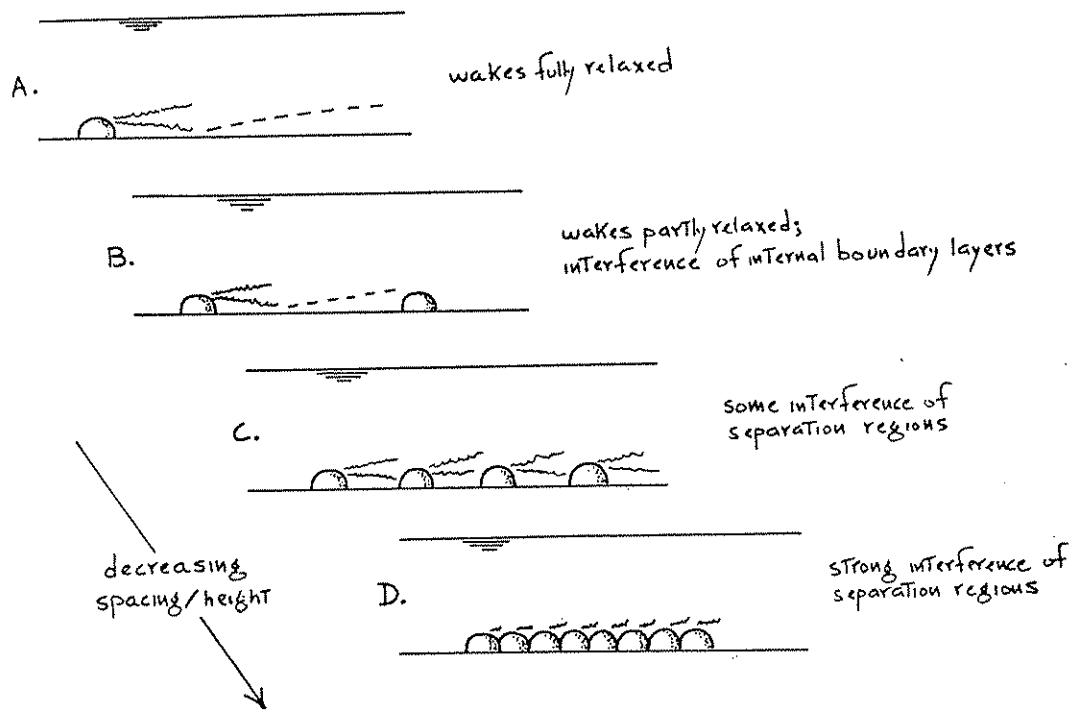

Figure 5.20 Changes in flow structure as roughness spacing decreases relative to roughness height.

The spatially averaged boundary shear stress τ_o is still dominantly viscous, as in the absence of roughness elements, but the contribution of pressure drag to τ_o increases with the roughness density. The flow could now be termed transitionally rough, although in a rather different sense from the use of that term in flow over close-packed roughness in earlier sections. Note also that the original flow, before emplacement of roughness elements, can itself be dynamically rough, if the bottom is covered with close-packed roughness that's much smaller than the large, isolated roughness we're adding. Then τ_o is dominated by pressure drag from the start, but this pressure drag is of two parts: a spatially uniform part produced by the underlying small and close-packed roughness, and a spatially nonuniform part produced by the large and isolated roughness. It takes only a low density of large roughness elements for their contribution to the pressure drag to outweigh that of the close-packed elements.

As we continue to add large roughness elements a point is reached where the wakes shed by the elements do not relax completely before encountering another roughness element downstream, and with some further increase in density most points in the near-bed flow are within wakes in various stages of relaxation (Figure 5.20B). Now there's no point on the bed that shows the relatively simple velocity profile of the original

smooth flow without roughness elements. This kind of flow is called wake-interference flow (Morris, 1955). Again you would have to take a large number of local velocity profiles and spatially average them to get a profile representative of the entire bed. Because most of the area of the bed is overlain by reattached and relaxing wakes, the spatially averaged profile shows two distinct segments: one, adjacent to the bed and extending upward for some fraction of the roughness height, represents the spatial average of the local wall-law profiles in the relaxing wakes, and the other, starting well above the tops of the large roughness elements and extending far above, represents the wall law above the zone in which the upward-diffusing wake turbulence blends into a spatially uniform layer--the case we treated at length in the earlier part of this chapter. These two distinctive parts of the profile tend to plot as semilog straight lines with a transition at heights somewhat below to somewhat above the tops of the roughness elements. See Nowell and Church (1979) for a good example. As the roughness spacing decreases, the height of the y = 0 level for the overall wall-law profile above the tops of the roughness elements rises higher and higher above the planar bottom.

With increasing roughness density, eventually most of the area of the bed between roughness elements is overlain by the parts of the wakes that lie upstream rather than downstream of reattachment (Figure 5.20C,D); this condition sets in when the ratio of roughness spacing to roughness height is of the order of ten or less. Well before this stage the lower straight-line segment of the spatially averaged velocity profile loses its distinctive character. The turbulent shear layers downstream of loci of separation then impinge mostly upon the surfaces of roughness elements downstream rather than on the planar bottom; viscous shear stresses on the planar bottom are almost nonexistent, and the geometry of the bottom in the areas between the roughness elements is irrelevant to the dynamics of the flow. For three-dimensional granular roughness this condition is maintained with no qualitative change as the elements become so closely spaced that their bases are touching--a good approximation to the condition of a loose granular bed treated in detail earlier. If the roughness consists of transverse ridges, however, the ratio of spacing to height can continue to decrease toward zero, and as it becomes smaller than about one the flow skims across the crests of the ridges and drives a circulation of stable vortices located in the deep and narrow troughs between the ridges; this is called skimming flow (Morris, 1955), and is not as important for our sedimentological purposes as the other kinds of flow.

Field Measurements

There have been few detailed studies of velocity and turbulence in large-scale natural flows, though innumerable routine determinations of velocity have been made in rivers in

order to establish the local relationship between stage (depth) and discharge. Most routine measurements are made using a propeller current meter lowered from a boat or a bridge. Each determination of velocity represents a value averaged over about 10-30 s, and the entire profile is measured over a period of a few minutes. Such data are not the most suitable to compare with measurements made under much more highly controlled conditions in the laboratory, and so there have been few attempts to test the supposition that results obtained in the laboratory with depths in the decimeter range can be extrapolated to flows in nature with depths in the range of meters or tens of meters.

One exception is a study made by the U.S. Geological Survey in the Columbia River (Savini and Bodhaine, 1971). In this study an array of ten equally spaced current meters on a rigid frame was used to make an accurate determination of the velocity profile at several sections of the river, and determinations were made at a single profiling point for periods of up to 66 minutes, with readings taken simultaneously from all ten current meters every minute. In the reaches studied, the flow was controlled by dams and was steady and nearly uniform. The bed was composed of lag gravel that was not moving when the measurements were made. There were therefore few complications in the flow attributable to bed forms, moving bed load, or high concentrations of suspended sediment. As far as is possible in the natural environment, therefore, conditions were ideal for comparison of natural velocity profiles with profiles determined over fixed rough beds in the laboratory. The only major deficiencies in the data are that measurements could not be made closer than 0.5 feet above the bed, and it was difficult to determine accurately the height of the lowest current meter above the bed. But neither of these is really a problem: as for the first point, 0.5 feet is of the same order as the diameter of the bed gravel, and as for the second, we should expect to have to juggle the origin up or down anyway to obtain the best straight-line semilog profile.

Results for the 66 minute profile are shown in Figures 5.21 and 5.22. If the depth-velocity data are plotted as reported, there is a definite departure from a logarithmic profile, but the data can be made to conform to a logarithmic velocity profile by adjusting the zero level to 16 cm below the bed level as recorded in the field. It is these adjusted data that are shown in Figure 5.21. The velocity data averaged over 66 minutes do conform very closely to the predicted logarithmic distribution.

This is not true, however, for any profile averaged over only one minute. Individual profiles show large deviations from logarithmic, and the deviations persist from one reading to the next for periods of several minutes. Such deviations are characteristic of field measurements made in deep rivers (for another example, see a study of the Mississippi River by Scott and Stephens, 1966) and are generally attributed to a combination of imprecision in positioning of the current meter, influence of large bed forms, and the effects of large-scale turbulence. In

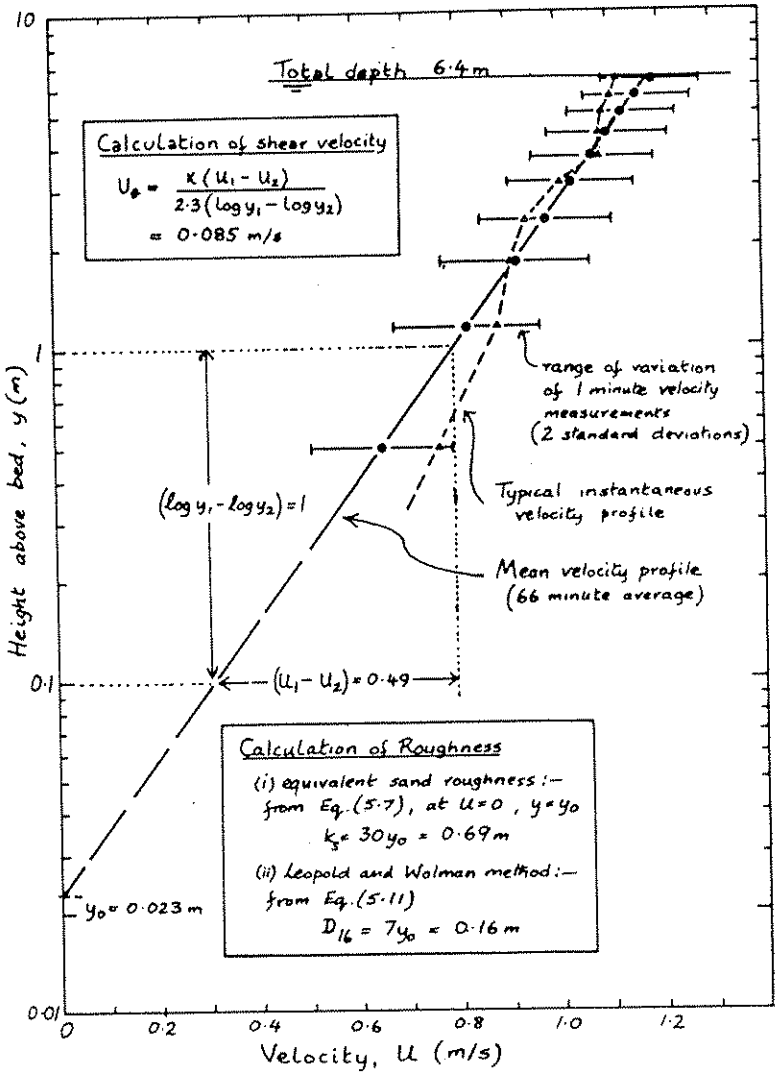

Figure 5.21 Velocity profile measured using an array of ten current meters in the Columbia River. Data from Savini and Bodhaine (1971). See text for discussion.

the case of the Columbia River measurements, however, it is clear that large-scale turbulence or eddies are the only reasonable explanation. The average velocity at this profile was about 1.0 m/s, and the depth and width of the river were 6.4 m and about 300 m, respectively. It can therefore be calculated that the largest eddies rotating about horizontal axes would move past a given current meter in about 5-10 seconds, and that the largest eddies rotating about vertical axes would move past in about 5-10 minutes. Thus this series of measurements points to the existence in wide rivers of eddies that rotate about vertical axes and have dimensions of the same order as the width of the river. In a

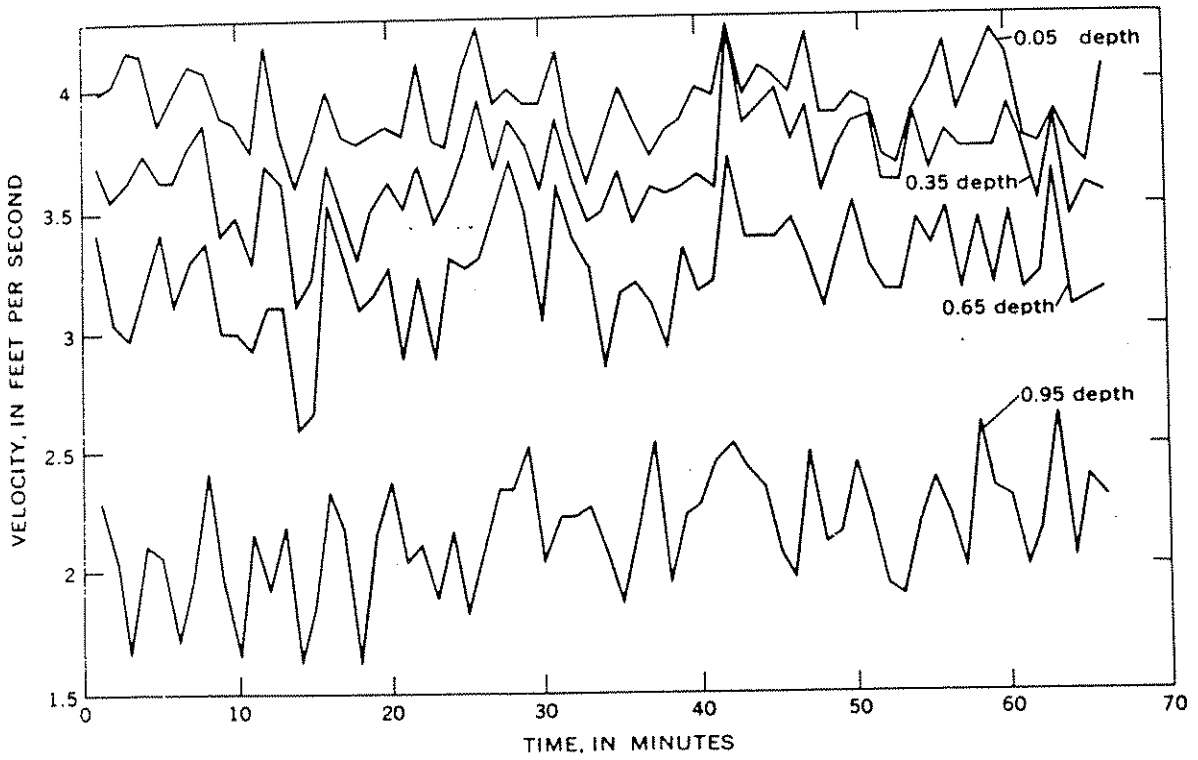

Figure 5.22 Fluctuation in velocity with time at four different depths measured at a single station in the Columbia River. From Savini and Bodhaine (1971, p. F20).

flume 1 m wide, operating at average velocities of the order of 0.5 m/s, precise measurements of the average velocity at a station can be obtained by averaging velocities observed for a period of about five seconds, but in a large river or tidal channel, for equivalent precision observations would have to be extended over a period of ten minutes or more--which is generally completely impractical.

A more significant matter in practice than the determination of the average velocity at a particular depth is the determination of the average velocity for the entire section, and the determination of the shear velocity u* from the measured velocity profile. For the measured section of the Columbia River the average velocity determined from all 66 profiles is 1.006 m/s. Average velocities determined from individual measured profiles varies from 0.851 m/s to 1.138 m/s (standard deviation 0.052). The coefficient of variation of about 5% is quite acceptable for field measurements. Shear velocities determined from individual profiles by linear regression of velocity on the logarithm of depth, however, show a much greater range of variation. The shear

velocity determined from the 66-minute average is 8.45 cm/s, but the shear velocity determined from individual profiles varies from 7 cm/s to more than 12 cm/s. The coefficient of variation is about 15%. The moral is that even under ideal field conditions it is much easier to obtain an accurate determination of average velocity than of shear velocity. In rivers, determination of shear velocity averaged over a reach is generally made from the average depth and slope (using Equation 1.17), but accurate determination of slope is also difficult, and the method cannot be used for other natural flows like tidal currents.

The hydraulic roughness can be determined from a measured velocity profile by making use of Equation (5.20). Because the numerical constants in this equation are those experimentally determined for sand grains glued to the wall of the channel, the value of k_s determined is unlikely to correspond closely to size of gravel (or height of bed forms) on the bed of a natural river channel. A number of authors have tried to use the available data on natural gravel-bed rivers to develop a form of Equation (5.20) that is more directly related to observed natural roughness. One such equation, that of Leopold and Wolman (see Leopold et al., 1964, p. 160), can be written

$$\frac{\bar{u}}{u_*} = 6 \log \frac{y}{D_{16}} + 5 \qquad (5.52)$$

Leopold and Wolman found that the roughness was mainly related to the size of the larger gravel clasts, so in Equation (5.52) the roughness is measured by D_{16}, the diameter exceeded by only 16% of the clasts.

Comparing the application of Equations (5.20) and (5.52) to the Columbia River data, we find that the equivalent sand roughness (from Equation 5.20) is 0.69 m, whereas the D_{16} value (from Equation 5.52) is 0.16 m. In fact, Savini and Bodhaine (1971) record that at this section of the Columbia River the measured maximum and mean sizes of the gravel on the bed were 0.28 m and 0.09 m, respectively, indicating an excellent agreement with the prediction from the formula given by Leopold and Wolman.

Once again it must be pointed out that determination of the hydraulic roughness from a single measured velocity profile in a large natural flow is likely to give highly inaccurate results. For example, the average of many individual determinations of equivalent sand roughness for the Columbia River data is 1.4 m, twice the value based upon the long-time-average velocity profile, and the coefficient of variation of values determined from single profiles is 60%.

CHAPTER 6. DYNAMICS OF SEDIMENT MOVEMENT

INTRODUCTION

Now that we have investigated the nature of fluid motions close to a solid boundary we can go on to consider how these motions affect a boundary composed of movable grains of sediment. The simplest case to investigate is the beginning of sediment movement--at this point, just before sediment has started to move, there is no reason why the concepts of "rigid-boundary hydraulics" should not be applied. This case is also important geologically, because it defines the flow conditions necessary to just move the largest grains present in a given deposit. Of course, the flow may actually have been stronger than that necessary to move the largest grains present, because other factors (e.g., availability) may limit the largest size of grains present--but at least we should be able to determine a minimum strength of flow required for a given clastic sediment.

As soon as sediment starts to move over the bed, everything becomes much more complicated. Grains may be moved not only by the fluid motion but also by being struck by other grains. When a large number of grains are moving, the nature of fluid motion close to the bed may be significantly altered. There may be important interactions between moving grains. Grains are locally piled up and scoured, to form bed configurations that further interact with the flow to change the pattern of sediment movement (Chapter 7).

To avoid some of these complications we will consider first some experimental results for a highly oversimplified case: the movement of a single grain over a bed composed of grains that have been fastened to the bed. These experiments provide some insight into the nature of particle movement, and what flow conditions are necessary, for example, to change particle motion from rolling or hopping close to the bed, to longer flights in which the particle is held up by fluid turbulence. We go on to consider some other important effects in the movement of grains near the bed, especially saltation.

We end this chapter with some considerations on the theory of sediment in suspension, and the complications that arise in trying to apply this theory to natural flows. And finally, we enquire whether the insights gained can be applied to the interpretation of sedimentary textures, particularly to the vexed question of grain-size distributions.

FORCES ACTING ON A PARTICLE IN THE BED

Introduction

We begin by considering the forces acting on a single grain located at the bed surface. Assuming that the sediment is

cohesionless, the forces are of two opposed kinds: those tending to hold the grain in place (the submerged weight of the grain), and those tending to lift, roll, or slide the grain out of its position in the bed (forces of fluid lift and drag). We note at once that both types of forces are highly variable, even in the simplest case observed in nature: steady uniform flow over a flat bed composed of well sorted grains.

The different kinds of fluid forces (lift and drag) combine to produce a resultant that acts downstream and at some angle to the bed. This resultant force can move the grain in one of three ways: (i) by lifting the grain off the grains beneath it, (ii) by sliding the grain along some path of "easiest movement" over the grains (i.e., downstream of it), or (iii) by rotating the grain about some "pivot" formed by one or two of the grains in the bed (Figure 6.1). In the first case the grain must rise up rather steeply from the bed, so lift forces must be at least as important as drag forces. In the second case the balance is between the component of fluid force acting upwards in the direction of easiest movement, on the one hand, and the component of gravity and the frictional force, acting in the opposite direction. In the third case the balance is between the moments of fluid forces tending to rotate the grain in the downflow direction, and the moment of gravity force tending to hold the grain in place in the bed. This third case has generally been considered to be the most realistic one, but analysis of either the second or third case leads to approximately the same conclusions, except for the different coefficients.

The gravity force acts through the center of gravity (C.G. in Fig. 6.1), but the position of the pivot and the direction of easiest movement vary greatly from grain to grain because of differences in size and shape of the grains and in local packing of the grains. The fluid force does not necessarily act through the center of gravity of the grain: in fact it may be expected to act through some point above the center of gravity, because the upper part of the grain is more exposed to fluid forces than the lower part. Furthermore, the fluid forces vary from grain to grain, being strongest for the most exposed grains, and they also fluctuate with time because of turbulent motions even within the viscous sublayer of a flow with steady time-average velocity. So it should be clear that any criterion that we can establish for the beginning of sediment movement will not be completely deterministic, but will be stochastic (statistical). Experimental investigations must be carefully designed to take this fact into account: in particular, by a careful statistical definition of exactly what is meant by the beginning of sediment movement.

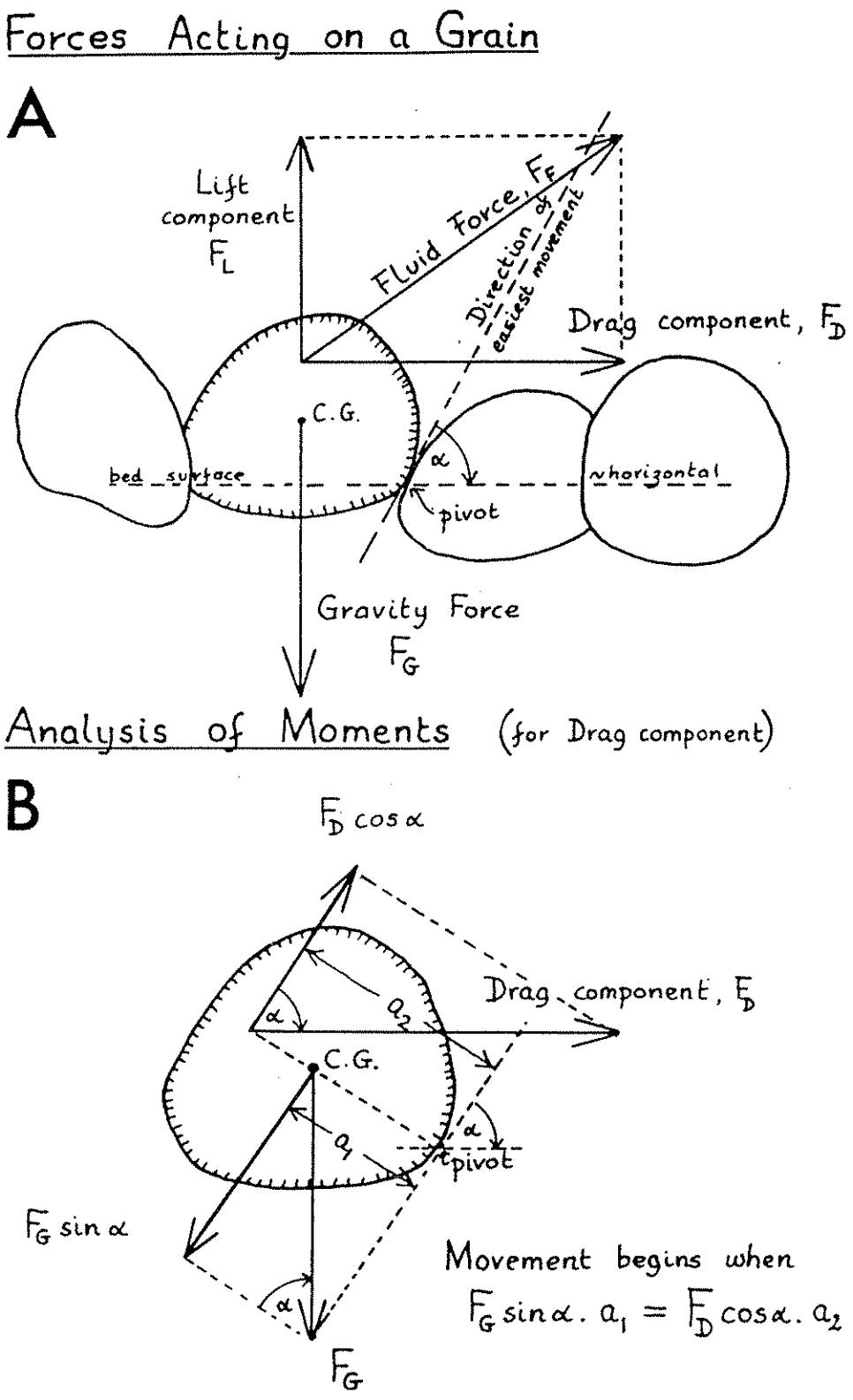

Figure 6.1 (A) Forces acting on a grain resting on a bed of similar grains. (B) Analysis of moments acting on a grain at the beginning of grain movement.

Gravity Force

The total gravity force acting on a grain is the volume times the submerged specific weight $\gamma_s-\gamma$. If D_n is the nominal diameter, the volume is $(\pi/6)D_n^3$, so the total gravity force F_G is

$$F_G = (\pi/6)\ D_n^3(\gamma_s-\gamma) \qquad (6.1)$$

The part of this force that opposes sliding of the grain in the direction of easiest movement is $F_G\sin\alpha$, where α is the angle that the direction of easiest movement makes with the horizontal (Figure 6.1). When sliding begins, this angle is determined not only by the geometry of the grains but also by their frictional characteristics.

Frictional Forces

In most published theoretical analyses of grain motion, friction between grains is not considered explicitly, but its effect is considered to be accounted for by the value chosen for α. The problem is analogous to that of the angle of repose of sands (for a review, see Statham, 1977): the surface of a sand slope can be built up only to a certain limiting angle, called the angle of initial yield. Beyond this angle, the downslope component of gravity forces acting on a surface layer of sand exceeds the resistance offered by a combination of frictional forces and "upslope" components of gravity that result from the interaction of the weight and geometry of the grains.

It is generally assumed that the angle α is the same as the angle of initial yield of a sand slope immersed in water, which for a typical sand is about 35° (it is less for spheres, more for highly angular materials; Carrigy, 1970). Miller and Byrne (1966) pointed out that the angle of repose for a single grain on a fixed bed composed of other grains is not necessarily (or generally) the same as the mass angle of repose assumed by a pile of grains. The angle for a single grain on a fixed bed of similar grains is larger, being in the range of 45° to 70° depending on sphericity and roundness (smaller values for more spherical and more rounded grains) and on sorting (smaller values for better sorted grains). That these larger values are in fact applicable to the beginning of grain movement has been confirmed experimentally by Fernandez Luque (1974; see also Abbott and Francis, 1977). For grains smaller than the average size in the (fixed) bed the angle is larger, and for grains larger than those in the bed the angle is smaller. The low value for grains larger than the average for the bed suggests the possibility that larger-than-average grains may actually be the easiest to move.

Fluid Forces

Fluid forces acting on a grain resting on the bed are of two kinds: (i) those due to viscous drag, acting mainly on the upper, exposed surface of the grain; and (ii) those due to the unequal distribution of dynamic pressure on the grain surface. Viscous forces are likely to be important at low boundary Reynolds numbers, $u_*D/\nu < 5$ (Figure 6.2).

It is convenient to distinguish two components of the fluid force, whatever its ultimate origin: drag (in the strict sense) acting parallel to the flow, and therefore parallel to the bed, and lift acting normal to the bed.

The drag force is relatively easy to understand: the principle is the same as for the drag forces considered in our discussion of settling in Chapter 2 and flow resistance in

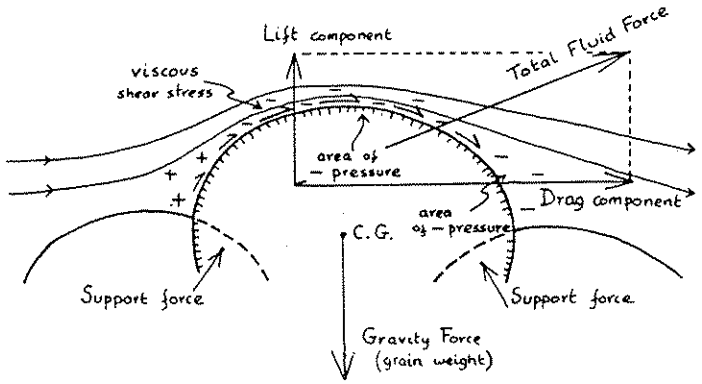

Figure 6.2 Forces acting on a grain at low boundary Reynolds numbers. The grain is enclosed in the viscous subiayer, and the velocities are locally small enough that there is no turbulent wake. Viscous drag is an important component of the total drag. Lift forces due to unequal pressure distribution are probably smaller than at larger Reynolds numbers. The resultant force acts along a line well above the center of gravity (C.G.). Plus and minus signs schematically indicate higher and lower pressures, respectively (not the actual sign of the pressure).

Chapter 5, except that there is the complication that not all parts of the cross section of the grain are equally exposed to the flow, because the lower part is somewhat shielded by the grains upstream. There are the further complications that the flow near the bed is characterized by a strong velocity gradient, and that flat grains may take up an imbricated orientation oblique to the flow. Thus, if we try to apply the usual drag equation (Equation 1.8),

$$F_D = C_D(\rho U^2/2)A$$

we have the problem that we do not know exactly what to choose as the drag coefficient C_D, as the "characteristic" velocity U, or as the "exposed" cross-sectional area A. Nevertheless, we expect that the same type of equation will hold, that the drag coefficient will be proportional to the conventional coefficient and will vary with Reynolds number in about the same way; Coleman (1967) has shown that this is in fact the case for a sphere resting on a bed of spheres. We also expect that the characteristic velocity will be some velocity close to the bed, which might perhaps be proportional to the shear velocity, and that the "exposed" area will be less than, but proportional to, the total cross-sectional area of the particle.

Our experience with settling further leads us to expect that it may be useful to distinguish between two different regimes: one characterized by relatively low boundary Reynolds numbers ($u*D/\nu < 5$), and therefore by grains entirely enclosed by essentially laminar flow in the viscous sublayer, with little or no flow separation behind the grains (Figure 6.2), and the other characterized by relatively high boundary Reynolds numbers, and therefore by grains that project up into the turbulent flow and produce a turbulent wake themselves (Figure 6.3). In the first case the drag coefficient and therefore the drag might be proportional to the boundary Reynolds number, and in the second case it might be almost independent of the boundary Reynolds number, especially in the range $u*D/\nu > 60$.

We saw in Chapter 4 that the lift force arises because of the asymmetry of flow around a grain resting on the bed. Because higher fluid velocities are developed over the top of the grain than underneath it, there is also an asymmetrical pressure distribution, with higher pressures on the lower surface of the grain (acting upward) than on the upper surface of the grain (acting downward); this results in a net upward lift force. We expect therefore that lift forces cannot act on grains that are freely suspended in a fluid, because flow around such particles is symmetrical about the line of flow, or almost so.

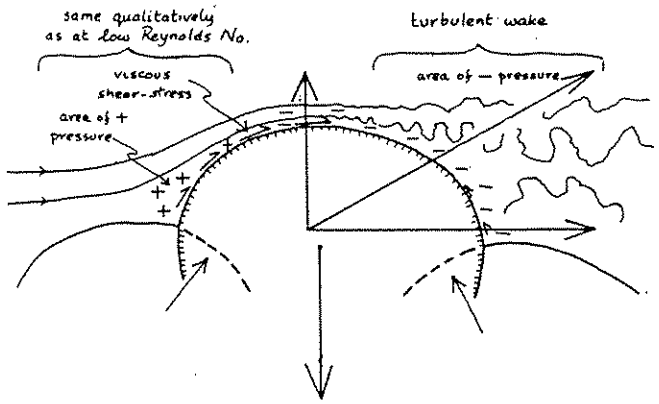

Figure 6.3 Forces acting on a grain at transitional boundary Reynolds numbers. The grain is still partly enclosed in the viscous sublayer, but local velocities are large enough to produce a turbulent wake behind the more exposed grains. Viscous drag and pressure distribution around the front of the grain differ little from those found at low Reynolds numbers, but viscous drag is very small in the turbulent wake. Lift forces approach 0.8 times the magnitude of the drag forces. The resultant force acts through, or close to, the center of gravity (C.G.). Significance of plus and minus signs is the same as in Figure 6.2.

The existence of the lift force and the fact that it decreases very rapidly as a grain rises up above the bed was verified experimentally by Chepil (1961) and by Willetts and Murray (1981). Chepil used a wind tunnel to measure the pressure distribution over the surface of spheres 0.3 to 5.1 cm in diameter embedded in, or suspended at, various heights over a gravel surface. The gravel surface was dynamically

fully rough, and flow over the surface produced a logarithmic velocity distribution with shear velocities ranging from 75 to 188 cm/s. A graphical summary of the results is shown in Figure 6.4. At zero height above the bed, lift was equal to about 80% of drag, but it decreased rapidly with height and disappeared virtually completely when the sphere was raised just a few sphere heights above the bed.

Willetts and Murray (1981) measured forces acting on a sphere in a wind and water tunnel using strain gauges. They observed large lift forces when the sphere was in contact with the wall, and when the gap was between 0.1 and 0.2 diameters wide. But negative lift forces (i.e., directed towards the wall) were observed at both smaller and larger gaps.

The lift force can be calculated for a few highly simplified cases. For example, a solution was obtained by Jeffreys (1929) for the case of irrotational inviscid flow around a cylinder lying on a plane surface with the axis normal to the flow. Figure 4.9 shows the calculated streamlines and pressure distribution for this case. The flow is symmetrical about the vertical plane (there is no flow separation because there is no viscosity) so theoretically there is no drag component in this case. It might be thought that this is so far removed from reality that the analysis can have no possible application to real fluids and grains, but this is not so. Although real fluids have viscosity, the inviscid-flow solution may be quite close to the truth for the case of very rapid fluid acceleration--as, for example, is produced by a turbulent eddy striking the bed.

The equation given by Jeffreys for the lift force (per unit length of the cylinder) is shown in Figure 4.9. We expect that for a given spherical grain the lift force will be given by an equation of the same general form as for the drag force:

$$F_L = C_L(\rho U^2/2)A$$

(In the case of unit length of a cylinder, A = D; in the case of a sphere, $A = \pi D^2/4$.) To get the resultant force on the grain we would simply add F_D and F_L vectorially. The question now is: How do we experimentally evaluate the coefficients of drag and lift?

Experimental Evaluation of Lift and Drag Coefficients

In the case of a hydrodynamically rough bed, for which viscous drag may be neglected, the drag and lift forces may be evaluated by measuring the pressure distribution over the grain surface, as was done by Chepil (1961). One of the earliest investigations of this kind was by Einstein and El-Samni (1949); we will review their work first, before returning to the work of Chepil and other more recent investigators, because their study led to the

development of several concepts used by Einstein and later workers in their theories of bed-load movement.

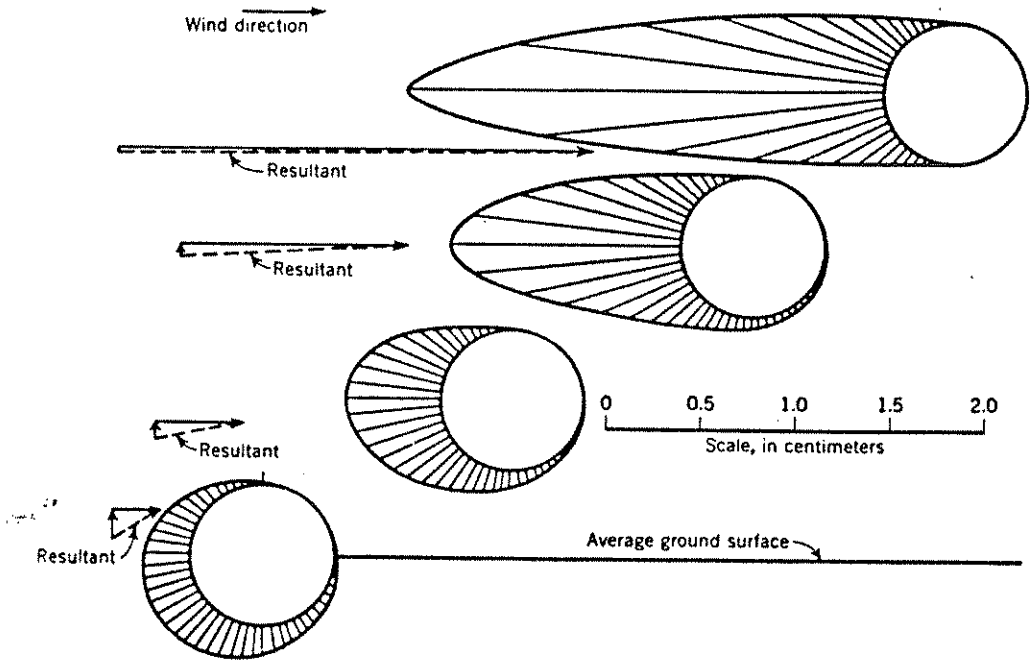

Figure 6.4 Pressure distribution over the surface of a sphere on or close to a rough surface (from Chepil, 1961). Reproduced from Soil Science Society of America Proceedings 25 (1961), p. 345, by permission of the Soil Science Society of America.

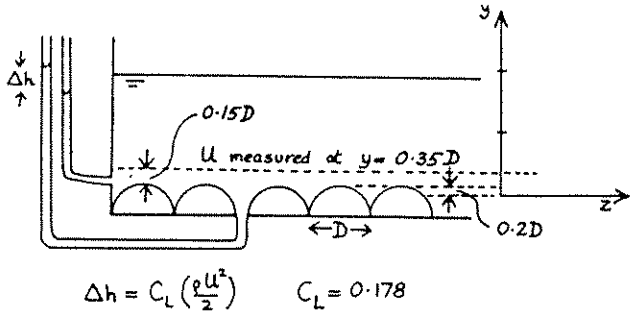

Figure 6.5 Experiments on hemispheres by Einstein and El-Samni (1949).

Einstein and El-Samni (1949) constructed an artificial bed composed of hemispheres 6.9 cm in diameter (Figure 6.5). The magnitude of the lift force was determined by means of pressure taps at the top and sides of hemispheres, from the relationship

$$\rho g \Delta h = C_L(\rho U^2/2)$$

where $\rho g \Delta h$ is the pressure difference between the top and sides of a hemisphere. As noted above, a problem arises about which value of U to use, as U is a function of height above the bed. Einstein and El-Samni found by trial and error that only one value of U gave a constant value for C_D: that measured at a height 0.15D above the tops of the hemispheres. A similar problem arises about where to define the "mean bed level"; in this case, Einstein and El-Samni found that velocity profiles were fitted by a logarithmic law only if height above the bed was measured from a level 0.20D below the tops of the hemispheres. So the value for U used in the lift equation is the value for y = (0.15 + 0.20)D = 0.35D. The experimentally determined value for C_L was 0.178.

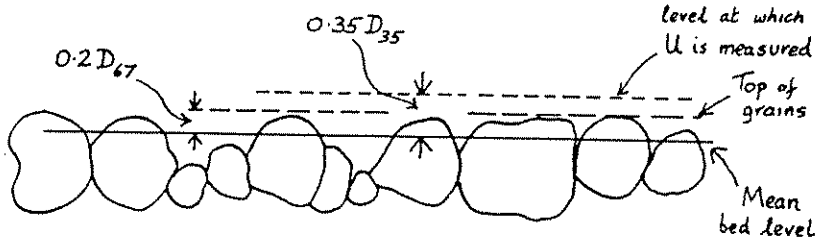

Figure 6.6 Experiments on natural grains by Einstein and El-Samni (1949).

These values for hemispheres were then compared with those for a natural gravel (Figure 6.6). Velocity plots indicated that the bed level should be taken at a level 0.12 cm below the tops of the gravel. Assuming that this is 0.2D, as for hemispheres, it was found that the value for D corresponds to the 67 percentile of the size distribution of the gravel (i.e, 67% of the gravel was finer than this). The lift coefficient was again found to be equal to 0.178 if U was chosen 0.35D above the mean bed level as defined above--but in this case the correct value was given only if D was chosen as the 35 percentile. These results explain why these particular percentiles were chosen by Einstein (1950) in developing his theories of bed-load movement.

We may note that these results indicate that for rough boundaries the correct velocity to use in the lift equation is directly proportional to the shear velocity. Making use of Equation (5.20),

$$\frac{\overline{u}}{u_*} = 5.75 \log_{10} \frac{y}{k_s} + 8.5 \qquad (6.2)$$

and setting $y = 0.35k_s$ (for a plane bed of well sorted sand grains, $D = k_s$) we obtain

$$\bar{u}_{0.35D} = (5.75 \log_{10} 0.35 + 8.5)u*$$

$$\approx 6u* \qquad (6.3)$$

Similar experiments have been performed by Chepil (1958, 1961), Coleman (1967), and Cheng and Clyde (1972, in Shen 1972), and the results have been reviewed by Benedict and Christensen (1972, in Shen, 1972). Chepil measured the pressure at many points over the surface of the hemisphere and determined the lift from those measurements by vector summation, a method more accurate than that used by Einstein and El-Samni. He showed that the method used by Einstein and El-Samni gave values for C_L that were larger than the true value, which in his experiments was 0.068. Chepil found that the ratio of lift to drag was about 0.8, but Cheng and Clyde found a larger value of about 2; possibly this is a result of different experimental bed configurations, as Chepil used hemispheres spaced 3 diameters apart whereas Cheng and Clyde used closely packed hemispheres (and measured forces using strain gauges). For isolated hemispheres on a plane boundary Flachsbart (1927) found that C_L/C_D was about 1.5. All of these experiments were run at high boundary Reynolds numbers, and it was found that the lift coefficient is not a strong function of Reynolds number within that range. Coleman (1967, 1977) and Coleman and Ellis (1976) measured the drag and lift coefficients for a single sphere resting on, or rolling past, a bed of similar close-packed spheres. They investigated a wide range of Reynolds numbers spanning the transition from laminar to fully turbulent flow at the boundary. For fully turbulent flow at the boundary, Einstein and El-Samni found that the zero velocity level was at 0.2D below the tops of the grains. From solid geometry, the elevation of the center of a sphere resting on close-packed spheres is 0.52D above this level, and Coleman and Ellis found that the velocity at this level was given by

$$\bar{u}_{0.52D} = 7.5u* \qquad ((6.4)$$

For low Reynolds numbers this velocity is not directly proportional to the shear velocity, but the ratio of the two, $\bar{u}/u*$, is proportional to the square root of a Reynolds number uD/ν defined on u. Drag and lift coefficients also vary with this Reynolds number. The drag coefficient varies in much the same way for a settling sphere (i.e., as shown in Figure 4.1) except that the curve is displaced slightly upwards. In other words, for equivalent Reynolds numbers the drag coefficient for a sphere resting on a boundary is slightly larger than that for a falling sphere.

Coleman (1967) reported that the lift coefficient actually becomes negative at low Reynolds numbers (i.e., laminar flows tend to press the sphere down onto the bed). This result was confirmed by Davies and Samad (1978), who suggested that the negative lift was due to flow beneath the sphere. Such flow is easier when a sphere rests on a bed of spheres than when it rests on a plane bed, and Davies and Samad found that negative lift was stronger in the former case. At high Reynolds numbers such negative lift is not observed, presumably because of the stronger velocity gradient close to the bed. At Reynolds numbers of 3,000-50,000 Willetts and Murray (1981) did not observe negative lift when a sphere was in contact with a plane wall, but they did observe it when the separation of the sphere from the wall was either very small (about 0.05 diameters) or larger than 0.2 diameters. It seems clear from these results that the exact geometry of the boundary, the separation of the grain from the wall, the Reynolds number, and probably also the roughness of the grain surfaces (cf. Willetts and Murray, 1981) may all have important effects on the relative magnitude of the lift and drag forces.

Another matter investigated in some of these experiments was the nature of the statistical variation in lift and drag forces. Most investigators have found that there is a close approach to a Normal distribution of both lift and drag. Cheng and Clyde reported that the coefficient of variation for lift (root mean square of lift divided by mean lift) was about 0.18 and independent of hydraulic conditions (depth and slope). They, and also other investigators, have found that the coefficient of variation for drag is somewhat larger and varies with Reynolds number.

As lift and drag forces fluctuate, some grains actually vibrate up and down in place. Cobbles on a stream bed might be abraded by this mechanism, as well as by rolling during transport (Schumm and Stevens, 1973).

INITIATION OF MOVEMENT

Balance of Forces

Grains begin to move on the bed when the combined lift and drag forces produced by the fluid become large enough to counteract the gravity and frictional forces that hold the grain in place. As we have seen, it is impossible to define the balance of forces or moments acting on grains uniquely for all grains: some grains lie in positions from which they are more easily lifted, slid, or rolled than others. It is equally impossible to define a single fluid force that applies to all grains: some grains are more exposed to the flow and subjected to larger fluid forces than other grains, and the fluid forces at the bed fluctuate with time because of turbulence in the flow. We begin by considering an average grain, in an average position on the bed, subjected to an average fluid force; we will return later to the problem of an appropriate definition of these averages.

To further simplify matters, we assume that friction prevents sliding of one grain past another and that the moving grain simply pivots about an axis normal to the flow direction. (Comparable theoretical analyses are given by Vanoni, 1975, p. 92-93, and by Helley, 1969.) The condition for the beginning of motion (Figure 6.1) is that the moments tending to rotate the grain downstream are just balanced by the moments (in the opposite sense) that tend to hold the grain in place.

To determine the fluid-force moment exactly we would have to sum all the products of the various kinds of fluid forces acting on the grain (e.g., lift and drag) times their normal distances from the lines of action to the pivot axis. We can simplify further by assuming that the bed is horizontal and by considering, at first, only drag forces. Then it is convenient to consider only those components of the gravity and drag forces that act normal to the line joining the pivot to the center of gravity of the grain. The total moment produced by summing body forces (like the gravity forces acting on each element of volume making up the grain) is the same as the total force, times the distance of the center of gravity from the pivot. We can readily see that if we divide the gravity force into two components, normal to and parallel to the line joining the pivot to the center of gravity, then the moment due to the second of these components must be equal to zero, as that component has a line of action passing through the pivot itself.

Let us write the condition for the beginning of movement as

$$a_1(F_G \sin\alpha) = a_2(F_D \cos\alpha) \qquad (6.5)$$

The left side of this equation is therefore the total moment due to gravity, and tends to rotate the grain upstream about the pivot, or to hold it in place against the moment due to fluid drag forces tending to rotate the grain downstream. The right side of the equation represents this fluid drag moment in a purely conventional way. The drag moment must actually be calculated as the integral of all the products of the drag forces acting on each element of the surface, times the normal distance of each of these forces from the pivot. But because we do not know the distribution of the drag forces over the surface of the grain, there is no way we can actually evaluate this integral. So it is represented conventionally simply as a product of the total component of drag, $F_D \cos\alpha$, that opposes the total component of gravity, $F_G \sin\alpha$, times a normal distance a_2. The value of a_2 cannot be determined analytically, so a_2 is actually a "fudge factor" chosen to make the equation balance.

The gravity force F_G may be written

$$F_G = c_1 D^3(\gamma_s - \gamma) \qquad (6.6)$$

where c_1 is the coefficient that takes account of shape and also of the fact that the measured diameter D is generally not equal to the nominal diameter D_n. The fluid drag force F_D may be assumed equal to the average boundary shear stress τ_o times the area of the grain, and may be written

$$F_D = c_2 D^2 \tau_o \tag{6.7}$$

where the coefficient c_2 takes into account not only the geometry and packing of the grains (which determines the "area of the grain") but also the variation of the drag coefficient. Thus c_2 may be expected to vary with boundary Reynolds number. Substituting Equations (6.6) and (6.7) for F_G and F_D into Equation (6.5) and writing $\tau_o = \tau_c$ for the critical condition gives

$$a_1 c_1 D^3 (\gamma_s - \gamma) \sin\alpha = a_2 c_2 D^2 \tau_c \cos\alpha$$

or, solving for τ_c,

$$\tau_c = \frac{a_1 c_1}{a_2 c_2} \tan\alpha \; D(\gamma_s - \gamma) \tag{6.8}$$

This can be arranged into a more useful form by dividing both sides by $D(\gamma_s - \gamma)$ to make the equation dimensionless:

$$\frac{\tau_c}{D(\gamma_s - \gamma)} = \beta$$

where β_c, the critical value of a dimensionless variable $\tau_o / D(\gamma_s - \gamma)$ called Shields' β or the Shields parameter, should be expected to be a function of grain geometry and boundary Reynolds number.

The analysis is not much different if lift is considered as well as drag, because there should be a proportionality between the two forces which also depends only on grain geometry and boundary Reynolds number.

It may be noted that in the derivation of the equations it has been assumed that the bed slope is negligibly small. If this is not the case, then it is easily shown that $\sin\alpha$ in the equation above should be replaced by $\sin(\alpha - \phi)$, where ϕ is the slope angle (positive in the downstream direction). If other conditions remain the same, therefore, increasing bed slope decreases the critical value of β.

Dimensional Analysis

The discussion in the preceding section leads inevitably to the conclusion that, although some insight may be gained by theoretical and experimental investigations of the forces acting on particles, there will always remain too many unknown coefficients (= fudge factors) to permit a satisfactory analytical approach to the problem of the beginning of sediment movement. In practice the only way to solve the problem is to investigate it by direct experimentation. It might be argued, in fact, that the main value of the preceding discussion has been to make clear what are the principal variables likely to affect the beginning of motion.

Restricting the investigation at first to the simplest case, that of incipient movement of almost spherical grains of almost uniform size on a grain bed, we may now list the major variables that characterize incipient movement as follows:

τ_c	the critical or threshold boundary shear stress needed to move particles on the bed;
ρ	the fluid density;
μ	the fluid viscosity;
D	the grain diameter;
$(\gamma_s-\gamma)$	the submerged specific weight of the grains.

Two points about these variables need further comment.

The first is the choice of the bottom shear stress as the critical hydraulic variable. In most of the preceding discussions, forces acting on grains were related to a velocity at the bed rather than to the shear stress. Why not use a velocity? One answer to this is that, after all, what is moving the grains is basically a force acting on the bed, so the boundary shear stress is a more logical choice than any velocity. Another point raised several times in the preceding discussion is that we have difficulty determining exactly what velocity we should choose: the most easily measured velocity (the mean velocity of flow U) is not clearly related to the velocity measured near the bed, which is what causes the grains to move. If we choose the mean velocity we should also add another variable, depth of flow, because the same mean velocities may give rise to different near-bed velocities, or shear stresses, if the flow depth is different. And finally, we have demonstrated in the preceding section (Equations 6.3 and 6.4) that the velocity at the grain level is proportional to the square root of the shear stress. Nevertheless, we must recognize that the choice of shear stress rather than mean velocity is ultimately an arbitrary choice.

The second point is that in listing the variables we have chosen to combine the acceleration due to gravity g and the density of the grain ρ_s into a single variable with the fluid density: $g(\rho_s-\rho) = (\gamma_s-\gamma)$. This is equivalent to assuming that the only important effect of both gravity and grain density is in controlling the submerged weight of the grain. We assume that gravity waves in the fluid are not important--which is equivalent to assuming that the flow is not shallow enough so that the motion of the fluid over the grains affects the free surface. This is clearly an invalid assumption for very shallow, gravel-bed rivers. We also assume unimportance of the inertial effects that must be involved when denser grains are immersed in an accelerated fluid. Although the classic experiments of Shields (see below) did include some runs with grains whose density differed considerably from that of quartz, experiments by Ward (1969) and Collins and Rigler (1982) demonstrate that the difference in density is not fully accounted for by the difference in submerged specific weight.

If we nevertheless assume for the moment that our list of variables is complete, we may write

$$f(\tau_c,\ \rho,\ \mu,\ D,\ \gamma_s-\gamma) = 0$$

and, using dimensional analysis, reduce the number of variables to only two:

$$f\left[\frac{\tau_c}{(\gamma_s-\gamma)D},\ \frac{u_* D}{\nu}\right] = 0 \qquad (6.9)$$

One can think of the curve expressed by this functional relationship (Figure 6.8) as giving the locus of points in a graph of Shields parameter vs. boundary Reynolds number that characterizes the condition of incipient movement. Then all points below this curve represent conditions for which fluid forces are insufficient to move grains, and all points above the curve represent conditions for which grains can be moved. We have already seen that the first of the two variables in Equation (6.9) is generally called Shields' β or the Shields parameter, and the second is the now-familiar boundary Reynolds number. (Bagnold, 1956, 1966, makes use of the same dimensionless number, but uses the symbol Θ.)

The boundary Reynolds number can be interpreted as being proportional to the ratio of the grain size to the thickness of the viscous sublayer (Figure 6.7). Its value therefore indicates the degree to which the grains project into the turbulent zone of the boundary layer, and, as discussed in the previous section, we expect that the drag and lift on the grain will be a function of this number or ratio, particularly for values less than 5 (i.e., for dynamically smooth boundaries).

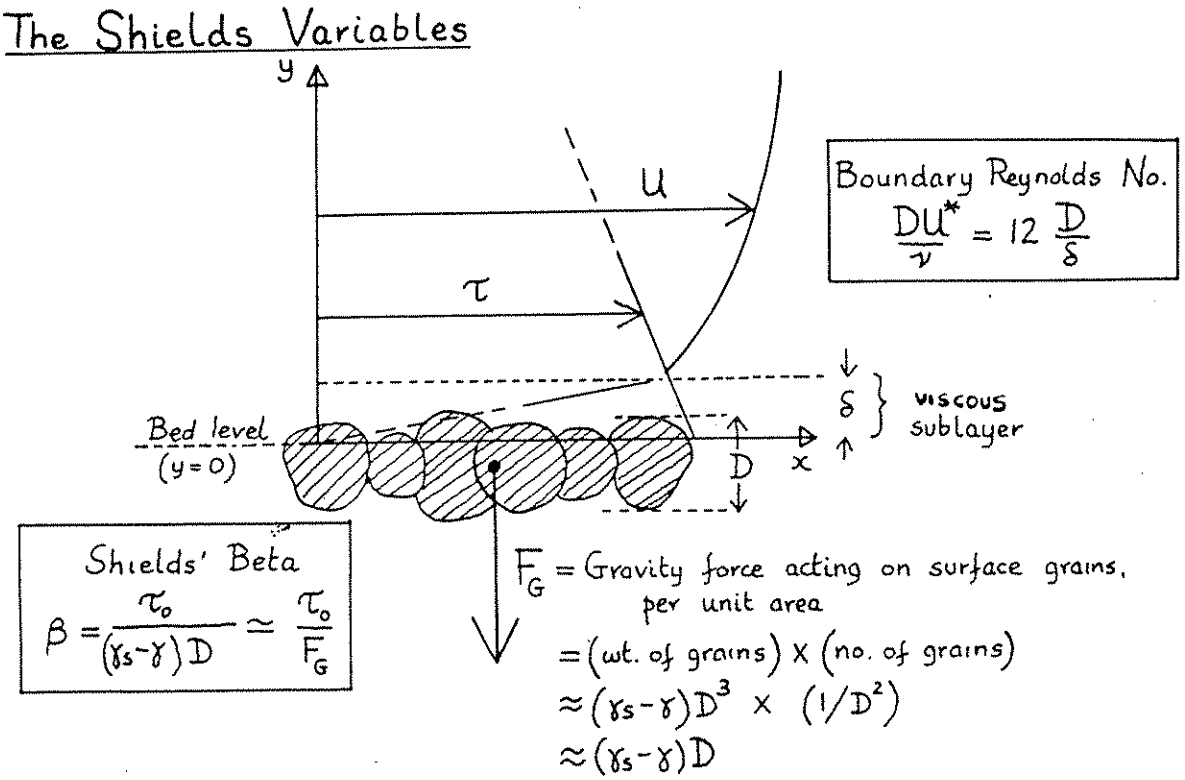

Figure 6.7 The Shields variables.

There is a practical disadvantage to using the boundary Reynolds number as the independent variable against which the Shields parameter is plotted: both of these two dimensionless numbers include shear stress and grain diameter. Yalin (1972) pointed out that dividing the square of the boundary Reynolds number by the Shields parameter gives a new parameter that does not include the shear stress:

$$\frac{\rho(\gamma_s-\gamma)D^3}{\mu^2}$$

This parameter, the Yalin parameter, can be regarded as the ratio of the submerged weight of the grain to the viscous forces acting on the grain. As the viscous forces get larger, the Yalin parameter gets smaller, and therefore it serves a function equivalent to that of the boundary Reynolds number but is more convenient to use.

Shields' β can be interpreted as the ratio between two forces per unit area (Figure 6.7). The shear stress τ_o is just the average drag force acting on a unit area of the bed, and we expect that for a given boundary Reynolds number this will be proportional to the lift force acting on a unit area of the bed. The variable $(\gamma_s-\gamma)D$ can be interpreted as proportional to the submerged weight of a single layer of grains underlying a unit area of the bed (F_G in Figure 6.7), and therefore it is proportional to the gravity forces that are opposed to fluid drag and lift forces acting on the surface layer of grains.

Experimental Results

The experimental results obtained by Shields (1936) are shown in Figure 6.8. We note first the considerable scatter in the points, and the fact that Shields had no data for boundary Reynolds numbers less than about 2 or greater than 600. It will help us to evaluate the results if we understand more clearly how they were obtained. Shields made his experiments in flumes 80 and 40 cm wide, with beds composed of granite fragments 0.85 mm to 2.4 mm in diameter, coal (S.G. 1.27) 1.8 mm to 2.5 mm in diameter, amber (S.G. 1.06) 1.6 mm in diameter, and barite (S.G. 4.2-4.3) 0.36 mm to 3.4 in diameter. He also made use of experimental data for sand determined by earlier workers (including Gilbert, 1914). Bottom shear stress was determined from Equation (1.16), $\tau_o = \gamma d \sin\phi$. The bed was carefully leveled before each run. Discharge and therefore mean velocity were increased in steps, and the slope was adjusted to maintain uniform flow. After grains began to move on the bed, bed load was collected in a trap at the end of the flume so that the rate of sediment transport for a given condition could be determined. For each bed material several observations were made at different discharges and rates of sediment transport, and the beginning of grain movement was determined not so much by direct observation as by plotting the measured rates of transport and extrapolating to the value of τ_o that corresponded to zero rate of transport. Shields observed that this corresponded to what other workers had described as "weak movement" of grains.

Shields himself noted that small ripples tend to form on the bed as soon as grains start to move. The presence of these ripples affects the rate of bed-load movement, and therefore there is some question about exactly what was being determined when Shields extrapolated the measured rates to zero: initiation of movement on a flat bed or on a rippled bed? It has been observed by other workers that the critical shear stress for initiation of motion on a rippled bed is greater than for that on a flat bed, although the mean velocity of flow is less (e.g., Rathbun and Goswami, 1966). The explanation is that ripples create form

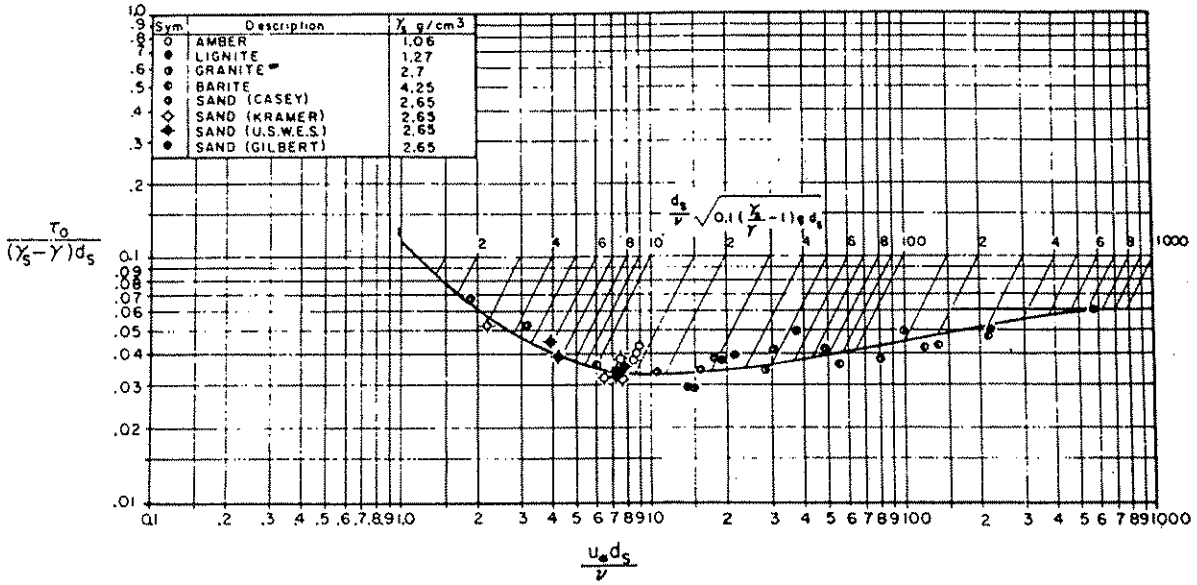

Figure 6.8 The Shields diagram, as modified by Vanoni (1964). To find the shear stress required to move a given sediment, calculate

$$(d_s/\nu)\sqrt{0.1\left(\frac{\gamma_s}{\gamma} - 1\right) g d_s}$$

locate this value on the scale given, find the intersection of the Shields curve, and read off the value of β from the ordinate. (In this figure d_s is the sediment grain size.)

resistance, which contributes most of the measured average bottom shear stress. If the depth does not change, the slope of the flume has to be increased to produce the shear stress needed to balance this form resistance and produce the same velocity. It is observed, however, that the slope and velocity needed to move grains on a rippled bed can be reduced below that necessary to move grains on a flat bed, because the phenomenon of flow separation over the ripples produces locally high and widely fluctuating shear stresses on the bed, which are large enough to move grains even at mean flow velocities lower than those required to move grains on a plane bed; see Chapter 7.

To make this more explicit, imagine that we set up two series of flume experiments, side by side, with exactly the same flow

depth and flow velocity, one with a flat sediment bed and one with a rippled bed. Start at a velocity so slow that there is no grain movement in either flume. Because of the large form drag on the rippled bed, slope and therefore boundary shear stress is much greater than for the flat bed. Now gradually increase flow velocity in both flumes while keeping flow depth constant but increasing the slope to maintain uniform flow. Boundary shear stress thus increases in both flumes, but is at all times greater on the rippled bed than on the flat bed. Grain movement starts first on the rippled bed; eventually, at a substantially higher flow velocity, grains begin to be moved on the flat bed also, but boundary shear stress on the flat bed at that point turns out to be lower than that for which grain movement began on the rippled bed.

The beginning of grain movement is a stochastic phenomenon that depends not only on the average fluid motions but also on the size of the turbulent deviations from the average. One experimental study that attempted to assess the stochastic basis of the beginning of grain movement was that of Grass (1970; see also Sutherland and Irvine, 1973). Grass used high-speed cinematography and a fluid-marker technique to determine (i) the fluctuations in shear stress within the viscous sublayer due to turbulence in the flow above, and (ii) the variations in the local instantaneous shear stress at which grains were actually observed to move from the bed. These variations were presumably caused by variations in the degree of grain exposure and local packing. Within the viscous sublayer the velocity gradient is almost constant. Determination of the velocity profile and therefore the gradient from the displacement of fluid markers permits determination of the shear stress from Equation (1.5), $\tau = \mu(du/dy)$. Observations using this technique are of course limited to low boundary Reynolds numbers, because at higher values there is no viscous sublayer.

Grass found that the coefficient of variation of the bottom shear stress was 0.4, and the coefficient of variation of the shear stress necessary to produce movement of grains of equal size and density was 0.3:

$$\frac{\sigma}{\overline{\tau}_o} = 0.4, \quad \frac{\sigma_c}{\overline{\tau}_c} = 0.3$$

where the sigmas are standard deviations. (In what follows we use a notation slightly different from elsewhere in these notes: τ_o is the instantaneous value of boundary shear stress on some local area of the bed, and $\overline{\tau}_o$, called τ_o elsewhere, is the time average of τ_o. An analogous notation holds for the critical values τ_c and $\overline{\tau}_c$ for incipient movement.) The condition for movement is that a large bottom shear stress (q standard deviations above the mean) coincides with a more unstable position of the grain (q standard

deviations below the mean):

$$\overline{\tau}_o + q\sigma = \overline{\tau}_c - q\sigma_c$$

or

$$\overline{\tau}_o + q(0.4\overline{\tau}_o) = \overline{\tau}_c - q(0.3\overline{\tau}_c)$$

$$\overline{\tau}_o = \frac{(1 - 0.3q)}{(1 + 0.4q)} \overline{\tau}_c$$

Choice of a value for q determines the probability of movement (large q corresponds to low probability). Grass found, in comparing his results with Shields' curve, that a choice of q = 0.625 corresponded to Shields' (unstated) choice of probabilities.

Other experimenters have tried to establish arbitrary but experimentally reproducible definitions of the beginning of movement. By observation of the bed through a microscope, Vanoni (1964) found that movement was intermittent on any small area of the bed, and when it did occur, it took place in local "bursts" with several grains moving at once. He defined the critical stage of movement in terms of four "burst" frequencies: (i) negligible ($<0.1\ s^{-1}$), (ii) small ($0.1\text{-}0.33\ s^{-1}$), (iii) critical ($0.33\text{-}1\ s^{-1}$), and (iv) general ($>1\ s^{-1}$). Neill (1968) and Yalin (1977) argued that kinematic similarity of movement of grains implies identity of the dimensionless parameter $N = nD^3/u*$, where n is the number of grains in motion per unit area and unit time. They suggested adopting 10^{-6} as a practical critical value of N, and pointed out that, for equal values of Shields' β, u* must be 30 times greater in air than in water, so that for equal N, n must be 30 times greater. This may explain why experimentally determined values of Shields' β are generally less for air than for water.

Finally, we may ask the almost philosophical question: For a given mean hydraulic condition, is there any size of sediment that can never be moved? According to Grass' approach, even the most stable grains on the bed can be moved (though rarely) by the largest turbulent fluctuations in bottom shear stress. From an investigation of the relationship between sediment transport rate and bottom shear stress at very low rates of transport, Paintal (1971) found that sediment transport rate was proportional to

shear stress raised to the 16th power! (See also Mantz, 1980.) So there is certainly a rather abrupt increase in the rate of sediment movement as the shear stress increases near threshold conditions. Paintal also concluded that there was no absolute "critical" shear stress below which movement of grains was impossible (see also He and Han, 1982). But common sense tells us, even though there are no supporting data, that in such a situation there is some range of flow below which nothing is ever moved, effectively.

Low Boundary Reynolds Numbers

Shields did not present any experimental results for low boundary Reynolds numbers (generally equivalent to fine grain sizes). He indicated that β in this region should be inversely proportional to the boundary Reynolds number:

$$\frac{\tau_c}{(\gamma_s-\gamma)D} = K_1 \frac{\nu}{u_* D}$$

or, rearranging and making use of the definition of u*,

$$\tau_c = K_2{}^3[\mu^2(\gamma_s-\gamma)^2/\rho]^{1/2} \qquad (6.10)$$

where K_1 and K_2 are constants. In other words, he expected that the critical shear stress needed to move a grain totally enclosed in the viscous sublayer would not depend on grain size.

Actual experimental work by Grass (1970), White (1970), Mantz (1973, 1977), and Yalin and Karahan (1979) has shown that this is not strictly true. White's data shown in Figure 6.9 indicate that below boundary Reynolds numbers of about 10, β does rise with decreasing Reynolds number, but the rise is slower than that predicted by Shields, thus indicating that the critical shear stress is still a weak function of the grain size. Therefore, at these grain sizes we might expect that the density difference between the grains and the fluid would play a more important role than grain size.

Collins and Rigler (1982) ran experiments on the initiation of motion of ilmenite, zircon, rutile, and cassiterite sands with specific gravities ranging from 4.1 to 7.0, and sizes from 0.1 to 0.3 mm. Boundary Reynolds numbers at the beginning of movement were in the range 1-5. They found that the density effect was overestimated by the Shields parameter, and also by the settling velocity, if the ratio u*/w was substituted for β. Strangely,

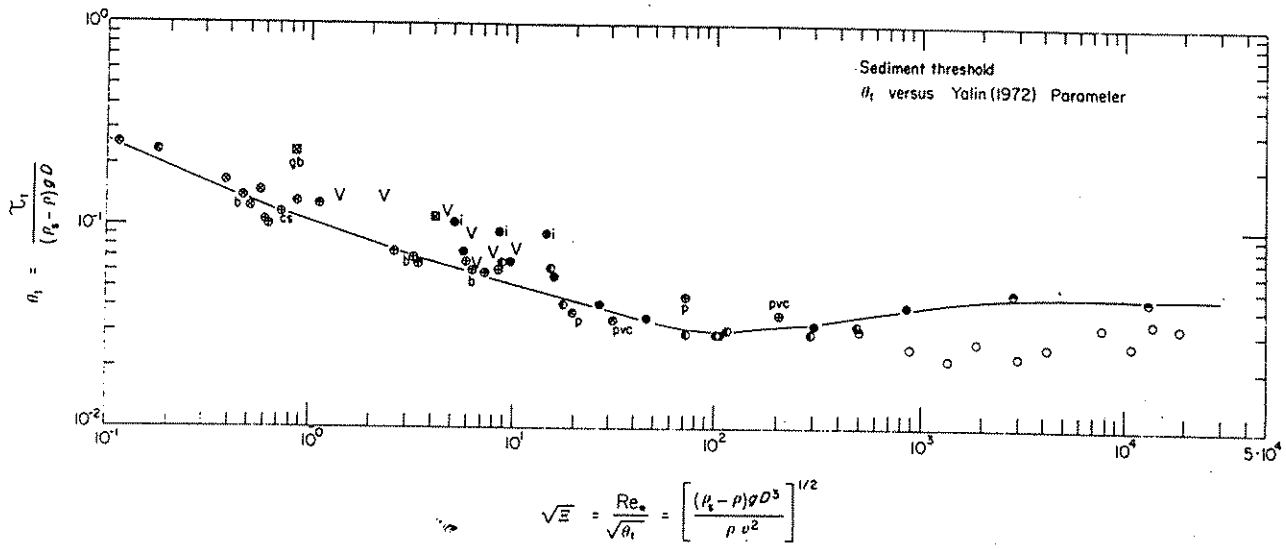

Figure 6.9 A new version of the Shields diagram using the Yalin parameter instead of the boundary Reynolds number, plotted against the Shields parameter (labeled θ_t in this diagram), and including the experimental data of White (1970) at low values of the Yalin parameter. The line through the data is the preferred line of Miller et al. (1977), from whom the diagram is taken. This paper and that of Yalin and Karahan (1979) should be consulted for a full discussion of recent data.

they found that initiation of motion was best predicted by a plot of shear stress (or shear velocity) directly against settling velocity. Their data showed that the critical value of u* was directly proportional to the 1/6 power of w, a result that is not dimensionally consistent, and which must therefore have a limited range of application. One can only conclude that the true effect of grain density is still not well understood.

High concentrations of heavy minerals in fine-grained natural sands are frequently observed on the backs of ripples. Grigg and Rathbun (1969) and McQuivey and Keefer (1969) suggested that the Shields theory predicts that if the shear stress is locally just at the critical value needed to move fine quartz grains, it will not be sufficient to move even finer grains of heavy minerals, which may have settled out of suspension along with the quartz grains because they both have about the same settling velocity. Thus the quartz grains would be removed and the heavies left behind as a thin lag deposit. If the results of Collins and

Rigler (1982) are correct, this theory must be revised, because they found that quartz and heavy-mineral grains with the same settling velocity started to move at the same critical shear stress.

High Boundary Reynolds Numbers

Shields' investigation of the beginning of grain movement was limited to boundary Reynolds numbers less than 600. For sediment of quartz density in water, this corresponds to sizes of about 7 mm. Shields concluded, without any real supporting evidence, that at higher boundary Reynolds numbers, β_c would be constant at a value of 0.06. This hypothesis that β_c approaches some constant critical value at high boundary Reynolds numbers is based on the analogy with the constant drag coefficient in pipe flow at sufficiently high Reynolds numbers and relative roughnesses (Figure 5.8).

There has been little subsequent experimental work at high boundary Reynolds numbers, but there have been many attempts to determine the critical shear stresses or velocities needed to move large grains (up to boulder size) from field observations (Fahnestock, 1963; Neill, 1968; Helley, 1969; Novak, 1973; Baker and Ritter, 1975; Bradley and Mears, 1980; Carling, 1983). Miller et al. (1977) have reviewed the experimental evidence, what little there is, and have argued that it indicates a value of β_c constant at about 0.045 rather than the value of 0.06 suggested by Shields (cf. Figure 6.9).

At high Reynolds numbers the critical shear velocity u_{*c} needed to move a grain on the bed should be directly proportional to the settling velocity w. Recall that the drag coefficient determined for the free fall of spheres was almost a constant (0.5) for a range of Reynolds numbers between 1000 and 200,000 (Chapter 4). In Chapter 2 we determined the relationship between w and D as

$$w = \left[\frac{4g(\rho_s-\rho)D}{3\rho C_D}\right]^{1/2} \qquad (6.11)$$

(This is just a rearrangement of Equation 2.1.) And for a constant value of 0.045 for β, it follows from Equation (6.11) that

$$u_{*c} = \left[\frac{0.045g(\rho_s-\rho)D}{\rho}\right]^{1/2} \qquad (6.12)$$

(Remember that $\tau_c = \rho u*_c^2$.) Therefore, combining Equations (6.11) and (6.12),

$$w/u*_c \simeq 30/C_D \qquad (6.13)$$

For spheres this ratio is about 8, and for less regular grains (with C_D somewhat larger than 0.5) it is about 7.

Geologists have a special interest in the critical conditions necessary for the transport of large grains, because of the problem of hydraulic interpretation of ancient gravels. Several considerations, besides the scarcity of good experimental data, limit the application of the Shields criterion to such problems: (i) Pebbles and cobbles are commonly moved by flows whose depth is quite small relative to the diameter of the grain. (ii) The problem is generally the interpretation of a few large grains set in a matrix of finer sands and gravels, rather than the interpretation of the average size of a well sorted deposit. (iii) The problem is not really what flow was required to initiate movement of such large grains, but what flow was capable of keeping them moving (see remarks below on grain "overpassing").

Strictly, the Shields criterion applies only to flows that are deep compared with the size of grains on the bed. Yalin (1977, p. 44) cites evidence that indicates that the velocity distribution is not logarithmic for flows in which the relative roughness (diameter/depth) is more than 1/6. Kellerhals (1967) found the limit to be somewhat higher: for natural gravel, his flume studies indicated that the usual logarithmic equations were valid, with the equivalent sand roughness k_s set equal to the 10 percentile of the bed material (the diameter exceeded by only 10% of the grains on the bed), over a range of relative roughnesses up to 1/3. At high relative roughnesses, not only is the velocity distribution (and therefore the distribution of drag forces on the grain) altered, but the large grains on the bed set up waves on the surface of the flow, thus dissipating part of the energy of the flow and changing the nature of the turbulent energy. It is difficult to predict a priori how this might affect β_c. Baker and Ritter (1975) thought that the field evidence indicated that β_c should be smaller for high relative roughnesses, and hypothesized that this is due to an increase in the proportion of lift to drag forces, but an experimental study by Bayazit (1978) shows the opposite effect: larger values of β_c were required to move spheres over a bed of similar spheres as relative roughness was increased.

Effect of Relative Protrusion of Grains and Poor Sorting

Shields' investigation, and most subsequent experimental studies, have been confined to well sorted sediments. But sediments may not be well sorted in nature. If there is a range

of grain sizes on the bed, the larger grains may be more easily moved because they are more exposed to the flow and because the position of the pivot about which they move is lower than for smaller grains. The finer grains may be shielded from the flow, and their movement obstructed by the larger grains. Alternatively, if the range of sizes is such that it is possible to move the smaller grains but not the larger grains, then progressive removal of the finer fraction may develop a protective cover consisting of a single layer of coarse grains on the bed surface (i.e., armor).

The effect of relative protrusion of the grain is not confined to beds in which there is a range of grain sizes. Grass's experiments indicated that even in well sorted sands, some grains are more easily moved than others. Fenton and Abbott (1977) made a detailed experimental study of the effect of raising one grain slightly above the level of the surrounding grains. They found that this reduced β_c to a value of about 0.01 when the test grain was actually resting on rather than forming a part of a bed composed of similar grains.

Where the bed material is poorly sorted, it might be expected that the larger grains protrude more into the flow, so that there should be circumstances for which it is easier to move the larger grains than the smaller grains. This was evaluated experimentally by Everts (1973) for the special case of uniform grains moving over a bed composed of stable uniform grains either smaller or larger than the moving grains. The experimental procedure was to prepare a uniform bed and determine the critical shear stress needed to start grain movement on that bed. Then, while maintaining shear stresses just less than critical, moving grains were introduced from upstream (Figure 6.10). Shear stress was progressively reduced until the introduced grains would no longer pass over the bed. Thus, what was determined was the minimum shear stress for overpassing, i.e., the minimum shear stress to keep grains moving over the bed, not the critical shear stress to initiate movement (Figure 6.11).

Everts observed that larger grains rolled over the bed, whereas grains of almost equal size bounded over the bed or became trapped in it. Grains both larger and smaller than the bed material would overpass. For the smaller grain sizes tested (0.13 mm to 0.51 mm), grains as small as about half the size of the bed material would overpass, as would grains as much as five times as large as the bed material (Figure 6.10). For the larger bed sizes (about 1 to 2 mm), the size range of the largest overpassing grains was proportionately less: sizes from about half to twice the bed sizes would overpass. The critical values of β_c for the bed were found to lie in the range from 0.02 to 0.05, depending on the boundary Reynolds number, but grains could be made to overpass at values of β from 0.005 to 0.05, with little effect of boundary Reynolds number being evident for the upper and lower limits (Figure 6.11). (It must be remembered that for a given shear stress the lower values of β correspond to larger sizes of overpassing grains.)

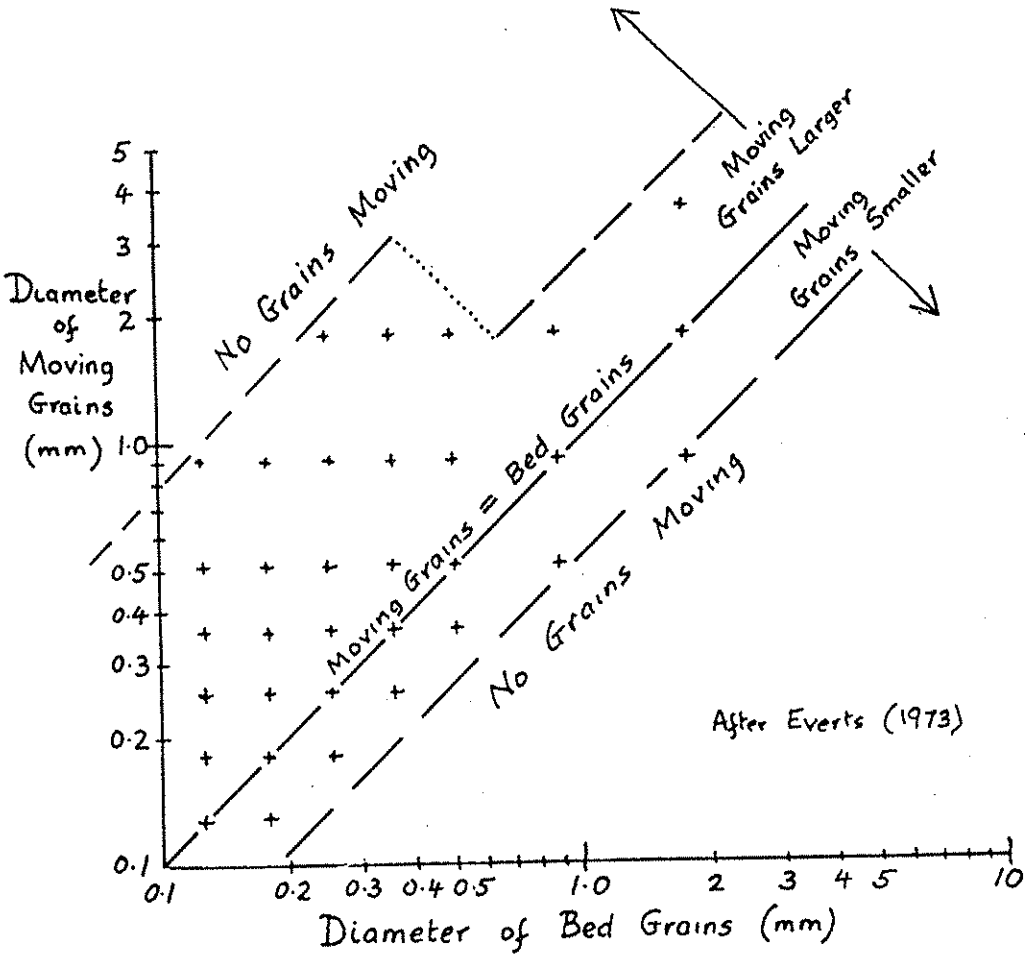

Figure 6.10 Size of grains able to move over (immobile) bed grains of a given size. After Everts (1973).

Everts suggested an application of these results to the observed inverse size grading observed in laminae produced by swash and backwash on beaches. Sediment carried in suspension up the beach by the highly turbulent swash drops to the bed as the swash reaches its limit and then begins to be entrained by the backwash. The larger grains are more easily moved over the bed, and hence are the last to be deposited as the backwash is finally dissipated, thus forming the observed inverse grading. Heavy minerals are the most difficult to entrain, both because of their small size and, more importantly, because of their high density, so they tend to be concentrated in the lower part of graded laminae. If the backwash is sufficiently strong, most of the light particles may be returned down the beach, leaving only a lag concentrate of heavy minerals.

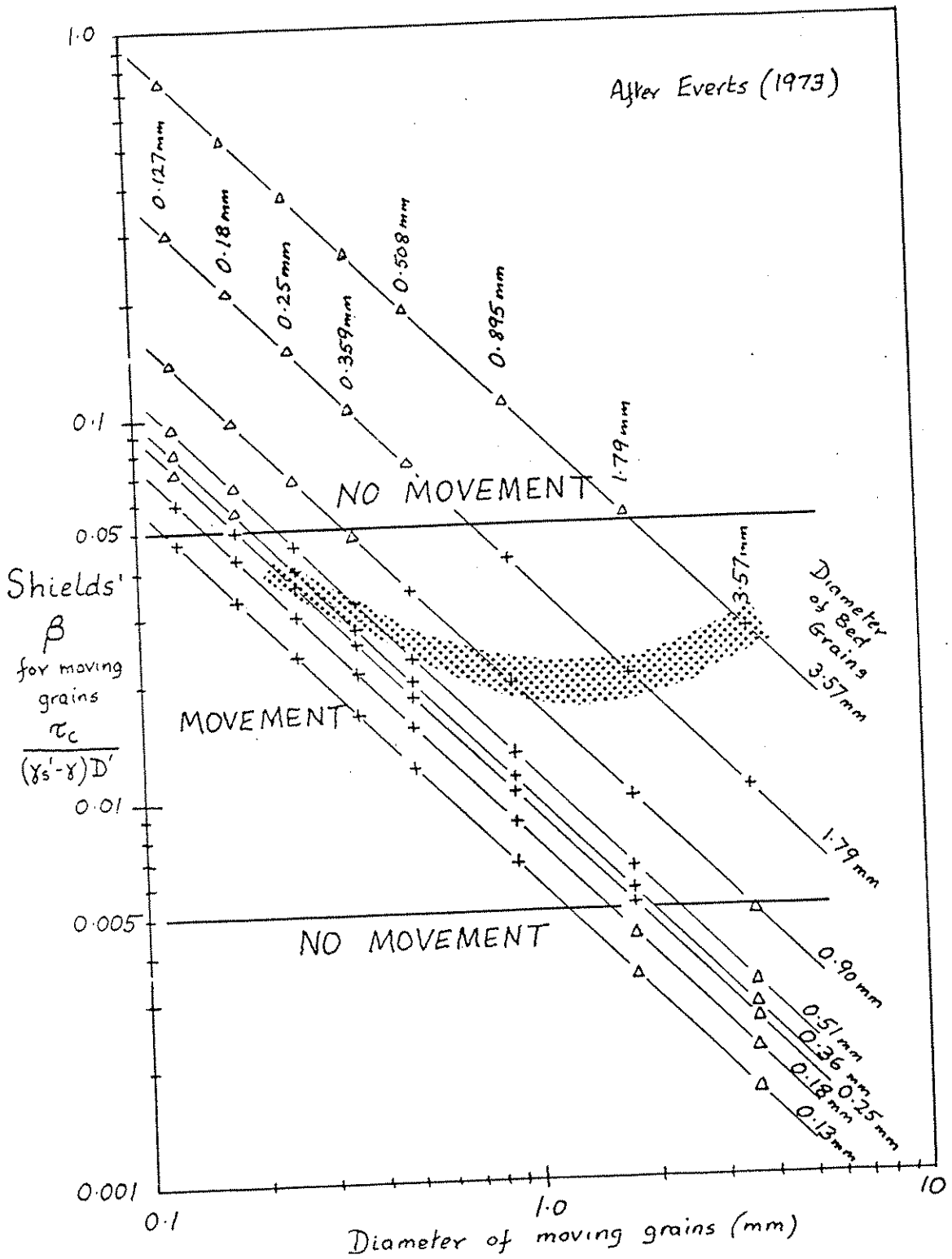

Figure 6.11 Shields' β necessary to move grains over (immobile) bed grains of a given diameter. Triangles indicate experimental runs in which there was no movement of grains; crosses indicate runs in which grains of the size indicated on the abscissa could move over bed grains whose size is indicated on the oblique lines. Shaded area indicates the Shields criterion for initial movement of grains on a bed composed of equal-size grains. After Everts (1973).

More recent investigations of the relative sizes of light and heavy minerals in laminae produced by swash and backwash have suggested, however, that the segregation of grains by size and density is more plausibly explained by Bagnold's mechanism of dispersive pressure (see below) than by the mechanism proposed by Everts (see Sallenger, 1979).

For many poorly sorted materials subject to only a limited range of shear stresses, the largest shear stresses may still not be large enough to remove the largest grains. The large grains remain behind as the finer grains are removed, to form a lag deposit which armors the bed and prevents further erosion. This phenomenon was investigated experimentally by Gessler (1967, and in Shen, 1971). Gessler assumed a critical local shear stress for movement of individual particles, and he further assumed that local bed shear stresses were Normally distributed (as indeed has been shown experimentally to be a fair approximation of the truth). The probability of erosion for a given grain size and a given average bed shear stress can then be calculated. These calculated probabilities were then compared with "observed" probabilities obtained from the ratio of frequencies of a particular size fraction in the original bed material to the frequencies of the same sizes in the armored surface layer. Gessler found that the best agreement was given by using a value of 0.57 for the coefficient of variation of the shear stress. This is larger than Grass' value, but this is to be expected because it implicitly includes variation in particle stability that was explicitly evaluated by Grass.

Another approach to the problem is to investigate the ratio betwen β_c for a given grain size in a uniform bed, and β_c for the same size when it is mixed with other sizes in a poorly sorted bed. Day (1980; see also White and Day, in Hey et al., 1982) found, for five different sediment mixtures, that the values of β_c required remained the same for the median grain size in the sediment mixtures but decreased towards the larger sizes, by the effect of protrusion, and increased towards the finer sizes, by the effect of shielding.

Organic Factors

Movement of grains may be influenced by biological activity in several different ways:

(i) Many grains produced by organic activity differ in their properties from their constituent mineral grains. Skeletal grains may have a much lower density than that of calcite or aragonite, because of a pore system filled with an organic substrate. This applies particularly to crinoid ossicles (Cain, 1968). Much mud may be bound into fecal pellets, of relatively large size and low density, whose dynamic behavior is quite different from that of

the clay and silt of which they are composed. Nevertheless, Fisher et al. (1979) found that the Shields criterion applies also to organic detritus.

(ii) Algae, both blue-greens and marine grasses, may bind fine sediment, making it more resistant to erosion.

(iii) Bioturbation may raise the threshold of erosion by increasing the adhesion of sediment grains. Grant et al. (1982) found that in fine intertidal sands there was a seasonal change in erodibility. In winter the critical conditions for erosion were well predicted by the Shields criterion, but in the summer biological reworking increased β_c, though generally by less than a factor of two.

MOVEMENT OF GRAINS OVER A BED

Introduction

When a flat bed of sand is prepared in a flume, and the flow strength is gradually increased until grains begin to move on the bed, a number of interesting phenomena can be observed. Grains move by hopping, rolling, and sliding. Grain movement is neither continuous nor uniform over the bed. There are short "bursts" of movement that affect a group of grains on one area of the bed. Grains move a short distance, stop, and then move again. Even when they are moving, they are generally not moving as fast as the fluid near the bed surface.

Transport of the surficial grains on a flat bed produces a distinctive microtopography, consisting of somewhat irregular and discontinuous ridges and depressions oriented roughly parallel to the flow. The spacing of these features on a sand bed is of the order of several millimeters, and the relief is very small, generally only a few grain diameters. But this lineated relief is a characteristic feature of transport of cohesionless grains over a flat bed, for grains ranging from silt sizes (Mantz, 1977) up to at least very coarse sand, and for hydraulic conditions ranging from just above the threshold of grain movement to high flow intensities that produce upper-regime, plane-bed conditions (Chapter 7).

The ridges and depressions are produced by the action of small but strong turbulent eddies on the bed (Sutherland, 1967). Exactly how this takes place is becoming clearer as the structure of turbulence close to the bed becomes better understood as a result of numerous recent laboratory studies. The observations were described briefly in Chapter 5, and their relevance for sediment movement has been discussed more thoroughly by Grass (1971, 1974), Karcz (1973), Jackson (1976), Sumer and Oguz (1978), Bridge (1978), Sumer and Deigaard (1981), and Leeder (1983a).

Most experimental observations have been made on boundaries that are dynamically smooth or transitionally rough, i.e., on boundaries characterized by a viscous sublayer that is at least poorly developed. But observations of dynamically rough boundaries (e.g., by Grass, 1971) show that even for flows without a viscous sublayer there exists a region close to the boundary (which Grass called the "inner zone", $y^+ < 40$) characterized by distinctive low-speed longitudinal streaks and a quasi-cyclic alternation of events that has come to be known as the "burst-sweep cycle" (see Chapter 5). As strong vortices with axes transverse to the flow approach the boundary, they produce pressure gradients that tend to lift up the streaks and eject them into the turbulent boundary layer. This "burst" of slow-moving fluid is capable of carrying small grains away from the bed to distances a few centimeters above the bed. Sumer and Oguz (1978) found that grains whose settling velocity was of the order of $0.5u_*$ were carried "in a single continuous motion" up to dimensionless elevations y^+ of 100-200. The slow-moving fluid in the burst then mixes with, and is accelerated by, the fluid in the outer zone, and some returns to the bed as a fast-moving vortex or "sweep" which in turn creates a new burst, and so on. The process is not strictly periodic, though on the average it displays a period and scale controlled mainly by the velocity and thickness of the turbulent boundary layer. If the period of bursts is T and the velocity far from the bed is U, then $UT/\delta \simeq 5$, where δ is the thickness of the boundary layer (in an open-channel flow, the depth of the flow).

The existence of the burst-sweep cycle suggests an explanation of the phenomena of grain movement described above. The "bursts" of movement of grains along the bed described by Vanoni (1964) probably correspond to fluid sweeps (not to the fluid bursts!) in the burst-sweep cycle, when velocity gradients close to the bed, and therefore shear stresses, are locally high. Grains tend to be swept to one side or the other of fast-moving fluid streaks to gather under slow-moving streaks and produce the characteristic current lineation observed on plane beds.

Bridge (1978) has suggested that, at sufficiently large scales of flow, bursts would be sufficiently large and strong to erode sand from the bed or eject sand-laden fluid away from the bed. Erosion would be followed by deposition of first the larger grains and then the smaller grains, resulting in a thin graded lamina with a sharp base. Laminae would be discontinuous, with dimensions comparable with the depth of the flow. They would vary somewhat in character depending on the grain size and rate of deposition. Perhaps this is the mechanism of formation of planar lamination by upper-regime plane-bed flows; Bridge's suggestion is interesting and needs to be confirmed or modified by detailed experimental observations.

For sand finer than about 0.6 mm, movement of grains over a flat bed eventually results in the formation of minor accumulations of grains that grow to form ripples (Chapter 7). The ripples then change the pattern of flow at the bed, and therefore

also the interaction of the flow and the moving sediment grains. Separation of flow takes place at the ripple crest, and the boundary layer is reestablished downstream of where the flow reattaches to the bed, on the stoss side of the next ripple downstream. Although the bed surface is now much more irregular, the same lineated surface seen on a flat bed can generally be observed on the upper stoss sides of ripples or larger bed forms.

Mode of Movement

Grains making up a substantial part of the movable bed of a stream are called bed material. Bed material in transport at a given time is called the bed-material load. Some, but generally not all, of the bed material moves very close to the bed, either in contact with it or rising only a few grain diameters above it This part of the bed-material load is known as the bed load (or contact load). Bed material can also be moved by being swept up into the main part of the flow by turbulence. This is the suspended load, which may also include a substantial quantity of very fine sediment, called wash load, that is not present in any quantity in the bed. The distinction between bed load and suspended load is important because of the fundamental physical difference in the mode of movement and the forces involved, but it is somewhat arbitrary: there is no sharp division between these two modes of movement, and a given grain at the bed surface may (if grain size and flow strength are within certain ranges) at some times travel as bed load and at other times travel as suspended load.

The relative proportions of the bed material that move as bed load and as suspended load depend upon the characteristics of the bed material (especially its size) and on the flow conditions. Very coarse bed material in rivers (gravel) generally moves as bed load, whereas fine to medium sands move predominantly as suspended load. The mode of movement of the coarser sand sizes generally varies depending on the hydraulic conditions: at low stages the coarser sand fractions move predominantly as bed load, whereas at high stages they are taken into suspension. Even at the same average discharge, sand of a given size may alternate between suspension and traction, as it is caught up by powerful eddies (for example, the separation eddies formed on the lee sides of major bed forms) or returns to the bed in less turbulent parts of the flow. Most sand sizes do not travel in continuous suspension: the very fact that these sizes constitute a major part of the bed material in most rivers indicates that they are taken into suspension only intermittently. To distinguish this mode of transport from the almost continuous suspension typical of wash load, which is generally composed of grains finer than fine sand, we may call the coarser part of the suspended load the intermittent suspension load.

Not only is there a continual exchange of grains between bed load and suspended load, there is also an exchange between the

moving bed load and the grains resting on the bed. This was neatly demonstrated in an experiment by Einstein (1950). After establishing an equilibrium condition with large grains (pebbles) being moved as bed load in a flume, the flow was stopped and the flume drained, and the surface layer of grains in part of the flume was coated with paint. After the equilibrium flow condition was reestablished it was observed not that grains were simply transported over the marked section from upstream, but that there was an exchange of grains: a number of unmarked grains came to rest in the marked section, and marked grains moved downstream. Observations of this kind led Einstein to postulate a stochastic model for grain movement based on the following assumptions: (i) that the probability of movement of a given grain depends on the size, shape, and weight of the grain and on the hydraulic conditions; (ii) that there is an equal probability that a moving grain might be redeposited on any part of the bed; and (iii) that the average distance traveled by grains does not depend on the flow conditions, but is equal to 100 grain diameters. The probability of movement of grains was calculated by using the observation of Einstein and El-Samni (1949) that the lift force was Normally distributed.

One way of observing how grains move as the flow intensity rises above the threshold condition is to study the movement of one loose grain over a bed composed of similar grains that have been fixed in position by the use of glue or cement. Such experiments have been reported by Meland and Norrman (1966), Francis (1973), and Abbott and Francis (1977). It may be objected that, because the bed is fixed, the true grain-exchange process that Einstein observed in flume experiments cannot take place. Another way to approach the problem is to examine the movement of labeled grains (fluorescent or radioactive tracers). In this case it is still possible to make observations on individual grains (see experiments by Grigg reported below), but generally this is not attempted. Instead average patterns of movement are observed and are compared with averages calculated from stochastic models that make various assumptions about the probability distributions of step lengths, rest periods, etc.

Because of the fundamental (albeit gradational) differences between the different types of sediment movement, it is important to develop criteria that will predict the predominant type of movement of a particular size of bed material under given hydraulic conditions.

Meland and Norrman (1966) distinguished three "stages" of grain motion: (i) In the stage of "stop-and-go" movement, the grain is periodically trapped between other grains on the bed. This stage follows initiation of motion and is particularly typical of grains smaller than the average bed material. At this stage a very small increase in u_* above the critical value produces a marked increase in the average rate of grain movement, which however is mainly controlled by the bed and grain size. (ii) In the stage of continuous movement in contact with the bed, the

the grain rolls or skims over the surface of the bed. (iii) In the highest stage, grains begin to be lifted up above the bed level or to make long jumps. Increases in grain velocity are roughly proportional to increases in shear velocity.

Francis (1973) also distinguished three modes of movement, although they do not correspond exactly with the stages described by Meland and Norrman: (i) rolling of grains in contact with the bed (roughly equivalent to stages i and ii of Meland and Norrman); (ii) saltation, with grains rising up to heights of about two to four grain diameters above the bed and then falling back along "ballistic" paths, as illustrated in Figure 6.12; and (iii) suspension, in which at first grains move in "leaps" that are distinguished from saltation by their length and sinuous trajectories (Figure 6.12) but as suspension becomes better developed the grains rise farther above the bed and return to it less often.

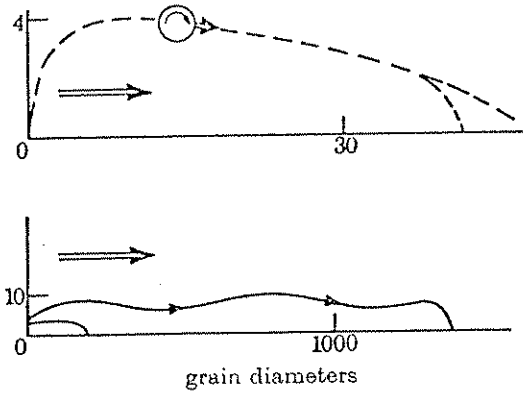

Figure 6.12 Sketches of typical grain trajectories, as observed by Francis (1973, Fig. 1). Above: saltation trajectory--note spinning of grain. Below: suspension trajectory (wavy line) with saltation trajectory shown to same scale for comparison.

Francis (1973) distinguished saltation from suspension on the basis of a qualitative assessment of the grain trajectory. Abbott and Francis (1977, p. 229) suggested a more rigorous definition: a grain is in saltation when it "jumps away from the bed and follows such a trajectory that its vertical acceleration is always directed downwards between the upward impulses sustained while in contact with the bed." If at any time the vertical acceleration is directed upwards, then the grain is regarded as being in suspension. According to this definition, whether or not a grain is in suspension cannot be determined simply from qualitative observation: a detailed analysis of the vertical component of its acceleration, based on high-speed photography of its trajectory,

is required. Further discussion of the nature of saltation (which is better developed in air than in water) will be deferred until we have examined some of the experimental results on the relation between flow intensity and rate of sediment movement. The mode of movement at shear velocities just above the threshold value $u*_c$ predicted by the Shields diagram was investigated by Abbott and Francis, with the results shown in Figure 6.13.

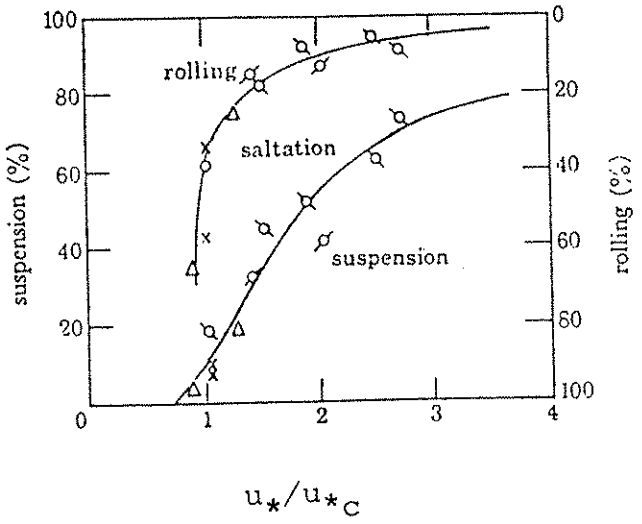

Figure 6.13 Modes of movement of a solitary grain moving over a fixed bed, as a function of dimensionless shear velocity $u*/u*_c$. Experimental results are for grains of different densities (different symbols) but all of nominal diameter 0.83 cm, in a flow 4.8 cm deep. (From Abbott and Francis, 1977, Fig. 1.)

The earliest grain movements, at $u*/u*_c$ of about 1 (corresponding to $u*/w$ about 0.15), are by rolling, but as flow intensity increases, saltation rapidly becomes the dominant mode of grain movement. By the time $u*/w$ has reached values of only about 0.3, about 50% of the grain trajectories are classified as being in the suspension mode, using the strict definition of Abbott and Francis (1977), but the grains follow paths that are still very close to the bed, and the average speed of the grains, U_G, is roughly proportional to the shear velocity. ($U_G/u*$ is about 6 to 8, indicating that the speed of the grain is almost equal to that of the flow close to the bed; see Equations 6.3 and 6.4.) At $u*/w = 0.5$ most trajectories would be classified by Abbott and Francis (1977) as in the suspension mode, but the grains are still moving mainly close to the bed in a mode that might be subjectively described by most observers as being more like saltation than true suspension.

As flow intensities are increased further, grain trajectories become longer and more irregular and the grains are carried higher into the flow. At these higher intensities it

seems more reasonable to normalize the average speed of grain movement by dividing by mean flow velocity U (a property of the main flow) than by dividing by shear velocity (a property of the flow just above the bed). Abbott and Francis (1977, and see Francis, 1973) found that for grains of equal density U_G/U was directly related to $w/u*$, the reciprocal of $u*/w$ (Figure 6.14). At $u*/w$ greater than 0.5 the average grain speed was actually higher than the mean flow velocity, because most trajectories carried the grains up into the higher and therefore more rapidly moving parts of the flow. (Earlier experiments reported by Francis, 1973, suggest that in most cases U_G/U does not approach 1 until $u*/w$ approaches 1.)

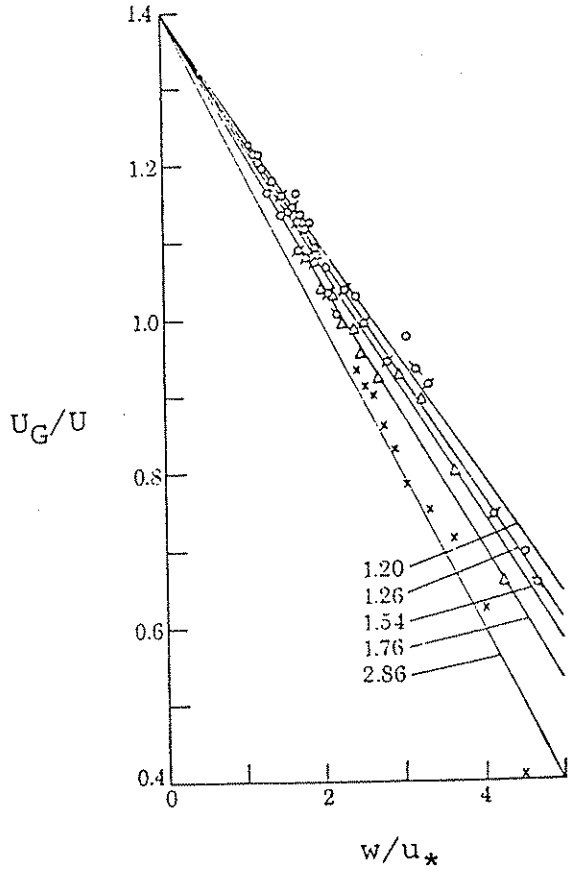

Figure 6.14 Plot of dimensionless grain speed U_G/U against the reciprocal of dimensionless shear velocity $u*/w$. Different symbols and lines refer to experimental grains of different specific gravities. From Abbott and Francis (1977, Figure 18). Note that as saltation becomes less important and suspension more important, the independent effect of grain density (not already accounted for by use of the settling velocity w) becomes less important.

It therefore appears that a conservative criterion for suspension is that

$$u_* > w \qquad (6.14)$$

This criterion can also be supported from arguments about the relation between the intensity of turbulence and the shear velocity. We might expect that grains would begin to be suspended when the root-mean-square of the vertical component of turbulence (rms v) is approximately equal to the settling velocity. Observations on turbulence intensity over both smooth and rough boundaries show that there is a maximum close to the bed and that the maximum values reached (of both horizontal and vertical rms) are proportional to the shear velocity (Blinco and Partheniades, 1971). The data of McQuivey and Richardson (1969) and Antonia and Luxton (1971) show that the maximum value of (rms v)/u_* is approximately equal to one and that this value does not depend strongly on the type of roughness. Therefore, the maximum value of rms v near the bed is approximately equal to the shear velocity, and it is to be expected that suspension becomes the dominant mechanism of sediment transport when both rms v and u_* are larger than the settling velocity. Middleton (1976) has argued that this criterion is also supported by a comparison of hydraulic measurements with the settling velocity of the largest grain sizes present in the suspended load of several rivers.

In his pioneer stochastic model for grain movement, Einstein (1950) postulated that the average distance travelled by a grain moving as bed load does not depend upon the flow intensity. Fernandez Luque (1974; see also Fernandez Luque and van Beek, 1976), in observations of grains moving over a loose flat bed at shear stresses only slightly larger than critical, found from direct observation that the average length of individual grain "steps" (or saltation jumps) was a constant equal to 16 times the grain diameter. Grains accelerated slightly at the beginning of each jump and decelerated upon returning to the bed, but generally did not come to rest. On the average a grain jumped about 18 times, for a total step length of 288 grain diameters, before coming to rest. The average velocity while moving was reduced by collisions with the bed surface to about 85% of the maximum velocity achieved in each jump.

Effect of Bed Forms

The presence of ripples or dunes probably has a major effect on measured grain speeds. The reason is that there is a high probability in this case that bed-load grains are trapped on the lee sides of the bed forms (see Chapter 7). The speed of a grain then depends mainly on the time the grain spends buried in the bed form, which in turn depends on the speed of bed-form movement. The average speed of a grain depends very little upon its speed while it is actually moving, but mostly on the speed of the bed form. This latter speed is of course determined by the number of

grains moving, as well as by the average speed of grain movement for the whole bed load. Thus, where there is a range of grain sizes moving as bed load over a flat bed the larger grains may move faster than the finer grains (up to a certain limit, as discussed in the previous section), but where a range of grain sizes moves as bed load over a rippled or duned bed the average speed of grains of all sizes is approximately the same, and is determined by the rate of movement of the bed forms.

Evidence that this is in fact the case has been obtained by R.W. Dalrymple (personal communication) for megarippled sand bars in the Bay of Fundy. The rate of movement of different grain-size fractions was determined by using different colors of fluorescent paint, and it was found that above a certain size all size fractions moved at the same rate. Below this size, finer sizes moved faster, indicating that this sand was in intermittent suspension and was therefore not always trapped on lee slopes but was bypassing a certain proportion of the bed forms.

The effect of bed forms on the movement of single grains labeled with a radioactive tracer was studied by Grigg (1970). He determined such statistical properties as the distribution of step lengths and the rest periods (periods when the grain was buried in the bed). He found, as expected, that there was a definite relation between the mean rest period and the rate of movement of the bed forms. There was also a direct relationship between mean step length and mean bed-form spacing (Figure 6.15), with only a minor grain-size effect (see also Nakagawa and Tsujimoto, 1980). For equal bed-form size the step length tends to be slightly longer on the average for finer grain sizes.

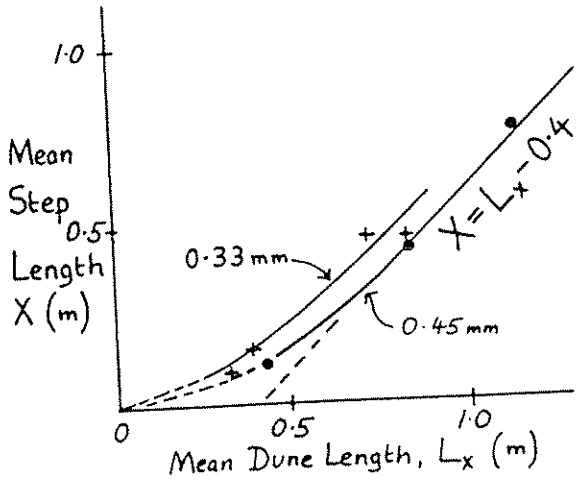

Figure 6.15 Relation between mean step length of grains and mean spacing of dunes. (After Grigg, 1970.)

A full discussion of theory and observations related to stochastic theories of bed-load movement goes beyond the scope of these notes; the reader is referred to papers by Crickmore and Lean (1962a, 1962b), Crickmore (1967), Yang and Sayre (1971a, 1971b), Rathbun and Nordin (1971), Hung and Shen (1976, 1979), Shen and Kikkawa (1980), and Cheong and Shen (1982). It is sufficient to indicate that Einstein's assumptions are not fully supported by recent studies and that further theoretical and experimental studies are currently under way in this field.

Effect of Shape

The movement of grains on the bed is strongly affected by their shape, and the effects are somewhat different from the effects of shape on settling velocity discussed in Chapter 4. The reason is that grains tend to become oriented on the bed by pivoting around other grains or resting against them, and they do not necessarily orient themselves with their maximum projection area normal to the flow, as they generally do during settling. Furthermore, certain shapes--notably prolate forms (rollers) but also disks--roll more easily than others.

An early experimental study of the effect of shape was made by Krumbein (1942) using artificial ellipsoidal grains, all with the same nominal diameter, in a flume with a smooth bed. Depth was held constant at 0.3 m and velocity was varied by changing the slope. Krumbein found that, for a given fluid velocity, spheres and rollers moved fastest. Within any one shape class (e.g., rollers) grain velocity increased with increasing sphericity; the shape effect was greatest at low fluid velocities and grain velocities, and was less important as particles tended to be taken into suspension.

Lane and Carlson (1954) found that pebbles lining the beds of Colorado drainage canals were sorted by both size and shape. In a given sample of bed pebbles the disk-shaped pebbles had substantially smaller volumes than the more spherical pebbles--the opposite of what would be the case if the pebbles had the same settling velocity--indicating that spherical pebbles rolled more easily and were more easily set in motion than disk-shaped pebbles, which tended to assume more stable, imbricated orientations on the bed.

Bradley et al. (1972) studied the effect of shape both in the field (Knik River, Alaska) and in the laboratory. They detected downstream sorting of shapes, with platy pebbles being the most easily transported, then elongate pebbles (rollers), and more equant pebbles being the least easily transported. They recognized that the anomalies in the shape effects observed in different field and laboratory investigations are probably caused by the different shape-sorting effects of grains moving by traction and by suspension. The readier transport of bladed pebbles can probably be explained by their observed "erratic-saltation" type

of motion, which tends to lift the bladed grains up into the flow, so that at sufficiently high fluid velocities their low settling velocity is more important than their poor rollability.

There is an interesting and still not fully explained difference between the behavior of sand-size grains and that of larger grains. Both sizes display upstream imbrication, but elongate sand grains are almost always oriented with the long axis parallel to the flow (and the blunt end pointing upstream; Dapples and Rominger, 1945), whereas pebbles are generally arranged with their long axes normal to the flow (except in conglomerates associated with turbidites, which presumably are deposited by mass flows).

RATE OF TRANSPORT OF BED LOAD

Derivation of a relationship between flow conditions and rate of movement of bed material is one of the classic problems of sedimentation engineering. Most published studies have adopted a strictly empirical approach to the problem in an attempt to solve practical design problems. The problem is frequently divided into two parts, corresponding to the two parts of the total load: the bed load and the suspended load. As the suspended load is relatively easily measured (see below), the most difficult part of the problem is to predict the rate of transport of bed load. The problem is a fundamental one for sedimentology too, because the rate of deposition or erosion at one place must be proportional to the downstream rate of change of sediment transport rate (see Chapter 7). We will not attempt to solve the problem here; instead we will indicate which of the variables are likely to be important and discuss briefly the derivation of one of the most successful of sediment-transport equations.

A commonly adopted approach to the problem is to try to list all the variables likely to be important in determining the rate of transport. This has been done, for example, by Willis and Coleman (1969), Southard (1971), and Yalin (1972). The list can be quite long, but if we consider that the acceleration due to gravity, the sediment and fluid density, and (to a lesser extent) the fluid viscosity are all essentially fixed for the movement of ordinary sand by water, the main variables left are grain size, mean flow velocity, and flow depth. The grain size determines the settling velocity (which could therefore be chosen instead of the grain size), and the flow depth and velocity determine the shear stress or shear velocity. Experience indicates that it is wise to include the depth as a separate variable, because as sediment rises higher above the bed, its rate of movement is less likely to be determined uniquely by the shear stress acting at the bed.

For very low rates of bed-load movement, however, the experiments of Meland and Norrman (1966), Francis (1973), Fernandez Luque (1974), Fernandez Luque and van Beek (1976), Abbott and Francis (1977), and Mantz (1980) have shown that the

average rate of movement U_G of individual grains can be predicted from the shear velocity together with the critical shear velocity needed to move the grain, which is really just a function of the grain size (see Figure 6.16). Mantz (1980) found that the sediment transport rate q_s, which is the average area P of grains moving over a unit area of the bed times the rate of grain movement U_G, can be expressed in dimensionless form as

$$G = P \frac{U_G}{u_*} \tag{6.15}$$

and that this is essentially a unique function of the Shields parameter except for some variation due to large differences in grain shape. G was found to be proportional to the seventeenth power of β.

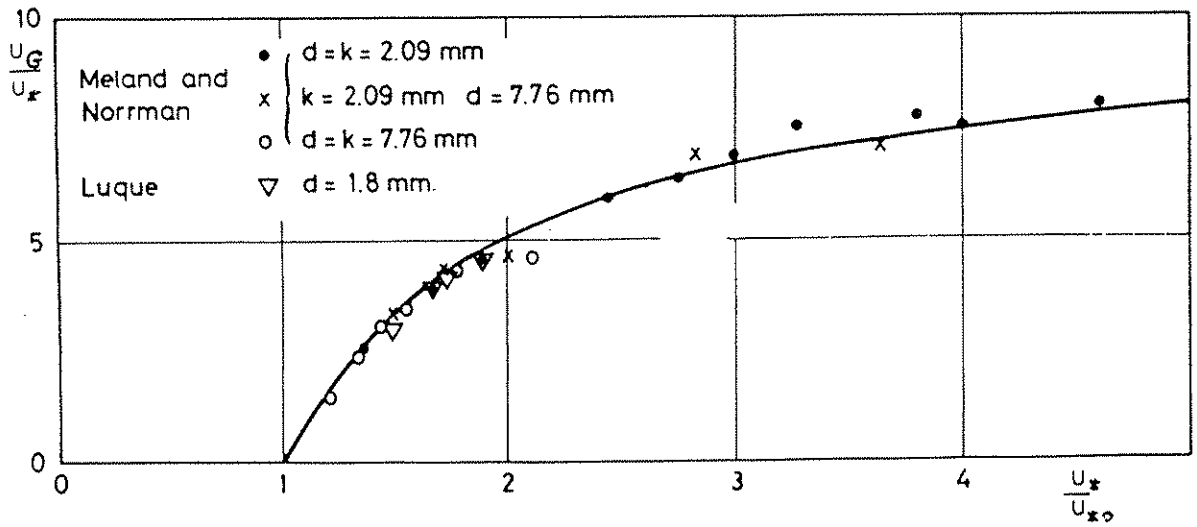

Figure 6.16 Plot of dimensionless grain velocity U_G against dimensionless shear velocity u_*/u_{*c}. After Fredsøe and Engelund (1976), who found that the data fell along the line $U_G/u_* = 10(1 - 0.7\ u_{*c}/u_*)$.

For higher sediment transport rates, it has been demonstrated experimentally that the shear velocity alone (and therefore the Shields parameter) is not an adequate variable to predict sediment transport rates. From the list given above, it might be expected that one would need at least three dimensionless variables (dimensionless versions of grain size, mean flow velocity, and

flow depth) to predict the sediment transport rate, just as they are needed to predict the occurrence of bed forms (Chapter 7). But for a limited range of conditions (transport of sand over dune-covered beds) Engelund and Hansen (1972) found it possible to reduce the number of dimensionless variables required from three to two:

$$\left(\frac{\rho_s-\rho}{\rho}\right)^2 \frac{q_s}{(gD^3)^{1/2}} = 0.05\left[\frac{u_*U^2}{(gD)^{5/2}}\right] \qquad (6.16)$$

The dimensionless variable on the left-hand side of Equation (6.16) is the volumetric sediment transport rate per unit width of channel, q_s, made dimensionless by use of the grain size D and combined with the density ratio (as also suggested by Willis and Coleman, 1969). The right-hand side combines two dimensionless ratios, one essentially a Shields parameter and the other a friction factor. The equation was derived partly from similarity considerations and was based on only a small amount of experimental data (largely taken from Guy et al., 1966). Details are given in the very readable book by Engelund and Hansen. It is surprising that the equation, based entirely on laboratory data, has been found to give very good results when tested in the field. The most important single fact to note is that sediment transport rate varies as a high power, roughly the fifth power of the mean velocity or the shear velocity. (Remember that, for a given flow depth, shear velocity is roughly proportional to the mean flow velocity.) Depth does not appear explicitly in the Engelund and Hansen formula, but it is present implicitly because the product on the right side includes both the shear velocity and the mean velocity.

SALTATION

Introduction

The term saltation, derived from the Latin verb meaning to jump or leap, was introduced into geology by McGee (1908, p. 199). The first detailed description was by Gilbert (1914), who regarded it as the dominant mode of stream traction. His description has been influential, and although we regard it as somewhat misleading, we include it here:

> "Viewed from the side, the saltation was seen to occupy at the bottom of the current a space with a definite upper limit, parallel to the sand bed. Within this space--the zone of saltation--the distribution of flying grains was systematic, the cloud being dense below and thin above, but not perceptibly varying from point to point along the bed. Viewed from above, the surface of

> the cloud seemed uniform and level, and it all appeared to be moving in the same direction. There was no suggestion of swirls in the current." (Gilbert, 1914, p. 27).

Gilbert therefore clearly distinguished saltation from both rolling and suspension, and stated that "each grain is projected from the bed with an initial velocity which gives it a trajectory analogous to that of a cannon ball" (Gilbert, 1914, p. 28).

Saltation is generally better developed in air than in water. The behavior of saltating grains in air has become well known through the experimental studies of Bagnold (1941), Chepil (1945), Zingg (1952), and others. The observed trajectories generally support the idea that the grain is raised up from the bed by a short-lived impulsive force, and that its subsequent path results mainly from the action of gravity and fluid drag, which decelerate the rise, produce an accelerating fall, and at the same time rapidly accelerate the grain to a horizontal velocity nearly equal to that of the moving fluid near the top of its trajectory.

Recently there has been a considerable revival of interest in the detailed mechanics of saltation, stimulated partly by the renewed interest in the physics of bed-load transport in water and partly by the problems of eolian transport of sediment on other planets. As a result of this recent activity, it has become clear that there are still quite a number of aspects of saltation that remain incompletely understood, including some quite fundamental questions:

(i) What causes the initial rise of saltating grains? Chepil (1945, 1961), among others, regarded hydrodynamic lift as the dominant mechanism. He showed that such forces act on a saltating grain only when it is in contact with the bed or very close to it. As soon as the grain rises from the bed, horizontal drag forces increase greatly, but lift forces drop almost to zero (Figure 6.4). Bagnold (1941, 1973), however, has tended to discount hydrodynamic lift, except perhaps while a saltating grain layer first develops, and to emphasize the importance of the impact of saltating grains as they return to the bed. The "impact" theory of saltation has recently been elaborated in theoretical models by Tsuchiya (1969, 1970), Reizes (1978), and Murphy and Hooshiari (1982).

(ii) Is true "ballistic" saltation a dominant mode of grain movement for bed load in water? Its importance in air is generally admitted, but there is much less agreement on its importance in water. Saltating grains rise much higher above the bed in air (about 0.1 m) than in water (only a few mm) because of the much greater effect of fluid drag and the reduced effect of grain inertia in water. Kalinske (1943) calculated that the height to which saltating grains would rise, for given grain size and shear velocity, should be inversely proportional to the fluid

density, i.e., grains should rise 800 times higher in air than in water. Also, the criterion for suspension developed in a previous section, $u_* = w$, implies that grains should be relatively easily taken into suspension in water, because of the much lower settling velocity of grains in water than in air. Therefore most engineering writers (Einstein, 1950; Einstein and Chien, 1955; Ippen, 1971; Vanoni, 1977) have assumed that suspension by turbulence is a much more important mechanism of sediment transport in rivers than saltation, even quite close to the bed. In contrast to this view, Bagnold (1956, 1973) has argued that true saltation is independent of turbulence, and that high concentrations of grains close to the bed tend to suppress turbulence and make saltation (and grain collisions) the dominant mechanism of sediment transport. In geology these ideas have been elaborated by Dzulynski and Sanders (1962, p. 88), who coined the term "traction carpet" for the dense "saltation zone" of Gilbert, which is not invaded by turbulent eddies of any size from the overlying turbulent flow, and by Moss (1972a, p. 162), who introduced the term "rheological layer" to describe essentially the same phenomenon:

> "As bed-load motion becomes more intense in sand-sized materials, a stage is reached wherein collisions between particles become inevitable and thereafter the load proceeds as a dense mass of colliding particles, buoyed up by the dispersive pressure thus generated.... This moving mass of particles behaves like a viscous fluid, but has a remarkably sharp boundary with the flow above and maintains almost constant thickness over quite large bed areas.... (It) will be called the "rheological layer."

(iii) How important are collisions between grains in bed-load transport? This question arises naturally from the preceding two. Most authors would agree that collisions between moving grains (as distinct from collisions between a moving grain and a grain resting on the bed) are of minor importance in eolian saltation. Such collisions have not been observed in high-speed photographic studies, and would not be expected because of the relatively great thickness and low concentration of the saltating grain layer. But in layers with a high concentration of grains close to the bed in water flows, collisions between grains are much more probable. Leeder (1979) calculated that even at flow intensities as low as $u_*/u_{*c} = 2$ (corresponding to $u_*/w = 0.3$) there is a high probability of collision between grains saltating in water. It seems inevitable that grain contacts will take place with high frequency close to the bed, unless prevented by viscous cushioning.

It is clear from this brief review that there is little consensus about the basic mechanisms and significance of saltation. What is important for air is not necessarily of equal

significance for water. In what follows we begin by reviewing some of the basic experimental data for saltation in air and then seeing how these observations compare with the predictions made by some simple theoretical models. We consider saltation in water only at very low grain concentrations and defer the problem of what happens at high concentrations until after we have considered theories of grain suspension by turbulence.

Saltation in Air

The general nature of the trajectories of saltating grains is known from descriptions by many investigators (Gilbert, 1914; Bagnold, 1941; Zingg, 1953). The trajectory shown in Figure 6.17 is taken from the paper by Maegley (1976), who describes it as a typical path of a medium sand grain saltating in air. Many authors have remarked on the steep angle at which grains leave the bed, as is well exemplified by the trajectories shown in Figures 6.12 and 6.17. Recently, however, White and Schulz (1977) measured the statistical distribution of lift-off angles and impact angles for saltating glass spheres in a wind tunnel and found that the average angle of lift-off was 50°, and less than 10% of the grains observed took off at an angle of more than 80°. The data are shown in Figure 6.18 together with the corresponding data on lift-off speed and impact speed. The steepness of the angle of ascent of the "average" trajectory has probably been somewhat exaggerated by some authors (though it is possible that natural grains tend to rise more steeply than perfect spheres because of a higher value of α, the angle of easiest movement discussed earlier in this chapter). The average angle of impact was 14°, close to the values mentioned by most earlier writers. Maximum velocities attained during lift-off were generally somewhat larger than the shear velocity.

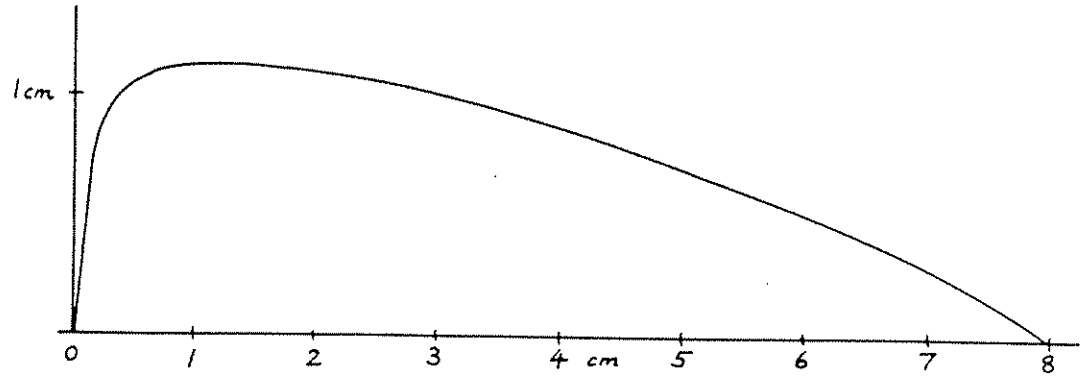

Figure 6.17 Typical path of a medium sand grain saltating in air (modified from Maegley, 1976). Note exaggeration of vertical scale.

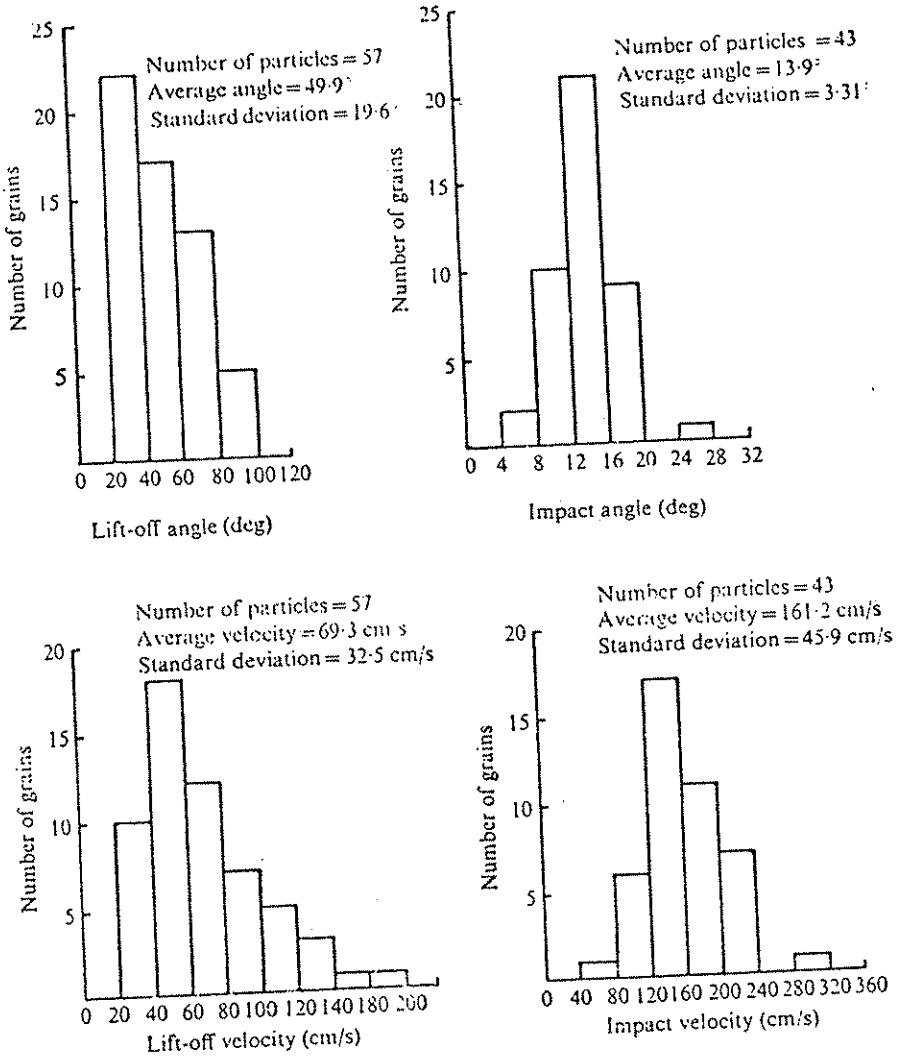

Figure 6.18 Distribution of value of lift-off angle impact angle, lift-off velocity, and impact velocity for a sample of spherical glass beads 0.5 mm in diameter saltating in a wind tunnel. Shear velocity was 40 cm/s. From White and Schulz (1977).

Even for a given sand and wind there is a considerable variation in the height to which saltating grains rise. The commonly held idea that the saltation zone has a well-defined upper limit is not supported by experimental data. Using a moderately well sorted sand bed, both Zingg (1953) and Williams (1964) found that the sediment discharge per unit cross-sectional area, q_s, varied as a negative exponential function of the height y above the bed

$$q_s = q_o \exp(-y/H)$$

where q_o is the sediment discharge at the bed ($y = 0$) and H is the mean height to which the grains rise, defined as the height below which the sediment discharge is half of the total.

Zingg (1953) found that H varies with both grain size and shear velocity, and determined an empirical equation of the type $H = \text{const}\ (D^3/2u*^{1/2})$. Williams found that H also depended on grain shape, and increased with increasing sphericity. Zingg found that for a given moderately well sorted sand bed the size of sand moving at progressively higher levels generally decreased, although the decrease was often not very marked above the lowest 5 cm. Thus, although coarser sands saltate to greater heights on the average, grains reaching the highest levels are generally the smallest grains in the population. The explanation for this effect is unclear, but possibly there is some tendency for smaller grains to rise higher after being struck by larger grains. The shear velocities in these experiments were approaching the magnitude of the settling velocities of the finest grains used, so possibly turbulent suspension might also have been a factor.

In the rising part of the trajectory the saltating grain is moving downstream more slowly than the surrounding fluid, which therefore exerts a drag force on the grain and accelerates it horizontally. The reverse is true in the falling part of the trajectory: the grain is moving faster than the surrounding fluid, so the fluid exerts a retarding force on the grain and is itself accelerated by the grain moving through it. It might therefore be expected that the velocity profile in the fluid is significantly modified by the presence of a layer of saltating grains close to the boundary. This has been confirmed in observations in wind tunnels reported by Bagnold (1941), Zingg (1953), and others (Figure 6.19). As discussed in Chapter 5 the velocity of air moving over a fixed rough bed varies logarithmically with height above the bed. Zero velocity corresponds to an intercept of y_o on the y axis, and y_o is directly related to the grain size (which in this case is equal to roughness, i.e., $D = k_s$) by the equation $D = 30y_o$, obtained by setting $D = k_s$ and $u = 0$ in Equation (5.20B). If $u*$ is changed, the slope of the velocity profile varies, but the intercept y_o does not. For air moving over a saltating grain layer a logarithmic profile is still observed, but there are two important modifications: (i) profiles for different shear velocities no longer converge on the point $(0, y_o)$ located on the y axis (where $u = 0$) but on a point (u_o', y_o') where u_o' is not equal to zero. and (ii) y_o' is much larger than y_o. Similar effects are observed for saltation in water; see Olivinskaya et al. (1973).

According to White and Schulz (1977), y_o' has been shown experimentally by Andres (unpublished thesis, 1970) to be 2.5D, i.e., $75y_o$. Movement of grains by saltation therefore increases the resistance of the bed even if the bed remains plane. If the resistance of the bed is measured by y_o or k_s (defined as $30y_o$), however, then this resistance is no longer a constant for a given grain size but depends on the shear velocity.

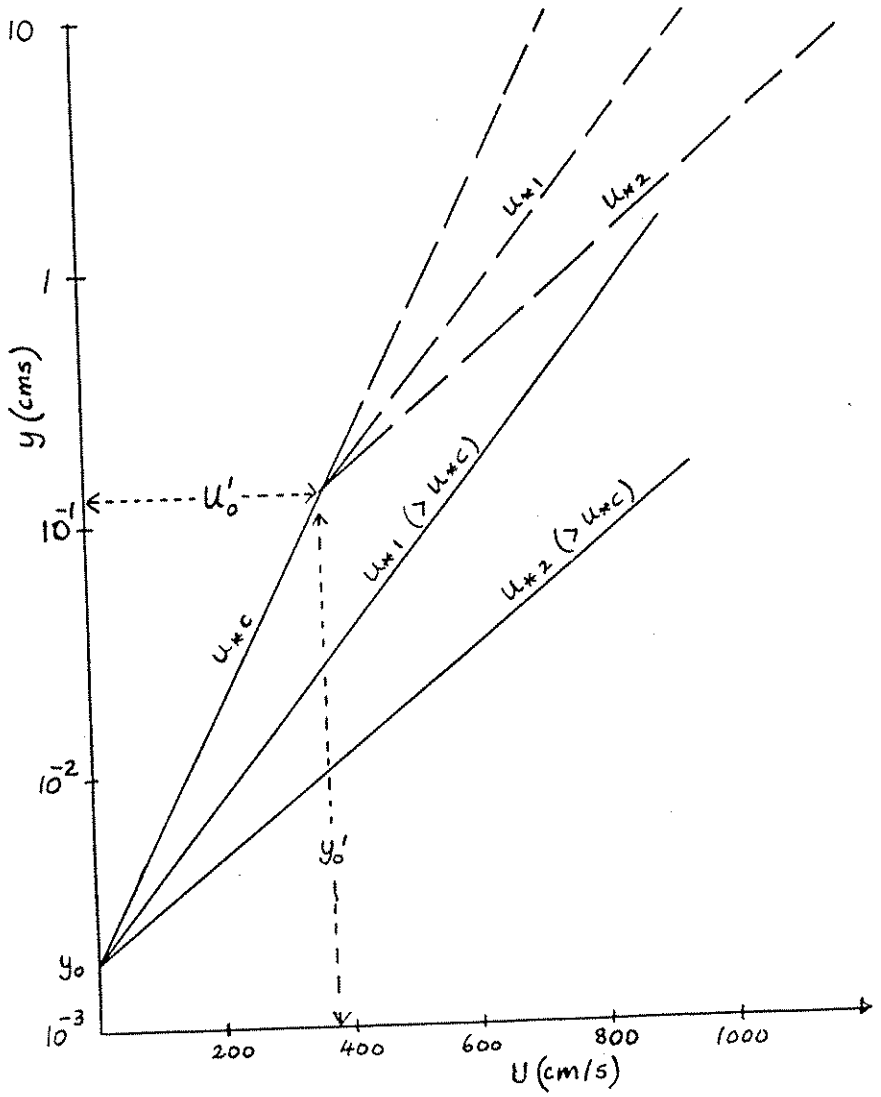

Figure 6.19 Typical velocity profiles observed close to the boundary in a wind tunnel. Solid lines show profiles observed where grains are fixed to the bed, and dashed lines show profiles observed where grains are saltating over a plane bed.

Owen (1964) suggested that the vertical component of lift-off velocity might be proportional to u_*, and so the height of rise of grains (neglecting air resistance) might be expected to be proportional to $u_*^2/2g$. So the effective value of k_s for a saltating boundary might be proportional to u_*^2 rather than to D. Owen plotted u/u_* against the logarithm of $2gy/u_*^2$ (a plot analogous to that of Figure 5.15, in that $u_*^2/2g$ can be viewed as a roughness length), and showed that the experimental data of Bagnold (1941), Chepil (1945), and Zingg (1953) did in fact plot as a straight line, with some scatter. As Zingg showed that the height of rise of a grain was proportional to $u_*^{1/2}$ rather than to u_*^2, and was also proportional to $D^{3/2}$, it is not surprising that

there was some scatter. Rather it is surprising that Owen's hypothesis leads to such good results.

One other aspect of the observed behavior of saltating grains must be considered before we turn to some of the theories of saltation. Rapid spinning of saltating grains has been observed by Bagnold (1941), Chepil (1945), and others. Spinning of grains is potentially important not only for the light it throws on the mechanism of ejection of the grain from the bed (as discussed by Danel et al., 1953) but also because spinning generates a lift force that acts while the grain is in flight. This effect of spinning is generally called the Magnus effect, though strictly this applies to spinning cylinders; the equivalent effect for spheres is sometimes called the Robins effect (Tritton, 1977, p. 124-126). The effect is easily explained qualitatively by reference to Figure 6.20. Rotation of the grain changes the streamlines so that they are no longer symmetrical about the grain. As shown in Figure 6.20, streamlines are closer together above the grain, implying that velocities are greater there than they are below the grain. From the Bernoulli equation (Chapter 3) it follows that the pressure is less above the grain than below, and the grain experiences a lift force. The variation in lift coefficient with rate of spinning is known (see Tritton, 1977, for a good summary), so the lift force can be calculated. White and Schulz (1977) could account for the observed saltation trajectories only by taking this effect into account. For most observed trajectories the rate of spinning could not be observed directly, but a good fit of observed trajectories to theoretical calculations could be made by assuming a rate of spin of several hundred revolutions per second. This is known from photographic studies to be about the right value for the spin. An example of their observations is shown in Figure 6.21.

The fact that saltating grains spin rapidly suggests that they rise from the bed by pivoting over bed grains. For grains in water there are some direct observations showing this (see below). This confirms that an analysis of initial movement in terms of moments is probably more realistic than one in terms of sliding or simple lift-off from the bed.

We can now return to the first of the two questions posed about the mechanism of saltation in air: What is the lift-off mechanism? Hydraulic forces (lift, or some combination of lift and drag) or grain impact, or some combination of the two? In the simple case where no other grains are moving, the fluid velocity impacting on a bed grain, and exerting lift or drag forces on it, should be proportional to the shear velocity. The force itself should be proportional to the shear velocity times the cross-sectional area of the grain, that is to $u*D^2$, and it should act only while the grain is close to the bed, say over a distance proportional to D^3. So the upward impulse (force times distance) is proportional to $u*D^3$, and it must overcome the inertia of the grain, which is proportional to the density times the volume, or D^3. Therefore the speed at which the grain leaves the bed should

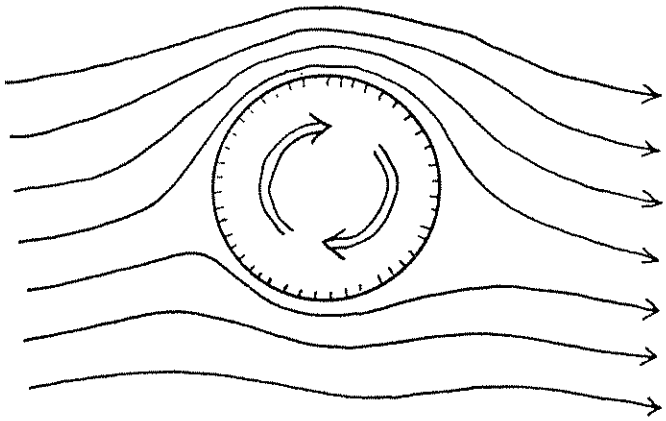

Figure 6.20 Streamlines for a fluid flowing around a spinning sphere. Crowding of streamlines above the sphere indicates a lower pressure there, and consequently a net lift force acting on the sphere.

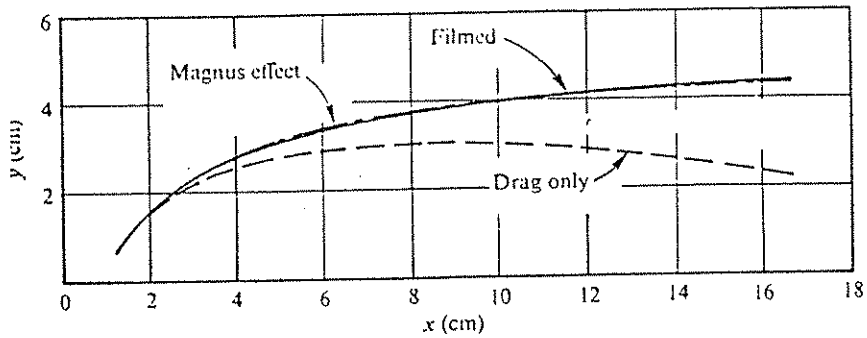

Figure 6.21 Trajectories of a saltating glass sphere calculated for the case of drag only (nonrotating sphere) and drag plus lift (a sphere rotating at 275 revolutions per second) compared with the observed trajectory. As can be seen, spinning of the grain produces a large effect both on the shape of the trajectory and on the maximum height to which the grain rises. (From White and Schulz, 1977, Fig. 3).

be proportional to u*, as Owen (1964) hypothesized (it should also be inversely proportional to the density), and it should not depend on the grain size. Experimental results do not confirm these predictions. Unfortunately this does not mean we can reject the hydraulic-lift hypothesis, because of a number of complicating factors: (i) As we have already seen, the velocity distribution close to the bed is modified by the presence of saltating grains. The velocity below y = 2.5D is no longer predictable from theory, although one might argue from the form of the velocity profile above this level (see White and Schulz, 1977, their Equation 6) that the velocity at bed level (say at y = 0.5D) should depend

more on D than on u*. (ii) The height to which grains rise depends on their rate of spin, which cannot be predicted.

One of the arguments used in favor of hydraulic lift forces has been the very steep angle of lift-off. The data indicate that angles are not as steep as has generally been supposed. In view of the evidence, reviewed earlier, that α (the angle of easiest movement of a grain surrounded by similar grains) is probably about 45 to 70° (rather than 30° as generally supposed) it seems that the lift-off angle of grains moved by any kind of short-lived impulse (lift, drag, or a shock resulting from grain impact) is likely to be just as steep.

The theoretical models of Tsuchiya (1969, 1970), Reizes (1978), and Murphy and Hooshiari (1982) certainly demonstrate that saltation can continue once started, without the necessity of any fluid lift or drag forces acting on grains resting on the bed, but they do not lead to any predictions about grain trajectories that can distinguish this hypothesis conclusively from the fluid-force hypothesis.

It must therefore be concluded that the question of the lift-off mechanism remains unresolved. It seems, however, to be quite open to experimental resolution by detailed observation in a wind tunnel. Do grains saltate without being struck by other grains and without themselves rebounding from the bed? As we shall see below, this <u>does</u> seem to be the case for saltation in water.

The second question concerned the nature and relative importance of saltation in water. Certain observations by Gordon et al. (1972), Fernandez Luque (1974), Fernandez Luque and van Beek (1976), and Abbott and Francis (1977) suggest that simple ballistic movement of grains, and movement by grains impacting on the bottom, may not be as important in water as some authors have held. Gordon et al. (1972) studied the saltation of spheres of diameter 6.6 mm and specific gravity 1.3 in a flow of water. Grain movement was made essentially two-dimensional by confining the flow within a flume only 7.9 mm wide. Observed trajectories were typical of saltation except that take-off angles were rather low, generally in the range of 10° to 35°. One reason for the low lift-off angle was that a saltating grain did not simply bounce off the loose grains on the bed; instead the moving grain rolled around the grain on the bed before lifting off to make another saltatory jump. There was a clear correlation between the fractional loss of kinetic energy and the angle of incidence in the collision, but the collisions were not simple elastic collisions; it seems clear that a combination of grain inertia and fluid drag forces was involved. Both Fernandez Luque (1974) and Abbott and Francis (1977), studying saltation in water, found that very few apparent saltations could be explained entirely as simple ballistic trajectories; some other kind of lift force was involved in most trajectories. These authors did not investigate Magnus effects, but it seems probable (particularly for the data reported

by Francis) that the main lift was provided by turbulence. Abbott and Francis (1977, p. 253) found that "there appears to be no effective elastic rebound between the bed and a moving grain impinging on it." Very few observed saltations immediately followed the return of a grain to the bed; most were preceded by some rolling. Furthermore, there seemed to be no difference in take-off velocity between grains rebounding from the bed and grains beginning a saltation from rest or rolling.

Murphy and Hooshiari (1982) studied the saltation of marbles 15.7 mm in diameter on a bed of similar but fixed marbles. The settling velocity, about 0.8 m/s, was much higher than the shear velocities needed to produce continuous saltation (0.08-0.11 m/s), so there is no doubt that saltation rather than suspension was the dominant mode of movement. In this case, grains appeared to be rebounding directly from the bed, though the exact mechanism of initial rise from the bed could not be studied by the stroboscopic technique used. Analysis of the trajectories indicated that they could be satisfactorily accounted for by a model that took into account gravity (and buoyancy), horizontal and vertical components of drag, and the added-mass effect that is produced by accelerating a solid through a fluid (Hamilton and Courtney, 1977). Magnus effects were not significant for grains of this size and shape in water. The observations suggest that bed impact forces are sufficient to produce the upward rise, and that lift forces are not necessary. If this is true (and it is not proven, because the bed was rigid in the model, not loose as it would be in nature) then there is the possibility that saltation of larger (gravel-size) grains in water may be different from that of sand in water. It may be that the saltation of gravel in water is more like that of sand in air than that of sand in water.

The observations described above were all made on flows in which very few grains were in saltation. Possibly fluid drag and lift play a much reduced role in initiating and maintaining saltation in a "traction carpet," but the observations certainly suggest severe limitations on a simple impact hypothesis for saltation at low concentrations in water, and they indicate a very significant role for turbulence in transport of sand as bed load.

SUSPENSION

Introduction

Suspended grains are held up above the bed by the turbulent motion of the fluid. The weight of the particle is therefore transmitted to the fluid (and increases the hydrostatic pressure at the bed) rather than being transmitted by grain contact to the solid part of the bed, as is the case for grains that roll or slide over the bed.

It should be noted that it is theoretically possible for grains to move through the fluid close to the bed without actually being in contact with the bed, and yet not be in suspension. This happens in true saltation: the ballistic motion of the grains results from fluid lift forces and/or grains striking the bed, but it is not at all dependent on turbulence--and in fact Francis (1973) has described saltation of grains in a laminar flow. It has also been postulated that grains may be held in a dispersed state close to the bed by actual collisions between grains or by near-misses that produce viscous forces with vertical components that hold the grains above the bed. This is the "dispersive pressure" of Bagnold (1956), the effectiveness of which is still very much a matter for debate.

We noted above that turbulence first becomes important in suspending grains when the vertical component of turbulence, whose strength is measured by the root-mean-square of the instantaneous velocity, becomes about equal to the settling velocity of the grains (Equation 6.14). This is so even if the turbulence is isotropic, so that the strength of the upward velocity components is the same as that of the downward components. Even in this case some grains will diffuse away from a region of high concentration, such as the bed itself or a layer of moving particles close to the bed.

Suspension by isotropic turbulence was investigated experimentally by Rouse (1939), who produced a close approximation to isotropic turbulence by vertically oscillating an array of square grids in a large-diameter vertical cylinder ("turbulence jar").

The rate of downward movement of grains, from a region in the fluid having a concentration C of uniformly sized grains, is

$$\begin{matrix}\text{rate of settling} \\ \text{(per unit volume)}\end{matrix} = -wC$$

(The positive y direction is upward.) We can make the assumption that the upward vertical diffusion of particles follows a Fickian diffusion law, like many other diffusion processes:

$$\begin{matrix}\text{rate of turbu-} \\ \text{lent diffusion} \\ \text{(per unit volume)}\end{matrix} = \varepsilon_s \frac{dC}{dy}$$

where ε_s is a diffusion coefficient, which should be constant in a field of isotropic turbulence of any particular type and strength.

Equating the two rates gives a formula for the vertical distribution of the concentration of suspended particles:

$$wC + \varepsilon_s \frac{dC}{dy} = 0 \qquad (6.17)$$

We expect that the diffusion coefficient will be proportional to, if not actually equal to, the corresponding coefficient for the diffusion of fluid momentum, i.e., the kinematic eddy viscosity (see Chapter 5), and therefore in a turbulence jar it should be proportional to the frequency of vertical oscillation of the grid. Rouse verified that this is the case, thus confirming the validity of the diffusion equation (see also experimental results reported by Antsyferov and Kos'yan, 1980).

Suspension in a Shear Flow

In nature we are much more interested in suspension in shear flows than in flows with isotropic turbulence. In a shear flow (for example, in a river), where turbulence is not even approximately isotropic except perhaps at large distances from the bed, we expect that the diffusion coefficient will vary in the y direction, so we need an expression that tells us how it varies with y before we can make use of Equation (6.17) to predict how the sediment concentration varies with y.

To find such an expression we assume the sediment diffusion coefficient ε_s to be proportional to the eddy viscosity ε, given by

$$\tau = \rho\varepsilon \frac{dU}{dy}$$

Assuming $\varepsilon_s = \beta\varepsilon$, then

$$\tau = \frac{\varepsilon_s \rho}{\beta} \frac{dU}{dy}$$

where β is a coefficient which we expect to be close to one. We know by Equation (1.20) that τ must vary linearly with y in a uniform open channel flow,

$$\tau = \tau_o \left(1 - \frac{y}{d}\right)$$

so

$$\varepsilon_s = \frac{\beta \tau_o}{\rho}\left(1 - \frac{y}{d}\right) \Big/ \frac{dU}{dy}$$

$$= \beta u_*^2 \left(1 - \frac{y}{d}\right) \Big/ \frac{dU}{dy}$$

Using the law of the wall $(du/dy) = u_*/\kappa y$ in differential form,

$$\varepsilon_s = \beta u_* \left(1 - \frac{y}{d}\right)\kappa y \qquad (6.18)$$

This is the relationship between ε_s and y that we need in order to solve Equation (6.17). Combining Equations (6.17) and (6.18) gives

$$\frac{dC}{C} = \frac{-w\ dy}{\beta \kappa u_* \left(1 - \frac{y}{d}\right) y} \qquad (6.19)$$

which may be integrated to give the equation first derived by Rouse (1937):

$$\ln C = \frac{w}{\beta \kappa u_*} \int_a^d \frac{dy}{\left(1 - \frac{y}{d}\right) y}$$

or

$$\frac{C}{C_a} = \left(\frac{d-y}{y}\ \frac{a}{d-a}\right)^z \qquad (6.20)$$

where

$$z = \frac{w}{\beta \kappa u_*} \qquad (6.21)$$

The exponent z is sometimes called the Rouse number.

Equation (6.20) gives the concentration of sediment of a given settling velocity w relative to its concentration C_a at some arbitrarily chosen level y = a (generally chosen to be close to the bed). The graph of the equation is shown in Figure 6.22. Because both β and κ are supposed to be constants, we expect that the main factor that determines the distribution of suspended sediment with height y above the bed is the ratio of the settling velocity w to the shear velocity u*. We have already suggested that a critical ratio of about one determines whether any grains will go into suspension: since β ≈ 1 and κ ≈ 0.4, w/u* less than one corresponds to z less than 2.5. We can see from Figure 6.22 that at values of z greater than 2.5 any sediment in suspension would be concentrated in a zone very close to the bed--and this tends to confirm our choice of w/u* as a suitable criterion for suspension.

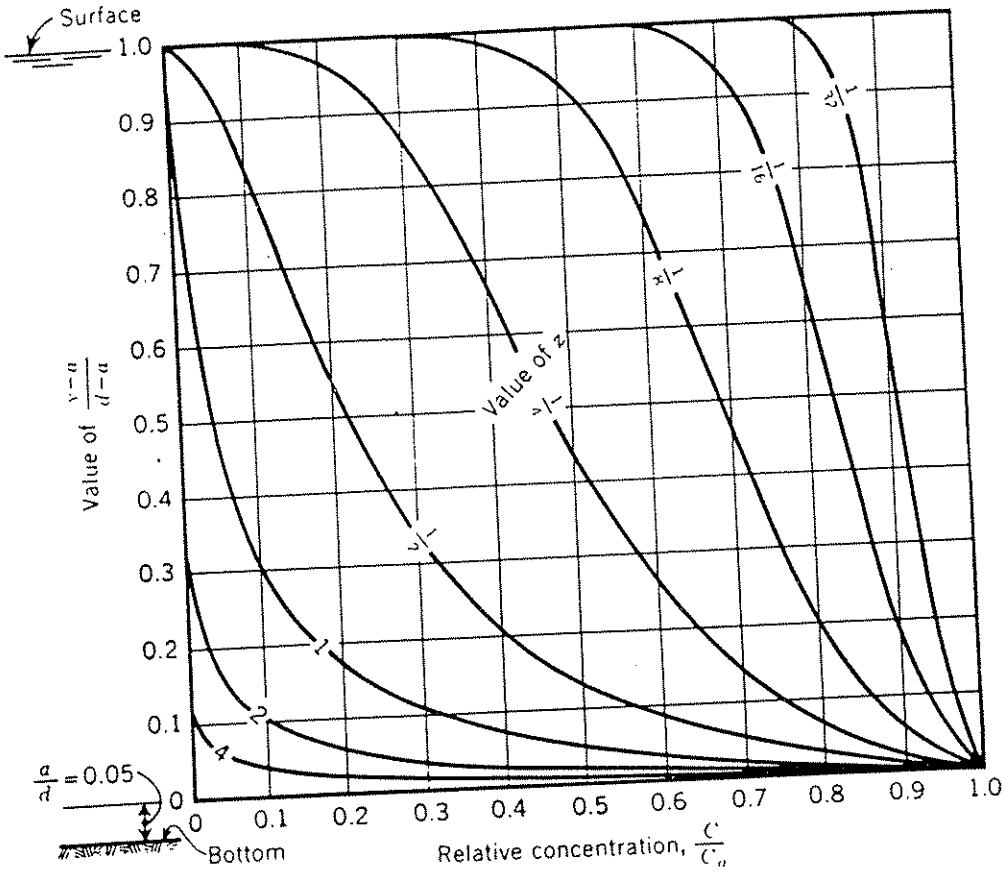

Figure 6.22 Distribution of relative concentration of suspended sediment with relative depth above the datum y = 0.05d. (After American Society of Civil Engineers, 1963.)

We should note that we expect the theory to fail very close to the bed, because a balance between passive upward turbulent diffusion and downward settling is not physically reasonable there: grain movements very near the bed are controlled by fluid lift and drag forces and turbulent bursts, and if concentrations are high these movements may be significantly affected by collisions or interactions between grains. But this is not a serious limitation if the theory successfully predicts concentrations over most of the flow depth (which in any event are the only ones that we can measure).

Experiments to test Equation (6.20) were reported by Vanoni (1946). These experiments were mostly run at relatively high velocities over a flat bed (either a sand bed or the floor of the flume itself) and at varying concentrations of sand. Vanoni found a general agreement between predicted and observed sediment concentrations.

It is worth considering for a moment what factors in natural channels affect the ratio $w/u*$ and therefore the vertical distribution of suspended sediment. We have seen in earlier chapters that, for a given grain size and shape, w is reduced by an increase in viscosity--which can be produced by a reduction in water temperature or an increase in the concentration of clay-size material (wash load) in suspension. Both of these effects tend to reduce z and make sediment more uniformly distributed in the vertical section of a river.

We have also seen that the ratio $U/u*$ is equal to $(8/f)^{1/2}$, by the definition of the friction factor f in Chapter 5, so for a given mean flow velocity an increase in shear velocity is produced by an increase in f--that is, an increase in the frictional resistance of the bed. Increase in shear velocity will also result in a more uniform distribution of suspended sediment in a vertical section. In sand-bed rivers, changes in f are produced mainly by changes in the relative roughness, which depends mainly on the nature and size of the bed forms. Large bed forms, such as dunes, produce high values of f, and therefore should tend to distribute the suspended sediment more uniformly in the vertical.

Unfortunately, it is difficult to test this prediction exactly, because in shallow rivers, where dune height can be as much as half the mean flow depth, the flow is no longer uniform over streamwise length scales of the order of the flow depth, and the velocity distributions show large perturbations from the logarithmic distribution that was assumed in deriving Equation (6.20). For the Rio Grande, in lower flow regimes with dunes on the bed, Nordin and Dempster (1963) concluded that the measured suspended-sediment concentrations were correctly predicted by Equation (6.20) even though the measured velocity distributions showed large deviations from logarithmic. In upper flow regimes, with a flat bed and generally higher suspended-sediment concentrations, the velocity distribution was logarithmic and the von Karman κ was reduced below its clear-water value of 0.38, just

as observed experimentally, but the measured distribution of suspended sediment was more uniform in the vertical than predicted by Equation (6.20). The reason for this is still not well understood.

The theory of suspension by turbulent flows outlined above is based on the assumption that the flow is steady. This may be a reasonable approximation for most rivers, but tidal currents change quite rapidly in both depth and speed over the tidal cycle. In experimental shear flows it has been shown that decelerating flows have larger turbulence intensities, and produce larger shear stresses on the bed, than steady flows. Decelerating flows therefore might be expected to be more erosive, and to have a higher capacity for suspended sediment, than steady or accelerating flows. Wimbush and Munk (1970), Gordon and Dohne (1973), Gordon (1975), Bohlen (1977), and McCave (1979) have reported measurements suggesting that turbulence intensities are higher than normal during deceleration of flows on both flood and ebb tides. Gordon (1975) and Bohlen (1977) have commented on the implications for transport of suspended sediment by tidal currents, but convincing direct evidence of the effect of deceleration on sediment transport by tidal currents is still lacking.

The theory of suspension given here is based on the assumption that turbulence diffuses sediment according to a Fickian diffusion law. Though this assumption is in reasonably good accord with experiment, it is not the only possible basis for a theory of sediment suspension. Alternative theories, based on different assumptions, are described by Nordin and McQuivey (in Shen, 1971), Drew (1975; see also Drew and Kogelman, 1975), Willis (1979), Herczynski and Pienkovska (1980), and McTigue (1981), among others.

Although the diffusional theory has been described as "the brightest analytical achievement to date in the field of river hydraulics" (Hsu et al., 1980; see also Kennedy, 1984, p. 1257), it is subject to a number of criticisms:

(i) The theory throws little light on the actual mechanisms of diffusion: it does not indicate how grains are lifted up from the bed, nor how they are supported by turbulent eddies. Attempts to understand the mechanism have met with only limited success, and there have been some widespread misconceptions about where the real problem lies. A simple time series of vertical components of turbulence, or statistics calculated from such a series (for example, root mean square and skewness of the velocity component) do not provide enough information to explain the observed diffusion (Ludwick and Domurat, 1982). The fact that diffusion away from the bed takes place against the gravity force that tends to return sediment to the bed, does not necessarily imply that the vertical component of turbulence is anisotropic, as asserted by Bagnold (1966). Leeder (1983a,b) has repeated Bagnold's arguments and has shown that the vertical component is anisotropic very close to the bed, which implies that the less common upward

motions are stronger than the more common downward motions in this region, as would be expected from the burst-sweep model. But even if the vertical component of turbulence is anisotropic close to the bed, it is clear from experimental data that it is nearly isotropic far from the bed. There must clearly be some mechanism that tends to trap sediment grains in the rising parts of eddies, and perhaps also transfer grains from one eddy to another. Such a mechanism has been discussed by Tooby et al. (1977) and Nielsen (1984).

It might seem "obvious" that a grain with settling velocity w enclosed within a vortex whose maximum tangential velocity is larger than w would tend to be carried with the fluid around the vortex, but ultimately to settle out of the vortex. In fact, as Tooby et al. (1977) have verified experimentally, this is not the case; in an ideal vortex, rotating about a horizontal axis, a grain within the rising limb describes a circular orbit, which ideally would be closed and would not exhibit any net downward motion (Figure 6.23). In the experiment, grains tended to spiral slowly outwards, so that they would ultimately diffuse out of the vortex, but it is expected that fine enough sediment will be trapped in vortices and will move with the vortex until it is dissipated. The mechanism is rather insensitive to the size of the trapped particles, and should tend to produce less vertical segregation by size than the classical diffusion theory predicts.

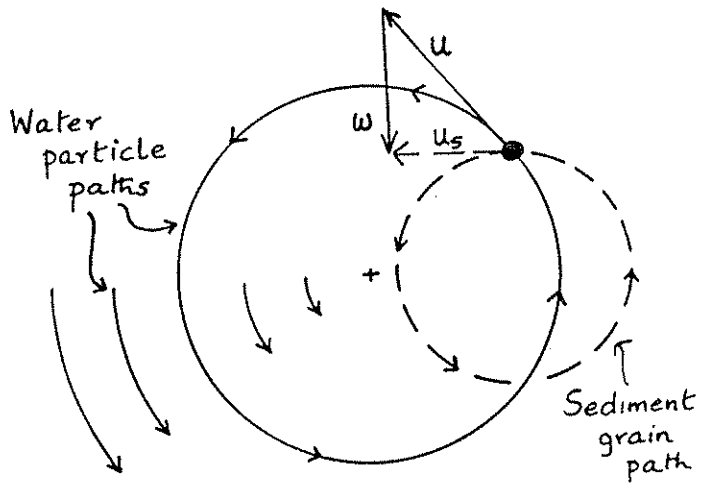

Figure 6.23 Path of a sediment grain moving in a fluid vortex. The tangential velocity of the fluid, u, is proportional to the distance from the center of the vortex. Simple vector addition of u and w, the settling velocity of the grain, predicts a circular sediment path, with no net settling of the grain.

(ii) Vanoni (1946, and many subsequent investigations reported and analyzed in Vanoni, 1975) found that in some experiments, particularly those in which there was a high concentration of coarse sediment close to the bed, the value of the supposedly universal von Kármán constant decreased from its accepted value of 0.38 to values as low as 0.2. He interpreted this as indicating that the presence of sand moving close to the boundary changed the structure of turbulence in the flow. There was, and has continued to be, considerable reluctance on the part of many workers to accept this result, though others (e.g., Einstein and Chien, 1955; Ippen, 1971; and Wang, 1981) have tried to develop theories to explain the effect.

Two general approaches have been taken by those who have tried to argue that von Kármán's constant is not really changed: (a) Coleman (1981; see also Coleman and Alonso, 1983; Lau, 1983) have suggested that there is no observed change if the logarithmic velocity distribution is fitted only to measurements closest to the boundary. According to Coleman, the apparent change is due to a departure from the logarithmic distribution in the outer part of the flow. Coleman claims that this departure is present near the surface even in clear-water flows, but becomes larger (for unspecified reasons) as the amount of suspended sediment increases. It seems unlikely that this can be entirely correct, however, because a change in κ has been observed in very carefully controlled experiments by Gust and Southard (1983) even in the case where there is only weak bed-load movement and no sediment in suspension. In these experiments the velocity distribution was observed very close to the boundary, and it is certain that the change in κ is not due to averaging the slope across the full depth of the flow. (b) Smith and McLean (1977b), Itakuri and Kishi (1980), Adams and Weatherly (1981), and DeVantier and Larock (1982) have suggested that because of the decrease of sediment concentration away from the bed there is also a decrease in the bulk density (of water plus sediment), and the resulting stable density stratification tends to suppress turbulent mixing in the vertical direction and therefore to change the nature of the velocity distribution. This mechanism is plausible, but it can hardly account for all cases in which an apparent reduction of κ has been observed: Gust and Southard (1983) have reported a reduction in κ with weak bed load and no suspended load; Gust (1976, and see references to earlier work) has reported that dilute suspensions of clays or long-molecule polymers cause a reduction in κ, and Elata and Ippen (1961) reported a reduction in κ in flows with neutrally buoyant particles.

(iii) Besides the uncertainty about κ several authors have reported large deviations of β from the expected value close to unity. There are reasons to expect that solid grains are not diffused at the same rate as fluid momentum, and that the ratio of the two rates of diffusion is not a constant but varies with the properties of both the sediment and the fluid turbulence. At present there is no satisfactory way to predict the value of β. Prediction presumably will become possible only when there is a better understanding of the mechanism of diffusion.

(iv) In the usual theory the sediment diffusion coefficient is assumed to be proportional to the eddy viscosity and the distribution with depth to be given by Equation (6.18). This equation predicts that ε_s (and ε) drop slowly to zero as the free surface is approached. Because sediment cannot diffuse through the free surface, ε_s must be equal to zero there. Coleman (1970) has, however, calculated ε_s directly from observed values of C and dC/dy using Equation (6.17). He found that there is a strong dependence on depth only near the bed; over most of the flow, and even quite close to the free surface, ε_s appears to be independent of depth. This appears to be true for both flume and river data (see further discussion below).

For all of these reasons, the diffusional theory of sediment suspension, though it is a better theory than that available for most aspects of sediment transport, must still be regarded as somewhat less than completely satisfactory.

Suspension at High Grain Concentrations (the Bed-Load Problem)

We have seen above that it is possible to distinguish two completely different mechanisms for lifting grains up from the bed and moving them in a fluid flow: saltation and suspension. Suspended grains are supported by fluid turbulence. The exact mechanism of saltation is in doubt, but it is clear that it is not directly related to turbulence. In air, the two mechanisms are quite distinct. In water, however, problems arise because of the difficulty in observing exactly how grains are transported in the zone of high sediment concentration close to the bed.

The problem has not been reduced by the prevailing confusion over nomenclature. To most authors, bed load is that part of the sediment load moving very close to the bed (Vanoni, 1975, p. 18). Einstein (1950) defined it as moving in "a flow layer, two grain diameters thick, immediately above the bed," but to other authors it consists of those grains that are supported by the bed and not by fluid turbulence (i.e., grains that are rolling, saltating, or moving as part of the "traction carpet"). Other definitions are much more vague, as for example the latest version in the AGI glossary (Bates and Jackson, 1980, p. 60):

> "The part of the total stream load that is moved on or immediately above the stream bed.... The part of the load that is not continuously in suspension or solution."

By this definition almost all of the sand transported by a river might be considered part of the bed load, because it spends at least part of the time on the bed, and is not transported continuously in suspension.

Actual measurements of "suspended load" in rivers are made by collecting samples of sediment-bearing water at different levels

within the flow, from near the surface to a level that is generally at least 0.5 ft (15 cm) above the bed. (See Vanoni, 1975, Chapter III, for a thorough discussion of sediment-measurement techniques.) "Bed load" may be sampled by the use of devices like the Helley-Smith bed-load sampler (Johnson et al., 1977) that trap all grains moving close to the bed. (Exactly how close depends on the size of the sampler; generally all grains moving with 0.3 ft (10 cm) of the bed are trapped.) Data obtained with such traps have generally been regarded as very unreliable, because moving bed forms interfere with proper operation of the trap. Recently, a small sand/gravel bed river, the East Fork River in Wyoming, has been fitted with a special bed-load trap, a small trench extended across the entire bed of the river, with a cover that may be closed in sections to passage of grains over the top or to trap grains that are not carried across the trench. Measurements made in this river have been discussed by Leopold and Emmett (1976, 1977) and Bagnold (1977).

In practical engineering terms, therefore, the bed load is the part of the load that moves within a few centimeters of the bed, and the suspended load is simply the part of the load that can be sampled by a "suspended-load" sampler. Discharge of suspended sediment is calculated from the samples by weighting the measured concentration by the local flow velocity and then averaging over the total sampled cross section. Corrections for the unmeasured part of the cross section (mainly the part close to the bed) are rarely applied. For most large muddy or sandy rivers it is assumed that the unmeasured suspended load and the bed load are a small part of the total sediment load; engineering experience confirms that this is a reasonable approximation, though it does not apply to rivers with bed material consisting mainly of coarse sand and gravel. Total sediment discharge has been actually measured in only a few small sandy rivers where it was possible to take the entire sediment load into suspension locally by constructing a special constricted and rough section of the river channel (a "turbulence flume"; see Vanoni, 1975, Chapter III). For these rivers it could be confirmed that, averaged over long periods of time (i.e., high discharges as well as low) the discharge of suspended load, sampled in the usual way at unmodified sections of the river, was by far the greater part of the total sediment discharge.

Sedimentologists, however, have reasons for taking a much greater interest in the sediment load close to the bed than practical hydraulic engineers: most of the sand that sedimentologists study must have been moving close to the bed before it became part of the preserved sedimentary record. We may therefore ask which processes are more important in determining the nature of the sedimentary deposit: the dominant transport mechanism (probably suspension for most medium to fine fluvial sands) or the mechanism of sediment movement just prior to deposition? The answer probably depends on which properties of the sedimentary deposit we are interested in: some, such as surface texture, probably depend mainly on the dominant mechanism

of transport; others, such as lamination, depend on the mechanism of deposition. For yet others, such as the nature of grain-size distributions, the answer is not yet clear.

As we have indicated several times in earlier discussions, there are reasons to believe that the mechanism of sediment movement in water must be modified by collisions (or at least some kind of interaction between grains, if not actual collisions) at high sediment concentrations. Bagnold (1954, 1956, 1966) concluded from experiments on shearing neutrally buoyant grains in the space (annulus) between two cylinders that interactions between grains became important at concentrations as low as 9% by volume. Grains sheared at higher concentrations exerted a pressure on the wall of the cylinders that was proportional to the shear stress applied. This pressure was called by Bagnold the dispersive pressure.

Bagnold (1973) has developed a theory of saltation and bed-load movement in which it is supposed that bed-load transport results entirely from collisions between grains. As grains rise into the moving fluid they are subjected to fluid drag, with the net result that an average thrust F is transferred from the fluid to the saltating grains. This same thrust is transferred from the moving grains to the bed, where it is transformed by grain collisions into an upward force sufficient to lift up the submerged weight W' of the saltating grains. Bagnold supposes that the transformation is accomplished by a mechanism similar to that acting between solid surfaces sliding past each other, and can therefore be described by an equation of the type $F/W' = \tan\alpha$. From his own experiments on shearing grains and from Francis' (1973) observations on saltating grains, Bagnold concludes that α has a value similar to that of the mass angle of repose, i.e., about 35° for natural sand grains.

The theory can be applied directly to calculate the thickness of the "zone of saltation" or "traction carpet" that can be driven along the bed of a river. If we suppose that the concentration of grains in this zone is about 25% by volume, then the submerged weight of the grains per unit area of the bed is

$$W' = 0.25\ (\gamma_s - \gamma)t_s$$

where t_s is the thickness of the "traction carpet." In rivers, where the direct effect of a downslope component of gravity acting on the grains themselves is negligible, F must be the shear stress exerted by the flow on the top of the "carpet" of moving grains (and ultimately transmitted by the "carpet" to the bed):

$$F = \gamma dS$$

Solving for t_s and remembering that tan $\alpha = 0.7$, $\rho_s = 2.65$ g/cm^3, and $\rho = 1.0$ g/cm^3,

$$t_s/d = 3.5\ S$$

The slope of large rivers is generally about 0.1% or less, so that thickness of the "traction carpet" should be less than one percent of the total depth, i.e., it should be a few centimeters at most.

Some authors have maintained that, at high sediment concentrations, turbulence is no longer effective in keeping sediment in suspension. This view does not seem to be supported by experimental investigation. Vanoni (1975, p. 83-91) summarized the results of investigations of the effect of sediment concentration on sediment suspension. In several of these, concentrations were high enough so that near the bed, grain interactions should have replaced turbulence as the main mechanism of grain support, according to Bagnold. Yet observed sediment distributions showed reasonable agreement with the predictions of the diffusion theory of suspension.

Quantitative investigations of the zone of high sediment concentration close to the bed have been made by Einstein and Chien (1955) and by Coleman (1969). Einstein and Chien ran experiments in which the bed was made of sand glued to the flume bottom, and sand of the same size was added to the flow up to high concentrations, but the amounts added were not sufficient to permit actual accumulation of sand on the bed. Conditions therefore approached, but were not identical with, upper-regime flat bed.

Einstein and Chien established that at high concentrations of relatively coarse sand both velocity and sediment concentration close to the bed differed from those measured in the outer part of the flow. Velocity distributions in the outer part of the flow were logarithmic, but with a reduced value of κ for flows with high sediment concentration close to the bed. Velocities close to the bed were higher than would be expected from the extrapolation to the bed of the logarithmic profiles measured in the outer part of the flow. Sediment concentrations at the bed were more nearly uniform than expected from extrapolation of trends in the outer part of the flow (Figure 6.24), and the deviation seemed to begin at a concentration by weight of about 10%. Einstein and Chien thought that the deviation could be at least partly explained by a reduction in the settling velocity of grains because of the high concentration and the proximity of the bed.

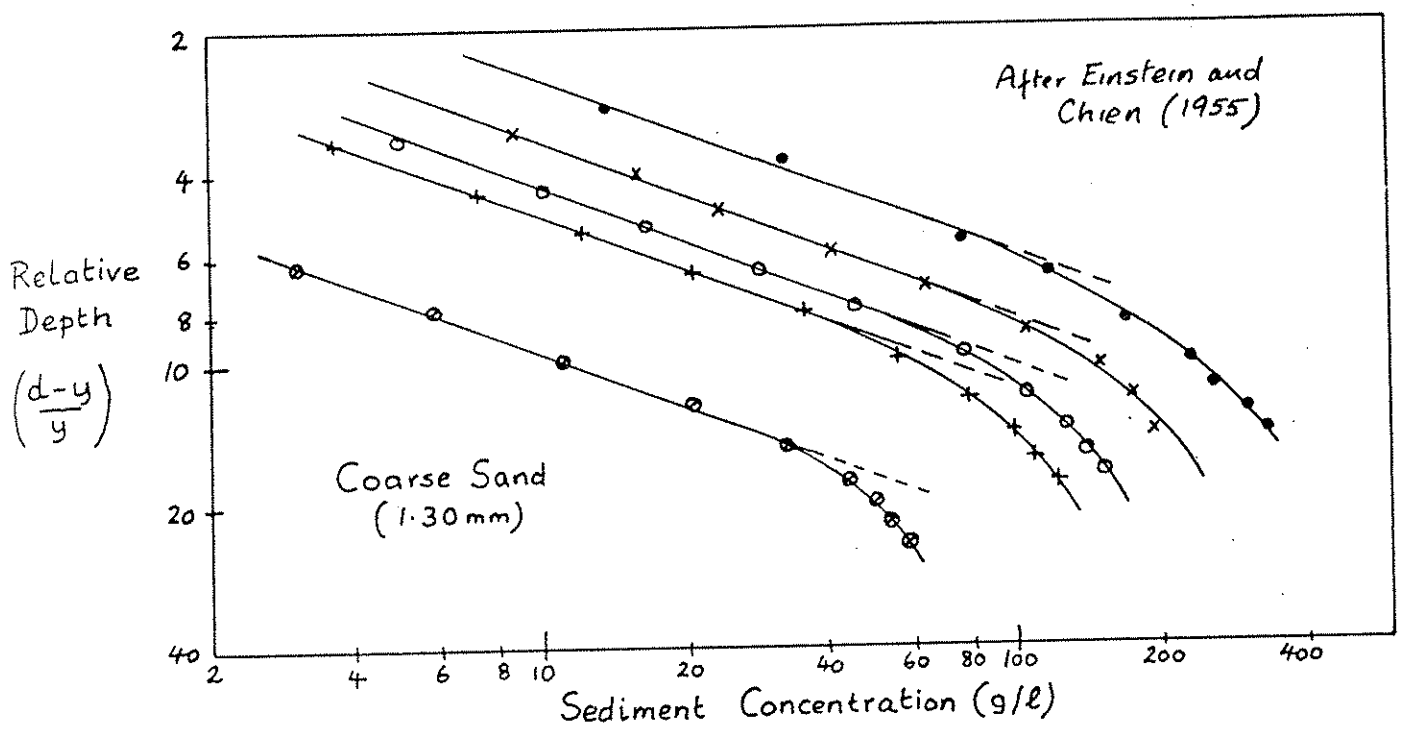

Figure 6.24 Sediment concentration (in grams per liter) plotted against relative depth, for five flows with different average concentrations of coarse sand. Data are from Einstein and Chien (1955). Note that sediment concentrations near the bed are more uniform and smaller than would be predicted from the diffusion theory of suspension. Deviation from theory begins at concentrations of about 4 to 10 weight percent (1.5 to 4 volume percent).

Coleman (1969) examined about seventy profiles of velocity and sediment concentration measured in both flumes and rivers, under conditions of both lower flow regime and upper flow regime. He too found that the profiles indicated that the flow should be divided into two parts. In the outer part of the flow the concentration declined exponentially with distance from the bed--which is <u>not</u> the result predicted by Equation (6.20) except <u>approximately</u> at small values of z. Close to the bed the values for concentration showed a deviation from the extrapolated exponential distribution, towards higher values of sediment concentration. The deviation began at a distance $\delta*$ from the boundary and at concentrations generally of the order of one percent by weight. Coleman called the region close to the bed the "inner suspension region." He found that its thickness, given by

frequently reached values of as much as 20% of the flow depth, where U_s is the maximum flow velocity (that at the water surface).

Coleman found that within the inner suspension region the sediment diffusion coefficient was proportional to y, as previously assumed, and was given by the relation $\varepsilon_s = wy$. In the outer part of the flow, however, Coleman found the ε_s was a constant.

Both Einstein and Chien's and Coleman's analysis of the available data indicate that the classical diffusion theory of suspension is oversimplified. Both velocity distribution and sediment concentration deviate from predicted values close to the bed, but the deviation begins at elevations well above those predicted for the top of the "traction carpet" and at concentrations well below those at which dispersive pressure should begin to replace turbulence as the dominant grain-support mechanism. There is little indication of a sharp boundary between a zone in which dispersive pressure is dominant and one in which turbulence is dominant. Nor is there any real indication that turbulence ceases to be important for the support of grains at high sediment concentrations. Recent observations both in rivers and in other large-scale natural flows (Jackson, 1976) support the idea that the same kind of "bursting" phenomenon takes place at the boundaries of these flows as have been observed in the laboratory. If high grain concentrations do tend to form a thin "traction carpet" close to the boundary, in which turbulence is suppressed, this zone must be constantly disrupted by the impact of large-scale eddies, just as the viscous sublayer is disrupted by small-scale sweeps along the boundary of a laboratory flume. Furthermore, grains reaching the top of the "traction carpet" would be exposed to the turbulence of the flow above, which in most rivers is sufficient to take fine to medium sand into suspension. We therefore expect a continuous transition from conditions very close to the bed, where grain interactions and dispersive pressure may be more important than turbulence, to regions of lower concentrations farther from the bed, where turbulence is the dominant support mechanism. Grains of medium sand size or finer should be continually exchanged between the bed and the suspended load. Only those grains too large to be taken into suspension are likely to be confined for most of their transport history to the zone very close to the bed.

INTERPRETATION OF SEDIMENT TEXTURES

Introduction

It is not expected that all aspects of sediment texture can be given a hydraulic interpretation. It is known that textures, such as grain size and shape, result from the complex interplay of three main factors:

(i) Inheritance of textures directly from source materials (preexisting sedimentary grains, or grains released from igneous or metamorphic rocks by weathering).

(ii) Production or strong modification of textures by abrasion. This is very important for sizes larger than sand and for some of the softer sand-sized particles. It is less important for quartz sand transported by water, although recent work by Moss (1972b; Moss et al., 1973) has shown that as the coarser quartz grains are transported away from the source they are reduced in size, predominantly by the splitting off of silt-size flakes bounded by sheeting surfaces that were present in the original grain.

(iii) Modification of textures by hydraulic sorting.

In these notes it is not appropriate to attempt any discussion of the first factor, and we confine our discussion of the second factor to a few remarks about surface texture. We do not mean to imply that we not think that inheritance, breakage, and abrasion are not important in determining sedimentary textures, but a full discussion of these factors would take us too far from the main theme of these notes.

One aspect of surface textures is worthy of note. Studies of the surface textures of sand grains from many natural environments (summarized in Krinsley and Doornkamp, 1973) has shown that many grains show textures that result from attrition of the surface produced by impact with other grains. Such attrition features are practically confined to grains larger than about 0.2 mm in diameter; they are most common on grains from eolian environments, beaches with moderate to high wave activity, and marine environments with strong tidal currents. They are not common on grains from fluvial environments. Furthermore, experimental studies (summarized in Middleton and Davis, 1979) suggest that in water such textures are produced much more readily by shearing at high grain concentrations than by turbulent agitation of grains in suspension.

In most natural subaqueous environments, grains less than 0.2 mm in diameter (with settling velocities less than 2 cm/s) can be readily taken into suspension if they can be moved at all, so it is not surprising that they lack surface textures produced by attrition. Swash and backwash on beaches are known to produce shearing of sand at high grain concentrations, and it has been argued by Komar (1978) that bed load is also more important than suspended load in transport by waves and longshore currents in the surf zone. This is compatible with the high frequency of attritional markings (poorly oriented V-shaped pits) observed on most beach sands.

The absence or scarcity of such markings on river sands, even on sands that have travelled for hundreds of kilometers down major rivers, therefore suggests that the dominant transport mechanism

of these sands is suspension rather than movement as part of a highly concentrated "traction carpet." In major rivers probably most of the sandy bed material can easily be taken into suspension during periods of flood. Discharge of suspended sediment increases as a high power of the flow velocity or discharge, so sand grains are transported most of the distance down a river in suspension rather than as part of the bed load.

Hydraulic Sorting

Some remarks can be made about the general nature of hydraulic sorting, before attempting specific interpretations. First we should note that total transport of an assemblage of sediment grains, in a flow system that has an upstream source and a downstream sink but no lateral exchange of sediment, does not result in hydraulic sorting. This is obviously true for mass movement of sediment (e.g., debris flows), but it also applies, for example, to movement of bed material in rivers. As we have seen, grains moving along the bed of a stream are constantly being deposited and reeroded; the probability of deposition and erosion is expected to be strongly influenced by the texture of the grains (their size and shape), and therefore there exists the potential for hydraulic sorting. However, if a steady state exists, such that there is a constant sediment discharge with no net deposition (or erosion), all particles crossing one cross section must be transported to a second cross section farther downstream, and there is no possibility of hydraulic sorting. These conditions may be closely approximated by the coarse bed load (gravel) of some rivers (e.g., Bradley, 1970; Bradley et al., 1972). The fact that some particles move through a reach faster than others does not, under these conditions, produce any strong downstream textural gradients: the same volume of sediment entering a reach from upstream must be leaving it downstream, and the most that can be produced in the way of textural change is a gradual coarsening of the bed load over a long period of time because of exchange with preexisting bed material.

In most natural environments, however, hydraulic sorting is possible, either because there is net deposition (or erosion) or because different grains are segregated laterally into different parts of the transportation system--for example, bed material is confined to channels and wash load is deposited in quantity only on flood plains. Thus, in any one part of the transportation system there is a possibility for the preferential entrapment of one or more texturally distinct parts of the total sediment load. Simple examples include the strong downstream size gradients observed in some rivers and alluvial fans, the cross-channel size gradients observed on point bars in some meandering rivers, and the progressive fining observed seaward of most beaches.

It should be noted that, in a sediment transport system in which there is net deposition, it is not necessary that there be hydraulic gradients in order to produce textural gradients in the

sediment deposited. This has been demonstrated by Swift et al. (1972; see also Swift and Ludwick, 1976) for a perhaps overidealized case of sediment being moved across a continental shelf by storms. It is not necessary to suppose that movement by storms acts in any preferred direction, or that storm action decreases in magnitude across the shelf. All that is necesssary in order to produce cross-shelf textural gradients is to assume that there is a source of sediment at the shoreline and a sink at the shelf break, that a certain proportion of sediment is deposited on the shelf (a minor sink), and that the probability of grains being deposited on the shelf is a function of their grain size. In this model, sediment is essentially diffused by random processes across the shelf, and coarser sediments accumulate on the shelf closest to the shoreline simply because it is probable that the coarser sediment will be trapped permanently in the shelf deposits in larger amounts than the finer sediments.

It is more obvious that textural sorting can take place if sediment is being transported down a hydraulic gradient. the clearest case is that of a downstream decrease in the competence of a stream. In this case, grains that are too large to be transported must be deposited upstream of a given point in the hydraulic gradient. A somewhat similar effect results from a downstream decrease in the capacity of a stream to transport a given size (or textural type) of grain. In this case, however, it may still be possible to transport some of the grains of that size that enter a reach, but because of the hydraulic gradient there will be a progressive decrease in the proportion of such grains that can be transported, because capacity (rate of sediment transport) is not a linear function of grain size.

Finally, it may be expected that the statistical distribution of grain sizes (and shapes) produced by any particular mechanism of hydraulic sorting will have characteristics determined by that hydraulic mechanism. Middleton (1970a) suggested that the operation of a repeated "sorting event"--like suspension and redeposition of sand by a single wave swash-backwash on a beach, which removes and/or adds some sediment to the "stock" (moving layer) originally present--leads in the long run to the development of a lognormal size distribution. Details of the hypothesis, which is based on purely statistical rather than hydraulic arguments, may be found in the original paper.

In nature it seems reasonable to postulate that the nature of the sorting event depends on the predominant mechanism of sediment transport. There are generally three ways in which sediment is transported over the bed of a stream: traction, intermittent suspension of grains that return frequently to the bed, and continuous suspension of grains that are only rarely trapped in the bed. Therefore even though there are no sharp distinctions between these three processes, during transportation the bed material is segregated into three different but overlapping fractions: a fraction distributed uniformly through the flow (by suspension), a fraction concentrated in the lower part of the flow

(by intermittent suspension), and a fraction moving in contact with the bed (by traction). If during transportation some of the sediment is lost from one or more of the fractions, and the amount that is lost depends upon the mechanism of transportation, then when the remaining sediment in the three fractions is recombined to form the bed material it might be expected that most bed materials would show three predominant textural "populations," each approximately lognormal (Figure 6.25). It is not clear a priori whether there would be a relatively abrupt transition from one lognormal population to another (truncated lognormal model, favored by Visher, 1969, and others) or the populations would overlap (overlapping lognormal model, favored by Tanner, 1964; Walger, 1962; and others), though the latter seems most likely. In fact, it is now well established that such populations do exist, and it is becoming clear from the detailed observations of Clark and Clark (1976) and Dalrymple (1976, personal communication) that the overlapping model generally provides a better fit than the truncated model.

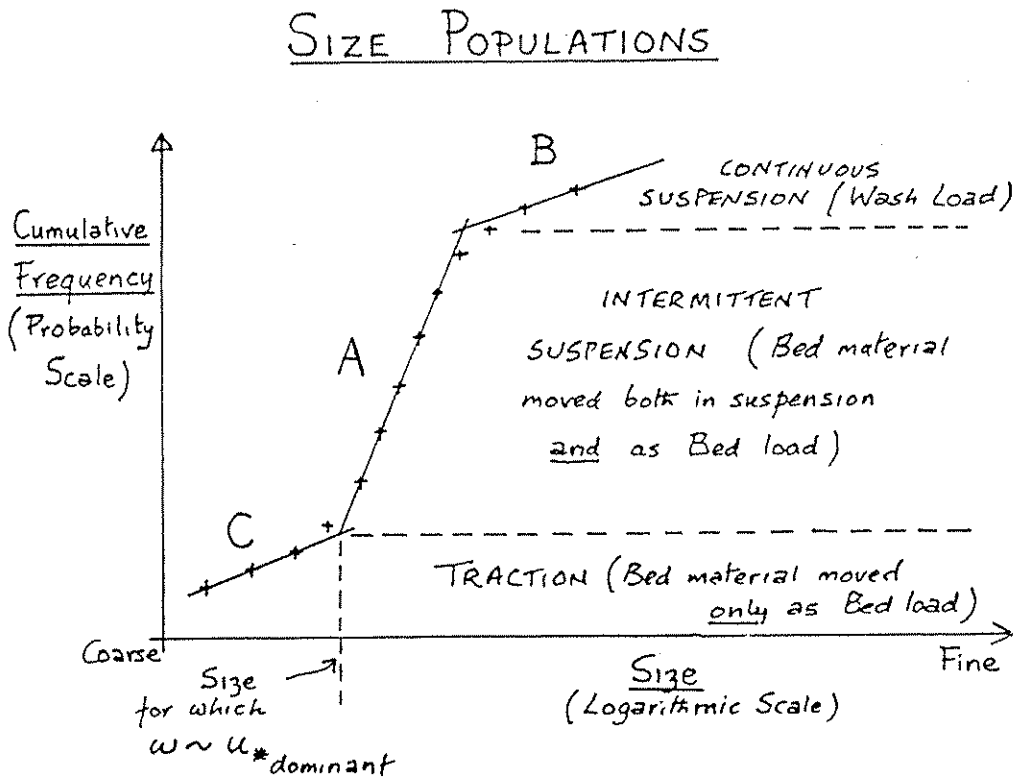

Figure 6.25 Typical size distribution, with cumulative frequency plotted on a probability scale and size on a logarithmic scale. An interpretation is shown in terms of three size populations produced by hydraulic sorting. A better separation of populations can probably be achieved by graphical dissection into overlapping Normal populations than by the simple fitting of straight line segments shown here.

In nature, interpretation of textural gradients or populations in terms of hydraulic sorting is greatly complicated by two important factors: (i) inheritance of textural characteristics produced in source materials by any of the three possible mechanisms listed at the beginning of this section, and (ii) the wide range of variability in both the type and the intensity of hydraulic mechanisms operating in most natural environments. The interpretation of any particular textural gradient or population is therefore likely to be controversial. The controversy can be resolved only by refining our understanding of the kinds of textural modification that it is reasonable to ascribe to each of the postulated mechanisms.

Characteristics of the Three Major Sediment Populations

Traction Population

Grains belonging to the traction population move only in contact with, or very close to, the bed. The range of characteristics of this population is likely to be defined by three main limiting conditions: (i) the availability of material, (ii) the competence of the stream, and (iii) the transition from traction to intermittent suspension as the dominant mode of transportation.

Availability is a very important factor governing both the proportion and the characteristics of the traction population. Because grains moving by traction travel much more slowly than those moving in suspension or intermittent suspension and have a far greater probability of being either temporarily or permanently deposited, it is expected that the proportion of the traction population will show a relatively rapid decrease in the downstream direction, even in the absence of any hydraulic gradient. Visher (1969), presumably basing his conclusions on samples collected from the lower reaches of major rivers, indicated that the traction population is absent from the bed material of most rivers. But published analyses show that it is present in the upper reaches of many rivers, and in some rivers (e.g., the Rio Grande) it can be shown that its amount decreases rapidly downstream (Middleton, 1976). A similar decrease in the proportion of the traction population away from the source can be documented for some intertidal sand bars in the Bay of Fundy (Dalrymple, personal communication).

The maximum size of the traction population is determined by the competence of the stream as defined by Shields' criterion. The minimum size (or, more correctly, the point of equal overlap with or transition to the intermittent-suspension population) is defined by the criterion for suspension discussed earlier (Equation 6.14). Thus, both limits to the population, insofar as they are not determined by availability, are determined by the shear velocity. It is therefore possible to determine the shear velocity from the size distribution by two different and independent methods, provided that sufficient coarse material

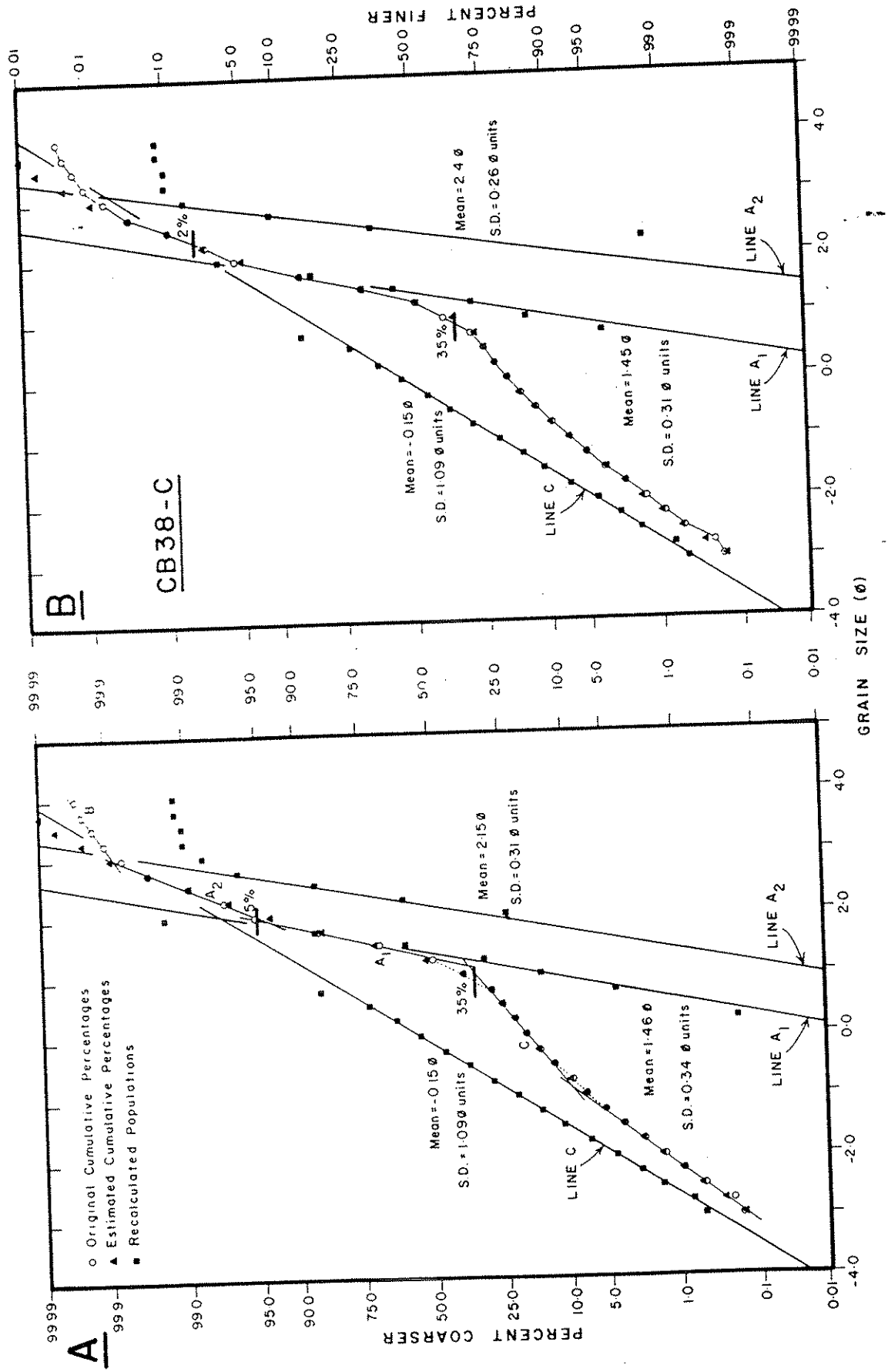

Figure 6.26 Example of an observed size distribution fitted by overlapping Normal distributions (unpublished data of R.W. Dalrymple). A is the first approximation in fitting three Normal distributions to the observed grain size distribution, and B is the second approximation. The three fitted populations are C (traction), and A_1 and A_2 (intermittent suspension). A small B (suspension) population is present, but has not been fitted.

about one percent) is present to define the traction population. Disagreement between the two methods suggests that the amount and properties of the traction population are limited by availability rather than by hydraulics. Absence of the traction population generally implies not low velocities but simply lack of availability or prior removal by hydraulic sorting.

After dissection of the cumulative size curve to separate the different lognormal populations present, it is generally observed that the traction population (if present) is much less well sorted than the intermittent-suspension population (see Figure 6.26 for an example). This is probably because sorting by traction is much less efficient than sorting by intermittent suspension. In particular it was noted above that where there are bed forms like ripples and dunes the rate of movement of the bed-load grains is determined mainly by the speed of movement of the ripples or dunes. In this case, grain size and shape have little effect on the rate of movement of bed load, provided that the flow is competent to move the largest grains present. Hydraulic sorting tends to remove the bed load completely (by deposition near the source) but not to differentiate strongly between the different grades or shapes of bed load, except perhaps in some environments where the bed load constitutes the greater part of the total load.

Intermittent-Suspension Population

In most sandy environments (rivers, littoral deposits, tidal sand bars) the intermittent-suspension population makes up by far the greatest part of the size distribution, simply because major deposits of sand generally can form only in environments where sand can be taken into suspension but does not remain in suspension long enough to permit its rapid removal from the environment.

The process of repeated suspension and redeposition is an efficient agent of hydraulic sorting. The diffusional theory of suspension, outlined above, can be used to calculate the size distribution of the material in suspension above any given bed material for a given hydraulic condition. The size distribution may be calculated for a given level above the bed, or for the total suspended load.

The necessary theory was developed by Einstein (1950), though he applied it to the more difficult task of predicting the rate of transport of suspended load rather than to predicting the size distribution. In order to predict the rate of transport of suspended material it is necessary to predict the absolute concentration of sediment at some level close to the bed--a very difficult task. But all that is needed in order to predict the size distribution is to assume that at some level very close to the bed the size distribution is very similar to that of the bed material. This assumption is almost certainly valid, with the

sole exception of the finest grain sizes (wash load), which in any case do not form part of the intermittent-suspension population.

The basic theory is outlined in Middleton (1976). Sengupta (1975) has presented some experimental data which confirm that it is possible to predict fairly successfully the size distribution higher in the flow from an observed size distribution close to the bed.

The size distribution of grains moving in intermittent suspension is shown, both by direct observation in rivers and by calculation, to be somewhat finer and better sorted than the bed material from which it is derived. Repeated removal of part of the bed material in suspension, when combined with selective (permanent) deposition of the unsuspended residue, therefore tends to shift the intermittent-suspension population towards the finer sizes and to improve its sorting.

The sorting of the intermittent-suspension population is to some extent controlled by the limits, in the environment, of the mechanism of intermittent suspension itself. The upper limit is defined by the size for which the settling velocity is greater than the dominant shear velocity. The lower limit is probably close to the size for which z in Equation (6.21) is so small that there is little vertical change in suspended-sediment concentration. (This corresponds very roughly to $z = 0.25$, or $w = 0.1\ u*$.) Grains with lower settling velocities would be rapidly winnowed out of the bed and easily carried away in suspension, to be deposited only in regions where the shear velocity remains low for long enough to permit settling of the grains through the water column.

Suspension Population

Probably more than for the other populations the properties of the suspension population depend on the properties of the source populations and on their modification by factors other than hydraulic sorting. Cohesion, flocculation, and organic factors (e.g., binding in feces produced by filter-feeding organisms) are probably all important. It is generally impossible to determine the true (depositional) size distribution for this population, even in sediments that have been deposited for only a short time. After the usual treatment with dispersing agents, the size distribution is generally determined to be poorly sorted and multimodal--but it is unlikely that this distribution bears much resemblance to the original size distribution, or much relation to the hydraulics of the environment.

Cross-Bedded Sands

Sands with trough cross-bedding generally have size distributions largely composed of an intermittent-suspension

population. At first it might seem that this observation implies a contradiction: trough cross-bedding was produced by the migration of dunes, and the sands in the cross-beds were trapped there because they were moving close to the bed and could not bypass the dune, as was possible for sediment moving in suspension higher in the flow. In fact, in some theories of sediment transport the bed load is defined as the sediment that moves through, rather than over, the bed forms, so it is expected that cross-bedded sands will be composed of bed load rather than suspended load.

The resolution of this apparent paradox must be a clear distinction between "bed load," as defined in theories of sediment movement, and "traction population," as determined from size distributions. At any one time and place on the stream bed, much of the sediment is moving close to the bed: if we define bed load as the sediment that is trapped in the lee of bed forms, all the sediment moving very close to the bed is bed load. But this sediment is composed of two different fractions: one fraction, generally a small part of the bed load, consists of grains that are so large that normally they can only move very close to the bed. Only very rarely, under exceptional flow conditions, or at times when an exceptionally strong eddy strikes the bed, can these grains rise high above the bed. This is the true traction population. A large fraction of the sediment moving close to the bed, at any particular place and time (i.e., a large fraction of the bed load), is composed of grains that can easily be carried up high above the bed; they can and will be moved in intermittent suspension for a substantial part of the time, though they also spend a part of the time moving close to the bed.

It is not yet known how frequently a grain must rise up above the bed in suspension before it becomes part of the intermittent-suspension population. It is clear, however, that the proportion of the grains moving as bed load is generally much larger than the proportion of traction population in the bed material.

CHAPTER 7. BED CONFIGURATIONS

INTRODUCTION

A striking characteristic of sediment transport on noncohesive beds is the development of geometrical forms or elements on a scale much larger than the grains themselves. These forms always show a strong element of regularity in arrangement, although usually they are irregular in detail. Most are elongated either parallel or transverse to the flow. Parallel-to-flow bed forms seem to be a manifestation of spiraling fluid motion, called secondary flow, that is parallel to the main flow and superimposed upon it. The convergent and divergent transverse components of near-bed flow may mold the bed into a series of ridges and troughs; the bed geometry in turn affects the structure of the flow, but not fundamentally. Transverse-to-flow bed forms, which are more commonly preserved in the sedimentary record, are dynamically more complicated in that they arise from a strong interaction between the flow and the bed. The nonuniformity of flow over transverse bed forms is not antecedent to the bed forms but comes about by the interaction between the flow and the bed; we'll see that these bed forms can be produced by uniform flow over a bed that is planar on the scale of grains. In this chapter we'll consider only transverse bed forms under unidirectional flows, but you should bear in mind that transverse bed forms under oscillatory flows are also interesting and important. See Clifton (1976), Harms et al. (1982), and Allen (1982, Vol. 1) for more information on oscillatory-flow bed forms.

Transverse bed forms move upstream or downstream at velocities much smaller than the flow velocity, by erosion of sediment at some points and deposition at other points. Most are at least crudely wave-shaped and are therefore often likened to waves. They are not waves in the dynamic sense, as water waves or sound waves are, although you'll see that they have certain wavelike properties in a kinematic as well as a geometric sense.

Geologists and engineers alike have marveled at bed forms. Apart from their intrinsic fascination as a physical phenomenon, bed forms are of practical importance: (i) they constitute obstacles to navigation and a threat to submarine structures; (ii) when present in a channel they are the most important determinant of flow resistance; (iii) they have an important and complicating effect on sediment transport rate; (iv) their existence leads to the development of some of the most common stratification features in sedimentary deposits, and these structures are one of the most useful tools available in the interpretation of ancient sedimentary environments.

Terminology for flow-produced bed forms is unsettled. Many distinguish between the overall bed geometry that exists at a given time in response to the flow (bed configuration) and any individual element of this overall geometry (bed form); some also

use a separate term (bed phase) for recognizably or qualitatively different kinds or categories of bed configurations that are produced over some range of flow and sediment conditions and are closely related in geometry and presumably in dynamics. It is also useful to have the term bed state for the aggregate or ensemble of like bed configurations that can be produced by a given mean flow over a given sediment bed: the bed configuration differs in detail, even from instant to instant, and the bed state can be viewed as the average of all the configurations possible. On the other hand, the term bedform (one word) is in common use for all of the different aspects of bed geometry distinguished above; we're engaged in a rearguard action against this broad usage.

Nature has given us a rich variety of bed states produced by the action of a steady sediment-transporting flow for a long enough time for the bed geometry to come into equilibrium with the flow. Over a wide range of conditions the bed forms that constitute these states are ripple-shaped forms that are generally oriented transverse to the flow and have gently sloping upstream surfaces and steeply sloping downstream surfaces. These bed forms move downstream by erosion on the upstream sides and deposition on the downstream sides. Others, like antidunes, are rounded and symmetrical undulations, also oriented transverse to the flow. These show strongly regular spacings. In certain ranges of flow conditions a planar transport surface is the stable bed configuration. (By the terminology introduced above, a plane bed is a bed configuration with no bed forms.)

The underlying reasons for the existence of bed forms are not obvious. At first thought it might seem that the natural mode of transport would be over a planar bed. Only in laminar flow, however, does transport in uniform flows invariably take place over a planar bed. In turbulent flow there can be stable plane-bed transport in certain ranges of flow conditions, but bed forms are the dominant geometry of transport surfaces in turbulent flows. The dynamics of bed forms is one of the most difficult problems in turbulent flow, for two reasons. First, turbulence structure is altered by the sediment in transport. More importantly, as the flow molds the bed by erosion and deposition the bed geometry thus generated changes the pattern and structure of the flow itself in fundamental ways; there is thus a strong interaction or feedback between the bed and the flow, and this is the essential element of complexity that makes theory so difficult.

Even aside from theory, the status of observational understanding of bed states leaves much to be desired. It is fairly easy to observe bed configurations in laboratory flumes, because it is a straightforward matter to put sand in a recirculating channel and then run a flow at a certain depth and discharge for long enough to let the bed geometry come into equilibrium with the flow. There have been many extensive series of flume experiments of this kind, and the major outlines are by

now well known. Even in the laboratory, however, there is room for improvement, because it's difficult to observe bed behavior when transport rates are high, and the usually small width-to-depth ratios of flumes tend to inhibit full development of the three-dimensional aspects of bed geometry, which if present are of crucial importance in determining the geometry of the sedimentary structures produced. And even the largest of flume experiments are restricted to flow depths at the lower end of the range of natural flow depths. So flume work can be expected to provide only an approximate idea of the behavior of bed forms that are important in natural flows. In nature, on the other hand, observational understanding of bed geometry as a function of flow and sediment has been limited both by the technical difficulties of making observations and by the typical unsteadiness of flow that causes bed geometry to lag behind the flow. This latter effect of disequilibrium is a major element of complexity that makes it much more difficult to decipher the relationships among bed phases.

This chapter has three areas of emphasis: (i) flow and grain movement over bed forms, (ii) empirical synthesis of field and laboratory data on bed states and bed phases, and (iii) the dynamics of bed configurations. First, however, in the next section we advance the discussion of open-channel flow a little, to cover some topics relevant to flow over bed forms.

MORE ON OPEN-CHANNEL FLOW

A little more material on open-channel flow, beyond what's in Chapters 1 and 5, will be useful in dealing with bed configurations. Specifically, after a brief section on the nature of flume experiments we'll examine some things about flow energy in bulk and the propagation of gravity waves on a free surface, and conclude with some comments on uniformity of sediment-transporting open-channel flow.

Flumes and Flume Experiments

Since much of what's known about bed configurations comes from flumes, a brief discussion of flumes and flume experiments might be useful here. Flumes are nothing more than long straight channels through which controllable discharges of water and sediment can be passed. Although some experiments have been made without recirculation of either water or sediment, in most flumes the water is recirculated, because of the fairly large discharges and long running times required. In some recirculating flumes the sediment is caught at the downstream end of the channel and separated from the water, and new sediment is fed into the flow at the upstream end at the same time. More commonly the sediment is recirculated as well, by pumping the sand-water mixture from the downstream end of the channel through a return pipe to the upstream end, so that the rate of introduction of sediment at the

head of the channel is constrained to be the same as the sediment discharge at the downstream end.

Two different kinds of runs with sediment recirculation are in turn possible: overfall and closed-circuit. In the overfall type the flow passes over a weir or through a grating at the downstream end of the channel into a sump whose water level is substantially lower than, and independent of, the water level in the channel. The sand-water mixture is then pumped from the sump to the upstream end of the channel. In the closed-circuit type the flow passes directly into a tailbox attached to the downstream end of the channel without interruption and is then recirculated.

In a flume with a closed-circuit arrangement, flow depth is fixed at the start of a run, independently of discharge, by the amount of water put into the system; in a flume with an overfall arrangement, adjustment of flow depth and flow velocity for a given discharge is more complicated, because a variable volume of water can be stored in the sump. It's generally accepted, however, that for sediment-transporting flow over a full sediment bed in either of these different arrangements (or in nonrecirculating flumes, for that matter) the flow characteristics and the bed state depend only on the final combination of depth and discharge, however established, and not on the way these conditions were established.

Flume experiments are not fully representative of streams for several reasons: (i) channel cross section is rectangular; (ii) sidewalls are straight and unerodible; (iii) width-to-depth ratio is usally too small; (iv) the channel is much too short; and (v) the greatest flow depths attainable are near the lower end of the range of natural flow depths. Of these, the shallowness of the flow is perhaps the most serious. Nonetheless, flume work has provided valuable information on various aspects of bed configurations--flow resistance, transport rates, geometry, and conditions for occurrence--at least since the time of the classic experiments by Gilbert (1914), largely because a wide range of bed configurations over a wide range of conditions of flow and sediment can be produced and studied easily.

Subcritical and Supercritical Flow

We noted in Chapter 3 that the Bernoulli equation is an expression of the work-energy theorem: the work done by the fluid pressure is equal to the change in kinetic energy of the fluid. In cases like this, if the change in kinetic energy is reversible a quantity called potential energy is defined as minus the work done, and then the sum of kinetic energy and potential energy, called mechanical energy, is unchanged or conserved. Forces for which this is true, like the fluid pressure in this case, are said to be conservative forces. Gravity is a good example: a thrown ball gains potential energy on its way up at the same rate it loses kinetic energy, provided that the frictional resistance of

the air is ignored. Frictional forces, on the other hand, degrade mechanical energy into heat energy.

Review the derivation of the Bernoulli equation (Equation 3.6) and you'll see that fluid pressure is a conservative force: in the absence of friction, the change in pressure potential energy per unit volume between two points 1 and 2 down a streamline, which is minus the work per unit volume $-(p_2-p_1)$ by the fluid pressure, is equal to the change in kinetic energy per unit volume, $(\rho/2)(v_2^2-v_1^2)$, so the two kinds of mechanical energy are interchangeable in this case also. It should therefore seem natural that when the fluid is in a gravity field a term for gravitational potential energy can be included in the Bernoulli equation as well. Since gravitational potential energy is mgh (where m is the mass of the body under consideration and h is the elevation relative to an arbitrary horizontal plane), the potential energy per unit volume is ρgh.

So in the expanded Bernoulli equation the mechanical energy per unit volume of fluid moving along a streamline, $v^2/2 + p + \rho gh$, is constant. This can be written a little more conveniently for our purposes as energy per unit weight of fluid E_w. Since weight equals volume multiplied by ρg,

$$E_w = \frac{v^2}{2g} + \frac{p}{\gamma} + h \qquad (7.1)$$

Note that each term has the dimensions of length; E_w is called the total head, and the terms on the right are called the velocity head, the pressure head, and the elevation head, respectively. In a real fluid, friction degrades mechanical energy to heat as the fluid moves along a streamline. This decrease in mechanical energy from point to point, expressed per unit weight of fluid, is called the head loss. If you add up all three terms on the right in Equation (7.1) the sum decreases downstream, no matter how the values of the individual terms change.

It would be nice to generalize Equation (7.1) so that it applies to an entire open-channel flow, not just to each streamline in it. The problem in doing this is that velocity, elevation, and pressure are not constant from point to point on a cross section. But if there are no strong fluid accelerations normal to the flow direction, pressure is close to being hydrostatically distributed: $p = \gamma(d-y)$. Then the sum of the elevation head and the pressure head can be written

$$h + \frac{p}{\gamma} = h_o + y + \frac{p}{\gamma}$$

$$= h_o + y + \frac{\gamma(d-y)}{\gamma}$$

$$= h_o + d$$

where h_o is the elevation of the channel bottom. Variations in pressure and elevation over the cross section are thus taken into account in Equation (7.1). Variation in velocity is still a problem, but in turbulent flows the velocity profile is so flat over most of the section that only a small correction need be made in order to replace v by the cross-sectional mean velocity U. Equation (7.1) can then be written between two different cross sections 1 and 2 in a channel flow that varies only slowly downstream as

$$\text{head loss} = (E_w)_2 - (E_w)_1$$

$$= \frac{U_2^2}{2g} + h_{o2} + d_2 - \left(\frac{U_1^2}{2g} + h_{o1} + d_1\right) \qquad (7.2)$$

A plot of E_w against downchannel position is called the energy grade line, and the slope of this line (or, generally, curve) is the energy gradient or <u>energy slope</u>.

In a uniform open-channel flow, for which both kinetic energy and potential energy are the same at every cross section but potential energy decreases downstream, the head loss is simply the rate of decrease of elevation head downsteam, or in other words the slope of the water surface and bed surface, which is then also equal to the energy slope.

It's often useful to apply Equation (7.2) to an open-channel flow that varies rapidly enough that there's little head loss but slowly enough that the hydrostatic-pressure approximation isn't too far wrong. Examples are a gentle rise or fall in the channel bed or a gentle expansion or contraction of the channel walls. In fact, the assumptions are not grossly unrealistic for bed forms, and should give at least a qualitative idea of what to expect by way of changes in depth and velocity of flow over a bed form. Such flows are said to be <u>rapidly varied</u>. Equation (7.2) becomes

$$\frac{U_2^2}{2g} + h_{o2} + d_2 = \frac{U_1^2}{2g} + h_{o1} + d_1 \qquad (7.3)$$

A convenient quantity to substitute into Equation (7.3) is $d + U^2/2g$, called the specific head H_o:

$$H_o = d + \frac{U^2}{2g} \qquad (7.4)$$

H_o is simply the head (i.e., flow energy per unit weight) relative to the channel bottom. Using H_o, Equation (7.3) becomes

$$H_{o2} + h_{o2} = H_{o1} + h_{o1}$$

or

$$H_{o2} = H_{o1} - (h_{o2} - h_{o1}) \qquad (7.5)$$

Now look at a unit slice parallel to the flow direction in a two-dimensional flow. (In other words, you don't have to worry about the sidewalls because they're far away relative to what's happening locally.) Discharge per unit width q is constant and equal to Ud. Substitution of $U = q/d$ into the definition for specific head eliminates U and provides a relation between d and H_o for each value of q:

$$H_o = \frac{q^2}{2gd^2} + d \qquad (7.6)$$

The family of curves of H_o vs. d for various values of q is called the specific-head diagram (Figure 7.1).

To illustrate the usefulness of this diagram, suppose that the flow approaching the step shown in Figure 7.2 is characterized by values of q, d, and H_o (i.e., discharge, depth, and flow energy) that plot at point P_1 in Figure 7.1, on the upper part of the curve for the given q. Since the bottom rises by a positive distance $\Delta h = h_{o2} - h_{o1}$, by Equation (7.5) the specific head H_{o2} associated with the flow downstream of the transition lies a distance Δh to the left of H_{o1} along the H_o axis; P_2 is the

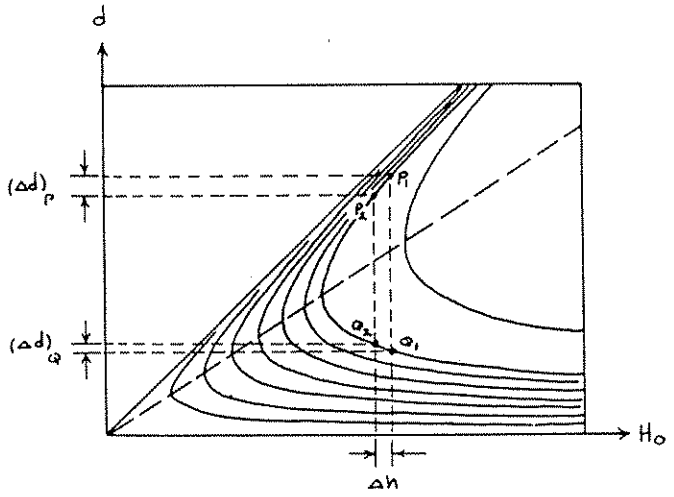

Figure 7.1 Specific-head diagram for rapidly varied two-dimensional open-channel flow. This is a plot of depth d against specific head H_o for several values of discharge per unit width q. See text for discussion.

corresponding point that represents the flow. Flow depth downstream of the step is therefore smaller by $(\Delta d)_P$ in Figure 7.1 than in the approaching flow, and by the relation $q = Ud$ the flow velocity is greater (Figure 7.2). By virtue of the doubly branched form of the curves in Figure 7.1 there can also be an approaching flow, represented by point Q_1 on the lower part of the same curve, with exactly the same discharge and flow energy but with smaller depth and higher velocity. In this case the flow downstream of the transition, represented by the point Q_2 found by moving a distance Δh leftward along the H_o axis as before, has depth greater by $(\Delta d)_Q$ than the approaching flow, and smaller velocity (Figure 7.3).

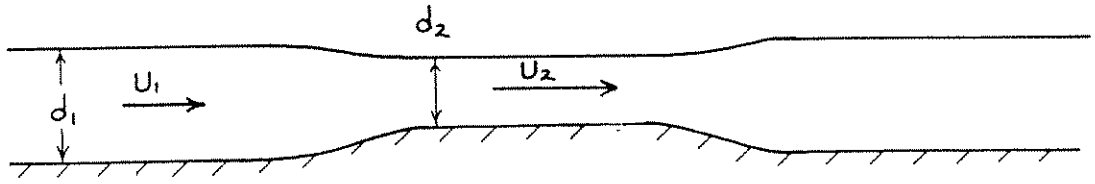

Figure 7.2 Behavior of depth and velocity of flow over a gentle rise in the channel bottom, when the approaching flow is subcritical.

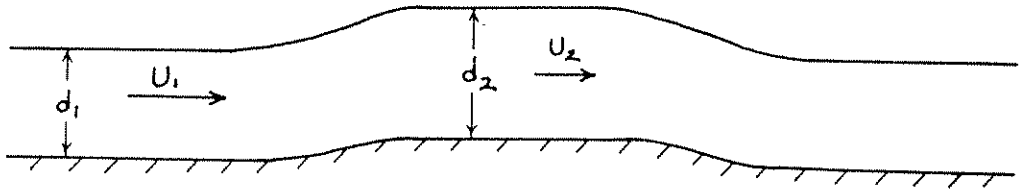

Figure 7.3 Behavior of depth and velocity of flow over a gentle rise in the channel bottom, when the approaching flow is supercritical.

For points at which the curves of d vs. H_o have vertical tangents, depth and velocity do not change in the transition. The equation for such points is found by differentiating the function in Equation (7.6) to find $dH_o/d(d)$, setting this derivative equal to zero, and solving for d as a function of H_o. The resulting curve is a straight line given by

$$H_o = \frac{3}{2} d \qquad (7.7)$$

Flows represented by this line are said to be critical flows. Flows corresponding to points above the line are subcritical (greater depths and lower velocities), and flows corresponding to points below the line are supercritical (smaller depths and higher velocities).

Thus, to every combination of discharge per unit width q and flow energy (represented by H_o) there correspond two different flow states, with different depth and velocity given by the two intersections of the curve of d vs. H_o for that q and the vertical line associated with that H_o. In some kinds of transitions the flow is forced all the way from one of these states to the other, thereby passing through the critical state during the transition. Any flow, whatever its origin and therefore whatever its depth and discharge, falls at some point on one of the curves in the specific-head diagram, and is therefore either supercritical or subcritical (or critical). The behavior of that flow in a transition is radically different depending on whether the flow is subcritical or supercritical. This difference in behavior is fundamentally a consequence of the requirement of conservation of flow energy expressed by Equation (7.2), together with the conservation-of-mass requirement that

$$q = \frac{U_1}{d_1} = \frac{U_2}{d_2} \tag{7.8}$$

For example, in the transition examined above, the variables U_1, d_1, h_{o1}, and h_{o2} are all given, and Equations (7.3) and (7.8) then specify exactly what combination of U_2 and d_2 must hold.

It happens that the condition for critical flow corresponds to a mean-flow Froude number $U/(gd)^{1/2}$ of unity. To verify this, simply substitute Equation (7.7), the condition for critical flow, into Equation (7.4), the definition for H_o, to obtain a relation between U and d for critical flow: $U^2 = gd$, or $Fr = 1$. Subcritical flows are characterized by Froude numbers less than one, and supercritical flows are characterized by Froude numbers greater than one.

There is an entirely separate relationship between mean-flow Froude number and open-channel flow, fundamentally unconnected with the above relationship, which is of greater importance in the study of bed forms. The celerity of shallow-water gravity waves (those with wavelength much greater than the water depth) propagating on the free surface of a liquid is given by $c = (gd)^{1/2}$. When the depth and velocity of the flow are such that U is equal to c, gravity waves propagating upstream (relative to the moving liquid) on the surface of the flow are stationary relative to the boundary (Figure 7.4). We'll see that such waves can interact with an erodible bed to produce a class of bed forms (antidunes) that are important in many channel flows having high velocities and shallow depths. Substituting U for c in the equation for the speed of propagation of surface gravity waves, again $U = (gd)^{1/2}$ or $Fr = 1$. A mean-flow Froude number of unity thus also specifies the condition that surface waves are stationary relative to the channel boundary.

Uniformity of Flow

If bed forms are present, the flow cannot be strictly uniform because bed forms can have heights that are a substantial fraction of the flow depth and spacings that are several times the flow depth. Flows of this kind can be uniform only in the looser sense that depths and velocities are constant from station to station along the flow when averaged over many bed forms in the vicinity of each station.

Flow over an erodible sediment bed in a channel tends automatically to produce uniform flow. To see this, suppose that the bed slope at the start of a flume run is too great for uniform flow. The flow would then have depth too small and velocity too large near the upstream end, and depth too large and velocity too

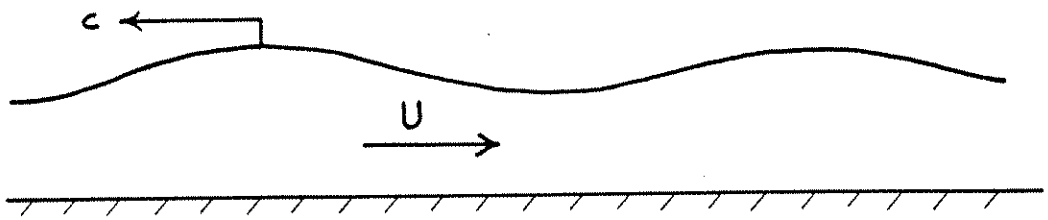

Figure 7.4 Relationship between flow velocity U and celerity c of shallow-water gravity waves propagating upstream in an open-channel flow.

small near the downstream end. Sediment transport rate would then be greater upstream than downstream, resulting in a pattern of erosion upstream and deposition downstream that would continue until depth, velocity, and sediment transport rate would each be uniform all along the channel. The result is the same if the bed slope starts out too small for uniform flow. The slope of the actual channel bottom in a flume run is therefore inconsequential (provided only that the channel bottom remains covered with sediment everywhere) because the flow adjusts the thickness of the layer or wedge of sediment along the channel until uniformity is attained. In flume work on bed configurations, adjustability of channel slope is convenient but not essential.

Remember from Chapter 5 (Equation 5.1) that for a given channel geometry the shear stress in uniform flow over a planar granular bed is uniquely specified by mean-flow Reynolds number and bed roughness. The same is true for a bed covered with bed forms, although three comments are in order: (i) the resistance diagram is not the same in its details as Figure 5.8 because of the differing roughness geometry; (ii) owing to the changes in details of bed geometry with time, the bed shear stress fluctuates irregularly with time around some average value; and (iii) the bed shear stress can be viewed as characterized by the roughness geometry, as in Chapter 5, but there's a new twist here: in fact the roughness geometry is itself determined by the forces exerted by the flow on its bed. Nonetheless, for some given mean flow depth and mean flow velocity in a flume experiment on bed configurations there will be a uniquely determined boundary shear stress after the bed has come to equilibrium with the flow, and therefore by Equation (1.16) a uniquely determined mean slope, characterized by either mean bed-surface slope or mean water-surface slope. From the preceding section, the energy slope will be the same as well.

If the flow is uniform in the presence of bed forms, then if we take profiles of the bed surface and the water surface and fit the "best" straight line to them, by some method like least squares, the lines are parallel. In fact, careful determination

of flow depth in a flume run necessitates just this kind of procedure. Slope and therefore boundary shear stress is easily determined by measuring the water-surface profile, finding the best-fit straight line, and comparing this with a preestablished horizontal reference plane. Since water-surface slope fluctuates with time around some average because of the slightly varying resistance properties of the bed configurations, reliable measurement of slopes requires either a very long channel or many determinations during a statistically uniform flow.

Hydraulic Regimes of Open-Channel Flow

In this section we draw together various phenomena of open-channel flow into a single graph, to give you an idea of the wide range of hydraulic regimes of flow that can exist. Figure 7.5 is a graph of mean flow depth against mean flow velocity for steady uniform open-channel flow in a wide rectangular channel. If bed roughness is present, its height is assumed to be a small fraction of the flow depth. Both depth and velocity span several decades, a far greater range than is found in the sediment-transporting flows encountered in natural flow environments. The value of a graph of this kind is that it helps to put into perspective the range of open-channel flows of interest to sedimentologists. The hydraulic regimes shown in Figure 7.5 are unrelated to the concept of "flow regimes" that is in common use in dealing with bed configurations; that concept will be discussed briefly in a later section of this chapter.

It's easy to plot curves in Figure 7.5 corresponding to $Fr = 1$, for the transition between subcritical flow and supercritical flow, and to $Re \simeq 500$, for the transition between laminar flow and turbulent flow (Chow, 1961). In a log-log plot like Figure 7.5 both of these conditions plot as straight lines; the line for $Fr = 1$ slopes upward to the right, and the line for $Re = 500$ slopes downward to the right. These two lines partition the graph into four sectors (Robertson and Rouse, 1941): turbulent subcritical in the upper left (the most important for sedimentological purposes); turbulent supercritical in the upper right (also important for sediment transport in shallow flows), laminar subcritical in the lower left, and laminar supercritical in the lower right.

In the lower part of Figure 7.5 are two curves (one for laminar flow and the other for turbulent flow) sloping upward to the right, below which steady, uniform open-channel flows cannot exist. These curves are defined by the condition that channel slope approaches the vertical, giving the greatest gravitational driving force possible. It's easy to get an exact solution for the curve that expresses this condition for laminar flow, by using Equation (1.23) to find the mean velocity U as a function of flow depth, fluid properties γ and μ, and channel slope angle ϕ,

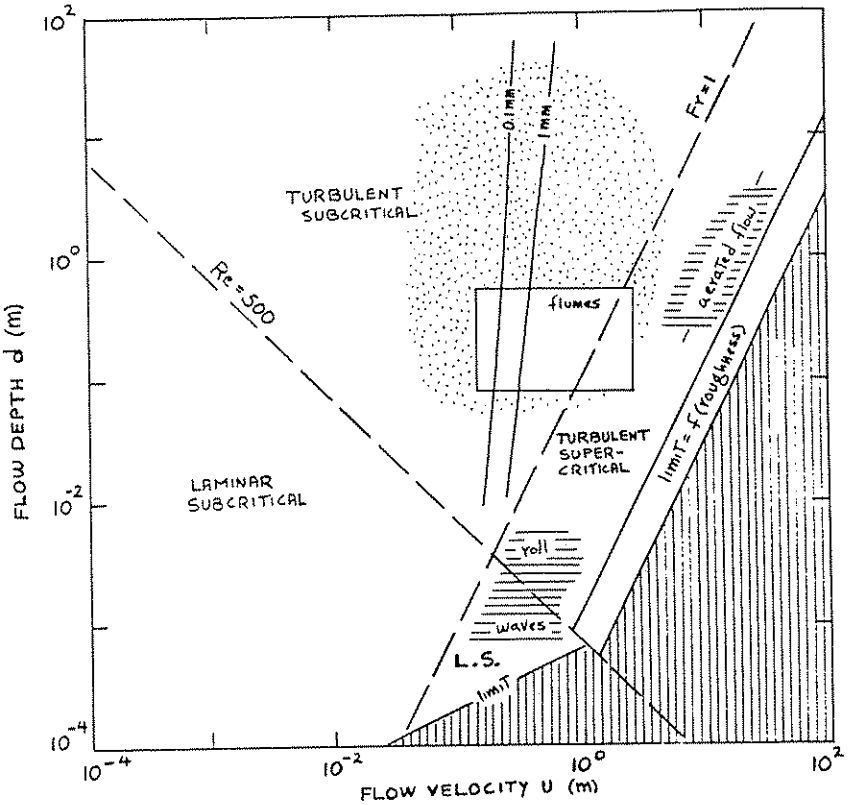

Figure 7.5 Hydraulic regimes of open-channel flow in a graph of mean flow depth vs. mean flow velocity. See text for explanation of curves.

$$U = \frac{\int_0^d u\,dy}{\int_0^d dy} = \frac{\gamma \sin\phi}{\mu} \frac{\int_0^d \left(yd - \frac{y^2}{2}\right) dy}{\int_0^d dy} = \frac{d^2 \gamma \sin\phi}{3\mu}$$

and then taking $\sin \phi = 1$, giving $U = d^2\gamma/3\mu$. This plots as a straight line in Figure 7.5. A sheet of rainwater running down a soapy windowpane is an example of flows represented by this line. It's not as easy to obtain the limiting curve for turbulent flows, because we have to work with a resistance diagram like that in Figure 5.8. The curve shown in Figure 7.5 was drawn in an approximate way by obtaining the friction factor f from the smooth-flow curve in Figure 5.8 and using that value together with $\tau_o = \gamma d$ in Equation (5.1). Figure 5.8 is for circular pipes, but it should be roughly applicable to open-channel flow provided that the pipe diameter is appropriately replaced. Four times the flow

depth was used in place of pipe diameter in computing the Reynolds number in Figure 5.8, because as noted in Chapter 5 the hydraulic radius of a circular pipe is one-fourth the pipe diameter, whereas the hydraulic radius of a very wide open-channel flow is just about equal to the flow depth. For rough flows the limiting curve in Figure 7.5 would be displaced upward somewhat, because the friction factor is greater for a given Reynolds number.

Also shown in Figure 7.5 are the equivalents of the Shields curve for incipient movement on planar sediment beds of 0.1 mm sand and 1 mm sand. These curves were drawn by converting threshold boundary shear stresses taken from Figure 6.9 into combinations of depth and velocity for threshold conditions, making use of the resistance diagram in Figure 5.8 in the same way as above. These curves could be extended into the laminar subcritical sector, but that sector is of no sedimentological importance anyway.

The region in Figure 7.5 of greatest sedimentological interest, in which sediment is transported by turbulent flows with moderate to high but not extremely high flow velocities and with flow depths at least an order of magnitude greater than the sediment size, is shaded by fine stippling. The little rectangle within this shaded area shows the typical depth-velocity range of flume experiments on sediment transport. In addition, shown by fine horizontal ruling are two separate areas: one for development of roll waves--the little waves with steep fronts and long backs you see when thin sheets of water flow down sloping surfaces under certain conditions--and the other for aerated flows, which develop when air is entrained downward from the free surface under conditions of very steep slopes and very high velocities, as in spillways below dams.

A FLUME EXPERIMENT ON BED CONFIGURATIONS

To get some idea of the bed configurations produced by a steady and uniform flow of water over a sand bed, and the succession of different kinds of bed configurations that appear as the flow strength is increased, imagine making a series of exploratory flume experiments on sand with some mean size between about 0.2 mm and 0.5 mm. In later sections we'll elaborate on many of the observations; this section is just intended as an orientation to some of the most important bed-configuration phenomena, in case you haven't had the chance to make systematic observations yourself. Place a layer of sand on the bottom of the channel (the bed need only be thick enough that even the deepest troughs of moving bed forms do not expose the rigid channel bottom) and then pass over the sand bed a series of steady uniform flows. Arrange each run to have the same mean flow depth (as great as the flume will allow, a large fraction of a meter if you're lucky) and increase the mean flow velocity slightly from run to run.

In each run, allow the flow to interact with the bed for a long enough time that the state of the bed is statistically steady; after this time the details of the bed configuration are in constant change but the average state of the bed remains the same. The time required for the flow and the bed to come into a new state of equilibrium might take from as little as a few minutes to as long as several days, depending on the rate of sediment transport, the size of the bed forms being developed, and the extent of modification of bed forms left over from the preceding run. You could speed the attainment of equilibrium a little by continually adjusting the slope of the whole channel to maintain uniform flow as the bed roughness changes, but these adjustments are not necessary: as noted above, the flow itself adjusts the bed for uniform flow by cutting and filling. But if you don't adjust the flume slope in this way you're likely to end up with a wedge of sand in the channel that tapers so sharply that the channel bottom is bare in the upper or lower reaches.

If before the first run you're impatient for results, the way to make bed forms develop fastest is to start with an irregular sediment bed. But it's more enlightening to start with a planar bed. (You can arrange one fairly easily by passing a straight horizontal scraper blade along the bed. If the blade is mounted on something that slides on the straight upper edges of the flume walls, you get a nice planar result.) Now turn on the pump and gradually increase the flow velocity--and remember to keep adjusting the slope of the channel to maintain uniform flow. The beginning of sediment movement would be in accordance with the Shields criterion (Chapter 6). Wait a while, and the flow will build very small irregularities at random points on the bed, not more than several grain diameters high, from which small ripples develop spontaneously (Southard and Dingler, 1971; Williams and Kemp, 1971, 1972).

You can help things along by poking your finger into the planar bed at some point to localize the first appearance of the ripples. The flow soon transforms the little mound you made with your finger into a miniature current ripple. The flow disturbance caused by this ripple scours the bed just downstream, and piles up enough sediment for another ripple to form, and so on until a beautiful widening train of downstream-growing ripples is formed (Figure 7.6). Little ripple trains like this, starting from various points on the bed, soon join together and pass through a complicated stage of development, finally to become fully developed ripples (Figure 7.7A). The stronger the grain transport, the sooner the ripples appear, and the faster they approach equilibrium. These ripples, which we'll later classify as <u>small ripples</u>, show generally triangular cross sections.

(Since we'll be using terms that describe ripple geometry throughout this chapter, we should stop right here and introduce these terms; refer to Figure 7.8. The region around the highest point on the ripple profile is the <u>crest</u>, and the region around the lowest point is the <u>trough</u>. The upstream-facing surface of

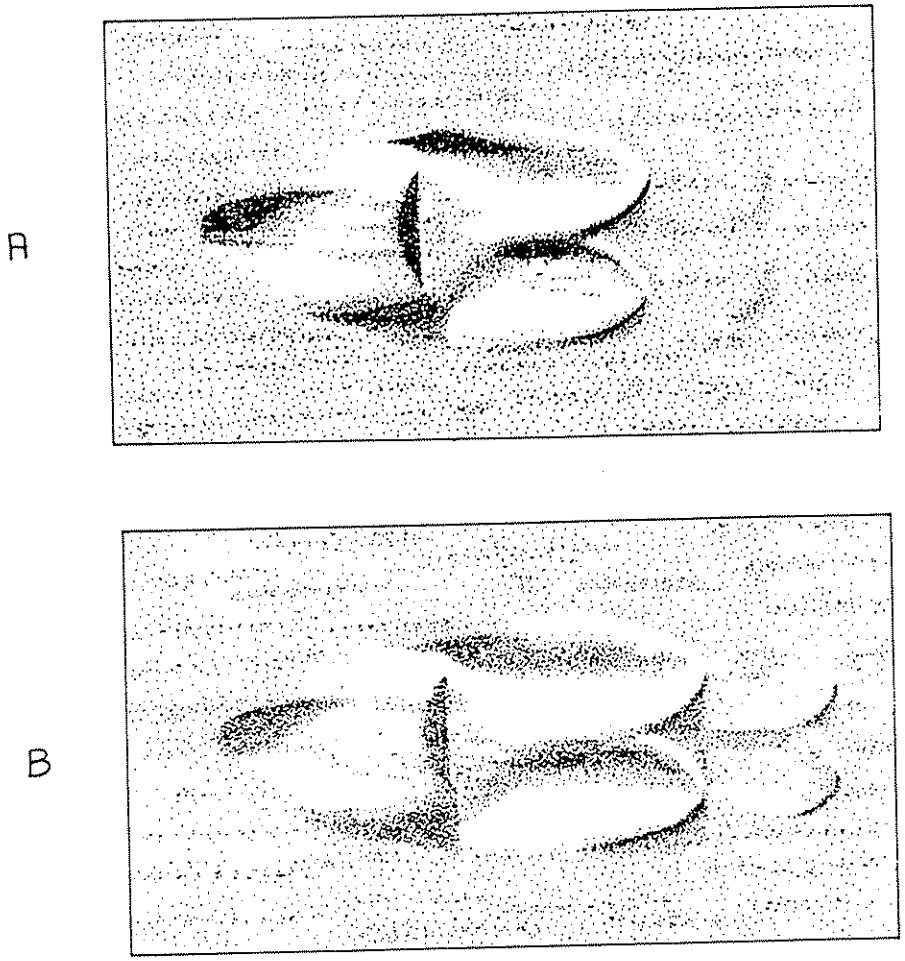

Figure 7.6 Two stages in the development of a train of ripples from a planar sand bed. Flow is from left to right, and light is from upper left. The picture in B was taken a short time after the picture in A. The depression in the left-hand part of the pictures was made by dragging a rod along the bed. The mound thus produced was modified by the flow to become a ripple. This ripple then produced additional ripples downstream. From photographs similar to those shown in Southard and Dingler (1971).

the ripple, extending from a trough to the next crest downstream, is the stoss surface; the downstream-facing surface, extending from a crest to the next trough downstream, is the lee surface. A well-defined and nearly planar segment of the lee surface, called the slip face, is usually a prominent part of the profile. The top of the slip face is marked by a sharp break in slope called the brink. There's often, but not always, a break in slope at the base of the slip face also. The top of the slip face is not

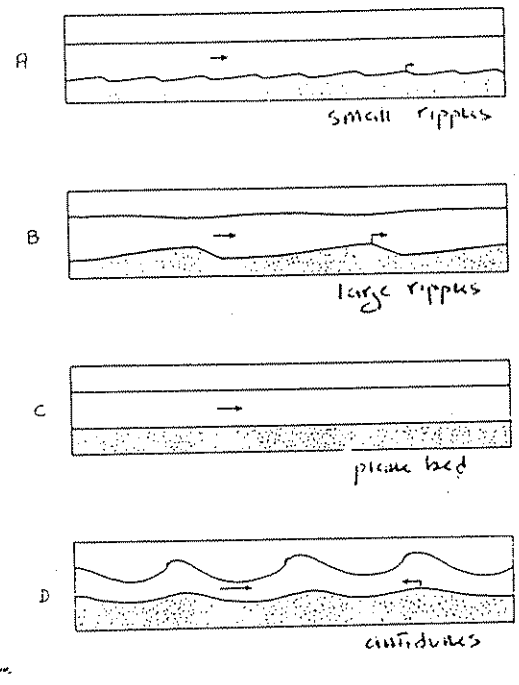

Figure 7.7 An exploratory flume experiment on bed configurations. A series of flows with increasing mean flow velocity but constant mean flow depth are set up over a bed of fine or medium sand. The generalized succession of bed phases observed after the bed and the flow have come to equilibrium is (A) small ripples; (B) large ripples; (C) plane bed; (D) antidunes. Arrows show qualitatively the mean flow velocity and the bed-form velocity.

always the highest point on the profile, and the base of the slip face is not always the lowest point on the profile. Such terminology can be made more precise and detailed; see Allen, 1968a.)

The stoss surfaces of small ripples are gently sloping, usually less than about 10° relative to the mean plane of the bed, and their lee surfaces are steeper, usually at or close to the angle of repose of the granular material in water. Crests and troughs are oriented dominantly transverse to the mean flow, but are irregular in detail in height and arrangement. The bed is said to be three-dimensional, rather than two-dimensional as it would be if the ripples were regular and straight-crested. The ripples move downstream by erosion of sediment from the stoss surface and deposition of sediment on the lee surface. With increasing current velocity an increasing fraction of the sediment load is carried in suspension above the ripples rather than being transferred as bed load from the stoss surface to the lee surface of the same ripple. Speed of ripple movement is

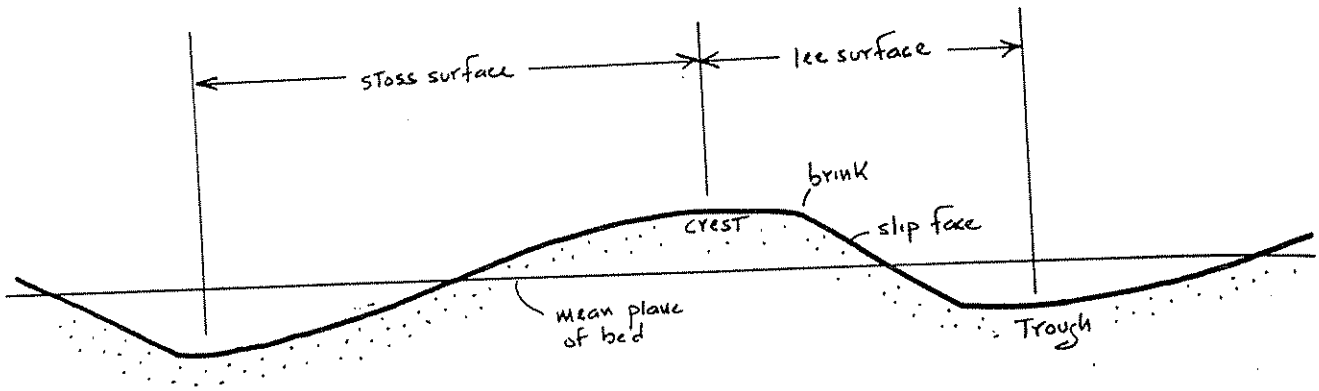

Figure 7.8 Terminology for ripple geometry in profile.

orders of magnitude less than the speed of the flow. The average spacing of ripples is of the order of 10-20 cm, and the average height is a few centimeters.

At a flow velocity that's a middling fraction of a meter per second (the exact value depending on flow velocity, grain size, and even water temperature), small ripples are replaced by larger bed forms generally called dunes or megaripples (we'll be calling them large ripples). These large ripples are broadly similar to small ripples in geometry and movement, but they are about an order of magnitude larger (Figure 7.7B). The transition from small ripples to large ripples is complete over a narrow range of only a few centimeters per second in flow velocity. Within this transition the bed geometry is complicated: the small ripples become slightly larger, with ill-defined larger forms intermingled, and then abruptly the larger forms become better organized and dominate the smaller forms.

You'd see that in the lower range of velocities that form large ripples the ratio of spacing to height is relatively large (larger than for small ripples), and the crests and troughs are fairly regular and continuous. With increasing flow velocity the large ripples become steeper and less regular. Also, with increasing flow velocity more sand is carried in suspension, obscuring the view of the bed except at the transparent sidewalls of the flume. Small ripples are superimposed upon the backs of large ripples, in the troughs and partway up the stoss slope. If we had a large enough flume at our disposal the large ripples would become large enough under some conditions of sand size and current velocity for smaller large ripples to be superimposed on larger large ripples.

With further increase in velocity the large ripples become lower and more rounded, over a fairly wide interval of flow velocity, until finally they disappear entirely, giving way to a planar bed surface over which abundant suspended load as well as

bed load is transported (Figure 7.7C). Judging from the appearance of the bed after the flow is abruptly brought to a stop, the transport surface is strikingly planar: relief is no greater than a few grain diameters. Since the bed is obscured, it's difficult to observe the mode of grain transport except through the sidewall, and you can't trust what you see there anyway because the boundary shear stress is unrepresentatively low in the corner.

As the flow velocity is increased still further over the planar bed, subdued standing waves appear on the water surface, and the resulting pattern of higher and lower near-bed flow velocity causes the bed to be molded correspondingly into a train of waves in phase with the water-surface waves. As the Froude number of the mean flow nears unity, these coupled bed and surface waves increase in amplitude and become unstable: they move slowly upstream and at the same time grow in amplitude, until they become so steep that they break abruptly, throwing much sediment into suspension (Figure 7.7D). The bed and water surface then revert to a planar or nearly planar condition, whereupon the waves build again and the cycle is repeated. Because of their upstream movement these forms were named antidunes by Gilbert (1914).

In an instructive variant of this flume experiment, increase the flow depth by a factor of two and cover the entire flow with a rigid planar sheet parallel to the mean plane of the bed. From the discussion in Chapter 5 it shouldn't surprise you that the flow structure in the lower half of the closed duct thus formed is not greatly different from that in the original open-channel flow; the differences are largely a consequence of the gross difference in roughness of the upper and lower boundaries when bed forms are present on the bed. If the sequence of runs is repeated with the top cover in place, the same succession of bed states is found except for one major difference: standing waves and antidunes would not appear, and plane-bed transport would be observed up to indefinitely high velocities. This should tip you off that the dynamics of antidunes is unrelated to the dynamics of ripples and the transition from ripples to a plane bed. The existence of antidunes is dependent upon the presence of the free surface, whereas the existence of ripples is independent of the presence of the free surface.

If you want to become an aficionado of flume studies on bed configurations there are lots of good papers to read. Some of these will be cited in the later section on empirical hydraulic relationships among the various bed states, but two deserve special mention at this point. The classic work of Gilbert (1914) still stands as one of the best of such studies, and the data are still widely used; unfortunately Gilbert didn't report the water temperature, and as we'll see later, that restricts the usefulness of the data somewhat. One of the largest and best-documented programs of flume experiments on bed configurations ever undertaken, made under the auspices of the U.S. Geological Survey in the 1950s and 1960s, is summarized by Guy et al. (1966).

FLOW AND SEDIMENT MOVEMENT OVER BED FORMS

Introduction

In this section we describe some of the important things about flow patterns and modes of grain movement over bed forms. This could be a large undertaking, and the discussion will have to be selective. It also has to be largely qualitative, because as we saw in Chapter 6 there is a definite limit to quantitative approaches to grain transport even when transport rates are low. In this section we'll concentrate on subaqueous ripples, small and large, although most of what's said applies to subaerial dunes as well. The literature dealing specifically with flow and grain movement over ripples is not large; although many make observations, few write specifically about them in much detail. As with so many areas in physical sedimentology, Allen (1968a, 1982) provides excellent and detailed review and discussion.

Flow Over Ripples

Pattern of Separated Flow over Ripples

Flow over ripples is dominated by separation at the crest or brink, reattachment in the trough, and boundary-layer redevelopment up the stoss surface of the next ripple downstream. The picture of separation downstream of a ripple (Figure 7.9) is largely similar to that shown in Figure 3.21B for flow through an expansion in a pipe, if the pipe is imagined to be replaced by a parallel-walled conduit and only the lower half is considered. In one way or another all the important things about flow and sediment movement over ripples are related to flow separation, so it's worth some more detailed discussion at this point.

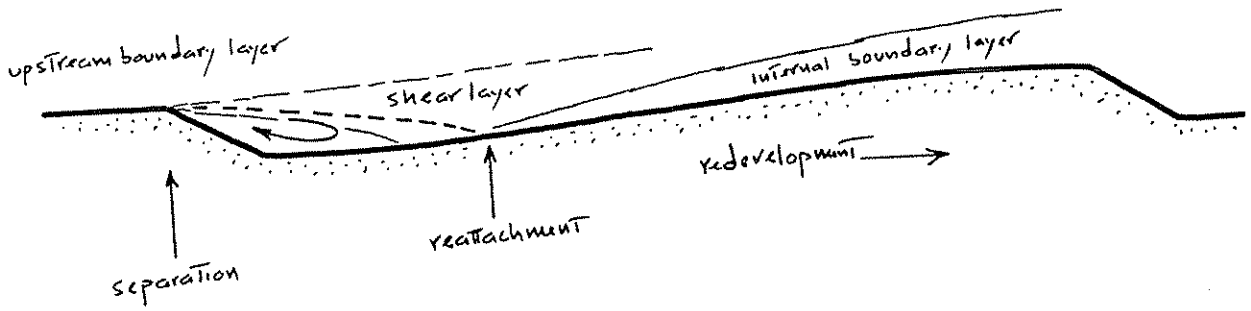

Figure 7.9 Elements of separating and reattaching flow over a ripple.

Separated flow over artificial small ripples or real but immobilized small ripples has been studied in the laboratory by Raudkivi (1963, 1966), Vanoni and Hwang (1967), and McQuorquodale and Giratella (1973). Systematic measurements of near-bed

velocity and turbulence, and especially of skin friction, over large ripples in nature are scarce; the most significant study is by Smith and McLean (1977). A similar kind of separated flow, that downstream of an abrupt downstream-facing step in a planar boundary, has had more detailed study (Bradshaw and Wong, 1972, and Etheridge and Kemp, 1979, among others). How well this flow over a negative step represents the flow over a ripple depends on the height-to-spacing ratio (i.e., the steepness) of the ripple: it should be much like flow over ripples with low steepness, but different in some important ways from flow over ripples with high steepness, owing to the appreciable slopes of the stoss surfaces both upstream and, more importantly, downstream of the step.

Separated flow over a negative step whose height is an appreciable fraction of the thickness of the flow upstream of it is one of the most complicated of turbulent flows. The strongly, even catastrophically, disrupted boundary layer has to be totally reorganized downstream of the step. It takes a surprisingly long distance downstream, as much as a few hundred step lengths, for the new boundary layer to become completely readjusted so that the turbulence structure is in accord with the picture described for an equilibrium turbulent boundary layer in Chapter 5. Moreover, you should expect the details, if not the overall phenomenon, to vary with step height H, upstream boundary-layer flow depth d, fluid properties ρ and μ, and mean upstream flow velocity U or boundary shear stress τ_o. So the flow structure should depend on both a mean-flow Reynolds number (or one defined on τ_o) and the ratio of step height to upstream flow depth, H/d. The dependence on Reynolds number is not substantial, basically for the same reasons discussed for velocity profiles in Chapter 5, but the dependence on H/d is strong. The picture is even more complicated for ripples, because of the varying bed slopes upstream and downstream of separation.

At low flow strengths just about all ripples have classically triangular profiles, but at higher flow strengths many have more rounded crests, and some are rather well streamlined, with separation pushed back to a point well downstream of the highest point on the profile. Even then, however, only a certain percentage of the ripples show rounded profiles. This variability in geometry and separation seems to be a result of strongly variable local flow patterns consequent upon the high degree of irregularity of neighboring ripples. Only when mean flow depth and mean flow velocity combine to produce small ripples or large ripples at mean-flow Froude numbers approaching unity (see the later section on hydraulic relationships) does the in-phase coupling of the ripples and the free surface lead to rounded profiles and absence or restriction of separation over all the ripples in the train.

Imagine taking a tour of a ripple profile by starting at a crest, sliding down the slip face, and then walking across the trough and up the stoss surface downstream. The flow you'd sense would differ greatly along the profile. This is something you

could actually do on a big sand wave in a river or a tidal current, with the right equipment and a spirit of adventure. On a subaerial dune you wouldn't even need that--although you might have to wait for a sand-moving wind. In a flume you'd have to put in little instruments, none of them perfect, as surrogates.

Turbulence rapidly develops on the shear surface extending downstream from the separation point at the ripple crest. The turbulent shear layer thus formed grows upward into the now-separated boundary layer above, and also downward. As the shear layer thickens, the sharp contrast in velocity across it is spread over a greater vertical distance. The mean-flow streamline that extends downstream from the locus of separation at the crest (called the dividing streamline) descends gently toward the trough, as the overall flow tries to follow the ripple profile. Remember that this streamline is defined only in a time-average sense; you'd have a difficult time locating it without careful measurements, because the shear layer is so strongly turbulent. At a point on the bed about ten step heights or a little less downstream, the shear layer meets the bed at some moderate angle. The shear layer is said to reattach to the boundary at that point. The stagnation point is well defined only in a time-average sense. (Technically we should be speaking of a stagnation line, again defined only in a time-average sense, rather than a stagnation point. One usually hears about reattachment points rather than reattachment lines, because the pattern of fluid motion is usually viewed in a streamwise cross section.) At reattachment the flow in the shear layer is divided: a small part is diverted upchannel, and the greater part continues downchannel, now in contact with the bed.

The space below the shear layer and upstream of the reattachment point is called the separation bubble (although it has nothing to do with bubbles sensu stricto). Turbulent mixing of fluid from the top of the separation bubble into the lower part of the shear layer, together with the upchannel diversion of a part of the shear layer at reattachment, combine to produce a weak vortex or roller, whose sense of circulation is shown by the arrow in Figure 7.9. As you moved down the lee face and out onto the trough you'd feel an irregular, eddying current in the opposite direction. This current is not nearly as strong as the main flow up above the ripple.

Near the reattachment line you'd feel the full effect of the turbulence in the shear layer. In the narrow reattachment zone the strong eddies generated in the shear layer impinge upon the bed in a seemingly random pattern and flatten out against it to cause temporarily very high local shear stresses. You'd feel strong puffs of flow trying to push you this way and that. But even though the shear stress is high at certain points and certain times, it's nearly zero on the average; the time-average component of velocity parallel to the bed is zero at the reattachment line, by definition, so the time-average local boundary shear stress is just about zero there also. Anisotropy in streamwise fluctuating

velocities at reattachment could make the shear stress average out to be nonzero there, but in any case the line of zero average boundary shear stress must be close by. Both the near-bed velocity and the average boundary shear stress increase sharply downstream from the reattachment zone, but the magnitudes of the fluctuations decrease noticeably.

The flow a short distance downstream of reattachment has a very complex structure. You can think in terms of three layers. (Oh, no; more layers.) (i) The shear layer developed by separation is now flowing in contact with the bed. (ii) Above the reattached shear layer is the original boundary-layer flow from upstream. This layer of flow maintains its identity rather well for long distances downstream of separation, even though it's being consumed from below. (iii) As it moves up the stoss surface, the flow in the reattached shear layer has to adjust itself to the presence of the boundary. This can be viewed as the development of a new boundary layer (called an internal boundary layer) upward from the bed in the downchannel direction. By the upward growth of this new boundary layer the presence of the boundary eventually alters the structure of the turbulence in both of the other two layers above. By this process the disturbed boundary layer is said to relax toward the new equilibrium state.

If a planar boundary extended indefinitely far downstream parallel to the mean flow direction, the new boundary layer would eventually develop to extend through the entire flow depth. In flow over a ripple, however, redevelopment is still incomplete by the time the flow reaches the crest, so the flow well above the crest senses little of the profound changes in near-bed flow. In the former case the velocity gradient and therefore the shear stress at the bed decrease gradually from a maximum just downstream of reattachment, where they had to rise sharply from zero, to their equilibrium values far downstream. In the case of ripples, on the other hand, the flow throughout the growing boundary layer and the degrading shear layer above it is accelerated as it's crowded upward over the upsloping stoss surface. It doesn't take much of a slope for this acceleration to cause an increase in both boundary shear stress and near-bed velocity up the stoss surface; consequently, the near-bed flow is strongest as it reaches the crest to separate again.

Figure 7.10 shows typical distributions of time-average local velocity, boundary shear stress, and boundary pressure over a ripple profile. Because of flow separation, vertical velocity profiles are greatly different just upstream and just downstream of the ripple crest. In the accelerated flow downstream of reattachment on the stoss surface, velocities in the lower part of the flow are less than they are at the crest, and a profile through the separation zone just downstream of the crest shows reverse velocities in the lower part of the flow. The average bed shear stress increases from zero at the reattachment point to a maximum at or near the ripple crest, and is actually directed upchannel beneath the separation vortex. Pressure at the boundary

is high downstream of reattachment and low at the crest, and therefore also in the separation zone; the net downstream pressure force (the form drag) on the ripple is typical of separated flow around bluff bodies, and greatly overshadows the net downstream force on the ripple due to the distribution of local boundary shear stress (skin friction).

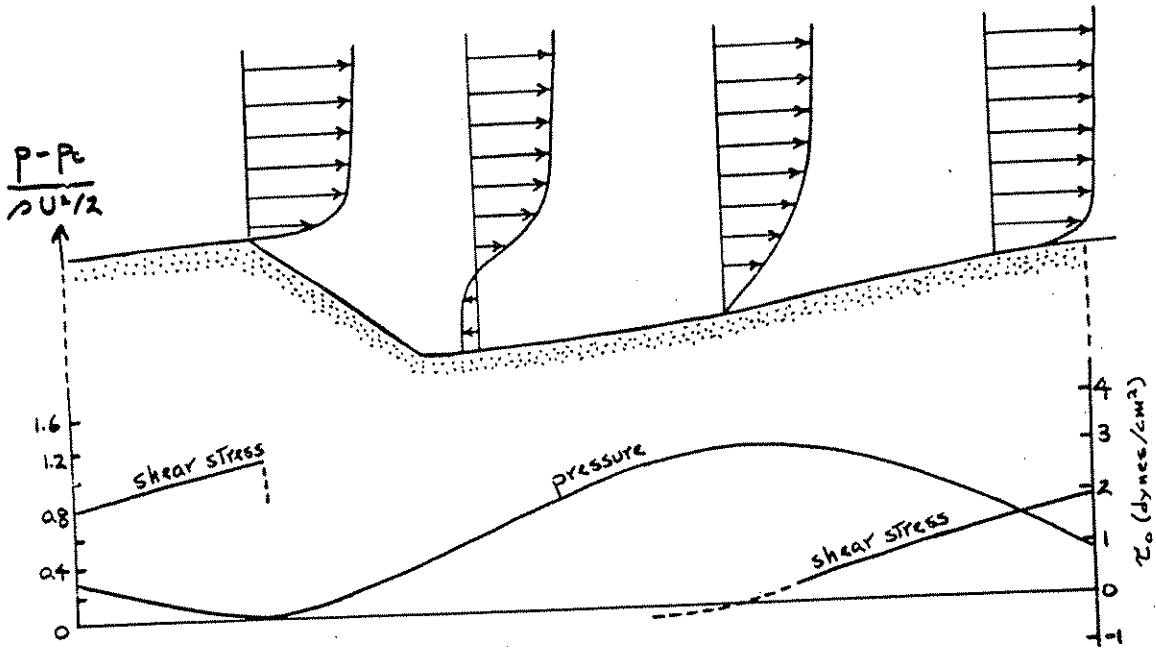

Figure 7.10 Distributions of velocity, bed shear stress τ_o, and bed-surface pressure p over a ripple. After Raudkivi (1963) and Vanoni and Hwang (1967), slightly schematized. Pressure is expressed in terms of pressure at the ripple crest, p_c, and mean flow velocity U (about 30 cm/s).

Velocity Profiles over Ripples

The material in the latter part of Chapter 5 on velocity profiles over rough beds is useful here in dealing with vertical profiles of time-average velocity over fields of ripple-shaped bed forms, large or small. It's natural to think about such profiles in two different ranges of height above the bed: well above the ripples, and close to the bed.

Think first about the velocity profile above a plane parallel to the mean bed level and one to two ripple heights above the ripple crests. Unless the ripple height is such a large fraction of the flow depth that the whole flow accelerates and decelerates as it passes over the ripples, such a velocity profile is almost the same wherever it's taken, because at this height the

upward-diffusing wake turbulence generated by flow separation at ripple crests is well blended spatially. In the following paragraphs we'll use the adjective integrated for such profiles (cf. Paola, 1983). These profiles characterize layers of the flow that blanket entire fields of bed forms without varying at the scale of those bed forms. If the flow depth is large relative to the ripple height the lower part of the integrated profile (and with little error the upper part also) is well described by Equation (5.29), the law of the wall for rough boundaries,

$$\frac{\bar{u}}{(u_*)_t} = A \ln \frac{y - (y_1)_t}{(y_o)_t} \qquad (7.9)$$

where A, the reciprocal of the von Kármán constant, has a value of about 2.5.

The boundary shear stress $(\tau_o)_t$ concealed in $(u*)_t$ in Equation (7.9) is the total shear stress the flow exerts on the rippled bed. Were you to invent a good way of measuring pressure and viscous shear stress at every point on the bed, you'd have to average over an area much larger than the scale of the ripples to get a representative value for $(\tau_o)_t$. Most of $(\tau_o)_t$ is form drag exerted on the ripples, not local stress exerted on the granular bed surface--called skin friction. This latter skin-friction component of the the total drag may be largely viscous drag, if the flow in the immediate vicinity of the bed is dynamically smooth, or it may itself be largely form drag, if the flow in the vicinity of the bed is dynamically rough. By analogy with the results in Chapter 5 for granular roughness, the roughness length $(y_o)_t$ associated with the integrated velocity profile in Equation (7.9) is proportional to the height of the ripples and is a small fraction thereof, the exact value depending on the shape (and most importantly the steepness) of the ripples. The displacement height $(y_1)_t$ is such that the origin for the velocity profile lies somewhat below the ripple crests. As the ratio of flow depth to ripple height decreases (but not to the point where there's no longer an integrated profile) it gets more difficult to distinguish between inner and outer layers of the flow, but the wall-law representation is still a good approximation.

Now look at the velocity profile near the bed at points on the stoss surface of a given ripple. At points well downstream from reattachment the velocity profile near the bed follows the law of the wall also, because of the upward development of the internal boundary layer at the expense of the turbulent wake downstream of separation. If the boundary Reynolds number based on the skin friction $(\tau_o)_s$ and the local granular roughness height is larger than about 10 the flow in the internal boundary layer is dynamically rough, and the velocity profile is given by

$$\frac{\bar{u}}{(u_*)_s} = A \ln \frac{y - (y_1)_s}{(y_o)_s} \qquad (7.10)$$

where $(\tau_o)_s$ in the shear velocity $(u*)_s$ is a local boundary shear stress that can be viewed as averaged over an area that's large compared with the granular roughness but small compared with the ripples themselves. We'll use the adjective local for profiles of this kind, because they apply only to particular points on the ripple. The profile in Equation (7.10) is characterized by values of roughness length $(y_o)_s$ and displacement height $(y_1)_s$ associated with the granular roughness, and both of these are smaller than the corresponding values associated with the integrated wall-law profile in Equation (7.9).

If the local boundary Reynolds number is much smaller, less than about 5, the local velocity profile is represented instead by the law of the wall for smooth flow, Equation (5.15),

$$\frac{\bar{u}}{(u_*)_s} = A \ln \frac{\rho(u_*)_s y}{\mu} + B \qquad (7.11)$$

where B has a value of about 5.1, as noted in Chapter 5. In this case the skin friction on the stoss surface of the ripple is mostly viscous drag rather than granular form drag. At intermediate boundary Reynolds numbers the velocity profile is represented by the law of the wall for transitionally rough flow. This can be put into the same form as the rough-flow profile (Equation 7.10) but with y_o then a function of the local boundary Reynolds number as well as the roughness height, and the skin friction is partly viscous drag and partly form drag. Whether the local flow in the growing boundary layer is smooth or rough, however, $(u*)_s$ in Equations (7.10) or (7.11) is much smaller than $(u*)_t$ in Equation (7.9), because whatever its nature the skin friction on the ripple surface is much smaller than the form drag on the ripples.

The local wall-law profile varies with distance up the stoss surface: as the flow in the internal boundary layer accelerates up the slope, the skin friction $(\tau_o)_s$ increases, as does the height to which the profile is applicable. You can be sure, however, that in a simple dimensional semilog plot with ln y on the vertical axis and u on the horizontal axis the slopes of the straight lines that represent the local wall-law profile are always much greater than the slope of the single straight line for the integrated wall-law profile that holds well above the level of the crests of the ripples, because $(u*)_t$ is much larger than $(u*)_s$; see Figure 7.11, which summarizes the relationship between the integrated profile and the local profile above a given point

on the stoss surface of a ripple. For how to find $(u*)_t$ and $(u*)_s$ from the slopes of the straight segments in this semilog plot, refer to the latter part of Chapter 5. In between the regions of applicability of the local wall-law profile near the bed and the integrated wall-law profile well above the ripples is a complicated region of the flow in which the velocity grades from one profile to the other. This region thins downstream along the stoss surface but is not consumed completely even when the flow reaches the next ripple crest downstream.

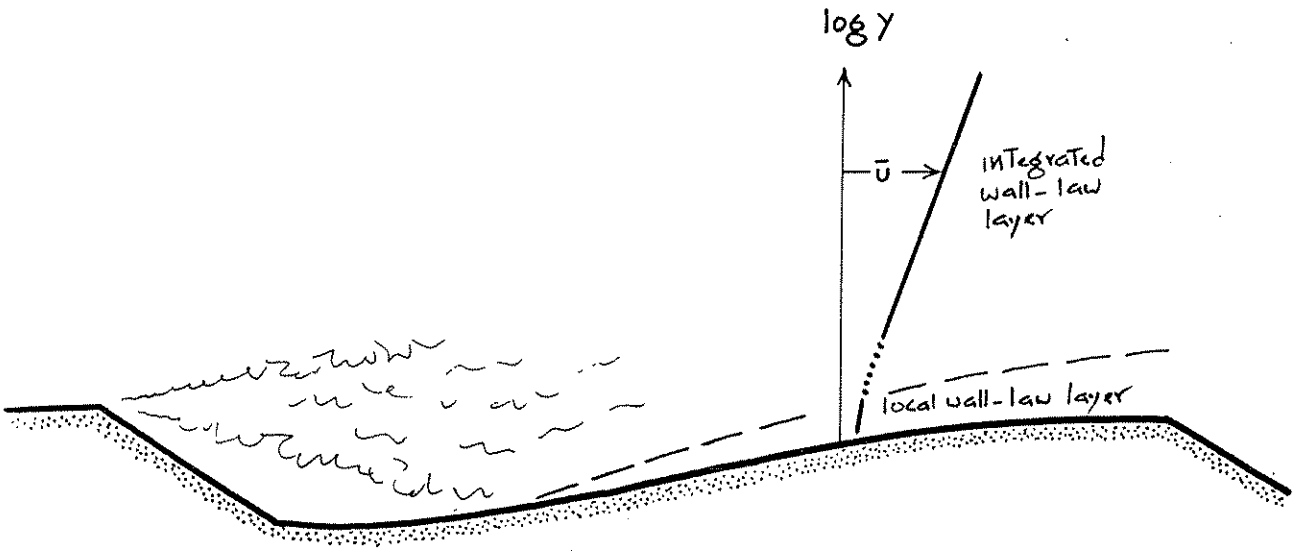

Figure 7.11 Relationship between the integrated wall-law layer and the local wall-law layer developed over a rippled bed.

Where small ripples are superimposed on much larger ripples the foregoing line of reasoning can be taken a step further. Large internal boundary layers develop on the stoss surfaces of the larger ripples in just the same way that small internal boundary layers develop on the smaller ripples. The smaller ripples, of which there presumably are a great number on the stoss surface of each larger ripple, act as local roughness beneath the internal boundary layer that develops up the stoss surface of each larger ripple. There is therefore a layer of the flow well above the crests of the smaller ripples but still well below the crests of the larger ripples in which the velocity follows an intermediate wall-law profile (Figure 7.12). This intermediate profile looks simultaneously like an integrated (although slowly varying) profile to a small observer stationed on one of the smaller ripples, but like a local profile to a large observer stationed on one of the larger ripples. This profile is

characterized by values of u_*, y_o, and y_1 intermediate between those of the integrated profile over the large ripples and those of the local profile over the smaller ripples. From the standpoint of the large ripples the intermediate value of u_* represents a local boundary shear stress, so in a sense it's skin friction even though form drag predominates over viscous drag. At the same time, the viscous drag and smaller-scale form drag associated with the sediment grains on the surfaces of the smaller ripples represent skin friction relative to the smaller ripples.

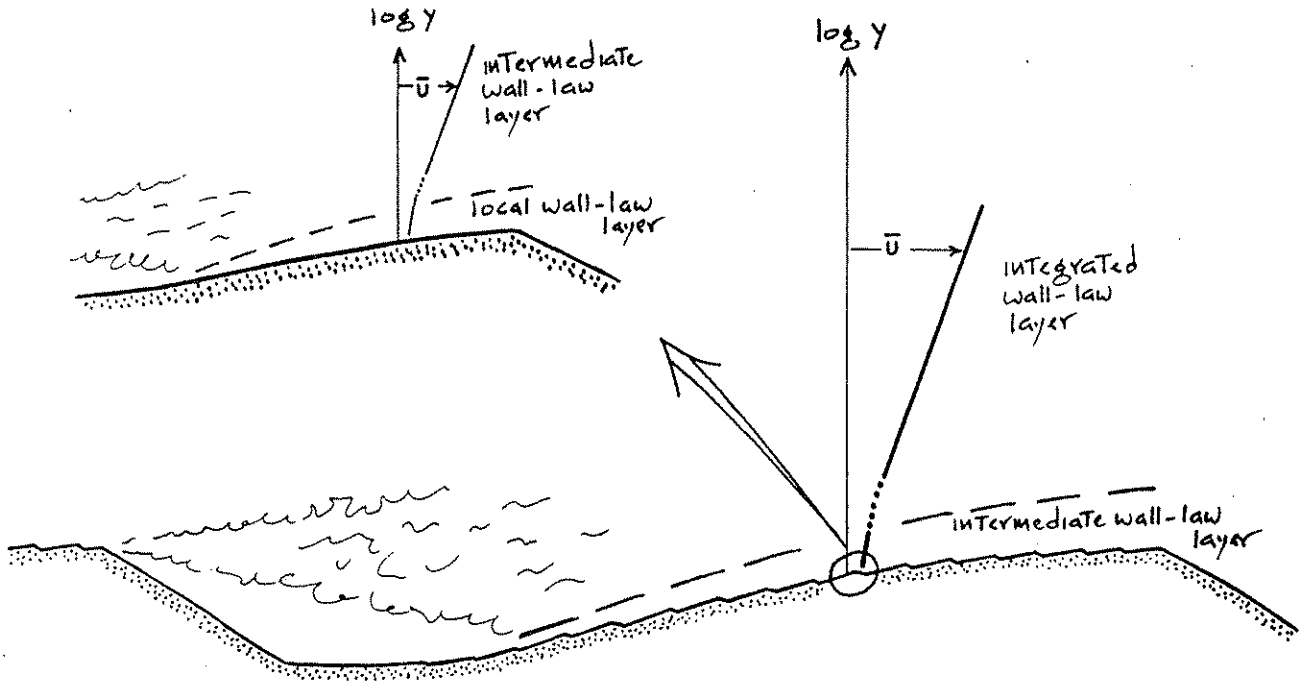

Figure 7.12 Intermediate wall-law layer developed over a rippled bed on which smaller ripples are superimposed on larger ripples. The intermediate layer acts as an integrated layer with respect to the smaller ripples but as a local layer with respect to the larger ripples.

The same ideas can even be extended to very large ripples (which would usually be called sand waves) on which two orders of smaller ripples with two greatly different scales are superimposed. There are then two different intermediate layers of the flow, of the kind just described, each with its own wall-law profile characterized by its own set of values of u_*, y_o, and y_1: one that's local relative to the largest ripples (the sand waves themselves) but integrated relative to the larger superimposed ripples and one that's local relative to the larger superimposed ripples but integrated relative to the smaller superimposed ripples.

You could take velocity profiles at a large number of points along the profile of one or more of the largest ripples present on the bed and average them all together to obtain a spatially averaged velocity profile. In a sense this spatially averaged profile represents the entire flow. Such averaging is not entirely satisfactory, for two reasons: (i) owing to growth of the internal boundary layer the near-bed part of the velocity profile varies with position along the ripple profile (even aside from the gross changes caused by separation and reattachment in the vicinity of the trough), and (ii) since the origin plane for the integrated wall-law region associated with ripples of a given order is parallel to the mean plane of the bed in the vicinity of those ripples, whereas the origin for the individual profiles is naturally taken at the bed surface itself, the base of the integrated wall-law profile is encountered at different heights in different places. The latter problem is not as serious as it seems, however, because at the height of even the lowest of such integrated wall-law regions, points at rather different heights plot close to each other on a logarithmic vertical axis. Provided that the ratio of spacing to height of the ripples of each order is large, so that separation bubbles occupy only a small fraction of the area of the bed, the spatially averaged profile in a semilog plot of height against velocity shows a series of straight-line segments connected by smooth transitions, just like the individual profiles--although the transitions are likely to be more gradual, for the two reasons noted above. The values for boundary shear stress obtained from these straight-line segments in the spatially averaged profile represent the spatial averages of the boundary shear stresses associated with each order of bed form present, ranging upward in scale from the grain roughness itself. For further details on such spatially averaged velocity profiles over ripples, see Smith and McLean (1977a).

Sediment Transport Over Ripples

Modes of Grain Movement Over Ripples

Even for a ripple of given size, formed under given conditions of sediment and flow, the mode of sediment transport varies greatly from place to place over the ripple profile. A repetition of your traverse across a ripple, this time just to watch the mode of sediment movement, would therefore be advantageous. Since the mode as well as the rate of sediment movement changes a lot more with increasing mean-flow velocity than does the structure of the flow, you may have to make more than one traverse.

The reattachment zone, where time-average flow and shear stress are near zero, is a good place to start, because time-average bed-load transport rate is near zero there. Strong eddies in the reattaching shear layer impinge upon the bed to cause strong but sporadic grain transport. At low mean-flow velocities sediment is shifted this way and that on the bed in

local pulses that strike seemingly at random. This is the site of first suspension of sediment as flow velocity gradually increases: swirls of sediment are put into suspension in puffs and gusts, and then the grains either settle directly back to the bed or are dispersed up into the flow. Downchannel from the mean position of the reattachment line these sporadic pulses of movement are directed more and more consistently downchannel and gradually give way to more uniform grain movement up the stoss slope. In the other direction they cease to be important just a short distance upchannel from reattachment, because flow in the separation vortex is relatively weak.

Grain movement up the stoss surface is much like that on a planar sediment bed, described in Chapter 6: it occurs as isolated pulses or "bursts" (an apt word, but probably confusing, because these pulses are only indirectly related to the bursts described in chapters 5 and 6) at low mean-flow velocities, and as a continuous sheet or layer at higher velocities. With increasing velocity the bed-load movement is obscured by sediment put into suspension in the trough or from ripples farther upstream. For as long as the bed can be seen, the stoss surface shows the characteristic longitudinal transport streaks described for plane-bed transport in Chapter 6. This should not surprise you, because flow conditions immediately above the planar stoss surface of a ripple are not much different from those over a more widespread planar bed. You'd also find that large ripples often have smaller ripples superimposed on their stoss slopes; this will be discussed in a little more detail in a later section.

At low flow velocities all the sediment transported as bed load to the brink is dumped there, tending to build the stoss surface forward over the top of the lee surface. This increases the lee slope angle there, and the sediment slips and flows down the lee surface as a grain flow (see Chapter 8) to restore a stable angle of repose. Grain flow is localized and sporadic when the rate of delivery is slow, but widespread and continuous at higher flow velocities (Allen, 1965). The result is a nearly planar lee surface, the slip face, with a break in slope not only at the top but also at the base, where the slip face builds forward onto the surface of the trough downstream.

At higher flow velocities some fraction of the grains transported near the bed up to the brink are carried out along or just above the shear surface downstream of the separation locus at the crest or brink. These grains then settle through the complicated turbulent flow field in the wake of the ripple and land at various points: on the slip face, in the trough, on the stoss surface of the next ripple downstream, or even on some ripple much farther downstream. Where the grains land depends on several things: the velocity of the flow, the settling velocity of the grains, the height of the grains above the bed as they first pass beyond the brink, and just which eddies the grains happen to fall through (Figure 7.13; Jopling, 1964, 1965; Allen, 1968b).

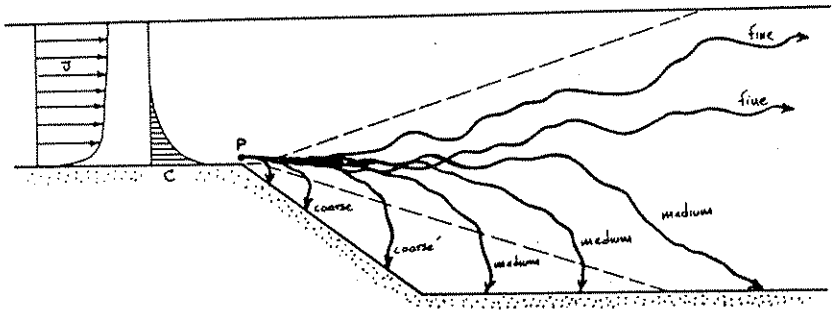

Figure 7.13 Very schematic picture of some representative trajectories of grains in suspension that pass through some point P over a ripple crest. Finer particles show less tendency to settle just downstream of the separation line, and their motion is more affected by turbulence. The dashed lines represent the mean position of the expanding shear layer.

To complicate things further, if the near-bed reverse flow in the separation vortex is strong enough it can move grains upchannel toward the base of the slip face. If in addition the reach of bed over which this current flows is long enough, a train of small upchannel-moving ripples is formed. The sediment moved by this current is swept up onto the lee surface to be deposited with the sediment flowing down from the brink. Lamination and grain-size distribution in the sediment deposited on the lower part of the slip face--and this is what's most likely to be preserved in the sedimentary record--are determined by the interplay of three modes of sediment delivery: (i) grain flow down the slip face; (ii) grain-by-grain deposition from suspension; and (iii) upchannel tractional transport by the reverse flow.

When the ripple geometry is three-dimensional many troughs show no well defined separation vortex, and patterns of flow and sediment transport are not as simple as outlined above. The bed surface near the base of the lee slope nonetheless usually feels flows that are much weaker than over the stoss slope, although these flows may have a substantial cross-stream component. In fields of large ripples, transverse flow in the lee of the ripples often produces trains of small ripples in troughs and on lee slopes, with crests oriented at a large and spatially variable angle to the crests of the large ripples.

Cycling of Sediment Within Ripples

It's easy to observe that a ripple moves downstream by transfer of sediment from the stoss surface to the lee surface, mostly as bed load. What's less obvious is that the sediment makes its way back through the moving ripple after deposition. Think about a grain that becomes entombed somewhere on the slip face (Figure 7.14). As the ripple moves downstream the horizontal distance between that grain and the stoss surface of the ripple decreases until the grain appears at the surface, to be transported as bed load up to the brink and deposited there to slide partway down the lee surface again. It's then interred again in the ripple, generally at a different level than before. Sediment grains are thus recycled episodically through the ripple, with relatively long periods of burial punctuated by relatively brief periods of transport. Using radioactive tracer techniques, Grigg (1970) was able to make direct measurements of probability distributions of the transport distances and rest periods involved.

An important implication of this grain recycling is that all the sediment in the ripple travels with that ripple; the average grain speed U_G is exactly the same as the velocity of advance of the ripple, which we'll call the bed-form velocity U_B. This is true, however, only if all the sediment moves as bed load, and even then only in the ideal case of a train of ripples of identical shape with troughs all at the same height relative to the mean plane of the bed. Most rippled beds show considerable variability in trough depth. This ensures that some of the grains deposited low on a particular lee surface that's building into an unusually deep trough will escape erosion not only by that ripple but perhaps also by one or more ripples following upstream. These grains are exhumed much later and are then cycled within some other ripple.

Even in a train of identical ripples, it's only at low flow velocities that all grains are cycled within a ripple. With increasing flow velocity grains begin to be put into suspension at some point during their period of transport over the ripple (predominantly in the trough or at the brink) and return to the bed beyond the influence of the near-bed reverse flow just downchannel from the base of the slip face, and are thus lost from that ripple forever. At the same time, grains put into suspension at points farther upstream are added to the ripple, either by settling directly onto the lee surface or by settling onto the stoss surface and moving as bed load to the lee surface.

Movement of Bed Forms

A fundamental characteristic of ripples is that they move downstream at some velocity U_B, by erosion on the stoss surface and deposition on the lee surface. This velocity is of interest because (i) it's an index of bed-load transport rate, because

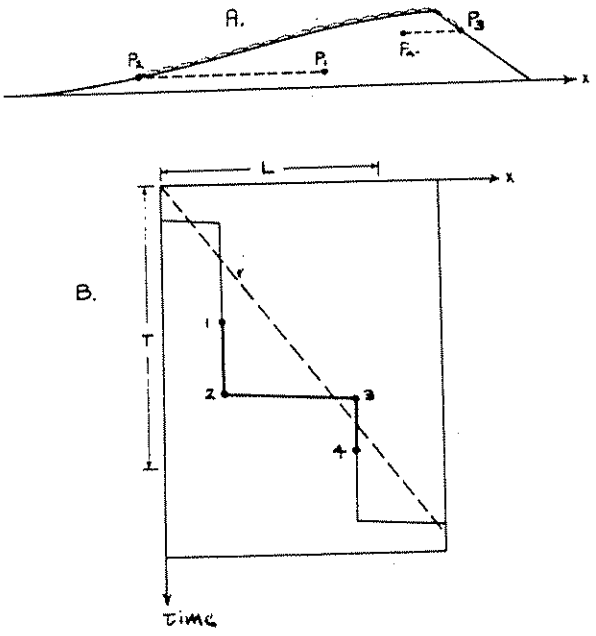

Figure 7.14 (A) Schematic representation of the transport path of a sediment grain relative to a moving ripple. At some time t_1 the grain is buried at point P_1 within the ripple. At a later time t_2 the grain is at the surface of the ripple at point P_2. Then in a relatively short time the grain is transported over the ripple to be deposited and buried at point P_3 at time t_3. At some later time t_4 the grain has moved upstream relative to the ripple to point P_4. (B) Time-distance graph of grain movement and ripple movement in A, showing positions of the given grain (solid line) and of the ripple crest (dashed line) with respect to downstream coordinate x. L is ripple spacing, and T_r is the time required for movement of the ripple past a fixed station. Step length is never greater than L, and rest period is never greater than T_r.

we've seen that most of the bed load moving on a ripple bed is cycled within the same ripple, and (ii) it's one of the determinants of the stratification geometry produced by ripple movement. This section addresses the measurement of U_B, along with some results, and also its use in estimating sediment transport rates. A discussion of its role in the geometry of sedimentary structures would take us too far afield; see papers by Allen (1970), Ashley et al. (1982), Rubin and Hunter (1982), and Harms et al. (1982, Chapter 3). At the end of this chapter we'll return to the dynamics underlying the downstream movement of ripples.

It's surprisingly difficult to characterize the downstream movement of ripples. If each ripple had an unchanging streamwise profile, U_B would be both well defined and readily measurable. Since most ripples have a fairly sharp break in slope at the brink, it's usually no problem to follow a distinguishable point on the profile as the ripple moves. But the profile shape changes as the pattern of sediment transport over the ripple changes, even if the profile area stays the same. This usually causes the position of the brink to change relative to the center of area of the ripple over just a short distance of movement, so even the position of a well defined point on the profile doesn't necessarily represent well the position of the ripple. Moreover, the profile area of a ripple itself is changed by several processes, which can act concurrently: (i) intensification of scour in a trough and deposition of the eroded sediment on the stoss surface or farther downstream; (ii) transfer of sediment from one ripple to another by either bed-load transport or suspended-load transport; (iii) overriding of one ripple by the next ripple upstream; (iv) division of one ripple into two, as a new trough develops on the stoss surface of a ripple as a result of some change in upstream flow pattern. The last two mechanisms imply that ripples don't live forever: they come into being, move for some distance that's usually a small number of ripple spacings, and then disappear.

A good way to apprehend the transitory existence of individual ripples is to generate a train of ripples in your flume and photograph them with a time-lapse movie camera as they move downstream. When you viewed the film at normal speed you'd see the ripples doing all sorts of crazy things that are hard to appreciate by real-time viewing; the moderately regular succession of ripples when viewed in a still picture is deceiving. Two other instructive things you could do are described in the following paragraphs.

You might stock up on sandwiches and caffeine, occupy a station somewhere along the channel, and for a large number of ripples measure the time T_r needed for two successive ripple crests to pass the station. After getting some rest you could then plot a cumulative distribution of T_r. (When multiplied by the spacing of the passing ripple, the inverse of T_r is a good representation of U_B.) Figure 7.15, measured by Southard et al. (1980), is such a curve. Note the wide range in passage times. It was found that hundreds of ripples would have had to be measured to obtain a stable cumulative curve, although substantially fewer were sufficient for a stable mean value.

To quantify the variability in ripple movement you might enlist a large number of volunteers to stand along the transparent sidewall and be responsible for keeping track of the positions of the ripples as a function of time. A plot of position vs. time would look like Figure 7.16, from which you can see that (i) for a given ripple U_B varies widely and irregularly with time; (ii) a

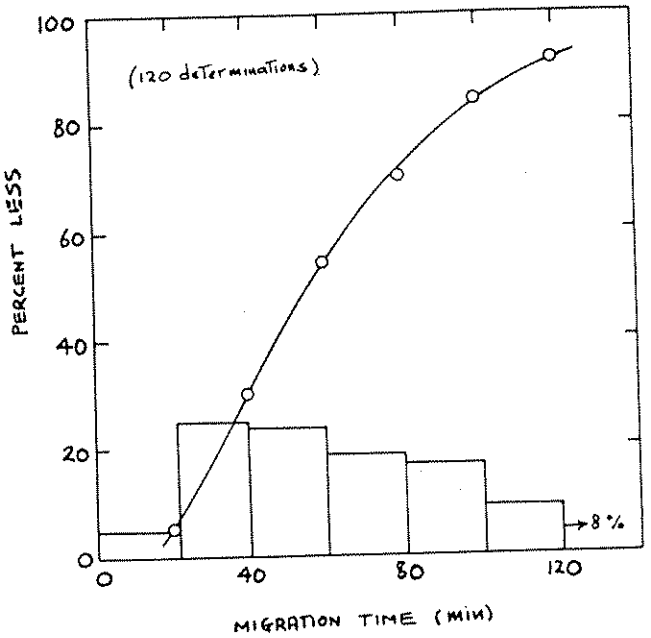

Figure 7.15 Histogram and cumulative curve of times for passage of two successive ripple crests past a fixed point, for 0.38 mm sand in a flow with mean flow depth 9.3 cm and mean flow velocity 29.2 cm/s. Data are from Southard et al. (1980).

given ripple exists for a distance of movement that's only a few ripple spacings; and (iii) ripples usually are born by division of one large ripple into two smaller ones, and usually die by becoming smaller and slower and then being overridden by a faster-moving ripple (on the average, deaths equal births). Despite all this variability, when considered as an aggregate the lines in the graph have a definite average slope, which is probably the best measure of U_B.

You should expect U_B to increase steeply with mean flow velocity U for a given sand, because bed-load transport rate increases steeply with flow strength (Chapter 6) and most of the bed load remains within individual ripples. The magnitude of this increase depends, however, on the concurrent change in ripple size, because the larger the ripple, the slower it moves for a given bed-load transport rate. The effect should therefore be most pronounced for current ripples, which vary little in size with flow conditions and sediment size. Systematic data on bed-form velocity as a function of flow strength and sediment size are surprisingly scarce, presumably owing to the difficulty of accurate measurement. Figure 7.17, a plot of U_B vs. U for three different sand sizes (Dillo, 1960), shows that U_B increases sharply with U for a given sand size, as expected. Note, however, that ripples in coarser sands move faster than ripples in finer

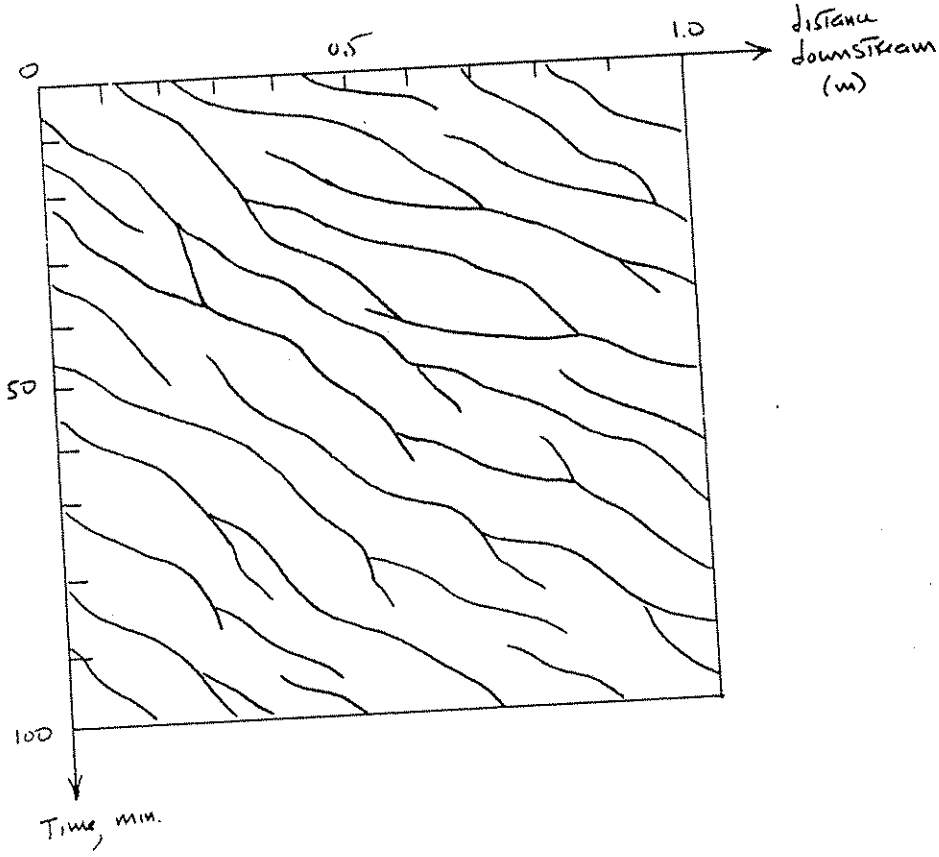

Figure 7.16 Positions of ripples in a space-time plot. The curves show positions of ripple crests as a function of time t and downstream position x. The flow is steady and uniform, and the bed state is unchanging on the average. (Schematic.)

sands. The reason for this seemingly anomalous behavior is unclear. There seem to be two possibilities: (i) the volume transport of sand as traction load in the accelerating flow over the stoss face of the ripple might be greater in coarser sand than in finer sand at a given mean flow velocity. (ii) The ripples in the coarser sand may have been smaller than in the finer sand, so that U_B is greater even though bed-load transport rate might have been smaller.

To the extent that the moving sediment is cycled within bed forms, the bed-load transport rate can be expressed in terms of the speed of movement of the bed forms. For ripples this is a good approximation, because bed-load transport rate is usually zero or nearly so at some point in the trough. Only if bed-load transport rate is nowhere zero over the bed-form profile, as is generally the case with antidunes, is this not true. To derive an expression for the bed-load transport rate associated with bed-form movements, consider a train of identical bed forms in which bed-load transport rate is zero in the troughs (Figure 7.18). The ripples have cross-sectional area A and

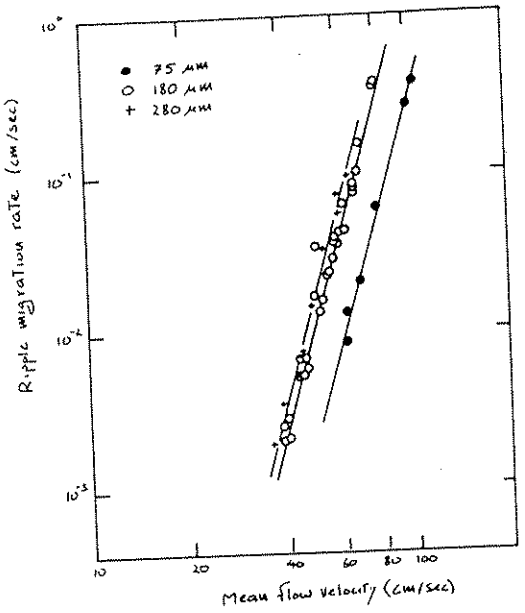

Figure 7.17 Plot of U_B against U for equilibrium current ripples in uniform flow, for three different sand sizes. Data are from Dillo (1960).

spacing (i.e., repeat distance of cross-section geometry) L. The time needed for passage of a bed form past a given point is T_r. The rate q_f, expressed per unit width normal to the flow, at which volume of sediment is moved downstream by bed-load transport within the ripples (remember that this involves stripping of sediment from the stoss surface, dumping at the crest, and slumping down the lee surface) is the same as the rate of downstream shift of the ripple cross section, except for a correction factor discussed below. A good way of thinking about this is to consider that the entire cross-sectional area of the ripple passes a given point on the bed in time $T_r = L/U_B$, so the average rate of passage of cross-sectional area past the point during this time is A/T_r, or, eliminating T_r, AU_B/L. So

$$q_f = K_1 \frac{AU_B}{L} \tag{7.12}$$

For a more elegant derivation of this result, see Simons et al. (1965).

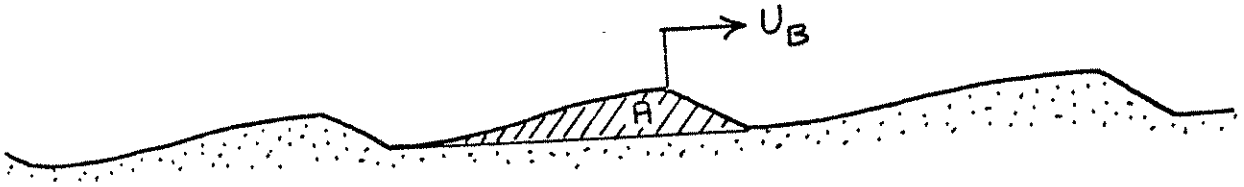

Figure 7.18 Definition sketch for derivation of a relation for bed-form transport rate.

The correction factor K_1 is needed because the transport rate is expressed as solids volume whereas bed volume is expressed as bulk volume, solids plus void space. It's easy to derive a relationship between solids volume V_s and bulk volume V_b in a sediment sample. Since voids volume and solids volume add up to total volume in a sediment, $V_v + V_s = V_b$, where V_v is voids volume. Also, the porosity λ is defined as $\lambda = V_v/V_b$. Combining these two equations to eliminate V_v gives the relationship between solids volume and bulk volume:

$$V_b = \frac{1}{1-\lambda} V_s \tag{7.13}$$

Since λ in equant and fairly well sorted sediments is on the order of 0.2-0.4, depending on both sorting and packing, the porosity correction factor $1/(1-\lambda)$ is always positive and a little larger than one. Using Equation (7.13), Equation (7.12) becomes

$$q_f = \frac{1}{1-\lambda} \frac{AU_B}{L} \tag{7.14}$$

In the rest of this chapter $1/(1-\lambda)$ will be written K_1 for convenience. If the bed forms have the shape of end-to-end triangles with height H, then $A = HL/2$ and Equation (7.14) becomes

$$q_f = K_1 \frac{HU_B}{2} \tag{7.15}$$

Rubin and Hunter (1982) proposed that q_f be called the bed-form transport rate and that the remainder of the bed-load transport rate, the part that bypasses the bed forms rather than being cycled within the same bed form, be called the throughgoing transport rate.

We've said that the bed-load transport rate (call it q_{sb}) is greatest at the crests of ripples. An expression for q_{sb} at a ripple crest can be derived on the assumption that all the bed load arriving at the crest is dumped there to slump down the lee face and build it forward (Figure 7.19). The slip-face angle is α and the horizontal distance of slip-face outbuilding is ζ. As before, ripple velocity is U_B and ripple height is H. The principle is that q_{sb} at the crest is equal to the time rate of addition of bulk sediment volume on the slip face. Since the increment in volume of the slip-face deposit is just the thickness of the slip-face deposit, $\zeta \sin\alpha$, times the length down the slip face, $H/\sin\alpha$,

$$q_{sb} = K_1 \frac{d}{dt}\left[(\zeta \sin\alpha)\ \frac{H}{\sin\alpha}\right] = K_1 \frac{d(\zeta H)}{dt} = K_1 H \frac{d\zeta}{dt} = K_1 H U_B \qquad (7.16)$$

By comparison of Equations (7.15) and (7.16) we have the neat result that, for ripples with triangular cross-section, bed-load transport at the crests is exactly twice the average value. This result seems first to have been derived by Bagnold (1941).

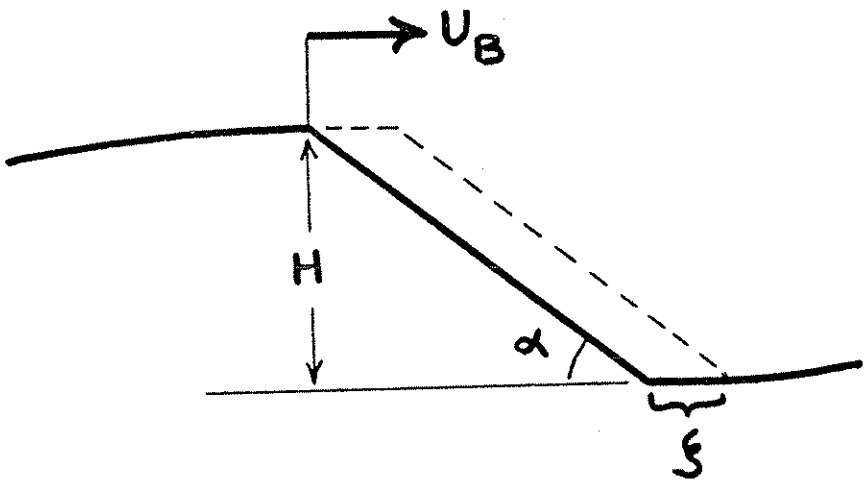

Figure 7.19 Definition sketch for derivation of a relation for bed-load transport rate at the crest of a ripple.

HYDRAULIC RELATIONS OF BED STATES

Introduction

A loose but useful analogy can be drawn between different patterns of flow around blunt bodies and kinds of bed geometries developed by flow over loose sediment beds. We saw in Chapters 2 and 4 that depending on a single dimensionless variable--the Reynolds number based on free-stream velocity and sphere diameter--there is a definite succession of qualitatively different flow patterns in flow past a sphere. Similarly, the exploratory experiment on bed configurations described in an earlier section indicates that as flow conditions change there is a succession of qualitatively different kinds of bed states, or bed phases. As in flow past a sphere, transitions between successive bed phases may be either abrupt or gradual.

It should seem natural to you at this point to make a dimensional analysis of bed states with a view toward developing a suitable set of dimensionless variables by which observations on equilibrium bed states in flumes or in natural flows can be represented. This systematizes and unifies disparate data on bed forms generated under a wide variety of flow and sediment conditions. Once the dimensionless variables that characterize the bed state are known, graphs can be plotted with these variables along the axes. A graph like this, which we'll call a bed-phase diagram, shows the ranges of existence, or the stability relations, of the various bed phases. They are analogous to the phase diagrams used by petrologists to represent the stability relations of mineral phases. We'll be able to draw graphs like this only for equilibrium bed states in steady uniform flows, but they serve as a reference for interpreting the more complicated cases, common in natural environments, of disequilibrium bed states in which changes in the bed geometry lag behind changes in the flow.

Important Variables

With the exploratory experiment described in an earlier section as a guide to the bed phases that must be taken into account, and with Chapters 4, 5, and 6 as a guide to the physical effects that might be important in flow and sediment transport over bed forms, we'll develop here a tentative list of the variables important for bed states. We assume as usual that the flow is steady and uniform, and also that the bed configuration is in equilibrium with the flow. If possible, some further simplication would be desirable at the outset in order to keep the list of variables workably short. If either an infinitely wide channel or an invariable channel cross-section shape is assumed, neither channel width nor anything about cross-sectional geometry is needed as a variable. We also assume that sediment texture is adequately taken into account solely by mean size; sorting and grain shape are in fact also important, but they will be assumed

here to be less important than mean size. To the extent that these last two simplifications are not grossly unrealistic, use of data from flows with varying channel cross-section shape and with sediment with varying sorting and grain shape shouldn't introduce great scatter in dimensionless plots of data on bed states.

Variables important in determining the bed state are those that characterize the flow, the sediment, and the fluid. As in many cases we've considered already in these notes, the fluid properties density ρ and viscosity μ must be included because of their effect on fluid forces both on the individual grains and on the bed forms themselves. Mean or median sediment size D must be included because of its effect on particle weight and therefore on the entrainment and settling properties of the grains, and also because it affects the roughness characteristics of the flow. Sediment density ρ_s is needed not only because it determines (together with ρ and g) the submerged weight per unit volume of the sediment, but also because it governs the inertial forces engendered by accelerations of sediment particles. The acceleration of gravity g must be included separately from its effect on submerged weight per unit volume because of its role in surface gravity waves. The three variables ρ, ρ_s, and g therefore all have to appear separately. This would be true even if there were no free surface, except that then it would be more natural to use γ_s, the weight per unit volume of the sediment, than g explicitly.

That leaves only variables that characterize the flow. One of these must express the scale of the flow normal to the bed; that one is most naturally the flow depth. You saw in Chapter 5 that the depth is needed for full characterization of the profile of the time-average velocity, which is one aspect of flow structure, although the velocity profile is independent of the depth in the inner region of the flow, near the bed. Similarly, it's clear from Chapter 6 that near-bed sediment transport over a planar bed is independent of the depth, but that other things about sediment transport, like the vertical distribution of suspended load, do depend on the depth. If flow structure and sediment transport depend in part on the depth, then it's reasonable to expect that the same is true of the bed configuration, so we should include flow depth in the list. We'll see presently that some things about bed configurations are depth-independent but others are not. The other flow variable must be a measure of flow strength, like mean velocity or bed shear stress. Only one of these two is needed, because if one is known the other can be found, provided that the flow depth, the nature of the grain roughness on the bed, and the fluid properties ρ and μ are specified; see the section on flow resistance in Chapter 5, and Equation (5.1) in particular. Flow and sediment transport are much more sensitive to changes to flow strength than to changes in flow depth, even when depth is important.

Mean flow velocity and boundary shear stress are equivalent ways of describing the strength of a flow of a given fluid at a

given flow depth over a bed with fixed roughness, because they are related through the frictional resistance characteristics of the flow, as expressed in a relationship like Equation (5.1). Therefore, since to specify the flow we must specify flow depth as well as one of the flow-strength variables, τ_o is determined if U and d are specified, and U is determined if τ_o and d are specified. But this statement is predicated upon a fixed bed roughness. If the flow is free to mold its bed into bed forms, there is a substantial reason for preferring U over τ_o as a measure of flow strength, as discussed in the following.

Suppose we set up a series of flows with increasing U but constant d over a loose sediment bed, as in the exploratory experiment on bed configurations in an earlier section. We would find that τ_o is not a monotonically increasing function of U. Bed configurations develop with increasing U in such a way that τ_o at first increases with increasing U in the sequence from small ripples through large ripples, then decreases in the transition to a plane bed, and then increases again. The reason for this is the greater flow resistance over ripples or dunes than over a planar bed at a given d and U, due to the much greater form drag involved in separated flow over the bed forms. Therefore, although to each U there corresponds one and only one τ_o, the converse is not always true: for a certain range of τ_o there is more than one value of U for a given τ_o (Figure 7.20; Brooks, 1958; Kennedy and Brooks, 1963). The troublesome consequence in representing data on bed states is that in plots involving τ_o there can be substantial overlapping of points for different bed phases in a certain range of τ_o simply because more than one bed phase can be associated with the same value of τ_o. Plots involving U, on the other hand, do not suffer from this effect. It therefore seems preferable to use U rather than τ_o in dimensional analysis of bed states.

Some discussion of independence of variables is relevant here. In the foregoing discussion we've purposely avoided use of the adjective "independent." In making a choice of important variables, three matters can be addressed: (i) Which variables characterize the bed state, in the sense that specification of those variables unambiguously identifies or corresponds to the state of sediment transport, whether those variables are imposed upon the system or are themselves fixed by the operation of the system? (ii) Which variables are truly independent, in the sense that they are imposed upon the flow system and are unaffected by its operation? (iii) Which variables govern the bed state, in the sense that they are mechanically directly responsible for sediment transport and bed configurations, whether or not they are independent?

Our goal in this section is to show as clearly and unambiguously as possible the hydraulic relationships among the various bed phases. If a one-to-one correspondence between bed states and combinations of variables is achieved, we then have a predictive capability, in that if we specify the nature of flow,

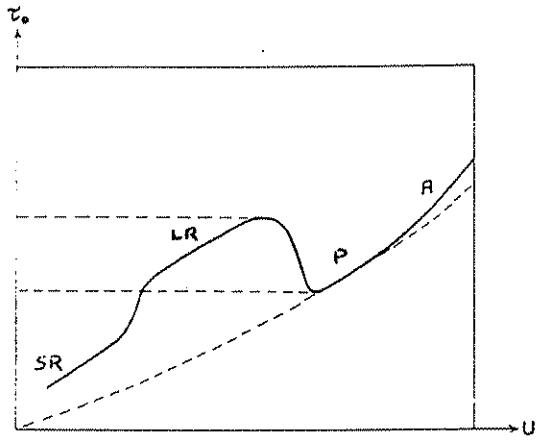

Figure 7.20 Schematic relationship between mean flow velocity U and boundary shear stress τ_o for a series of equilibrium uniform flows over a full sediment bed at constant mean flow depth. In the range of τ_o falling within the horizontal dashed lines, three values of U are possible for any given τ_o. The dashed curve represents the relationship between τ_o and U for the same succession of flows but over a rigid plane bed with sand-grain roughness of the same diameter as the loose sediment. Letters designate bed phases associated with the various segments of the curve: SR, small ripples; LR, large ripples; P, plane bed; A, antidunes.

the sediment, and the fluid, we can be confident that the graphs predict the bed state that would result. Unambiguous characterization is the most important consideration here. In this respect, U is better than τ_o as a flow-strength variable because of the ambiguity discussed above.

Independence need not be a criterion in our choice of variables, because a given set of variables can equally well describe the bed state whether any given variable in the set is dependent or independent. The bed state is a function of the nature of the flow but not of how it is arranged or established. Independence of variables depends to a great extent on the nature of the sediment-transporting system. For example, in an extremely long channel (many kilometers, say) carrying a steady uniform flow, even though the flow might prefer a different slope for a given discharge, the slope adjusts so slowly that it can be considered fixed. Discharge and slope are therefore independent variables, and U and d are dependent upon them. In a similar but much shorter channel (a laboratory flume, say) the slope can change so rapidly by erosion and deposition along the channel that the flow cannot be considered uniform until the slope has reached a state of adjustment to the imposed discharge; discharge is an

independent variable, but slope is now dependent, in the sense that it cannot be preselected except approximately by adjusting the flow depth. In constant-volume recirculating flumes, both discharge and depth are independent and slope is dependent. In terms of prediction, we lose nothing by choice of U and d whether or not they are independent variables in a given kind of flow system.

With regard to governing variables, it might seem better to use τ_o for the reason that it represents the actual force on the boundary, which is what moves the sediment in the first place. In fact, however, on beds with large roughness elements like bed forms only a small part of τ_o represents the skin friction directly responsible for sediment transport, the rest being the form drag on the roughness elements. So use of τ_o does not bring us much closer to the actual dynamics of the bed configurations. Both U and τ_o are surrogate variables, in the sense that they are not directly responsible for particle transport and bed-configuration dynamics, as are near-bed flow structure and the distribution of skin friction. Both U and τ_o are merely ways of parameterizing these complicated effects for the purpose of empirical characterization. Another disadvantage of using τ_o is that errors in measurement are much greater than for U, with correspondingly greater scatter in bed-phase stability plots.

Another flow-strength variable in common use is flow power (or stream power) per unit bed area, P; this represents the rate at which the flow does work on a unit area of the boundary. For a steady uniform flow, flow power is simply the product of mean velocity and boundary shear stress, $\tau_o U$. Although as we've already seen in Chapter 5 it is in some ways illuminating to view the flow in terms of rate of energy expenditure rather than directly in terms of forces and motions, flow power embodies nothing new, because like any expression for mechanical energy it is nothing more than a function of the forces and motions. At least with regard to bed configurations, flow power provides no better a framework for representing stability relations than either U or τ_o. And because τ_o is involved, flow power also suffers from the multiple-valued behavior discussed above.

Dimensionless Depth-Velocity-Size Diagram

We now have the following list of variables that should characterize the bed state:

d	mean flow depth
U	mean flow velocity
D	mean or median sediment size
ρ_s	sediment density
ρ	fluid density
μ	fluid viscosity
g	acceleration of gravity

Dimensional analysis provides a set of four equivalent dimensionless variables. One set (Southard, 1971) has the sedimentologically most meaningful variables--depth, velocity, and sediment size--separated into dimensionless variables that could be viewed as dimensionless depth, dimensionless velocity, and dimensionless sediment size, denoted here by d^o, U^o, and D^o, respectively:

$$\left(\frac{\rho^2 g}{\mu^2}\right)^{1/3} d, \left(\frac{\rho}{\mu g}\right)^{1/3} U, \left(\frac{\rho^2 g}{\mu^2}\right)^{1/3} D, \frac{\rho_s}{\rho}$$

The third of these is a form of the Yalin parameter introduced in Chapter 6. A different but equivalent set, which has the advantage of being more directly related to the physics of the flow, contains the Reynolds number $\rho Ud/\mu$, the Froude number $U/(gd)^{1/2}$, the relative roughness d/D, and again the density ratio ρ_s/ρ.

Data on bed states for all combinations of fluid, sediment, and gravity are plotted most naturally in a series of three-dimensional graphs, one for each value of ρ_s/ρ. Each graph is filled exhaustively and mutually exclusively with stability regions for the various bed phases. Boundaries between bed phases are either well defined surfaces or transitional zones. One of these graphs includes the important case of quartz-density sand in water. This particular graph will be called the dimensionless depth-velocity-size diagram in the rest of this chapter. Keep in mind, however, that there's one of these graphs for every density ratio. The only other density ratio for which much is known about bed configurations is that of quartz-density sand in air. (For eolian bed configurations the variable that desribes the vertical scale of the flow might be wind-tunnel height. In the atmosphere, however, the surface mixed layer is usually so thick relative to bed-form height and the mean-flow Reynolds number is so large that flow depth is not an important variable. The vertical density structure of the atmosphere is a further complicating factor that's usually not present in liquid flows--except perhaps in turbidity currents.) Of the variables ρ, μ, and g that enter into each of the four dimensionless variables d^o, U^o, D^o, and ρ_s/ρ, ρ and g are very nearly constant for all flows of water at the Earth's surface. The same cannot be said, however, about μ. One of the many remarkable properties of water is that its viscosity varies unusually strongly with temperature. Over the range of natural water temperatures, say from 0°C to 30°C, μ varies by a factor of about 2.2. This corresponds to a variation by a factor of about 1.7 for d^o and D^o and by a factor of about 1.3 for U^o. A graph using just the dimensional variables d, U, and D should therefore be expected to show considerable scatter if the data cover a range of water temperatures.

Since it's difficult for the mind to attach much significance to values of d^o, U^o, and D^o, in presenting and discussing sections through the dimensionless depth-velocity-size diagram below we've chosen to convert the dimensionless variables to values of d, U, and D corresponding to a reference water temperature of 10°C. That allows you to get some concrete idea of flow and sediment conditions. But remember that if such graphs are to be used for other water temperatures some recomputation is needed. For example, for flow depth,

$$d^o = d_T\left(\frac{\rho_T^{\,2} g}{\mu_T^{\,2}}\right)^{1/3} = d_{10}\left(\frac{\rho_{10}^{\,2} g}{\mu_{10}^{\,2}}\right)^{1/3}$$

where the subscript T denotes the value at the desired temperature and the subscript 10 denotes values at a temperature of 10°C. Solving this equation for d_T, assuming g to be constant, and using values for μ_{10} and ρ_{10} in cgs units,

$$d_T = d_{10}\left(\frac{\rho_{10}/\rho_T}{\mu_{10}/\mu_T}\right)^{2/3} = 18.02\ d_{10}\left(\frac{\mu_T}{\rho_T}\right)^{2/3} \qquad (7.17)$$

This equation gives you the depth in centimeters at a given water temperature that is equivalent to the depth in centimeters at 10°C. The depths are equivalent in the sense that both flows have the same dimensionless depth. The numerical constant is not dimensionless, and would have to be changed if you work with a different system of units. The corresponding equations for flow velocity and sediment size are

$$U_T = U_{10}\left(\frac{\rho_{10}/\rho_T}{\mu_{10}/\mu_T}\right)^{1/3} = 4.24\ U_{10}\left(\frac{\mu_T}{\rho_T}\right)^{1/3} \qquad (7.18)$$

$$D_T = D_{10}\left(\frac{\rho_{10}/\rho_T}{\mu_{10}/\mu_T}\right)^{2/3} = 18.02\ D_{10}\left(\frac{\rho_T}{\mu_T}\right)^{2/3} \qquad (7.19)$$

Equations (7.17), (7.18), and (7.19) help you to plot a given data point for some water temperature T onto the 10°-standardized dimensionless depth-velocity-size diagram, and also to convert points on that diagram to some water temperature of interest to you.

Two kinds of section through the dimensionless depth-velocity-size diagram are most useful for visualizing relationships among bed phases: depth-velocity diagrams for a given sediment size, and size-velocity diagrams for a given flow depth. The former arise naturally from flume work, because usually a large number of runs with various depths and velocities are made for a given sand size.

Three depth-velocity diagrams are shown in Figure 7.21 and three velocity-size diagrams are shown in Figure 7.22. These are representative selections from a much larger number being compiled by one of the writers in an unfinished synthesis of all flume studies on equilibrium bed configurations in which the bed geometry is described and the water temperature is reported. They include much more data than earlier versions of the same diagram shown in the earlier edition of these notes (Middleton and Southard, 1977) and by Harms et al. (1975, 1982), so the phase boundaries are better defined and more trustworthy even though they're not drafted in smoothly. Figures 7.23 and 7.24 are cartoon versions of the same figures; they show no data points and the boundaries are somewhat schematic, but we hope they convey the relationships more clearly.

The first depth-velocity diagram (Figures 7.21A and 7.23A), for sands with mean size 0.10-0.14 mm, shows fields for only three phases: small ripples, upper-regime plane bed, and antidunes. The boundary representing the abrupt transition between ripples and upper plane bed is steeper than that representing the gradual transition from upper plane bed to antidunes. The latter boundary is shown extending downward to truncate the former. As flow velocity is increased over small ripples at shallow depths, surface gravity waves develop to be in phase with the ripples. The surface waves gradually become the dominant effect, and the bed forms move upstream as antidunes. The same effect is seen in the diagram for medium sand (Figures 7.21B and 7.23B). On the left are two boundaries, not shown, between movement and no movement. One is the Shields curve for beginning of grain movement on a plane bed, appropriately transformed onto this graph. The other, farther to the left, describes the minimum flow velocity needed to maintain equilibrium movement of preexisting small ripples.

The next depth-velocity diagram (Figures 7.21B and 7.23B), for 0.50-0.64 mm sand, shows an additional field for large ripples, with a lower-velocity boundary that slopes more steeply than the higher-velocity boundary. As flow depths become very shallow it is increasingly difficult to differentiate between small ripples and large ripples. Truncation of the large-ripple field by antidunes is clear. Again there are two kinds of boundary between movement and no movement, not shown. This graph pertains to the exploratory flume experiment described earlier.

In the last depth-velocity diagram (Figures 7.21C and 7.23C), for 1.3-1.8 mm sand, a lower-regime plane-bed phase replaces

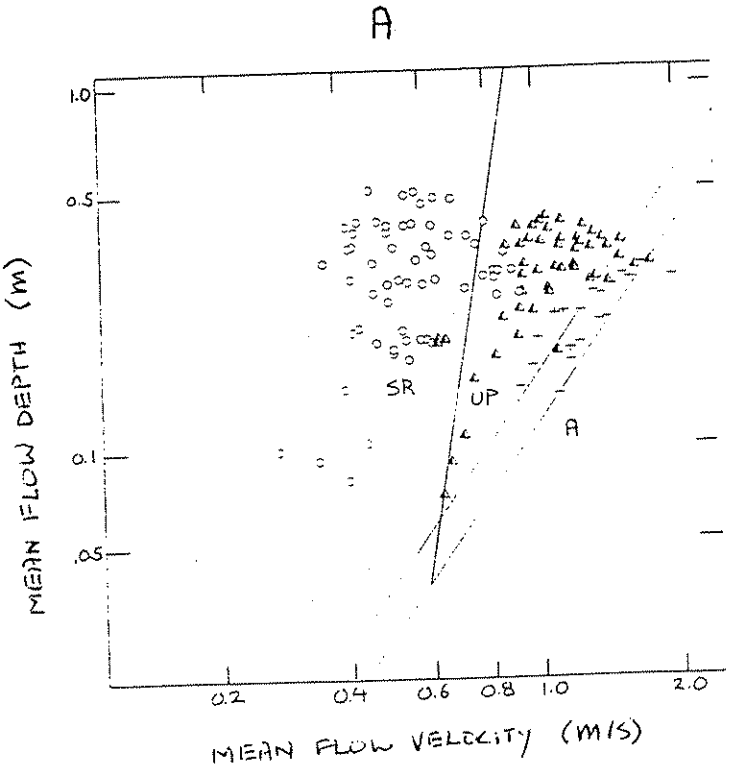

Figure 7.21 Three depth-velocity sections through the dimensionless depth-velocity-size diagram for stability fields of equilibrium bed phases developed in steady uniform flow of water over quartz-density sediment (ρ_s/ρ = 2.65). Flow depth and flow velocity are standardized to 10°C water temperature, as explained in the text. (A) (above) 0.10-0.14 mm sediment; (B) (opposite page) 0.50-0.64 mm sediment; (C) (opposite page) 1.30-1.80 mm sediment. Explanation of symbols: open circles, small ripples (SR); solid circles, large ripples (LR); half-open circles, undifferentiated ripples; half-open triangles, upper plane bed (UP); plus signs, antidunes (A); open diamonds, lower plane bed (LP).

B

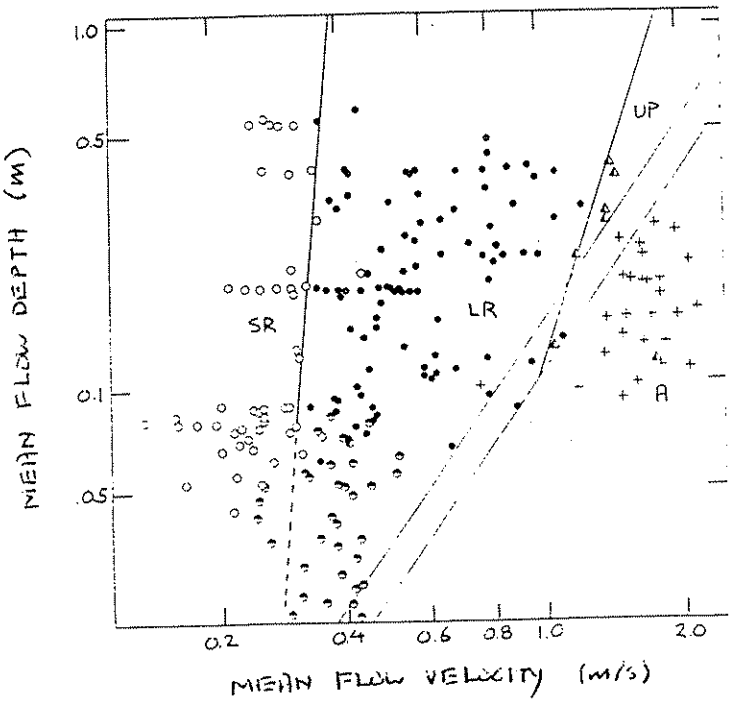
1.0
0.5
0.1
.05
MEAN FLOW DEPTH (M)
SR
LR
A
UP
0.2
0.4
0.6
0.8
1.0
2.0
MEAN FLOW VELOCITY (M/S)

C

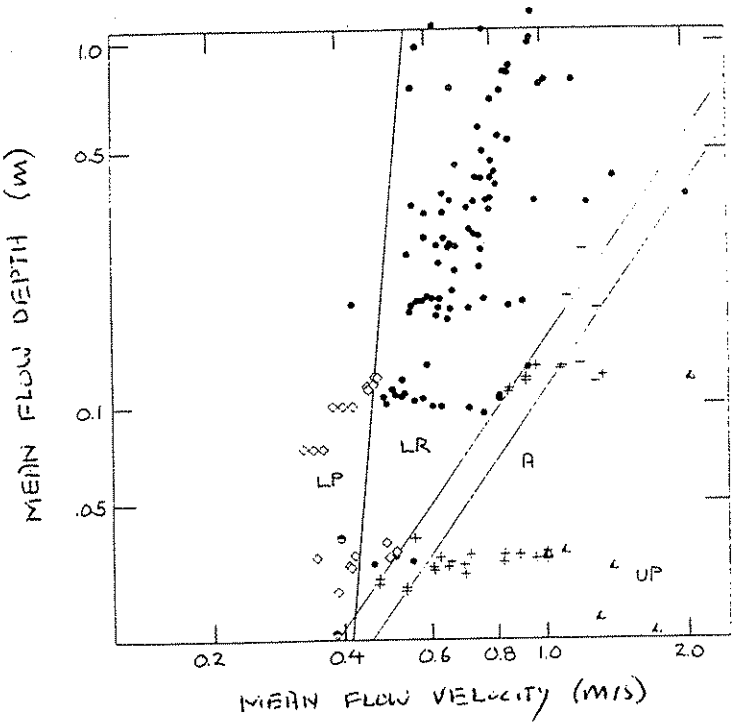
1.0
0.5
0.1
.05
MEAN FLOW DEPTH (M)
LP
LR
A
UP
0.2
0.4
0.6
0.8
1.0
2.0
MEAN FLOW VELOCITY (M/S)

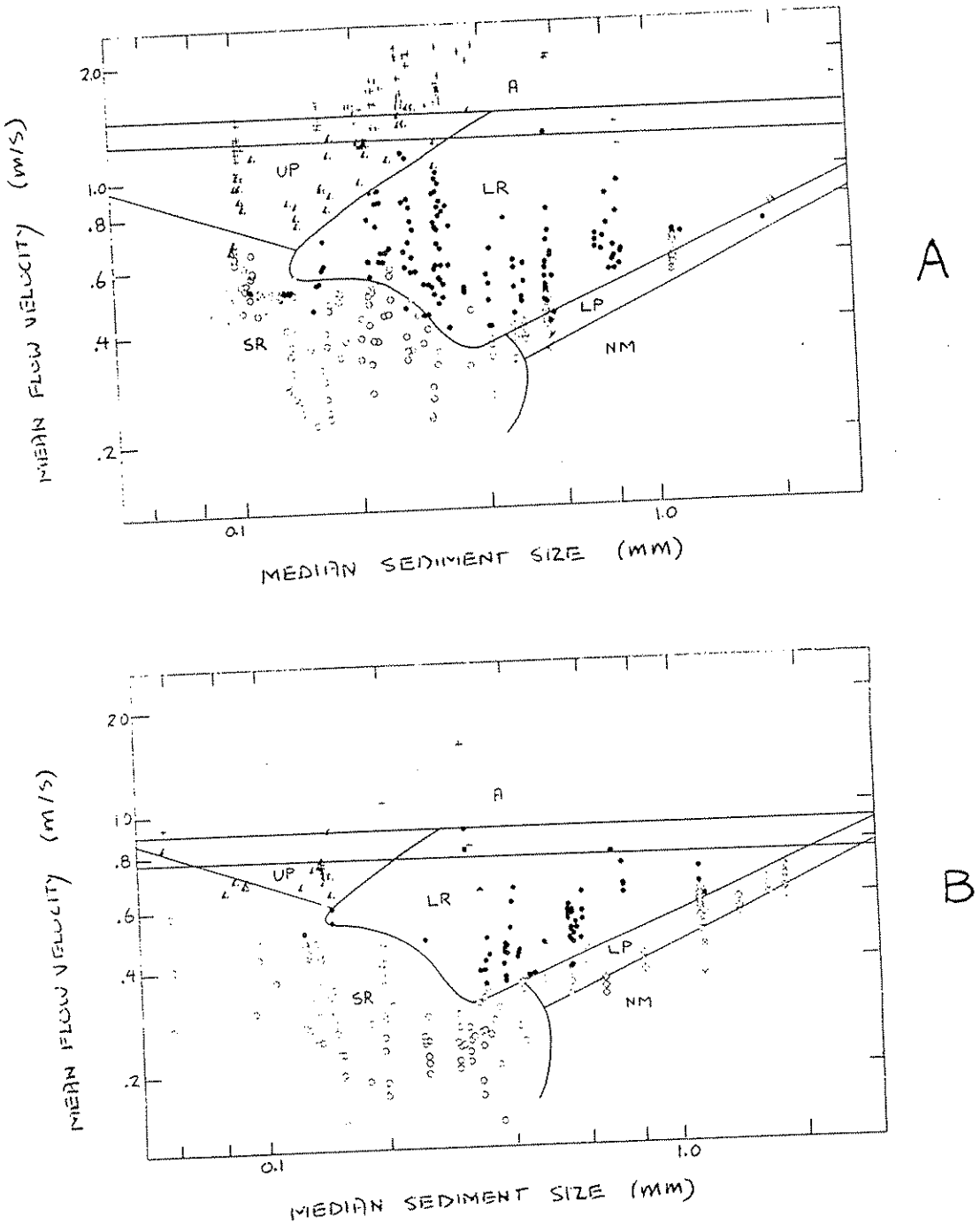

Figure 7.22 Two velocity-size sections through the dimensionless depth-velocity-size diagram for stability fields of equilibrium bed phases developed in steady uniform flow of water over quartz-density sediment ($\rho_s/\rho = 2.65$). Flow velocity and sediment size are standardized to 10°C water temperature, as explained in the text. (A) flow depth 0.16-0.25 m; (B) flow depth 0.06-0.10 m. Symbols: X marks, no movement on a plane bed; others as defined in Figure 7.21.

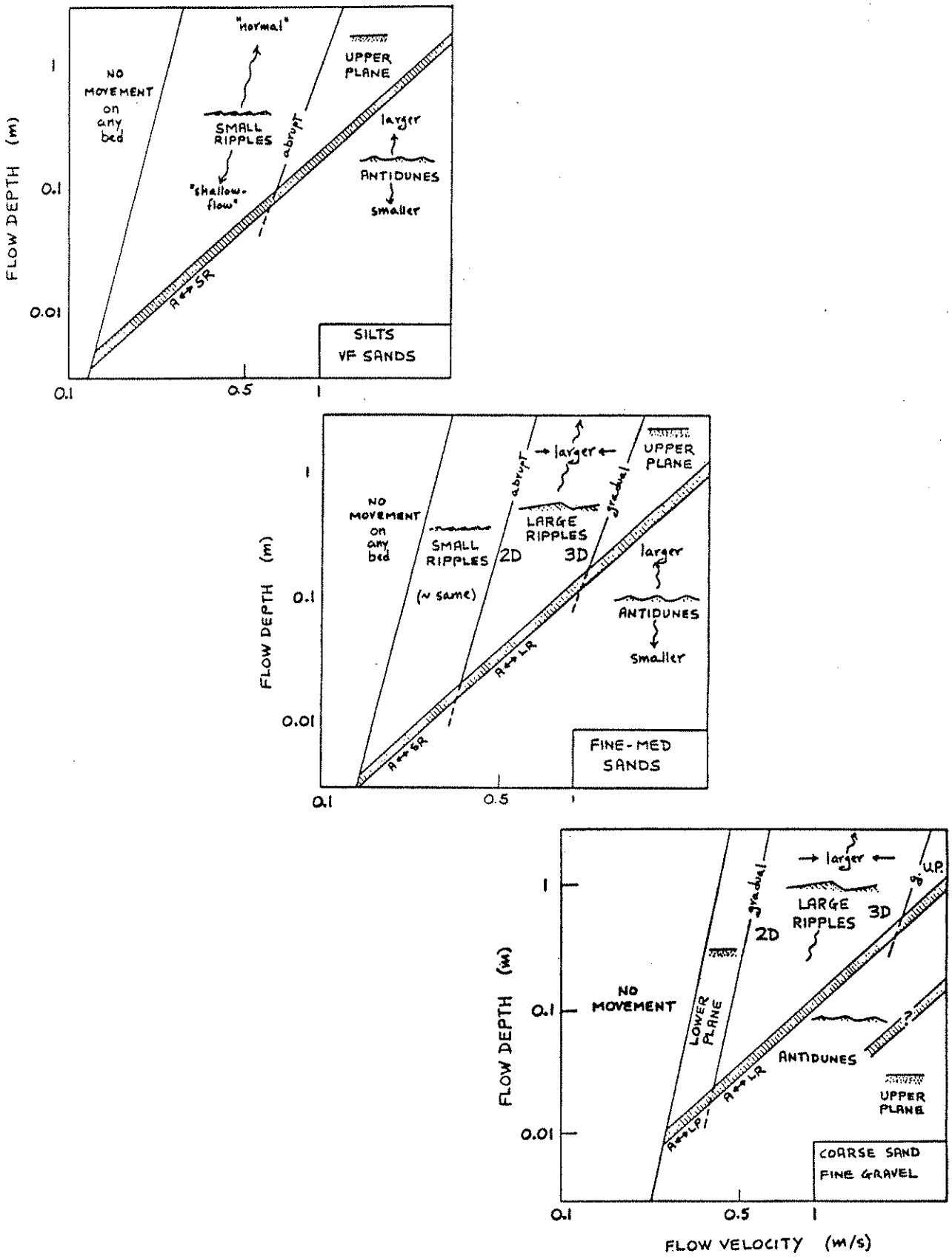

Fig. 23 Cartoon versions of the three depth-velocity sections in Figure 7.21.

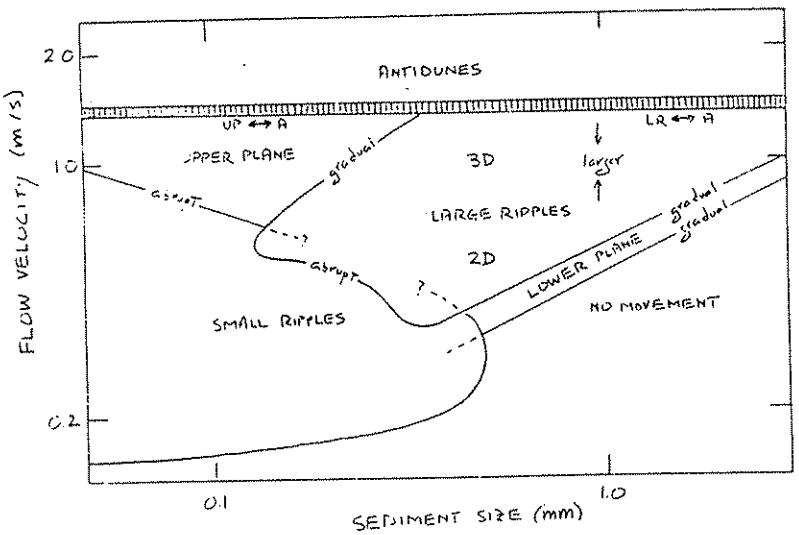

Figure 7.24 Cartoon version of the size-velocity section for a flow depth of 0.16-0.25 m in Figure 7.22.

small ripples at low flow velocities. Points for upper-regime plane bed would be present beyond the upper right corner of the graph if data at sufficiently high flow velocities were available. Upper-regime plane beds succeed antidune beds with increasing flow velocity and decreasing depth in the lower right corner of the graph; apparently the bed becomes planar once again as the Froude number becomes sufficiently greater than one. The boundary between no movement and lower-regime plane bed corresponds to the Shields criterion. The lower-regime plane bed involves much weaker grain movement than the upper-regime plane bed. With increasing flow velocity, low straight-crested large ripples gradually develop on the lower-regime plane bed.

The velocity-size sections (Figures 7.22 and 7.24) are better for visualizing the relationships among bed phases as a function of sediment size. These sections, for two narrow ranges of flow depth with abundant data, show the following features. Small ripples are stable over a wide range of sediment sizes finer than about 0.6 mm. The range of flow velocities for which small ripples are stable narrows with increasing sediment size; the small-ripple field terminates against fields for plane beds with or without movement. Relationships at the coarse-sediment end of the small-ripple field are difficult to study because in these sand sizes it takes a long time for the bed to adjust to an ultimately stable condition (Costello and Southard, 1981). In medium sands small ripples give way abruptly to large ripples with increasing flow velocity, but in sediment finer than this, small ripples give way (also abruptly) to upper-regime plane bed. Although not ideally well constrained, the boundary between small ripples and upper-regime plane bed clearly rises to higher

velocities with decreasing sediment size.

Large ripples are the stable phase over a wide range of flow velocities in sediments from medium sand size up to indefinitely coarse gravel sizes. Flow velocities for large ripples increase with increasing sediment size. In the finer sediment sizes, large ripples pass fairly slowly into upper-regime plane bed with increasing flow velocity. The boundary between large ripples and upper-regime plane bed slopes upward to higher flow velocities with increasing sediment size until truncated by the antidune boundary. Below the large-ripple field at sediment sizes greater than about 0.6 mm is a narrow field for lower-regime plane bed. The lower boundary of this field is given by the Shields curve. There is considerable scatter in this part of the diagram, for two reasons: (i) as we saw in Chapter 6, the threshold for sediment movement is not well defined, and (ii) with increasing flow velocity large ripples make their appearance as flat, low bed forms, and drawing the line between lower-regime plane bed and large ripples leaves room for individual judgment. The boundary for threshold of movement on a plane bed continues under the ripple field, although it's not shown. If the flow velocity is gradually decreased over preexisting ripples generated at higher flow velocities, stable small ripples can be maintained at flow velocities well below those for the threshold of grain movement on a plane bed.

At high flow velocities antidunes are the stable bed phase for all sediment sizes. The minimum velocity for antidunes depends on the flow depth. The two horizontal lines in the upper part of the graphs are for mean-flow Froude number of 0.84 and 1.0. (In Kennedy's (1963) analysis, a Froude number of 0.84 is the lowest for which antidunes should be stable.) This range of Froude numbers represents well the transition from low-Froude-number bed forms to antidunes. As the flow depth decreases, these lines of constant Froude number descend in the velocity-size sections. At flow depths even smaller than those for the sections in Figure 7.22 the antidune "curtain" descends so far that very little of the field for large ripples is unaffected. Conversely, in flows much deeper than in Figure 7.22 very high flow velocities are needed for antidunes to form.

The shape of the boundary between small ripples and large ripples in Figure 7.22 is noteworthy. There is a triple point among small ripples, large ripples, and upper-regime plane bed at a sediment size of about 0.2 mm (this size varies only slightly with flow depth) and a flow velocity that increases with increasing flow depth. From the location of the data points in this region it seems inescapable that the field for large ripples forms a beak pointing toward finer sizes and that the boundary between small ripples and upper-regime plane bed intersects this beak well above its almost horizontal lower boundary curve. It's tempting to speculate that the boundary between small ripples and upper-regime plane bed passes unaffected beneath the field for large ripples at this triple point to emerge at coarser sediment

sizes and flower flow velocities as the boundary between small ripples and lower-regime plane bed. There's some evidence in support of this: even by casual experiments in a very short channel it's easy to observe the transition from small ripples to upper-regime plane bed at flow velocities considerably greater than at the boundary between small ripples and large ripples, provided only that the channel is so short (less than about two meters) that the development of large ripples is suppressed. This speculation leads to another: that the stability fields for small ripples and large ripples are controlled by dynamically separate effects, and the particular position of the boundary between the two is the outcome of a contest for dominance between two competing effects.

You can see by comparing the two velocity-size diagrams for different depths in Figure 7.22 that all the boundaries rise with increasing flow depth, as you should expect from the slopes of the boundaries in the depth-velocity sections in Figure 7.21. But the boundaries don't rise at the same rate, so the shapes of the stability fields change noticeably with increasing flow depth, even for this very limited range of depths. This tells you that the different velocity-size sections can't be made to coincide merely by translating one section relative to another; this in turn means that three dimensions are needed to represent bed-phase stability fields. The long search for the perfect two-dimensional bed-phase graph is doomed to failure.

Flume data are so limited in flow depth that you could count on your fingers and toes the number of data points on one of these velocity-size sections for depths around a meter. The positions of these points are consistent with extrapolations of the boundaries shown on more densely populated sections like those in Figure 7.22, but they don't provide much guidance to where the boundaries go as depth increases by, say, an order of magnitude to 10 m. Rubin and McCulloch (1980) have synthesized their own data and those of others into the depth-velocity-size diagram shown in Figure 7.25. This graph extends from the range that's well constrained by flume data into the lesser-known greater depths characteristic of important natural flow environments. The left-hand vertical panel in Figure 7.25 is the same velocity-size diagram shown for flume data in Figure 7.22, and the horizontal panel is the depth-velocity diagram of Figure 7.21 for half-millimeter sand, extended to flow depths of some tens of meters. The right-hand vertical panel shows a velocity-size section for a flow depth of 20 m; the relationships are similar to those in Figure 7.22 except that, as expected, the field for large ripples is fatter and its boundaries are at higher flow velocities. Rubin and McCulloch schematically contoured the field for large ripples for ripple height H, with the following results: (i) for a given flow depth and flow velocity, H increases with sediment size; (ii) for a given sediment size and flow velocity, H increases with increasing flow depth; (iii) for a given flow depth and sediment size, H first increases and then decreases with increasing flow velocity.

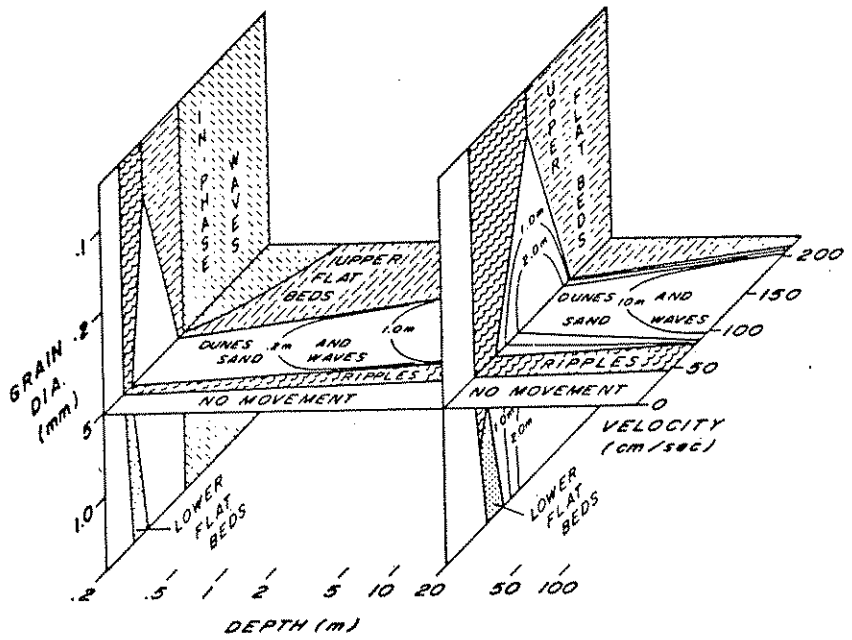

Figure 7.25 Schematic depth-velocity-size diagram showing stability fields for bed phases in steady unidirectional water flows with a wide range of flow depths in flumes and natural environments. From Rubin and McCulloch (1980).

Remember that boundary shear stress τ_o can be used in place of mean flow velocity U in representing bed-state data, although you should expect some overlap of ripple points and upper-regime-plane-bed and antidune points because of the multiple-value effect discussed earlier in this section. Figure 7.26 is a plot of bed-phase stability fields in a graph of Shields parameter against dimensionless sediment size from many sources of flume data (Allen, 1982). Since the Shields parameter contains both τ_o and D, this plot is skewed relative to one in which shear stress is nondimensionalized without use of D, but the relationships are qualitatively the same. (A good substitute dimensionless bed shear stress that doesn't contain D is $\tau_o/(\rho\mu^2 g^2)^{1/3}$ or, using $\gamma_s-\gamma$ in place of g, $\tau_o[\rho/(\gamma_s-\gamma)^2\mu^2]^{1/3}$.) Note the large region of overlap between the fields for large and small ripples, on the one hand, and for upper-regime plane bed and antidunes, on the other hand. This overlap isn't present between the fields for small ripples and large ripples, because τ_o is a monotonically increasing function of U there. Remember also that in a plot like this, just as in those in Figure 7.22, some dependence on dimensionless flow depth should be expected. Since the range of flow depths in flume work is so limited (most of the data fall in a range that spans much less than an order of magnitude in flow depth), a systematic section-by-section comparison would be needed to pin down the changes with depth.

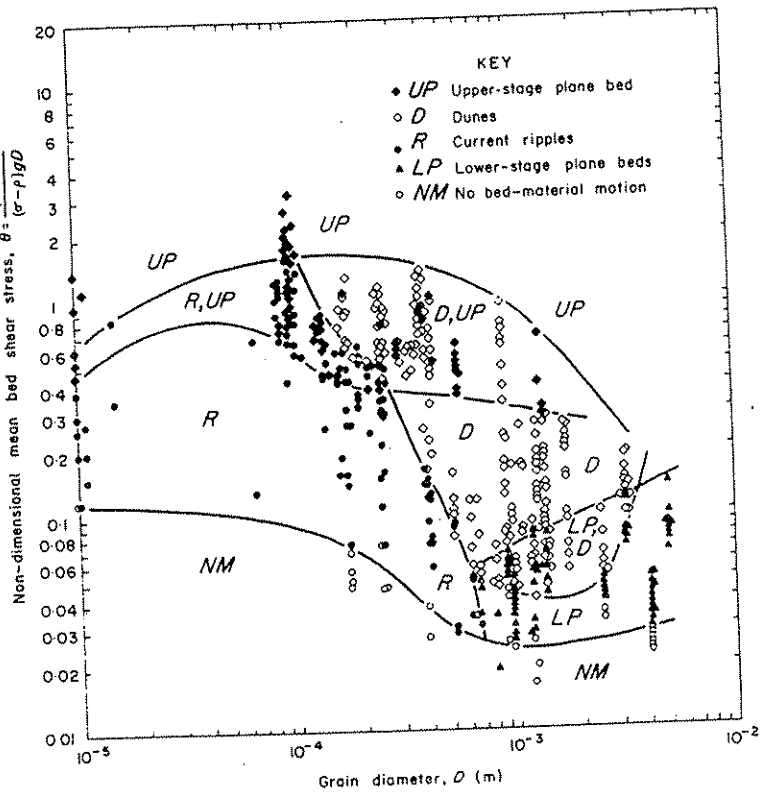

Figure 7.26 Stability fields for bed phases in steady unidirectional water flows, in a graph of Shields parameter against dimensionless sediment size (size standardized to 25°C water temperature). From Allen (1982, Vol. 1, p. 340).

Flow Regimes

This is the place to be more specific about the terms lower flow regime and upper flow regime we've used a few times already. Simons and Richardson (1963) proposed that bed phases be classified into a lower flow regime and an upper flow regime based on the transition from the rugged ripple-like bed phases (small ripples and large ripples, in our terminology) formed at relatively low flow strengths and the the less rugged bed phases (upper plane bed and antidunes) formed at high flow strengths (Figure 7-22A). The motivation for this classification was not so much the sharp distinction in bed geometry in itself as the great decrease in flow resistance in passing from the lower flow regime to the upper flow regime. Geologists have found the distinction useful not only in terms of the differing bed geometry but also in terms of the consequent great difference in sedimentary structures produced: with the minor exception of lower-regime plane beds, lower-regime conditions give rise to cross-stratified structures, whereas upper-regime conditions give rise mostly to planar lamination. (Antidunes can produce cross-stratification, but the lamination is usually obscure and the preservation potential is low; see, e.g., Middleton, 1965; Hand et al., 1969; Skipper, 1971.)

In terms of bed-configuration dynamics, it's also natural to divide bed phases into two groups in a different way based on the importance of a free surface (Figure 7.22B). Small ripples, large ripples, and plane bed are bed phases whose occurrence is independent of the existence of a free surface; recall that in the exploratory flume exeriments described earlier in this chapter the existence of ripples was not affected by placing a board over the water surface. These bed phases could therefore be termed free-surface-independent bed phases. Antidunes, on the other hand, are dependent upon the existence of a free surface, and could therefore be termed a free-surface-dependent bed phase.

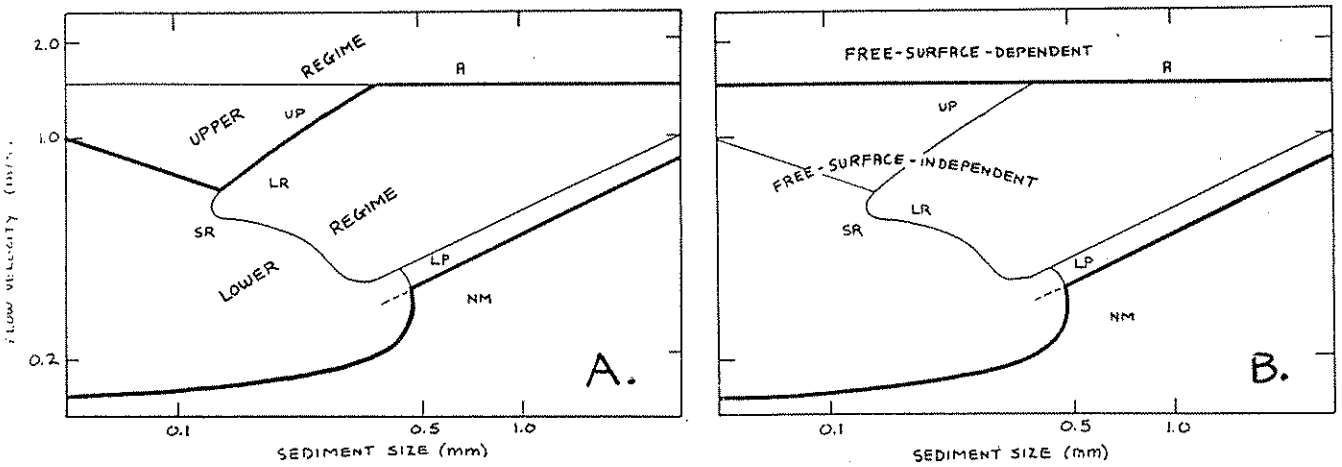

Figure 7.27 Two ways of classifying bed phases into flow regimes. A. Velocity-size diagram for a flow depth of about half a meter (see Figure 7.22) showing the customary division into an upper flow regime and a lower flow regime based on the transition from ripple bed phases (small ripples and large ripples) to upper plane bed or antidunes. B. The same velocity-size diagram showing an alternative division into a lower group of bed phases (lower plane bed, small ripples, large ripples, and upper plane bed) whose dynamics are independent of the existence of a free surface and an upper bed phase (antidunes) whose dynamics are dependent upon the existence of a free surface.

RIPPLES UNDER UNIDIRECTIONAL WATER FLOWS: PROBLEMS OF GEOMETRY AND CLASSIFICATION

Introduction

Ripples sensu lato vary widely in size, from centimeters to thousands of meters in spacing, and also substantially in plan pattern. Their unifying characteristics are orientation transverse to the flow, downstream movement, and asymmetry of profile. We're using the term ripple in a broad sense here for all bed forms with these characteristics. This usage is not widespread: most would restrict the term ripple to small-scale

features also called current ripples. But there's no generally accepted single term for the broad but readily distinguishable class of ripple-like features, and no other that's ripe for adoption or adaptation.

Of central importance in the classification of ripples is a universal break in scale between bed forms we've called small ripples and large ripples earlier in this chapter, following the usage of Harms et al. (1982). Ripples with spacings of half a meter, give or take a decimeter or two, are extremely uncommon except in two situations: in very shallow flows at velocities that would produce large ripples in deeper flows, and over a narrow transitional zone with confused bed geometries between small ripples and large ripples. This statement needs two qualifications: (i) as discussed in an earlier section, ripples associated with a given dimensionless bed state are larger in higher-viscosity fluids, and (ii) although data are scanty, the scales of all ripples are smaller for larger values of ρ_s/ρ. For given water temperature and ρ_s/ρ, however, the break between small ripples and large ripples is fundamental. It would be nice to have terms for the two kinds of ripples that are not so closely tied to size; it's awkward to have to talk about small large ripples and large large ripples. Microripples and megaripples would be nice, but the latter term is too firmly associated with a more specific meaning. This is not the place to try to erect new terminology anyway.

Both the classification and the general characteristics of ripples are closely bound up with dynamics. In this section we'll consider some aspects of both of these topics but stop short of a frontal assault on dynamics. A more systematic but still incomplete discussion of dynamics is reserved for the following section.

Small Ripples

Figures 7.21 and 7.23 show that, in flows of water-viscosity fluid over quartz-density sediment, small ripples are stable over a wide range of sediment sizes at low to moderate flow velocities. Toward coarser sizes the small-ripple stability field pinches out in the coarse sand range. Toward finer sizes the relationships are less well defined. Robust small ripples like those in sands have been studied in sediments with sizes down to 0.02 mm (standardized to 10°C water) by Jopling and Forbes (1979) and Mantz (1978, 1981), and tenuous ripples have been reported in sizes down to less than 0.01 mm by Kalinske and Hsia (1945) and Rees (1966). The inevitable increase in cohesion with decreasing size makes it unclear whether the absence of ripples in very fine sediment is a consequence of bed-form dynamics or is only a reflection of the unavailability of loose sediment to be moved as bed load. Grazer (1982) addressed this question in a model study of ripples in fine sediments by use of higher-viscosity fluid to decrease the effective size of the sediment without decreasing the actual size and therefore without introducing cohesion. Ripples not greatly different from those in coarser silts developed and persisted even in

noncohesive sediment with effectively 5 μm size, suggesting that it is cohesion rather than ripple dynamics that accounts for the absence of ripples in very fine sediments.

Since small ripples are easily studied in even small flumes, it would seem that data on their characteristics should be abundant. In fact, although small ripples have been observed and measured in innumerable flume runs, no definitive or unified picture of spacing, height, velocity, and plan geometry has emerged. There seem to be several reasons for this: (i) As noted in an earlier section, the ripples of a given bed state are so variable in their characteristics that tens or even hundreds must be measured to obtain reliable estimates of these characteristics. (ii) Measures of size and shape are open to varying definitions, so there is no certainty that what one investigator means by, say, ripple height or ripple spacing is the same as what another means. (iii) There can be a large element of subjectivity in the very recognition of a ripple. Along a streamwise bed profile of ripples, most local maxima represent well defined ripples, but there are always many lesser maxima that require some subjective judgment as to whether they qualify as official ripples. This uncertainty in the static profile is a manifestation of the short lifetimes of ripples; most ripples come into being and then disappear within a distance of movement of only a few ripple spacings. A snapshot always catches many in transition. (iv) Plan pattern depends on the width-to-depth ratio of the channel, and this varies greatly in flume work. Plan variability of ripples in a channel narrower than the average ripple spacing can never be great. As width-to-depth ratio increases, secondary circulations inherent in flow in walled channels at first accentuate the variability in plan pattern, but this effect becomes unimportant at width-to-depth ratios greater than something like 10.

Average spacing L of small ripples shows little variation over their entire range of existence. The relationship $L = 1000\ D$, derived by Yalin (1977) by assuming that L is independent of flow depth d and that the ratio L/D is only a weak function of the boundary Reynolds number u_*D/ν, is often cited. It seems unjustified, however, because it predicts, for example, that the spacing of ripples in 0.5 mm sand should be ten times that of ripples in 0.05 mm silt, which is clearly not the case, the spacings differing by much less than a factor of two with much scatter of the available data. For example, in the study by Jopling and Forbes (1979), with a 10° sediment size of 0.063 mm, the 10° average spacing in nine small-ripple runs over a wide range of flow velocities was 18.5 cm, whereas in the study by Guy et al. (1966), with a 10° sediment size of 0.45 mm, the 10° average spacing in nine small-ripple runs over a wide range of flow velocities was 26.0 cm. Ripple size thus increases by a factor of only 1.4 for an increase in sediment size by a factor of more than 7--a very weak dependence. A unified plot of dimensionless ripple spacing $L(\rho^2 g/\mu^2)^{1/3}$ against dimensionless depth, velocity, and sediment size has yet to be made, but it seems clear that dimensionless spacing would not differ greatly over most of the phase vol-

ume occupied by small ripples in the dimensionless depth-velocity-size diagram. This remarkable circumstance indicates that L, when expressed in dimensionless form, is independent not only of flow depth but also flow velocity and sediment size. The dynamical controls on ripple spacing, whatever they are, are almost unchanged over a wide range of flow and sediment conditions.

Remember that the unscaled size of ripples depends on the water temperature, because of the effect of viscosity. Look at the change in ripple size that you'd see if, for a given flow over a given sediment bed, you changed only the water temperature but kept the flow depth and flow velocity the same. You thereby change the dimensionless depth, velocity, and sediment size and move to a different point in the dimensionless depth-velocity-size diagram. Assume that this change keeps you in the ripple stability field. Since dimensionless height H^o and spacing L^o of ripples are almost constant throughout most of the small-ripple stability field,

$$L^o = \text{const}_1 = L\left(\frac{\rho^2 g}{\mu^2}\right)^{1/3}$$

$$H^o = \text{const}_2 = H\left(\frac{\rho^2 g}{\mu^2}\right)^{1/3}$$

So L and H are approximately proportional to the two-thirds power of μ/ρ. Using the approximate values for μ and ρ for water, you can check for yourself that the size of small ripples should therefore decrease by a factor of about 1.5 from 0°C to 20°C.

There seems to have been almost no systematic consideration of the effect of density ratio ρ_s/ρ on the characteristics of ripples--or on their existence, for that matter. The concentration of effort on quartz-density sand in water and air is understandable from the standpoint of sedimentology, but it's shortsighted from the standpoint of understanding the fundamental dynamics of bed forms. How can one expect to understand a phenomenon fully when one observes it through two narrow windows spaced far apart? The few measurements of bed-form characteristics that have been made for ρ_s/ρ substantially different from 2.65 suggest that small ripples are larger for $\rho_s/\rho < 2.65$ (Bagnold, 1955) and smaller for $\rho_s/\rho > 2.65$ (Brady and Jobson, 1973). The gap in ρ_s/ρ between sand in air and sand in water is large (Figure 7.28). It's not clear whether eolian ripples are dynamically related to subaqueous small ripples, in the sense that the two could be traced continuously from one to the other in the full four-dimensional phase diagram (appropriately modifed for, say, flow in a closed duct to take account of the different flow geometries in wind and open-channel flow). In experiments with styrofoam beads in a wind tunnel (for which ρ_s/ρ is about the same as mineral-

density sand in the Venusian atmosphere) Southard et al. (1982) found a total absence of small-scale ripples. Since that value of ρ_s/ρ is intermediate between those for sand in water and for sand in air, this result suggests that eolian ripples are not the same phenomenon as small ripples in water.

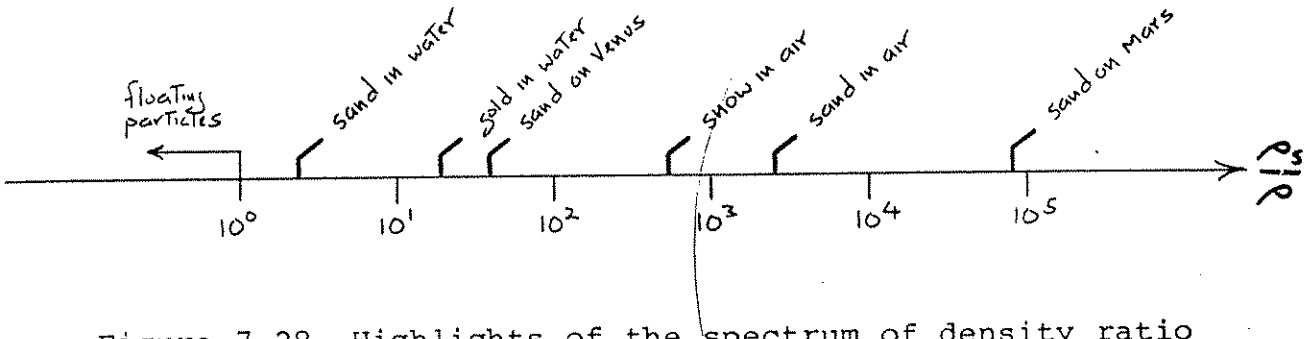

Figure 7.28 Highlights of the spectrum of density ratio ρ_s/ρ

When fully developed, small ripples are always less than ideally two-dimensional crests and troughs vary substantially in elevation in the cross-stream direction, and in plan view crests do not extend far in the cross-stream direction before dying out or joining with another. Small ripples initially develop two-dimensionally from a planar bed, however, if their loci of development are arranged beforehand to be regular: all that's needed is an initial series of straight and uniform cross-stream grooves or ridges. Irregularities in the regular two-dimensional pattern eventually develop at certain points and then grow and spread rapidly downstream. A possible clue to the nature of the instability of the initial two-dimensional pattern is the observation that the configuration becomes three-dimensional only where the bed is thick enough that troughs are mostly floored with movable sediment. If the mean thickness of the sediment bed in a flume is so thin that troughs are everywhere underlain by a rigid planar surface, crests are continuous and show only slight differences in sinuosity and crest elevation.

In rigid-trough ripples a regularizing mechanism is clear. If a short segment of a crest is made to loop upstream, the increased transport rate on the stoss surface there acts to advance that segment faster and straighten the crest. Likewise, if a crest is made slightly higher along a short segment the resulting divergence of flow around the salient tends to spread the sediment laterally from the high area, thus reducing the height. In erodible-trough ripples there must be a counteracting mechanism that tends to accentuate irregularities; this mechanism is presumably related to uneven scour in downstream troughs caused by crest irregularities, which in turn affects the height and movement speed of crests still farther downstream. In this case the depth an advancing ripple must fill depends not only on the elevation of

the crest of that ripple but also on the elevation of the trough downstream, which is a function of local flow and is not constrained by the rigid bottom. The resulting irregular pattern is sedimentologically significant, in that it is the dominant control on the geometry of cross-stratification that results from deposition on rippled beds, but it is not fundamental to the existence and scale of the ripples themselves.

Large Ripples

Classification of the bed forms we're calling large ripples has been controversial. Some workers, exemplified by Boothroyd and Hubbard (1974) and Dalrymple et al. (1978)--and the author of the present chapter, before he began to change his mind a few years ago--have believed that there are two kinds of large-scale ripple-like bed forms: megaripples (often called dunes in flume experiments) and sand waves. Others, most notably Allen (1968a) and Rubin and McCulloch (1980), have taken the position that all of these large-scale bed forms are fundamentally the same in terms of dynamics, differing smoothly (but not necessarily uniformly) in size and shape as a function of flow conditions and sediment size. We're copping out by using the term large ripple for both megaripples and sand waves and leaving open the question of a possible distinction.

In natural flow environments large ripples have been studied more widely in tidal currents than in large rivers, because of their greater accessibility to observation and measurement in intertidal environments. In most of these intertidal flows the degree of tidal-current asymmetry is sufficient to make the asymmetry in sediment transport very great remember that sediment transport rate is an extremely steep function of flow strength. In most such flows the bed forms are therefore effectively the same as unidirectional-flow ripples, with only minor modification by the reverse current. We'll restrict our comments here to these effectively unidirectional-flow large ripples. Noteworthy studies of large ripples in tidal currents have been made by Klein (1970), Klein and Whaley (1972), Boothroyd and Hubbard (1975), Dalrymple et al. (1978), and Rubin and McCulloch (1980). Except for Rubin and McCulloch, these authors have contended not only that the two kinds of large ripples are different in size, shape, and formative flow conditions, but that there is a gap in characteristics between them, implying a fundamental difference in dynamics.

Our impression is that at least in some cases the distinction between megaripples and sand waves has been made only by the criterion of superimposition of smaller large ripples on larger large ripples. This seems not to be a valid criterion, because irrespective of the dynamics of the largest ripples there can be no superimposition until the scale of the largest ripples is large enough for development of smaller large ripples on their stoss surfaces. Another problem is that of the correlation that devel-

ops between sediment size and flow conditions in some local area; segregation of sand sizes by the currents tends to select, out of the three-dimensional continuum of flow conditions and sediment sizes possible, only a certain subset in any given area. So just the presence of a scarcity or even a break in the continuum of ripple sizes and shapes in some local area doesn't necessarily imply a corresponding fundamental break in dynamics. In this view, recognition of such a break would necessitate data from studies in many different areas--or from a flume, in which flow and sediment can be varied continuously, but that flume would have to be bigger than anyone has now or is likely ever to have.

DYNAMICS OF BED CONFIGURATIONS

Introduction

How is it that a turbulent flow molds a bed of loose sediment into stable bed forms? The subject of bed-configuration dynamics has long been one of frustration and controversy. The fundamental difficulty is easy to state: it has to do with the difficulty of specifying adequately how sediment transport rate varies from place to place over a geometrically irregular transport surface. Before elaborating, we should make clear what we mean by the sediment transport rate at a point. In Chapter 6 we dealt briefly with the rate at which sediment is transported past a given cross section of the flow, in solids volume per unit width of the flow; it's usually denoted by q_s. Here we need to think about how the "point" value of the volumetric transport rate, which you can view as the sediment transport rate over an arbitrarily small local area of the bed (again expressed per unit width of flow), varies from point to point on a nonplanar sediment bed. We'll denote this by q_s also.

The velocity profile and the local bed shear stress (i.e., the skin friction) at some point on a nonplanar sediment bed, and their time variation, are not likely to be the same as at a point on a featureless, planar bed with the same discharge and depth above it. This is because the details of forces and motions in accelerating and decelerating boundary layers are substantially different than in nonaccelerating boundary layers. You've seen this for the grossly nonuniform flows around bluff bodies like spheres and cylinders in Chapter 4, but the effect is substantial even when much smaller accelerations or decelerations are caused by mild streamwise gradients in fluid pressure. The structure of the flow above any point tends to be inherited from upstream as the flow adjusts toward new conditions, so the flow at the given point depends in a complicated way on the shape of the bed for a long distance upstream. So even if q_s could be assumed to be in local equilibrium with the spatially varying flow, it couldn't be specified in any simple way as a function of position. Furthermore, q_s is likely not to be in equilibrium with local flow conditions, because a finite distance is needed for load to be dropped out or picked up as transport capacity changes. This distance

should be expected to be greater for suspended load than for bed load, but it can't be assumed to be negligible even for the latter.

The development of bed forms depends on the variation in q_s over the bed-form profile. In turn, q_s depends on the flow, and if an adequate expression for q_s as a function of position could be found it could be combined with the kinematic constraint imposed by conservation of sediment volume to give an equation that could be solved for the evolution of any initial bed geometry to a steady equilibrium geometry. But q_s cannot be specified so simply; as we've seen, it is itself a function of the bed configuration for which we're trying to solve.

In the face of this depressing prospect many investigators have attempted with some limited success to glean physical understanding of the dynamics of bed configurations by making various simplifying assumptions that allow q_s to be expressed in a form that leads to mathematically tractable equations. Not many of these attempts have led to greatly improved understanding of the problem. This is a field of endeavor marked by an understandable scarcity of satisfying or useful results.

In this section we concentrate not so much on a detailed review of the literature on bed-configuration dynamics as on the physical effects related to the existence, shape, size, and movement of bed forms. We'll deal with each of these four aspects of dynamics in the following sections. The aim is to give you some appreciation of the potential and limitations of the various approaches to the problem of bed-configuration dynamics. It turns out to be easier to account qualitatively for shape and movement than for existence and size. As a necessary preliminary we first derive the sediment conservation equation, a kinematic relation expressing conservation of sediment volume (or mass) that must hold in any sediment-transporting system.

Sediment Conservation Equation

In any flow that transports sediment the volume or mass of transported sediment must be conserved. This requirement leads to a purely kinematic relationship that must hold irrespective of the dynamics of sediment transport. We'll concentrate on a two-dimensional flow (one that varies in two dimensions only, downstream and upward from the bed but not in the cross-stream direction), but the principle is the same for a flow that varies in all three directions.

Consider a small rectangular region R of the sediment bed, with unit width normal to the flow and with length Δx in the flow direction (Figure 7.29). The area of R is Δx because of the unit width. Denote by h the elevation of the bed above some arbitrary horizontal datum plane. Transport of sediment at any cross section can be expressed by q_s, the volumetric sediment transport

rate per unit width of flow; this may include sediment moving as bed load or in suspension. Let the depth-averaged volume concentration of the load be C. (Strictly, C includes the concentration of bed load as well as suspended load.) The difference between q_s at the downstream boundary of R, $(q_s)_{out}$, and at the upstream boundary of R, $(q_s)_{in}$, is Δq_s: $(q_s)_{out} - (q_s)_{in} = \Delta q_s$.

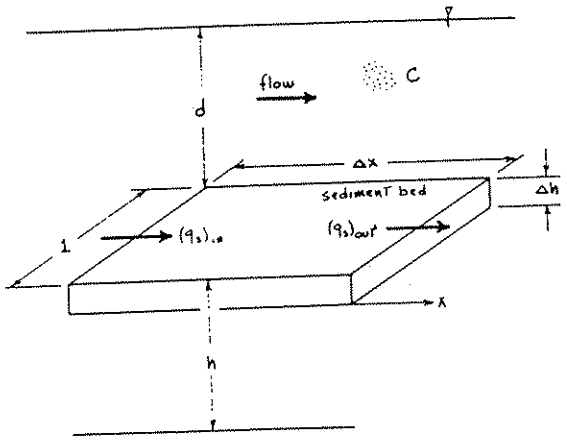

Figure 7.29 Definition sketch for derivation of the sediment conservation equation.

Any change Δh in bed elevation during some time interval Δt is caused by storage of sediment in R (deposition, or aggradation) or removal of sediment from R (erosion, or degradation). This change can be viewed as the sum of two contributions. One of these, Δh_s, is caused by downstream change in q_s: if q_s is greater across the upstream face than across the downstream face of R, then sediment must be stored in R, but if q_s is smaller, then sediment must be removed from storage in R. The other contribution, Δh_t, is caused by temporal change in C: if the concentration of transported sediment is decreasing with time, then there must be deposition on all areas of the bed, but if the concentration is increasing, then there must be erosion (assuming that sediment is not being added to the flow from above). The bulk volume $\Delta h_s \Delta x$ of aggraded or degraded bed in R due to downstream variation in q_s is equal to Δt times $(q_s)_{in} - (q_s)_{out}$, the rate of sediment storage due to the difference in transport rates across the upstream and downstream boundaries of R, with a correction for the porosity effect (Equation 7.13):

$$h_s \Delta x = \Delta t[(q_s)_{in} - (q_s)_{out}] = -K_1 \Delta q_s \Delta t \qquad (7.20)$$

The porosity correction factor $1/(1-\lambda)$, again denoted by K_1, is needed because the volume of transported sediment is measured in

solids volume whereas volume of bed sediment is measured in bulk volume, solids plus void space. The bulk volume of aggraded bed in R due to temporal variation in C is equal to minus the total change in volume of suspended sediment above R, again corrected for the porosity effect:

$$\Delta h_t \Delta x = -K_1 d \Delta C \Delta x \tag{7.21}$$

where d is flow depth. Using Equations (7.20) and (7.21), the average rate of change of bed elevation with time over R, $\Delta h/\Delta t$, can now be written

$$\frac{\Delta h}{\Delta t} = \frac{\Delta h_s}{\Delta t} + \frac{\Delta h_t}{\Delta t} = -K_1\left(\frac{\Delta q_s}{\Delta x} + d\,\frac{\Delta C}{\Delta t}\right) \tag{7.22}$$

In the limit, as $\Delta x \to 0$, Equation (7.22) becomes

$$\frac{\partial h}{\partial t} = -K_1\left(\frac{\partial q_s}{\partial x} + d\,\frac{\partial C}{\partial t}\right) \tag{7.23}$$

This differential equation is a volume-balance relationship that must hold at every point on the bed regardless of the sediment-transport dynamics. It relates the time rate of change of bed elevation at a point, $\partial h/\partial t$, to the downstream rate of change of sediment transport rate at that point, $\partial q_s/\partial x$, and the time rate of change of total suspended-sediment concentration in the flow, $\partial C/\partial t$. It's usually called the sediment conservation equation, or the sediment continuity equation. Its use is essential in thinking about the temporal changes in bed geometry consequent upon spatial changes in transport rate. If C does not change with time, Equation (7.23) becomes

$$\frac{\partial h}{\partial t} = -K_1\,\frac{\partial q_s}{\partial x} \tag{7.24}$$

Rate of change of bed elevation is then directly proportional to minus the downstream rate of change of sediment transport rate. If q_s decreases downstream for any reason, the bed is aggraded; if q_s increases downstream, the bed is degraded.

Movement of Bed Forms

Armed with the sediment conservation equation and all that's been said in Chapters 5 and 6 about flow and sediment transport in turbulent boundary layers, what can we do about accounting for the existence, size, shape, and movement of loose-sediment bed forms? Look first at movement, because that's the most straightforward. Consider a hypothetical bed form like that in Figure 7.30A, one element in a train of similar bed forms. We'll assume that the bed is in equilibrium with a steady sediment-transporting flow, and that the bed form moves downstream with unchanging size and shape. Equation (7.24) associates with the movement of the bed form a particular pattern of variation of q_s over the bed-form profile in the following way. For the bed form to move downstream it's a kinematic necessity that $\partial h/\partial t$ be negative on the upstream side of the bed form and positive on the downstream side (Figure 7.30B). Note that $\partial h/\partial t$ is zero at the crest and trough and has its greatest absolute value at points of steepest slope on the bed-form profile. By Equation (7.24), $\partial q_s/\partial x$ must vary with x in a sense just opposite to the variation in $\partial h/\partial t$ (Figure 7.30C), and therefore q_s itself must be greatest at the bed-form crest and least in the trough (Figure 7.30D). No zero point is shown on the q_s axis in Figure 7.30D, because any position of the curve is consistent with that of the curve for $\partial q_s/\partial x$ in Figure 7.30C. On ripple bed forms, q_s is zero or nearly so in the trough, and may even be negative if the reverse flow in the separation zone is strong enough. Over antidunes, on the other hand, there may not be much relative variation in q_s over the bed-form profile. If the bed form is to move downstream q_s must increase up the stoss surface from the trough to the crest and must decrease down the lee surface from the crest to the next trough.

In any flow of a low-viscosity fluid like air or water with a velocity large enough to transport sediment, Reynolds numbers of flow over even small ridges or mounds on the bed are large enough for substantial front-to-back asymmetry in local bed shear stress. Look back at Figures 4.3 and 4.10 and the accompanying text. Beginning at Reynolds numbers of about 10 the spacing of streamlines is closer, and therefore the skin friction is greater, on the front side of a cylinder or a sphere than on the back. This becomes more pronounced with increasing Reynolds number, and when flow separation eventually develops, the skin friction on the back is negligible. The effects are qualitatively the same for any ridge or mound on a sediment bed. So provided that the free surface remains approximately planar above the bed form, any bed form--even one whose height is only a few grain diameters--should have larger q_s on the upstream side than on the downstream side, with a maximum near the crest and a minimum somewhere in the trough. From Figure 7.30D it's clear that this distribution of q_s guarantees downstream movement. This distribution of q_s is not likely to be exactly the one needed for maintenance of bed-form shape, but that's a matter for the next section; the bed form

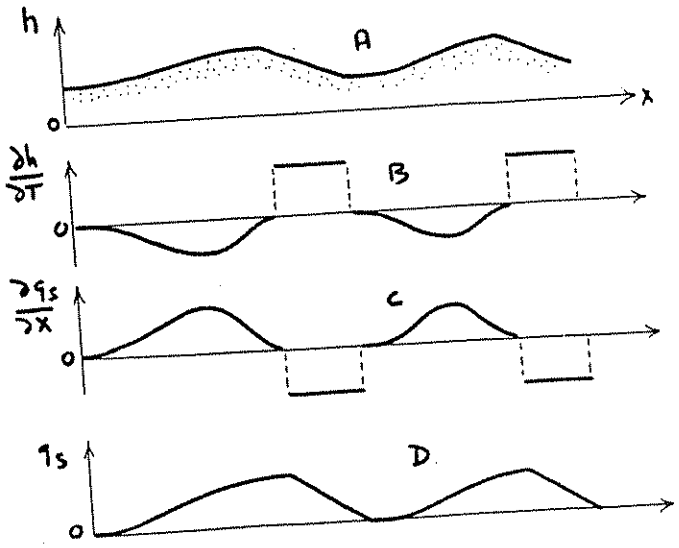

Figure 7.30 Variation of (A) h, (B) $\partial h/\partial t$, (C) $\partial q_s/\partial x$, and (D) q_s over a hypothetical unchanging bed form in a low-Froude-number flow.

always moves downstream even if its shape tends to change at the same time.

If mean-flow Froude numbers are close to unity, surface gravity waves interact with the bed to produce stationary or slowly shifting bed waves that are in phase or almost in phase with the water-surface waves. For these upstream-shifting bed forms, called antidunes, the interaction of the free-surface wave and the bed-surface wave is such that q_s decreases up the upstream slope and increases down the downstream slope, resulting in upstream movement. No capsule statement can be made at this point that elucidates the dynamical reasons for this variation of q_s.

We've shown (i) what the variation in q_s has to be over a bed-form profile for the bed form to move and (ii) that in the case of ripples the expected variations in q_s are in accord with the bed-form movement actually observed. This may seem like a self-evident or trivial exercise, but it shows how we can get some insight into the behavior of bed forms by combining ideas about sediment transport with the sediment conservation equation, and it points the way toward other problems that aren't as easy to deal with.

Shape of Bed Forms

Introduction

A striking characteristic of ripples, large and small, is their asymmetrical profile, with a gently sloping upstream surface and a steeper, nearly angle-of-repose slip face on the downstream surface. Typically the bed profile shows a sharp angle at the top and bottom of the slip face--although reverse flow in the separation eddy can smooth out the slope break at the base. If the breaks in bed slope at the top and base of the slip face are ideally sharp, they represent jumps or discontinuities in $\partial h/\partial t$ and therefore by Equation (7.24) in $\partial q_s/\partial x$ as well. Both h and q_s show kinks in their profiles at these points.

The Profile Shape of Ripples

In this section we'll show how the asymmetrical profile shape of ripples can be accounted for by combining the sediment conservation equation with a very general assumption about the physics of the sediment transport, namely that q_s increases with increasing flow strength. As in the preceding section, look at a hypothetical bed form in a train of identical bed forms (Figure 7.31). In this section we'll start with a symmetrical bed form and consider how its profile changes with time. We'll restrict consideration to flows with low Froude number, so that the water surface remains nearly planar whatever the bed geometry. The following line of reasoning was first presented by Exner (1925).

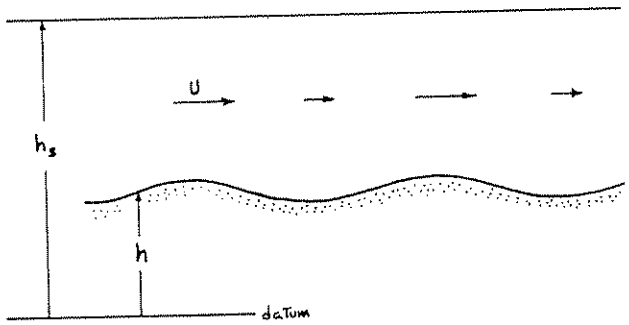

Figure 7.31 Definition sketch for analysis of the evolution of bed-form shape.

The strategy will be to develop a relationship between bed elevation h and sediment transport rate q_s, in order to put the sediment conservation equation into a form that can be solved for bed elevation as a function of position and time. As discussed above, ultimately we'd like to be able to supply enough physics for this approach to lead to insights about how bed forms grow. For now we'll be content with very simple assumptions about q_s that will lead to understanding of bed-form shape but not bed-form growth.

The mathematically simplest assumption we can make about q_s is that it's directly proportional to some variable that describes the flow strength above the point at which q_s is measured. Using mean flow velocity U as this flow-strength variable,

$$q_s = K_2 U \tag{7.25}$$

where K_2 is some constant. This has some serious shortcomings: (i) there is a finite U for which q_s becomes nonzero, and at smaller U no sediment is moved; (ii) q_s does not vary linearly with U even when U is strong enough to move sediment; (iii) if U rather than the skin friction is to be used to characterize q_s, the flow depth d must also be specified in the function. Notwithstanding these difficulties, this is a workable assumption for the task at at hand, because it contains a large element of truth and it permits insight into how the bed evolves. More sophisticated assumptions would lead to the same qualitative results on the evolution of bed-form shape but would necessitate working with equations that are much more difficult to solve. Furthermore, the fact that even such an oversimplified assumption about q_s accounts well for the evolution of bed-form shape is revealing in itself.

Using Equation (7.25) the sediment conservation equation (Equation 7.24) can be written

$$\frac{\partial h}{\partial t} = -K_1 K_2 \frac{\partial U}{\partial x} \tag{7.26}$$

where K_1 is again the porosity correction factor $1/(1-\lambda)$. Conservation of fluid volume in the flow requires that, per unit width,

$$Ud = U(h_s - h) = K_3 \tag{7.27}$$

where h_s is water-surface elevation above the same arbitrary datum as for h, and K_3 is another constant. Equation (7.27) says that where the flow is deeper over some two-dimensional bed configuration the velocity is smaller, and where the flow is shallower the velocity is greater, so by Equation (7.26) there is deposition or erosion depending on the sign of $\partial U/\partial x$. Combining Equations (7.26) and (7.27),

$$\frac{\partial h}{\partial t} = -\frac{K_1 K_2 K_3}{(h_s - h)^2} \frac{\partial (h_s - h)}{\partial x} \qquad (7.28)$$

Assuming h_s to be constant (a reasonable assumption for flows at low Froude numbers) and writing K for the constant $K_1K_2K_3$, Equation (7.28) becomes

$$\frac{\partial h}{\partial t} = \frac{K}{(h_s - h)^2} \frac{\partial h}{\partial x} \qquad (7.29)$$

You can verify for yourself that the solution to this fairly simple partial differential equation is

$$h_s - h = f\left[\frac{Kt}{(h_s - h)^2} - x\right] \qquad (7.30)$$

where f is an arbitrary function. To investigate the change in bed geometry with time, Exner (1925) assumed an initial bed topography given by a cosine function:

$$h = A_o + A_1 \cos \frac{2\pi x}{L} \qquad (7.31)$$

where L is the spacing of the sinusoidal bed forms, and A_o and A_1 are constants. This is what the bed profile at time t = 0 would be if Equation (7.30) is specialized in such a way that the bed profile as a function of x and t is

$$h = A_o + A_1 \cos \frac{2\pi}{L}\left[x - \frac{K_1 K_2 t}{(h_s - h)^2}\right] \qquad (7.32)$$

Figure 7.32 shows how the initial sinusoidal bed profile is modified with time according to Equation (7.32). The upstream slope of the bed form becomes gentler and the downstream slope becomes steeper, until finally the downstream slope passes through the vertical and an overhang develops. If this were a real bed form a slip face would develop when the slope angle of the downstream side reaches the angle of repose. What's less clear

from Figure 7.32 is that the bed form doesn't change in height as it changes in shape--but you can see from Equation (7.32) that the highest point on the bed form always has a height $h = A_o + A_1$, because the maximum value of the cosine function is one. This just means that the oversimplified assumption about q_s is inadequate to address the problem of bed-form growth.

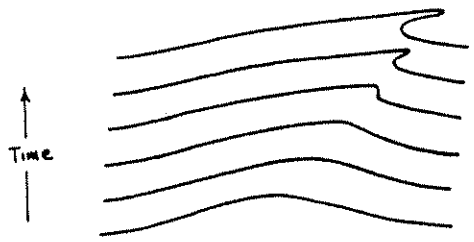

Figure 7.32 Evolution of an initially sinusoidal bed form with time. After Exner (1925).

So even a very simple assumption about the dependence of q_s on the flow accounts for the tendency for an originally symmetrical bed-form profile to evolve into the markedly asymmetrical profile characteristic of ripples. If we use a different function in Equations (7.31) and (7.32) to represent a different symmetrical or nearly symmetrical initial profile, the end result is just about the same. It's easy to observe just this kind of profile development in the laboratory: mold a long and low symmetrical ridge transverse to the flow on the sand bed of your flume, turn up the discharge until the sand moves, and then watch the profile as it's transformed gradually into a ripple, just as in Figure 7.32.

Bed Forms as Kinematic Waves

Another way of showing that low-Froude-number bed forms develop shapes characteristic of current ripples is to view bed forms as kinematic waves (Costello and Southard, 1981). The development in this section generalizes that in the last section, and it also serves to emphasize the significance of the discontinuities in $\partial h/\partial t$ and $\partial q_s/\partial x$ noted in the last section.

Kinematic waves (Lighthill and Whitham, 1955; Whitham, 1974) can exist in any unidirectional transport system in which there is a relationship between flow (quantity passing some point per unit time) and concentration (quantity per unit distance). Use of the term "wave" is appropriate because a property (bed elevation, in the case of bed forms) is propagated or carried in a way describable by a wave equation, but the waves are not dynamic waves like water waves or sound waves. Even a subject like highway traffic flow, in which the flow variable is the number of cars passing a given point per unit time and the concentration variable

variable is the number of cars per unit length of the road, lends itself to this approach. Have you ever seen those stop-and-start waves working their way back against the direction of traffic flow? They're kinematic waves.

In sand-transporting flows the kinematic-wave relationship holds between sediment transport rate q_s and bed height h. The wave property arises directly from the sediment conservation equation, Equation (7.24), and so the existence of waves is independent of the particular form of the sediment-transport dynamics. Assume as an approximation that for a given mean flow depth and velocity, q_s is a function of h but not of x or t: $q_s = f(h)$. This is certainly not true in detail, because we've seen that q_s depends on bed geometry as well as on bed height, but q_s must indeed increase strongly with h. This assumption is about like the assumption $q_s = K_2U$ in the preceding section but a little more general. By the chain rule for differentiation, $\partial q_s/\partial x = (dq_s/dh)(\partial h/\partial x)$ if we assume that q_s does not vary with x apart from its variation with h. (This assumption is not a good one for flow over bed forms, as we've seen, but it permits some valuable qualitative insights.) Denoting the derivative dq_s/dh by R and introducing this into the sediment conservation equation (Equation 7.24),

$$\frac{\partial h}{\partial t} + K_1 R \frac{\partial h}{\partial x} = 0 \qquad (7.33)$$

Solutions to Equation (7.33) are of the form $h = f(x-K_1Rt)$. The form of the argument of the function tips you off to the wave property of the solution. These solutions can be viewed as describing point "wavelets," each moving along the x axis with velocity K_1R and carrying a certain constant value of bed height, and the continuum of these wavelets can be viewed as a bed-elevation wave, or a bed form.

With Equation (7.33) can be associated a family of curves in a graph of downstream position x vs. time t, each curve giving the time and space history of a particular wavelet. These are straight lines with slopes equal to the wavelet velocity K_1R. Such lines are called characteristics. If q_s were a linear function of h, R would be constant, all the characteristics would be parallel, each wavelet would carry a constant value of h at a constant velocity, and the bed-elevation wave (i.e., the bed-form profile) would not change in shape as it moves downstream. It will be shown below, however, that q_s is not linear in h, so R itself is a function of h. The characteristics are still straight lines, but their slopes depend upon h. Wavelets carrying different values of h move at different speeds, and the bed-elevation wave changes shape as it moves.

To see what the curve of $q_s = f(h)$ is like, go back to the assumption made about q_s in the preceding section, $q_s = K_2U$. Combining Equations (7.25) and (7.27),

$$q_s = K_1K_2 \frac{1}{h_s - h}$$

Since both K_1 and K_2 are positive constants and $h_s > h$ by definition, this plots as a concave-upward curve in a graph of q_s vs. h. You'll see in the following that any curve for q_s that's concave upward in this graph, not just this particular one, leads to the characteristically asymmetrical ripple profile.

Evolution of bed-form shape can best be visualized by means of the x-t graph of characteristics (Figure 7.33). Assume any concave-upward curve of q_s vs. h (Figure 7.33B), so that R increases with increasing h. If a mound is placed on a planar bed (Figure 7.33C), its continued evolution can be traced with the aid of Figure 7.33A. On the upstream side of the mound, between x_1 and x_2, h and therefore R increases. The slopes of the corresponding characteristics in Figure 7.33A diverge to the right between x_1 and x_2 for times later than t_o. On the downstream side of the mound, between x_2 and x_3, h and therefore R decreases, and the characteristics in Figure 7.33A converge between x_2 and x_3 for times later than t_o. Because of this pattern of divergence and convergence, a short time later than t_o the mound becomes asymmetrical, with a more gently sloping upstream face and a more steeply sloping downstream face, as indicated by the closer spacing of the characteristics between x_1 and x_2 and the wider spacing between x_2 and x_3.

Characteristics must actually intersect at some time later than t_o and at a certain value of x; in Figure 7.33A this intersection first sets in at point P. Thus, at times and places represented by points along some curve extending to the right of point P there are two values of bed elevation at the same point on the bed. Such a jump discontinuity in bed elevation--and therefore, by Equation (7.24), also in sediment transport rate--is termed a shock wave. An example at some time t_1 is shown in Figure 7.33D. In reality, before the bed topography evolves to reach this physically impossible situation, wherein a single point on the bed has two different elevations, an angle-of-repose slip face develops. A migrating ripple-shaped bed form with a well defined slip face is thus a kinematic shock wave in which the discontinuities in bed elevation and sediment transport rate are spread over the horizontal distance between the brink and the base of the lee face.

If there are no bed forms coming along from upstream to change the profile of sediment transport rate, then the contrast in bed elevations between the intersecting characteristics becomes

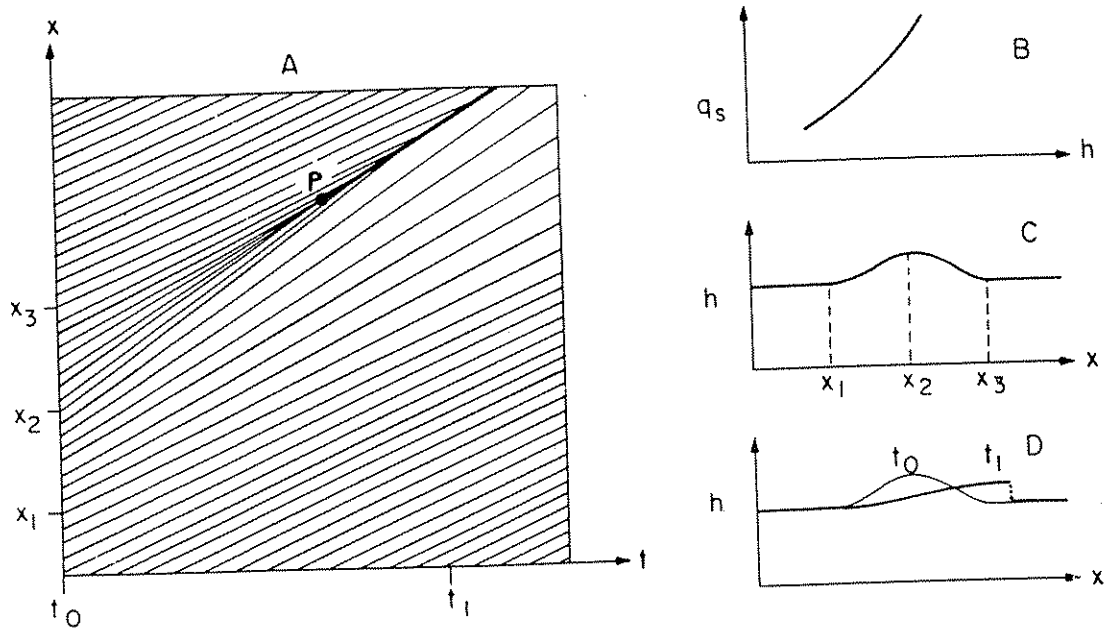

Figure 7.33 Development of a ripple-shaped kinematic shock wave from an isolated mound on a sediment bed. (A) Space-time plot of characteristics. (B) Schematic curve of sediment transport rate as a function of bed elevation. (C) Initial streamwise profile of the bed mound. (D) Evolution of the bed mound with time into a shock discontinuity. From Costello and Southard (1981).

smaller and smaller with time to the right along the shock-wave curve in Figure 7.33A, so the bed form becomes lower as it moves. Since the bed form has constant volume, it becomes longer at the same time it becomes lower. Thus, as the shock wave moves it becomes flattened or attenuated.

In reality, wherever local slopes of the bed become nonnegligible q_s is a function of x as well as h. The characteristics are then curves rather than straight lines. As is seen from the foregoing development, this situation inevitably develops during the evolution of any positive feature on the bed, even if the initial slopes are extremely small. But the approach outlined above is still qualitatively applicable.

A given bed form in a train of identical moving bed forms does not necessarily decay in the way described above, because the pattern of flow structure and therefore of sediment transport on the stoss surface keeps being shifted downstream by the advance of the next bed form upstream, and this acts to maintain the height of the shock. Ripples in a moving train can therefore be viewed as coupled or strongly interacting kinematic shock waves.

Growth of Bed Forms

Introduction

It's more difficult to account for the growth of bed forms than for their movement and shape. Here we'll follow the same approach as before, that of combining sediment-transport dynamics with the sediment conservation equation, but it won't lead to as satisfying results. This is because bed-form growth and decay, or more generally the stability of bed configurations, depends on the interaction of flow and sediment transport in ways too complicated to be expressed or parameterized by local conditions like flow velocity, boundary shear stress, bed elevation, or bed slope: it involves the entire bed configuration, not just local variations in h and q_s.

After describing a hypothetical flume experiment to examine some of the physical effects that have to be explained, we'll again examine the qualitative kinematic constraints imposed on q_s during bed-form growth, and then review some of the attempts that have been made to account for the existence of bed forms by deriving and solving equations for bed-form growth based on various assumptions about transport dynamics.

Hypothetical Flume Experiment

Make a long series of low transverse ridges on a sand bed in your flume (Figure 7.34). It makes no difference whether these are initially symmetrical or asymmetrical, because you've already seen that the flow soon gives the profile of a transverse ridge a ripple shape, whatever its initial shape. It helps if you give the ridges an initial spacing that's not greatly different from what you know beforehand about equilibrium ripple spacing (if any) corresponding to the conditions of flow and sediment size you're going to use, because then you maximize the duration of your experiment by reducing the tendency for the bed forms to change their spacing by dividing and merging. If you make the train of initial ridges very regular, the ripples will stay very much alike for a long time as they evolve. Eventually the inevitable irregularities in initial bed geometry (together with the stochastic nature of the grain transport itself) lead to the irregular geometry characteristic of real bed forms, but this irregularity is not essential to the existence of the bed forms. We emphasize that this experiment is a valid way of thinking about the physics of growth and decay of ripples within the context of the initial spacing you choose, although in general you can't expect these ripples to be happy with the given spacing forever even if at first they grow rather than decay.

Pass a sand-moving current over the ridges, and keep track of the elevations of crests and troughs. Under some conditions (Figure 7.34A) bed-form height increases as the troughs become deeper and the crests become higher. Stoss surfaces become

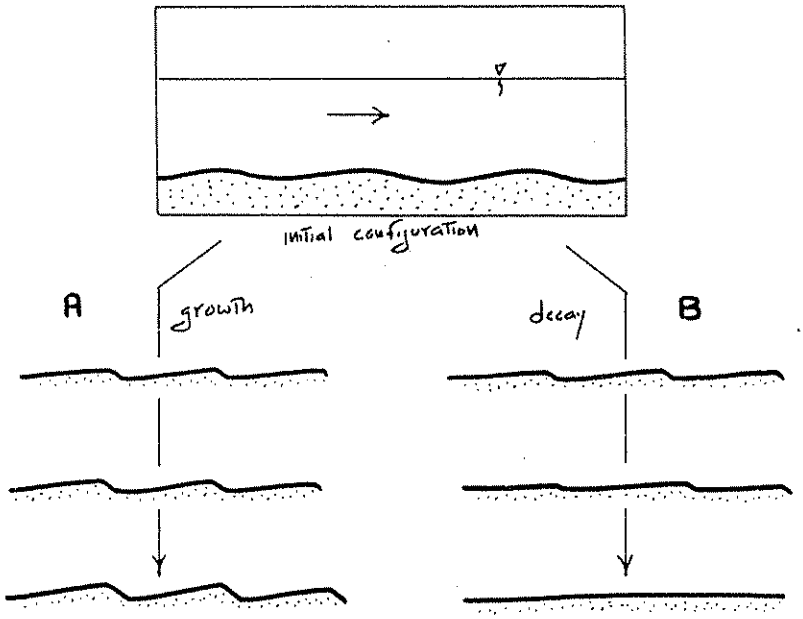

Figure 7.34 Hypothetical flume experiment on growth and decay of a train of artificially constructed bed forms.

steeper as well, because bed-form spacing is strongly locked in to the original value and won't change, at least not until after a long running time. The lee surface is likely to become a slip face almost from the beginning, as you've already seen, and then stay that way. Associated with the increase in crest elevation and decrease in trough elevation is an increase in the volume of sand contained in the ripple per unit width (volume being measured upward from a plane coincident with the bed-form troughs). Time-lapse motion-picture photography of the ripples as they move is a good way of appreciating the changes in bed-form height and stoss-surface steepness. If you know something beforehand about equilibrium height of ripples as a function of flow conditions and sediment size, you could first generate a set of low ripples under one set of flow conditions and then change the flow conditions to what you know will make higher ripples, and then sit back and watch.

Now make a second run in which you start out with a train of initially high and steep ridges (Figure 7.34B). The bed forms rapidly become aymmetrical as before, and sediment transport and ripple movement are qualitatively the same as before, but the bed forms are degraded as they move downstream: there is a gradual increase in trough elevation and decrease in crest elevation, and a corresponding gradual decrease in bed-form volume and also in the steepness of the stoss surface. Depending on sediment size and flow conditions, the ripples may stabilize at some equilibrium

height, shape, and velocity, or they may become more and more like fast-moving sediment sheets with small downstream steps until ultimately the bed is transformed into a planar transport surface.

Both kinds of run are an approximate simulation of what happens when an equilibrium ripple bed configuration is subjected to a change in flow conditions. They leave out the effects of adjustment in ripple spacing by gradual accentuation of inevitable small irregularities in the profile and then division of one ripple into two, or fusion of two ripples into one. But they illustrate an important principle of bed-configuration stability: if very small disturbances grow larger, then some nonplanar bed configuration will be the stable one under those conditions of flow and sediment, whereas if a preexisting nonplanar bed configuration is degraded to a planar transport surface, then upper-regime plane bed or lower-regime plane bed is the stable configuration. An analysis of how the ripple trains grow or decay in experiments like this should therefore provide insight into the dynamics of bed-form stability.

Conditions for Growth and Decay of Bed Forms

In this section we'll reason as far as possible about the conditions for growth and decay of bed-form trains, like those in the hypothetical experiment described above. We'll take the x direction downstream and measure bed height from some plane parallel to the plane representing the mean bed surface and lying well below it. We'll restrict ourselves to indefinitely long trains of two-dimensional flow-transverse bed forms in a transport system that's uniform in the large, in the sense that q_s averaged over an entire bed form does not change in the downstream direction (Figure 7.35).

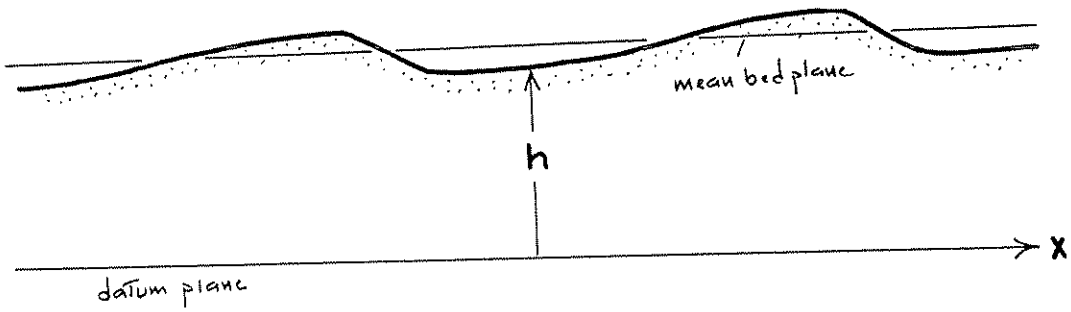

Figure 7.35 Definition sketch for analysis of growth and decay of bed-form trains in steady uniform flow.

The bed-form profile may or may not be changing. In either case, $\int h dx$ evaluated between two equivalent points on successive bed forms is constant. This expresses the condition that the bed is not aggrading or degrading on the average. If crests get higher, troughs have to get deeper in such a way that the mean bed elevation stays the same.

It's instructive to consider first the reference case of an unchanging profile. In the following, refer to Figure 7.36 (which is fundamentally the same as Figure 7.30).

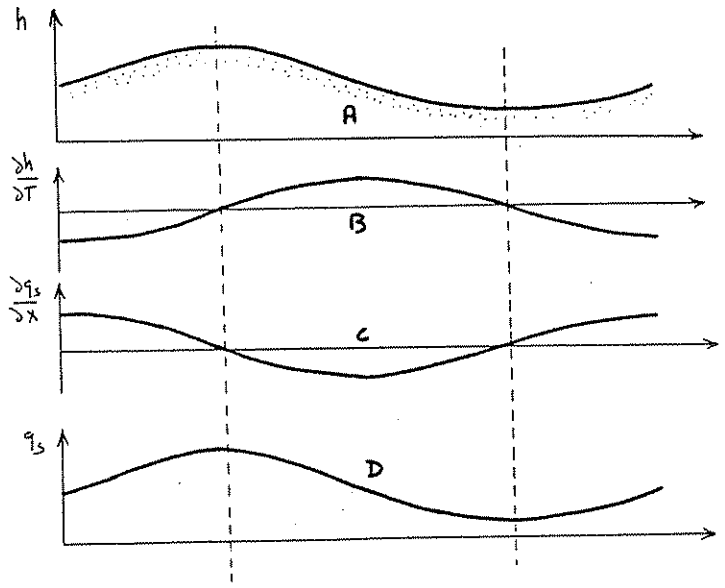

Figure 7.36 Profiles of (A) h, (B) $\partial h/\partial t$, (C) $\partial q_s/\partial x$, and (D) q_s for an unchanging ripple train in steady uniform flow. For simplicity, the bed-elevation profile is shown as a sine curve: the results are qualitatively the same for any periodic bed profile.

The kinematic condition for an unchanging profile is that

$$h = f(x-U_B t) \qquad (7.34)$$

where U_B is a constant and f is some periodic function that represents the bed profile at a given time. The argument $x-U_B t$ in the function implies that the profile propagates or shifts downstream at speed U_B as an unchanging wave form; U_B is therefore basically the same as the bed-form velocity used earlier in this chapter. To see the consequences of this condition, assume for now that the bed profile is a sine wave:

$$h = \sin(x-U_B t) \tag{7.35}$$

There's really no loss of generality in doing this, because any periodic bed profile can be represented as a Fourier sum of sinusoidal components; at the end of this paragraph we'll revert to a general periodic function f. Differentiating Equation (7.35) with respect to t,

$$\frac{\partial h}{\partial t} = \frac{\partial}{\partial t}\sin(x-U_B t) = \frac{d[\sin(x-U_B t)]}{d(x-U_B t)}\,\frac{\partial(x-U_B t)}{\partial t} = U_B \cos(x-U_B t) \tag{7.36}$$

by use of the chain rule for partial differentiation. Note that $\partial h/\partial t$ in Equation (7.36) is 90° out of phase with h in Equation (7.34), if the phase angle is measured in the downstream direction. In other words, the peak of the function in Equation (7.36) is offset downstream from that of the function in Equation (7.34) by one-quarter of a wavelength. (If you're not sure about the phase relationships, plot the four curves $y = \cos x$, $y = \sin x$, $y = -\cos x$, and $y = -\sin x$ and watch the sine wave shift along the x axis by 90°, i.e., one-quarter of a wavelength, each time.) Now to find $\partial q_s/\partial x$ substitute Equation (7.36) into the sediment conservation equation, Equation (7.24):

$$\frac{\partial q_s}{\partial x} = -\frac{1}{K_1}\frac{\partial h}{\partial t} = -\frac{U_B}{K_1}\cos(x-U_B t) \tag{7.37}$$

Note that $\partial q_s/\partial x$ in Equation (7.37) is 270° out of phase with h in Equation (7.34) because of the minus sign, i.e., the crest of the $\partial q_s/\partial x$ profile is one-quarter of a wavelength upstream of the crest of the bed-elevation profile. Integrating $\partial q_s/\partial x$ in Equation (7.37) with respect to x,

$$q_s(x,t) = \int \frac{\partial q_s}{\partial x}\,dx = \frac{U_B}{K_1}\int \cos(x-U_B t)\,dx$$

$$= \frac{U_B}{K_1}\sin(x-U_B t) + c_1(t) \tag{7.38}$$

where $c_1(t)$ is a constant of integration that in general could be a function of t, but isn't in this case because we're assuming steady flow. (The constant of integration has to be a function of

t because the integration is a "partial integration" of a function of two variables with respect to just one of those variables, while holding $U_B t$ constant.) Note that q_s is in phase with the bed profile and differs only by a multiplicative constant U_B/K_1 and an additive constant c_1.

To summarize, for an unchanging bed profile $h(x,t) = f(x-ct)$ and $q_s(x,t) = (U_B/K_1 f(x-U_B t) + c_1$, where c_1 is just a constant that relates the average bed elevation to the average sediment transport rate. The variation of q_s is in phase with the bed profile and has the same shape except for the constant factor U_B/K_1. Remember that this is all just a kinematic necessity; we haven't said anything about how q_s and h interact dynamically to produce the particular patterns observed.

From here on we'll concentrate on lower-flow-regime ripple bed forms. You've seen that if suspended-load transport is unimportant, lower-regime bed forms are dominated by slip faces that represent shock discontinuities. These discontinuities are associated with major flow separation over the bed form, but in a sense they are independent of the flow separation, in that they are a consequence of the steep increase in q_s with flow strength. Disregarding minor reverse flow in the lee eddy, q_s is zero from the toe of the slip face downstream to the reattachment point. If the profile is unchanging with time this stretch of bed must be horizontal: within it q_s is independent of both x and t because it's identically zero there, so h, which differs from q_s only by a multiplicative and an additive constant (compare Equations 7.34 and 7.38), is constant in x and t there. This stretch of bed with $q_s = 0$ may not be quite the lowest in the profile, because of some upchannel-directed sediment transport just upchannel of the reattachment zone, but it can safely be assumed so without affecting the conclusions of this section. Likewise, there's no dynamical requirement that the brink at the top of the slip face is the highest point on the profile, even if the profile is unchanging with time, but since there's such a strong tendency for flow separation to develop upstream of a negatively sloping surface, the brink should be just about the highest point on the profile. It's therefore convenient to let the slip-face height represent the bed-form height H, and it's also convenient to let the rate of downstream advance of the brink represent the velocity U_B of the ripple.

The presence of the shock discontinuity represented by the slip face imposes a further kinematic relationship that must hold among bed-form height, bed-form velocity, and the value of q_s at the brink:

$$(q_s)_{brink} = K_1 H U_B \qquad (7.39)$$

This is exactly the same as Equation (7.16); if you go back and review the derivation of that equation you'll see that it holds for the present situation as well, provided that all of the load is dumped at the break in slope at the brink to build the slip face forward. Equation (7.39) holds generally, not just for an unchanging profile. Note that the slip-face angle drops out of the expression. This is consistent with the idea that the slip face is just the physical manifestation of a shock discontinuity in q_s. The sediment delivered to the crest could just as well be falling off a cliff, in terms of the kinematics of the phenomenon.

In the light of all this bed-form kinematics let's see what can be done about accounting for the results of the hypothetical experiment. In the first run the bed forms started out too low and grew to some stable greater height, and they changed their shape in the process. After the bed forms reached equilibrium the distributions of h, $\partial h/\partial t$, $\partial q_s/\partial x$, and q_s must have been as shown in Figure 7.37B, which is qualitatively the same as Figure 7.30. Note the discontinuities in $\partial h/\partial t$ and $\partial q_s/\partial x$, reflecting the sharp kinks in bed elevation and transport rate at the top and bottom of the slip face. While the ripple train was adjusting, these curves must have been as shown in Figure 7.37A. The differences between Figure 7.37A and Figure 7.37B look minor, but they're very significant for ripple growth. Large differences shouldn't be expected anyway, because change in ripple shape and height is slow relative to ripple movement.

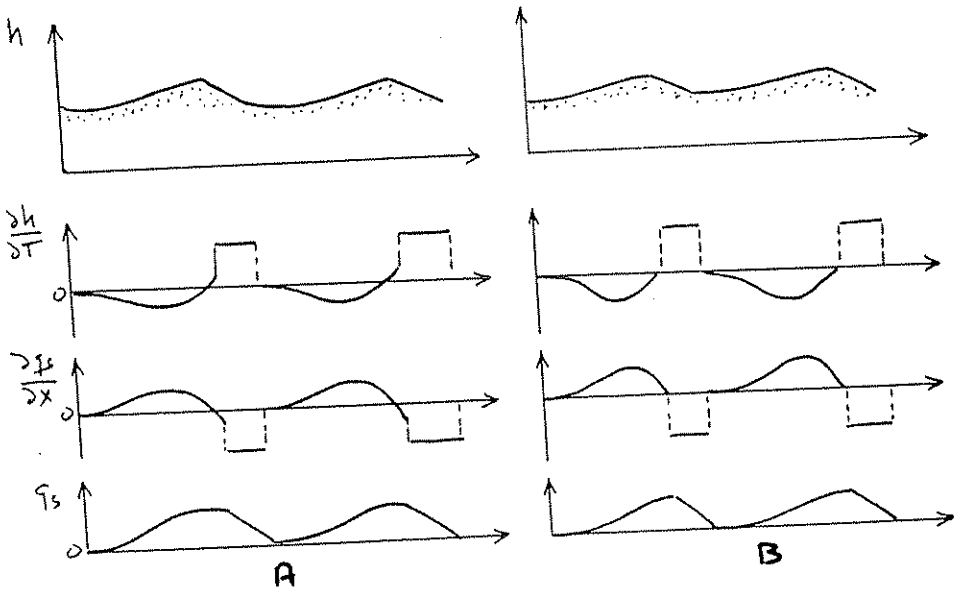

Figure 7.37 Profiles of h, $\partial h/\partial t$, $\partial q_s/\partial x$, and q_s for a train of ripples increasing in height. (A) Ripples are adjusting in height. (B) Ripples have reached equilibrium. See text for explanation.

The maximum in q_s on the stoss slope is located a little upstream of the brink rather than right at it. This leads to upward growth of the upper stoss surface during migration. Also, there's a downchannel slope to the bed between the base of the slip face and the low point on the profile. These two differences reflect stronger-than-equilibrium scour in the reattachment zone and just downstream, leading to a temporal lowering of bed elevation in the trough. The extra sediment produced by this scour is transported up the stoss surface to steepen the upper part. The slip face lengthens as it builds into the deepening trough, making ripple height greater. By Equation (7.39), U_B tends to decrease as the slip face lengthens, and this augments the tendency for increased trough scour, because the reattachment zone passes more slowly along the bed in the trough as it's driven downstream by the next ripple coming along. Eventually the geometry and sediment transport adjust to the new flow, and a picture qualitatively like that of Figure 7.36B is reestablished with a greater ripple height and a different ripple shape.

In the second run the bed forms started out too large and shrank either to some stable smaller height or were degraded completely. Figure 7.38 shows the distributions of h, $\partial h/\partial t$, $\partial q_s/\partial x$, and q_s as the ripples were changing. If the ripples reached equilibrium in the run, Figure 7.38A can be compared with Figure 7.38B for the stable smaller ripples. If not, then Figure 7.38A evolves into an uninteresting graph, not shown, in which h and q_s are positive and constant, and $\partial h/\partial t$ and $\partial q_s/\partial x$ are zero. Note in Figure 7.38A that q_s is increasing at all points up the stoss surface from reattachment. Since $\partial q_s/\partial x$ is still positive at the brink $\partial h/\partial t$ is negative there, so the crest elevation is decreasing with time. Scour in the trough is weaker than needed to maintain trough depth, so the bed slopes upward at all points downchannel of the base of the slip face, although no sediment is moved on the stretch of bed from there to the reattachment point. Trough elevation increases as the slip face becomes shorter by building onto the upsloping trough surface, so both ripple height and ripple volume decrease. By Equation (7.39), U_B tends to increase as the slip face becomes shorter, and this augments the weakening of scour in the trough because it causes the reattachment zone to sweep more rapidly downchannel.

In summary, changes in ripple height, shape, and velocity can be viewed in terms of the interaction among three related but distinguishable factors: (i) the dependence of q_s on flow structure along the reach of bed extending from the reattachment point up the stoss surface to the brink; (ii) the rate at which the zones of differing flow structure downstream of the point of flow separation are swept along the bed surface by the advancing crest upstream, as specified by the relation expressed by Equation (7.39) among slip-face height, ripple velocity, and sediment transport rate at the brink; and (iii) the slope of the trough surface onto which the slip face builds. We haven't solved any problems of bed-form stability here; we've only shown what factors are involved. Nonetheless, this line of approach is nonetheless

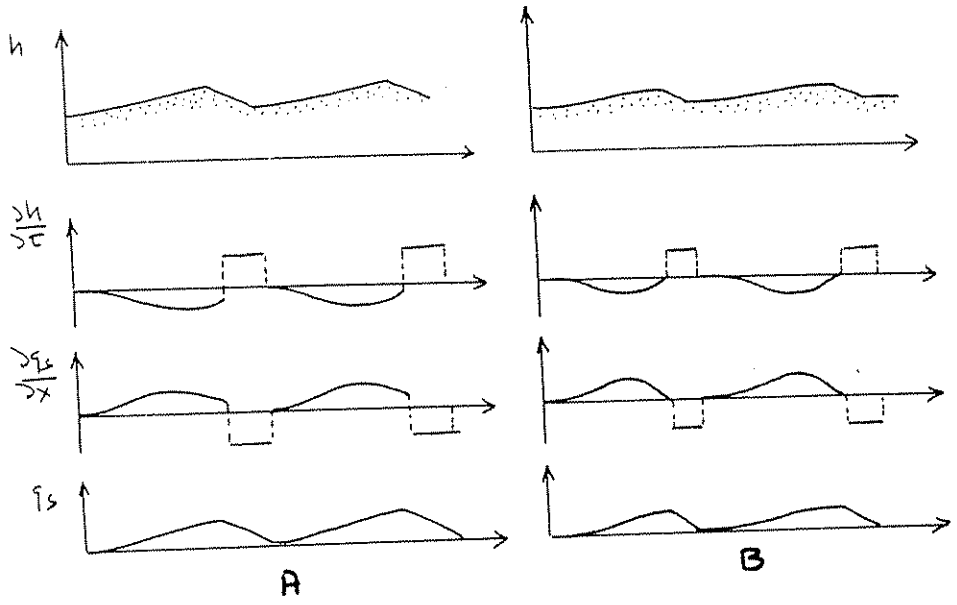

Figure 7.38 Profiles of h, $\partial h/\partial t$, $\partial q_s/\partial x$, and q_s for a train of ripples decreasing in height. (A) Ripples are adjusting in height. (B) Ripples have reached equilibrium. See text for explanation.

in that it aids in an understanding of the problem.

Stability Analyses

In order to understand the existence of bed forms, various investigators have resorted to stability analysis, a mathematical technique (useful in many areas of applied mathematics) wherein a partial differential equation is somehow developed that gives the rate of growth of a periodic disturbance or perturbation introduced onto the bed surface. The assumption is that if the rate of growth of the perturbation is positive the perturbation is amplified with time, and bed forms eventually develop. If, on the other hand, the perturbation is damped, then a plane bed should be the only stable bed configuration. The differential equation is of the same kind as used in the preceding sections. It comes about by supplying a relationship for q_s as a function of flow, which can be used to put the sediment conservation equation into a solvable form. This equation has to go beyond the oversimplified assumptions made in the section on shape of ripples, because we saw that those assumptions account only for change in ripple shape, not in ripple volume.

The great advantage of the stability approach is that it can be developed for perturbations with amplitude very small compared to wavelength, so that bed slopes are very small. It is then more

likely that relationships for sediment transport that are not grossly unrealistic can be specified. By the same token, however, without further analysis this approach gives no information on the nature of the resulting bed configuration when the perturbation is amplified to the extent that that the small-amplitude assumption is no longer valid. There is the possibility, however, that an estimate of the spacing of the resulting bed forms can be obtained by determining the wavelength of the perturbation that shows the fastest rate of growth.

It is worth mentioning four different attempts, among others, along the above lines to account for observed bed configurations: those by Kennedy (1963, 1969), Smith (1970), and Engelund (1970); see also Engelund and Fredsøe (1974) and Richards (1980).

Kennedy's analysis, which is most relevant to bed configurations at mean-flow Froude numbers close to one, assumes inviscid flow with a wavy free surface over a wavy boundary. By making simple assumptions about sediment transport rate as a function of near-bed velocity Kennedy developed a framework that accounts well for the occurrence of antidunes--bed forms whose behavior is dependent upon the presence of the free surface. The theory does not so much predict the bed configuration as provide a rational framework in which to account for it: as do many later analyses by others, the analysis involves a parameter called the lag distance (the distance by which local sediment transport rate lags behind the local velocity at the bed) that would have to be supplied by either experiment or additional theory. For the stability of antidunes, the theory works well with physically realistic assumptions about the lag distance in that it succeeds in accounting for the observed spacing of antidunes. As might be expected from the essential role of the presence of the wavy free surface in the analysis, the theory is less successful in accounting for dunes. Kennedy's work stimulated many subsequent attempts along the same lines.

Smith (1970) developed a stability analysis to deal specifically with flow at Froude numbers low enough that free-surface effects are negligible. Making suitable assumptions about nature of the flow (eddy-viscous flow of real fluid) and about sediment transport rate as a function of flow, Smith developed an equation that when linearized by retaining only the most significant terms is amenable to stability analysis. The result is that, for these not grossly unrealistic assumptions about flow and sediment transport, a positive growth rate, and therefore development of ripple-like bed configurations, is predicted for all flows strong enough to transport sediment. This is a rather fundamental and satisfying way to account for the existence of ripple-like bed configurations under reasonably realistic assumptions about flow and sediment transport. But even aside from the usual problem of not being able to take finite-amplitude effects into account without further theory, the analysis does not account for the existence of plane-bed stability at the higher flow strengths.

Engelund (1970; see also Fredsøe, 1974, and Engelund and Fredsøe, 1974), in a somewhat different approach also involving an eddy-viscous fluid, but taking account of the distinction between suspended-load transport and bed-load transport, was able to account well for the transition from large ripples to plane bed as a function of both grain size and flow strength. Richards (1980), using a more realistic description of the structure of turbulence near the bed, was able to account for the separate existence of small ripples and large ripples by predicting the occurrence of two separate modes of instability, one (for small ripples) dependent on the bed roughness and the other (for large ripples) dependent on the flow depth.

CHAPTER 8. SEDIMENT GRAVITY FLOWS

INTRODUCTION

Definitions

Almost all flows of geophysical importance are produced by the effect of gravity, either directly or indirectly. One category of fluid gravity flows has traditionally been called density currents. These are currents due to gravity acting on relatively small differences in density between different layers of fluid. Thus a stream of cold water flowing beneath warmer water in a lake is a density current, but a river is not (because the density difference between warm and cold water is small but the density difference between water and air is large compared with that of either fluid). The density differences that drive density currents are commonly due to differences in temperature, salinity, or suspended sediment (or some combination of these three: for example, the famous density currents observed in Lake Mead and Swiss lakes are frequently caused by the combined action of lower temperature and high suspended-sediment concentration in the river inflows, as compared with the lake water). Density currents due to suspended sediment have commonly been called turbidity currents by geologists.

There is, however, a fundamental distinction between gravity currents composed of sediment-fluid mixtures and those in which only fluids are involved. In the case of sediment gravity flows, gravity acting on the sediment particles moves the fluid, whereas in fluid gravity flows it is gravity acting on the fluid that moves the fluid. In the former the sediment moves the fluid and in the latter the fluid moves the sediment (if any sediment movement is involved).

Autosuspension

In turbidity currents, which are undoubtedly the most common type of sediment gravity flow, the situation is not quite as simple as indicated above. First the flow must be initiated by some event that takes a large volume of sediment into suspension. The suspended particles are supported by the fluid, which therefore acts as though it has a density higher than that of the surrounding sediment-free fluid. The effective density difference, combined with the action of gravity, produces a lateral flow; this fluid motion in turn produces turbulence in the fluid, which tends to hold the sediment in suspension and thus prevent the turbidity current from becoming dissipated by deposition. The maintenance of turbulence, and therefore of suspension and of the flow of the turbidity current, depends on a constant input of energy, which is derived by flow of the current downslope.

Many authors have followed Knapp (1938) and Bagnold (1962) in arguing that there should exist a condition where the input of gravitational energy is just sufficient to sustain the turbulence necessary to keep the sediment in suspension (and to overcome the frictional resistance at the lower and upper boundaries of the flow). In this case, the turbidity current would continue to flow downslope as a steady uniform flow, without either depositing or eroding sediment, until either the supply of suspension was exhausted or the slope changed. This ideal condition has been called by Bagnold (1962) autosuspension: autosuspension prevails when gravity acting on the solid particles provides just enough kinetic energy to maintain the turbulence that is necessary to keep the particles in suspension. Theoretically, autosuspension is not restricted to turbidity currents. In fact, Bagnold appears to have developed the idea (also suggested by Knapp, 1938) originally for application to rivers. Fine sediment added to a river is taken into suspension (as wash load) and adds to the apparent density or effective specific weight of the river water; this adds to the downslope component of gravity and causes the river to flow faster until the force of resistance again balances the downslope gravity component (see analysis of this force balance in Chapter 1). The increased speed of the river also gives rise to an increased intensity of the vertical turbulent fluctuations that hold the sediment in suspension. Ideally it seems that there should be a grain size at which the increment in turbulence produced by the added speed of the river is just sufficient to hold the added sediment in a condition of continuous suspension.

We will argue below that it is not really possible to draw up the simple kind of energy budget required by this theory. But first let us follow the attempts made by Bagnold to quantify the theory and provide a numerical criterion for autosuspension.

First we calculate the total energy needed to hold grains of sediment in suspension. The grains are falling relative to the fluid at a velocity w, so in order to keep them in suspension the fluid must be lifting them at the same rate. The submerged weight of grains per unit volume of fluid is

$$C(\rho_s-\rho)g$$

where C is the volume concentration of the grains. So the power expended in raising this mass in unit time is

$$C(\rho_s-\rho)gw$$

Note, in passing, that it is the fluid (water) that must perform work at this rate on the sediment.

Next we consider how the mixture of sediment and water might have a power that is larger than that of the water by itself. The force acting on the fluid alone is the downslope component of gravity acting on the difference in density between the fluid and the overlying fluid--which is generally assumed to be zero in the case of turbidity currents, though it is the main driving force in rivers. The added gravity component resulting from sediment in the fluid-sediment mixture is $C(\rho_s-\rho)gS$, and to obtain the power contributed we multiply by the average speed U of movement downslope. It is next claimed that autosuspension will result when the power contributed by the sediment-fluid mixture is equal to that expended (by the fluid alone) in maintaining the suspension, i.e., when

$$C(\rho_s-\rho)gw = C(\rho_s-\rho)gSU$$

or

$$w = SU \qquad (8.1)$$

This is the result given by Knapp (1938) and by Bagnold (1962). For large rivers $S = \tan\phi \approx \sin\phi$ is of the order of 0.001 and U is of the order of 100 cm/s, so w is of the order of 0.1 cm/s. The prediction therefore is that sediment grains about 0.03 mm in diameter should be in autosuspension, and finer grains should be contributing energy to the flow rather than requiring energy from the flow for their suspension, as larger grains do.

A test of this criterion was provided by an experiment carried out by Southard and Mackintosh (1981). These authors circulated water through a closed pipe. The main straight test section was first kept horizontal, and fine sediment was added until the concentration of suspended sediment had reached a limited value, and the excess sediment supplied had formed a plane bed on the bottom of the pipe section. Because the pipe was horizontal there was no net contribution to the energy of the flowing mixture from gravity acting on the sediment: the power required to keep the sediment suspended came from the flow itself, and was ultimately derived from the pump that provided the pressure gradient driving the flow. Next, the pipe was tilted at an angle sufficient to satisfy (and in some runs, substantially exceed) the criterion of Equation (8.1). The mean flow velocity and the energy slope remained essentially unchanged over the test section. At this point one would have expected that the concentration of sediment in suspension would have increased, because sediment could have been taken up from the bed without needing any additional contribution of energy from the flowing fluid. In fact the concentration did not increase in any of the five runs with five different sizes of sediment (ranging from 0.014 to 0.096 mm). The results clearly invalidate the criterion

of Equation (8.1), at least as regards its possible application to pipe and river flow. It has been argued by Pantin (1982) that this is because the wrong criterion was tested, and by Parker (1982b) that the result does not necessarily mean that the criterion cannot be applied, at least as a necessary if not a sufficient criterion, for the occurrence of autosuspension in turbidity currents, but the original paper, and the discussion by Parker (1982a) and by Paola and Southard (1983) make it clear that the criterion itself was derived from a highly oversimplified model of the energy balance in the flow of a sediment-water mixture.

The trouble with calculations of this kind is that they neglect all the other effects that the sediment may have on the flow. It is easy to show by means of calculations like those given above that the energy required to suspend the sediment in a river (or turbidity current) is a very small fraction of the total amount of energy expended by the flow. Rubey (1933a) calculated that it was only about 2-3%. Most of the energy of the flow goes to overcome the resistance of the boundaries: because the resistance of the boundaries is what produces turbulence, this includes the energy that produces turbulent motions and is ultimately dissipated as heat. Only a small part of the energy in turbulence can be put to the sedimentologically useful task of suspending sediment, and in particular it seems unlikely that the high-frequency, small-scale part of the turbulence spectrum, which contains a substantial part of the turbulent energy, has much influence on grain suspension. So any disturbance of the way in which turbulence is generated at the boundary of the flow, and of the distribution of energy within different frequency ranges of the turbulent energy spectrum, might have a major effect on the energy available to suspend sediment. Adding fine sediment to a river increases the effective viscosity of the water, alters the settling behavior of the coarser grains being moved, and demonstrably can produce major changes in the bed configuration (Simons et al., 1965). These changes, and particularly those affecting the bed configuration and the concentration of coarser grains close to the bed, probably produce substantial changes in the structure of the turbulence of the flow, and therefore alter the energy structure of the flow to a degree that is large compared with the energy input produced by adding the fine sediment in the first place. Changes in the bed configuration can easily produce a change in resistance (and therefore kinetic energy) by as much as 50-100%, as compared with the 2-3% of the total energy used in maintaining sediment in suspension.

How much sediment is carried in suspension also depends critically upon the nature of the processes acting at the lower boundary, that is, on the mechanisms by which sediment is deposited on or eroded from the bed. We saw in Chapter 6 that these mechanisms are closely linked to the generation of turbulence at the boundary, and that the way in which the presence of sediment moving in relatively high concentration along the boundary affects the turbulence and the exchange of sediment with the bed are still not at all well understood.

Because of all these complications it is not surprising that it is difficult to define a condition for autosuspension. But we may ask, is the concept itself a useful one? In the case of rivers, the answer is probably no. Despite assertions to the contrary, there are no known aspects of river flow which can definitely be attributed to the additional potential energy added to the flow by the suspended sediment. But, though we may have little hope of understanding the concept of autosuspension clearly enough to formulate a numerical criterion, the concept itself does seem to have some merit for turbidity currents. We can illustrate this by considering two possible end members in the turbidity-current continuum. In the first, sediment is taken into suspension by an initial catastrophic event, which produces a mixed turbulent mass of water and sediment. If this mass of dispersed sediment overlies a horizontal bed, it simply spreads out in all directions, and as the turbulence generated by the initial disturbance decays, the sediment is deposited. Little additional turbulence is generated by the flow itself, and the flow is soon dissipated. If the mass of dispersed sediment is generated on a slope, however, it begins to flow down the slope and one of two things happens: the motion of the flow either does or does not generate enough turbulence to maintain the sediment (or at least a substantial part of it) in suspension. If not enough turbulence is generated, the sediment is deposited not far from the source (this is in fact the model of deposition from a turbidity current elaborated by Scheidegger and Potter, 1965). But if enough turbulence is generated it is possible for the flow to travel great distances without the total loss of the suspended sediment due to decay of the intial turbulence. In fact, we expect that, as the flow moves down slope, the characteristics of the initial sediment dispersion have less and less control on the characteristics of the turbidity current.

The possible evolution of a cloud of suspension generated on a submarine slope has been examined in a qualitative fashion by many geologists concerned with erosion by, or deposition from, turbidity currents. Recently a more quantitative analysis has been attempted by Chu et al. (1979, 1980), Pantin (1979), and Parker (1982a). We do not have the space to examine any of these analyses in detail; they are in any event based on some dubious assumptions, particularly (in the case of Pantin and Parker) regarding a criterion of autosuspension. In general, however, the analyses suggest the following possible line of evolution of a turbidity current. As suggested above, either the current will dissipate (flows in the "subsiding field" of Pantin's analysis; flows that fail to "ignite" in Parker's analysis) or they will accelerate and grow. In Pantin's analysis, flows that are generated by sufficiently strong initial events pass through an "exploding field" but eventually enter a field of stability corresponding to autosuspension. In Parker's analysis, corresponding flows "ignite" and accelerate and entrain sediment up to some "catastrophic state" which Parker believes will be limited by factors not included in his formal analysis. Factors that limit the growth of "exploding" or "catastrophic" turbidity

currents are those that limit the ability of the turbidity current to pick up more sediment by erosion of the bed, and those that increase drag forces and produce rapid mixing of the current with the overlying sea water at the upper interface of the current (see below). Ultimately, of course, the current is dissipated by flowing onto regions of very low slope, where the further input of potential gravitational energy becomes too low to compensate for the energy loss due to friction. But the evidence from marine geology indicates clearly that large turbidity currents carrying sediment at least as coarse as very fine sand can travel for thousands of kilometers (and for many hours) over very low slopes. It does not seem unreasonable to describe such currents as being in a state of "autosuspension" even though we may not yet be able to formulate exactly in mechanical terms exactly what this means.

TYPES OF SEDIMENT GRAVITY FLOWS

Up to this point we have assumed that before sediment can be moved by gravity to produce a sediment gravity flow it must be taken into suspension by turbulence. But this is not necessarily the case: any mechanism that will disperse sediment within a fluid to the point where the whole sediment-fluid mixture can be sheared like a fluid will permit the formation of a sediment gravity flow. It seems possible to hold sediment in a dispersed state in one of three ways, besides turbulence: interaction of the grains themselves (producing what Bagnold has called "dispersive pressure"), (ii) by the upward movement of fluids escaping from between the grains, after initial liquefaction of a mass of sediment, and (iii) by the presence of a fine matrix that has sufficient strength to prevent the settling of the coarser grains through it. Thus, Middleton and Hampton (1973, 1976) have classsified sediment gravity flows into four ideal types, depending on the mechanism of grain support (Figure 8.1): (i) turbidity currents (grains supported by fluid turbulence), (ii) grain flows (grains supported by grain interaction, either by actual collisions betweens grains--the inertial regime--or by viscous forces produced by near approaches of grains to each other--the viscous regime), (iii) liquefied sediment flows (originally called fluidized sediment flows; grains supported by upward movement of intergranular fluid), and (iv) debris flows (grains supported by matrix strength).

The four types of sediment support mechanisms are not mutally exclusive, and it is thought that in most cases more than one mechanism is important. At different stages in the history of the same flow one or another mechanism might be dominant (Figure 8.2). For example, a mass of sediment might be liquefied, perhaps by an earthquake or by pressure surges associated with a major storm, and as it begins to flow downslope the grains are supported at first by the upward loss of pore fluid. As the liquefied mass accelerates downslope, internal shear should produce a component of dispersive pressure, though the dominant grain-support mechanism might continue to be loss of pore fluid. Further

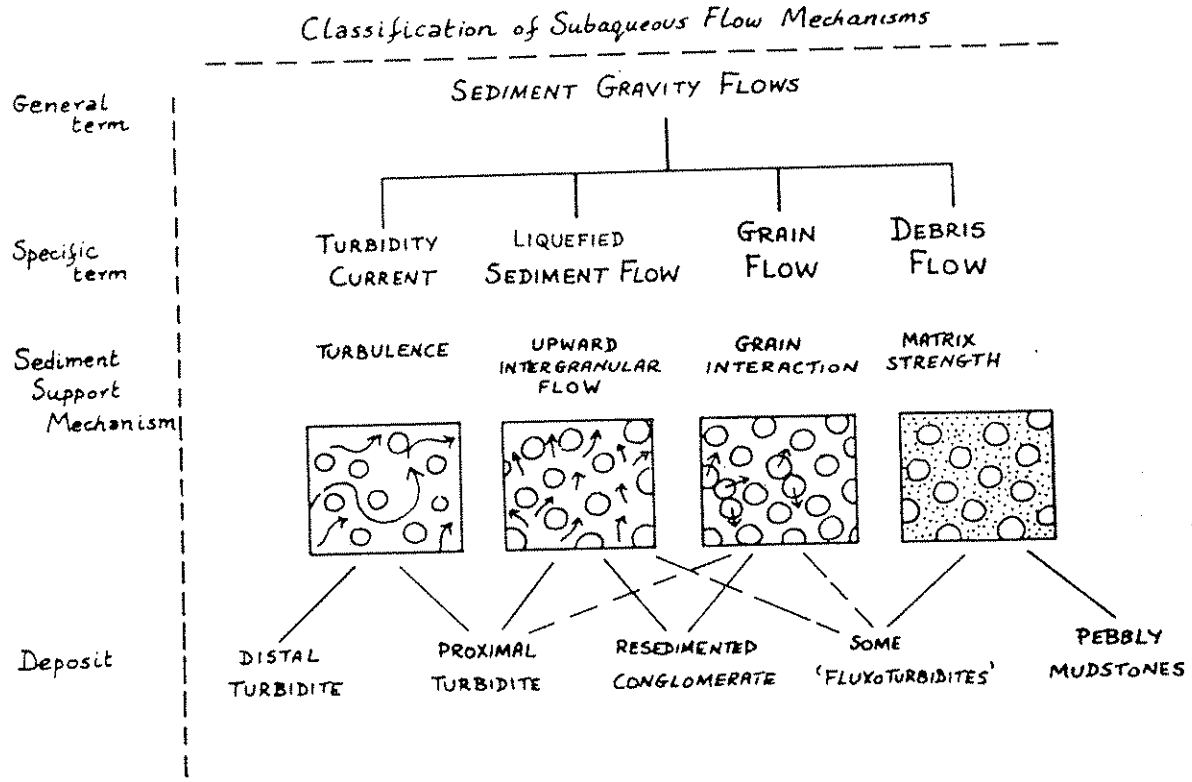

Figure 8.1 Classification of subaqueous sediment gravity flows (modified slightly from Middleton and Hampton, 1973).

acceleration might result in the moving sediment-water mass becoming turbulent, thus producing a high-density turbidity current. Mixing of water into the flow or deposition of some of the sediment (or some combination of both) might either cause a gradual dilution of the main flow to form a turbidity current of relatively low density, or it might produce a separate low-density flow associated with the original high-density flow. Conversely, as a turbidity current moves onto lower slopes and begins to slow down, the coarser sediment might become concentrated into the lower part of the flow, and with further deceleration that part of the flow might become separated by a discontinuity in size and concentration from the rest of the flow. As the lower part of the flow slows still further, it might cease to be turbulent, and in the last stages of movement, as the mass of sediment "freezes" from the bottom up, the grains might be supported mainly by the upward loss of pore fluids. In this case, therefore, the main stage of turbidity-current flow gives way, during the early stages of sediment deposition, to a transient stage of liquefied sediment flow.

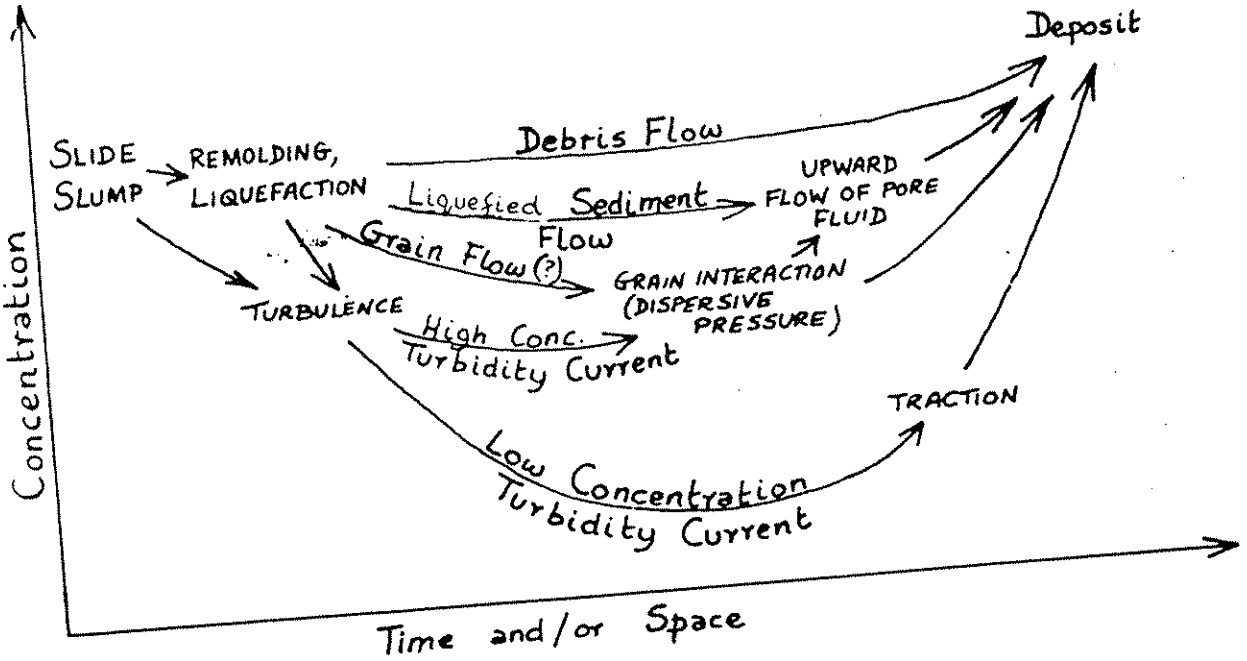

Figure 8.2 Hypothetical evolution of a single sediment gravity flow in time and space (modified slightly from Middleton and Hampton, 1973).

The type of flow prevailing during deposition of the sediment might not be the same as the type that was most important for the greater part of the duration of the flow; it might be that the preserved characteristics of the sediment bed were more strongly affected by the last few moments of flow than they were by the much longer period of flow that preceded deposition. In the same way, it has been argued in Chapter 6 that most river sand is transported most of the distance between source area and point of deposition in suspension--though sedimentary structures such as planar lamination or cross-lamination indicate that the final stage of transportation, just before deposition, was not as suspended load but as bed load or as grain flows avalanching down the slip faces of ripples or dunes.

Since the concepts and terminology of sediment gravity flows were originally systematized by Middleton and Hampton in 1973, several papers have appeared which present somewhat different terminologies for the different types of flow (Carter, 1975; Nardin et al., 1979; Lowe, 1979, 1982). Although the new classifications may have some merit, we do not believe that these papers have suggested any new fundamental mechanisms for sediment

support, besides those proposed by Middleton and Hampton (1973) and discussed briefly above. A further mechanism, not fully discussed in the original paper, is that of buoyancy, and the application of this mechanism to debris flow has been discussed by Hampton (1979) and Pierson (1981). Although no new mechanisms have been proposed, there have been substantial improvements in our understanding of the hydraulics of sediment gravity flows and in the mechanisms of highly concentrated flows such as grain flows and debris flows. We will discuss these advances briefly in the remainder of this chapter.

HYDRAULICS OF SEDIMENT GRAVITY FLOWS

To what extent does the hydraulic behavior of sediment gravity flows differ from that of fluid gravity flows like rivers, and to what extent does it depend on the mechanism of sediment support, i.e., on the specific type of sediment gravity flow? To answer this question we need to review the derivation of the main hydraulic equations given in Chapters 1 and 5.

Steady Uniform Flow

Consider first the equations for a steady uniform flow of a gravity flow of thickness d and density $(\rho+\Delta\rho)$, moving beneath a fluid of density ρ down a surface with slope S (Figure 8.3). The downslope component of gravity acting on a control volume of unit length and width is

$$F_G = \Delta\rho g d S$$

and the force of resistance is the sum of the resistance at the upper and lower boundaries of the flow:

$$F_R = \tau_o + \tau_i$$

So, for steady uniform flow

$$\tau_o + \tau_i = \Delta\rho g d S$$

We now set

$$\tau_o = \frac{f_o}{4} \frac{(\rho+\Delta\rho)U^2}{2}$$

$$\tau_i = \frac{f_i}{4} \frac{(\rho+\Delta\rho)U^2}{2}$$

(all we are doing is assuming that the shear stress at the lower and upper interface is proportional to the kinetic energy of the moving gravity flow--and we are using f/4 as the proportionality factor). We can now write an equation for the average velocity of the gravity flow:

$$U = \sqrt{\frac{8g}{f_o+f_i}} \sqrt{\frac{\Delta\rho}{(\rho+\Delta\rho)}} \sqrt{dS} \qquad (8.2)$$

$$= \sqrt{\frac{8g'}{f_o+f_i}} \sqrt{dS}\ , \quad g' = g\ \frac{\Delta\rho}{(\rho+\Delta\rho)}$$

This is the gravity-flow equivalent of the Chézy equation for rivers (Equation 5.2). In fact, it reduces to this equation if we assume that the resistance at the upper interface is negligible, $f_i = 0$, and that the density of the air above the river water is also negligible, $\Delta\rho/(\rho+\Delta\rho) = 1$, or $g' = g$. This gives the Chézy equation as in Chapter 1:

$$U = \sqrt{\frac{8g}{f_o}} \sqrt{dS}$$

$$= C\sqrt{dS}$$

The formal similarity of the equations for rivers and for gravity flows should not distract us from the fact that there may be important differences between the behavior of the two types of flows: in gravity flows, everything depends on the behavior of

the two resistance coefficients, f_o and f_i. In clear-water open-channel flows with a fixed bed, the behavior of f_o is well known: it is a constant provided the flow is turbulent, the bed is hydraulically rough, and the relative roughness d/k_s, where k_s is the height of the roughness elements, is a constant. In rivers, f_o is more difficult to predict because of the interaction between the flow and the bed material; in fact, it cannot be predicted accurately in the present state of knowledge. Bed forms produced by the flow and high concentrations of sand-size sediment moving close to the bed both modify f_o in ways not fully understood.

So before we can apply Equation (8.2) to gravity flows we need to understand how f_o and f_i vary with such factors as the main hydraulic variables (Reynolds number and Froude number) and the type and concentration of sediment in the flow. Even more fundamentally, we should ask whether the mechanism of grain support may not produce a completely different relationship between the shear stress and the kinetic energy, or average velocity of flow. We know that in ordinary open-channel flows the relationship

$$\tau_o = \frac{f}{4}\frac{\rho U^2}{2}$$

(with f roughly constant) is valid only for fully turbulent flows. For laminar flows, for example, a quite different relationship holds. Referring to Chapter 1, and integrating the equation for the velocity of laminar flow down an inclined plane, Equation (1.21), to obtain the discharge gives

$$Q = \frac{\gamma' d^3}{3\mu}$$

or

$$U = \frac{\gamma' d^2}{3\mu} \qquad (8.3)$$

$$= \frac{d\tau_o}{3\gamma}$$

In this case, therefore, the bottom shear stress is directly proportional to the average velocity, rather than to the square of

the average velocity.

For density currents due to salinity, it has been found experimentally (as might be expected) that f_o varies with Reynolds number for laminar flows but depends only on the relative roughness for fully turbulent flows moving over a rough bed. The effect of the bottom on density currents, and presumably also on turbidity currents, is therefore essentially the same as it is for rivers. The velocity distribution below the level of maximum velocity (Figure 8.3) has also been found to be logarithmic, as it is in rivers.

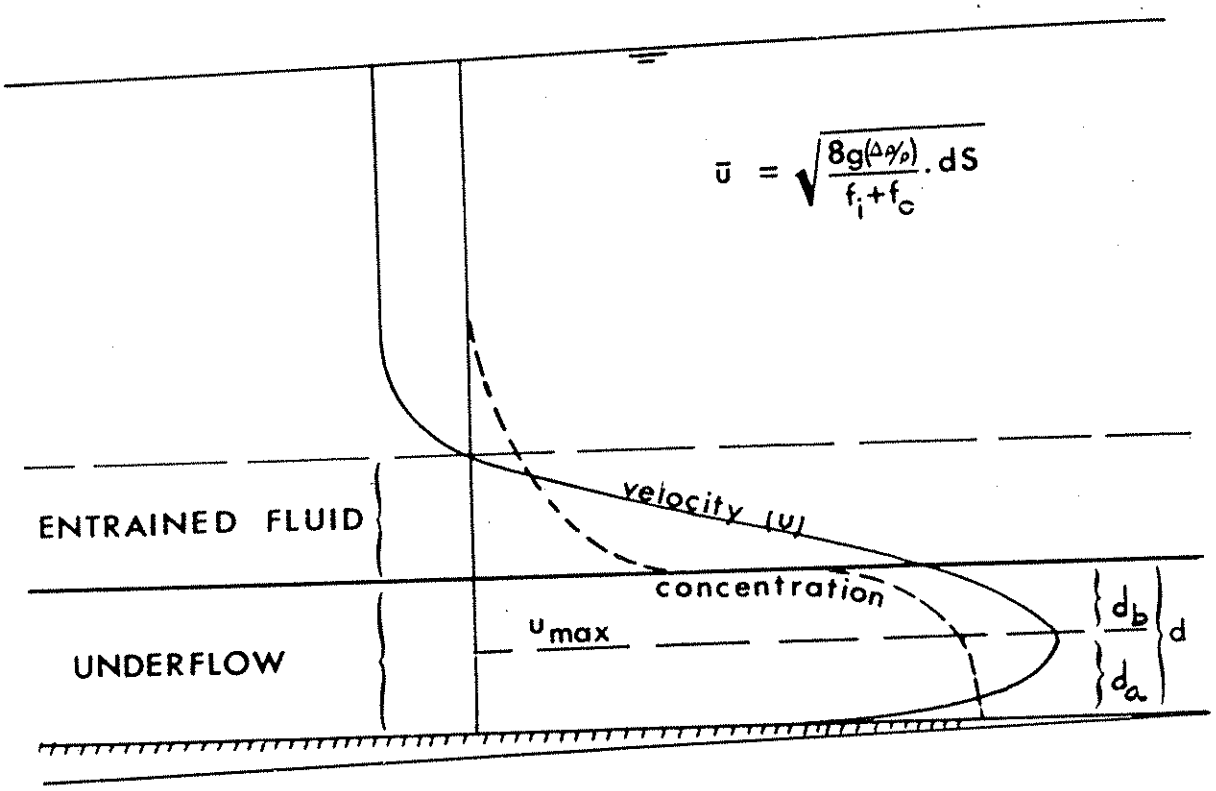

Figure 8.3 Steady uniform flow of a turbidity current.

The factors controlling f_i are more complex (for a review, see Turner, 1973; Fischer et al., 1979). The resistance at a boundary between two miscible fluids is due mainly to mixing across the boundary with resulting exchange of momentum and dragging (entrainment) of a layer of fluid just above the density interface in the direction of the flow. The resistance depends on the degree of turbulent mixing across the interface, and this in turn depends on the density contrast across the interface and on the velocity and scale of the current. The main variables can be included in a form of Froude number, called the densiometric Froude number:

$$Fr' = \frac{U}{(g'd)^{1/2}} \qquad (8.4)$$

where $g' = g(\rho_s-\rho)/\rho$. In general, experimental studies indicate that mixing and resistance (as characterized by f_i) increase as Fr' increases, but remain fairly low provided that Fr' is less than one. At Fr' ≈ 1, however, mixing and resistance increase markedly. It is thought that the Reynolds number also has some effect on f_i, though it is much less than the effect of the densiometric Froude number; f_i actually seems to decrease somewhat as the Reynolds number increases.

We can divide a gravity flow into two parts using the level at which the velocity achieves a maximum and the average shear stress falls to zero (Figure 8.3). Assuming that the density of the underflow does not depend on height above the bed (an assumption that probably corresponds only roughly to reality), then for a uniform flow the shear stress varies linearly with depth (see Chapter 1), and it follows that the ratio between the thicknesses of the upper part of the flow (d_b) and the lower part of the flow (d_a) is the same as the ratio between the shear stresses at the upper and lower boundaries, which in turn is the same as the ratio between f_i and f_o:

$$d_b/d_a = \tau_i/\tau_o = f_i/f_o$$

The velocity distribution in the lower part of the flow is logarithmic, and determined by the roughness of the bottom, but the velocity distribution in the upper part of the flow is determined by mixing at the upper interface. The same applies to the velocity distribution at the boundary of a jet of one fluid in another, and so it is not surprising to find that experimental work has confirmed that the velocity distribution in the upper parts of saline density currents (and fine-grained turbidity currents) is an exponential distribution (a Gaussian distribution), just as it is at the boundaries of jets.

If we combine Equations (8.1) and (8.2) we find

$$Fr' = \frac{U}{(g'd)^{1/2}} = \left(\frac{8S}{f_o+f_i}\right)^{1/2} \qquad (8.5)$$

from which it is clear that the main control on the densiometric Froude number is the slope. As the slope increases, the densiometric Froude number increases, and therefore so does the degree of mixing. For Fr'>1 (supercritical flow), f_i increases rapidly, and there is a great deal of mixing at the upper interface. (For large turbidity currents, we may guess that f_o+f_i will be about 0.01, so that supercritical flows might be found on quite low slopes, of the order of 0.001--the flow should certainly be supercritical in submarine canyons and on the steep parts of submarine fans.) For such flows f_i will be in larger than f_o, so the maximum velocity will be the lower part of the flow. It is expected that on steep slopes turbidity currents will tend toward some natural upper limit of Fr': as the slope becomes steep and Fr' greater than one, f_i will increase rapidly, thus tending to limit further increases in Fr' (Equation 8.5). It should also be noted that it is not strictly possible to have a uniform flow under these conditions: because fluid is being rapidly mixed into the flow, the flow becomes diluted and expands in thickness as it moves down a steep slope.

The outlines of the theory given above have been known for some time and have not been substantially modified by any recent advances. It must be remembered that it is not clear how far the concepts of boundary resistance and mixing across density gradients, which were developed and tested experimentally for Newtonian fluids, have to be modified for highly concentrated two-phase flows, so the theory can be applied only with caution to high-concentration sediment gravity flows, though it should apply pretty well to low-concentration turbidity currents. Even so, the theory simply avoids the real question (already discussed earlier in this chapter) about how sediment is entrained by or depositied from a sediment gravity flow. In a gravity flow composed of dense fluid, the density can be assumed to be constant, or solely a function of the degree of mixing with the less dense fluid (water); but in a sediment gravity flow it may also increase or decrease as sediment is eroded by or deposited from the flow.

A summary of how the basic hydraulic equations may be used to model the behavior of turbidity currents in the ocean is given by Komar (1977). It is hard to reconstruct the properties of the flow simply from a knowledge of the thickness, grain size, and geographical extent of the deposit, because too many variables (e.g., flow depth and density) remain unknown. Good examples of what can be done are provided by Stow and Bowen (1980) and Van Tassell (1981).

The Head of the Flow

A special feature of many of the sediment gravity flows of interest to geologists is that they are not strictly steady flows but rather are unsteady surges produced by some event of limited duration, such as slumping or liquefaction of sediment. A surge produced by such an event may be divided into three main regions:

(i) the head of the flow, which is advancing into still water, (ii) the body of the flow, behind the head, where flow may approximate the steady, uniform condition, and (iii) the tail of the flow, where the flow may still be approximately uniform but the thickness, and probably also the sediment concentration, is gradually diminishing (with distance from the head). As the flow moves past any one point on the bed, therefore, flow conditions will change from unsteady and nonuniform (as the head passes), to roughly steady and uniform (as the body passes), to slowly varying. Most studies have focussed on the nature of the head, where flow is expected to differ most from steady, uniform conditions.

The basic equations for surges were developed on the basis of momentum and dimensional analysis, and experimental studies on salt-water surges released from locks, by O'Brien and Cherno (1934), Keulegan (1957), and Daley and Pracht (1968). The basis for a simple momentum analysis of a surge released from a lock into a horizontal channel is shown in Figure 8.4.

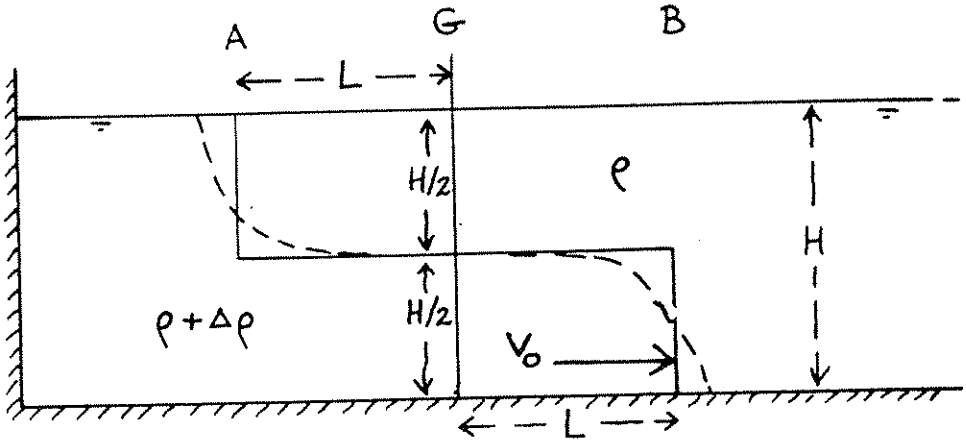

Figure 8.4 Schematic view of a gravity surge released from a lock (on the left) by removal of a gate, G. The solid line is the idealized shape of the surge, whose real shape is close to that of the dashed line.

A fluid of density $\rho+\Delta\rho$ is originally confined within a lock. The lock gate connects with a horizontal channel filled with a fluid of density ρ. The depth of fluid in both lock and channel is H. After removal of the lock gate, the denser fluid flows into the channel and forms an underflow, whose thickness is observed to be about H/2. The head of the underflow moves at an initial speed V_o.

We can obtain an expression for V_o by considering the change in potential energy (due to lowering of the center of mass of the denser fluid between sections A and B), and equating this to the

increase in kinetic energy due to accelerating two masses of fluid from rest to V_o, between sections A and B.

The column of fluid originally between A and B was 2LH, and had potential energy $(\rho+\Delta\rho)gLH(H/2) + \rho gLH(H/2)$. After the surge has moved into position, the potential energy is $(\rho+\Delta\rho)gLH(H/4) + \rho gLH(3H/4)$, so the change in potential energy is

$$\frac{\Delta\rho g L H^2}{4}$$

The kinetic energy of the surge of denser water below, and of the surge of lighter water moving above it in the opposite direction, is approximately

$$\text{kinetic energy} = 1/2\ (\text{mass})\ V_o^2$$

$$= \frac{[(\rho+\Delta\rho)LH + \rho LH]\ V_o^2}{2}$$

Equating the two and solving for V_o gives

$$V_o^2 = \frac{gLH^2}{2(2\rho+\Delta\rho)LH}$$

$$\simeq \frac{1}{4}\ \frac{\Delta\rho}{\rho+\Delta\rho}\ gH$$

So

$$V_o \simeq 0.5\left[\left(\frac{\Delta\rho}{\rho+\Delta\rho}\right)gH\right]^{1/2} \qquad (8.6)$$

Although this result has been obtained using what might seem to be rather crude approximations, experimental studies show that it fits the observations rather closely. Keulegan (1958) and Barr (1967) both made extensive studies of the effect of lock length, channel width, fluid viscosity, etc. and found that fluid viscosity reduced the initial velocity; the only modification

required was to change the constant from 0.5 to 0.46 (Keulegan) or to 0.47 (Barr).

Keulegan also found that, after the surge emerges some distance from the lock, it develops a distinct head. If the thickness of the head is h, Keulegan found that its speed V could be expressed by an equation somewhat similar to Equation (8.6):

$$V = 0.7\left[\frac{\Delta\rho}{(\rho+\Delta\rho)}\ gh\right]^{1/2} \qquad (8.7)$$

It should be noted that this equation essentially states that the densiometric Froude number for a gravity-current head moving on a level surface is a constant (0.7). Middleton (1966) showed that turbidity-current surges are very similar to those of saline water, and that the same equations describe the speed of the head.

When the head is allowed to form by releasing a steady discharge of denser fluid on a constant slope, the head grows in thickness until it moves down the slope followed by a flow that is almost uniform in thickness. The steeper the slope, the greater the thickness of the head needed to move the head at almost the same speed as the uniform flow behind it. The response of the head thickness and of the uniform-flow thickness to increases in slope are therefore different: for a given discharge, a greater slope requires a greater head thickness, though the uniform flow thins because of an increase in mean velocity.

On relatively steep slopes (greater than 0.01) the average velocity of the current behind the head was observed to be somewhat larger than that of the head itself. As the head is not observed to be increasing in volume, this implies that denser fluid is constantly being lost from the head; and this was observed to be taking place in a turbulent wake formed in the lee of the head (Figure 8.5). This observation has considerable significance for the evolution of turbidity currents, because it provides a mechanism for transferring the coarsest sediment into the head, and trapping it there until deposition takes place. Fluid plus sediment is constantly being transferred into the head, but when the mixture is lost from the turbulent wake in the rear of the head, the coarsest sediment is likely to drop back down into the body of the current and thus be recycled into the head. Simpson (1982) reported that generally about 15% of the denser fluid delivered into the head is lost in this way.

Wilkinson and Wood (1972) showed that on a very gentle slope the motion of the head is ultimately controlled by friction, and that the speed asymptotically approaches that of the uniform flow in the body of the current. This seems contrary to the analysis of Komar (1972), who thought that on low slopes the head might "outrun," and thus become thinner than, the body.

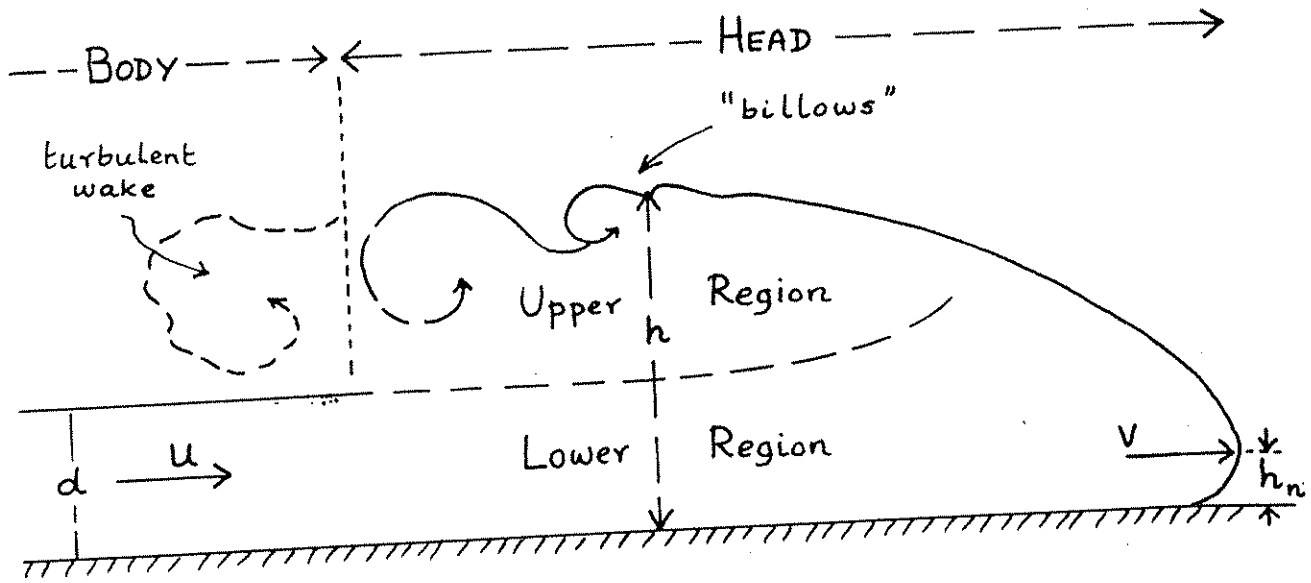

Figure 8.5 The head and front part of the body of a gravity flow. The head has a distinctive shape and a thickness h. At the front there is an overhang of height h_n. Towards the upper front of the head the interface becomes unstable and develops distinct "billows," which roll up to form large vortices that separate from the rear of the head to yield a turbulent wake. As a result the rear part of the head may be divided into two regions: (i) a lower region, which is really a continuation of the flow from the body, in which little mixing is taking place, and (ii) an upper region with intense turbulence and mixing. Dense fluid is constantly lost from the upper region, at a rate of about 15% of that supplied to the head. After Britter and Simpson (1978).

Since 1966 there have been a large number of experimental studies of gravity-current heads. The most important theoretical paper is probably that of Benjamin (1968), and the most important experimental studies are those of Simpson and his associates (Simpson, 1969, 1972; Simpson and Britter, 1979, 1980; Britter and Linden, 1980; Britter and Simpson, 1978, 1981; Beghin, Hopfinger and Britter, 1981; Huppert and Simpson, 1980). Besides their application to turbidity currents in water, these studies also have application to sediment gravity flows in air, particularly to powder snow avalanches (for an excellent review see Hopfinger, 1983). Processes operating in density-current heads (or "fronts") are also of interest to meteorologists and oceanographers, and to igneous petrologists (Irvine, 1980). As can be seen from the small selection of citations given, the literature is already too large for a short review (for a more complete review see Simpson, 1982). In what follows, we will just pick out a few highlights of the recent results.

Gravity-current heads are observed in the laboratory to have a distinct overhang at the front, due to friction at the bed (viscous effects) (Figure 8.5). The overhang implies that the current overrides some of the lighter fluid, and Allen (1971) hypothesized that this fluid would be mixed into the current and would have an important effect in diluting the current. Simpson (1972) showed experimentally, however, that the degree of overhang decreases as the scale of the current increases: if the height to the overhang is h_n, then

$$h_n/h = 0.61\ Re^{-0.23}$$

For laboratory flows where $Re \approx 10^4$ the overhang is of the order of 10%, but for large natural flows it might be much less (though Simpson and Britter, 1980, suggest that a limiting value of 12% is consistent with some atmospheric data.) By moving the floor of the flume at the same speed as the head, Simpson was able to eliminate the overhang completely and determine the angle between the base of the head and the boundary. This should be the same angle that would be observed if viscosity was not important. The angle was $\pi/8$, not $\pi/3$ as had previously been predicted by von Kármán (1940) and Benjamin (1968). It should be noted, however, that Daley and Pracht (1968) claimed to have confirmed von Kármán's result by numerical simulation of an inviscid flow.

Not only did use of a moving floor eliminate the overhang of the head, it also made the head almost two-dimensional. Normally, the head is observed in experiments to have a distinct three-dimensional structure, with distinct lobes separated by clefts. Simpson (1972) found that the distance b between clefts is related to the head thickness and Reynolds number by

$$b/h = 7.4\ Re^{-0.39}$$

The lobe-like nature of the head, therefore, also becomes somewhat less important at larger scales. Observations of dust storms and inferences from mapping current marks and tool marks cut by the heads of turbidity currents suggest, however, that the lobe-like shape of the head remains well developed even in large natural flows.

One question is how Equation (8.7) might be modified by flow on a slope. Middleton (1966) found little effect experimentally up to slopes of 0.04. A small effect was reported by Daley and Pracht (1968) in their simulation experiments. Britter and Linden (1980) found that for a constant downslope flux of heavy fluid, Q, the head velocity was constant for slopes greater than 0.01, and for slopes steeper than 0.09 was given by

$$V = 1.5\left(\frac{\Delta\rho}{\rho}gQ\right)^{1/3} \qquad (8.8)$$

When a surge is released in a channel, the main body of the fluid behind the head is contained in a "slug" which is actually formed by the reflection of the surge of lighter fluid from the back wall of the lock. This wave or slug eventually overtakes the head at a distance of about 10 lock lengths from the start of the surge (Simpson, 1982). This is a special example of a gravity current with a variable inflow, for which some more general results have been given by Maxworthy (1983). If the flow rate is suddenly increased, solitary waves are formed behind the head, and eventually overtake it.

One geometry of flow that may have considerable geological importance is the emergence of a gravity flow from a channel onto a flat or slightly sloping surface (as would be expected at the mouths of distributary channels on submarine fan surfaces). Most of the attention by mechanicians has been given to spreading of dense fluids in all directions away from an initial cloud (Beghin et al., 1981). This is also of interest in geology, but mainly for application to pyroclastic flows (movement of ash clouds, base surges, etc.). Luthi (1981) describes some model experiments on unconfined turbidity currents moving down a slope of 5°, but there seems to be plenty of scope for further studies of this sort. This is the type of flow described by Bates (1953) as hyperpycnal jets, but it has been little studied by engineers or those interested in deltas.

Gravity flows display a great variety of phenomena--in fact, a wider variety of phenomena than those shown by ordinary free-surface flows. For further information the reader should consult the books by Turner (1973) and Yih (1980).

SPECIAL FEATURES OF HIGH-CONCENTRATION FLOWS

Introduction

All four of the types of sediment-support mechanisms distinguished by Middleton and Hampton (1973) might theoretically operate when sediment is present at very high concentrations. In addition, such high concentrations are generally thought to be a necessary condition for liquefied sediment flow, grain flow, or debris flow.

The basic problem presented by the flow of very highly concentrated sediment-fluid mixtures can be simply stated in terms of the familiar Navier-Coulomb criterion for yield of a granular material (e.g., Jaeger, 1971):

$$\tau_c = C + (\sigma - p)\tan\alpha \qquad (8.9)$$

Here τ_c is the critical shear stress needed for failure (i.e., flow), C is the cohesion, σ is the normal stress, p is the pore pressure, and α is the angle of internal friction. The quantity σ-p is called the effective normal stress, and is generally the total stress minus the hydrostatic pressure, or in other words the stress due to the submerged weight of the grains. It follows from Equation (8.9) that if the cohesion is small the angle of slope down which a flow of grains is possible is the same as the angle of internal friction. It makes no difference whether flow takes place in a vacuum, in air, or in water. The only factors that can make a flow possible at angles substantially lower than the angle of internal friction are (i) the presence of fluid between the grains that is denser than the fluid overlying the flow, or (ii) addition of a shear stress not due simply to the downslope component of the weight of the grains themselves. These factors were discussed at length by Middleton (1970b). For subaerial flows the first factor can reduce the angle required for flow from the normal internal friction angle of about 30° to 10-15°, but a corresponding reduction is not possible for subaqueous flows.

There seem basically to be three ways around this problem:

(i) We can increase the pore pressure, so that it approaches the total pressure. In general such a high pore pressure is soon dissipated by flow of the fluid out of the pores. Nevertheless, it may be possible for a significant flow to take place before the pore pressure is lost, particularly if a substantial thickness of sand is involved (for then a correspondingly large volume of fluid must be lost from the pores to restore hydrostatic pressure). This is the basic mechanism for liquefied flows.

The fluid may be prevented from flowing out of the pores if it is made sufficiently viscous or cohesive, by mixing in substantial quantities of mud. In this case the critical angle for flow is determined largely by the cohesion and strength (effective pressure times the friction coefficient) of the mud, while the larger grains in the flow are transported by a combination of the strength of the mud (which opposes settling of the large grains) and buoyancy. The buoyancy force acting on a large grain is that which results not just from the displaced fluid, but from the displaced fluid-sediment mixture (Hampton, 1979; Pierson, 1981). As the grains may be only a little more dense than the mixture, very large grains (boulders even) may be transported by this mechanism. This is the Johnson-Hampton hypothesis for explaining both subaerial and subaqueous debris flows.

(ii) It might be that, as the concentration of grains decreases, there is a decrease in the angle of internal friction, or even a complete change in the nature of the relationship between deformation and effective stress. It was, however, proposed by Bagnold (1954, 1956, 1973) that this does not happen, and that the relationship between effective normal stress (which Bagnold calls "dispersive pressure") and shear stress continues to be related to the angle of internal friction of the grains, down to concentrations at least as low as 9% by volume. In Bagnold's terminology and notation, Equation (8.9) is replaced by

$$T = P \tan\alpha \qquad (8.10)$$

where T is the shear stress transmitted by the grains and P is the dispersive pressure normal to this shear stress.

(iii) The third way to reduce the angle required for flow is to reduce the angle of internal friction, by mechanisms that are not generally well defined. The mobility of large avalanches, not only on earth but also on Mars and even on the Moon, appears to require that there be some way of doing this that does not depend on the presence of a fluid to provide liquefaction or a lubricating "cushion" beneath the avalanche (Hsu, 1975).

Recently a substantial number of workers have begun to study the flow of highly concentrated grain dispersions and to construct new models of the flow behavior (rheology) of such mixtures. These theories have not yet been developed far enough to solve the types of problems that interest sedimentologists, but there is little doubt that future solutions of such problems will have to make use of such theories. We cannot discuss them in detail in these notes but will give the main references and indicate briefly some of the basic physics on which they are based.

Liquefied Sediment Flows

The distinction between liquefaction and fluidization, as well as some of the properties of liquefied sediment, were discussed in Chapter 4. To develop hydraulic equations for flows of liquefied sediment, the main question is: what is the rheological equation relating shear stress to velocity for such flows?

Experiments on highly concentrated mixtures of sand and water have shown (Davidson et al., 1977) that these mixtures generally behave like fluids with greatly increased viscosity but little or no shear strength (i.e., like Newtonian fluids). For high concentrations (greater than 10%) Roscoe (1953) gave a semi-empirical equation relating the ratio between the viscosity of the sediment dispersion μ_s and the viscosity of the grain-free fluid μ to the volume concentration C of (well sorted) grains:

$$\mu_s/\mu = (1 - 1.35C)^{-2.5} \qquad (8.11)$$

This equation gives viscosity ratios of about 15 for volume concentrations of 50%. Higher values are to be expected as concentrations approach the limiting value of about 55% (freshly deposited sands have a porosity of about 45%), and there are also departures from Newtonian behavior at very high concentrations.

The question of the effective viscosity of highly concentrated sand-water mixtures is important, because it bears on the question of whether or not liquefied sediment flows are likely to remain essentially laminar or become turbulent and be transformed into highly concentrated turbidity currents. For Newtonian fluids the criterion defining the onset of turbulence is the Reynolds number (Chapter 3). Defining the Reynolds number for a gravity flow as

$$Re = \frac{\rho U d}{\mu_s}$$

the critical value for the transition from laminar to turbulent flow is close to that for open-channel flows (about 500 or a little larger; Harleman, 1961). It is clear, therefore, that even if we allow for an increase in viscosity by a factor of 100 times (to 1 poise), the critical Reynolds number is exceeded when the product of average velocity and depth exceeds 500 cm^2/s. This will obviously be the case even for flows that are of quite small scale.

Thus we may conclude that it is very unlikely that large liquefied sediment flows can move down any substantial slope (such as found typically in submarine canyons or on the upper parts of submarine fans) without becoming turbulent. After the flow has become fully turbulent, there is no reason to suppose that the hydraulics will differ substantially from that of other less concentrated turbidity currents.

A further question is whether or not there is any minimum slope necessary for the continued movement of a liquefied sediment flow. If the sediment dispersion behaves like a true Newtonian fluid, then it is capable of flow down any slope, no matter how small. But it may be expected that highly concentrated sand-water mixtures will not be perfect Newtonian fluids but will instead show some properties like those of debris flows or grain flows (see discussion below). Nevertheless, field observations (summarized in Middleton, 1969; Lowe, 1976a) indicate that flow of liquefied sand is certainly possible on slopes as low as three degrees (slopes of 0.05).

Most of the work done recently on liquefaction has been on the conditions necessary for the liquefaction of sands by earthquakes and wave action (e.g., Seed et al., 1978; Dalrymple, 1979). The concept of liquefaction and the associated landsliding mechanisms have been used to explain the slope morphology of the Mississippi and other deltas (Bouma, 1981).

Grain Flows

Bagnold (1956) gave a theoretical derivation of equations for the shearing of grain dispersions in a fluid, based upon highly simplified models. He distinguished two different regimes: (i) In the viscous regime, dispersive pressure is produced by viscous forces due to near approaches of the grains to each other (with or without actual touching of the grains), so that the viscosity of the fluid is important but the density of the grains is not. The basic relationships he derived are more easily obtained by dimensional analysis. (ii) In the inertial regime, dispersive pressure is produced by actual collisions between the grains, and the presence of the fluid has little effect.

For neutrally buoyant particles in the viscous regime, the important parameters are the shear stress τ. the viscosity of the fluid μ, the rate of shear dU/dy, the diameter of the particles D, and the average spacing of the particles S (a measure of the volume concentration, with the dimensions of length). In Bagnold's notation, which is here followed as closely as possible, script letters are parameters that depend on both grains and fluid, capital letters are parameters that depend only on grains, and lower-case letters are parameters that depend only on the fluid.

Dimensional analysis gives

$$\mathcal{T} = f(\mu,\ dU/dy,\ D,\ S)$$

$$f\left(\frac{\mu \dfrac{dU}{dy}}{\mathcal{T}},\ L\right) = 0$$

where $L = D/S$ is a dimensionless measure of concentration. Bagnold found experimentally that the actual form of the function was

$$(\mu\ dU/dy)/\mathcal{T} = 0.445\ L^{-3/2} \qquad (8.12)$$

In the inertial regime the viscosity can be neglected but the density of the grains must be considered, giving

$$T = f(\rho_s,\ D,\ S,\ dU/dy)$$

$$f\left[\frac{D^2\left(\frac{dU}{dy}\right)^2 \rho_s}{T},\ L\right] = 0$$

and from experiments, Bagnold found that the form of the function is

$$\frac{\rho_s D^2 \left(\frac{dU}{dy}\right)^2}{T} = \frac{77}{L^2} \qquad (8.13)$$

The shear stress T transmitted by the grains is related to the dispersive pressure P (also transmitted by the grains) by the equation

$$T = P \tan\alpha$$

where α is an angle of internal friction. Originally Bagnold stated that $\tan\alpha$ is 0.75 in the viscous regime but could be as low as 0.32 in the inertial regime. More recently he has stated (Bagnold, 1973) that he now believes that he was misled by his experiment on spherical grains (which have a lower angle of internal friction than natural grains) into thinking that the values for spheres applied generally, and that the correct value for natural sand grains in the inertial regime is the same as the value obtained from "angle-of-repose" experiments, that is, $\tan\alpha = 0.63$.

A dispersion that responds to shear in the way described by Bagnold's theory can itself be regarded as a "fluid" (this is what is meant by describing such theories as continuum models), but the fluid the equation describes has markedly non-Newtonian properties. For example, in the inertial regime the shear stress is proportional to the square of the rate of shear, and also to the square of the grain size and concentration. Equation (8.13) has the form

$$T = (\text{coefficient})\ (dU/dy)^2$$

which may be compared with the equation for a Newtonian fluid:

$$\tau = \mu(dU/dy)$$

or, looking ahead, with the equation of a Bingham plastic, which is used in the Johnson-Hampton model of debris flows:

$$\tau = \tau_c + \mu_s(dU/dy)$$

If we are willing to assume that the coefficients do not change with depth--and for grain flows this means making the rather large assumption that grain size and concentration do not vary vertically in the flow--then we can use these three equations to derive the velocity distribution in grain flows or debris flows, in the same way that we derived the velocity distribution for a viscous fluid in Chapter 1 (p. 1-23 to 1-24). For inertial grain flow the velocity distribution has the form

$$\frac{U_{max} - U}{U_{max}} = 1 - \frac{U}{U_{max}} = \left(1 - \frac{y}{d}\right)^{3/2}$$

For a Bingham plastic the velocity distribution has the same form as for a viscous fluid (with μ_s substituted for μ) up to that value of y where the shear stress becomes equal to the strength of the plastic. Above this no shearing of the debris can take place and the velocity therefore remains constant. The three velocity distributions are compared in Figure 8.6 (in this figure it is arbitrarily assumed that the strength of the Bingham plastic is exceeded only at $y/d < 0.4$). For comparison, a typical logarithmic velocity profile in turbulent flow (calculated assuming a rough bed and $U_{max} = 25u*$) is also shown.

In calculating all of these profiles the no-slip condition has been assumed, i.e., $u = 0$ at $y = 0$. This is known to be correct for true fluids (whether in viscous or turbulent flow), but it is not clear that it is always the case for grain flows or debris flows. We would actually expect some slip at the boundary for a dispersion of grains flowing over a smooth boundary.

The equations relating shear stress and rate of deformation, which were used to calculate the velocity profiles shown, are examples of constitutive equations. The science of rheology concerns itself with the correct formulation of such equations; the subject is a complicated one, as can be quickly discovered by referring to any text that considers in detail the problems involved in the formulation of the full constitutive equations for even such a simple substance as a Newtonian fluid.

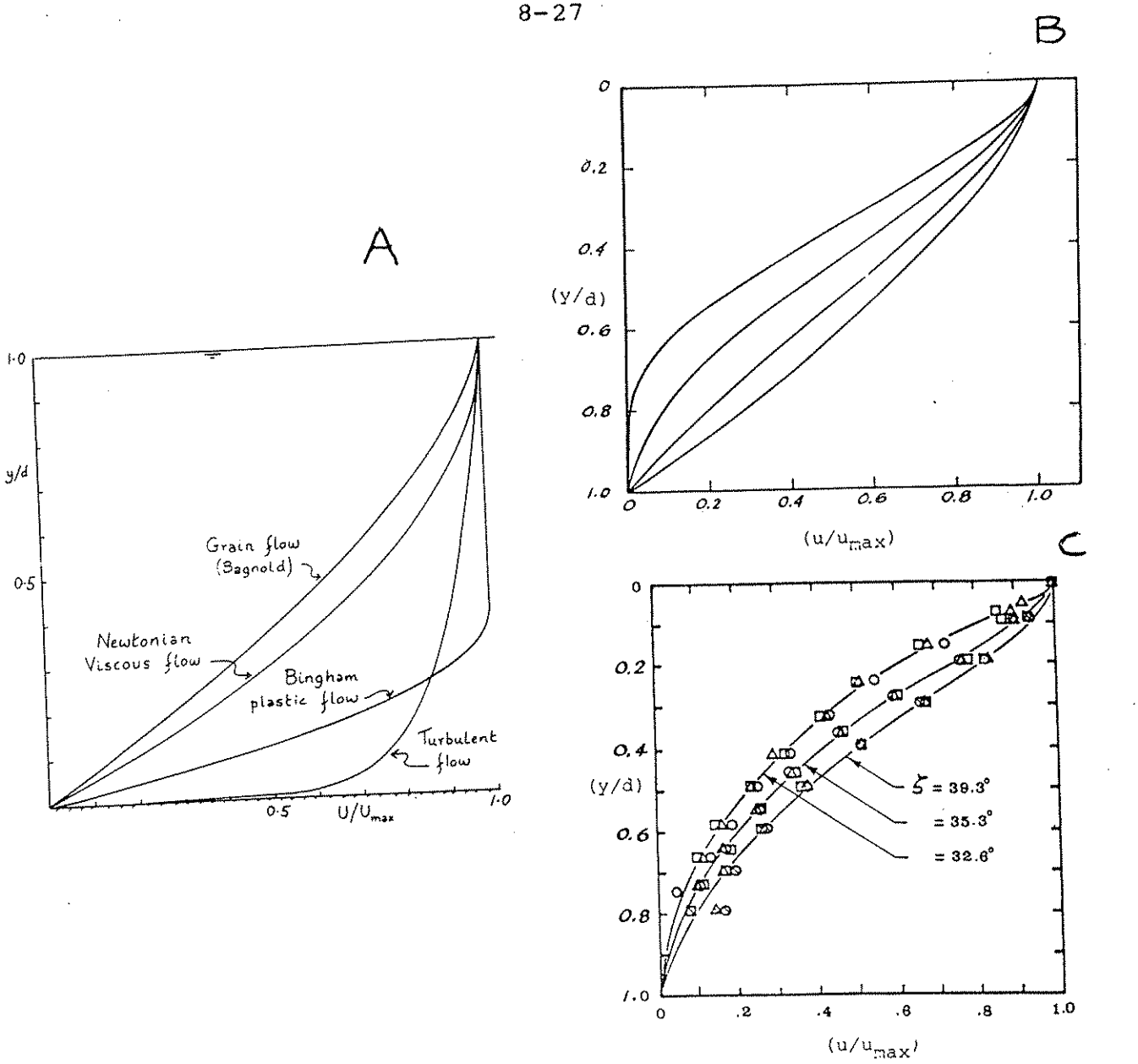

Figure 8.6 Nondimensional velocity profiles for grain flows, compared with those for other types of flows. A. Grain-flow velocity profile derived from Bagnold's theory (inertial regime) compared with profiles for viscous fluid, turbulent fluid, and Bingham plastic (see text). B. Theoretical grain-flow profiles from Savage (1979): the top curve is for no variation in concentration through the flow, and the other curves are increasing concentration gradients. C. Observed profiles for flow down chutes inclined at angles of 32.6°, 35.3°, and 39.3°. In A, y is measured up from the base of the flow, and in B and C it is measured down from the top of the flow. In A, the highest rates of shear in all types of flows are at the bed. In B and C, because of the boundary conditions, they are found in the upper part of the flows.

(Equation 1.5 is a much simplified version of the full equations, applicable strictly only to two-dimensional flows.)

Formulation and testing of the correct constitutive equations for grain flow is currently an active field of research by several workers. The most important recent advance is the work of Savage (1979, 1982; Savage and Jeffrey, 1981; Savage and McKeown, 1983; Jenkins and Savage, 1983; see also Haff, 1983, and references cited in these papers). Savage's work was inspired by the practical problems of the flow of granular solids in chutes, hoppers, and bins. His 1979 paper contains a very thorough review of previous engineering studies of these phenomena. His work, however, deals with the general form of the flow equations, taking the up the problem essentially where Bagnold's work stops. All the theoretical work has been directed towards flows in Bagnold's inertial regime. The main result has been to develop generalized constitutive equations and test them by determining experimentally the types of velocity distributions and other flow phenomena that can be predicted from the equations.

Several different forms of the constitutive equations have been developed. At first the form of the equations was based on assumptions which are difficult to test directly, and whose physical significance was not clear. In later theoretical developments attempts have been made to derive the form of the constitutive equations more or less directly from a physical model of collisions between grains in a sheared dispersion (Savage and Jeffrey, 1981; Jenkins and Savage, 1983). The theory is still in a state of development, and as it stands does nothing to resolve the basic geological problem: according to Savage's theory, grain flows should not be able to flow down slopes less than the angle of internal shearing of the grains. It is not predicted that this angle decreases markedly at high shear rates.

In the flow of granular solids in the inertial regime there is a much closer analogy between the grains and molecules of an ideal gas (in the statistical theory of gases) than there was between fluid particles and molecules in the "mixing-length" theories of turbulence originally developed by Prandtl (and now of historical significance only). Some of these analogies have been explored by Haff (1983). He suggests, in particular, that an important dependent variable, besides the mean flow velocity, is the mean random fluctuating velocity of an individual grain. This is analogous to the thermal velocity of molecules in the statistical theory of gases. An important difference between molecules and grains is that grains can never be fully elastic, and because of this, processes that depend on the transmission of "thermal" vibrations are much more rapidly damped out in grain flows than they are in gases.

From this model of a grain flow it is also possible to deduce the acoustic velocity, i.e., the speed at which sound or other vibrations will be transmitted through the grain dispersion. The speed is quite slow, because it depends mainly on the time

taken for grains to travel the distance S between grains. If v is the "thermal" velocity of the grains and D is the diameter of the grains, then the speed of sound, C, is given by

$$C \propto v \frac{D}{s}$$

From this it can be deduced that most grain flows move at supersonic speeds. This may have hitherto unexplored consequences for the nature of these flows.

Melosh (1979, 1983) has proposed, as a solution to the problem of apparent high grain-flow mobility on low slopes, a mechanism he calls "acoustic fluidization." The term is unfortunate, as the mechanism has nothing to do with support of grains by an upward flow of interstitial fluid. For this reason we will substitute the term acoustic mobilization of grain flows. The mechanism involves grain vibrations similar to those Haff (1983) calls intense "thermal" velocities of the grains, but there is a difference. In acoustic mobilization it is assumed that the grains are so close together that the vibrations are transmitted directly through grains in contact with each other, rather than by grain collisions (Figure 8.7). Acoustic energy originally transmitted to the debris, by some initial catastrophic event, is assumed to be lost at a rate low enough to permit the flow to take place while the weight of the grains is essentially supported by sound waves propagating through the solid grains themselves. If this mechanism for grain support is confirmed by further work it should perhaps be considered as a new, fifth mechanism, in addition to the four originally proposed by Middleton and Hampton (1973). Perhaps the two mechanisms are not really as distinct as Melosh proposed: perhaps grain flows tend to become more mobile as the "thermal" velocity of the grains increases. The pressure of a gas increases as the thermal velocity of the molecules increases, and although the viscosity also increases, it does not do so to the same extent. Pressure exists even if the gas is not sheared. Similarly one might hypothesize that grains might be supported for a while by "thermal" vibrations not directly related to collisions produced by shear.

Debris Flows

The work of Johnson (1970) and Hampton (1972, 1975) made it clear that many of the features of some subaerial debris flows can be explained by the assumption that the sediment-water mixture has properties approximated by an ideal (Bingham) plastic. For such a substance the shear stress is related to velocity by an equation of the type

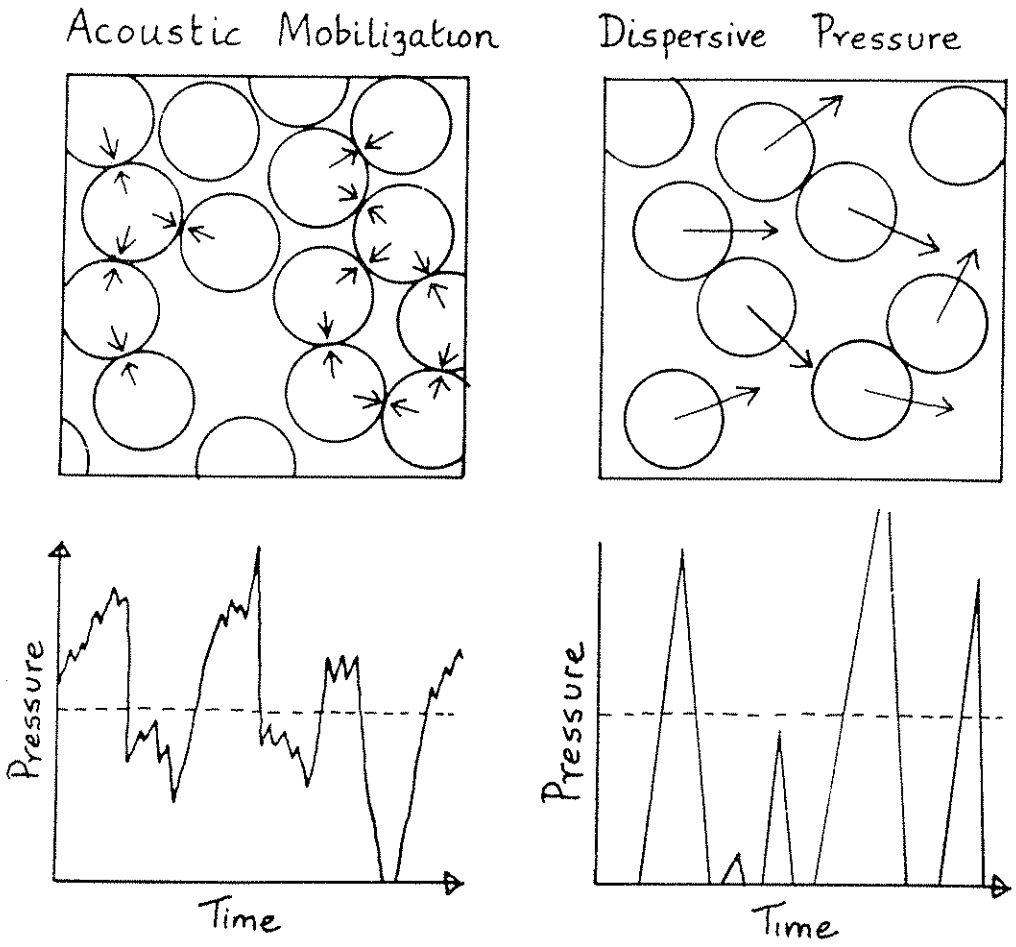

Figure 8.7 Acoustic mobilization (left) compared schematically with dispersive pressure (right). In acoustic mobilization, sound waves are transmitted through the debris, from contact to contact of grains, causing the pressure to fluctuate about a value large enough to support the weight of the grains above. In dispersive pressure, shearing of the grain dispersion produces grain collisions, which support the weight of the grains. After Melosh (1983).

$$\tau = \tau_c + \mu_s \frac{dU}{dy} \qquad (8.14)$$

where τ_c is the critical shear stress that must be exceeded before any deformation (and therefore flow) is possible and μ_s is the viscosity of the sediment-water mixture. The model may be made

more explicit by assuming that the critical shear stress is made up of two components, a cohesion component (due to the presence of fine-grained cohesive clay particles in the matrix of the flow) and a component related to the internal normal effective stress equation of the type given earlier (Equation 8.9); the resulting model is called a Coulomb-viscous model.

It seems clear from observation of subaerial debris flows that such flows are capable of movement at speeds up to several meters per second. Flows are generated on slopes that are commonly steeper than 10° but can extend out onto slopes as low as one or two degrees (0.015 to 0.05). In most observed cases flow is laminar rather than turbulent.

The peculiar flow properties of some debris flows result from the presence of a fine-grained matrix. The fine particles have two important functions: (i) They impart a very high viscosity to the muddy matrix; because of this the matrix is not easily lost from the pore spaces between the larger particles. The high viscosity of the matrix also gives average flow velocities that remain moderately low, even for relatively large-scale flows (too low to produce a transition to turbulent flow). (ii) The muddy matrix has high cohesion and therefore sufficient strength to support the larger grains in the flow. Depending on the combination of matrix strength and dispersive pressure, grains as large as boulders may be transported, even by flows that are traveling quite slowly. The larger grains are not necessarily concentrated near the base of the flow, and in fact they may even project out of the matrix at the top of the flow, so long as the total gravity force acting on them (gravity minus buoyancy) is not greater than the strength of the matrix beneath the grain.

For a Bingham plastic the transition from laminar to turbulent flow depends not only on a Reynolds number but also on the Bingham number

$$B = \frac{\tau_c d}{\mu_s U} \qquad (8.15)$$

The critical relation is displayed in Figure 8.8. (Hampton, 1972, gives a full discussion of this diagram; his version is marred by a mistake in labeling the two scales.) From inspection of Figure 8.8 it is seen that, for Bingham numbers as large as 100, well within the range of possible values for natural debris-flow materials, the critical Reynold numbers rises as high as 50,000. The experimental data are not abundant and do not extend to very large Bingham numbers, but it appears that at large Bingham numbers the boundary between laminar flow and turbulent flow approximates the relationship

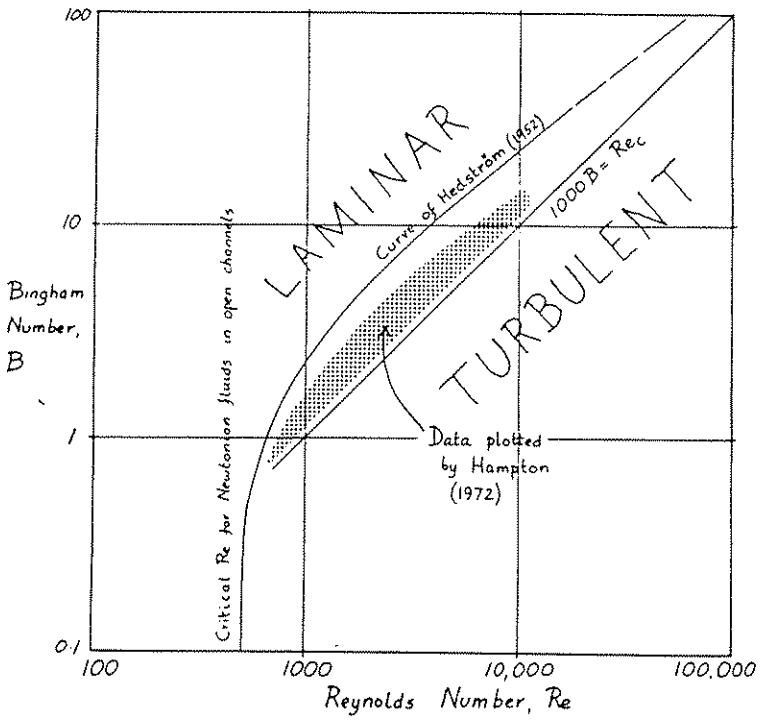

Figure 8.8 Relation of Bingham number to critical Reynolds number for turbulence in a Bingham plastic. Based on Hampton (1972). Experimental data are for pipe flow, but scales have been adjusted to the correct values for turbidity currents, using the thickness of the flow as the length scale.

$$1000\ B = Re_c$$

which is equivalent to the condition for turbulence

$$\rho U^2/\tau_c > 1000 \qquad (8.16)$$

(see also Enos, 1977). Hiscott and Middleton (1979, p. 319) have suggested that this dimensionless number should be called the Hampton number. (It is interesting that this criterion does not include the viscosity or the flow thickness.)

So for typical shear strengths of 10^4 dynes/cm^2 (see Johnson, 1970, for determination of shear strength of some natural debris flows), turbulence would not begin until the flow reached speeds in excess of 3 m/s. Using Equation (8.7) Sharp and Nobles (1953) estimated the viscosity of two observed debris flows to be about 10^4 poise. Using a more conservative value of 10^3 poise and applying Equation (8.3) suggests that these velocities might be reached on relatively steep slopes (0.05) by subaerial flows thicker than about 1.5 m. For subaqueous flows somewhat

greater thicknesses would be required. These calculations are necessarily only very rough, because the properties of large submarine debris flows can only be very roughly estimated. They are sufficient to show that small-scale and medium-scale debris flows are probably laminar but that it is likely that large-scale flows might be at least partly turbulent.

Laminar debris flows will exhibit the phenomenon of a "rigid plug" in the interior of the flow. There will necessarily be a region within a subaqueous debris flow where the shear stress falls below the strength of the debris. The debris in this central part of the flow will therefore not deform, but will be carried along by the flow as a rigid plug.

Up to this point we have assumed that subaqueous debris flows will have properties similar to those of subaerial debris flows. It is to be expected, however, that many sediment gravity flows will contain some fine-grained material and will therefore have a watery "matrix" with some strength, even though the concentration and therefore the strength will be much less than those exhibited by the more spectacular subaerial debris flows. Hampton (1975) has argued that a flow with less than 10 percent by weight of clay might have sufficient strength to support sand grains, and thus to form fine-grained (sandy) submarine debris flow.

Hampton (1975) presented data showing that sea water with only 15% kaolinite was competent to support sand grains up to 0.5 mm in size. Such a clay-water matrix has a strength of only about 10 dynes/cm^2, and a viscosity only a few times larger than that of water. It is clear, therefore, that even relatively small flows (for example, about one meter in thickness) will easily reach velocities sufficient to cause turbulence (for example, velocities of about one meter per second) on the slopes typical of submarine canyons. Once turbulence is initiated it will spread throughout the flow and eliminate any rigid plug that may have been formed in the center of the flow: in a turbulent flow, the <u>average</u> shear stress still falls to zero at the level of the velocity maximum, but the actual shear stress varies widely as a result of the penetration of large eddies into the central part of the flow. Flows with a low concentration of mud in the "matrix" are therefore unlikely to travel down steep submarine slopes as laminar debris flows, but they may revert from turbulent turbidity currents to laminar debris flows as they move away from the steeper, channelized parts of submarine fans to the flatter distal parts of fans or basin plains.

It is interesting to note that a Bingham-plastic model for low-density turbidity currents (in Lake Mead) was developed as early as 1941 by Einstein. His suggestion was not followed up at the time, probably because subsequent experiments showed that low-density, fine-grained turbidity currents (composed of clay suspensions) were fully turbulent throughout, and did not display

the central rigid plug that Einstein predicted. But Einstein's idea might still have some validity for small-scale flows with a high concentration of fine cohesive sediment.

It should be noted that a turbulent muddy gravity flow that is also carrying a substantial load of sand has some properties in common with both turbidity currents and debris flows. As the hydraulic properties would be mainly determined by the turbulence, such a flow should be called a turbidity current. But turbulence would not be the only mechanism supporting the coarser (sand) grains, since Hampton's experiments have shown that the muddy matrix retains some strength even while it is being sheared. The result would be damping of the small-scale, high-frequency part of the turbulence spectrum and retention of sand in dispersion, held up by the strength of the matrix, even if the intensity of the turbulence in the flow was too low to support it.

The main problem with the theory outlined above is that many observed modern subaerial debris flows, and not a few suspected ancient submarine debris flows, lack an essential ingredient of the Johnson-Hampton model, namely a substantial amount of fine-grained, cohesive matrix. Some of the best-documented examples have been described by Japanese workers, who have made careful studies of modern active debris flows by setting up remotely controlled instrument networks in steep gullies where debris flows are known to occur frequently (see for example Okuda et al., 1980). The main theoretical analysis has been by Takahashi (1978, 1980, and see his review paper, 1981). Takahashi regards many debris flows as being flows in which not only matrix strength and buoyancy but also grain interactions support the grains. In fact, for most cases Takahashi finds that Bagnold's theory (Equation 8.12) explains the observed characteristics of Japanese debris flows better than the Johnson-Hampton model does. It nevertheless remains true that the Takahashi-Bagnold theory has difficulty explaining the movement of debris flows on slopes less than about 10-15°, unless they are driven by an overlying stream flow.

In summary, geological evidence and even direct observation in the case of some subaerial debris flows and rock avalanches suggests that highly concentrated grain dispersions can flow considerable distances on slopes as low as a few degrees. In spite of recent advances in the theory of grain flows and debris flows, the explanation of this phenomenon is still not clear.

REFERENCES

Abbott, J.E., and Francis, J.R.D., 1977, Saltation and suspension trajectories of solid grains in a water stream: Philos. Trans. Roy. Soc. London, 284, 225-254.

Adams, C.E., Jr., and Weatherly, G.L., 1981, Some effects of suspended sediment stratification on an oceanic bottom boundary layer: J. Geophys. Res., 86, 4161-4172.

Allen, J.R.L., 1965, Sedimentation to the lee of small underwater sand waves; an experimental study: J. Geol., 73, 95-116.

Allen, J.R.L., 1968a, Current Ripples; Their Relation to Patterns of Water and Sediment Motion: Amsterdam, North Holland, 433 p.

Allen, J.R.L., 1968b, The diffusion of grains in the lee of ripples, dunes, and sand deltas: J. Sed. Petrol., 38, 621-633.

Allen, J.R.L., 1970, A quantitative model of climbing ripples and their cross-laminated deposits: Sedimentology, 14, 5-26.

Allen, J.R.L., 1971, Mixing at turbidity current heads, and its geological implications: J. Sed. Petrol., 41, 97-113.

Allen, J.R.L., 1982, Sedimentary Structures; Their Character and Physical Basis: Amsterdam, Elsevier, 2 vols.

American Society of Civil Engineers, Task Committee on Preparation of Sedimentation Manual, 1962, Introduction and Properties of Sediment: Proc. Am. Soc. Civ. Eng., J. Hydraul. Div., 88(4), 77-107.

American Society of Civil Engineers, Task Committee on Preparation of Sedimentation Manual, 1963, Suspension of Sediment: Proc. Am. Soc. Civ. Eng., J. Hydraul. Div., 89(5), 45-76.

Antonia, R.A., and Luxton, R.E., 1971, The response of a turbulent boundary layer to a step change in surface roughness, Part 1, smooth to rough: J. Fluid Mech., 48, 721-761.

Antsyferov, S.M., and Kos'yan, R.D., 1980, Sediments suspended in stream flow: Proc. Am. Soc. Civ. Eng., J. Hydraul. Div., 106, 313-330.

Ashley, G.M., Southard, J.B., and Boothroyd, J.C., 1982, Deposition of climbing-ripple beds: A flume simulation: Sedimentology, 29, 67-79.

Baba, J., and Komar, P.D., 1981a, Settling velocities of irregular grains at low Reynolds numbers: J. Sed. Petrol., 51, 121-128.

Baba, J., and Komar, P.D., 1981b, Measurement and analysis of settling velocities of natural quartz grains: J. Sed. Petrol., 51, 631-640.

Bagnold, R.A., 1941, The Physics of Blown Sand and Desert Dunes: London, Methuen, 265 p.

Bagnold, R.A., 1954, Experiments on a gravity-free dispersion of large solid spheres in a Newtonian fluid under shear: Proc. Roy. Soc. London, A225, 49-63.

Bagnold, R.A., 1955, Some flume experiments on large grains but little denser than the transporting fluid, and their implications: Proc. Inst. Civ. Eng. (London), Part 3, 174-205.

Bagnold, R.A., 1956, The flow of cohesionless grains in fluids: Philos. Trans. Roy. Soc. London, A249, 235-297.

Bagnold, R.A., 1962, Auto-suspension of transported sediment; turbidity currents: Proc. Roy. Soc. London, A265, 315-319.

Bagnold, R.A., 1966, An approach to the sediment transport problem from general physics: U.S. Geol. Surv. Prof. Paper 422-I, 37 p.

Bagnold, R.A., 1973, The nature of saltation and of "bed load" transport in water: Proc. Roy. Soc. London, A332, 473-504.

Bagnold, R.A., 1977, Bed load transport by natural rivers: Water Resour.

Res., 13, 303-312.
Baker, V.R., and Ritter, D.F., 1975, Competence of rivers to transport coarse bedload material: Bull. Geol. Soc. Am., 86, 975-978.
Barr, D.I.H., 1967, Densiometric exchange flow in rectangular channels. III. Large scale experiments: Houille Blanche, 22, 619-631.
Batchelor, G.K., 1967, An Introduction to Fluid Dynamics: Cambridge Univ. Press, 615 p.
Bates, C.C., 1953, Rational theory of delta formation: Bull. Am. Assoc. Petrol. Geol., 37, 2119-2162.
Bates, R.L., and Jackson, J.A., eds., 1980, Glossary of Geology: Am. Geol. Inst., 2nd ed., 749 p.
Bayazit, M., 1978, Scour of bed material in very rough channels: Proc. Am. Soc. Civ. Eng., J. Hydraul. Div., 104(9), 1345-1349.
Beghin, P., Hopfinger, E.J., and Britter, R.E., 1981, Gravitational convection from instantaneous sources on inclined boundaries: J. Fluid Mech., 107, 407-422.
Benjamin, T. Brooke, 1968, Gravity currents and related phenomena: J. Fluid Mech., 31, 209-248.
Blinco, P.H., and Partheniades, E., 1971, Turbulence characteristics in free surface flows over smooth and rough boundaries: J. Hydraul. Res., 9(8), 43-69.
Bohlen, W.F., 1977, Shear stress and sediment transport in unsteady turbulent flows: in Wiley, M., ed., Estuarine Processes, Vol. 1, Uses, Stresses, and Adaptation to the Estuary, 109-123: N.Y., Academic Press, Vol. 2, 541 p.
Boillat, J.L., and Graf, W.H., 1981, Settling velocity of spherical particles in calm water: Proc. Am. Soc. Civ. Eng., J. Hydraul. Div., 107, 1123-1131.
Boothroyd, J.C., and Hubbard, D.K., 1975, Genesis of bedforms in meso-tidal estuaries: in Cronin, L.E., ed., Estuarine Research, Vol. 2, Geology and Engineering, 217-235: N.Y., Academic Press, 587 p.
Bouma, A.H., ed., 1981, Offshore geologic hazards: Amer. Assoc. Petrol. Geol., Education Course Notes, No. 18.
Bradley, W.C., 1970, Effect of weathering on abrasion of granitic gravel, Colorado River (Texas): Bull. Geol. Soc. Am., 81, 61-80.
Bradley, W.C., Fahnestock, R.K., and Rowekamp, E.T., 1972, Coarse sediment transport by flood flows on Knik River, Alaska: Bull. Geol. Soc. Am., 83, 1261-1284.
Bradley, W.C., and Mears, A.I., 1980, Calculations of flows needed to transport coarse fraction of Boulder Creek alluvium at Boulder, Colorado: Bull. Geol. Soc. Am., Part II, 91, 1057-1090.
Bradshaw, P., and Wong, F.Y.F., 1972, The reattachment and relaxation of a turbulent shear layer: J. Fluid Mech., 52, 113-135.
Brady, L.L., and Jobson, H.E., 1973, An experimental study of heavy-mineral segregation under alluvial-flow conditions: U.S. Geol. Surv. Prof. Paper 562-K, 38 p.
Bridge, J. S., 1978, Origin of horizontal lamination under turbulent boundary layers: Sed. Geol., 20, 1-16.
Britter, R.E., and Linden, P.F., 1980, The motion of the front of a gravity current travelling down an incline: J. Fluid Mech., 99, 531-543.
Britter, R.E., and Simpson, J.E., 1978, Experiments on the dynamics of a gravity current head: J. Fluid Mech., 88, 223-240.
Britter, R.E., and Simpson, J.E., 1981, A note on the structure of the head of an intrusive gravity current: J. Fluid Mech., 112, 459-466.
Brooks, N.H., 1958, Mechanics of streams with movable beds of fine sand: Trans. Am. Soc. Civ. Eng., 123, 526-549.

Buckingham, E., 1914, On physically similar systems; illustrations of the use of dimensional equations: Phys. Rev., Ser. 2, 4, 345-376.
Buckingham, E., 1915, Model experiments and the forms of empirical equations: Trans. Am. Soc. Mech. Eng., 37, 263-292.
Cain, J.D.B., 1968, Aspects of the depositional environment and paleoecology of crinoidal limestones: Scott. J. Geol., 4, 191-208.
Cantwell, B.J., 1981, Organized motion in turbulent flow: Ann. Rev. Fluid Mech., 13, 457-515.
Carling, P.A., 1983, Threshold of coarse sediment transport in broad and narrow natural streams: Earth Surf. Processes and Landforms, 8, 1-18.
Carrigy, M.A., 1970, Experiments on the angles of repose of granular materials: Sedimentology, 14, 147-158.
Carter, R.M., 1975, A discussion and classification of subaqueous mass-transport with particular application to grain-flow, slurry-flow and fluxo-turbidites: Earth Sci. Rev., 11, 145-177.
Chase, R.R.P., 1979, Settling behavior of natural aquatic particulates: Limnol. Oceanogr., 24, 417-426.
Cheong, H.-F., and Shen, H.-W., 1982, Statistical properties of sediment movement: Am. Soc. Civ. Eng., J. Hydraul. Eng., 109, 1577-1589.
Chepil, W.S., 1945, Dynamics of wind erosion, I, Nature of movement of soil by wind: Soil Sci., 60, 305-320.
Chepil, W.S., 1958, The use of evenly spaced hemispheres to evaluate hydrodynamic forces on a soil surface: Trans. Am. Geophys. Union, 39, 397-404.
Chepil, W.S., 1961, The use of spheres to measure lift and drag on wind-eroded soil grains: Proc. Soil Sci. Soc. Am., 25, 343-345.
Chow, V.T., 1961, Open-channel flow: in Streeter, V.L., Handbook of Fluid Dynamics, Chapter 24, 59 p.: N.Y., McGraw-Hill.
Chu, F.H., Pilkey, W.D., and Pilkey, O.H., 1979, An analytical study of turbidity current steady flow: Mar. Geol., 33, 205-220.
Chu, W.F., Pilkey, O.H., and Pilkey, W.D., 1980, A turbidity current model: Am. Soc. Civ. Eng., Civil Engineering in the Oceans, IV, 416-432.
Clark, M.W., and Clark, I., 1976, A sedimentological pattern recognition problem: in Merriam, D.F., ed., Quantitative Techniques for the Analysis of Sediments, 121-141: N.Y., Pergamon Press, 174 p.
Clifton, H.E., 1976, Wave-formed sedimentary structures--a conceptual model: Soc. Econ. Pal. Min., Spec. Publ. 24, 126-148.
Coe, H.S., and Clevenger, G.H., 1916, Methods for determining the capacities of slime-settling tanks: Trans. Am. Inst. Min. Metall. Eng., 55, 356-384.
Coleman, N.L., 1967, A theoretical and experimental study of drag and lift forces acting on a sphere resting on a hypothetical stream bed: Int. Assoc. Hydraul. Res., 12th Congress, Proc., 3, 184-192.
Coleman, N.L., 1969, A new examination of sediment suspension in open channels: J. Hydraul. Res., 7, 67-82.
Coleman, N.L., 1970, Flume studies of the sediment transfer coefficient: Water Resour. Res., 6, 801-809.
Coleman, N.L., 1977, Extension of the drag coefficient function for a stationary sphere on a boundary of similar spheres: Houille Blanche, 32, 325-328.
Coleman, N.L., 1981, Velocity profiles with suspended sediment: J. Hydraul. Res., 19, 211-229.
Coleman, N.L., and Alonso, C.V., 1983, Two-dimensional channel flows over rough surfaces: Am. Soc. Civ. Eng., J. Hydraul. Eng., 109, 175-188.
Coleman, N.L., and Ellis, W.M., 1976, Model study of the drag coefficient of a streambed particle: Proc. 3rd Fed. Interagency Sedimentation Conf., Denver, Colo., March 22-25, 1976, Sedimentation Comm., Water Resources Comm., p. 4-1

to 4-11.
Collins, M.B., and Rigler, J.K., 1982, The use of settling velocity in defining the initiation of motion of heavy mineral grains under unidirectional flow: Sedimentology, 29, 419-426.
Costello, W.R., and Southard, J.B., 1981, Flume experiments on lower-flow-regime bed forms in coarse sand: J. Sed. Petrol., 51, 849-864.
Coulson, J.M., and Richardson, J.F., 1955, Chemical Engineering, Vol. 2: N.Y., McGraw-Hill, 775 p.
Crickmore, M.J., 1967, Measurement of sand transport in rivers with special reference to tracer methods: Sedimentology, 8, 175-228.
Crickmore, M.J., and Lean, G.H., 1962a, The measurement of sand transport by means of radioactive tracers: Proc. Roy. Soc. London, A266, 402-421.
Crickmore, M.J., and Lean, G.H., 1962b, The measurement of sand transport by the time-integration method with radioactive tracers: Proc. Roy. Soc. London, A270, 27-47.
Daley, B.J., and Pracht, W.E., 1968, Numerical study of density-current surges: Phys. Fluids, 11, 15-30.
Dalrymple, R.W., 1979, Wave-induced liquefaction: a modern example from the Bay of Fundy: Sedimentology, 26, 835-844.
Dalrymple, R.W., Knight, R.J., and Lambiase, J.J., 1978, Bedforms and their hydraulic stability relationships in a tidal environment, Bay of Fundy, Canada: Nature, 275, 100-104.
Danel, P., Durand, R., and Condolies, E., 1953, Introduction à l'étude de la saltation: Houille Blanche, 8, 815-829. (Trans. by D.J. Hebert, 1955.)
Dapples, E.C., and Rominger, J.F., 1945, Orientation analysis of fine-grained clastic sediments--a progress report: J. Geol., 53, 246-261.
Davidson, J.F., Harrison, D., and Guestes de Carvalho, J.R.F., 1977, On the liquidlike behavior of fluidized beds: Ann. Rev. Fluid Mech., 9, 55-86.
Davies, T.R.H., and Samad, M.F.A., 1978, Fluid dynamic lift on a bed particle: Proc. Am. Soc. Civ. Eng., J. Hydraul. Div., 104, 1171-1182.
Day, T.J., 1980, A study of initial motion characteristics of particles in graded bed material: Geol. Surv. Can. Pap. 80-1A, 281-286.
DeVantier, B.A., and Larock, B.E., 1984, Sediment transport in stratified turbulent flow: Am. Soc. Civ. Eng., J. Hydraul. Eng., 109, 1622-1635.
Dillo, H.-G., 1960, Sandwanderung in Tideflussen: Technische Hochschule Hannover, Franzius-Institut fur Grund- und Wasserbau, Mitt., 17, 135-253.
Drew, D.A., 1975, Turbulent sediment transport over a flat bottom using momentum balance: J. Appl. Mech., E42, 38-44.
Drew, D.A., and Kogelman, S., 1975, Turbulent sediment transport using momentum balance--the strong turbulence approximation: Appl. Sci. Res., 30, 279-290.
Dzulynski, S., and Sanders, J.E., 1962, Current marks on firm mud bottoms: Trans. Conn. Acad. Arts Sci., 42, 57-96.
Einstein, H.A., 1950, The bed-load function for sediment transportation in open channel flows: U.S. Dept. Agric., Tech. Bull. 1026, 70 p. (reprinted as Appendix B in Shen, H.W., ed., 1972, Sedimentation, Fort Collins, Colorado).
Einstein, H.A., and Chien, N., 1955, Effects of heavy sediment concentration near the bed on velocity and sediment distribution: U.S. Army Corps of Engrs., Missouri River Div., M.R.D. Sediment Series No. 8, 76 p.
Einstein, H.A., and El-Samni, E.A., 1949, Hydrodynamic forces on a rough wall: Rev. Mod. Phys., 21, 520-524.
Elata, C., and Ippen, A.T., 1961, The dynamics of open channel flow with suspensions of neutrally buoyant particles: Mass. Inst. Technol., Hydrodynam-

ics Lab., Tech. Rep. 45.
Engelund, F., 1970, Instability of erodible beds: J. Fluid Mech., 42, 225-244.
Engelund, F., and Fredsøe, J. 1974, Transition from dunes to plane bed in alluvial channels: Tech. Univ. Denmark, Inst. Hydraul. Eng., Series Paper 4.
Engelund, F., and Fredsøe, J., 1976, A sediment transport model for straight alluvial channels: Nord. Hydrol., 7, 293-306.
Engelund, F., and Hansen, E., 1972, A monograph on sediment transport in alluvial streams: Copenhagen, Teknisk Forlag, 3rd ed., 62 p.
Enos, P., 1977, Flow regimes in debris flow: Sedimentology, 24, 133-142.
Etheridge, D.W., and Kemp, P.H., 1978, Measurements of turbulent flow downstream of a rearward-facing step: J. Fluid Mech., 86, 545-566.
Everts, C.H., 1973, Particle overpassing on flat granular boundaries: Proc. Am. Soc. Civ. Eng., J. Waterways Harbors Div., 99, 425-438.
Exner, F.M., 1925, Über die Wechselwirkung zwishchen Wasser und Geschiebe in Flussen: Sitzungsber. Akad. Wiss. Wien, Math.-Naturwiss. Kl., Abt. IIa, 134, 166-204.
Fahnestock, R.K., 1963, Morphology and hydrology of a glacial stream--White River, Mount Rainier, Washington: U.S. Geol. Surv. Prof. Paper 422-A, 70 p.
Fenton, J.D., and Abbott, J.E., 1977, Initial movement of grains on a stream bed: the effect of relative protrusion: Proc. Roy. Soc. London, A352, 523-537.
Fernandez Luque, R., 1974, Erosion and Transport of Bed-Load Sediment: Ph.D. Thesis, Technical Highschool, Delft, Holland, Krips. Repro. B.V., Meppel, 65 p. plus tables and figs.
Fernandez Luque, R., and Van Beek, R., 1976, Erosion and transport of bed-load sediment: J. Hydraul. Res., 14, 127-144.
Fischer, H.B., et al., 1979, Mixing in Inland and Coastal Waters: N.Y., Academic Press, 483 p.
Fisher, J.S., Pickral, J., and Odum, W.E., 1979, Organic detritus particles: Initiation of motion criteria: J. Oceanogr., 24, 529-532.
Fok-Pun, L., and Komar, P.D., 1983, Settling velocities of planktonic foraminifera: Density variations and shape effects: J. Foraminiferal Res., 13, 60-68.
Francis, J.R.D., 1973, Experiments on the motion of solitary grains along the bed of a water-stream: Proc. Roy. Soc. London, A332, 443-471.
Fredsoe, J., 1974, On the development of dunes in erodible channels: J. Fluid. Mech., 64, 1-16.
Futterer, E., 1978, Untersuchungen uber die Sink- und Transportgeschwindigkeit biogener Hartteile: Abh. Neues Jahrb. Geol. Palaontol., 155, 318-359.
Gessler, J., 1967, The beginning of bedload movement of mixtures investigated as natural armoring in channels: Calif. Inst. Technol., W.M. Keck Laboratory of Hydraulics Water Resources, Translation T-5 (by E.A. Prych), 89 p.
Gibbs, R.J., Matthew, M.D., and Link, D.A., 1971, The relation between sphere size and settling velocity: J. Sed. Petrol., 41, 7-18.
Gilbert, G.K., 1914, The transportation of debris by running water: U.S. Geol. Surv. Prof. Paper 86, 263 p.
Gordon, C.M., 1975, Sediment entrainment and suspension in a turbulent tidal flow: Mar. Geol., 18, M57-M64.
Gordon, C.M., and Dohne, C.F., 1973, Some observations on turbulent flows in a tidal estuary: J. Geophys. Res., 78, 1971-1978.
Gordon, R., Carmichael, J.B., and Isackson, F.J., Saltation of plastic balls in a "one-dimensional" flume: Water Resour. Res., 8, 444-459.

Graf, W.H., 1971, Hydraulics of Sediment Transport: N.Y., McGraw-Hill, 513 p.

Grant, W.D., Boyer, L.F., and Sanford, L.P., 1982, The effects of bioturbation on the initiation of motion of intertidal sands: J. Mar. Res., 40, 659-677.

Grass, A.J., 1970, Initial instability of fine bed sand: Proc. Am. Soc. Civ. Eng., J. Hydraul. Div., 96, 619-632.

Grass, A.J., 1971, Structural features of turbulent flow over smooth and rough boundaries: J. Fluid Mech., 4, 149-190.

Grass, A.J., 1974, Transport of fine sand on a flat bed: turbulence and suspension mechanics: Tech. Univ. Denmark, Proc. Euromech. 48, 33-34.

Grazer, R.A., 1982, Experimental study of current ripples using medium silt: Mass. Inst. Technol., S.M. Dissertation, 131 p.

Grigg, N.S., 1970, Motion of single particles in alluvial channels: Proc. Am. Soc. Civ. Eng., J. Hydraul. Div., 96, 2501-2518.

Grigg, N.S., and Rathbun, R.E., 1969, Hydraulic equivalence of minerals with a consideration of the reentrainment process: U.S. Geol. Surv. Prof. Paper 650-B, 77-80.

Gust, G., 1976, Observations on a turbulent-drag reduction in dilute suspension of clay in sea-water: J. Fluid Mech., 75, 29-47.

Gust, G., and Southard, J.B., 1983, Effects of weak bed load on the universal law of the wall: J. Geophys. Res., 88, 5939-5952.

Guy, H.P., Simons, D.B., and Richardson, E.V., 1966, Summary of alluvial channel data from flume experiments, 1956-61: U.S. Geol. Surv. Prof. Paper 462-I, 96 p.

Haff, P.K., 1983, Grain flow as a fluid-mechanical phenomenon: J. Fluid Mech., 134, 401-430.

Hallermeier, R.J., 1981, Terminal settling velocity of commonly occurring sand grains: Sedimentology, 28, 859-865.

Hamilton, W.S., and Courtney, G.L., 1977, Added mass of sphere starting upward near floor: Proc. Am. Soc. Civ. Eng., J. Eng. Mech. Div., 103, 79-97.

Hampton, M.A., 1972, The role of subaqueous debris flow in generating turbidity currents: J. Sed. Petrol., 42, 775-793.

Hampton, M.A., 1975, Competence of fine-grained debris flows: J. Sed. Petrol., 45, 637-648.

Hampton, M.A., 1979, Buoyancy in debris flows: J. Sed. Petrol., 49, 753-758.

Hand, B.M., Wessel, J.M., and Hayes, M.O., 1969, Antidunes in the Mount Toby Conglomerate (Triassic), Massachusetts: J. Sed. Petrol., 39, 1310-1316.

Harleman, D.R.F., 1961, Stratified flow: in Streeter, V.L., ed., Handbook of Fluid Dynamics, Chapter 26, 21 p: N.Y., McGraw-Hill.

Harms, J.C., Southard, J.B., Spearing, D.R., and Walker, R.G., 1975, Depositional environments as interpreted from primary sedimentary structures and stratification sequences: Soc. Econ. Pal. Min., Short Course 2, 161 p.

Harms, J.C., Southard, J.B., and Walker, R.G., 1982, Structures and sequences in clastic rocks: Soc. Econ. Pal. Min., Short Course 9, variously paged.

Hawley, N., 1982, Settling velocity distribution of natural aggregates: J. Geophys. Res., 87, 9489-9498.

He, M.-M., and Han, Q.-W., 1982, Stochastic model of incipient sedimentation: Proc. Am. Soc. Civ. Eng., J. Hydraul. Div., 108, 211-224.

Helley, E.J., 1969, Field measurement of the initiation of large particle motion in Blue Creek, near Klamath, California: U.S. Geol. Surv., Prof. Paper 562-G, 19 p.

Herczynski, R., and Pienkovska, I., 1980, Toward a statistical theory of suspension: Ann. Rev. Fluid Mech., 12, 237-269.

Hey, R.D., Bathurst, J.C., and Thorne, C.R., eds., 1982, Gravel Bed Rivers; Fluvial Processes, Engineering and Management: N.Y., Wiley, 875 p.
Hinze, J.O., 1975, Turbulence: N.Y., McGraw Hill, 2nd ed., 790 p.
Hiscott, R.N., and Middleton, G.V., 1979, Depositional mechanics of thick-bedded sandstones at the base of a submarine slope, Tourelle Formation (Lower Ordovician), Quebec, Canada: Soc. Econ. Pal. Min., Spec. Publ. 27, 307-326.
Hoerner, S.F., 1965, Fluid Dynamic Drag: Published by the author, 148 Busteed, Midland Park, New Jersey.
Hopfinger, E.J., 1983, Snow avalanche motion and related phenomena: Ann. Rev. Fluid Mech., 15, 47-76.
Hsu, K.J., 1975, Catastrophic debris streams (Sturzstroms) generated by rock-falls: Bull. Geol. Soc. Am., 86, 129-140.
Hsu, S.-T., van der Beken, A., Landweber, L., and Kennedy, J.F., 1980, Sediment suspension in turbulent pipe flow: Proc. Am. Soc. Civ. Eng., J. Hydraul. Div., 106, 1783-1793.
Huffman, G.D., and Bradshaw, P., 1972, A note on von Karman's constant in low Reynolds number turbulent flows: J. Fluid Mech., 53, 45-60.
Hung, C.S., and Shen, H.-W., 1976, Stochastic models of sediment motion on flat bed: Proc. Am. Soc. Civ. Eng., J. Hydraul. Div., 102, 1745-1759.
Hung, C.S., and Shen, H.-W., 1979, Statistical analysis of sediment motions on dunes: Proc. Am. Soc. Civ. Eng., J. Hydraul. Div., 105, 212-227.
Huppert, H.E., and Simpson, J.E., 1980, The slumping of gravity currents: J. Fluid Mech., 99, 785-799.
Ippen, A.T., 1971, A new look at sedimentation in turbulent streams: J. Boston Soc. Civ. Eng., 58, 131-161.
Irvine, J.N., 1980, Magmatic density currents and cumulus processes: Am. J. Sci., A280, 1-58.
Itakura, T., and Kishi, T., 1980, Open channel flow with suspended sediments: Proc. Am. Soc. Civ. Eng., J. Hydraul. Div., 106, 1325-1343.
Izakson, A., 1937, Formula for the velocity distribution near a wall [in Russian]: Zh. Eksp. Teor. Fiz, 7, 919-924.
Jackson, P.S., 1981, On the displacement height in the logarithmic velocity profile: J. Fluid Mech., 111, 15-25.
Jackson, R.G., 1976, Sedimentological and fluid dynamic implications of the turbulent bursting phenomenon in geophysical flows: J. Fluid Mech., 77, 531-560.
Jaeger, J.C., 1969, Elasticity, Fracture and Flow, with Engineering and Geological Applications: N.Y., Wiley, 3rd ed., 268 p.
Jeffreys, H., 1929, On the transportation of sediment by streams: Proc. Cambridge Philos. Soc., 25, 272-276.
Jenkins, J.G., and Savage, S.B., 1983, A theory for the rapid flow of identical, smooth, nearly elastic spherical particles: J. Fluid Mech., 130, 187-202.
Johnson, A.M., 1970, Physical Processes in Geology: San Francisco, Freeman, 577 p.
Johnson, C.W., Engleman, R.L., Smith, J.P., and Hanson, C.L., 1977, Helley-Smith bed-load sampler: Proc. Am. Soc. Civ. Eng., J. Hydraul. Div., 103, 1214-1221.
Johnson, R.G., 1974, Particulate matter at the sediment-water interface in coastal environments: J. Mar. Res., 32, 313-330.
Jopling, A.V., 1964, Laboratory study of the sorting processes related to flow separation: J. Geophys. Res., 69, 3403-3418.
Jopling, A.V., 1965, Laboratory study of the distribution of grain sizes in

cross-bedded deposits: Soc. Econ. Pal. Min., Spec. Publ. 12, 53-65.
Jopling, A.V., and Forbes, D.L., 1979, Flume study of silt transportation and deposition: Geogr. Ann., 61A, 67-85.
Kalinske, A.A., 1943, Turbulence and the transport of sand and silt by wind: Ann. N.Y. Acad. Sci., 44, 41-54.
Kalinske, A.A., and Hsia, C.H., 1945, Study of transportation of fine sediments by flowing water: Univ. Iowa, Studies in Engineering, Bull. 29, 30 p.
Karcz, I., 1973, Reflections on the origin of some small-scale longitudinal streambed scours: in Morisawa M., ed., Fluvial Geomorphology, Proc. 4th Annual Geomorphology Symposium, Publications in Geomorphology, State Univ. of New York at Binghamton, 149-173.
Kellerhels, R., 1967, Stable channels with gravel-paved beds: Proc. Am. Soc. Civ. Eng., J. Waterways Harbors Div., 93, 63-83.
Kennedy, J.F., 1963, The mechanics of dunes and antidunes in erodible-bed channels: J. Fluid Mech., 16, 521-544.
Kennedy, J.F., 1969, The formation of sediment ripples, dunes, and antidunes: Ann. Rev. Fluid Mech., 16, 521-544.
Kennedy, J.F., 1984, Reflections on rivers, research and Rouse: Am. Soc. Civ. Eng., J. Hydraul. Eng., 109, 1254-1271.
Kennedy, J.F., and Brooks, N.H., 1963, Laboratory study of an alluvial stream at constant discharge: U.S. Dept. Agric., Agric. Res. Serv., Misc. Publ. 970, Proc. Federal Inter-Agency Sedimentation Conf., 320-330.
Keulegan, G.H., 1957, Twelfth progress report on model laws for density currents: An experimental study of the motion of saline water from locks into fresh water channels: U.S. Nat. Bur. Stand., Rep. 5168, 21 p.
Keulegan, G.H., 1958, Thirteenth progress report on model laws for density currents: The motion of saline fronts in still water: U.S. Nat. Bur. Stand., Rep. 5831, 29 p.
Klein, G. deV., 1970, Depositional and dispersal dynamics of intertidal sand bars: J. Sed. Petrol., 40, 1095-1127.
Klein, G. deV., and Whaley, M.L., 1972, Hydraulic parameters controlling bedform migration on an intertidal sand body: Bull. Geol. Soc. Am., 83, 3465-3470.
Kline, S.J., 1965, Similitude and Approximation Theory: N.Y., McGraw-Hill, 229 p.
Knapp, R.T., 1938, Energy-balance in stream flows carrying suspended load: Trans. Am. Geophys. Union, 19, 501-505.
Komar, P.D., 1972, Relative significance of head and body spill from a channelized turbidity current: Bull. Geol. Soc. Am., 83, 1151-1156.
Komar, P.D., 1977, Computer simulation of turbidity current flow and the study of deep-sea channels and fan sedimentation: in Goldberg, E.D., et al., eds, The Sea, Vol. 6, Marine Modelling, 603-621: N.Y., John Wiley, 1048 p.
Komar, P.D., 1978, Relative quantities of suspension versus bed-load transport on beaches: J. Sed. Petrol., 48, 921-932.
Komar, P.D., 1981, The applicability of the Gibbs equation for grain settling velocities to conditions other than quartz grains in water: J. Sed. Petrol., 51, 1125-1132.
Komar, P.D., and Reimers, C.E., 1978, Grain shape effects on settling rates: J. Geol., 86, 193-209.
Kranck, K., 1975, Sediment deposition from flocculated suspensions: Sedimentology, 22, 111-123.
Krinsley, D.H., and Doornkamp, J.C., 1973, Atlas of Quartz Sand Surface Textures: Cambridge Univ. Press, 91 p.

Krumbein, W.C., 1942, Settling velocity and flume-behavior of non-spherical particles: Trans. Am. Geophys. Union, 23, 621-632.
Kuenen, Ph.H., 1950, Turbidity currents of high density: 18th Int. Geol. Congr., London, Repts., Pt. 8, 44-52.
Laird, M.G., 1970, Vertical sheet structures--a new indicator of sedimentary fabric: J. Sed. Petrol., 40, 428-434.
Lane, E.W., and Carlson, E.J., 1954, Some observations on the effect of particle shape on the movement of coarse sediments: Trans. Am. Geophys. Union, 35, 453-462.
Langhaar, H.L., 1951, Dimensional Analysis and Theory of Models: N.Y., Wiley, 166 p.
Lau, Y.L., 1983, Suspended sediment effect on flow resistance: Am. Soc. Civ. Eng., J. Hydraul. Eng., 109, 757-763.
Laufer, J., 1954, The structure of turbulence in fully developed pipe flow: Nat. Advis. Comm. Aeronaut., Rep. 1174, 18 p.
Leeder, M.R., 1979, "Bedload" dynamics: grain-grain interactions in water flows: Earth Surf. Processes, 4, 229-240.
Leeder, M.R., 1983a, On the interactions between turbulent flow, sediment transport and bedform mechanics in channelized flow: Int. Assoc. Sedimentologists, Spec. Publ. 6, 5-18.
Leeder, M.R., 1983b, On the dynamics of sediment suspension by residual Reynolds stresses--confirmation of Bagnold's theory: Sedimentology, 30, 485-491.
Leopold, L.B., and Emmett, W.W., 1976, Bedload measurements, East Fork River, Wyoming: Proc. Nat. Acad. Sci., 73, 1000-1004.
Leopold, L.B., and Emmett, W.W., 1977, 1976 Bedload measurements, East Fork River, Wyoming: Proc. Nat. Acad. Sci., 74, 2644-2648.
Leopold, L.B., Wolman, M.G., and Miller, J.P., 1964, Fluvial Processes in Geomorphology: San Francisco, Freeman, 522 p.
Lighthill, M.J., and Whitham, G.B., 1955, On kinematic waves. I. Flood movement in long rivers: Proc. Roy. Soc. London, A229, 281-316.
Lin, C.C., 1955, The Theory of Hydrodynamic Stability: Cambridge Univ. Press, 155 p.
Lowe, D.R., 1975, Water escape structures in coarse-grained sediments: Sedimentology, 22, 157-204.
Lowe, D.R., 1976a, Subaqueous liquefied and fluidized sediment flows and their deposits: Sedimentology, 23, 285-308.
Lowe, D.R., 1976b, Grain flow and grain flow deposits: J. Sed. Petrol., 46, 188-199.
Lowe, D.R., 1979, Sediment gravity flows: Their classification and some problems of application to natural flows and deposits: Soc. Econ. Pal. Min., Spec. Publ. 27, 75-82.
Lowe, D.R., 1982, Sediment gravity flows: Two depositional models with special reference to the deposits of higher density turbidity currents: J. Sed. Petrol., 52, 279-297.
Ludwick, J.C., and Domurat, G.W., 1982, A deterministic model of the vertical component of sediment motion in a turbulent fluid: Mar. Geol., 45, 1-15.
Lugt, H.J., 1983, Autorotation: Ann. Rev. Fluid Mech., 15, 123-147.
Luthi, S., 1981, Experiments on non-channelized turbidity currents and their deposits: Mar. Geol., 40, M59-M68.
Maegley, W.J., 1976, Saltation and Martian sandstorms: Rev. Geophys. Space Phys., 14, 135-142.
Maiklem, W.R., 1968, Some hydraulic properties of bioclastic carbonate grains: Sedimentology, 10, 101-109.

Mantz, P.A., 1973, Cohesionless, fine graded, flaked sediment transport by water: Nature Phys. Sci., 246, 14-16.
Mantz, P. A., 1977, Incipient transport of fine grains and flakes by fluids--extended Shields diagram: Proc. Am. Soc. Civ. Eng., J. Hydraul. Div., 103, 601-615.
Mantz, P.A., 1978, Bedforms produced by fine cohesionless, granular and flaky sediments under subcritical water flows: Sedimentology, 25, 83-103.
Mantz, P.A., 1980, Low sediment transport rates over flat beds, Proc. Am. Soc. Civ. Eng., J. Hydraul. Div., 106, 1173-1190.
Mantz, P.A., 1981, Laboratory flume experiments on the transport of cohesionless silicon silts by water streams: Proc. Inst. Civ. Eng. (London), Part 2, 69, 977-994.
Maxworthy, T., 1983, Gravity currents with variable flow: J. Fluid Mech., 128, 247-257.
McCave, I.N., 1979, Tidal currents at the North Hines Lightship, southern North Sea: Flow directions and turbulence in relation to maintenance of sand bars: Mar. Geol., 31, 101-113.
McGee, W.J., 1908, Outlines of hydrology: Bull. Geol. Soc. Am., 19, 193-220.
McNown, J.S., and Lin, P.N., 1952, Sediment concentration and fall velocity: Proc. 2nd Midwestern Conf. Fluid Mech., Ohio State Univ., Columbus, Ohio, 401-411.
McQuivey, R.S., and Keefer, T.N., 1969, The relation of turbulence to deposition of magnetite over ripples: U.S. Geol. Surv. Prof. Paper 650-D, 244-247.
McQuivey, R.S., and Richardson, E.V., 1969, Some turbulence measurements in open-channel flows: Proc. Am. Soc. Civ. Eng., J. Hydraul. Div., 95, 209-223.
McQuorquodale, J.A., and Giratella, M.K., 1973, Flow over natural and artificial ripples: Proc. 15th Congr. Int. Assoc. Hydraul. Res., Istanbul, 1, 167-172.
McTaggart, K.C., 1960, The mobility of nuees ardentes: Am. J. Sci., 258, 369-382.
McTigue, D.F., 1981, Mixture theory for suspended sediment transport: Proc. Am. Soc. Civ. Eng., J. Hydraul. Div., 107, 659-673.
Mehta, A.J., Lee, J., and Christensen, B.A., 1980, Fall velocity of shells as coastal sediment: Proc. Am. Soc. Civ. Eng., J. Hydraul. Div., 106, 1727-1744.
Meland, N., and Norrman, J.O., 1966, Transport velocities of single particles in bed-load motion: Geogr. Ann., A48, 165-182.
Melosh, H.J., 1979, Acoustic fluidization: a new geologic process?: J. Geophys. Res., 84, 7513-7520.
Melosh, H.J., 1983, Acoustic fluidization: Am. Sci., 71, 158-164.
Middleton, G.V., 1965, Antidune cross-bedding in a large flume: J. Sed. Petrol., 35, 922-927.
Middleton, G.V., 1966, Experiments on density and turbidity currents. I, Motion of the head: Can. J. Earth Sci., 3, 523-546.
Middleton, G.V., 1969, Grain flows and other mass movements down slopes: Lecture 11 in Stanley, D.J., ed., The New Concepts of Continental Margin Sedimentation, Am. Geol. Inst., Short Course Lecture Notes.
Middleton, G.V., 1970a, Generation of the log-normal frequency distribution in sediments: in Romanova, M.A., and Sarmanov, O.V., eds., Topics in Mathematical Geology, 34-42: N.Y., Consultants Bureau, 281 p.
Middleton, G.V., 1970b, Experimental studies related to the problems of flysch

sedimentation: Geol. Assoc. Can. Spec. Paper 7, 253-272.
Middleton, G.V., 1976, Hydraulic interpretation of sand size distributions: J. Geol., 84, 405-426.
Middleton, G.V., and Davis, P.M., 1979, Surface textures and rounding of quartz sand grains on intertidal sandbars, Bay of Fundy, Nova Scotia: Can. J. Earth Sci., 16, 2071-2085.
Middleton, G.V., and Hampton, M.A., 1973, Sediment gravity flows: mechanics of flow and deposition: in Middleton, G.V., and Bouma, A.H., eds., Turbidites and Deep-Water Sedimentation, Soc. Econ. Pal. Min., Short Course 1, 1-38.
Middleton, G.V., and Hampton, M.A., 1976, Subaqueous sediment transport and deposition by sediment gravity flows: in Stanley, D.J., and Swift, D.J.P., eds., Marine Sediment Transport and Environmental Management, 197-218: N.Y., Wiley, 602 p.
Middleton, G.V., and Southard, J.B., 1977, Mechanics of sediment movement: Soc. Econ. Pal. Min., Short Course 3, variously paged.
Miller, M.C., McCave, I.N., and Komar, P.D., 1977, Threshold of sediment motion under unidirectional currents: Sedimentology, 24, 507-527.
Miller, R.L., and Byrne, R.J., 1966, The angle of repose for a single grain on a fixed rough bed: Sedimentology, 6, 303-314.
Millikan, C.B., 1939, A critical discussion of turbulent flows in channels and circular tubes: Fifth Int. Congr. Appl. Mech., Cambridge, Mass., 386-392.
Monin, A.S., and Yaglom, A.M., 1971, Statistical Fluid Mechanics, Vol. 1: Cambridge, Mass., MIT Press, 769 p.
Morris, H.M., 1955, Flow in rough conduits: Trans. Am. Soc. Civ. Eng., 120, 373-398.
Moss, A.J., 1972a, Bed-load sediments: Sedimentology, 18, 159-219.
Moss, A.J., 1972b, Initial fluviatile fragmentation of granitic quartz: J. Sed. Petrol., 42, 905-916.
Moss, A.J., Walker, P.H., and Hutka, J., 1973, Fragmentation of granitic quartz in water: Sedimentology, 20, 489-511.
Moss, A.J., and Walker, P.H., 1978, Particle transport by continental water flows in relation to erosion, depositon, soils, and human activities: Sed. Geol., 20, 81-139.
Murphy, P.J., and Hooshiari, H., 1982, Saltation in water dynamics: Proc. Am. Soc. Civ. Eng., J. Hydraul. Div., 108, 1251-1267.
Nakagawa, H., and Tsujimoto, T., 1980, Statistical analysis of sediment motions on dunes--discussion: Proc. Am. Soc. Civ. Eng., J. Hydraul. Div., 106, 221-226.
Nardin, T.R., Heim, F.J., Gorsline, D.S., and Edwards, B.D., 1979, A review of mass movement processes, sediment and acoustic characteristics, and contrasts in slope and base-of-slope systems versus canyon-fan-basin floor systems: Soc. Econ. Pal. Min., Spec. Publ. 27, 61-73.
Neill, C.R., 1968, Note on initial movement of coarse uniform bed-material: J. Hydraul. Res., 6, 173-176.
Nielsen, P., 1984, On the motion of suspended sand particles: J. Geophys. Res., 89, 616-626.
Nikuradse, J., 1932, Gesetzmässigkeiten der Turbulente Strömung in glatten Rohren: VDI Forschungsheft 356.
Nikuradse, J., 1933, Strömungsgesetze in rauhen Rohren: VDI Forschungsheft 361, 22 p (transl.: Nat. Advis. Comm. Aeronaut., Tech. Memo 1292, Nov. 1950).
Nordin, C.F., Jr., and Dempster, G.R., Jr., 1963, Vertical distribution of velocity and suspended sediment, Middle Rio Grande, New Mexico: U.S. Geol.

Surv., Prof. Paper 462-B, 20 p.
Novak, I.D., 1973, Predicting coarse sediment transport: The Hjulstrom curve revisited: in Morisawa, M., ed., Fluvial Geomorphology, State Univ. of N.Y. at Binghamton, Publ. in Geomorphology, 13-25.
Nowell, A.R.M., and Church, M., 1979, Turbulent flow in a depth-limited boundary layer: J. Geophys. Res., 84, 4816-4824.
O'Brien, M.P., and Cherno, J., 1934, Model law for motion of salt water through fresh: Trans. Am. Soc. Civ. Eng., 99, 576-594.
Okuda, S., et al., 1980, Observations on the motion of a debris flow and its geomorphic effects: Z. Geomorph., Supplement Band 35, 142-163.
Olivinskaya, S.K., Pivovarov, A.A., and Rossinskiy, K.I., 1974, Experimental study of the effect of saltation load on flow kinematics: Soviet Hydrology, Selected Papers, 1973, no. 2, 163-168.
O'Neill, M.E., 1981, Small particles in viscous media: Sci. Progr., 67, 149-184.
Owen, P.R., 1964, Saltation of uniform grains in air: J. Fluid Mech., 20, 225-242.
Paintal, A.S., 1971, Concept of critical shear stress in loose boundary open channels: J. Hydraul. Res., 9, 91-114.
Pantin, H.M., 1979, Interaction between velocity and effective density in turbidity flow: phase-plane analysis, with criteria for autosuspension: Mar. Geol., 31, 59-99.
Pantin, H.M., 1982, Comments on: Experimental test of autosuspension: Earth Surf. Processes and Landforms, 7, 503-505.
Paola, C., 1983, Flow and skin friction over natural rough beds: Mass. Inst. Technol., Dept. of Earth and Plan. Sci., Ph.D. Dissertation, 347 p.
Paola, C., and Southard, J.B., 1983, Autosuspension and the energetics of two-phase flows: Reply to comments on "Experimental test of autosuspension" by J.B. Southard and M.E. Mackintosh: Earth Surf. Processes and Landforms, 8, 273-279.
Parker, G., 1982a, Conditions for recognition of catastrophically erosive turbidity currents: Mar. Geol., 46, 307-327.
Parker, G., 1982b, Discussion of: Experimental test of autosuspension (Southard and Mackintosh, 1981): Earth Surf. Processes and Landforms, 7, 507-510.
Pierson, T.C., 1981, Dominant particle support mechanism in debris flows at Mt. Thomas, New Zealand, and its implications for flow mobility: Sedimentology, 28, 49-60.
Rathbun, R.E., and Goswami, A., 1966, Discussion of Sediment Transportation Mechanics: Initiation of Motion: Proc. Am. Soc. Civ. Eng., J. Hydraul. Div., 92, 251-253.
Rathbun, R.E., and Nordin, C.F., Jr., 1971, Tracer studies of sediment transport processes: Proc. Am. Soc. Civ. Eng., J. Hydraul. Div., 97, 1305-1316.
Raudkivi, A.J., 1963, Study of sediment ripple formation: Proc. Am. Soc. Civ. Eng., J. Hydraul. Div., 89(HY6), 15-33.
Raudkivi, A.J., 1966, Bed forms in alluvial channels: J. Fluid Mech., 26, 507-514.
Rees, A.I., 1966, Some flume experiments with a fine silt: Sedimentology, 6, 209-240.
Reizes, J. A., 1978, Numerical study of continuous saltation: Proc. Am. Soc. Civ. Eng., J. Hydraul. Div., 104, 1305-1321.
Reynolds, D.L., 1954, Fluidization as a geological process and its bearing on the problem of intrusive granites: Am. J. Sci., 252, 577-614.

Reynolds, O., 1883, An experimental investigation of the circumstances which determine whether the motion of water shall be direct or sinuous, and the law of resistance in parallel channels: Philos. Trans. Roy. Soc. London, 174, 935-982.

Riabouchinsky, D.P., 1935, Thirty years of theoretical and experimental work in fluid mechanics: J. Roy. Aeronaut. Soc., 39, 282-348, 377-444.

Richards, K.J., 1980, The formation of ripples and dunes on an erodible bed: J. Fluid Mech., 99, 597-618.

Richardson, J.F., and Meikle, R.A., 1961, Sedimentation and fluidisation--Part III: The sedimentation of uniform fine particles and of two-component mixtures of solids: Trans. Inst. Chem. Eng. (London), 39, 348-356.

Richardson, J.F., and Zaki, W.N., 1954, Sedimentation and fluidisation: Trans. Inst. Chem. Eng. (London), 32, 35-53.

Riley, S.J., and Bryant, T., 1979, The relationship between settling velocity and grain size values: J. Geol. Soc. Australia, 26, 313-315.

Robertson, J.M., and Rouse, H., 1941, On the four regimes of open-channel flow: Civ. Eng, 11, 169-171.

Roscoe, R., 1953, Suspensions: in Hermans, J.J., ed., Flow Properties of Disperse Systems, 1-38: N.Y., Interscience, 445 p.

Rouse, H., 1937, Modern conceptions of the mechanics of turbulence: Trans. Am. Soc. Civ. Eng., 102, 436-505.

Rouse, H., 1939, Experiments on the mechanics of sediment suspension: 5th Int. Congr. Appl. Mech., Cambridge Mass., 550-554.

Rubey, W.W., 1933a, Equilibrium conditions in debris-laden streams: Trans. Am. Geophys. Union, 14th Ann. Mtg., 497-505.

Rubey, W.W., 1933b, Settling velocities of gravel, sand, and silt: Am. J. Sci., 25, 325-338.

Rubin, D.M., and Hunter, R.S., 1982, Bedform climbing in theory and nature: Sedimentology, 29, 121-138.

Rubin, D.M., and McCulloch, D.S., 1980, Single and superimposed bedforms: a synthesis of San Francisco Bay and flume observations: Sed. Geol., 26, 207-231.

Sallenger, A.H., 1979, Inverse grading and hydraulic equivalence in grain flow deposits: J. Sed. Petrol., 49, 553-562.

Savage, S.B., 1979, Gravity flow of cohesionless granular materials in chutes and channels: J. Fluid Mech., 92, 53-96.

Savage, S.B., 1982, Granular flows down rough inclines--review and extension: in Jenkins, J.T., and Satake, M., eds., U.S./Japan Seminar on New Models and Constitutive Relations in the Mechanics of Granular Materials, Cornell University, August 23-27, 1982: Amsterdam, Elsevier, 364 p.

Savage, S.B., and Jeffrey, D.J., 1981, The stress tensor in a granular flow at high shear rates: J. Fluid Mech., 110, 255-272.

Savage, S.B., and McKeown, S., 1983, Shear stresses developed during rapid shear of concentrated suspensions of large spherical particles between concentric cyinders: J. Fluid Mech., 127, 453-472.

Savini, J., and Bodhaine, G.L., 1971, Analysis of current-meter data at Columbia River gauging stations, Washington and Oregon: U.S. Geol. Surv. Water-Supply Paper 1869-F, 59 p.

Scheidegger, A.E., and Potter, P.E., 1965, Textural studies of graded bedding, observation and theory: Sedimentology, 5, 289-304.

Schiller, L., 1932, Fallversuche mit Kugeln und Scheiben: in Schiller, L., ed., Handbuch der Experimentalphysik, Vol. 4, Hydro- und Aeromechanik, Part 2, Widerstand und Auftrieb, 339-398: Leipzig, Akademische Verlagsgesellschaft, 443 p.

Schubauer, G.B., and Skramstad, H.K., 1947, Laminar boundary-layer oscillations and stability of laminar flow: J. Aeronaut. Sci., 14(2), 69-78.
Schumm, S.A., and Stevens, M.A., 1973, Abrasion in place: a mechanism for rounding and size reduction of coarse sediments in rocks: Geology, 1, 37-40.
Scott, C.H., and Stephens, H.D., 1966, Special sediment investigations, Mississippi River at St. Louis, Missouri, 1961-63: U.S. Geol. Surv., Water-Supply Paper 1819-J, 35 p.
Sedov, L.I., 1959, Similarity and Dimensional Methods in Mechanics: N.Y., Academic Press, 363 p.
Seed, H.B., Pyke, R., and Mertin, G.R., 1978, Effect of multi-directional shaking on pore pressure development in sands: Proc. Am. Soc. Civ. Eng., J. Geotech. Eng. Div., 104, 27-44.
Sengupta, S., 1975, Size-sorting during suspension transportation: lognormality and other characteristics: Sedimentology, 22, 257-273.
Sharp, R.P., and Nobles, L.H., 1953, Mudflow of 1941 at Wrightwood, Southern California: Bull. Geol. Soc. Am., 64, 547-560.
Shen, H.W., ed., 1971, River Mechanics: Privately printed, H.W. Shen, P.O. Box 606, Fort Collins, Colo. 80521, 2 vols.
Shen, H.W., ed., 1972, Sedimentation Symposium to Honor Prof. H.A. Einstein: Privately printed, H.W. Shen, P.O. Box 606, Fort Collins, Colo. 80521.
Shen, H.W., and Kikkawa, H., eds., 1980, Application of stochastic processes in sediment transport: Littleton, Colorado, Water Resources Publ., 18 chapters and 2 appendices (separately paged).
Shields, A., 1936, Anwendung der Ähnlichkeitsmechanik und der Turbulenzforschung auf die Geschiebebewegung: Preuss. Versuchanstalt für Wasserbau und Schiffbau (Berlin), Mitteilungen, v. 26, 26 p. (Transl.: W.P. Ott and J.C. van Uchelen, U.S. Dept. Agric., Soil Conserv. Serv. Coop. Lab., Calif. Inst. Technol.)
Shreve, R.L., 1968, The Blackhawk landslide: Geol. Soc. Am. Spec. Paper 108, 47 p.
Simons, D.B., and Richardson, E.V., 1963, Forms of bed roughness in alluvial channels: Trans. Am. Soc. Civ. Eng., 128, Part I, 284-302.
Simons, D.B., Richardson, E.V., and Nordin, C.F., Jr., 1965, Sedimentary structures generated by flow in alluvial channels: Soc. Econ. Pal. Min., Spec. Publ. 12, 34-52.
Simpson, A., 1983, Wind-induced vibrations of overhead power transmission lines: Sci. Progr., 68, 285-308.
Simpson, J.E., 1969, A comparison between laboratory and atmospheric density currents: Q. J. Roy. Meteorol. Soc., 95, 758-765.
Simpson, J.E., 1972, Effects of the lower boundary at the head of a gravity current: J. Fluid Mech., 53, 759-768.
Simpson, J.E., 1982, Gravity currents in the laboratory, atmosphere and ocean: Ann. Rev. Fluid Mech., 14, 213-234.
Simpson, J.E., and Britter, R.E., 1979, The dynamics of the head of the gravity current advancing over a horizontal surface: J. Fluid Mech., 94, 477-495.
Simpson, J.E., and Britter, R.E., 1980, A laboratory study of an atmospheric mesofront: Q. J. Roy. Meteorol. Soc., 106, 485-500.
Simpson, R.L., 1970, Characteristics of turbulent boundary layers at low Reynolds numbers with and without transpiration: J. Fluid Mech., 42, 769-802.
Skipper, K., 1971, Antidune cross-stratification in a turbidite sequence, Cloridorme Formation, Gaspe, Quebec: Sedimentology, 17, 51-68.
Slingerland, R., 1982, Discussion of the applicability of the Gibbs equation:

J. Sed. Petrol., 52, 1025.
Smith, J.D., 1970, Stability of a sand bed subjected to a shear flow of low Froude number: J. Geophys. Res., 75, 5928-5939.
Smith, J.D., and McLean, S.R., 1977a, Spatially averaged flow over a wavy surface: J. Geophys. Res., 82, 1735-1746.
Smith, J.D., and McLean, S.R., 1977b, Boundary layer adjustments to bottom topography and suspended sediment: in Nihoul, J.C.J., ed., Bottom Turbulence, 123-151: Amsterdam, Elsevier, 306 p.
Smith, N.D., and Syvitski, J.P.M., 1982, Sedimentation in a glacier-fed lake: the role of pelletization on the deposition of fine-grained suspensates: J. Sed. Petrol., 52, 503-513.
Sneed, E.D., and Folk, R.L., 1958, Pebbles in the lower Colorado River, Texas—A study in particle morphogenesis: J. Geol., 66, 114-150.
Southard, J.B., 1971, Representation of bed configurations in depth-velocity-size diagrams: J. Sed. Petrol., 41, 903-915.
Southard, J.B., Boguchwal, L.A., and Romea, R.D., 1980, Test of scale modeling of sediment transport in steady unidirectional flow: Earth Surf. Processes, 5, 17-23.
Southard, J.B., and Dingler, J.R., 1971, Flume study of ripple propagation behind mounds on flat sand beds: Sedimentology, 16, 251-263.
Southard, J.B., and Mackintosh, M.E., 1981, Experimental test of autosuspension: Earth Surf. Processes and Landforms, 6, 103-111.
Southard, J.B., Walker, J.D., and Nozette, S.D., 1982, Wind-tunnel modeling of transport threshold and saltation on Venus: Int. Assoc. Sedimentologists, 11th Int. Congress on Sedimentology, Abstracts of Papers, p. 63.
Statham, I., 1977, Earth Surface Sediment Transport: Oxford, Clarendon Press, 184 p.
Stauffer, P.H., 1967, Grain-flow deposits and their implications, Santa Ynez mountains, California: J. Sed. Petrol., 37, 487-508.
Stow, D.A.V., and Bowen, A.J., 1980, A physical model for the transport and sorting of fine-grained sediment by turbidity currents: Sedimentology, 27, 31-46.
Stringham, G.E., Simons, D.B., and Guy, H.P., 1969, The behavior of large particles falling in quiescent liquids: U.S. Geol. Surv. Prof. Paper 562-C, 36 p.
Sumer, B.M., and Deigaard, R., 1981, Particle motions near the bottom in turbulent flow in an open channel, Part 2: J. Fluid Mech., 109, 311-337.
Sumer, B.M., and Oguz, B., 1978, Particle motions near the bottom in turbulent flow in an open channel: J. Fluid Mech., 86, 109-128.
Sutherland, A.J., 1967, Proposed mechanism for sediment entrainment by turbulent flows: J. Geophys. Res., 72, 6183-6194.
Sutherland, A.J., and Irvine, H.M., 1973, A probabilistic approach to the initiation of movement of non-cohesive sediments: Int. Assoc. Hydraul. Res., Proc. Int. Symp. on River Mechanics, A34-1 to A34-11.
Swift, D.J.P., and Ludwick, J.C., 1976, Substrate response to hydraulic process: Grain-size frequency distributions and bed forms: in Stanley, D.J., and Swift, D.J.P., eds., Marine Sediment Transport and Environmental Management, 159-196: N.Y., Wiley, 602 p.
Swift, D.J.P., Ludwick, J.C., and Boehmer, W.R., 1972, Shelf sediment transport: a probability model: in Swift, D.J.P., Duane, D.B., and Pilkey, O.H., eds., Shelf Sediment Transport: Process and Pattern, 195-223: Stroudsburg, Pa., Dowden, Hutchinson and Ross, 656 p.
Takahashi, T., 1978, Mechanical characteristics of debris flow: Proc. Am. Soc. Civ. Eng., J. Hydraul. Div., 104, 1153-1169.

Takahashi, T., 1980, Debris flow on prismatic open channel: Proc. Am. Soc. Civ. Eng., J. Hydraul. Div., 106, 381-396.
Takahashi, T., 1981, Debris flow: Ann. Rev. Fluid Mech., 13, 57-77.
Tanner, W.F., 1964, Modification of sediment size distributions: J. Sed. Petrol., 34, 156-164.
Tennekes, H., and Lumley, J.L., 1972, A First Course in Turbulence: Cambridge, Mass., MIT Press, 300 p.
Thom, A.S., 1971, Momentum absorption by vegetation. Q. J. Roy. Meteorol. Soc, 97, 414-428.
Thorpe, H.R., 1965, The effect of concentration on the terminal fall velocity of particles in suspension: Proc. Roy. Soc. Edinburgh, 67, 9-24.
Tooby, P.F., Wick, G.L., and Isaacs, J.D., 1977, The motion of a small sphere in a rotating velocity field: a possible mechanism for suspending particles in turbulence: J. Geophys. Res., 82, 2096-2100.
Tritton, D.J., 1977, Physical Fluid Dynamics: N.Y., Van Nostrand Reinhold, 362 p.
Tsuchiya, Y., 1969, Mechanics of the successive saltation of a sand particle on a granular bed in a turbulent stream: Kyoto Univ., Bull. Disaster Prevention Res. Inst., 19, Part 1, No. 152, 31-44.
Tsuchiya, Y., 1970, On the mechanics of saltation of a spherical sand particle in a turbulent stream: Kyoto Univ., Bull. Disaster Prevention Res. Inst., 19, No. 5, 52-57.
Turner, J.S., 1973, Buoyancy Effects in Fluids: Cambridge Univ. Press, 367 p.
Van Tassell, J., 1981, Silver abyssal plain carbonate turbidite: Flow characteristics: J. Geol., 89, 317-333.
Vanoni, V.A., 1946, Transportation of sediment in suspension: Trans. Am. Soc. Civ. Engrs., 111, 67-133.
Vanoni, V.A., 1964, Measurements of critical shear stress for entraining fine sediments in a boundary layer: Calif. Inst. Technol., W.M. Keck Lab. of Hydraulics and Water Resources, Rept. KH-R-7, 47 p.
Vanoni, V.A., ed., 1975, Sedimentation Engineering: Am. Soc. Civil Engrs., Manuals and Reports on Engineering Practice, No. 54, 745 p.
Vanoni, V.A., and Hwang, L.S., 1967, Relation between bed forms and friction in streams: Proc. Am. Soc. Civ. Eng., J. Hydraul. Div., 93(3), 121-144.
Visher, G.S., 1969, Grain size distributions and depositional processes: J. Sed. Petrol., 39, 1074-1106.
Vogel, S., 1981, Life in Moving Fluids: The Physical Biology of Flow: Princeton Univ. Press, 352 p.
von Kármán, T., 1940, The engineer grapples with non-linear problems: Bull. Am. Math. Soc., 46, 615-683.
Walger, E., 1962, Die Korngrössenverteilung von Einzellagen sandiger Sedimente und ihre genetische Bedeutung: Geol. Rundsch., 51, 55-563.
Wallis, G.B., 1969, One-dimensional Two-phase Flow: N.Y., McGraw-Hill, 408 p.
Wang, S.-Y., 1981, Variation of von Karman constant in sediment-laden flow: Proc. Am. Soc. Civ. Eng., J. Hydraul. Div., 107, 407-417.
Ward, B.D., 1969, Relative density effects on incipient bed movement: Water Resour. Res., 5, 1090-1096.
Warg, J.B., 1973, An analysis of methods for calculating constant terminal-settling velocities of spheres in liquids: Math. Geol., 5, 59-72.
Watson, R.L., 1969, Modified Rubey's Law accurately predicts sediment settling velocities: Water Resour. Res., 5, 1147-1150.
White, B.R., and Schulz, J.C., 1977, Magnus effect in saltation: J. Fluid Mech., 81, 497-512.

White, S.J., 1970, Plane bed thresholds of fine grained sediments: Nature, 228, 152-153.
Whitham, G.B., 1974, Linear and Nonlinear Waves: N.Y., Wiley, 636 p.
Wilhelm, R.H., and Kwauk, M., 1948, Fluidization of solid particles: Chem. Eng. Progr., 44, 201-218.
Wilkinson, D.L., and Wood, I.R., 1972, Some observations on the motion of the head of a density current: J. Hydraul. Res., 10, 305-324.
Willetts, B.B., and Murray, C.G., 1981, Lift exerted on stationary spheres in turbulent flow: J. Fluid Mech., 105, 487-505.
Williams, G., 1964, Some aspects of the eolian saltation load: Sedimentology, 3, 257-287.
Williams, P.B., and Kemp, P.H., 1971, Initiation of ripples on flat sediment beds: Proc. Am. Soc. Civ. Eng., J. Hydraul. Div., 97(4), 505-522.
Williams, P.B., and Kemp, P.H., 1972, Initiation of ripples by artificial disturbances: Proc. Am. Soc. Civ. Eng., J. Hydraul. Div., 98, 1057-1070.
Willis, J.C., 1979, Suspended load from error-function models: Proc. Am. Soc. Civ. Eng., J. Hydraul. Div., 105, 801-816.
Willis, J.C., and Coleman, N.L., 1969, Unification of data on sediment transport in flumes by similarity principles: Water Resour. Res., 5, 1330-1336.
Willmarth, W.W., Hawk, N.E., and Harvey, R.L., 1964, Steady and unsteady motions and wakes of freely falling disks: Phys. Fluids, 7, 197-208.
Wimbush, M., and Munk, W., 1970, The benthic boundary layer: in Maxwell, A.E., ed., The Sea, Vol. 4, Part 1, Ch. 19, 731-758: N.Y., Wiley-Interscience, 791 p.
Yalin, M.S., 1972, Mechanics of Sediment Transport: Oxford, Pergamon, 290 p.
Yalin, M.S., 1977, Mechanics of Sediment Transport: Oxford, Pergamon, 2nd ed., 298 p.
Yalin, M.S., and Karahan, E., 1979, Inception of sediment transport: Proc. Am. Soc. Civ. Eng., J. Hydraul. Div., 106, 1173-1190.
Yang, C.T., and Sayre, W.W., 1971a, Stochastic model for sand dispersion: Proc. Am. Soc. Civ. Eng., J. Hydraul. Div., 97, 265-288.
Yang, C.T., and Sayre, W.W., 1971b, Longitudinal dispersion of bed material particles: Proc. Am. Soc. Civ. Eng., J. Hydraul. Div., 97, 907-921.
Yih, C.-S., 1980, Stratified Flows: N.Y., Academic Press, 418 p.
Zingg, A.W., 1952, Wind tunnel studies of the movement of sedimentary material: State Univ. of Iowa, Proc. Hydraulics Conf., Studies in Engineering, Bull. 34, 111-136.
Zingg, A.W., 1953, Some characteristics of aeolian sand movement by saltation process: Centre Nationale de la Recherche Scientifique, Editions, 13, 197-208.

APPENDIX 1 Scale Modeling of Flow Past a Sphere

Suppose you want to study the drag force exerted by a flow of water past a sphere 0.1 mm in diameter by means of a model grapefruit-size sphere 10 cm in diameter in a wind tunnel. To do this, all you need to do is adjust the wind velocity in the wind tunnel so that the Reynolds number $\rho UD/\mu$ is the same as for the flow of water past the small sphere:

$$\frac{\rho_m U_m D_m}{\mu_m} = \frac{\rho_o U_o D_o}{\mu_o} \qquad \text{(A1.1)}$$

where m denotes the large model sphere in air and o denotes the small original sphere in water. Assuming a temperature of 20°C for both air and water, you have the following values of the quantities in Equation (A1.1):

$$\begin{aligned} D_o &= 0.01 \text{ cm} \\ D_m &= 10 \text{ cm} \\ \rho_o &= 1.00 \text{ g/cm}^3 \\ \rho_m &= 1.20 \times 10^{-3} \text{ g/cm}^3 \\ \mu_o &= 1.00 \times 10^{-2} \text{ poise} \\ \mu_m &= 1181 \times 10^{-4} \text{ poise} \end{aligned}$$

So Equation (A1.1) becomes

$$U_m \simeq 1.5 \times 10^{-2} U_o \qquad \text{(A1.2)}$$

Equation (A1.2) tells you what wind velocity you need in the wind tunnel to model a given water velocity around the small sphere. Suppose you're interested in a water velocity of 50 cm/s. You'd need a wind velocity of 0.75 cm/s around the model sphere--just a hint of a breeze. All the details of fluid motions and forces around the big sphere will be exactly the same as around the little sphere, when expressed in dimensionless form. For example, with an appropriate smoke injector you could get a good idea of the flow patterns, and then scale all the velocities down by Equation (A1.2). Positions are conveniently specified in dimensionless form by dividing the distance from the center of the sphere by the sphere diameter. With regard to the total drag force, the dimensionless drag force $F_D/\rho^2 D^2$ would be the same for both spheres, and by plugging in the appropriate values of ρ, U, and D you could predict the drag force on the little sphere in water by measuring the drag force on the big sphere in air.

APPENDIX 2 Hydraulic radius of a circular pipe and a rectangular channel of infinite width

Applying the definition for the hydraulic radius, $R_H = A/P$, to the case of a pipe with circular cross section,

$$R_H = \frac{A}{P} = \frac{\pi D^2/4}{\pi D} = \frac{D}{4}$$

The hydraulic radius of a circular pipe is one-fourth the pipe diameter.

Applying the definition for the hydraulic radius to a rectangular channel of width b and depth d,

$$R_H = \frac{A}{P} = \frac{bd}{b + 2d}$$

As the width increases relative to the depth, the term 2d in the denominator on the right becomes negligible relative to the term b, so

$$R_H \longrightarrow \frac{bd}{b} = d$$

The hydraulic radius of an infinitely wide channel is equal to the flow depth.

APPENDIX 3 Evaluating the Constant of Integration in Equation (5.14) to Obtain the Constant B in Equation (5.15A), the Law of the Wall for a Smooth Boundary Outside the Viscous Sublayer and Buffer Layer

Think in terms of the height δ' at which the turbulence-dominated profile and the viscosity-dominated profile intersect each other; see Figure A3.1, which is a schematic version of Figure 5.13. This point lies about in the middle of the buffer layer, and represents in an approximate way the thickness of the viscosity-dominated layer next to the boundary. Just like the viscous-sublayer thickness δ_v (see the section on smooth flow and rough flow), the intersection height δ' is a function only of τ_o, ρ, and μ, so the dimensionles form of δ', $\rho u_* \delta'/\mu$, equals a constant; call it C.

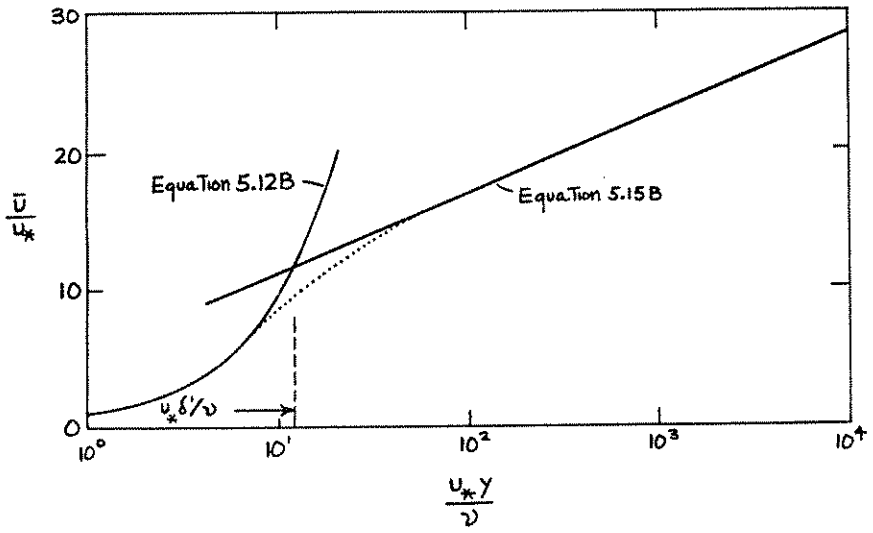

Figure A3.1 Schematic plot of $\bar{u}/u_*$ against $\rho u_* y/\mu$ for the inner layer in smooth flow, showing the intersection of Equation (5.12B) for the viscosity-dominated part of the profile with Equation (5.15B) for the turbulence-dominated part of the profile.

Let the boundary condition for evaluation of A_1 in Equation (5.14) be that at $y = \delta'$

$$\frac{\bar{u}}{u_*} = A \ln \delta' + A_1 \qquad \text{(A3.1)}$$

But from Equation (5.12B), for the viscosity-dominated profile, we know also that at this same height

$$\frac{\bar{u}}{u_*} = \frac{\rho u_* \delta'}{\mu} \qquad \text{(A3.2)}$$

Eliminating $\bar{u}/u*$ by setting the right side of Equation (A3.1) and (A3.2) equal and then solving for A_1,

$$A_1 = \frac{\rho u_* \delta'}{\mu} - A \ln \delta' \qquad \text{(A3.3)}$$

Substituting this value for A_1 into Equation (5.14) and making some rearrangements with the objective of putting the right side into a form with A $\ln(\rho u*/y\mu)$ plus a constant,

$$\begin{aligned}
\frac{\bar{u}}{u_*} &= A \ln y + A_1 \\
&= A \ln y - A \ln \delta' + \frac{\rho u_* \delta'}{\mu} \\
&= A \ln \frac{y}{\delta'} + \frac{\rho u_* \delta'}{\mu} \\
&= A \ln \left[\frac{y}{C \frac{\mu}{\rho u_*}} \right] + C \\
&= A \ln \frac{\rho u_* y}{\mu} + A \ln \frac{1}{C} + C \\
&= A \ln \frac{\rho u_* y}{\mu} + B
\end{aligned}$$

we again obtain Equation (5.15A), and we see that $B = A \ln(1/C) + C$ is a constant that's a function of the dimensionless intersection height C introduced above. The constant B can thus be viewed as a constant that's directly related to the thickness of the viscosity-dominated layer near the boundary, which by Reynolds-number similarity should be nearly the same for a wide range of mean-flow Reynolds numbers.

APPENDIX 4 Integrating Equation (5.27) to Obtain Equations (5.28) and (5.29)

Equation (5.27) is the differential form of the law of the wall for rough boundaries, written in terms of the displacement height y_1 in order to take into account the linear part of the multiplicative function f(D/y) that corrects for proximity to the roughness elements. Here are some details on how to get from Equation (5.27) to the equivalent integral forms, Equations (5.28) and (5.29).

Integrating Equation (5.27) with respect to y,

$$\overline{u} = Au_* \int \frac{1}{y - y_1}\, dy \qquad \text{(A4.1)}$$

By the chain rule for differentiation,

$$\frac{d(y - y_1)}{dx} = \frac{d(y - y_1)}{dy}\,\frac{dy}{dx}$$

(where x is an irrelevant additional variable), so in terms of differentials,

$$dy = \frac{1}{d(y - y_1)/dy}\, d(y - y_1) = \frac{1}{\frac{dy}{dy} - \frac{dy_1}{dy}}\, d(y - y_1) = d(y - y_1)$$

since y_1 isn't a function of y. Replacing dy by $d(y-y_1)$ in Equation (A4.1),

$$\overline{u} = Au_* \int \frac{1}{y - y_1}\, d(y - y_1) \qquad \text{(A4.2)}$$

Dividing both sides of Equation (A4.2) by u* and then evaluating the integral,

$$\frac{\bar{u}}{u_*} = A \ln(y - y_1) + c_1 \qquad (A4.3)$$

where c_1 is a constant of integration which in fully rough flow shouldn't depend on the boundary Reynolds number. By splitting c_1 into two parts, $-A \ln D + B'$, Equation (A4.3) can be put into the form

$$\frac{\bar{u}}{u_*} = A \ln \frac{y - y_1}{D} + B' \qquad (A4.4)$$

which is Equation (5.28). Alternatively, by writing $B' = -A \ln c_2$, where c_2 is a constant, Equation (A4.4) becomes

$$\frac{\bar{u}}{u_*} = A \ln \frac{y - y_1}{D} - A \ln c_2$$

$$= A \ln \frac{y - y_1}{c_2 D} \qquad (A4.5)$$

If we denote $c_2 D$ by y_o, Equation (A4.5) becomes

$$\frac{\bar{u}}{u_*} = A \ln \frac{y - y_1}{y_o} \qquad (A4.6)$$

which is Equation (5.29). The constant c_2 is just the ratio of the roughness length y_o, introduced earlier, to the actual roughness height D.

APPENDIX 5 Finding τ_o and y_1 from a Measured Profile of Mean Velocity in the Inner Layer

As an example of how to find u* from the velocity profile, look at a representative example of the velocity profiles measured by Nikuradse (1933) in his classic experiments on flow resistance in sand-roughened pipes. You might object that sedimentologists aren't much interested in pipe flow, but remember that the law of the wall holds just as well in sand-roughened open channels as in sand-roughened pipes--and for that matter, just as well in bed-form-roughened open channels provided that the bed-form height is a small fraction of the flow depth.

Profile A in Figure A5.1 shows $\overline{u}$ vs. ln y for a flow with cross-section mean velocity U of 8.2 m/s through a pipe with diameter 0.1 m onto which uniform 0.4 mm sand had been glued (Nikuradse, 1933, Table 10, Column 8). The flow was fully rough, because the boundary Reynolds number was 230. The y = 0 level is taken to be at the tops of the grains.

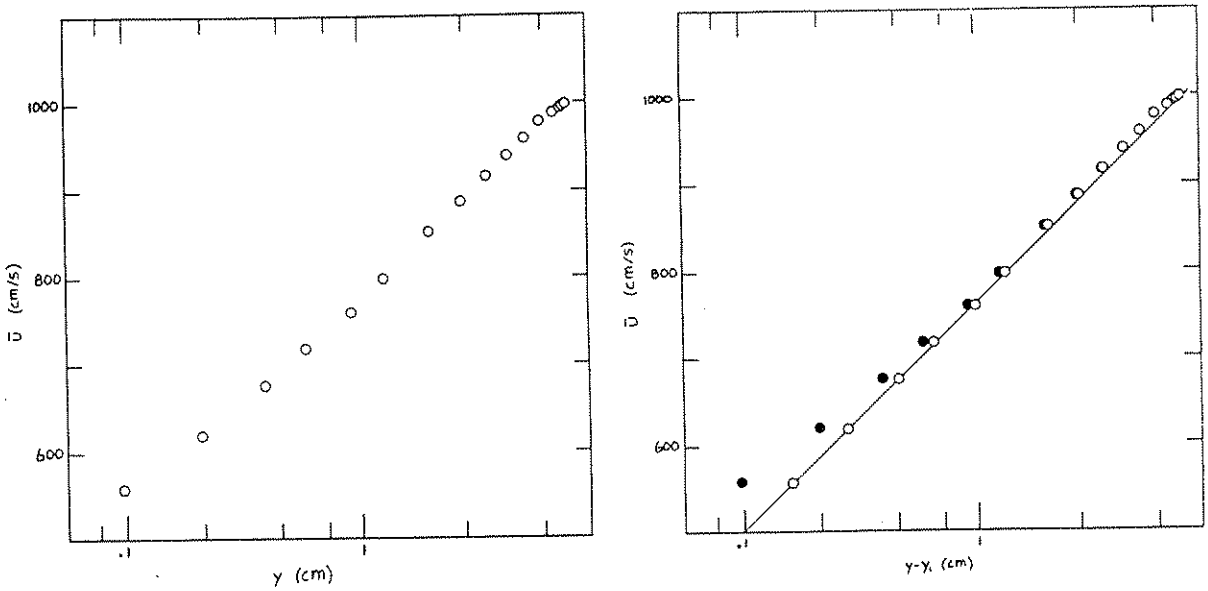

Figure A5.1 Profile of $\overline{u}$ vs. ln y measured by Nikuradse (1933) in fully rough flow in a circular pipe lined with a monolayer of uniform, well rounded sand grains. A. y = 0 level taken at the tops of the grains. B. y = 0 level taken a distance below the tops of the grains that minimizes the sums of the squares of the deviations of the points from the least-squares straight line.

The first thing to do is straighten the profile as much as possible by adjusting the y = 0 level. We did this by trial and error, by moving the y = 0 level up or down slightly and each time fitting a least-squares straight line through the six points that extend up to a height 0.2 times the pipe radius until the sum of

the squares of the deviations of the measured points from the least-squares straight line was a minimum. This shifts the y = 0 level downward a distance of 0.57 mm toward the wall of the pipe, and results in Profile B in Figure A5.1. The slope of this best least-squares line for $\overline{u}$ vs. $\ln(y-y_1)$ is 289.7 (if y and y_1 are measured in centimeters and $\overline{u}$ in centimeters per second), so by Equation (5.30) u* should be 50.3 cm/s. The value of u* actually measured by Nikuradse for this run was 49.0 cm/s, so our estimate is satisfactorily close.

With so few points in the profile, however, it doesn't take much error in velocity measurements to throw off the estimate of u* appreciably. Figure A5.2 shows a graph of the ratio of measured u* to estimated u* for the six of Nikuradse's velocity profiles (including the one used above) that meet the conditions Re* > 100 (fully rough flow) and r/D > 60 (roughness elements only a small fraction of pipe radius). In each of these six profiles there are six points for which y > D and y < 0.2r. (We avoided Nikuradse's smooth and transitional flows, because for those it's not clear how to adjust the profile for roughness-height effects in the inner part of the inner layer, and if we neglect that part, there aren't enough measured points in the outer part of the inner layer, for which y >> D and y < 0.2r, to establish a reliable straight line.) The ratio of measured u* to estimated u* ranges from 0.965 to 1.084, the average being about 1.023. We note in passing that if profile points up through y = 0.5r are included, the average ratio of u* values decreases to 0.95. So the velocity profile expressed in inner coordinates deviates nonnegligibly from a straight line outside the log layer, even though to one's eye the curve still looks like a good extension of the inner-layer semilog straight line.

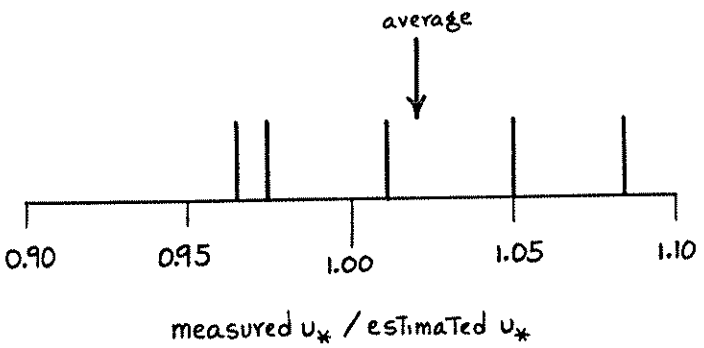

Figure A5.2 Graph of the ratio of measured u* to estimated u* for the six velocity profiles measured by Nikuradse for which Re > 100 and r/D > 60.

APPENDIX 6 Finding B', y_o, and k_s from a Profile of Mean Velocity Measured in the Inner Layer

Assume that you've already adjusted the y = 0 level by trial and error to make your measured profile as nearly a straight line as possible in a semilog plot, as in Appendix 5. You can find the value of the constant B' in Equation (5.28) that's associated with the particular geometry of roughness of the bed above which you measured your velocity profile. Don't expect it to be equal to 8.5, as in Equation (5.20B), even if you've done a fine job of measuring the profile, because the roughness geometry is not likely to be the same as that used by Nikuradse (1933), on which the value of 8.5 is based.

Compare the equation for your best least-squares straight line,

$$\bar{u} = m \ln(y - y_1) + b \qquad \text{(A6.1)}$$

where m is the slope and b is the $\ln(y-y_1)$ intercept, with Equation (5.28),

$$\frac{\bar{u}}{u_*} = A \ln \frac{y - y_1}{D} + B' \qquad \text{(A6.2)}$$

Put Equation (A6.1) into the same form as Equation (A6.2) by dividing both sides by u* and getting D into the log term:

$$\frac{\bar{u}}{u_*} = \frac{m}{u_*} \ln(y - y_1) + \frac{b}{u_*}$$

$$= \frac{m}{u_*} \ln(y - y_1) - \frac{m}{u_*} \ln D + \frac{m}{u_*} \ln D + \frac{b}{u_*}$$

$$= \frac{m}{u_*} \ln \frac{y - y_1}{D} + \frac{m}{u_*} \ln D + \frac{b}{u_*} \qquad \text{(A6.3)}$$

If you compare Equations (A6.3) and (A6.1), you see that

$$B' = \frac{b + m \ln D}{u_*} \qquad (A6.4)$$

(and also that A = m/u*, although that's not of interest here.) With Equation (A6.4) you can find B' once you know u* (see Appendix 5). If the bed grains aren't extremely well sorted, there's a question about which size in the bed-sediment size distribution to use for D. It seems natural to use some percentile coarser than the median, on the theory that it's the coarser grains that stick up higher and are more effective as roughness elements. The value of B' you get using Equation (A6.4) depends on this choice of representative roughness size.

Finding the roughness length y_o is a parallel problem, but with the difference that your estimate of y_o is independent of the problem of the choice of sediment size to represent D. Start again with the best-fit straight line, Equation (A6.1), and put it into the same form as Equation (5.29), which we repeat here as

$$\frac{\bar{u}}{u_*} = A \ln \frac{y - y_1}{y_o} \qquad (A6.5)$$

by dividing both sides by u* and then rearranging the right side to get rid of the separate constant:

$$\begin{aligned}
\frac{\bar{u}}{u_*} &= \frac{m}{u_*} \ln(y - y_1) + \frac{b}{u_*} \\
&= \frac{m}{u_*} \ln(y - y_1) + \frac{m}{u_*}\left(\frac{u_*}{m}\frac{b}{u_*}\right) \\
&= \frac{m}{u_*}\left[\ln(y - y_1) + \frac{b}{m}\right] \\
&= \frac{m}{u_*}\left[\ln(y - y_1) + \ln e^{b/m}\right] \\
&= \frac{m}{u_*}\left[\ln (y - y_1)\, e^{b/m}\right] \qquad (A6.6)
\end{aligned}$$

If you compare Equations (A6.5) and (A6.6), you see that

$$y_o = e^{-b/m} \qquad \text{(A6.7)}$$

By Equation (A6.7) you can find y_o for your particular case of bed-roughness geometry when you know the slope m and intercept b of the best straight-line fit of your velocity profile (Equation A6.1).

Finding the equivalent sand roughness k_s is easy now that you have Equation (A6.4). Simply substitute the value of 8.5 for B' and replace D by k_s, and then solve for k_s:

$$k_s = \exp\left(\frac{8.5\ u_* - b}{m}\right) \qquad \text{(A6.8)}$$

Instead of finding B' in accordance with the actual value of D, you're finding a fictitious value of D (and calling it k_s) in accordance with the conventional uniform-sand-roughness value of B'.

APPENDIX 7 A Different Way of Matching Inner-Layer and Outer-Layer Velocity Profiles

There's another slightly different way to see how the matching of inner-layer and outer-layer velocity profiles works (Clauser, 1956; Monin and Yaglom, 1975). It's straightforward but involves more mathematics.

In the outer layer (Equation 5.32),

$$\frac{U_s - \overline{u}}{u_*} = f_1\left(\frac{y}{d}\right) = f_1(q_1) \qquad \text{(A7.1)}$$

and in the inner layer (Equation 5.8)

$$\frac{\overline{u}}{u_*} = f_2\left(\frac{\rho u_* y}{\mu}\right) = f_2\left(\frac{y}{d}\ \ \frac{\rho u_* d}{\mu}\right) = f_2(q_1 q_3) \qquad \text{(A7.2)}$$

where for convenience y/d is called q_1 and $\rho u_* d/\mu$ is called q_3. In the overlap layer, Equations (A7.1) and (A7.2) hold simultaneously. Add them together:

$$\frac{U_s}{u_*} = f_1(q_1) + f_2(q_1 q_3) = f_3(q_3) \qquad \text{(A7.3)}$$

The function f_3 is there on the right because U_s/u_* is not a function of y but is a function of $\rho u_* d/\mu$. Differentiate Equation (IV.3) twice, first with respect to q_3,

$$\frac{\partial}{\partial q_3}\left[f_1(q_1)\right] + \frac{\partial}{\partial q_3}\left[f_2(q_1 q_3)\right] = \frac{\partial}{\partial q_3}\left[f_3(q_3)\right]$$

$$0 + q_1\, f_2'(q_1 q_3) = f_3'(q_3) \qquad \text{(A7.4)}$$

and then the result, Equation (A7.4), with respect to q_1:

$$\frac{\partial}{\partial q_1}\left[q_1\ f_2'(q_1q_3)\right] = \frac{\partial}{\partial q_1}\left[f_3(q_3)\right]$$

$$q_1\ \frac{\partial}{\partial q_1}\left[f_2'(q_1q_3)\right] = f_2'(q_1q_3)\ \frac{\partial q_1}{\partial q_1} = 0$$

$$q_1q_3\ f_2''(q_1q_3) + f_2'(q_1q_3) = 0 \qquad \text{(A7.5)}$$

Equation (A7.5) is a simple differential equation whose solution you can readily verify is

$$f_2(q_1q_3) = c_1\ \ln\ q_1q_3 + c_3 \qquad \text{(A7.6)}$$

or, in the original variables,

$$\frac{\overline{u}}{u_*} = c_1\ \ln\ \frac{\rho u_* y}{\mu} + c_3 \qquad \text{(A7.7)}$$

Equation (A7.7) is the same as the law of the wall, Equation (5.15).

Writing Equation (A7.6) in the form

$$f_2(q_1q_3) = c_1\ \ln\ q_1 + c_1\ \ln\ q_3 + c_3$$

and comparing this with Equation (A7.3), namely

$$f_2(q_1q_3) = f_3(q_3) - f_1(q_1)$$

we see that

$$f_1(q_1) = -c_1\ \ln\ q_1 + c_4 \qquad \text{(A7.8)}$$

or in original variables,

$$\frac{U_s - \bar{u}}{u_*} = -c_1 \ln \frac{y}{d} + c_4 \qquad \text{(A7.9)}$$

where c_4 is a positive constant different from c_3. Equation (A7.9) is Equation (5.38), the logarithmic part of the velocity-defect law in the overlap layer.

INDEX